DEPARTMENT OF ORGANIC CHEMISTRY

DÉPARTEMENT DE CHIMIE ORGANIQUE

Chemical investigation of three Cameroonian medicinal plants with antileishmanial potency: *Endodesmia calophylloides* Benth., *Pentadesma butyracea* Sabine (Clusiaceae) and *Adenia lobata* (Jacq.) Engl. (Passifloraceae)- Phytodrug preformulation trial

By:

GARBA KOFFI Jean
Master in Organic Chemistry
Registration number: 09Y849
Under the Direction of

LENTA NDJAKOU Bruno
Professor

July 2022

DEPARTEMENT DE CHIMIE ORGANIQUE
DEPARTMENT OF ORGANIC CHEMISTRY

ATTESTATION DE CORRECTION DE MEMOIRE DE THESE DE DOCTORAT/*Ph.D* DE MONSIEUR GARBA KOFFI Jean

<u>Titre de thèse</u>: Chemical investigation of three Cameroonian medicinal plants with antileishmanial potency: *Endodesmia calophylloides* Benth., *Pentadesma butyracea* Sabine (Clusiaceae) and *Adenia lobata* (Jacq.) Engl. (Passifloraceae)- Phytodrug preformulation trial

Nous soussignés, enseignants ci-dessous nommés, membres du jury de soutenance de thèse de Doctorat/*Ph.D* de Monsieur **GARBA KOFFI Jean**, Matricule 09Y849, attestons que ce candidat a bel et bien pris en compte dans la mouture finale de sa thèse, toutes corrections et recommandations qui lui ont été faites au cours de sa soutenance en date du 15 Juillet 2022.

En foi de quoi, la présente attestation de correction lui est délivrée pour servir et valoir ce que de droit.
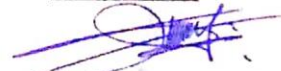
Fait à Yaoundé, le 2 9 JUIL 2022

<u>Le Jury :</u>

<u>Le Président :</u>

Wandji Jean
Professeur

<u>Le rapporteur :</u>

<u>Les membres</u>

Dr. Nbazoa Dyana Céline

prof nkeo fou

CERTIFICATION

I, the undersigned, **LENTA NDJAKOU Bruno** (Professor) certify that the work presented in this thesis was carried out in the Laboratory of Natural Substances of Therapeutic Interest and Organic Synthesis of the Higher Teacher Training College of the University of Yaoundé 1, under my supervision.

This work has never been presented to a jury as part of a thesis or dissertation.

In witness whereof, this certificate is issued to him to serve and assert that of right.

Yaoundé ……………………………

Supervisor

UNIVERSITÉ DE YAOUNDÉ I		THE UNIVERSITY OF YAOUNDE I
Faculté des Sciences		Faculty of Science
Division de la Programmation et du Suivi des Activités Académiques		Division of Programming and Follow-up of Academic Affaires
LISTE DES ENSEIGNANTS PERMANENTS		LIST OF PERMANENT TEACHING STAFF

Academic year 2021/2022
(Per Departement and per grade)
Revised date 22th June 2022

ADMINISTRATION

DEAN: TCHOUANKEU Jean-Claude, *Associate professor*
VICE-DEAN / DPSAA: ATCHADE Alex de Théodore, *Associate Professor*
VICE-DEAN / DSSE: NYEGUE Maximillienne Ascencion*, Professor*
VICE-DEAN / DRC: ABOSSOLO Monique, *Associate Professor*
Head of Division of Administrative and Financial Affairs: NDOYE FOE Florentine Marie Chantal., *Associate Professor*
Head of Division of Academics Affairs, admission and research DAASR: AJEAGAH Gideon AGHAINDUM, *Professor*

1- DEPARTMENT OF BIOCHEMISTRY (BC) (39)

N°	NOMS ET PRÉNOMS	GRADE	OBSERVATIONS
1	BIGOGA DAIGA Jude	Professor	On duty
2	BOUDJEKO Thaddée	Professor	On duty
3	FEKAM BOYOM Fabrice	Professor	On duty
4	FOKOU Elie	Professor	On duty
5	KANSCI Germain	Professor	On duty
6	MBACHAM FON Wilfried	Professor	On duty
7	MOUNDIPA FEWOU Paul	Professor	*Head of Department*
8	OBEN Julius ENYONG	Professor	On duty
9	ACHU Merci BIH	Associate Professor	On duty
10	ATOGHO Barbara Mma	Associate Professor	On duty
11	AZANTSA KINGUE GABIN BORIS	Associate Professor	On duty
12	BELINGA née NDOYE FOE M. C. F.	Associate Professor	*Head DAF / FS*
13	DJUIDJE NGOUNOUE Marcelline	Associate Professor	On duty
14	EFFA NNOMO Pierre	Associate Professor	On duty
15	EWANE Cécile Anne	Associate Professor	On duty
16	KOTUE KAPTUE Charles	Lecturer	On duty
17	MOFOR née TEUGWA Clotilde	Associate Professor	*Dean FS/UDs*
18	NANA Louise épouse WAKAM	Associate Professor	On duty
19	NGONDI Judith Laure	Associate Professor	On duty
20	NGUEFACK Julienne	Associate Professor	On duty
21	NJAYOU Frédéric Nico	Associate Professor	On duty
22	TCHANA KOUATCHOUA Angèle	Associate Professor	On duty
23	AKINDEH MBUH NJI	Lecturer	On duty
24	BEBEE Fadimatou	Lecturer	On duty

25	BEBOY EDJENGUELE Sara Nathalie	Lecturer	On duty
26	DAKOLE DABOY Charles	Lecturer	On duty
27	DJUIKWO NKONGA Ruth Viviane	Lecturer	On duty
28	DONGMO LEKAGNE Joseph Blaise	Lecturer	On duty
29	FONKOUA Martin	Lecturer	On duty
30	KOUOH ELOMBO Ferdinand	Lecturer	On duty
31	LUNGA Paul KEILAH	Lecturer	On duty
32	MANANGA Marlyse Joséphine	Lecturer	On duty
33	MBONG ANGIE M. Mary Anne	Lecturer	On duty
34	OWONA AYISSI Vincent Brice	Lecturer	On duty
35	Palmer MASUMBE NETONGO	Lecturer	On duty
36	PECHANGOU NSANGOU Sylvain	Lecturer	On duty
37	WILFRIED ANGIE Abia	Lecturer	On duty

38	FOUPOUAPOUOGNIGNI Yacuba	Assistant Lecturer	On duty
39	MBOUCHE FANMOE Marceline Joëlle	Assistant Lecturer	On duty

2- DEPARTMENT OF BIOLOGY AND ANIMAL PHYSIOLOGY (BAP) (51)

1	AJEAGAH Gideon AGHAINDUM	Professor	*Vice-Dean / DSSE*
2	BILONG BILONG Charles-Félix	Professor	***Head of Department***
3	DIMO Théophile	Professor	On duty
4	DJIETO LORDON Champlain	Professor	On duty
5	DZEUFIET DJOMENI Paul Désiré	Professor	On duty
6	ESSOMBA née NTSAMA MBALA	Professor	Vice Dean*/FMSB/UYI*
7	FOMENA Abraham	Professor	On duty
8	KEUKEUNOU Sévilor	Professor	On duty
9	NJAMEN Dieudonné	Professor	On duty
10	NJIOKOU Flobert	Professor	On duty
11	NOLA Moïse	Professor	On duty
12	TAN Paul VERNYUY	Professor	On duty
13	TCHUEM TCHUENTE Louis Albert	Professor	*Inspector of service Coord.Progr./MINSANTE*
14	ZEBAZE TOGOUET Serge Hubert	Professor	On duty

15	ALENE Désirée Chantal	Associate Professor	On duty
16	BILANDA Danielle Claude	Associate Professor	On duty
17	DJIOGUE Séfirin	Associate Professor	On duty
18	JATSA BOUKENG Hermine épse MEGAPTCHE	Associate Professor	On duty
19	LEKEUFACK FOLEFACK Guy B.	Associate Professor	On duty
20	MBENOUN MASSE Paul Serge	Associate Professor	On duty
21	MEGNEKOU Rosette	Associate Professor	On duty
22	MONY Ruth épse NTONE	Associate Professor	On duty
23	NGUEGUIM TSOFACK Florence	Associate Professor	On duty
24	NGUEMBOK	Associate Professor	On duty
25	TOMBI Jeannette	Associate Professor	On duty

26	ATSAMO Albert Donatien	Lecturer	On duty
27	BASSOCK BAYIHA Etienne Didier	Lecturer	On duty
28	DONFACK Mireille	Lecturer	On duty
29	ESSAMA MBIDA Désirée Sandrine	Lecturer	On duty
30	ETEME ENAMA Serge	Lecturer	On duty
31	FEUGANG YOUMSSI François	Lecturer	On duty
32	GONWOUO NONO Legrand	Lecturer	On duty
33	GOUNOUE KAMKUMO Raceline	Lecturer	On duty
34	KANDEDA KAVAYE Antoine	Lecturer	On duty
35	KOGA MANG DOBARA	Lecturer	On duty
36	LEME BANOCK Lucie	Lecturer	On duty
37	MAHOB Raymond Joseph	Lecturer	On duty
38	METCHI DONFACK Mirelle Epse GHOUMO	Lecturer	On duty
39	MOUNGANG Luciane Marlyse	Lecturer	On duty
40	MVEYO NDANKEU Yves Patrick	Lecturer	On duty
41	NGOUATEU KENFACK Omer Bébé	Lecturer	On duty
42	NJUA Clarisse Yafi	Lecturer	*Head of Div. UBA*
43	NOAH EWOTI Olive Vivien	Lecturer	On duty
44	TADU Zephyrin	Lecturer	On duty
45	TAMSA ARFAO Antoine	Lecturer	On duty
46	YEDE	Lecturer	On duty
47	YOUNOUSSA LAME	Lecturer	On duty

48	AMBANG NDZENGUE Georgia Elna	Assistant Lecturer	On duty
49	FOKAM Alvine C. Epse KEGNE	Assistant Lecturer	On duty
50	MAPON NSANGOU Indou	Assistant Lecturer	On duty
51	NWANE Philippe Bienvenu	Assistant Lecturer	On duty

3- DEPARTMENT OF BIOLOGY AND VEGETAL PHYSIOLOGY (BVP) (33)

1	AMBANG Zachée	Professor	*Head of DAARS/UYII*
2	DJOCGOUE Pierre François	Professor	On duty
3	MOSSEBO Dominique Claude	Professor	On duty
4	MBOLO Marie	Professor	On duty
5	YOUMBI Emmanuel	Professor	**Head of Department**
6	ZAPFACK Louis	Professor	On duty

7	ANGONI Hyacinthe	Associate Professor	On duty
8	BIYE Elvire Hortense	Associate Professor	On duty
9	MALA Armand William	Associate Professor	On duty
10	MBARGA BINDZI Marie Alain	Associate Professor	*DAAC/ UDla*
11	NDONGO BEKOLO	Associate Professor	*CE / MINRESI*
12	NGODO MELINGUI Jean Baptiste	Associate Professor	On duty
13	NGONKEU MAGAPTCHE Eddy L.	Associate Professor	On duty
14	TONFACK Libert Brice	Associate Professor	On duty
15	TSOATA Esaïe	Associate Professor	On duty

16	ONANA JEAN MICHEL	Associate Professor	On duty

17	DJEUANI Astride Carole	Lecturer	On duty
18	GOMANDJE Christelle	Lecturer	On duty
19	GONMADGE Christelle	Lecturer	On duty
20	MAFFO MAFFO Nicole Liliane	Lecturer	On duty
21	MAHBOU SOMO TOUKAM. Gabriel	Lecturer	On duty
22	NGALLE Hermine BILLE	Lecturer	On duty
23	NNANGA MEBENGA Ruth Laure	Lecturer	On duty
24	NOUKEU KOUAKAM Armelle	Lecturer	On duty
25	NSOM ZAMBO Epse PIAL Annie C.	Lecturer	*On secondment to UNESCO Mali*
26	GODSWILL NTSOMBAH NTSEFONG	Lecturer	On duty
27	KABELONG BANAHO Louis-Paul-Roger	Lecturer	On duty
28	KONO Léon Dieudonné	Lecturer	On duty
29	LIBALAH Moses BAKONCK	Lecturer	On duty
30	LIKENG-LI-NGUE Benoit C	Lecturer	On duty
31	TAEDOUNG Evariste Hermann	Lecturer	On duty
32	TEMEGNE NONO Carine	Lecturer	On duty
33	MANGA NDJAGA Jude	Assistant Lecturer	On duty

4- DEPARTMENT OF INORGANIC CHEMISTRY (IC) (31)

1	AGWARA ONDOH Moïse	Professor	*Head of Department*
2	Florence UFI CHINJE Epse MELO	Professor	*Rector Univ. Ngaoundere*
3	GHOGOMU Paul MINGO	Professor	*Minister in Charge of Miss. PR*
4	NANSEU Njiki Charles Péguy	Professor	On duty
5	NDIFON Peter TEKE	Professor	*CT MINRESI*
6	NDIKONTAR Maurice KOR	Professor	*Vice-Dean Univ. Bamenda*
7	NENWA Justin	Professor	On duty
8	NGAMENI Emmanuel	Professor	*Dean FS UDs*
9	NGOMO Horace MANGA	Professor	*Vice Chancelor/UB*

10	ACAYANKA Elie	Associate Professor	On duty
11	EMADACK Alphonse	Associate Professor	On duty
12	KAMGANG YOUBI Georges	Associate Professor	On duty
13	KEMMEGNE MBOUGUEM Jean C.	Associate Professor	On duty
14	KENNE DEDZO GUSTAVE	Associate Professor	On duty
15	KONG SAKEO	Associate Professor	On duty
16	MBEY Jean Aime	Associate Professor	On duty
17	NDI NSAMI Julius	Associate Professor	On duty
18	NEBAH nee NDOSIRI Bridget NDOYE	Associate Professor	*CT/ MINFEM*

19	NJIOMOU C. épse DJANGANG	Associate Professor	On duty
20	NJOYA Dayirou	Associate Professor	On duty
21	NYAMEN Linda Dyorisse	Associate Professor	On duty
22	PABOUDAM GBAMBIE A.	Associate Professor	On duty
23	TCHAKOUTE KOUAMO Hervé	Associate Professor	On duty

24	BELIBI BELIBI Placide Désiré	Lecturer	*CS/ ENS Bertoua*
25	CHEUMANI YONA Arnaud M.	Lecturer	On duty
26	KOUOTOU DAOUDA	Lecturer	On duty
27	MAKON Thomas Beauregard	Lecturer	On duty
28	NCHIMI NONO KATIA	Lecturer	On duty
29	NJANKWA NJABONG N. Eric	Lecturer	On duty
30	PATOUOSSA ISSOFA	Lecturer	On duty
31	SIEWE Jean Mermoz	Lecturer	On duty

5- DEPARTMENT OF ORGANIC CHEMISTRY (OC) (38)			
1	DONGO Etienne	Professor	*Vice-Dean/FSE/UYI*
2	MBAZOA née DJAMA Céline	Professor	On duty
3	NGOUELA Silvère Augustin	Professor	*Head of Department UDs*
4	NYASSE Barthélemy	Professor	On duty
5	PEGNYEMB Dieudonné Emmanuel	Professor	**Head of Department** *Director/ MINESUP*
6	WANDJI Jean	Professor	On duty

7	Alex de Théodore ATCHADE	Associate Professor	*Vice-Dean / DPSAA*
8	AMBASSA Pantaléon	Associate Professor	On duty
9	EYONG Kenneth OBEN	Associate Professor	On duty
10	FOLEFOC Gabriel NGOSONG	Associate Professor	On duty
11	FOTSO WABO Ghislain	Associate Professor	On duty
12	KAMTO Eutrophe Le Doux	Associate Professor	On duty
13	KEUMEDJIO Félix	Associate Professor	On duty
14	KEUMOGNE Marguerite	Associate Professor	On duty
15	KOUAM Jacques	Associate Professor	On duty
16	MKOUNGA Pierre	Associate Professor	On duty
17	MVOT AKAK CARINE	Associate Professor	On duty
18	NGO MBING Joséphine	Associate Professor	*Vice/Direct. MINERESI*
19	NGONO BIKOBO Dominique Serge	Associate Professor	*C.E/MINESUP*
20	NOTE LOUGBOT Olivier Placide	Associate Professor	*DAAC of U. Bertoua*
21	NOUNGOUE TCHAMO Diderot	Associate Professor	On duty
22	TABOPDA KUATE Turibio	Associate Professor	On duty
23	TAGATSING FOTSING Maurice	Associate Professor	On duty
24	TCHOUANKEU Jean-Claude	Associate Professor	*Dean /FS/ UYI*
25	YANKEP Emmanuel	Associate Professor	On duty
26	ZONDENDEGOUMBA Ernestine	Associate Professor	On duty

27	MESSI Angélique Nicolas	Lecturer	On duty
28	NGNINTEDO Dominique	Lecturer	On duty

29	NGOMO Orléans	Lecturer	On duty
30	OUAHOUO WACHE Blandine M.	Lecturer	On duty
31	SIELINOU TEDJON Valérie	Lecturer	On duty
32	TCHAMGOUE Joseph	Lecturer	On duty
33	TSAMO Armelle	Lecturer	On duty
34	TSEMEUGNE Joseph	Lecturer	On duty

35	MUNVERA MFIFEN Aristide	Associate Professor	On duty
36	NONO Cardy	Assistant Lecturer	On duty
37	OUETE NANTCHOUANG Judith	Assistant Lecturer	On duty
38	TSAFFACK Maurice	Assistant Lecturer	On duty

6- DEPARTMENT OF INFORMATIC (IN) (22)

1	ATSA ETOUNDI Roger	Professor	*Chief of Div. MINESUP*
2	FOUDA NDJODO Marcel Laurent	Professor	*Head Dpt ENS/Head IGA.MINESUP Chef*

3	NDOUNDAM Réné	Associate professor	On duty
4	TSOPZE Norbert	Associate professor	On duty

5	ABESSOLO ALO'O Gislain	Lecturer	*Deputy Director/ MINFOPRA*
6	AMINOU Halidou	Lecturer	**Head of Department**
7	DJAM Xaviera YOUH - KIMBI	Lecturer	On duty
8	DOMGA KOMGUEM Rodrigue	Lecturer	On duty
9	EBELE Serge Alain	Lecturer	On duty
10	HAMZA Adamou	Lecturer	On duty
11	JIOMEKONG AZANZI Fidel	Lecturer	On duty
12	KOUOKAM KOUOKAM E. A.	Lecturer	On duty
13	MELATAGIA YONTA Paulin	Lecturer	On duty
14	MONTHE DJIADEU Valery M.	Lecturer	On duty
15	OLE OLE Daniel Claude Delort	Lecturer	*C/D Enset. Ebolowa*
16	TAPAMO Hyppolite	Lecturer	On duty

17	BAYEM Jacques Narcisse	Assistant Lecturer	On duty
18	EKODECK Stéphane Gaël Raymond	Assistant Lecturer	On duty
19	MAKEMBE. S. Oswald	Assistant Lecturer	On duty
20	MESSI NGUELE Thomas	Assistant Lecturer	On duty
21	NKONDOCK. MI. BAHANACK.N.	Assistant Lecturer	On duty
22	NZEKON NZEKO'O Armel Jacques	Assistant Lecturer	On duty

7- DEPARTMENT OF MATHEMATICS (MA) (31)

1	AYISSI Raoult Domingo	Professor	**Head of Department**
2	EMVUDU WONO Yves S.	Professor	*Inspector MINESUP*

3	KIANPI Maurice	Associate Professor	On duty

4	MBANG Joseph	Associate Professor	On duty
5	MBEHOU Mohamed	Associate Professor	On duty
6	MBELE BIDIMA Martin Ledoux	Associate Professor	On duty
7	NOUNDJEU Pierre	Associate Professor	*Chief of service of programs & Degrees*
8	TAKAM SOH Patrice	Associate Professor	On duty
9	TCHAPNDA NJABO Sophonie B.	Associate Professor	*Director/AIMS Rwanda*
10	TCHOUNDJA Edgar Landry	Associate Professor	On duty

11	AGHOUKENG JIOFACK Jean Gérard	Lecturer	*Chief Cellule MINEPAT*
12	BOGSO Antoine marie	Lecturer	On duty
13	CHENDJOU Gilbert	Lecturer	On duty
14	DJIADEU NGAHA Michel	Lecturer	On duty
15	DOUANLA YONTA Herman	Lecturer	On duty
16	KIKI Maxime Armand	Lecturer	On duty
17	MBAKOP Guy Merlin	Lecturer	On duty
18	MENGUE MENGUE David Joe	Lecturer	On duty
19	NGUEFACK Bernard	Lecturer	On duty
20	NIMPA PEFOUKEU Romain	Lecturer	On duty
21	OGADOA AMASSAYOGA	Lecturer	On duty
22	POLA DOUNDOU Emmanuel	Lecturer	On duty
23	TECHEUTIA Daniel Duviol	Lecturer	On duty
24	TETSADJIO TCHILEPECK M. E.	Lecturer	On duty

25	BITYE MVONDO Esther Claudine	Assistant Lecturer	On duty
26	FOKAM Jean Marcel	Assistant Lecturer	On duty
27	LOUMNGAM KAMGA Victor	Assistant Lecturer	On duty
28	MBATAKOU Salomon Joseph	Assistant Lecturer	On duty
29	MBIAKOP Hilaire George	Assistant Lecturer	On duty
30	MEFENZA NOUNTU Thiery	Assistant Lecturer	On duty
31	TCHEUTIA Daniel Duviol	Assistant Lecturer	On duty

8- DEPARTMENT OF MICROBIOLOGY (MIB) (22)

1	ESSIA NGANG Jean Justin	Professor	*Head of Department*
2	NYEGUE Maximilienne Ascension	Professor	*Vice Dean/DSSE/FS*
3	NWAGA Dieudonné M.	Professor	On duty

4	ASSAM ASSAM Jean Paul	Associate professor	On duty
5	BOUGNOM Blaise Pascal	Associate professor	On duty
6	BOYOMO ONANA	Associate professor	On duty
7	KOUITCHEU MABEKU Laure Brigitte Epse KOUAM	Associate professor	On duty
8	RIWOM Sara Honorine	Associate professor	On duty
9	SADO KAMDEM Sylvain Leroy	Associate professor	On duty

10	BODA Maurice	Lecturer	On duty
11	ESSONO OBOUGOU Germain G.	Lecturer	On duty
12	NJIKI BIKOÏ Jacky	Lecturer	On duty
13	TCHIKOUA Roger	Lecturer	On duty
14	ESSONO Damien Marie	Lecturer	On duty
15	LAMYE Glory MOH	Lecturer	On duty
16	MEYIN A EBONG Solange	Lecturer	On duty
17	NKOUDOU ZE Nardis	Lecturer	On duty
18	TAMACHO KWEYANG Blandine P.	Lecturer	On duty
19	TOBOLBAÏ Richard	Lecturer	On duty
20	MONI NDEBI Esther Del Florence	Assistant Lecturer	On duty
21	NKOUE TONG ABRAHAM	Assistant Lecturer	On duty
22	SAKE NGANE Carole Stéphanie	Assistant Lecturer	On duty

9. DEPARTMENT OF PHYSICS (PHY) (43)

1	BEN- BOLIE Germain Hubert	Professor	On duty
2	DJUIDJE KENMOE épouse ALOYEM	Professor	On duty
3	EKOBENA FOUDA Henri Paul	Professor	*Vice Rector. UN*
4	ESSIMBI ZOBO Bernard	Professor	On duty
5	KOFANE Timoléon Crépin	Professor	On duty
6	NANA ENGO Serge Guy	Professor	On duty
7	NANA NBENDJO Blaise	Professor	On duty
8	NDJAKA Jean Marie Bienvenu	Professor	***Head of Department***
9	NOUAYOU Robert	Professor	On duty
10	NJANDJOCK NOUCK Philippe	Professor	On duty
11	PEMHA Elkana	Professor	On duty
12	TABOD Charles TABOD	Professor	*Dean Univ/Bda*
13	TCHAWOUA Clément	Professor	On duty
14	WOAFO Paul	Professor	On duty
15	ZEKENG Serge Sylvain	Professor	On duty

16	BIYA MOTTO Frédéric	Associate Professor	*DG/HYDRO Mekin*
17	BODO Bertrand	Associate Professor	On duty
18	ENYEGUE A NYAM épse BELINGA	Associate Professor	On duty
19	EYEBE FOUDA Jean sire	Associate Professor	On duty
20	FEWO Serge Ibraïd	Associate Professor	On duty
21	HONA Jacques	Associate Professor	On duty
22	MBINACK Clément	Associate Professor	On duty
23	NDOP Joseph	Associate Professor	On duty
24	SAIDOU	Associate Professor	*MINERESI*
25	SIEWE SIEWE Martin	Associate Professor	On duty
26	SIMO Elie	Associate Professor	On duty
27	VONDOU Derbetini Appolinaire	Associate Professor	On duty

28	WAKATA née BEYA Annie	Associate Professor	*Director/ ENS/UYI*

29	ABDOURAHIMI	Lecturer	On duty
30	AYISSI EYEBE Guy François Valérie	Lecturer	On duty
31	CHAMANI Roméo	Lecturer	On duty
32	EDONGUE HERVAIS	Lecturer	On duty
33	FOUEDJIO David	Lecturer	*Chief Cell. MINADER*
34	MELI'I Joelle Larissa	Lecturer	On duty
35	MVOGO ALAIN	Lecturer	On duty
36	OBOUNOU Marcel	Lecturer	*DA/Univ Inter Etat/Sangmalima*
37	OTTOU ABE Martin Thiery	Lecturer	On duty
38	TEYOU NGOUPOU Ariel	Lecturer	On duty
39	WOULACHE Rosalie Laure	Lecturer	On duty

40	KAMENI NEMA TCHOUA Modeste	Assistant Lecturer	On duty
41	LAMARA Maurice	Assistant Lecturer	On duty
42	NGA ONGODO Dieudonné	Assistant Lecturer	On duty
43	WANDJI NYAMSI William	Assistant Lecturer	On duty

10- DEPARTMENT OF EARTH SCIENCES (ES) (42)

1	BITOM Dieudonné	Professor	*Dean / FASA / UDs*
2	FOUATEU Rose épse YONGUE	Professor	On duty
3	NDAM NGOUPAYOU Jules-Remy	Professor	On duty
4	NDJIGUI Paul Désiré	Professor	***Head of Department***
5	NGOS III Simon	Professor	*DAAC/Uma*
6	NKOUMBOU Charles	Professor	On duty
7	NZENTI Jean-Paul	Professor	On duty

8	ABOSSOLO née ANGUE Monique	Associate Professor	*Vice-Dean / DRC*
9	BISSO Dieudonné	Associate Professor	*Director/Project Barrage Memve'ele*
10	EKOMANE Emile	Associate Professor	On duty
11	FUH Calistus Gentry	Associate Professor	*Sec. D'Etat/MINMIDT*
12	GANNO Sylvestre	Associate Professor	On duty
13	GHOGOMU Richard TANWI	Associate Professor	*HOD*/Uma
14	MOUNDI Amidou	Associate Professor	*CT/ MINIMDT*
15	NGO BIDJECK Louise Marie	Associate Professor	On duty
16	NGUEUTCHOUA Gabriel	Associate Professor	CEA/MINRESI
17	NJILAH Isaac KONFOR	Associate Professor	On duty
18	NYECK Bruno	Associate Professor	On duty
19	ONANA Vincent Laurent	Associate Professor	*Chief service*
20	TCHAKOUNTE J. épse NUMBEM	Associate Professor	*Chief Cell/MINRESI*
21	TCHOUANKOUE Jean-Pierre	Associate Professor	On duty
22	TEMDJIM Robert	Associate Professor	On duty
23	YENE ATANGANA Joseph Q.	Associate Professor	*Chief Div. /MINTP*
24	ZO'O ZAME Philémon	Associate Professor	*DG/ART*

25	ANABA ONANA Achille Basile	Lecturer	On duty
26	BEKOA Etienne	Lecturer	On duty
27	ELISE SABABA	Lecturer	On duty
28	ESSONO Jean	Lecturer	On duty
29	EYONG JOHN TAKEM	Lecturer	On duty
30	MANDEM TAMTO Lionelle E.	Lecturer	On duty
31	MBESSE CECILE OLIVE	Lecturer	On duty
32	MBIDA YEM	Lecturer	On duty
33	METANG Victor	Lecturer	On duty
34	MINYEM Dieudonné-Lucien	Lecturer	*CD/Uma*
35	NGO BELNOUN Rose Noël	Lecturer	On duty
36	NOMO NEGUE Emmanuel	Lecturer	On duty
37	NTSAMA ATANGANA Jacqueline	Lecturer	On duty
38	TCHAPTCHET TCHATO De P.	Lecturer	On duty
39	TEHNA Nathanaël	Lecturer	On duty
40	TEMGA Jean Pierre	Lecturer	On duty
41	MBANGA NYOBE Jules	Lecturer	On duty
42	NGO'O ZE Arnoud	Assistant Lecturer	On duty

Breakdown of teachers from the Faculty of Sciences of the University of Yaoundé I

	NUMBER OF TEACHERS				
DEPARTMENT	**Professors**	**Associate Professor**	**Lecturer**	**Assistant Lecturer**	**Total**
BCH	08 (00)	14 (10)	15 (05)	02 (01)	**39 (16)**
BPA	14 (01)	11 (07)	22 (07)	04 (02)	**51 (17)**
BPV	06 (01)	10 (01)	16 (09)	01 (0)	**33 (11)**
CI	9 (01)	14 (04)	08 (01)	00 (0)	**31 (06)**
CO	06 (01)	20 (04)	08 (03)	04 (01)	**38 (09)**
IN	02 (0)	02 (0)	12 (01)	06 (0)	**22 (01)**
MAT	02 (0)	08 (0)	14 (01)	07 (01)	**31 (02)**
MIB	03 (0)	06 (02)	10 (03)	03 (02)	**22 (08)**
PHY	15 (0)	13 (02)	11 (03)	04 (0)	**43 (06)**
ST	07 (01)	16 (03)	18 (04)	01 (0)	**42 (08)**
Total	**72 (07)**	**114 (33)**	**134 (37)**	**32 (07)**	**352 (84)**

For a total of **352 (**84**)** of which:

- Professors **72 (07)**
- Associate Professor **114 (**33**)**
- Lecturer **134 (37)**
- Assistant Lecturer **32 (**07**)**

( ) = Number of Women **84**

DECLARATION

I GARBA KOFFI Jean, Registration number: 09Y849, Department of Organic Chemistry, Faculty of Science of The University of Yaoundé I, hereby declare that, this work titled: **"Chemical investigation of three Cameroonian medicinal plants with antileishmanial potency:** *Endodesmia calophylloides* **Benth.,** *Pentadesma butyracea* **Sabine (Clusiaceae) and** *Adenia lobata* **(Jacq.) Engl. (Passifloraceae)-Phytodrug preformulation trail''** is my original work. It has not been presented in any application for a degree or any academic pursuit. I have sincerely acknowledged all borrowed ideas nationally and internationally by citations.

Signature:_____   **Date:** _____

DEDICATION

To my wife **ETOGO TIMA Nadège**

To my children**: GARBA KOFFI Samuel Yanis and KOFFI Gabriel Yohan Soleil**

To my Parents: Mr. and Mrs. **NGARBA KOFFI**

ACKNOWLEDGMENTS

Thank you all for making the lab a great place to work. I wish you all the best of luck, and much success in your research.

TABLE OF CONTENTS

LIST OF ABBREVIATIONS, ACRONYMS AND SYMBOLS

brd	**:**	**broad doublet**
brs	:	**broad singlet**
CC	:	**Column Chromatography**
°C	:	**Degree Celsius**
^{13}C	:	**Carbone 13**
^{13}C NMR		**Carbon 13 Nuclear Magnetic Resonance**
COSY	:	**COrrelation SpectroscopY**
d	:	**doublet**
dd	:	**doublet of doublets**
DEPT	:	**Distortionless Enhancement by Polarization Transfer**
^{1}D and ^{2}D NMR		**One and Two Dimensional Nuclear Magnetic Resonance**
EC$_{50}$	:	**Effective Concentration fifty**
^{1}H	:	**Proton**
HMBC	:	**Heteronuclear Multiple Bond Connectivity**
^{1}H NMR		**Proton Nuclear Magnetic Resonance**
HR-ESI-MS	:	**High Resolution- ElectroSpray Ionization-Mass Spectrometry**
HSQC	:	**Heteronuclear Single Quantum Coherence**
Hz	:	**Hertz**
IC$_{50}$	:	**Inhibitory Concentration fifty**
IR	:	**Infra Red**
J	:	**Coupling constant in Hertz**
m	:	**multiplet**
MHz	:	**Megahertz**
MIC	:	**Minimum Inhibitory Concentration**
MS	:	**Mass spectrometry**
m/z	:	**Atomic mass/charge ratio**
m. p	:	**melting point**
NHC		**National Herbarium of Cameroon**
PED	:	**Pays En voie de Développement**
ppm		**Part-per-million**
OMS	:	**Organisation Mondiale de la Santé**
s	:	**singlet**

t	:	**triplet**
TLC	:	**Thin-layer chromotography**
UNICEF	:	**United Nations International Children Emergency Fund**
UV	:	**Ultra Violet**
WHO	:	**World Health Organization**
$\varDelta$	:	**Chemical shift scale in ppm**
v_{max}	:	**maximum frequency**

LIST OF TABLES

LIST OF FIGURES

LIST OF SCHEMES

ABSTRACT

This thesis reports the chemical investigation of the extracts of three Cameroonian medicinal plants with antileishmanial potency: *Endodesmia calophylloides*, *Pentadesma butyracea* (Clusiaceae) and *Adenia lobata* (Passifloraceae), which showed potent antileishmanial activity *in vitro* during preliminary screening against *Leishmania donovani* 1S (MHOM/SD/62/1S) promastigotes (IC_{50} values ranging from 5.96-26.43 μg/mL) and with good selectivity towards Raw 264.7 macrophage and Vero Cells (SI>4.11). The bioguided fractionation of CH_2Cl_2-MeOH (1:1) extracts of *E. calophylloides* (Stem bark and leaves), *P. butyracea* (Stem bark and fruits) and *A. lobata* (Stem bark) led to fractions which were also tested for their antileishmanial activity against the same strain and showed good to moderate activities with IC_{50} values ranging from 2.71 to 100 μg/mL. Purification of these fractions using successive columns chromatography led to the isolation of forty compounds. The methods used for the isolation of compounds were mainly liquid-liquid partition, flash chromatography and columns chromatography. Their structures were established using spectroscopic methods (HR-MS, 1D and 2D NMR, IR). From the CH_2Cl_2-MeOH (1:1) extract of the stem bark of *A. lobata* eight compounds including a new ceramide derivative named adeniamide (**54**), together with D-mannitol (**88**), germanicol ester caffeoyl (**55**), octacosanoic acid (**85**), β-sitosterol-3-*O*-β-D-glucopyranoside (**92**), a mixture of stigmasterol (**90** and β-sitosterol (**91**), and vanillic acid (**73**) were isolated. The purification of CH_2Cl_2-MeOH (1:1) extract of the stem bark of *E. Calophylloides* led to the isolation of fourteen compounds including friedelin (**56**), absicic acid β-D-glucoside (**70**), tachioside (**71**), the mixture (1:3) of tachioside (**71**) and isotachioside (**72**), morelloflavone (**67**), lupenone (**63**), 2′,3′-dihydroxypropyl triacontanoate (**87**), 1,5-dihydroxy-3-methoxyxanthone (**75**), cerin (**58**), marsformoxide B (**59**), the mixture (1:1) isoxanthochymol (**69a**) and cycloxanthochymol (**69b**), canophyllol (**57**) and koaburaside (**73**). The CH_2Cl_2-MeOH (1:1) extract of the leaves of *E. Calophylloides* afforded seven compounds including lupeol (**62**), β-amyrin (**60**), 4′-methylamentoflavone (**65**) and amentoflavone (**66**), β-amyrin palmitate (**61**), 3,3′-*O*-dimethylellagic acid (**89**) and tetracosanoic acid (**86**). The CH_2Cl_2-MeOH (1:1) extract of the fruits of *P. butyracea* led to the isolation of nine compounds including daphnifolin (**77**), norathyriol (**76**), epicathechin (**68**), methyl citrate (**84**), β-sitosterol-3-*O*-β-D-glucopyranoside (**92**), stigmasterol (**90**), tovopyrifolin C (**78**), cowagarcinone B (**80**), and α-mangostin (**79**). The CH_2Cl_2/MeOH (1:1) extract of the stem bark of *P. butyracea* has led to the isolation of eight compounds including daphnifolin (**77**), stigmasterol (**90**), α-mangostin (**79**), lupeol (**62**),

betulin (**64**), tovophyllin A (**82**), 1,3,7-trihydroxyxanthone (**83**), and 9-hydroxycalabaxanthone (**81**).

The compounds were tested for their antileishmanial activity against the same strain and daphnifolin (**77**), epicathechin (**68**), α-mangostin (**79**), 9-hydroxycalabaxanthone (**81**), germanicol caffeoyl ester (**55**), the mixture (1:1) of isoxanthochymol (**69a**)/cycloxanthochymol (**69b**) and the mixture (1:3) of tachioside (**71**)/isotachioside (**72**) exhibited potent antileismanial activity with IC_{50} between 2.0 and 9.0 μg/mL, and good selectivity towards Raw 264.7 macrophage cells and Vero Cells (SI> 2.4).

In order to pre-formulate a phytodrug, the acute toxicity was assessed using the protocol of the OCDE (2001) following guideline 423 on the hydroethanolic extract of *E. calophylloides*. Nine not pregnant adult female rats of the *wistar* strain were used for this purpose. Results on acute oral toxicity of hydroethanolic extract of stem bark did not show intoxication syndrome in rats at doses of 2000 and 5000 mg/kg. In rats given the extract, no deaths were observed for fourteen days after administration of the extract suggesting that, the LD_{50} is greater than 5000 mg/kg (OCDE, 2001). No clinical signs of toxicity were observed on the behavior, the body weight of the animals, and on the weight of the liver, kidney, spleen, heart and lungs after administration of the test substance during the fourteen days of experimentation. Thus, according to the Globally Harmonized Classification System (GHCS), the hydroethanolic extract of *E. calophylloides* can be classified in category 5 of non-toxic substances because of its harmlessness.

Keywords: *Endodesmia calophylloides*, *Pentadesma butyracea*, *Adenia lobata*, antileishmanial, cytotoxicity, acute toxicity, phytodrugs.

RESUME

Cette thèse porte sur l'investigation chimique des extraits de trois plantes médicinales Camerounaises à potentiel antileishmanial: *Endodesmia calophylloides*, *Pentadesma butyracea* (Clusiaceae) et *Adenia lobata* (Passifloraceae), lesquelles ont montré une bonne activité antiparasitaire *in vitro* lors d'un criblage préliminaire sur la souche *Leishmania donovani* 1S (MHOM/SD/62/1S) promastigotes (CI$_{50}$ allant de 5,96 à 26,43 μg/mL) et une bonne sélectivité vis-à-vis des macrophages Raw 264.7 et des cellules *Vero* (SI>4,11). Le fractionnement bioguidé des extraits au mélange CH$_2$Cl$_2$-MeOH (1:1) de *E. calophylloides* (écorce du tronc et feuilles), *P. butyracea* (écorce du tronc et fruits) et *A. lobata* (écorce du tronc) a conduit à des fractions qui ont été testées pour leur activité antileishmaniale sur la même souche et ont montré des activités bonnes à modérées avec des valeurs de CI$_{50}$ allant de 2,71 à 100 μg/mL. La purification de ces fractions par chromatographie sur colonne a permis d'isoler quarante composés. Les méthodes utilisées pour l'isolement des composés étaient principalement la partition liquide-liquide, la chromatographie sous pression réduite et la chromatographie sur colonne. Leurs structures ont été établies à l'aide de méthodes spectroscopiques (HR-MS, RMN 1D et 2D, IR). De l'extrait au mélange CH$_2$Cl$_2$-MeOH (1:1) de l'écorce du tronc de *A. lobata*, huit composés dont un dérivé nouveau de céramide appelé adeniamide (**54**), ensemble avec le D-mannitol (**88**), le germanicol ester caffeoyl (**55**), l'acide octacosanoïque (**85**), Le β-sitostérol-3-*O*-β-D-glucopyranoside (**92**), un mélange de stigmastérol (**90**) et de β-sitostérol (**91**) et l'acide vanillique (**74**) ont été isolés. La purification de l'extrait du mélange CH$_2$Cl$_2$-MeOH (1:1) de l'écorce du tronc de *E. calophylloides* a conduit à quatorze composés dont la friedeline (**56**), l'acide absicique β-D-glucoside (**70**), le tachioside (**71**), le mélange (1:3) de tachioside (**71**) et isotachioside (**72**), la morelloflavone (**67**), la lupénone (**63**), le triacontanoate de 2′,3′-dihydroxypropyle (**87**), le 1,5-dihydroxy-3-méthoxyxanthone (**75**), la cérine (**58**), le marsformoxyde B (**59**), le mélange (1:1) isoxanthochymol (**69a**) et cycloxanthochymol (**69b**), canophyllol (**57**) et le koaburaside (**73**). L'extrait au CH$_2$Cl$_2$-MeOH (1:1) des feuilles de *E. calophylloides* a fourni sept composés dont le lupéol (**62**), la β-amyrine (**60**), la 4′-méthylamentoflavone (**65**) et l'amentoflavone (**66**), la β-amyrine palmitate (**61**), l'acide 3,3′-*O*-diméthylellagique (**89**) et l'acide tetracosanoïque (**86**). L'extrait au CH$_2$Cl$_2$-MeOH (1:1) des fruits de *P. butyracea* a conduit à l'isolement de neuf composés dont la daphnifoline (**77**), le norathyriol (**76**), l'épicathéchine (**68**), le citrate de méthyle (**84**), le β-sitostérol-3-*O*-β-D-glucopyranoside (**92**), le stigmasitotérol (**90**), la tovopyrifoline C (**78**), la cowagarcinone B (**80**) et l'α-mangostin (**79**). L'extrait au CH$_2$Cl$_2$-

MeOH (1:1) de l'écorce du tronc de *P. butyracea* a fourni huit composés dont la daphnifoline (**77**), le stigmastérol (**90**), l'α-mangostin (**79**), le lupéol (**62**), la bétuline (**64**), la tovophylline A (**82**), la 1,3,7-trihydroxyxanthone (**83**) et la 9-hydroxycalabaxanthone (**81**).

Les composés isolés ont été testés sur la même souche et la daphnifoline (**76**), l'épicathéchine (**68**), l'α-mangostin (**79**), la 9-hydroxycalabaxanthone (**81**), le germanicolcaffeoyl ester (**55**), le mélange (1:1) d'isoxanthochymol (**69a**)/cycloxanthochymol (**69b**) et le mélange (1:3) du tachioside (**71**)/isotachioside (**72**) ont présenté une très bonne activité antileismaniale avec des valeurs de CI$_{50}$ entre 2,0 et 9,0 μg/mL et une bonne sélectivité envers les cellules macrophages Raw 264.7 et les cellules *Vero* (SI> 2.4).

En vue de pré-formuler un phytomédicament, la toxicité aiguë a été évaluée selon le protocole de l'OCDE (2001) suivant la directive 423 sur l'extrait hydroéthanolique de *E. calophylloides*. Neuf rats femelles adultes non enceintes de souche *wistar* ont été utilisés à cette fin. Les résultats de la toxicité orale aiguë de cet extrait n'ont montré aucun de signe d'intoxication chez le rat aux doses de 2000 et 5000 mg/kg. Chez les rats ayant reçu l'extrait, aucun décès n'a été observé pendant quatorze jours après l'administration de l'extrait, ce qui suggère que la DL$_{50}$ est supérieure à 5000 mg/Kg (OCDE, 2001). Aucun signe clinique de toxicité n'a été observé sur le comportement, le poids corporel des animaux, et sur le poids du foie, des reins, de la rate, du cœur et des poumons après administration de la substance d'essai pendant les quatorze jours d'expérimentation. Ainsi, selon le système général de classification harmonisé (SGCH), l'extrait hydroéthanolique de *E. calophylloides* peut être classé dans la catégorie 5 des substances non toxiques en raison de son innocuité.

Mots clés: *Endodesmia calophylloides*, *Pentadesma butyracea*, *Adenia lobata*, activité antileishmaniale, cytotoxicité, toxicité aiguë, phytomédicaments

GENERAL INTRODUCTION

Leishmaniasis is an infectious disease that occurs in countries with tropical and temperate climates. It is transmitted to humans by the bite of sandflies infected with protozoa of the genus *Leishmania*. It is a complex infectious disease with a varied spectrum of clinical manifestations, which range from self-healing cutaneous ulceration to progressive and lethal visceral infection (Torres-Guerrero *et al*., 2017). It is prevalent in more than 98 endemic countries in the world with an estimated annual incidence of almost 0.2 to 0.4 million new cases of visceral manifestation and 0.7 to 1.2 million new cases of cutaneous form (WHO, 2018). The current treatment includes pentavalent antimonials, meglumine antimoniate (glucantime), and sodium stibogluconate as the first line treatment. Amphotericin B, pentamidine, paromomycin, and miltefosine are equally used as second line drugs (Goto and Lindoso, 2010; Rodrigues *et al*., 2015). Despite these treatment options, the emergence of resistance, toxicity and high cost of the current treatment and the absence of a suitable vaccine reveal the urgent need of alternative chemotherapeutic agents. In this context, more interest has been given to the search of new lead drugs from plants.

Several plant families such as Clusiaceae, Fabaceae, Lauraceae, Meliaceae, Moraceae, Celastraceae, Bignoniaceae, Berberidaceae, Asteraceae, Apocynaceae, Annonaceae, Euphorbiaceae, Rubiaceae and Rutaceae, are used in traditional medicine for the treatment of several pathologies, including leishmaniasis, because they are less toxic and available. What would be interesting to embark on their investigation with a view to finding drugs against this disease (Rocha *et al*., 2005). In addition, some phenolic compounds isolated from *Allanblackia monticola* and *Symphonia globulifera* belonging to the Clusiaceae family, also exhibited good leismanicidal activities against *Leishmania donovani* (MHOM/ET/67/L82) amastigostes with IC$_{50}$ values ranging between 0.16-1.40 μM (Lenta *et al*., 2007).

To the best of our knowledge no antileishmanial investigation on *E. calophylloides, P. butyracea* and *A. lobata* have been reported so far. In our continuous search for bioactive compounds from Cameroonian medicinal plants, we undertook as part of this thesis, the investigation of the stem bark of *A. lobata*, the leaves and the stem bark of *E. calophylloides* and stem bark and fruits of *P. butyracea*.

This research was motivated by the fact that *E. calophylloides*, *P. butyracea*, and *A. lobata* were reported to be used in traditional medicine for skin and hair care, and in the manufacture of soap for healing qualities, filariae and hemorrhoids (Hutchinson and Dalziel, 1954; Dencausse *et al*., 1995; Konkon *et al*., 2012; Sarkodie *et al*., 2013). In addition, despite its many uses, the plant *A. lobata* has not been the subject of any chemical studies to our knowledge.

The general objective of this work was been to search for active and non-toxic extracts, fractions or molecules that could be used in the preformulation of new therapeutic agents for the treatment of leishmaniasis. Specifically, our work consisted of:

- Harvest, extract and evaluate the biological activity of extracts and fractions from plants;

- Isolate and purify compounds from active extracts and fractions;

- Evaluate acute toxicity and preformulate a phytodrug trial.

This thesis, which summarizes the essence of our work, has three main parts:

- A first part covers the bibliographic review with a brief overview on leihmaniasis, and a brief botanical description on the plants studied as well as the previous chemical and biological works;

- A second part devoted to the results and discussion;

- A third part which describes the equipment and various techniques used as to achieve our set objectives.

CHAPTER I: BIBLIOGRAPHIC STUDY

CHAPTER I: BIBLIOGRAPHIC STUDY

I.1 General information on leishmaniasis

I.1.1 Definition

Leishmaniasis is a skin or visceral diseases caused by flagellated protozoa belonging to the genus *Leishmania* of the Trypanosomidae family and transmitted by the bite of female sandflies (Aubry and Gaüzère, 2020; Dedet, 2003).

There are 4 main forms of the disease: visceral leishmaniasis (VL, also known as kala-azar), post-kala-azar dermal leishmaniasis (PKDL), cutaneous leishmaniasis (CL) and mucocutaneous leishmaniasis (MCL). CL is the most common form of the disease while VL is the most serious and is almost always fatal if untreated (WHO, 2020; Aubry and Gaüzère, 2020).

I.1.2 Epidemiology

Widely distributed worlwide, leishmaniases have an intertropical geographical distribution, but largely spilling over into the temperate zones of southern Europe, North Africa, Asia and America. Present on four continents, they affect 88 countries, amongst which 72 of the most underdeveloped. The population exposed to the risk of leishmaniasis is estimated at 370 million people and the number of new cases diagnosed annually (all clinical forms combined), is estimated between 1.5 and 2 million (WHO, 2020; Aubry and Gaüzère, 2020).

In 2018, 253,435 new cases of CL and 17,223 new cases of VL were reported to WHO. Over 90% of new reported cases of CL originated from the Eastern Mediterranean Region (74%) and the Region of the Americas (18%) with the Eastern Mediterranean Region and Algeria constituting an eco-epidemiological focus, as they alone report 79% (198,109) of all cases of CL. Seven countries (Afghanistan, Algeria, Brazil, Iraq, Pakistan, Syrian Arab Republic and Islamic Republic of Iran) each reported > 10,000 cases of CL, or 70% of cases worldwide. Nepal reported 1 case of CL in 2008, 1 indigenous case in 2016 and 19 cases in 2018 (WHO, 2020; Aubry and Gaüzère, 2020).

CL and VL have been reported in Cameroon and studies have revealed the presence of about 20 sandfly species. In fact, the first case of CL was described in 1930 at the Northern part of the country and the first case of VL was described in 1976 in the Center part of the country. However, over time studies on leishmaniasis are becoming scarce, very scanty data and data poorly documented. Cameroon is currently classified among the countries with no

data available on leishmaniasis (Ngouateu *et al*., 2022; Yemeli *et al*., 2021; Kimutai *et al*., 2009).

Figure 1 belows shows the regions where CL and VL cases have been already described or where the presence of the vector has been reported leishmaniasis in Cameroon.

Figure 1: Cameroon regions with indication of reported leishmaniasis cases and/or where sandflies have been collected. Reports available on: sandflies (circles); cutaneous leishmaniasis (triangles) and visceral leishmaniasis (stars) (Ngouateu *et al*., 2022).

I.1.3 The parasite

The parasite is a tissue flagellate protozoan which presents during its life cycle two distinct evolutionary stages:

● The amastigote stage: which intramacrophagic, without an exteriorized flagellum and found in vertebrate hosts including humans;

● The promastigote stage: which free and mobile thanks to its flagellum, found in the intestine of the sandfly and in culture medium (Anofel, 2014).

I.1.3.1 The amastigotes

The amastigote forms are ovoid, has a diameter between 2 µm to 6 µm and show in optical microscopy after staining with May-Grünwald-Giemsa two characteristic purple inclusions: the rounded nucleus and the kinetoplast (origin of the flagellum) in a darker rod (Figure 2) (Anofel, 2014).
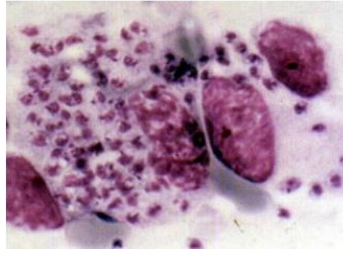
Figure 2: *Leishmania* **amastigotes in macrophages (Anofel, 2014).**

I.1.3.2 The promastigotes

During culturing at 24 to 28 °C, on NNN medium (Novy, McNeal, Nicolle) or others, the amastigotes transform into promastigotes as in the vector's intestine. During the exponential culture phase, the so-called procyclic promastigotes multiply by longitudinal scissiparity (Figure 3) (Anofel, 2014).

Figure 3: Promastigotes of *Leishmania* **in culture (Anofel, 2014).**

The parasite reservoirs vary according to the leishmania species and the regions concerned (Table 1) (Dedet, 2001).

Table I: Some parasite reservoirs depending on the Leishmania species and the regions concerned (Gentilini, 1993).

Clinical form	Parasite	Regions	Reservoirs
Visceral leishmaniasis	*L. donovani*	India, China, Iraq, Syria, Kenya	Man
	L. infantum	Mediterranean Basin	Dog
	L. chagasi	Central Asia, China, South America	Wild canids
Old world cutaneous leishmaniasis	*L. tropica*	Central Asia, Middle East,	Man,
	L. killicki	Greece, Morocco, Tunisia, Turkey,	Dog
	L. major	Central Asia, Middle East, India, Africa	Rodents
New World Cutaneous	*L. mexicana*	Central America	Rodents
	L. venezuenlis	Venezuela	Unknown

Leishmaniasis	*L. guyanensis*	French Guiana	Lazy
	L. panamensis	Central America	Lazy
	L. peruviana	Peru	Dog
	L. lainsoni	Brazil	Agouti
Diffuse cutaneous	*L. pifanoi*	Venezuela	Rodents
leishmaniasis	*L. amazonensis*	Colombia, Brazil	Rodents
	L. aethiopica	Ethiopia, Kenya, Tanzania	Damans
Mucocutaneous	*L. braziliznsis*	Wide distribution (from Costa Rica to	Unknown
leishmaniasis	*L. donovani*	Argentina)	Man, Dog
		Chad, Sudan	

I.1.4 Agent vector

The sandfly is a small 2 to 3 mm long diptera, having the appearance of a very small hairy mosquito, yellowish in color, with large black eyes, lanceolate wings, fringed with long hairs which are raised at rest and able to pass through the mesh of a mosquito net. The hematophagous female bites both humans and animals, ensuring the transmission of leishmaniasis since she needs blood for the development of her eggs. Sandflies shelter themselves from light and wind during the day and become active at night (Figure 4) (Aubry and Gaüzère, 2020; Anofel, 2014).

ⓘ Phlebotomus papatasi, Female © ECDC/Photographer
SPECIES NAME/CLASSIFICATION: *Phlebotomus* spp. (Diptera: Psychodidae)
COMMON NAME: Sand fly

Figure 4: Picture of a sandfly

I.1.4 Life cycle of the *Leishmania* parasite

Leishmaniasis is transmitted by the bite of infected female phlebotomine sandflies. The sandflies inject the infective stage (promastigotes) from their proboscis to their host during blood meals (1). Promastigotes that reach through punctured wound are phagocytized by macrophages (2) and other types of mononuclear phagocytic cells. Promastigotes

transform in these cells into the tissue stage of the parasite (amastigotes) (3), which multiply by simple division and proceed to infect other mononuclear phagocytic cells (4). The parasite, host, and other factors determine whether the infection becomes symptomatic, cutaneous or visceral leishmaniasis. Sandflies become infected by ingesting infected cells during blood meals (5, 6). In sandflies, amastigotes transform into promastigotes, develop in the gut (7) (in the hindgut for leishmanial organisms in the Viannia subgenus; in the midgut for organisms in the *Leishmania* subgenus), and migrate to the proboscis (8) (Borghi *et al*., 2016). The following figure 5 presents the life cycle of the *Leishmania* parasite.
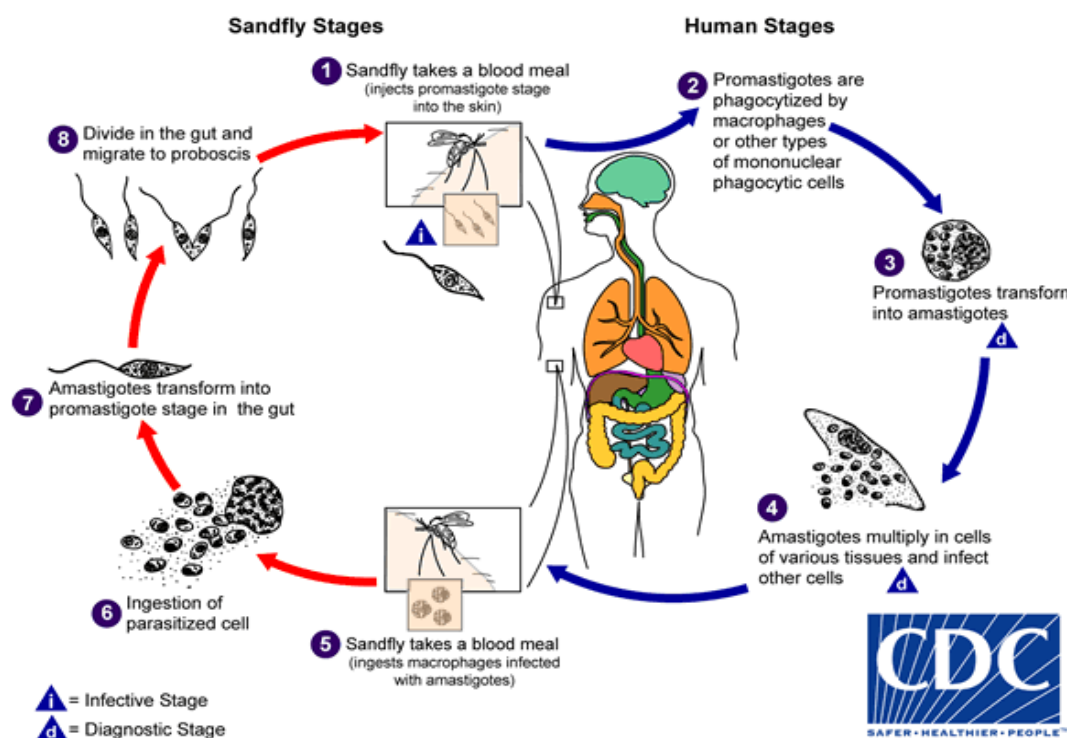
Figure 5: Life cycle of *Leishmania* parasite

I.1.5 Symptoms and different forms of leishmaniasis

Symptoms of leishmaniasis are skin sores that appear a few weeks or months after the bite of the sandfly. We can also cite other manifestations such as fever, anemia, involvement of the liver and spleen (splenomegaly which is the enlargement of the spleen). There are generally four main forms of leishmaniasis: visceral leishmaniasis, localized cutaneous leishmaniasis, diffuse cutaneous leishmaniasis and mucocutaneous leishmaniasis (Aubry and Gaüzère, 2020).

I.1.5.1 Visceral leishmaniasis

The endemic disease is caused by *Leishmania donovani* and its main reservoir is humans. It is an epidemic in Sudan, Ethiopia, India, Nepal, Bangladesh (Marty, 2010; Anofel, 2014). The infantile form affects children aged 2 to 3 years. After an incubation period of 1 to 2 months, it settles insidiously with rapid deterioration in the general condition. The condition phase includes an irregular fever associated with anaemia causing extreme pallor and is fatal if left untreated (Dedet, 2003). The increasingly common adult form has a more abrupt onset than in children. The condition period is similar, atypical forms are frequent (gastrointestinal, respiratory or cutaneous) particularly in immunocompromised individuals (Dedet, 2001). Figure 6 shows the clinical appearance of a child with visceral leishmaniasis.

Figure 6: Clinical appearance of a child with visceral leishmaniasis (Anofel, 2014)

I.1.5.2 Localized cutaneous leishmaniasis

It is the most common form that causes skin lesions, mainly ulcers, on exposed parts of the body leaving permanent scars and severe disabilities. This form is due to the species *L. mexicana*, *L. panamensis*, *L. amazonensis*, *L. peruviana*, *L. braziliensis* or *L. guyanensis*. More than two-thirds of cases occur in the following six countries: Afghanistan, Algeria, Brazil, Colombia, the Syrian Arab Republic and the Islamic Republic of Iran (Biomnis, 2012; Anofel, 2014). Figure 7 shows the clinical appearance of a person with localized cutaneous leishmaniasis.

Figure 7: Clinical appearance of a person with localized cutaneous leishmaniasis.

(Anofel, 2014)

I.1.5.3 Diffuse cutaneous leishmaniasis

Diffuse cutaneous leishmaniasis is infrequent and caused by *L. amazonensis* in South America and *L. aethiopica* in East Africa (Anofel, 2014). They are linked to the deficit in the host's cellular immunity and result in lumpy lesions distributed throughout the body which are reminiscent of lepromatous leprosy (Dedet, 2003). This form of leishmaniasis is rebellious to classical antileishmanians. In France (Guyana), cutaneous forms due to *L. guyanensis* are observed (Anofel, 2014). Since acquired immunosuppression states have increased, a few cases of LCD have been reported with species such as *L. major*, *L. braziliensis*, even *L. infantum* (Aubry *et al*, 2020). (Figure 9).

Figure 8: Clinical appearance of a person with diffuse cutaneous leishmaniasis
(Anofel, 2014)

I.1.5.4 Mucocutaneous leishmaniasis

Geographically limited to the South American continent, mucocutaneaous leishmaniasis, called Espundia, is caused by *L. braziliensis* (WHO, 2018). The skin lesion resembles that of cutaneous leishmaniasis, but after healing, the parasite can secondarily reach the mucous membranes of the face, cartilage of the nose or ear, lips or mucous membranes of

the oropharynx leading to facial mutilation and sometimes death (Marty, 2010). Figure 10 shows a person with muco-cutaneous leishmaniasis.
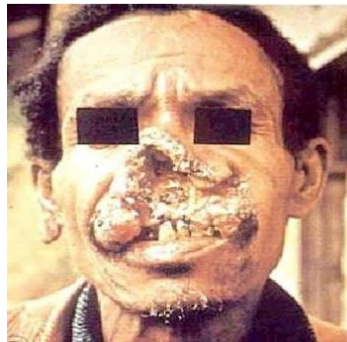
Figure 9: Clinical appearance of a person with mucocutaneous leishmaniasis (Anofel, 2014)

Leishmaniasis is amongst the diseases which are decimating the population in large numbers. Despite the devastating effects of the disease, there exist treatments and means of prevention.

I.1.6 Diagnosis of leishmaniasis

Conventional diagnosis depends on microscopic examination by direct identification of amastigotes from Giemsa-stained lesion smears of biopsies, scrapings, or impression smears. Amastigotes are observed as round or oval bodies, 2-4 μm in diameter, with characterised nuclei and kinetoplasts in tissue(s) aspirated from different organs like spleen, lymph nodes, liver, skin, and can also be done by culturing parasites from these sites. However, this suction examination process is not comfortable for patients and also the method of isolating the parasite from the culture is time-consuming, expensive, and difficult to perform (Thakur *et al*., 2020; Elmahallawy *et al*., 2014).

I.1.7 Treatment of leishmaniasis

Several drugs are used in the treatment of leishmaniasis. We can cite:

- **Pentavalent antimony derivatives or pentavalent antimony salts**

In this category we have meglumine antimonate (**1**) and sodium stibiogluconate (**2**) known in pharmacies respectively under the trade names of glucantime and pentostam respectively (Aubry and Gaüzère, 2020).

$$(1) \qquad (2)$$
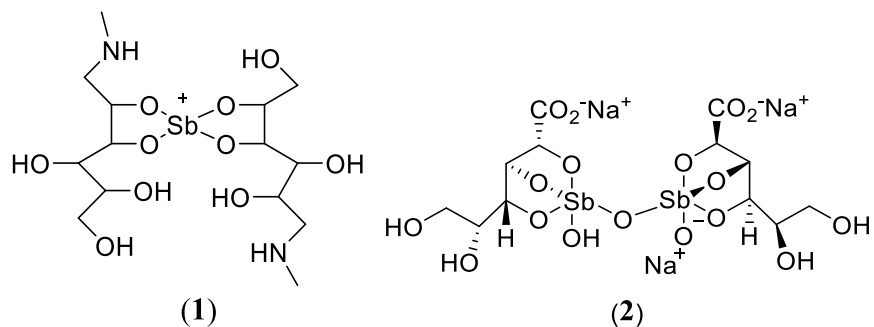
- Miltefosine

Miltefosine (3) commonly known as impavido in pharmacies is the first oral drug available for the treatment of visceral and cutaneous leishmaniasis (Aubry *et al*, 2020; Anofel, 2014).

$$(3)$$
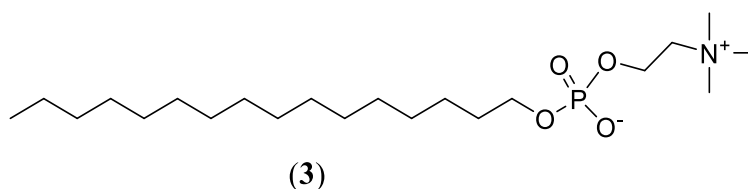
- Amphotéricine B (**4**)

We have ampho B deoxycholate known in pharmacies as fungizone and liposomal ampho B known as ambisome. It represents a powerful antileishmanian used in the treatment of severe leishmaniasis (visceral and mucous membranes) or forms which are resistant to antimonials. It is also less toxic than antimony-based treatments and can be used in children and in vulnerable individuals (pregnant women, immunocompromised individuals including patients infected with HIV) (Aubry and Gaüzère, 2020; Anofel, 2014).

$$(4)$$
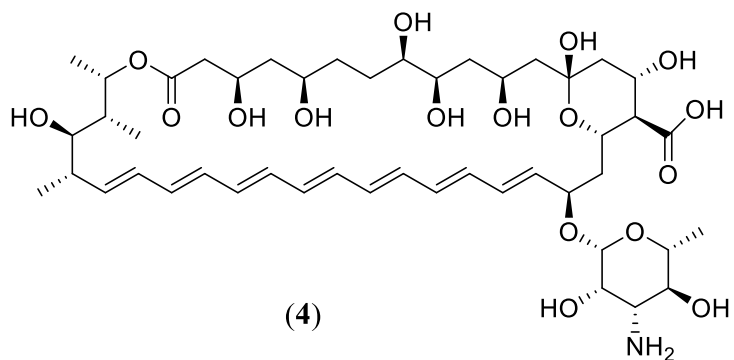
- Pentamidine salts

This is the case with pentamidine isethionate (**5**) known in pharmacies as pentacarinat. It is now mainly used as a first-line drug in the treatment of certain forms of cutaneous leishmaniasis in short course (Aubry and Gaüzère, 2020; Anofel, 2014).

(5)
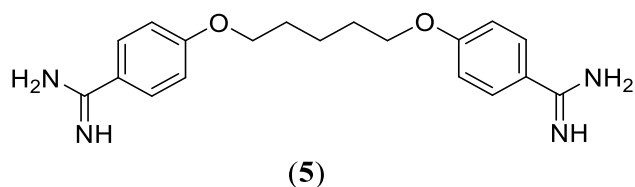
- Paramomycin (5)

It is an expensive but effective treatment for fighting leishmaniasis (Aubry and Gaüzère, 2020).

(6)
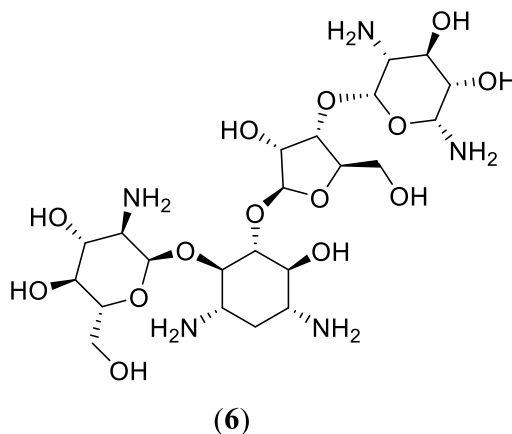
I.1.8 Prevention

The fight against wild reservoirs is illusory and campaigns to eliminate carrier dogs are only of temporary effectiveness. Individual prophylactic measures are intended to prevent the bite of sandflies. They consist of home and peri-domiciliary spraying of synthetic pyrethroids and the use of mosquito nets impregnated with pyrethroids (Dedet, 2003; Anofel, 2014). The wearing of insecticidal collars in dogs in outbreaks of visceral leishmaniasis caused by *L. infantum* is recommended (Aubry and Gaüzère, 2020; Anofel, 2014).

Plants are reservoirs of bioactive compounds, which are known to be chemically balanced, effective and less harmful compared to synthetic drugs. The current resistance and toxic effects of available drugs have led to the tendency to evaluate the anti-leishmanial effect of various plant extracts and their compounds (Ullah *et al*., 2016).

I.1.9 Information on formulation

Based on new drugs development, it is essential to appropriately transpose drug dosage from one animal species to the another. This animal dose should not be extrapolated to a human equivalent dose (HED) by a simple conversion based on the body weight. It is advisable to use the body surface area standardization (BSA) method as it is a more appropriate conversion method of drug dosage from animals to human doses. BSA is well correlated in several mammalian species with several biological parameters, including oxygen

utilization, calorie expenditure, basal rate, blood volume, circulating plasma proteins, and kidney functions (Reagan-Shaw *et al*., 2007). The formular for Dose translation from animal to human studies was derived as seen below:

Formula for Dose Translation Based on BSA
HED (mg/kg) = Animal dose (mg/kg) $\times \dfrac{Animal\ Km}{Human\ Km}$

The following table illustrates the conversion of animal doses into HED based on the BSA method.

Table II: Conversion of animal doses to HED based on BSA (Reagan-Shaw *et al*., 2007)

Species	Weight (Kg)	BSA (m^2)	Km factor
Human			
Adult	60	1.6	37
Child	20	0.8	25
Baboom	12	0.6	20
Dog	10	0.5	20
Monkey	3	0.24	12
Rabbit	1.8	0.15	12
Guinea pig	0.4	0.05	8
Rat	0.15	0.025	6
Hamster	0.08	0.02	5
Mouse	0.02	0.007	3

I.2. Botanical and ethnobotanical overview of the studied plants

I.2.1. Clusiaceae

The Guttifereae also called Clusiaceae are a family of woody plants native to tropical regions. They are composed of 49 genera and 1610 species and constitute in many aspects a group particularly interesting for the study of floral diversification (Adam, 1971; Troupin, 1978).

They are trees, shrubs, grasses and rarely lianas. The plants of this family are easily recognizable by the yellow or orange resinous latex which flows from the notches (barks) of the barks, flowers and fruits (Letouzey, 1982; Bamps, 1970).

The leaves are opposite, sometimes whorled or alternate, simple, not stipulated, with resin glands and canals, usually furnished with thin parallel and tight veins (Letouzey, 1982; Bamps, 1970).

The flowers are very often unisexual and hermaphrodite. They consist of imbricated sepals, imbricated or contorted petals which are sometimes stripped. The stamens are numerous and grouped in phalanges. The ovary is sessile and superior (Letouzey, 1982; Héfin, 1980).

The fruits are drupes or capsules containing one or more seeds without albumen per compartment. The embryo is relatively large but with very small cotyledons (Letouzey, 1982; Aubreville, 1950).

The wood is hard, firm with medium-sized pores whose rays are clearly visible while the parenchyma is generally arranged in concentric lines or in bands which are sometimes visible (Adam, 1971; Héfin, 1980; Busson, 1965).

The Guttifereae can thus be grouped into subfamilies, tribes and genera, the most common of which are: *Endodesmia*, *Garcinia*, *Allanblakia*, *Symphonia*, *Pentadesma*, *Kielmyera*, *Mammea* etc. (Hutchinson, 1973; Waterman, 1986).

I.2.1.1 *Endodesmia*

The genus *Endodesmia* belonging to the family Guttifereae, is an African monotype genus represented by the only species *Endodesmia calophylloides* Benth. This tree is found in Cameroon, Nigeria, Gabon and Angola (Hutchinson et Dalziel, 1954; Stevens, 1980).

I.2.1.1.1 *Endodesmia calophylloides*

I.2.1.1.1.1 Botanical description

E. Calophylloides commonly called «M'fass» by the Ewondo and Bulu population in Cameroon and «bonason» in Nigeria. It is a small river tree of 17 m high with a thin bole, it has whole, and smooth branches with evanescent flowering nature. Its leaves are oval with a rather obtuse slender acuity. Its flowers include not only nectar and pollen, but also resin, which is very rarely seen outside the family. The fruit is a single-seeded berry with a well-developed exocarp, a fibrous or fleshy mesocarp and a testa consisting of a stony layer and a spongy layer (Burkill, 1985; Bittrich and Amaral, 1997; Normand, 2014). The figure below shows the leaves and bark of the trunk of *E. calophylloides.*

(a): trunk, (b): leaves, (c): stem bark

Figure 10: Picture of *Endodesmia calophylloides*

I.2.1.1.1.2 Geographical distribution

The species occurs in Africa, especially in Gabon, Equatorial Guinea, Democratic Republic of Congo, Congo Brazzaville, Central African Republic, Angola, Nigeria and Cameroon (Hutchinson and Dalziel, 1954; Pellegrin, 1959). In Cameroon, *E. calophylloides* is known under different names: Tsatsa among the Yabassi and Kepkpa among the Baka pygmies (Office national de développement des forêts du Cameroun, 1998; Normand, 2014). According to the information available at the National Herbarium of Cameroon (NHC), this species has already been collected in several regions of the country (Table III).

Table III: Geographical distribution of *E. Calophylloïdes* Benth in Cameroon

Region	Place	Localisation	Sources
South-West	Mundemba	5º 03′N; 8º 48′E Altitude: 50 m Korup national park forest	NHC
South	Kribi	2º 55′N ; 9º 58′E About 7 km from Kribi in an old forestry exploitation ground	
Littoral	Eboné-Ekomtolo	4º 50′N; 9º 54′E Altitude: 520 m Situated in the Bakaka forest at 4km from Eboné-Ekomtolo	

Center	Ntui	-	Ngouamegne *et al.,* 2008
	Mbalmayo		
East	Dja	Dja reserve	NHC

I.2.1.1.1.3 Classification APG III (2009)

From the point of view of the general classification of Guttiferae and of the genus *Endodesmia*, the systematic position of *E. calophylloides* is as follows:

Kingdom: Plantae

Branch: Spermatophytes

Sub-branch: Angiospermes

 Class: Dicotylédones

Order: Malpighiales

Family: *Clusiaceae*

Sub family: *Kielmeyeroideae*

Tribe: *Endodesmieae*

Genus: *Endodesmia*

Specie: *Endodesmia calophylloides* Benth.

I.2.1.1.1.4 Uses of de *Endodesmia calophylloides*

Plants of the genus *Endodesmia* are widely used in several fields of life: traditional medicine, economic, ornamental and artisanal.

I.2.1.1.1.4.1 Economical plan

The wood of *E. calophylloides* is exploited by Cameroonian forestry companies and marketed under the name Kpakpa Ele and code 1691 (Office national de développement des forests du Cameroun, 1998).

I.2.1.1.1.4.2 Ornamental and artisanal plan

It is a very hard wood, appreciated in cabinetmaking and for the manufacture of canoes and frames in Melanesia (Schultes *et al*., 1990).

I.2.1.1.1.4.3 In traditional medicine

This plant is traditionally used for the treatment of a wide range of disorders such as eye-instillation and against filariae (Hutchinson and Dalziel, 1954).

I.2.1.2 *Pentadesma*

The genus *Pentadesma* belongs to the tribe Symphonieae, the subfamily Moronobeoideae and the family Clusiaceae. 15 species belonging to this genus are known, amongst which four African species: *P. butyracea* Sabine with a large geographical distribution; *P. grandifolia* E.G.Baker only present in Nigeria, Cameroon and Gabon; *P. lebrunii* Staner only known in Democratic Republic of Congo and Burundi, and *P. reyndersii* Spirlet endemic of Rwanda. All species of the genus produce an edible fat (Sultanbawa, 1980; Ouattara, 1999; White and Abernethy, 1996). Different parts of *Pentadesma* species are used in tropical African medicine for the treatment of coughs, fevers, bronchitis, venereal diseases and viral infections (Iwu, 1993).

I.2.1.2.1 *Pentadesma butyracea*

I.2.1.2.1.1 Botanical description

P. butyracea commonly called «butter tree», is a long-lived tree that often reaches 20–35 m in height and 80-100 cm diameter at breast height with bole straight (without buttresses) and horizontal branches (Ouattara 1999; White and Abernethy, 1996). Its latex is yellow or orange-yellow while its bark is rough, deeply cracked and exudes a thick resinous juice of reddish yellow color. The leaves are 10-22 cm long, 3.5-7 cm broad, with numerous close parallel and lateral nerves; the flowers are large, white or sometimes reddish; the fruits are broadly ellipsoid, pointed, about 15 cm long and 10 cm large (Hutchinson and Dalziel, 1954).

I.2.1.2.1.2 Geographical distribution

The figure below shows the fruit and trunk of *P. butyracea.*
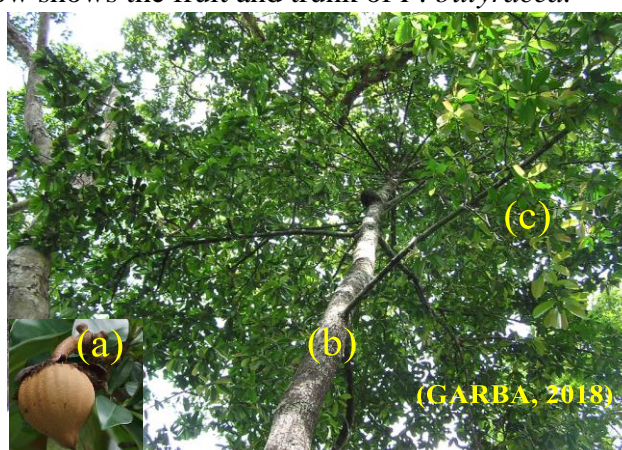
(a): fruit (b): trunk (c): leaves
Figure 11: Picture of *Pentadesma butyracea*

Table IV: Geographical distribution of *P. butyracea* in Cameroon

Region	Place	Sources
South-West	Mamfe	NHC
	Toko	
	Mundemba	
	Bamuso	
	Limbe	
	Kumba	
South	Bipindi	
	Lolodorf	
	Akom 2	
	Campo	
	Mintom 2	
	Lokoundje	
Littoral	Douala 4	
	Edéa	
West	Bazou	

I.2.1.2.1.3 Classification APG III (2009)

Kingdom   Plantae

Subkingdom   Tracheobionta

Superdivision   Spermatophyta

Division   Magnoliophyta

Class   Magnoliopsida

Subclass   Dilleniidae

Order   Theales

Family   Clusiaceae ⁄ Guttiferae

Tribe   Symphonieae

Genus   *Pentadesma*

Species   *Pentadesma butyracea* Sabine

I.2.1.2.1.4 Uses of *Pentadesma butyracea*

I.2.1.2.1.4.1 Economic plan

The seeds are used to make a yellowish edible butter used mainly as fat in culinary preparations that women substitute for shea butter (Dah-dovonon, 2002)

I.2.1.2.1.4.2 Ornamental and artisanal plan

Studies carried out on planing, deformation, probing, mortising, turning and sanding have shown that the wood of *P. butyracea*, has good mechanical properties, similar to those of caïlcedrat (*Khaya senegalensis*) and of iroko (*Milicia excelsa*) (Ewédjè, 2012; Rachman *et al*., 1987).

I.2.1.2.1.4.3 In traditional medicine

Pentadesma butyracea is used in traditional medicine as massage oil, in skin and hair care and in the manufacture of soap for its softening, lubricating and healing qualities (Dencausse *et al*., 1995). It is used to delay the ageing of skin in patented cosmetic preparation (Courtin, 1986). Different parts of this plant are used in tropical African medicine for the treatment of coughs, fevers, bronchitis, venereal diseases and viral infections (Iwu, 1993).

In the western part of Cameroon, an infusion of the stem bark is used to treat fever (Sinsin *et al*., 2003).

In Gabon, the macerated bark is used as lotions for the treatment of the parasitic diseases of the skin and as an antidiarrhetic (Raponda-Walker and Sillans, 1961).

In Ghana, the decoction of the roots is used to fight against intestinal worms and the decoction of the bark is used as a purgative (Tchobo *et al*., 2007).

In Congo-Brazzaville, the bark is sometimes taken as an aphrodisiac (Sinsin *et al*., 2003).

In Liberia the decoction of the root is used as a vermifuge (Sinsin *et al*., 2003).

In Sierra Leone the leaves after roasting and crushing are given to children to relieve constipation (Sinsin *et al*., 2003).

I.2.2 Passifloraceae

The Passifloraceae is a family of dicotyledonous plants. They are divided into 19 genera with about 600 species. This family includes: shrubs, trees, herbaceous plants, climbing plants and lianas. In the latter, the attachment to the support is done through spiral and axillary tendrils, corresponding to sterile pedicels (Killip, 1938; Quotig, 2011). Worldwide, about 14 genera and over 370 species have been described. Among the genera of the Passifloraceae family, we can cite: *Ancistrothyrsus, Androsiphonia, Barteria, Basananthe, Crossostemma, Deidamia, Dilkea, Efulensia, Hollrungia, Mitostemma, Paropsia, Paropsiopsis, Passiflora, Schlechterina, Smeathmannia, Tetrastylis, Tryphostemma, Viridivia and Adenia* due to its frequent use in traditional medicine (Quotig, 2011).

I.2.2.1 *Adenia*

Adenia is a genus of flowering plants in the Passifloraceae family, native mainly to tropical Africa, Madagascar and Asia (Feuillet, 1989). Some species of the genus *Adenia* are xerophytes and is divided into six sections comprising about 95 species, of which about 60 are on the African continent, 20 in Madagascar and 15 in Asia (Scmelzer and Gurib-fakim, 2008). These species come in various forms: lianas, trees, shrubs, etc and occupy different types of habitats be it the certain African deserts or the dense forests of South-East Asia (Hearn, 2006). The genus *Adenia* has about 95 known species, that is to say 47 species described among which: *Adenia aculeata, Adenia cissampeloides, Adenia cladosepala, Adenia digitata, Adenia ellenbeckii, Adenia firingalavense, Adenia fruticosa, Adenia glauca, Adenia globosa, Adenia goetzii, Adenia keramanthus, Adenia lanceolata, Adenia oblongifolia, Adenia olaboenis, Adenia pechuelii, Adenia racemosa, Adenia spinosa, Adenia stenodactyla, Adenia venenata, Adenia volkensii, Adenia lobata* (Scmelzer and Gurib-fakim, 2008). The latter will be the subject of our study.

I.2.2.2 *Adenia lobata*

I.2.2.2.1 Botanical description

A. lobata with vernacular name Gawna in the Masa language in Cameroon and Chad, is a large liana, usually dioecious, whose stem reaches 45 m long and up to 12 cm in diameter, smooth or with tubercles; its bark is green to red-brown; its sap is clear, turning red and its stems have simple or fidid tendrils up to 25 cm long. The leaves of this plant are alternate, simple; stipules triangular, 0.5-1 mm long and rapidly falling. The flowers are unisexual, regular, yellowish; its pedicel 5-40 mm long; its calyx with tube 5-15 mm long and triangular lobes are 7-15 mm long. The fruit is an obovoid to globose or ellipsoid capsule 3-8 cm long, leathery or fleshy, yellow, smooth or bumpy, 20-150-seeded. Seeds are broadly ellipsoid to orbicular, 5 mm long, punctate (Burkill, 1997; De Wilde, 1975).

Figure 12: Picture of liana of *Adenia lobata*

I.2.2.2.2 Geographical distribution

Adenia lobata occurs from East Senegal to Ethiopia and South of Africa to Mozambique (Robyns, 1995). *A. lobata* occurs in rainforests, secondary forests, forest edges, gallery forests, periodically flooded and marshy forests and on rocky outcrops, from sea level up to 1800m altitude (Neuwinger, 2004). In Cameroon this species is localized in several regions. The following table V gives some regions and location where *Adenia lobata* is found.

Table V: Geographical distribution of *A. lobata* in Cameroon

Region	Place	Localisation	Species	Sources
Center	Ngoumou	Otoutoumou	*Adenia lobata*	NHC
	Akonolinga	15km south of Djouo		
East	Akok Bikele	Near Akok Bikele		
East	Matchéboum	Matchéboum near Abong Mbang		
South	Campo	25 km SE Campo. IGN. Kribi.		

I.2.2.2.3 Classification APG III (2009)

Kingdom: **Plantae**

Clade: Tracheophytes

Order: Malpighiales

Family: Passifloraceae

Subfamily: Passifloroideae

Tribe: Passifloreae

Genus: *Adenia*

Species   *Adenia lobata* (Jacq.) Engl.

I.2.2.2.4 Uses of *Adenia lobata*

Several species of the genus *Adenia* are widely used in several areas of life such as: food, craft or ornament, agricultural, economically and medicinal.

I.2.2.2.4.1 As food

In DR Congo the cooked minced leaves of *Adenia lobata* are eaten as a vegetable. Stem fluid can be drunk as a drink (Atindehou *et al*., 2002). In West and Central Africa, as well as in Tanzania and Angola, the stems, bark, fruits or juice of *Adenia lobata* are used to poison fish (Atindehou *et al*., 2002).

I.2.2.2.4.2 On the artisanal and ornamental plan

In Cameroon, the stem sections of *Adenia lobata* are used as sponges (Adjanohoum *et al*., 1986).

In DR Congo, the stem of *A. lobata* serves as a cord (Bouquet *et al*., 1974).

I.2.2.2.4.3 In traditional medicine

In Togo, a decoction of *Adenia lobata* twigs is drunk or used as a bath to treat malaria (Aké *et al*., 1985). The young leaves of *A. lobata*, lightly roasted, are applied on abscesses and then covered with leaves (Ulubelen *et al*., 1982). In Senegal, the leafy stems of *A. lobata* are heat dried and applied to wounds caused by guinea worms in order to remove them. The Tendas of Senegal drink a soup made from the leaves to reduce fever in children; a decoction of the leaves is also used to wash patients suffering from malaria (Fernandes and Fernandes, 1978). In Ivory Coast and Congo, the leaves of *A. lobata* are eaten with palm oil and salt to treat palpitations. The juice of the leaf is used as local application or in washing against

rheumatic pain, rib and abdominal pain while the maceration in water of the leafy twigs is taken to treat cough, bronchitis and fever (Adjanohoum *et al*., 1986). In Ghana the leaves of *A. lobata* are used to treat hemorrhoids topically (Aké *et al*., 1985; Atindehou *et al*., 2002). In Ivory Coast and Congo, the juice of the leaves and stem of *A. lobata* is used to treat trypanosomiasis, and is applied to insect bites. Enemas made from pulped twigs are administered for their diuretic properties and to treat jaundice and fainting (Adjanohoum *et al*, 1986). In D.R Congo, a decoction of *A. lobata* leaves is drunk to treat delusional flushes. The juice of the stems of *A. lobata* is also taken to treat gastrointestinal problems (Adjanohoum *et al*., 1979).

In view of the various uses in traditional medicine of the species described above in the treatment of several diseases, many research teams have invested in the chemical study of species of these genera and have evaluated the different compounds for their biological potentials.

I.3 Previous chemical and biological investigation on the selected plants

I.3.1 *Adenia lobata* (Jacq.) Engl.
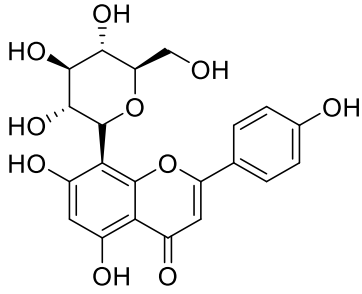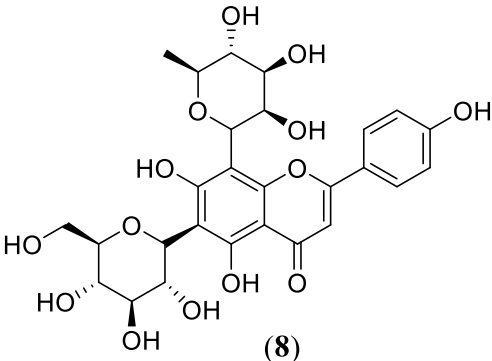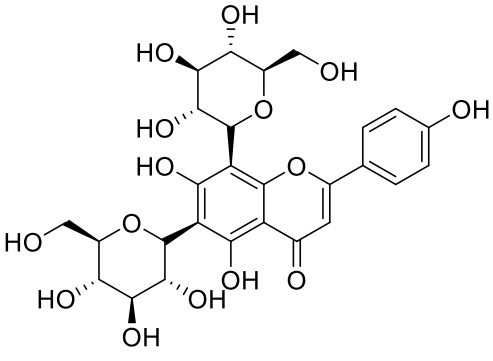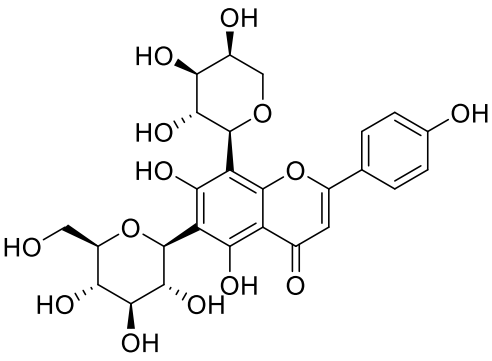
I.3.1.1 Previous chemical studies of species of the genus *Adenia*

The chemical works carried out up to date with a view to determine the chemical composition of plants of the genus *Adenia* has enabled the isolation and characterization of several secondary metabolites, in particular: flavonoids, cyanogenic heterosides, and triterpenes.

I.3.1.1.1 Flavonoids

The flavonoids isolated from the genus *Adenia* are generally glycosylated. The table VI below shows some of them.
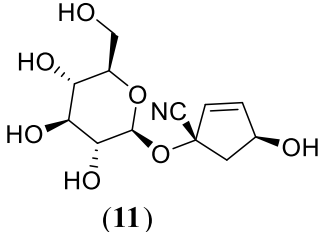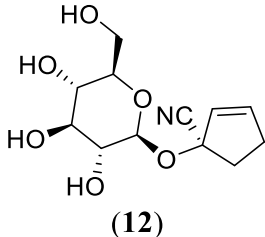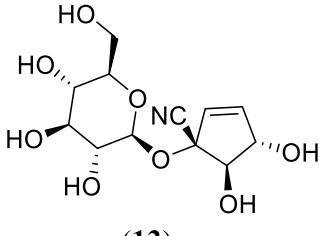
Table VI: Some flavonoids isolated from the genus *Adenia*

Structures	Names	Sources	References
(7)	Vitexin		
(8)	Violanthin	Leaves of *Adenia lobata*	Scmelzer *et al.*, 2008
(9)	Vicenin-2		
(10)	Schaftoside.		

I.3.1.1.2 Cyanogenic heterosides

Cyanogenic glycosides, cyanoglycosides or cyanogenic heterosides, are very widespread plant toxins (phytotoxins), from the group of glycosides (Chaouli, 2013). The table below shows some of them.
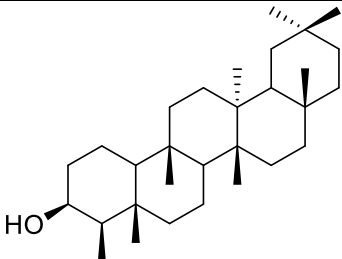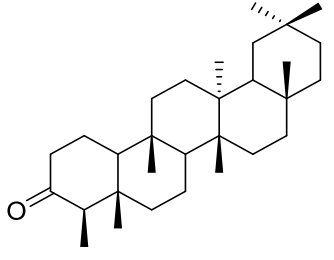
Table VI: Some cyanogenic heterosides isolated from the genus *Adenia*

Structures	Names	Sources	References
(11)	Tetraphyllin B	Leaves, stem, fruit and roots of Ade*nia cissampeloides*	Morah, 1988
(12)	Tetraphyllin A	The aerial parts of *Adenia globosa*	Jaroszewski *et al.*, 1985
(13)	Gynocardin	leaves of *Adenia lobata*	Tantisewie *et al.*, 1969

I.3.1.1.3 Triterpenoids

Triterpenes are natural C_{30} compounds resulting from the cyclization of squalene (Bruneton, 1999). The table VIII below shows two of them, isolated from *Adenia* species

Table VIII: Some isolated triterpenes from the genus *Adenia*

Structures	Names	Sources	References
(14)	Friedelan-3-ol	*Adenia cissampeloides*	(Spencer *et al.*,1987)
(15)	Friedelin		

Certain compounds isolated and extracted from the genus *Adenia* have exhibited a diverse range of biological activities.

I.3.1.2 Previous biological work on the genus *Adenia*

Biological works carried out on *A. lobata* has confirmed certain therapeutic virtues.

The aqueous and ethanolic extracts of stem bark of *Adenia lobata* showed activity on the NF54 strain of *Plasmodium falciparum* with IC_{50} value of 14.57 ± 1.16 μg/mL and 9.69 ± 0.38 μg/mL, respectively (Kipré *et al.*, 2018).

The ethanolic extract of the wood of *A. lobata* has been tested for its antiplasmodial activity *in vitro* against K1 resistant to chloroquine strains of *P. falciparum* with an IC_{50} value of 125 μg/mL (Sarah *et al.*, 2000).

The aqueous and ethanolic extracts of stem bark of *A. lobata* showed activity on *P. falciparum* strain K1 with IC_{50} values of 15.88 ± 1.41 μg/mL and 25.1 ± 0.71 μg/mL, respectively (Kipré *et al.*, 2018).

70% of the ethanolic extract of *A. lobata* showed better antisalmonella activity in vitro with a minimum inhibitory concentration of between 8 and 64 μg/mL (Fowa *et al.*, 2019).

The ethanolic extract of the wood of *A. lobata* showed antiplasmodial activity against the K1 strain of *Plasmodium falciaprum*, resistant to chloroquine with an IC_{50} value of 125 μg/mL (Marshall *et al.*, 2000)

The dichloromethane extract of the leaves of *A. lobata* showed good activities against other protozoan parasites such as *Trypanosoma brucei* (EC_{50} of 3.1 μg/mL) and *Leishmania donovani* (EC_{50} of 50 μg/mL) (Okpekon *et al.*, 2004).

I.3.2 *Endodesmia calophylloides* Benth.
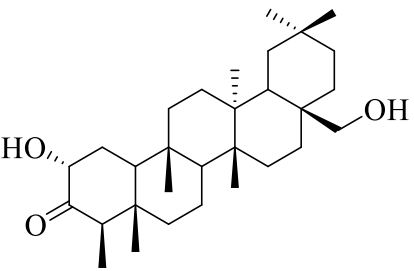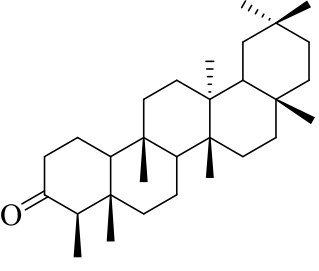
I.3.2.1 Previous chemical work done on *Endodesmia calophylloides*
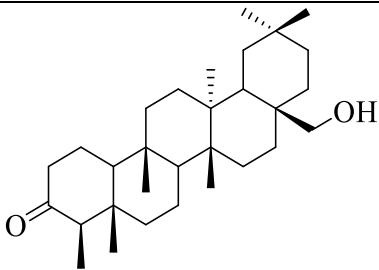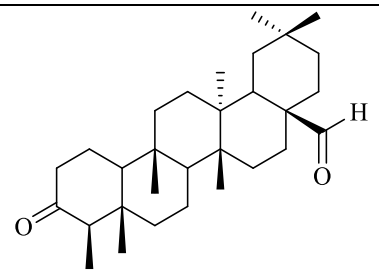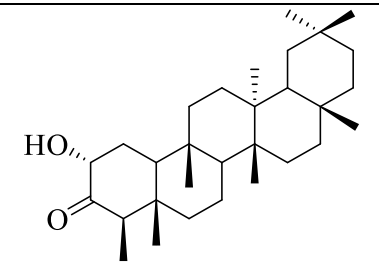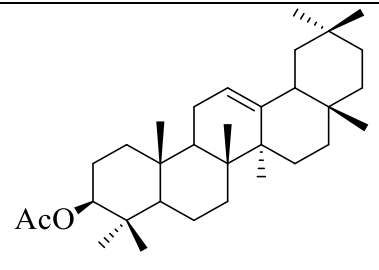
Previous chemical studies performed on *E. calophylloides* have led to the isolation and characterization of secondary metabolites belonging to several classes of compounds such as xanthones, terpenoids, biflavonoids and polyprenylated benzophenones (Ngouamegne *et al.*, 2008).

I.3.2.1.1 Pentacyclic triterpenoids

Triterpenes are natural C_{30} compounds resulting from the cyclization of squalene (Bruneton, 1999). The triterpenes isolated from *E. calophylloides* belong mainly to the friedelane series. The table IX below shows some triterpènes.

Table IX: Some triterpenes isolated from the bark of the trunk of *Endodesmia calophylloides*
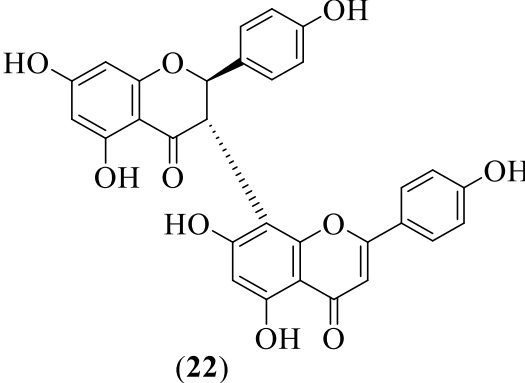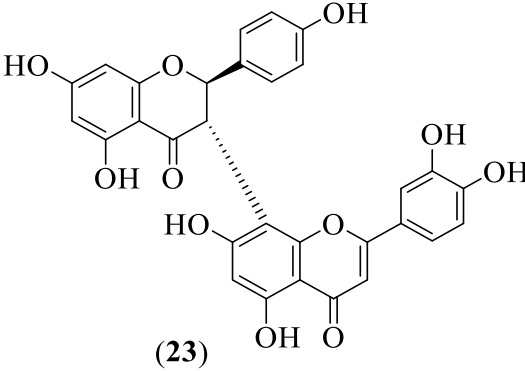
Structures	Names	Sources	References
(16)	Endodesmiadiol		
(15)	Friedelin		

(18)	Canophyllol		
(19)	canophyllal	Stem bark of *E. calophylloides*	Ngouamegne *et al.,* 2008
(20)	Cerin		
(21)	3*β*-Acetoxyoleanolic acid		

I.3.2.1.2 Biflavonoids

Biflavonoids are obtained by the condensation of identical flavonoid units (homologous dimers or homobiflavonoids) or of flavonoid units belonging to different classes (mixed dimers or hetero biflavonoids) (Yong, 1992). Most of the biflavonoids isolated from Clusiaceae have a 3 → 8″ junction, which is characteristic of this family (Taher *et al*., 2005). The table X below shows some bioflavonoids.
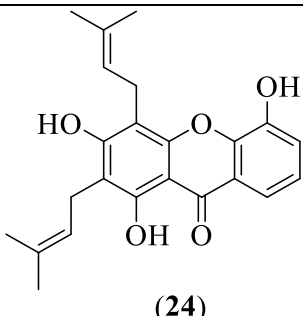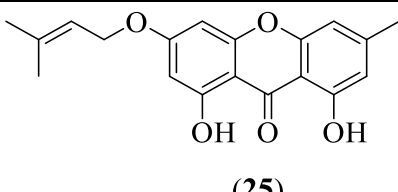
Table X: Some biflavonoids isolated from *Endodesmia calophylloides*

Structures	Names	Sources	References
(**22**)	Volkensiflavone	Stem bark of *E. calophylloides*	Ngouamegne *et al.*, 2008
(**23**)	Morelloflavone		

I.3.2.1.3 Xanthones

The xanthones isolated from Clusiaceae can be classified into two broad groups: simple oxygenated xanthones and prenylated xanthones (Table XI).
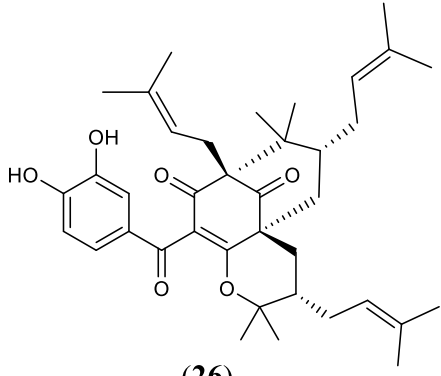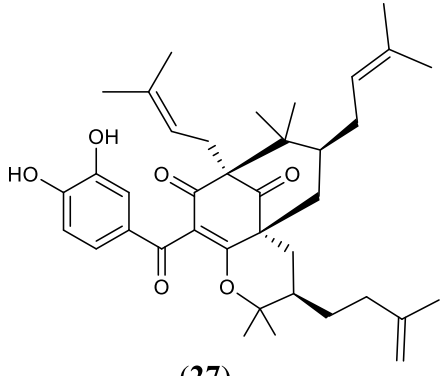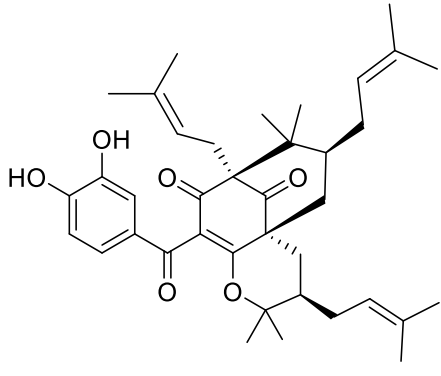
Table XI: Some xanthones isolated from *Endodesmia calophylloides*
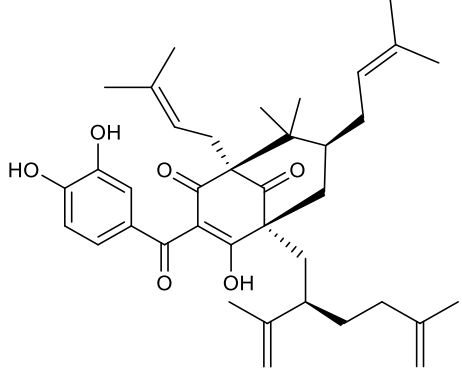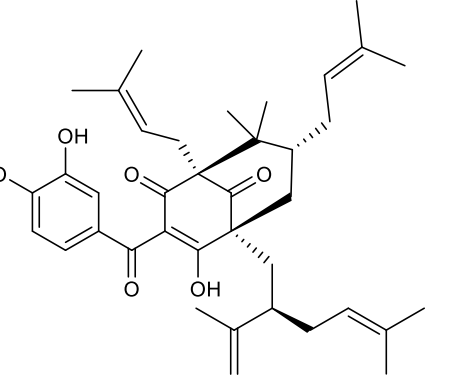
Structures	Names	Sources	References
(**24**)	8-Deoxygartanin	Stem bark of *E. calophylloides*	Ngouamegne *et al.*, 2008
(**25**)	1,8-Dihydroxy-3-isoprenyloxy-6-methylxanthone		

I.3.2.1.4 Benzophenones

The benzophenones isolated from *E. calophylloides* are polyprenylated benzophenones (Table XII).

Table XII: Some Benzophenones isolated from *Endodesmia calophylloides*

Structures	Names	Sources	References
(**26**)	Cambogin	Stem bark *E. calophylloides*	Ngouamegne *et al.*, 2008
(**27**)	Cycloxanthochymol		
(**28**)	Isoxanthochymol		

 (29)	Xanthochymol		
 (30)	Guttiferone E		

Certain compounds isolated and extracted from *E. calophylloides* have exhibited a diverse range of biological activities.

I.3.2.2 Previous biological work on *Endodesmia calophylloides*

Several extracts and isolated compounds from *E. calophylloides* were tested on *P. falciparum* strain W2 by Ngouamegne and collaborators in 2008 with the aim of evaluating their antiplasmodial activities. Thus, the hexane, ethyl acetate and methanol extract of the stem bark of *E. calophylloides* showed inhibitory concentrations IC_{50} (in μg/mL) of 9.3 ± 1.0; 7.4 ± 0.6; 12.8 ± 1.0 respectively.

Compounds isolated from the bark of the trunk of *E. calophylloides*, namely endodesmiadiol (**16**), friedelin (**17**), canophyllol (**18**), canophyllal (**19**), cerin (**20**), morelloflavone (**23**), 8-dexoygartanin (**24**), showed inhibitory concentrations IC_{50} against *P. falciparum* W2 between 7.2 and 23.6 μM (Ngouamegne *et al.*, 2008).

I.3.3 *Pentadesma butyracea* Sabine

I.3.3.1 Previous chemical work on *Pentadesma butyracea*
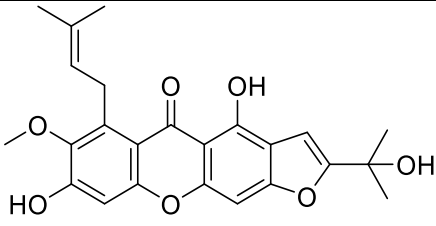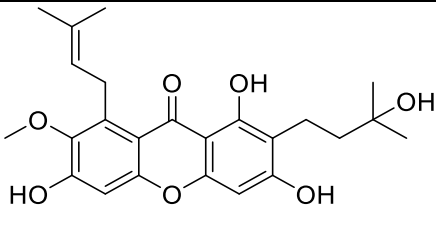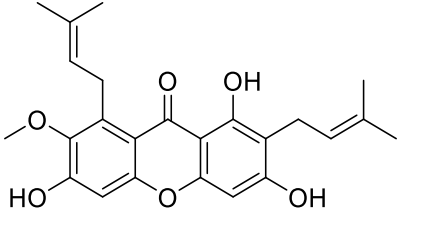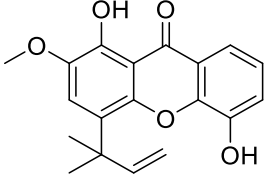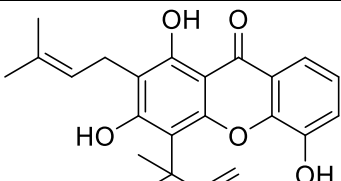
Previous chemical studies performed on *Pentadesma butyracea* have led to the isolation and characterization of secondary metabolites belonging to several classes of
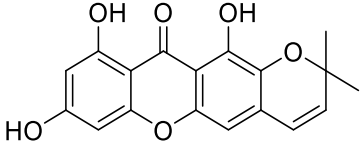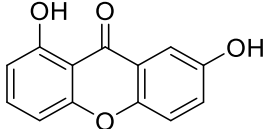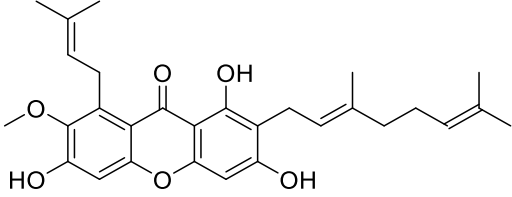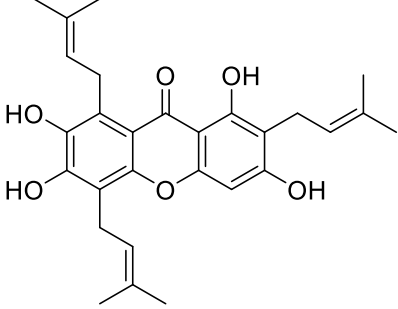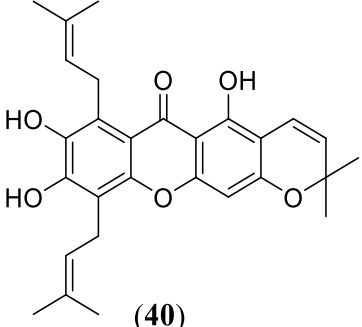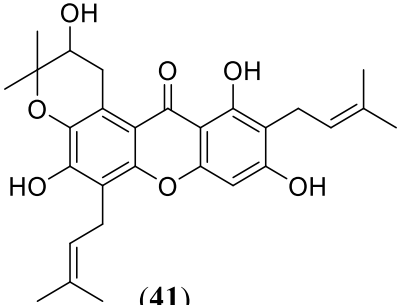
compounds such as xanthones, flavonoids, steroids, polyprenylated benzophenones and triterpenoids (Tala *et al.*, 2013; Lenta *et al.*, 2011; Wabo *et al.*, 2010; Zelefack *et al.*, 2009).
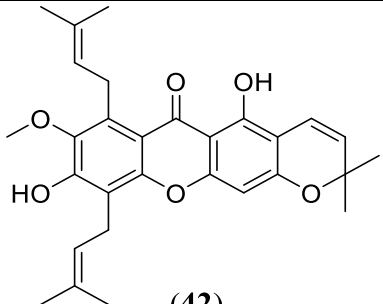
I.3.3.1.1 Xanthones

The xanthones isolated from Clusiaceae can be classified into two broad groups: Simple oxygenated xanthones and prenylated xanthones (Table XIII).

Table XIII: Some xanthones isolated from *Pentadesma butyracea*

Structures	Names	Sources	References
(31)	pentadexanthone	Fruit of *Pentadesma butyracea*	Lenta *et al.*, 2011
(32)	Cratoxylone		
(33)	*α*-mangostin		
(34)	Butyraxanthone F	leaves of *Pentadesma butyracea*	Tala *et al.*, 2013
(35)	Allanxanthone A		
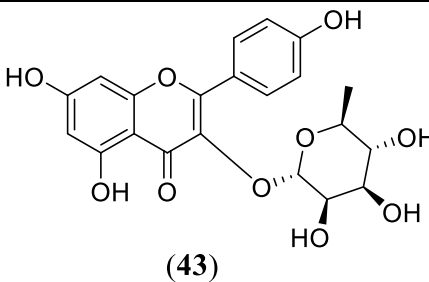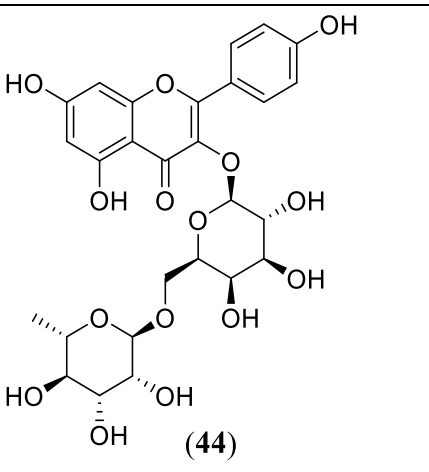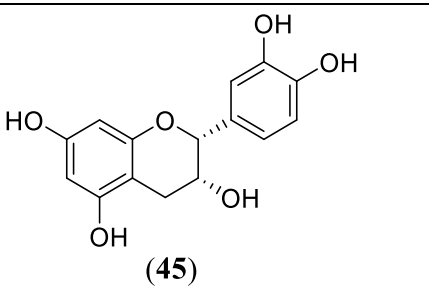
(36)	Butyraxanthone E	roots of *Pentadesma butyracea*	Wabo *et al.*, 2010
(37)	1,7-dihydroxyxanthone		
(38)	Butyraxanthone A	stem bark of *Pentadesma butyracea*	Zelefack *et al.*, 2009
(39)	garcinone E		
(40)	Butyraxanthone B		
(41)	Butyraxanthone C		

Structures	Names	Sources	References
(**42**)	Magostanin		

I.3.3.1.2 Flavonoids

Several flavonoids were isolated from *P. butyracea* (Table XIV).
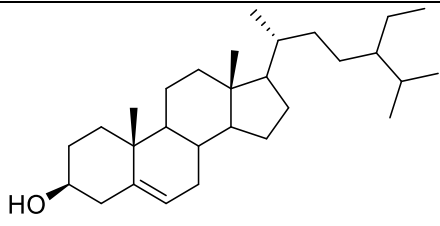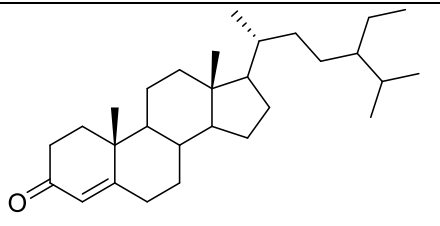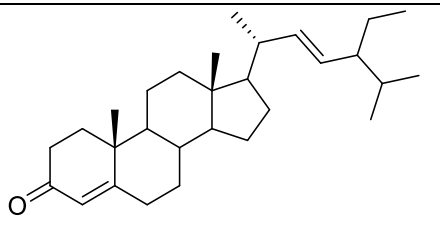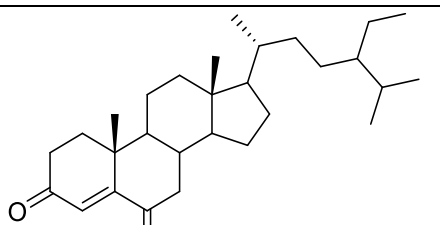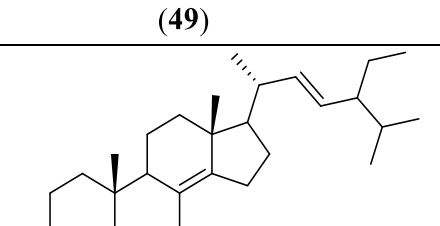
Table XIV: Some flavonoids isolated from *Pentadesma butyracea*

Structures	Names	Sources	References
(**43**)	Kaempferin	leaves of *Pentadesma butyracea*	Tala *et al*., 2013
(**44**)	Kaempferol-3-*O*-*α*-L-rhamnopyranosyl-(1-->6)-*β*-D-galactopyranoside		
(**45**)	(−)-epicathechin	Fruit of *Pentadesma butyracea*	Lenta *et al*., 2011

I.3.3.1.3 steroids

Steroids are secondary alcohols of animal and vegetable origin, the basic skeleton of which varies from C_{27} to C_{29} (Table XV).

Table XV: Some steroids isolated from *Pentadesma butyracea*

Structures	Names	Sources	References
 (**46**)	*β*-sitosterol	leaves of *Pentadesma butyracea*	Tala *et al*., 2013
 (**47**)	Stigmasta-4-en-3-one		
 (**48**)	Stigmasta-4,22-dien-3-one		
 (**49**)	Stigmasta-4-en-3,6-dione		
 (**50**)	Ergosta-4,6,8,22-tetraen-3-one		

I.3.3.1.4 Benzophenones

30-*epi*-cambogin (**51**) has been isolated from the leaves and roots of *Pentadesma butyracea* (Tala *et al*., 2013; Wabo *et al*., 2010)

(**51**)
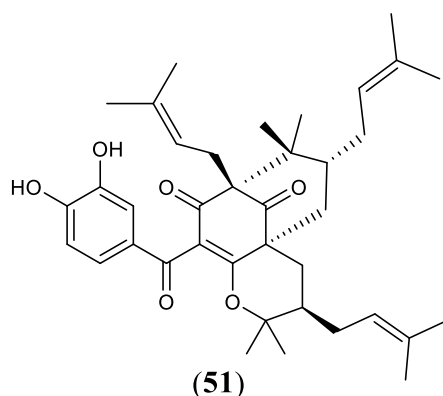
I.3.3.1.5 triterpenoids

Lupeol (**52**) has been isolated from the fruit and leaves of *Pentadesma butyracea* (Lenta *et al.*, 2011; Tala *et al.*, 2013).

(**52**)
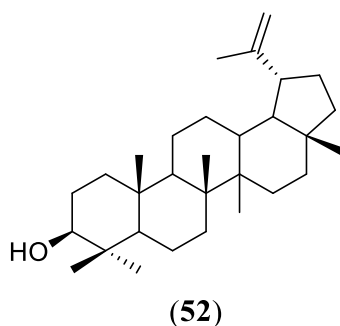
I.3.3.2 Previous biological work on *Pentadesma butyracea*

Butyraxanthone B (**40**), butyraxanthone C (**41**), mangostanin (**42**), garcinone E (**39**), and lupeol (**52**) isolated from the stem bark of *P. butyracea*, showed inhibitory concentrations (IC$_{50}$) between 1.9 and 3.0 μg/mL aginst the FcB1 *Plasmodium falciparum* chloroquine-resistant strain (Zelefack *et al.*, 2009).

Butyraxanthone E (**36**) and 30-*epi*-cambogin (**51**) isolated from the roots of *P. butyracea*, showed moderate antiproliferative activity against *Drosophila* S2 cells with IC$_{50}$ values of 6.27 and 2.74 μg/mL, respectively (Wabo *et al.*, 2010).

The methanol extract and ethyl acetate fraction of the fruit of *P. butyracea* showed inhibitory concentrations (IC$_{50}$) against W2 *Plasmodium falciparum* strain (in μg/mL) of 1.83 $\pm$ 0.17; 2.77 $\pm$ 0.09 respectively. Compounds isolated from this same part of the plant namely pentadexanthone, cratoxylone, α-mangostin, garcinone E, also showed inhibitory concentrations (IC$_{50}$) on the same strain between 0.41 and 3.0 μM (Lenta *et al.*, 2011).

Taking into account the fact that most of the active isolated compounds as well as the new derivative of *A. lobata* belong respectively to the families of ceramides and xanthones, it is therefore important to give a brief overview on these two classes of secondary metabolites.

I.4 Brief overview of ceramides

Glycosphingolipids, a class of natural products, were firstly described in the second half of the last century. The German physician J. L. W. Tudichum was able to isolate an organic base that he called sphingosine in addition to sugar and fatty acids by fractional crystallization of alcoholic brain extracts. The structure was elucidated by Carter in 1947. The isolation and naming of further brain lipids such as ceramide, sphingomyelin, and cerebroside are also attributed to Tudichum (Kolter and Sandhoff, 1999).

I.4.1 Definition and structure

Ceramide is composed of sphingosine, which is an amide-linked to a fatty acyl chain, varying in length from C_{14} to C_{26} (Saddoughi *et al*., 2008).
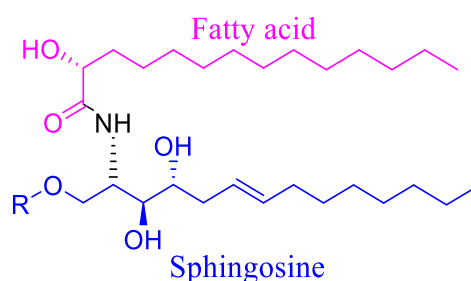
R=H or R= single sugar (either glucose or galactose) (Kihara, 2016).

I.4.2 Biosynthesis of ceramides

The condensation of the amino acid L-serine with an activated fatty acid such as a derivative of coenzyme A to give 3-ketosphinganine is catalyzed by serine palmitoyltransferase (SPT). SPT is a pyridoxal phosphate dependent enzyme and is mechanically linked to aminolevulinate synthase, which catalyzes the initial reaction of heme biosynthesis. Serine palmitoyltransferase has a lower activity than subsequent enzymes in ceramide biosynthesis and catalyzes the rate-determining step of this metabolic pathway. It preferably uses coenzyme A esters of fatty acids with a chain length of C_{16} atoms so that a long chain base with a C_{18} chain is formed. Serine palmitoyltransferase is the only ceramide biosynthesised enzyme for which sequence data is available in yeast and humans. In the following NADPH dependent reaction, 3-ketosphinganine is reduced to D-erythro-sphinganine by 3 ketosphinganine reductase. Finally, sphinganine N acyltransferase acylates sphinganine is converted to dihydroceramide. The enzyme exhibits selectivity towards stearic acid activated by coenzyme A and is also capable of acylating sphingosine formed in the recovery pathway from sphingolipid degradation (Kolter and Sandhoff, 1999). The following scheme shows the biosynthesis of ceramides.
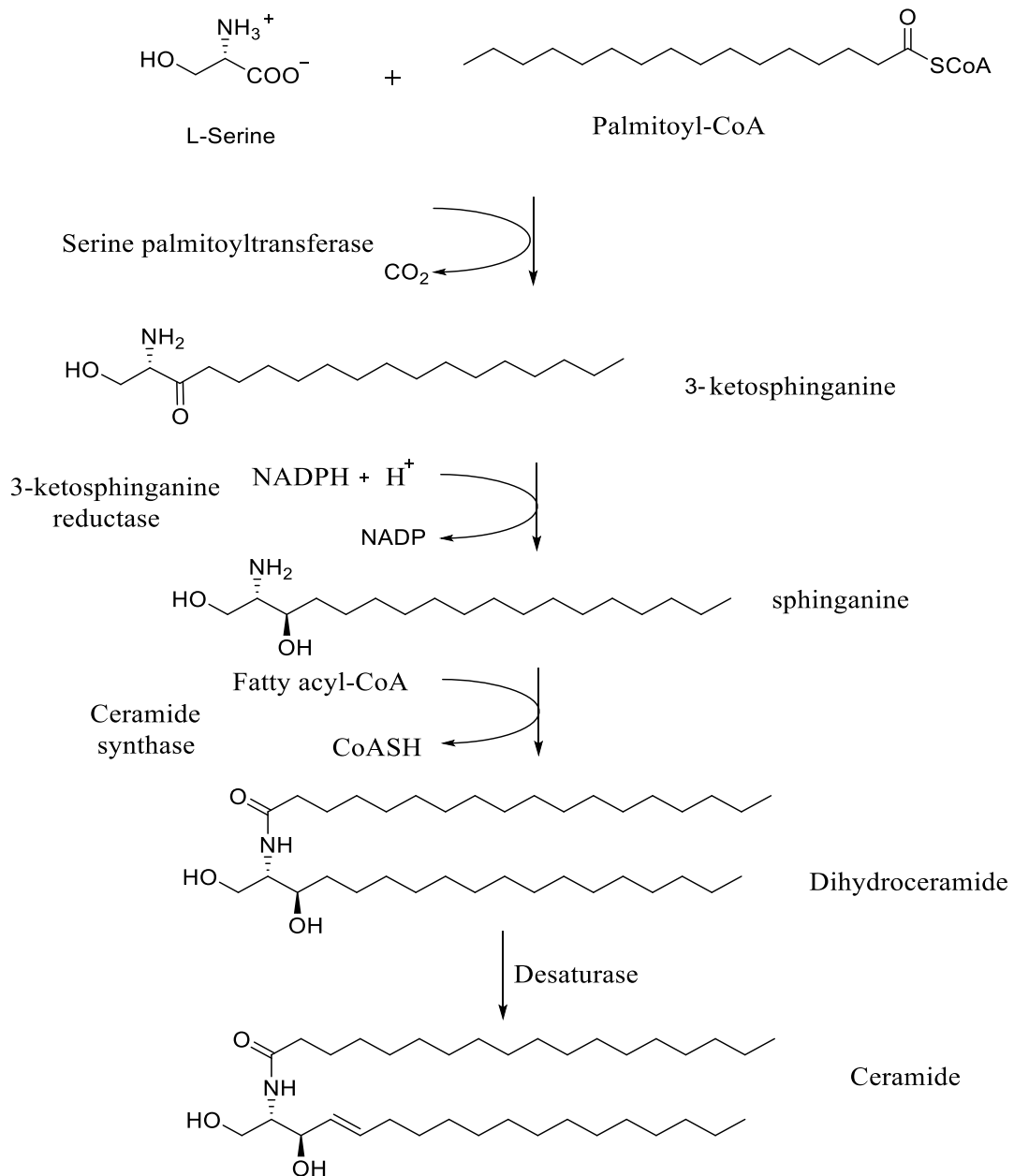
Scheme 1: Biosynthetic pathway for ceramide (Kolter and Sandhof, 1999; Merrill and Sandhoff, 2002).

I.4.3 Biological function of ceramides

Ceramides are predominantly lipids of human epidermal stratum corneum, acting as the water barrier to prevent loss of body water. They are classified into two groups, free ceramides and protein-bound ones (Masuda and Mori, 2005). In addition to their contribution to membrane structure, a growing body of literature suggests that dietary sphingolipids have protective effects against colon cancer (Zhu *et al.*, 2013).

I.4.4 General method for the structural elucidation of ceramides

A ceramide is a sphingolipid resulting from the combination of a fatty acid with sphingosine via an amide bond. Determining their structure amounts to finding the length of the sphingosine part and the fatty acid part. Several techniques such as: mass spectrometry (MS), infrared spectrometry (IR) and nuclear magnetic resonance (NMR) are used for this.

I.4.4.1 Infrared spectroscopy

Infrared analysis makes it possible to demonstrate the presence of a hydroxyl group, a secondary amide, an aliphatic chain and an olefinic functional group. Thus, an absorption around 3605 cm^{-1} indicates the presence of a hydroxyl group, that around 3434, 1657 and 1510 cm^{-1} suggest an amide functional group. In addition to this, the absorption band close to 2928, 2855 and 1450 cm^{-1} suggests the presence of an aliphatic chain of ceramides. While an absorption band close to 1467 cm^{-1} is due to the presence of an olefinic functional group (Yaoita *et al.*, 2002; Shaiq Ali *et al.*, 2006; Bankeu *et al.*, 2010).

I.4.4.2 Mass spectrometry

High resolution mass spectrometry can determine the molecular formula and the number of unsaturations of a ceramide. Often used techniques are: High Resolution Electrospray Ion Mass Spectrometry (HR-ESI-MS), High-Resolution Electron Ionization Mass Spectrometry (HR-EI-MS), High Resolution Fast Atomic Bombardment Mass Spectrometry (HR-FAB-MS) (Yaoita *et al.*, 2002; Muralidhar *et al.*, 2005; Shaiq Ali *et al.*, 2006; Bankeu *et al.*, 2010).

I.4.4.3 Proton nuclear magnetic resonance spectroscopy

On the ^{1}H NMR spectrum of ceramides, some characteristic signals appear: the resonance of the terminal methyl groups (-CH$_3$) of the two side chains appear as a triplet between δ_H 0.84-0.86 with the coupling constant between 7.0-7.8 Hz depending on the solvent. A broad signal between δ_H 1.26–1.40 corresponding to the sequence of the methylene (-CH$_2$-) groups in the fatty acid and sphingosine parts. The signal of a proton attached to the (H – N) amide function appearing as a doublet at approximately δ_H 8.55 (1H, d, J = 9.0 Hz). The Ha and Hb resonances of hydroxymethylene at position 1 appear as a pair of double doublets (dd) around δ_H 4.49 and 4.41 (J = 10.5, 6.0 Hz). The resonance of the olefinic proton appears as a pair of doublets of triplets or as multiplets close to δ_H 5.52 and 5.48. If one of the J values of these protons is around 14.5 Hz, this reveals the E configuration (Yaoita *et al.*, 2002; Cateni *et al.*, 2003; Muralidhar *et al.*, 2005; Shaiq Ali *et al.*, 2006; Bankeu *et al.*, 2010; Ebede *et al.*, 2019; Kagho *et al.*, 2020).

I.4.4.4 Carbon nuclear magnetic resonance spectroscopy

The ^{13}C NMR of ceramides also shows some characteristic signals, amongst which we have: primary methyls of the two side chains appearing around δ_C 14.0-14.5 (-CH$_3$), a signal corresponding to the sequence of methylene groups in the fatty acid parts and sphingosine between δ_C 22.6-31.0 (-CH$_2$-). The olefinic carbon signals appear in the range of δ_C 127.0 to 135.0 (Cateni *et al.*, 2003; Muralidhar *et al.*, 2005; Bankeu *et al.*, 2010; Ebede *et al.*, 2019; Kagho *et al.*, 2020). The olefinic double bond will take on a *trans* configuration depending on the chemical shifts of its allylic carbons at δ_C 33.9 and 32.7, respectively which are greater than 29 ppm (Teinkela *et al.*, 2019). Typically, signals of a carbon next to a *trans* double bond appear between δ_C 32 and 33 (Ai-Qun *et al.* 2010; Huang *et al.*, 2010), while those of a cis double bond appear between δ_C 27 and 28 (Liu *et al.*, 1999). The carbonyl resonance of the amide appears to be close to δ_C 175.0-176.2. The signal of an oxymethylene (C-1) appears between δ_C 62.1-68.5 (Cateni *et al.*, 2003; Muralidhar *et al.*, 2005; Bankeu *et al.*, 2010; Ebede *et al.*, 2019; Kagho *et al.*, 2020).

I.4.4.5 Chemical degradative methods in the structural determination of ceramides

The length of the fatty acid and sphingosine chains are determined by methanolysis coupled by HR-ESI-MS analysis. The ceramide is dissolved in pyridine and heated at reflux (70°C) for 18 hours in a methanolic solution containing 0.9N hydrochloric acid, with magnetic stirring. The reaction medium is neutralized with an aqueous solution of sodium carbonate (Na$_2$CO$_3$). The fatty acid methyl ester (FAME) obtained with a long chain base (LCB) from the methanolysis is extracted with chloroform (CHCl$_3$) and this layer is concentrated and subjected to analysis by gas chromatography-spectrometry of mass (GCMS) to determine the nature of FAME or High resolution electrospray ion mass spectrometry to determine the nature of LCB (Kamga *et al.*, 2010).

To determine the position of the double bond in one of the long chains of a ceramide, an additional reaction is required. For this, the compound is dissolved in carbon disulfide and iodine is added to the solution. A small volume of the resulting mixture is stored at 60 °C for 40 h in a small sealed vial. The reaction is then quenched with aqueous Na$_2$S$_2$O$_3$ (5%), and the mixture is extracted with *n*-hexane. The extract is concentrated to give the dimethyldisulfide (DMDS) derivative of ceramide. The FAB positive ion mass spectrum of the DMDS derivative of ceramide shows a remarkable fragment ion peak due to the cleavage of the bond between carbons bearing a methylthio group. These data indicate the position of the double bond in the LCB or in the FAME of the ceramide (Bankeu *et al.*, 2010).

I.5 Brief overview of xanthones

I.5.1 Definition and structure

Xanthones and their derivatives are widely distributed in nature and are isolated from several natural sources such as plants, lichens, fungi. The term xanthone comes from the Greek word "xanthos" which means yellow. They are oxygenated heterocycles whose basic skeleton is symmetrical dibenzo-γ-pyrone (**53**). Hydroxyl, methoxyl, prenyl, glycosyl etc. groups are frequently encountered as substituents on the xanthonic nucleus. Oxygenated carbons 1,3 or 1,4 belong to nucleus A (acetate derivative) and nucleus B (shikimate derivative) carries oxygen at C-5, C-6, C-7 or C-8 (Masters and Bräse, 2012; Silva and Pinto, 2005).

(53)
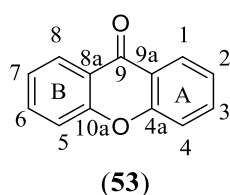
I.5.2 Biosynthesis of xanthones

Xanthones are biosynthelized following two differents pathways: the polyacetic and the mixed (polyacetic and shikimic) pathways (Bennett and Lee, 1989).

I.5.2.1 Polyacetic biosynthesis of xanthones

This biosynthetic pathway is common in lower plants (lichens, bacteria). It starts from acetylcoenzyme A, then leads through malonyl coenzyme A, to a polyester of variable length called polyacetate. This polyester generates by cyclization (Claisen reaction then condensation), the xanthonic skeleton. This mechanism is illustrated by Scheme 2 (Bennett and Lee, 1989).

Scheme 2: Polyacetic biosynthesis of xanthones
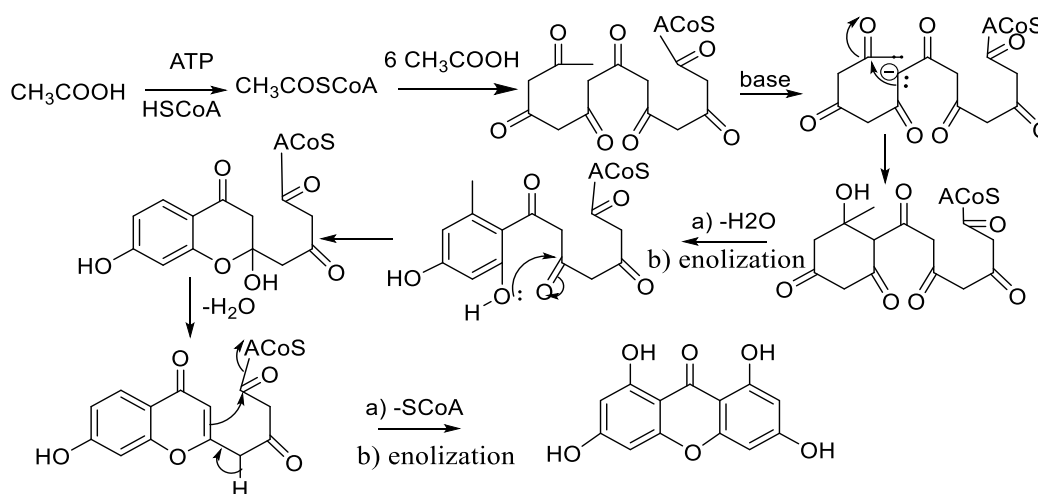
I.5.2.2 Mixed acetate-shikimate biosynthesis of xanthones

In plants, the xanthone nucleus is synthesized by a mixed acetate-shikimate pathway. Biosynthesis is initiated by benzophenone synthase (BPS), a type III polyketide synthesis, which catalyzes the condensation of benzoyl and 3-hydroxybenzoyl-CoA with three molecules of malonylCoA to give 2,4,6-trihydroxybenzophenone and 2,3′,4,6-tetrahydroxybenzophenone (2,3′,4,6-tetraHB) respectively. The product (2,4,6-trihydroxybenzophenone) has been shown to be converted to 2,3′,4,6-tetraHB by the activity of benzophenone 3-hydroxylase (B3′-H) (Schmidt and Beerhues, 2000; Liu *et al.*, 2003). The 2,3′,4,6-tetraHB intermediate key undergoes regioselective intramolecular coupling reactions of *para* or *ortho* C-O to the 3-hydroxyl group to give 1,3,7 and 1,3,5-trihydroxyxanthones, respectively, as the cell cultures of *Hypericum androsaemum* and *Centaurium erythraea* (scheme) (Peters *et al.*, 1997).
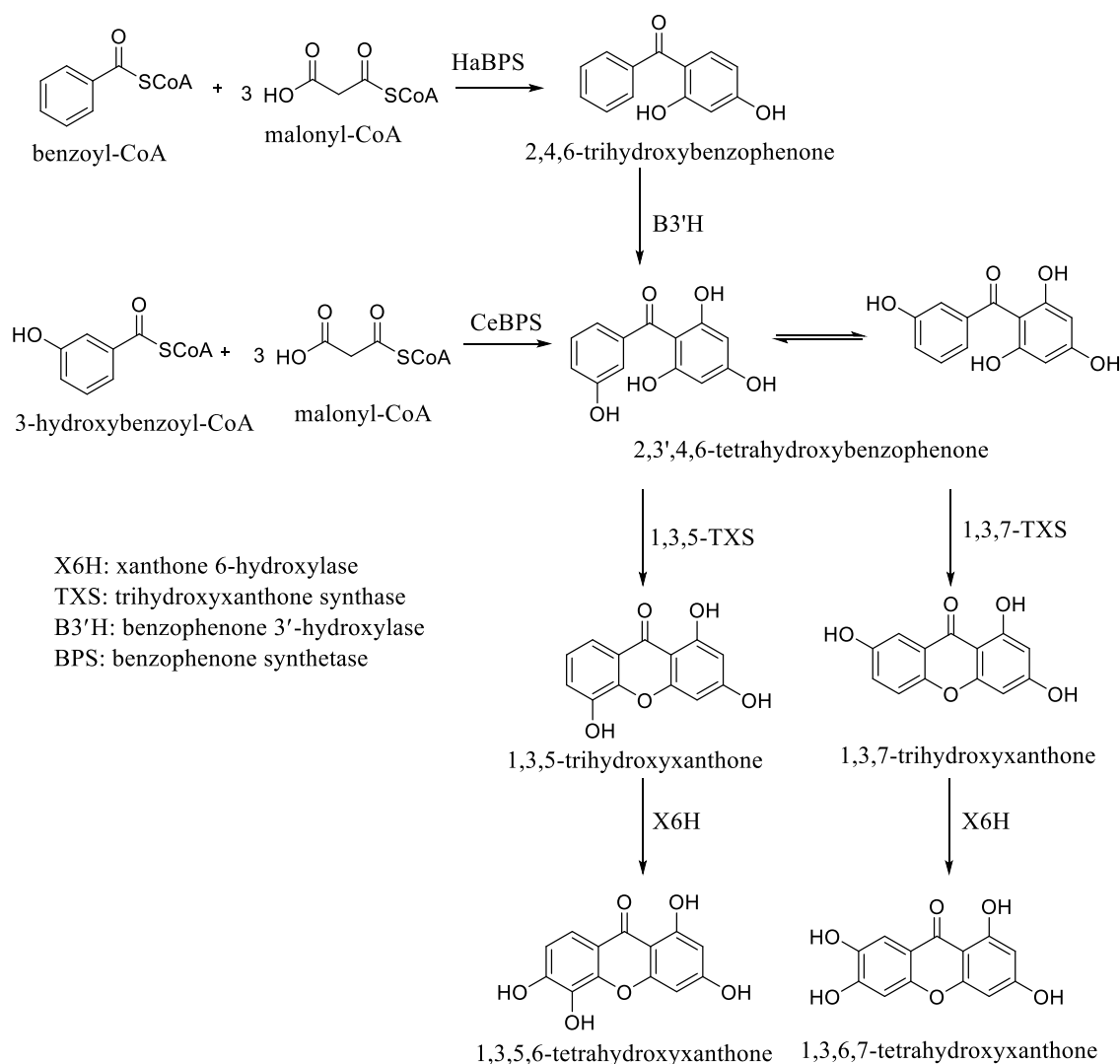
Scheme 3: Mixed acetate-shikimate biosynthesis of xanthones (Peters *et al.*, 1997)

I.5.3 Biological function of xanthones

Several studies have shown that xanthones are endowed with various biological and physiological activities such as: antiplasmodial, antibacterial and antiproliferative, anti-inflammatory, hypoglycemeic activities (Zelefack *et al*., 2009; Wabo *et al*., 2010; Lenta *et al*., 2011; Negi *et al*., 2013).

I.5.4 General method for the structural elucidation of xanthones

Spectroscopic methods (IR, UV, Mass, NMR) make it possible to quickly determine the structures of xanthones.

I.5.4.1 Infrared spectroscopy

It provides information on the hydroxyl group which is easily identifiable with a band around 3420 cm^{-1} and the carbonyl group around 1660 cm^{-1}. The band of the carbonyl group is displaced towards 1620 cm^{-1} when there is a hydroxyl group in position 1 or 8. An oxygenated substituent fixed at C-3 or C-6 on the xanthonic ring induced by a mesomeric effect, leads to a decrease in the frequency of the carbonyl elongation. The absorptions in the vicinity of 1610 and 1590 cm^{-1}, highlight the aromatic nucleus (Silva and Pinto, 2005; Lenta *et al*., 2011).

I.5.4.2 Ultraviolet spectroscopy

Visible ultraviolet is a useful spectroscopic technique for locating free hydroxyl groups of xanthones. In particular, the OH group at position 3, which is easily detected by the addition of NaOAc which results in a bathochromic shift of 300–330 nm bands with increasing intensity. Three or four bands of maximum absorption are always found in the region 220–410 nm and it should be noted that all bands show high intensity. Most substances show marked absorption in regions of 400 nm, which explains their yellow color (Negi *et al*., 2013).

I.5.4.3 Proton nuclear magnetic resonance spectroscopy

The ^{1}H NMR spectrum appears mainly in the range 0 to 12 ppm downstream of the TMS reference signal. The integral of the signal is proportional to the number of protons present. The number and relative position of acetyl and methoxy groups can be determined by observing the shift in the position of aromatic proton uptake which occurs upon replacement of the methoxy group with an acetyl group. Signals between δ_H 2.40–2.50 indicate acetylation at the periphery of the carbonyl group (position 1 or 8) because the other acetyl signals are between δ_H 2.30 and 2.35. The presence of the OH group at δ_H 12-13 also confirms the

hydroxyl substitution at 1 or 8. But when these positions are unsubstituted, aromatic protons appear in the vicinity of δ_H 7.70–8.05 (Negi *et al*., 2013). The presence of one of the substituents (hydroxyl, alkoxy and alkyl) on the xanthonic ring (42) causes a shielding of the protons in *ortho* at δ_H 0.55, in *meta* at δ_H 0.15 and in *para* at δ_H 0.50. Moreover the interactions between the protons 3,4; 1,2 and 2,3 respectively induce an *ortho* coupling of about 8.5; 8.0 and 7.0 Hz. On the other hand, the *meta* coupling constant varies between 1.7 and 1.1 Hz for the 1,3 and 2,4 position respectively (Silva and Pinto, 2005). The hydroxylated protons of several oxygenated xanthones resonate in the region of 9.25-13.35 ppm. The following table XVI gives certain chemical shifts depending on the position of the chemical groups.

Table XVI: Hydroxyl proton resonances of oxygenated xanthones (Silva and Pinto, 2005).

δ (ppm)	Oxygenated pattern
9.25-9.45	2- or 7-OH with OR[a)] in 1- or 8-position
9.35-9.60	4- or 5-OH with OR[a)] in *ortho* ou *para* position
9.70-10.05	2- or 7- OH
10.35-10.55	4- or 5- OH
	3- or 6-OH with OR[a)] in 4- or 5-position
10.80-11.10	3- or 6- OH
11.45-12.00	1- et 8- OH
	1- or 8-OH with OR[a)] in 4- or 5-position
12.50-12.90	1- or 8-OH
12.90-13.25	1- or 8-OH with OR[a)] in 3- and 6-position
	1- or 8-OH with OCH_3 in 8- or 1-position

[a)]R=H or CH_3

I.5.4.4 Carbon nuclear magnetic resonance spectroscopy

The carbon where the hydroxyl group is attached resonates between 29-35 ppm downfield relative to the value of unsubstituted xanthone. The carbons *ortho* to the hydroxyl group move upwards from 9.7 to 17.9 ppm. An ortho substituent effect in 2-, 3- and 4-hydroxy or methoxyxanthones is almost twice that of the other *ortho* carbon. The high field shifts of the *ortho* carbons, facing the incorporated γ-pyrone ring, are almost twice as large as those of the carbons in the opposite direction. This indicates a preferred electron release to the γ-pyrone system. The presence of a 1-hydroxyl group, involved in an intermolecular hydrogen bond with the carbonyl group, implies an electronic redistribution of electrons responsible for a de-shielding in C-9 (carbonyl carbon) δ_C approximately 5 ppm and a shielding in C-8a δ_C appreciably 3 ppm, whereas a double chelation (1,8-dihydroxy) implies a falling field of

approximately 10 ppm (no chelation δ_C appreciably 174-175 ppm, monochelation δ_C appreciably 179-180 ppm, bischelation δ_C substantially 184-185ppm); the presence of electron donor substituents conjugated to the carbonyl group is responsible for shielding its carbon atom (C-9). The greatest of these effects is observed when a 3-hydroxy group is present (approximately 2 ppm in the field); the agreement between predicted and observed chemical shifts is particularly poor for the *ortho* and vicinal oxy-substituted units resulting from orthosteric effects; the resonances of methoxyl carbons constitute a useful diagnoses for the localization of methoxyl groups on the xanthonic ring. Resonances of methoxyl carbon appear around 55-56 ppm, but when this group is surrounded by two *ortho* substituents, it is shifted down to δ_C 60-62 ppm, due to orthosteric crowding (Silva and Pinto, 2005). The following table XVII gives the increments relating to the chemical shifts of the carbons of a xanthone as a function of the position of the group OH.

Table XVII: Increments relating to the chemical shifts of the carbons of a xanthone as a function of the position of the OH group (Frahm and Chaudhuri, 1979).

Carbon relative to hydroxy group	Carbon in ring position	Increment (ppm)
C-*ipso*	1, 8	+ 35,5±0,5
	2, 3, 4, 5, 6, 7	+29,3±1,0
C-*ortho*	1, 4, 5, 8	-16,0±1.5
	8b, 4a, 4b, 8a	-11,5±1.5
C-*meta*	1,8	+1,0±1.0
	8a, 8b	+1,0±1.0
	4a, 4b	+0,5±1.0
C-*para*	1, 4, 5, 8	-10,5±1.0
	8b, 4a, 4b, 8a	-7,0±1.0

Despite all the work that has already been done on medicinal plants with anti-leishmanial properties, many species are still not or little investigated. This is why as part of our research work, we undertook the chemical investigation of three Cameroonian medicinal plants guided by the antileishmanial activity.

CHAPTER II: RESULTS AND DISCUSSION

II.1 Bioguided study by the antileishmanial activity of *E. calophylloides*, *P. butyracea* and *A. lobata*

II.1.1 Harvesting, extraction and isolation

The stem bark and leaves of *E. calophylloides* Benth., the stem bark and fruits of *P. butyracea* Sabine and the stem bark of *A. lobata* (Jacq.) Engl. were harvested in May-October 2018 at Mbalmayo, Bazou and Ngoumou, respectively, in the Center and West Region of Cameroon. The plant materials were identified by Mr. Victor Nana, botanist at the National Herbarium of Cameroon, by comparison with the voucher specimens formerly kept at the National Herbarium under the registration number 29528/HNC, 6861/SRF/Cam and 43292/HNC, respectively.

The air-dried and ground stem bark of *E. calophylloides* (3.5 kg) was extracted with the mixture CH_2Cl_2-MeOH (1:1, 2×10L) (2 days, repeated three times) at room temperature. The extract was freed from solvent under vacuum at low temperature (40°C) to afford 341.9 g of crude extract.

The air-dried and ground leaves of *E. calophylloides* (5.2 kg) was extracted with the mixture CH_2Cl_2-MeOH (1:1, 4×10L) (2 days repeated two times) at room temperature. The extract was freed from solvent under vacuum at low temperature (40ºC) to afford 587.2 g of crude extract.

After drying and grinding, we obtained 4,8 kg of powdered fruits and 3.5 Kg of powdered stem barks of *P. butyracea,* that were macerated in CH_2Cl_2/MeOH (1:1, 15L) twice for 48 hours at room temperature each, to give 210.7 g and 190.8g of the CH_2Cl_2/MeOH crude extract after evaporation of solvent under reduced pressure respectively.

The stem bark of *A. lobata* was chopped, air-dried and ground. The resulting powder (1.1 kg) was extracted by maceration with CH_2Cl_2-MeOH (1:1) (10 L) (2 days, repeated three times) at room temperature. The extract was freed from solvent under vacuum at low temperature (40°C) to give 114.1 g of crude extract.

These extracts were submitted for preliminary screening on *Leishmania donovani* 1S (MHOM/SD/62/1S) promastigotes strain.

The results of the preliminary screening are summarised in the table XVIII below.

Table XVIII: Results of the antileishmanial screening on extracts of *E. calophylloides*, *P. butyracea*, *A. lobata*

Families	Species	Plant parts	Extracts	IC$_{50}$ (μg/mL)	Classification (Camacho *et al.*, 2003)
Guttiferae	*E. calophylloides*	Stem bark	CH$_2$Cl$_2$/MeOH (1:1)	24.33	Good activity
		Leaves	CH$_2$Cl$_2$/MeOH (1:1)	17.75	Good activity
	P. butyracea	stem bark	CH$_2$Cl$_2$/MeOH (1:1)	5.96	High activity
		Fruits	CH$_2$Cl$_2$/MeOH (1:1)	26.43	Good activity
Passifloraceae	*A. lobata*	Stem bark	CH$_2$Cl$_2$/MeOH (1:1)	21.17	Good activity

Camacho *et al.*, 2003 (IC$_{50}$ < 10 μg/mL, extract is highly active; 10 < IC$_{50}$ < 50 μg/mL, extract has a good activity; 50 < IC$_{50}$ <100 μg/mL, extract is moderately active; IC$_{50}$ > 100 μg/mL, extract is inactive).

After this screening, extracts of *E. calophylloides*, *P. butyracea* and *A. lobata* showed interesting antileishmanial activity, and therefore were the subject of further study.

Fractionation and purification of the active extracts of *E. calophylloides* (bark of the trunk and leaves), yielded 20 compounds, summarized in the following scheme 4 and scheme 5 respectively.

Stem bark
of *Endodesmia calophylloides*

-Drying
-Crushing

Powder
3.2 kg

-Maceration with CH_2Cl_2/MeOH (1:1)
30 L   -Filtration, evaporation

Crude extract of stem bark
of *Endodesmia calophylloides*
340.1 g
24.33μg/mL

Antileishmanial
screening

Liquid-liquid partition

n-Hex CH_2Cl_2 EtOAc   *n*-BuOH H_2O

F1
32.1 g
21.91μg/mL

F2
29.3 g
21.31μg/mL

F3
93.9 g
9.19μg/mL

F4
85.4 g
45.77μg/mL

F5
95.8 g
> 100

CC over SiO_2
(0.063-0.2 mm)
n-hexane/EtOAc (1:0-0:1), and
EtOAc/MeOH (1:0-0:1)

CC over SiO_2
(0.063-0.2 mm)

CC over SiO_2
(0.063-0.2 mm)
and Sephadex
LH-20
EtOAc/MeOH mixture (1:0-0:1)

CC over SiO_2
(0.063-0.2 mm),
Sephadex LH-20 and
C_{18}-reversed phase

ECT1
137.3 mg
>50

ECT2
15.2 mg
>50

ECT3
150.1 mg
4.77μg/mL

ECTF21
15.5 mg
>50

CH_2Cl_2/MeOH
(3:7)

n-hexane/EtOAc (9:1-0:1), and
EtOAc/MeOH mixture (1:0-0:1)

EC9
49.9 mg
>50

ECTF24
15.7 mg
44.77μg/mL

ECTF33
659.2 mg
>50

ECTF22
4.4 mg
>50

ECT14
5.1 mg
>50

ECT23
3.8 mg
>50

EtOAc/MeOH/H_2O (9:1:0.5-7:3:1)

ECTF3
10.2 mg
>50

ECTF41
7.9 mg
>50

ECTF42
5.2 mg
8.66μg/mL

ECTF93
10.8 mg
>50

— IC_{50} against *Leishmania donovani* promatigostes

Scheme 4: Bioguided isolation of active compounds from the CH2Cl2/MeOH (1:1) crude extract of the stem bark of *E. calophylloides* against *Leishmania donovani* 1S (MHOM/SD/62/1S) promastigotes

```
                    ┌─────────────────────────┐
                    │        Leaves           │
                    │ of Endodesmia calophylloides │
                    └─────────────────────────┘
                              │  -Drying
                              │  -Crushing
                    ┌─────────────────┐
                    │     Powder      │
                    │     5.2 kg      │
                    └─────────────────┘
```

-Maceration with CH_2Cl_2/MeOH (1:1) 35 L
-Filtration, evaporation

Crude extract of leaves
of *Endodesmia calophylloides*
580.1 g
24.33 μg/mL

Antileishmanial screening ← → Vaccum liquid chromatography SiO_2 (0.063-0.2 mm)

n-Hex	Hex/EtOAc (75:25)	Hex/EtOAc (1:1-75:25)	EtOAc	EtOAc/MeOH (9:1-4:1)	EtOAc/MeOH (1:1-0:1)
F1 17.1 g > 100	F2 83.5 g 22.74 μg/mL	F3 18.6 g 47.77 μg/mL	F4 21.2 g > 100	F5 33.1 g > 100	F6 18.3 g > 100

CC over SiO_2 (0.063-0.2 mm) and Sephadex LH-20

CC over SiO_2 (0.063-0.2 mm)

n-hexane/EtOAc (9:1-0:1), and EtOAc/MeOH mixture (1:0-0:1)

ECF43
178.9 mg
>50

ECF44
3.0 mg
>50

ECF6
500.1mg
>50

n-hexane/EtOAc (9:1-0:1)

ECF1
15.6 mg
44.43 μg/mL

ECF23
18.2 mg
>50

──── IC_{50} against *Leishmania donovani* promatigostes

Scheme 5: Bioguided isolation of active compounds from the CH_2Cl_2/MeOH (1:1) crude extract of the leaves of *E. calophylloides* against *Leishmania donovani* 1S (MHOM/SD/62/1S) promastigotes

The fractionation and purification of the active extracts of *P. butyracea* (bark of the trunk and fruits), made it possible to obtain 15 compounds, summarized in the following scheme 6 and scheme 7 respectively.
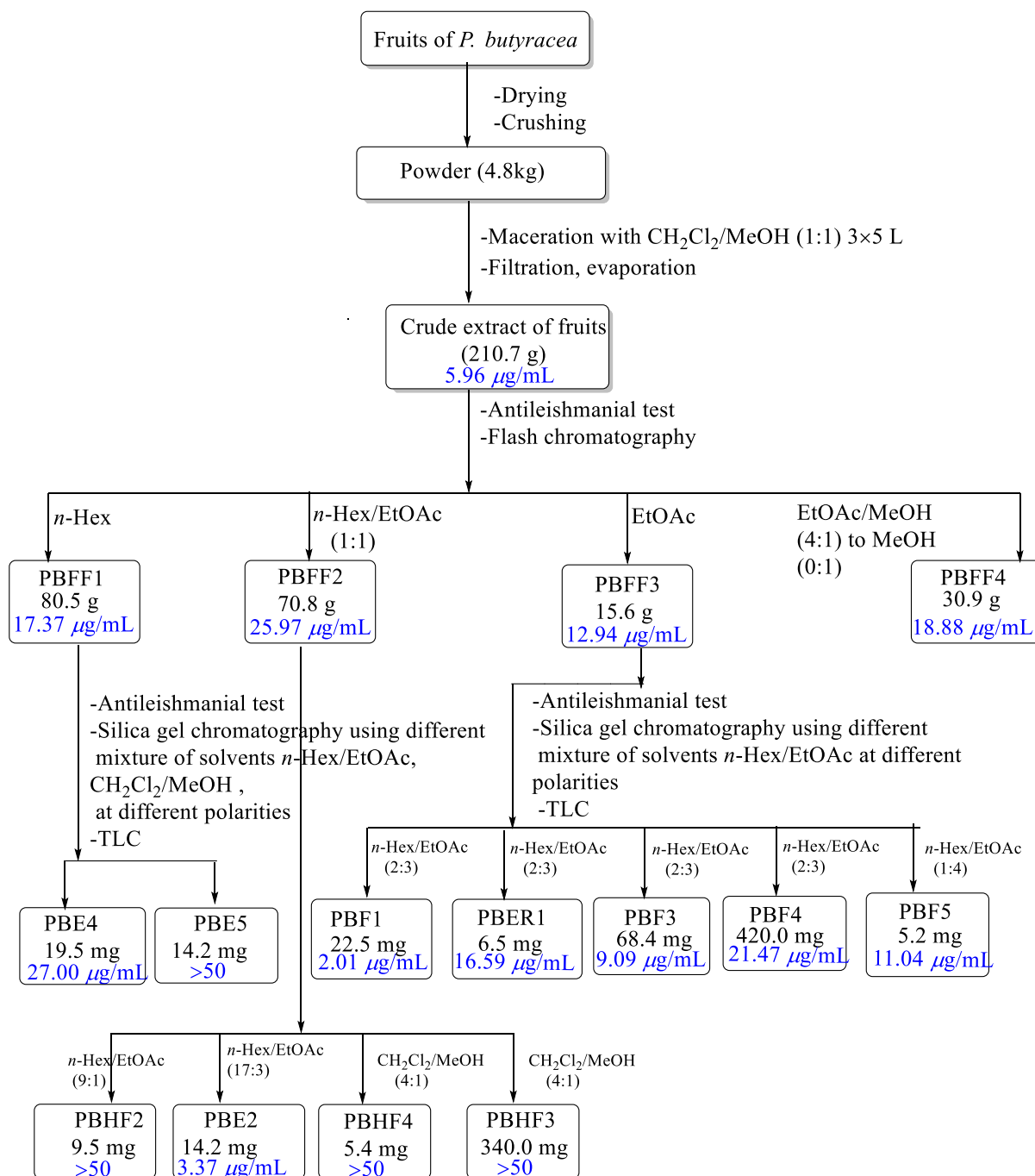
IC_{50} against *Leishmania donovani* promatigostes

Scheme 6: Bioguided isolation of active compounds from the CH₂Cl₂/MeOH (1:1) crude extract of the fruits of *P. butyracea* against *Leishmania donovani* 1S (MHOM/SD/62/1S) promastigotes
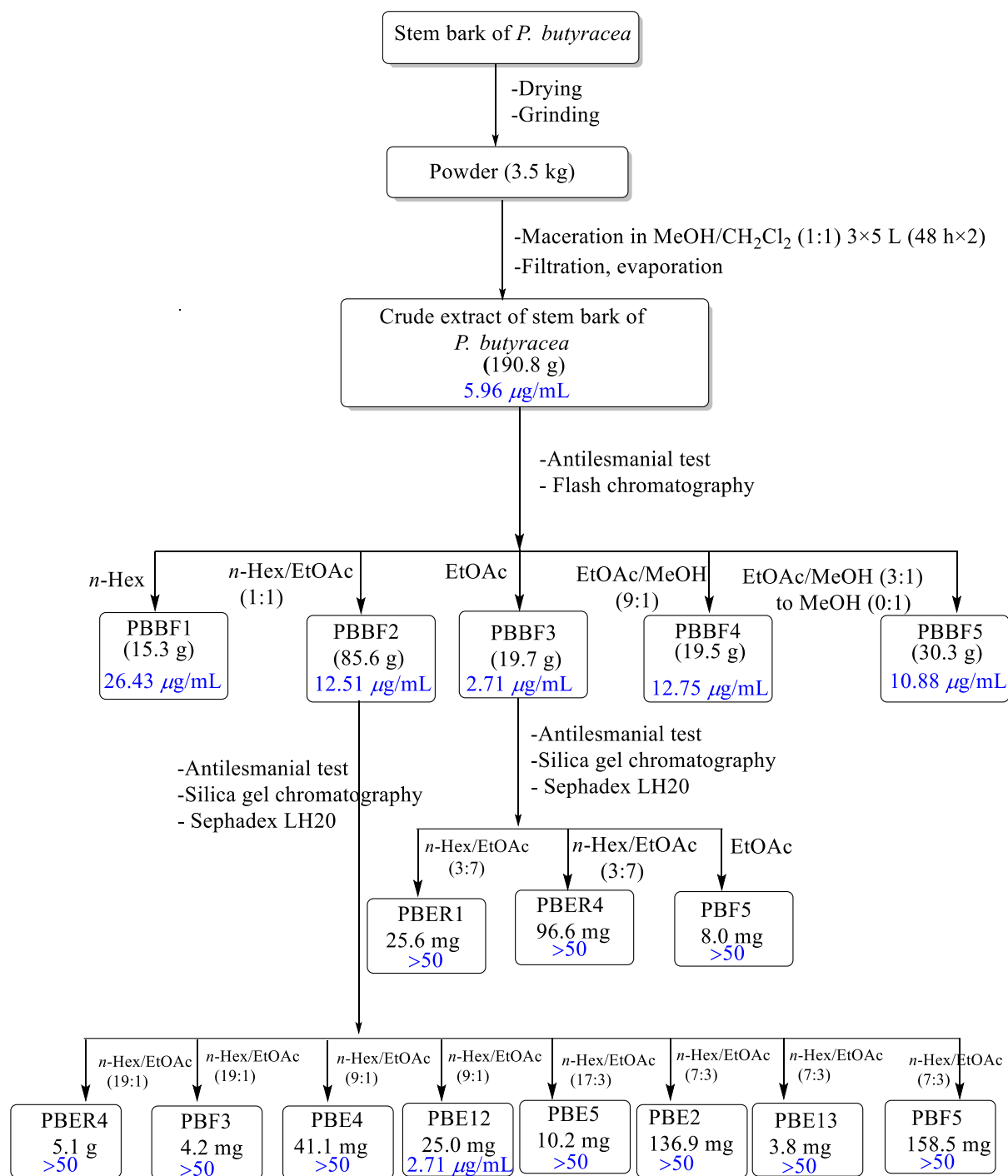
Scheme 7: Bioguided isolation of active compounds from the CH2Cl2/MeOH (1:1) crude extract of the stem bark of *P. butyracea* against *Leishmania donovani* 1S (MHOM/SD/62/1S) promastigotes

The fractionation and purification of the active extracts of *A. lobata* (bark of the trunk), made it possible to obtain 09 compounds, summarized in the following scheme.
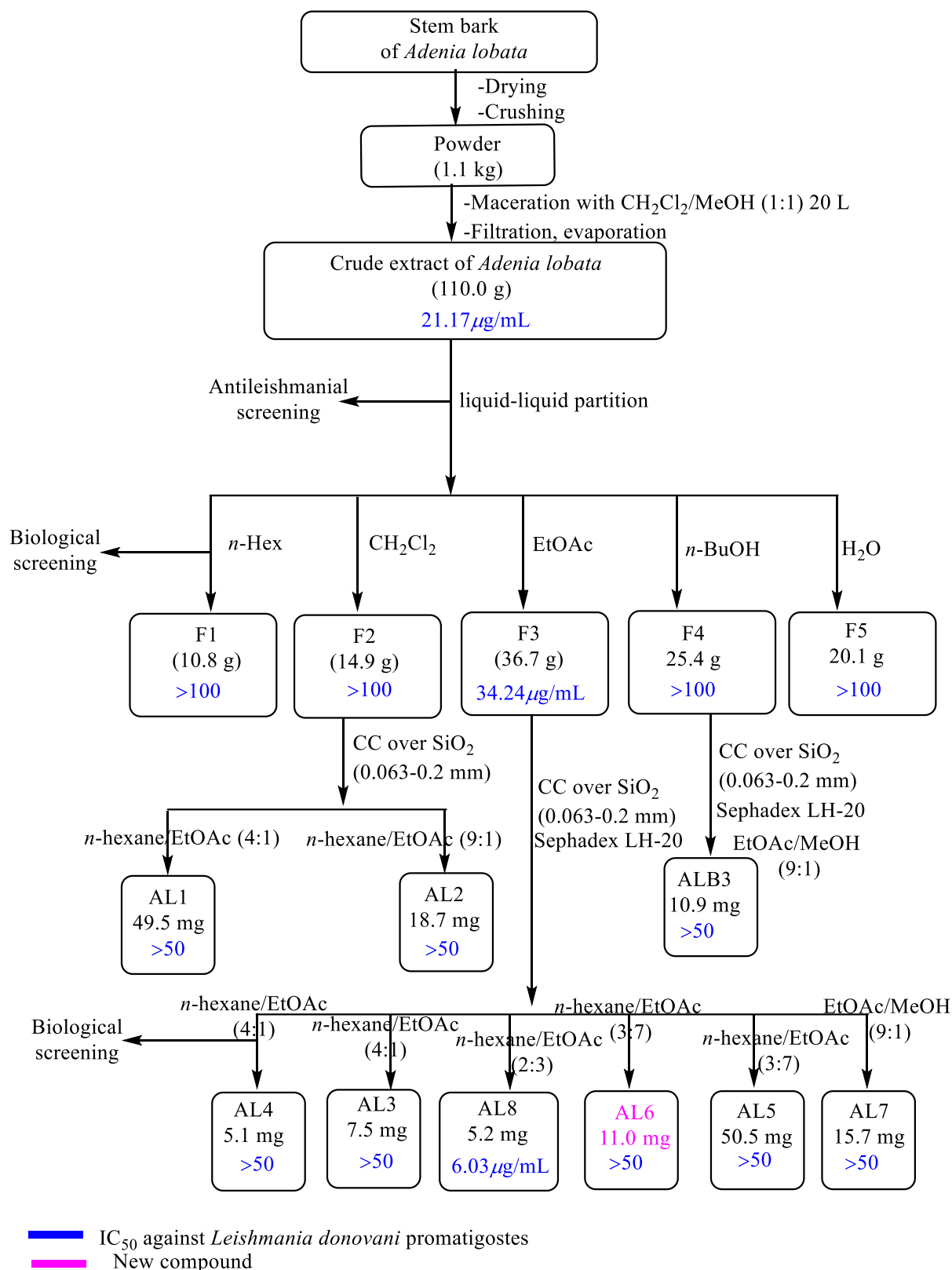
Scheme 8: Bioguided isolation of active compounds from the CH2Cl2/MeOH (1:1) crude extract of the stem bark of *A. lobata* against *Leishmania donovani* 1S (MHOM/SD/62/1S) promastigotes

II.1.2 Structural study of the isolated compounds

The structural determination of the isolated compounds was made by analysis of their spectral data, and by comparison of their spectroscopic and physical data with those described in the literature or by comparison with authentic samples available in our laboratory. Thus, we obtained from the 3 plants, 40 compounds belonging to 12 classes of secondary metabolites:

- 01 ceramide (AL6);
- 09 xanthones (PBER1, PBF1, PBE2=PBHF9, PBE12, PBHF3, PBHF4, PBE6, PBE13 and ECTF24);
- 10 triterpenoids (ECT1= ECF21=AL4, ECF1= PBE1=AL2, ECT2, ECF23, ECTF23, EC1, PBE5, ECTF22, ECTF21 and AL8);
- 04 flavonoids (ECF43, ECF44, ECTF33 and PBER4);
- 04 phenolic compounds (ECTF41, ECTF42, ECTF93 and ALB3);
- 02 benzophenones (ECTF3a and ECTF3b);
- 03 steroids (PBF5, EC4 and EC6);
- 03 fatty acids (AL3, EC8 and PBF4);
- 01 ellagic acid (EC9);
- 01 Sugar (AL7);
- 01 monoglyceride (ECT14);
- 01glucosylated sesquiterpenoid (ECTF44).

II.2. Characterization and identification of compounds from *E. calophylloides*, *P. butyracea* and *A. lobata*

II.2.1.1. Ceramides

II.2.1.1.1. Structure determination of AL6

AL6 was obtained as a white amorphous solid, $[\alpha]_D^{24}$ -5.9 (*c* 0.001, MeOH). The molecular formula, $C_{42}H_{83}NO_5$, implying two degrees of unsaturation, was deduced from its HR-ESI-MS (positive mode) spectrum (figure 13), which showed the protonated ion peak [M+H]$^+$ at *m/z* 682.6352 (calculated 682.6349 for $C_{42}H_{84}NO_5$). The IR spectrum (Figure 14) exhibited characteristic absorption bands for hydroxy groups (3398 cm^{-1}), a carbonyl of amide (1638 cm^{-1}) and C=C double bond (1463 cm^{-1}).

The ^{1}H NMR spectrum (Figure 15) displays several signals, including a triplet of six protons at δ_H 0.85 (6H, t, *J* = 6.9 Hz) assigned to the two terminal methyl groups, a broad signal between δ_H 1.27-1.40 corresponding to the sequence of methylene groups in the fatty

acid and amino-triol parts, the signals of an exchangeable proton N-H appearing as a doublet at δ_H 8.58 (1H, d, J = 9.0 Hz) and a proton of an *N*-methine group at δ_H 5.11 (1H, m). In addition, the ^{1}H NMR spectrum of compound **AL6** exhibited characteristic signals of three oxymethine protons at δ_H 4.36 (1H, dd, J = 11.2, 6.2 Hz), 4.28 (1H, m), and 4.62 (1H, dd, J = 7.7, 3.9 Hz) and two oxymethylene protons at δ_H 4.51 (1H, m) and 4.42 (1H, m). The signals of a pair of olefinic protons at δ_H 5.48 (1H, dt, J = 15.3 Hz) and 5.50 (1H, dt, J = 15.3 Hz) revealed the presence of a double bond in this compound. This olefinic double bond was assigned a *trans* configuration based on the coupling constant at J = 15.3 Hz (Ebede *et al*., 2019). This ^{1}H NMR data is close to those of phytoceramides (Kagho *et al*., 2020).

The ^{13}C NMR spectrum (Figure 16) of compound **AL6** exhibits characteristic signals of three oxymethine carbons at δ_C 76.5, 72.8 and 72.3 and one oxymethylene carbon at δ_C 61.8. The signals of carbons of an *N*-methine group at δ_C 52.8 and an amide carbonyl at δ_C 175.0 further confirmed it ceramide nature (Kagho *et al*., 2020). The signals of a pair of olefinic carbons at δ_C 130.5 and 130.6 reveal the presence of a double bond. This olefinic double bond was assigned as *trans* configuration based on the chemical shifts of its allylic carbons C-5 and C-8 (δ_C 33.9 and 32.7). Typically, the signal of a carbon next to a *trans* double bond appears between δ_C 32 and 33, while that of a *cis* double bond appears between δ_C 27 and 28 (Bankeu *et al*., 2010; Teinkela *et al*. 2019). In addition, ^{13}C NMR spectrum also displays signals including a signal of two methyl carbons at δ_C 14.0 assigned to the two terminal methyl groups, an broad signal between δ_C 25.6-31.9 corresponding to the sequence of methylene groups in the fatty acid and amino-triol parts of skeleton of ceramide.

The double bond was deduiced to be at C-6 and C-7 on the LCB part of the ceramide using HMBC (Figure 19), HSQC (Figure 17) spectra. In fact, this HMBC spectrum exhibited correlation from the methine proton at δ_H 4.36 (H-3) to the carbons at δ_C 33.9 (C-5), 130.5 (C-6), and from the methylene protons at δ_H 1.93 (H-5) to the carbon at δ_C 130.5 (C-6). In addition, the N-H proton at δ_H 8.58 correlates with the C=O of the amide group (δ_C 175.0) and the methylene protons at δ_H 4.42 (H-1b) and 4.51 (H-1a) showed connectivities with the methine at δ_C 52.8 (C-2).

The presence of the double bond at this position was further strengthened by the following observed COSY correlations (Figure 18) of H-3/H-4, H-4/H-5 and H-5/H-6.

All of this information allows us to propose the following sub-structure:
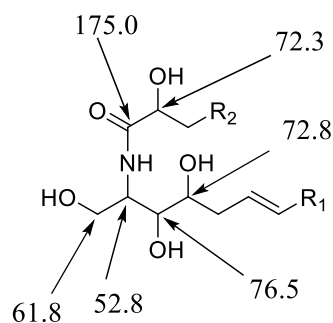
Methanolysis of compound **AL6** (scheme 9) was carried out to determine the length of the two chains in. The reaction gave a fatty acid methyl ester (FAME) and a long chain base (LCB), which were characterized by HR-ESI-MS analysis (Figure 20). The pseudo-molecular ion peak $[M+H]^+$ at *m/z* 330.3029 (calculated for $C_{19}H_{40}NO_3$, 330.3008) corresponding to the molecular formula $C_{19}H_{39}NO_3$ containing one double-bond equivalence was assigned to the long base chain (LCB) moiety.
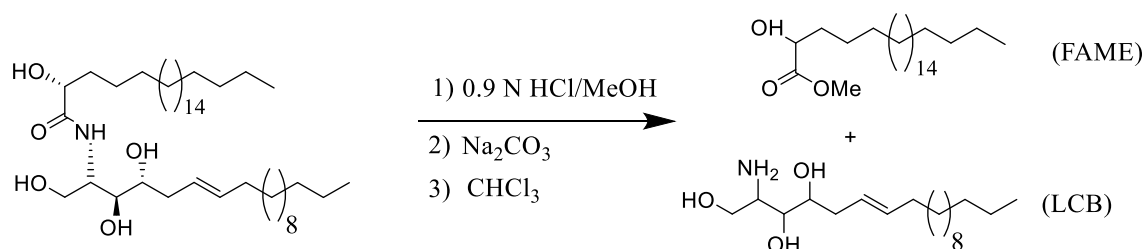
Scheme 9: Methanolysis reaction of compound AL6

The relative configurations at C-2, C-3, C-4, and C-2′ were determined to be (*S*), (*S*), (*R*), and (*R*), respectively, by configuration biosynthesis from serie and comparison of the ^{1}H and ^{13}C NMR data of compound **AL6** (Table XIX) with those obtained from the literature (Kolter and Sandhof, 1999; Bankeu *et al*., 2010)**.** The fragmentation pattern of compound **AL6** (Scheme 11) indicates the fragments observed at *m/z* 240, 354, 357, and 527 to further confirm the structure.
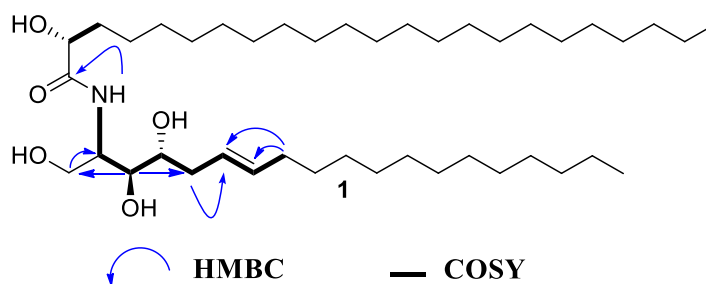
Scheme 10: Selected HMBC and COSY correlations of compound AL6
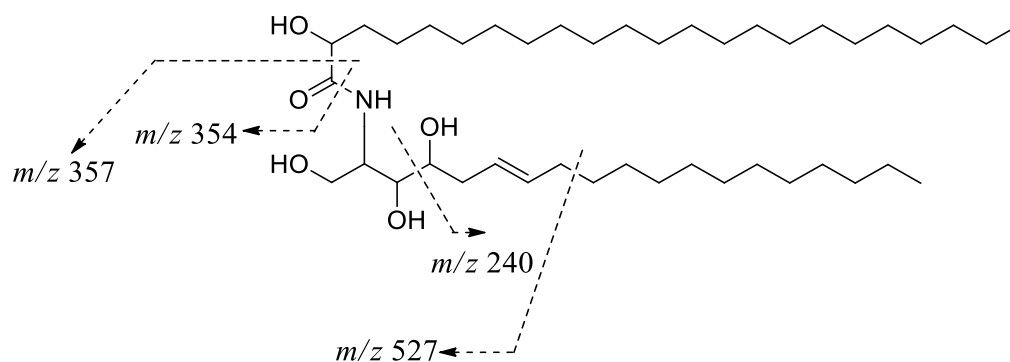
Scheme 11: Mass fragmentation pattern for compound AL6

Thus, compound **AL6** was fully characterized as (2*S*,3*R*,4*R*,6*E*)-2-[(2′R)-2′-hydroxytetracosanoylamino]-1,3,4-nonadecanetriol-6-ene, with the given name adeniamide (**54**).
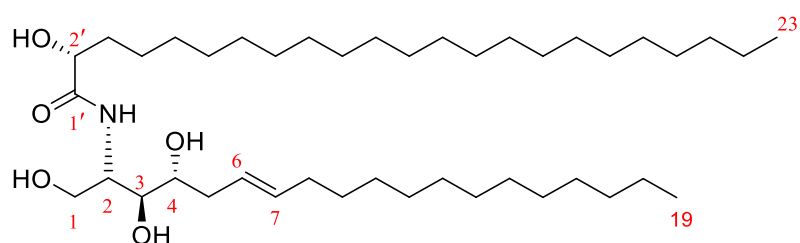
(**54**)

Table XIX: ^{1}H (500 MHz) and ^{13}C (125 MHz) NMR data of compound AL6 (C$_5$D$_5$N)

Position	δ_H (nH, m, *J* in Hz)	δ_C
1a	4.51 (1H, m)	
1b	4.42 (1H, m)	61.8
2	5.11 (1H, m)	52.8
3	4.36 (1H, dd, *J* = 11.2, 6.2 Hz)	76.5
4	4.28 (1H, m)	72.8
5a	1.93 (1H, m)	
5b	2.17 (1H, m)	33.9
6	5.48 (1H, dt, *J* = 15.3 Hz)	130.5
7	5.50 (1H, dt, *J* = 15.3 Hz)	130.6
8	1.98 (2H, m)	32.7
9-18	1.27 (20H, brs)	25.6-31.9
19	0.85 (3H, t, *J* = 6.9 Hz)	14.0
1′	-	175.0
2′	4.62 (1H, dd, *J* = 7.7, 3.9 Hz)	72.3
3′a	2.03 (1H, m)	
3′b	2.23 (1H, m)	35.5
4′-22′	1.27-1.40 (38H, brs)	25.6-31.9
23′	0.85 (3H, t, *J* = 6.9 Hz)	14.0
NH	8.58 (1H, d, *J* = 9.0 Hz)	-
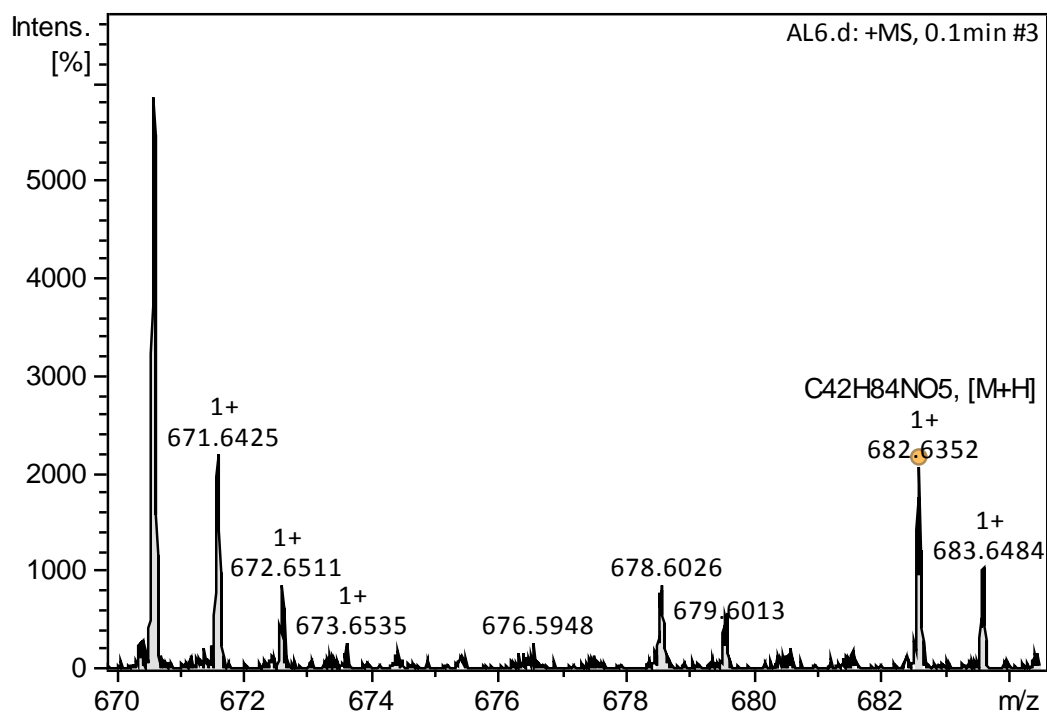
Figure 13: HR-ESI-MS spectrum of compound AL6
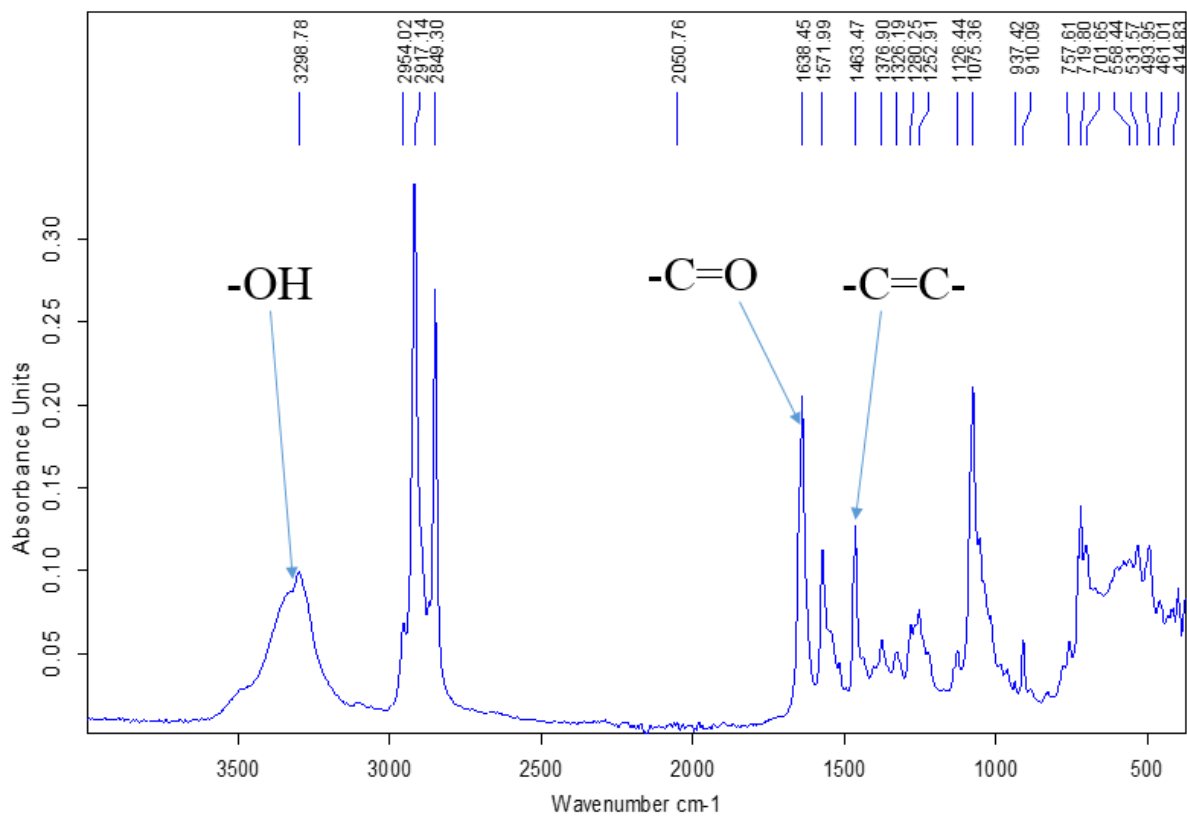
Figure 14: IR spectrum of compound AL6
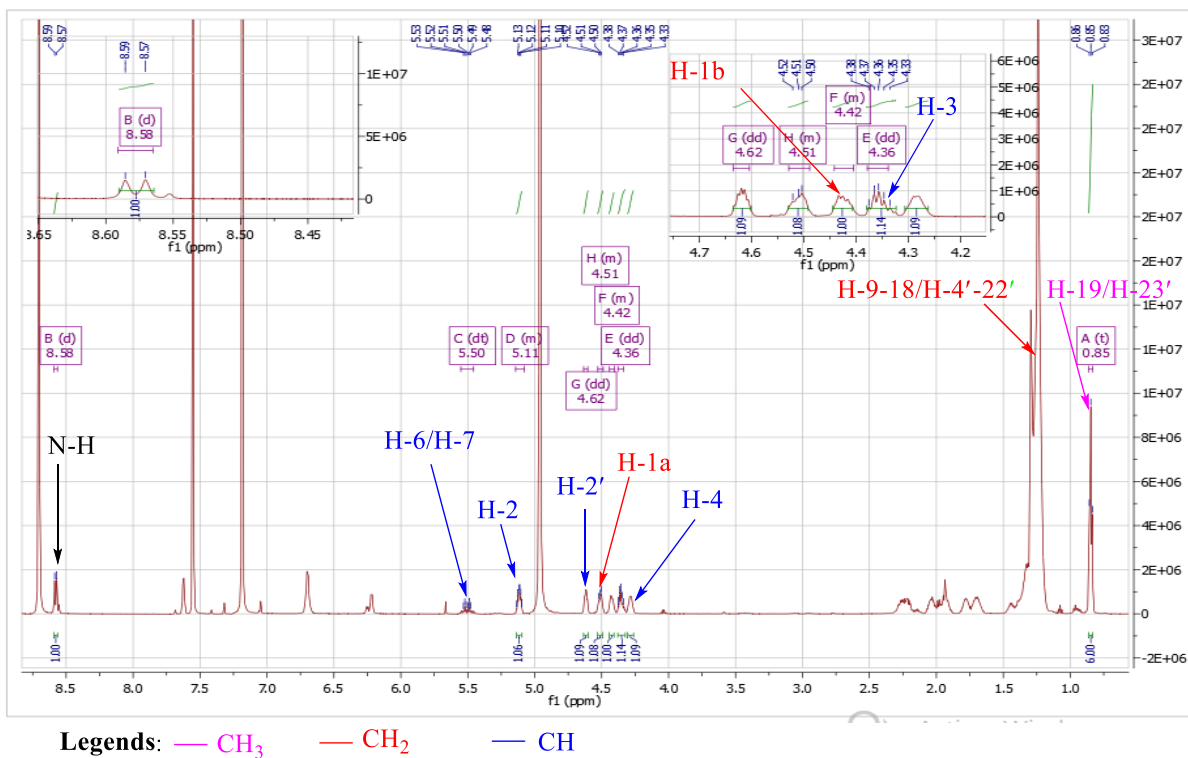
Figure 15: ^{1}H NMR spectrum (C$_5$D$_5$N, 500 MHz) of compound AL6
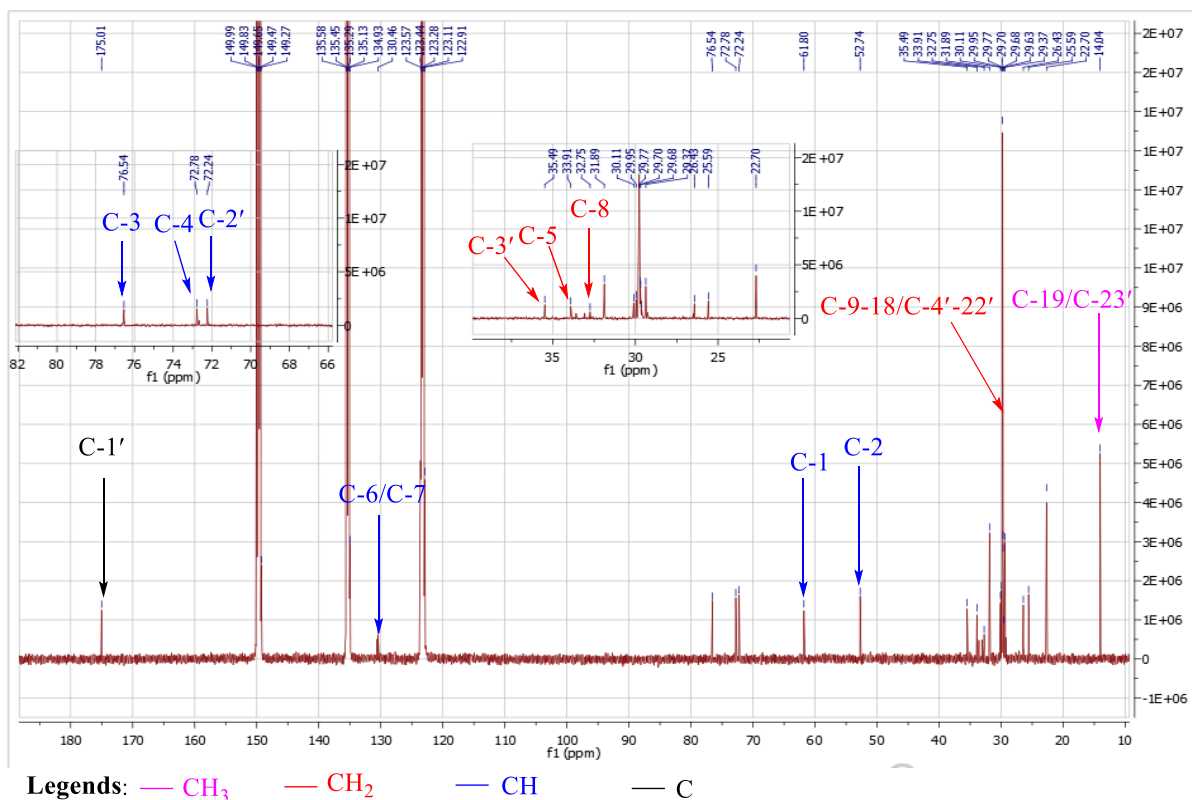
Figure 16: ^{13}C NMR spectrum (C$_5$D$_5$N, 125 MHz) of compound AL6
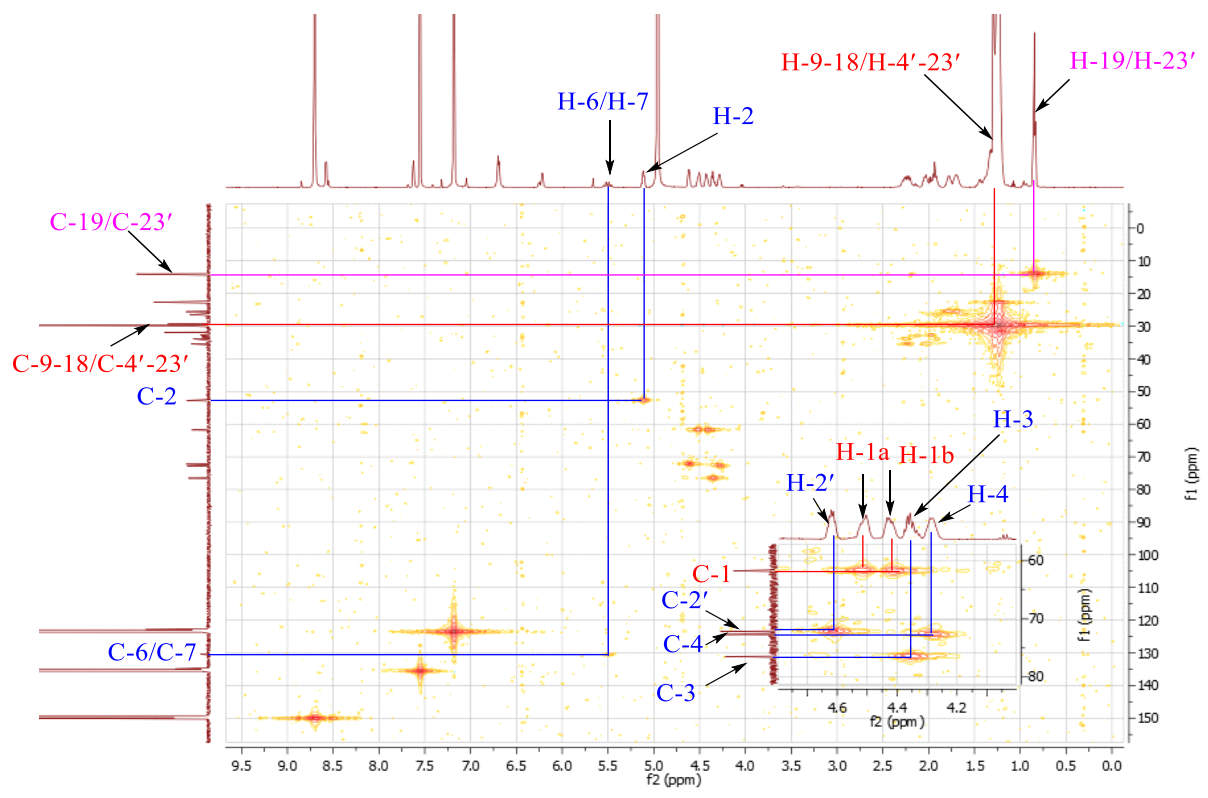
Figure 17: HSQC spectrum of compound AL6
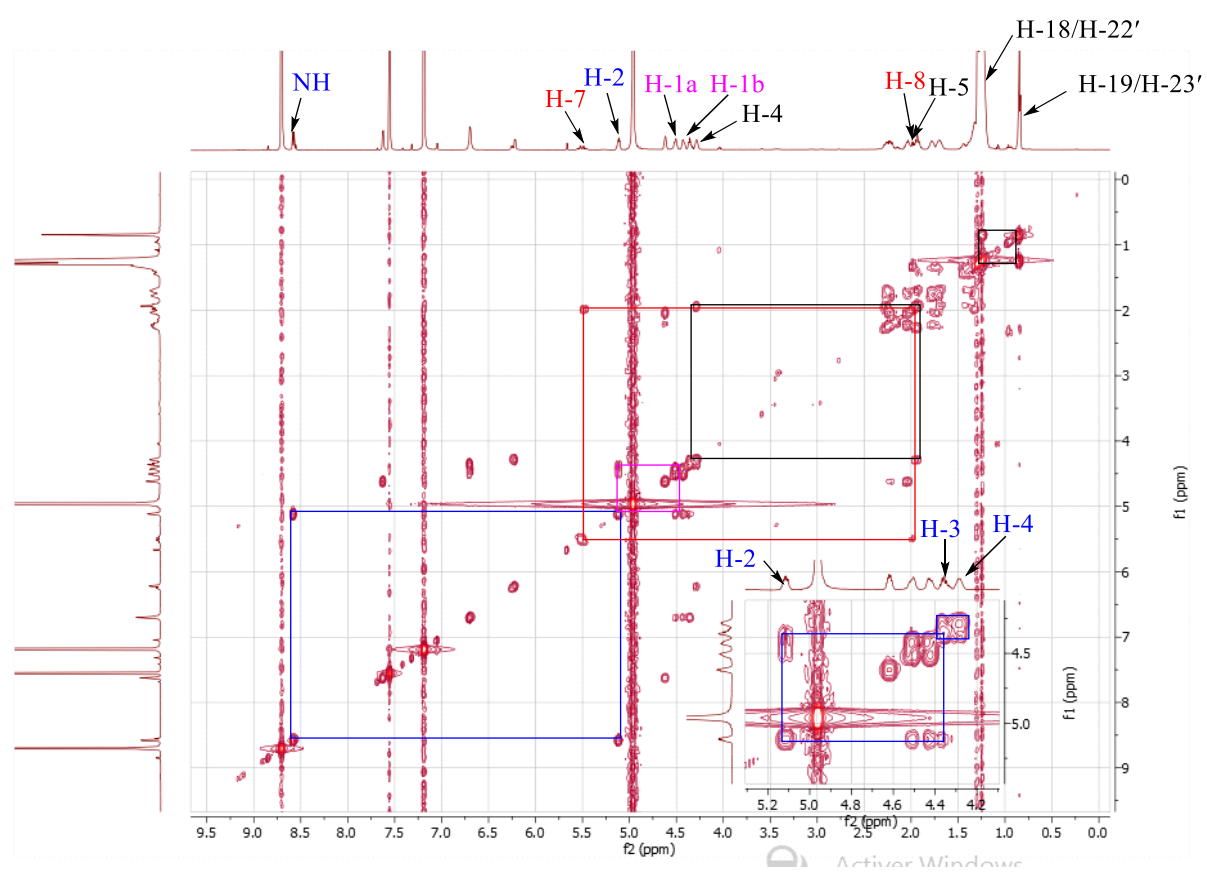
Figure 18: COSY spectrum of compound AL6
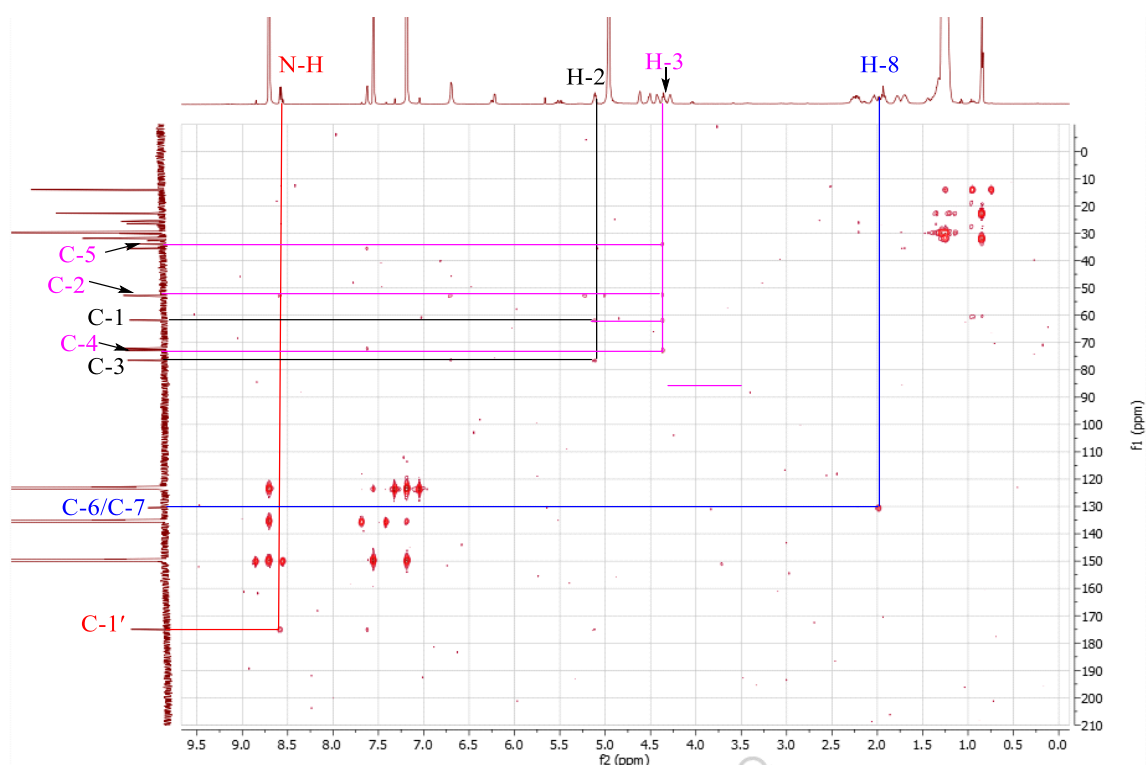
Figure 19: HMBC spectrum of compound AL6
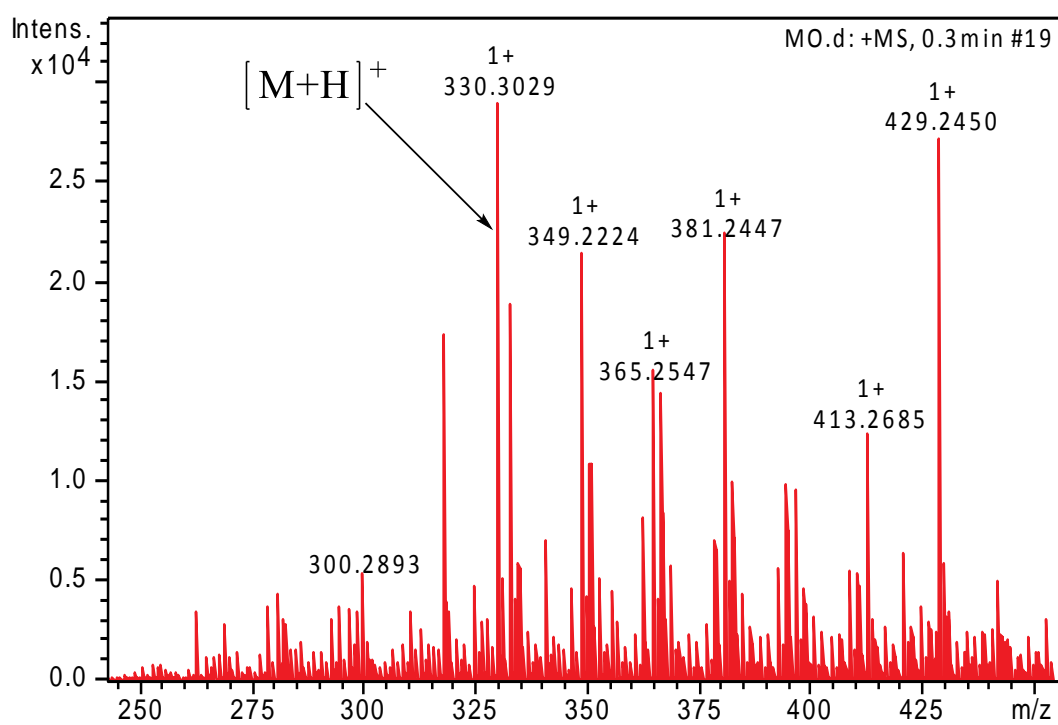
Figure 20: HR-ESI-MS spectrum of the methanolysis of compound AL6

II.2.1.2. Triterpenoids

II.2.1.2.1 Identification of AL8

AL8 was obtained as a greenish amorphous solid. It is soluble in chloroform and responds positively to the Liebermann-Burchard test, giving a red coloration, characteristic of triterpenes. Its HR-ESI mass spectrum in positive mode (Figure 21) shows the peak of the sodium adduct $[M+Na]^+$ at m/z 611.4114 corresponding to the molecular formula $C_{39}H_{56}O_4Na$ (calculated for 611.4179), containing twelve unsaturations.

On its fully decoupled broadband ^{13}C NMR spectrum (Figure 23), 39 signals of 39 carbon atoms were distinguished and sorted with the DEPT135 technique (Figure 26) as follow:

- eight methyl carbons at δ_C 14.6, 16.1, 16.7, 16.8, 25.3, 28.0, 29.2 and 31.4.

- ten methine carbons at δ_C 114.4, 115.5, 122.4, 144.3, 116.5, 129.8, 81.2, 55.6, 51.1 and 38.4.

 - ten methylene carbons at δ_C 18.2; 21.2; 23.8; 26.2; 27.5; 33.4; 34.5; 37.4; 37.7 and 38.7.

- eleven quaternary carbons, including one carbon of an ester group at δ_C 167.5; olefinic and aromatic carbons at δ_C 142.7; 143.7; 146.1; 127.8 respectively and other quaternary carbons at δ_C 43.4; 40.8; 38.1; 37.2; 34.4 and 32.4.

The chemical shifts at δ_C 129.8 and 142.7 are characteristic of pentacyclic triterpenes of the olean-18-ene type (Mahato and Kundu, 1994).

Its ^1H NMR spectrum (Figure 22) shows:

- eight singlets each integrating for 3 protons and attributable to methyl protons of pentacyclic triterpenes at δ_H: 0.87; 0.90; 0.91; 1.07; 0.73; 1.00; 0.92 and 0.93;

- a singlet at 4.85 (1H, s) attributable to a proton bound to a sp^2 carbon;

- a signal at 2.25 (1H, d, $J = 11.0$ Hz) attributable to an α proton of an ethylenic group;

- signals of a *trans*-configured double bond at δ_H 7.54 (1H, d, $J = 15.9$Hz) and 6.25 (1H, d, $J = 15.9$Hz), that of 1,3,4- trisubstituted aromatic ring at δ_H 7.00 (1H, dd, $J = 8.2$; 1.7 Hz), 6.85 (1H, d, $J = 8.2$ Hz) and 7.08 (1H, d, $J = 1.7$ Hz), indicated the presence of cinnamoyl fragment (Ragasa *et al*., 2011).

All of the above data allows us to propose the following substructures:

SS_2　　　　　　　　　SS_1
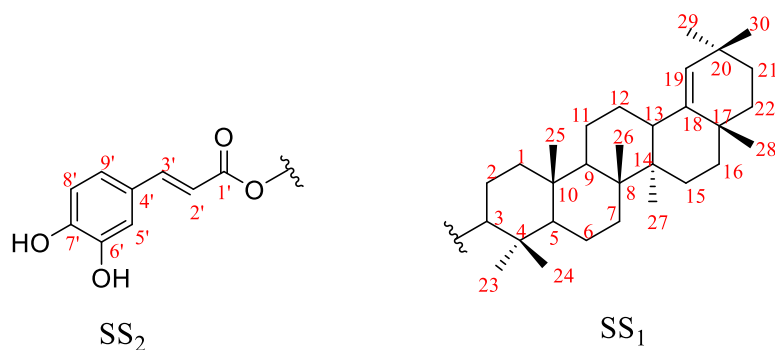
These two substructures was confirmed with the correlations observed on the HMBC (Figure 24) and COSY (Figure 25) spectra. Indeed, on the HMBC spectrum, we observe correlations between:

-the proton H-3′ (δ_H 7.54) and carbons C-1′ (δ_C 167.5); C-9′ (δ_C 122.4); C-8′ (δ_C 115.5) and C-5′ (δ_C 114.4 and C-4′ (δ_C 127.8);

-the proton H-9′ (δ_H 7.00) and carbons C-5′ (δ_C 114.4); C-3′ (δ_C 144.3) and C-7′ (δ_C 146.1);

-the proton H-2′ (δ_H 6.25) and carbons C-3′ (δ_C 144.3); C-1′ (δ_C 167.5);

-the proton H-8′ (δ_H 6.85) and carbons C-4′ (δ_C 127.8); C-6′ (δ_C 143.7); C-7′ (δ_C 146.1); C-9′ (δ_C 122.4);

-the proton H-5′ (δ_H 7.08) and carbons C-9′ (δ_C 122.4); C-3′ (δ_C 144.3); C-7′ (δ_C 146.1);- the proton H-19 (δ_H 4.80) and C-13 carbons (δ_C 38.7); C-17 (δ_C 34.4) and C-29 (δ_C 31.4);
- the proton H-5 (δ_H 0.85) and carbon C-3 (δ_C 81.2).

Also on its COSY spectrum (figure 28), we observe correlations between:
- the proton H-3′ (δ_H 7.54) and the proton H-2′ (δ_H 6.25);
- the proton H-9′ (δ_H 7.00) and the proton H-8′ (δ_H 6.85);
- the proton H-3 (δ_H 4.55) and the proton H-2 (δ_H 1.71);
- the proton H-5 (δ_H 0.85) and the proton H-6 (δ_H 1.40);
- the proton H-13 (δ_H 2.25) and the proton H-12 (δ_H 1.20).
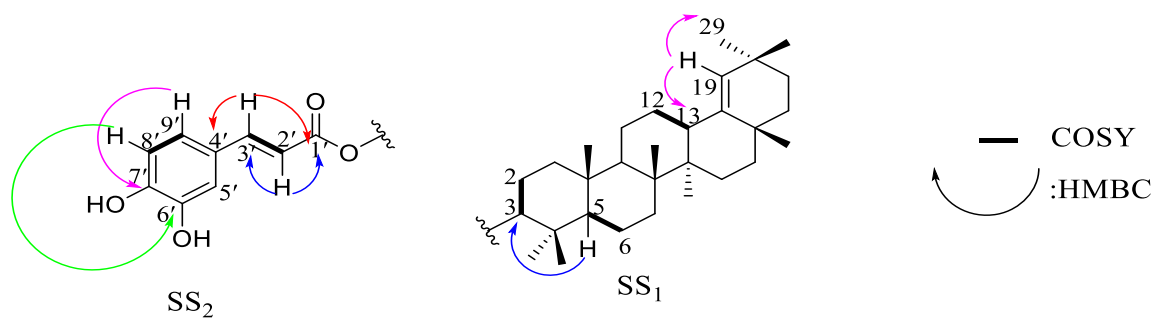
The cinnamoyl fragment (SS2) was linked to the triterpene skeleton (SS1) follow the HMBC correlation from proton H-3 (δ_H 4.55) to C-1′ carbons (δ_C 167.5); C-24 (δ_C 16.8) and C-23 (δ_C 28.0).
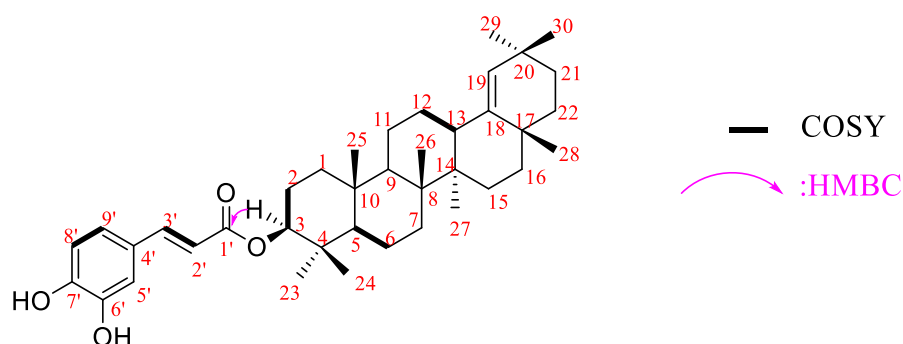
Scheme 12: Selected HMBC and COSY correlations of compound AL8

All these spectral data, compared to those of the literature, allowed to assign to AL8 the structure (**55**), which is that of germanicol caffeoyl ester, previously isolated from the leaves of *Barringtonia asiatica* by Ragasa *et al* in 2011.

(**55**)
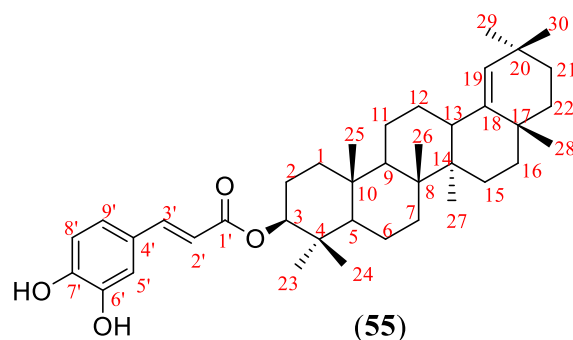
Table XX: Spectral data (CDCl₃, 500 MHz ¹H; 125 MHz ¹³C) of AL8 compared to those (CDCl₃, 600 MHz ¹H; 150 MHz ¹³C) of germanicol caffeoyl ester (Ragasa *et al.*, 2011)

N°	AL8 δ_C	AL8 δ_H (nH, m, *J* in Hz)	germanicol caffeoyl ester δ_C	germanicol caffeoyl ester δ_H (nH, m, *J* in Hz)
1	38.4	1.08	38.4	1.05
2	23.8	1.71	23.8	1.68
3	81.2	4.55 (1H, dd, *J* =9.4, 7.1 Hz)	81.2	4.59 (1H, dd, *J* = 9.6, 7.2 Hz)
4	38.1	/	38.1	/
5	55.6	0.85	55.6	0.82
6	18.2	1.40	18.2	1.40
7	34.5	1.36	34.5	1.36
8	40.8	/	40.8	/
9	51.1	1.32	51.1	1.30
10	37.4	/	37.4	/
11	21.2	1.30	21.2	1.30
12	26.2	1.20	26.2	1.20
13	38.7	2.25 (1H, brd, *J* = 10.0 Hz)	38.7	2.26
14	43.4	/	43.4	/
15	27.5	1.08	27.5	1.08
16	37.7	1.32	37.7	1.32
17	34.4	/	34.4	/
18	142.7	/	142.7	/
19	129.8	4.85 (1H, s)	129.8	4.85 (1H, s)
20	32.4	/	32.4	/
21	33.4	1.32	33.4	1.32
22	37.2	1.51	37.2	1.40
23	28.0	0.87 (3H, s)	28.0	0.87 (3H, s)
24	16.8	0.90 (3H, s)	16.8	0.90 (3H, s)
25	16.7	0.91 (3H, s)	16.7	0.91 (3H, s)
26	16.1	1.07 (3H, s)	16.1	1.07 (3H, s)
27	14.6	0.73 (3H, s)	14.6	0.73 (3H, s)
28	25.3	1.00 (3H, s)	25.3	1.00 (3H, s)
29	31,4	0.92 (3H, s)	31.4	0.93 (3H, s)
30	29.2	0.93 (3H, s)	29.2	0.94 (3H, s)
1′	167.5	/	167.5	/
2′	116.5	6.25 (1H, d, *J* = 15.9 Hz)	116.5	6.25 (1H, d, *J* = 15.6 Hz)
3′	144. 3	7.54 (1H, d, *J* = 15.9 Hz)	144.3	7.54 (1H, d, *J* = 15.6 Hz)
4′	127.8	/	127.8	/
5′	114.4	7.08 (1H, d, *J* = 1.7 Hz)	114.4	7.09 (1H, d, *J* = 1.8 Hz)
6′	143.7	/	143.7	/
7′	146.1	/	146.1	/
8′	115.5	6.85 (1H, d, *J* = 8.2 Hz)	115.5	6.85 (1H, d, *J* = 7.8 Hz)
9′	122.4	7.00 (1H, dd, *J* = 8.2, 1.7 Hz)	122.4	6.99 (1H, dd, *J* = 7.8, 1.8 Hz)
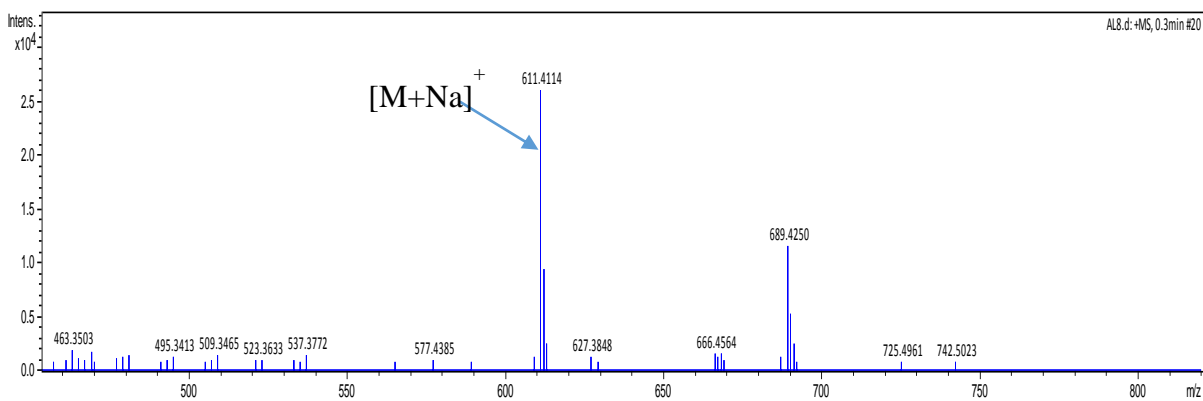
Figure 21: HR-ESI-MS spectrum of compound AL8
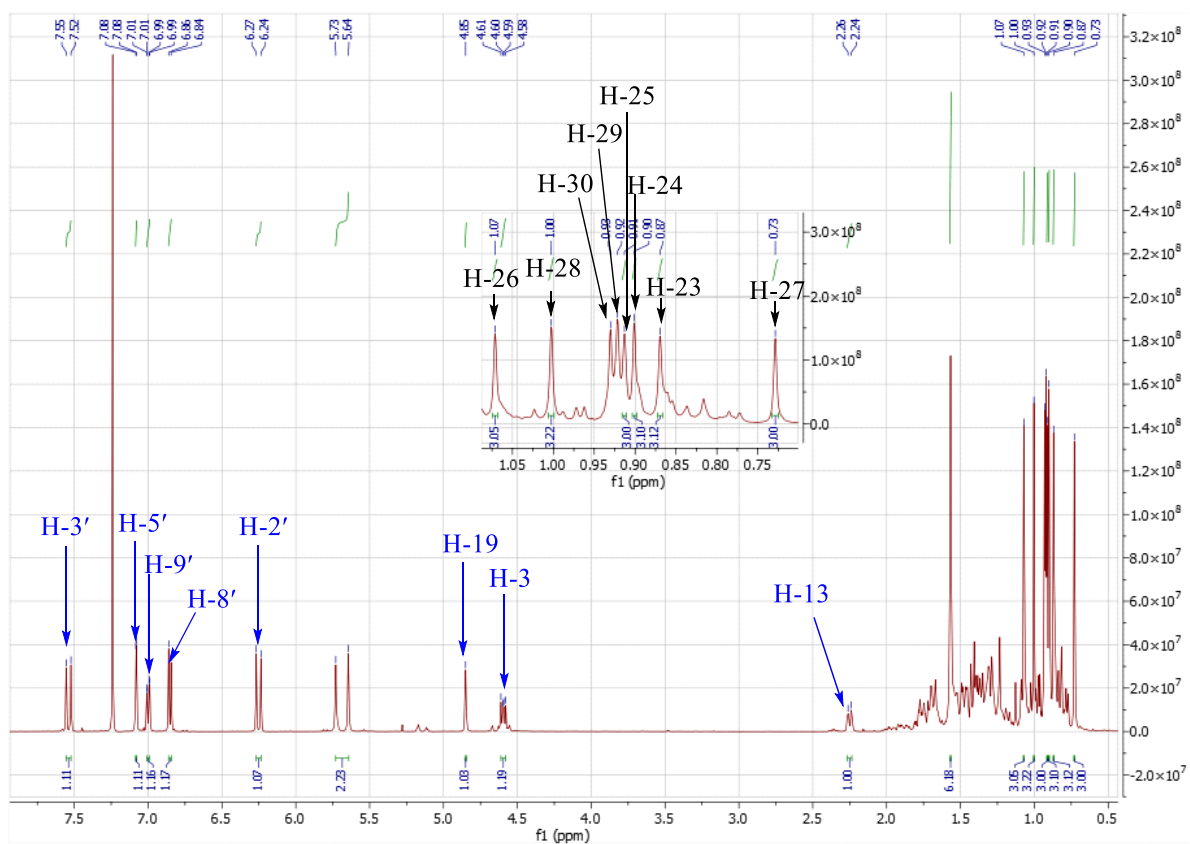
Figure 22: ^{1}H NMR spectrum (CDCl$_3$, 500 MHz) of compound AL8
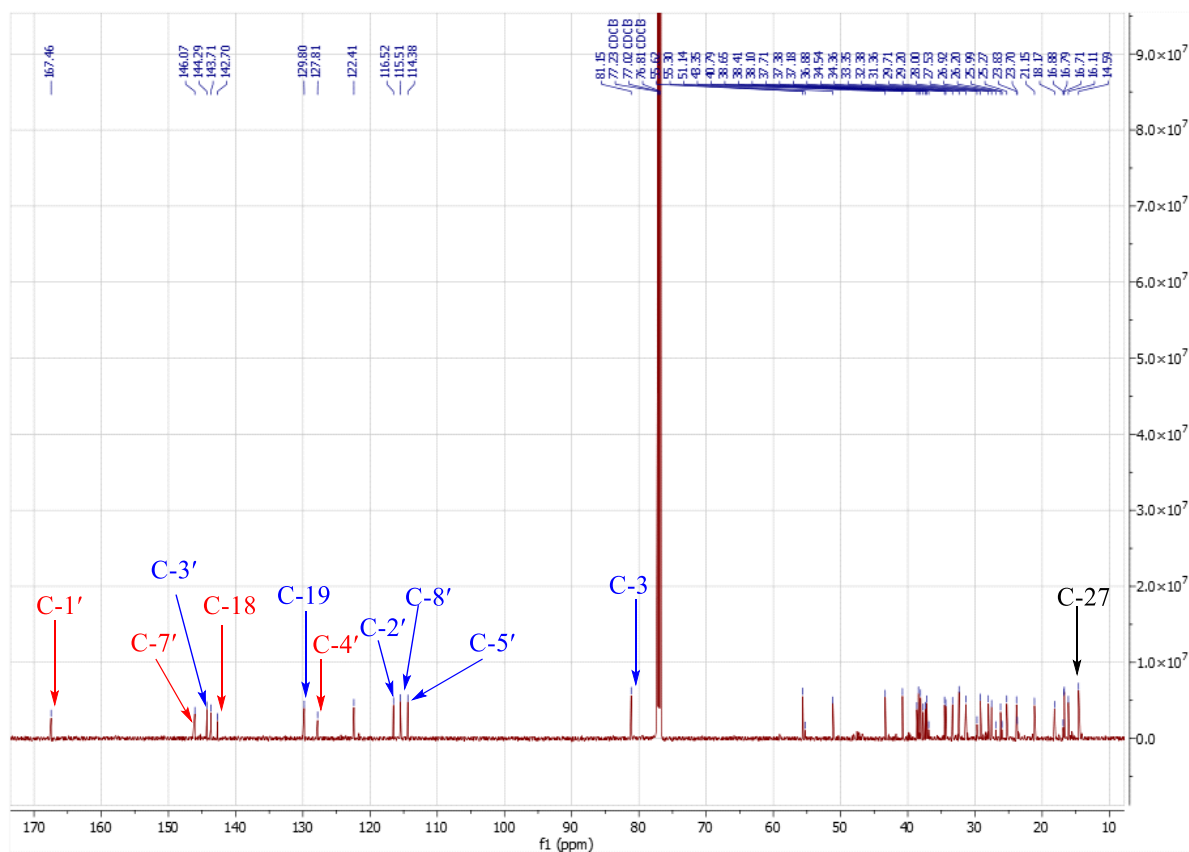
Figure 23: ^{13}C NMR spectrum (CDCl$_3$, 125 MHz) of compound AL8
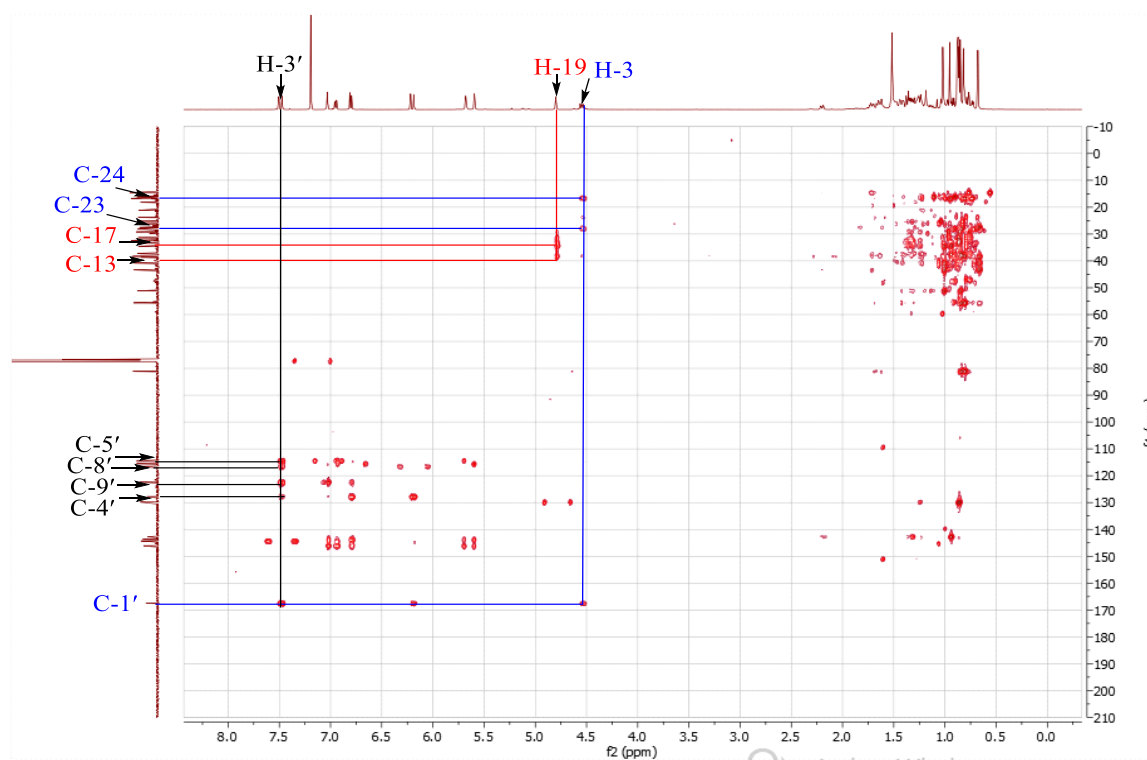
Figure 24: HMBC spectrum of compound AL8
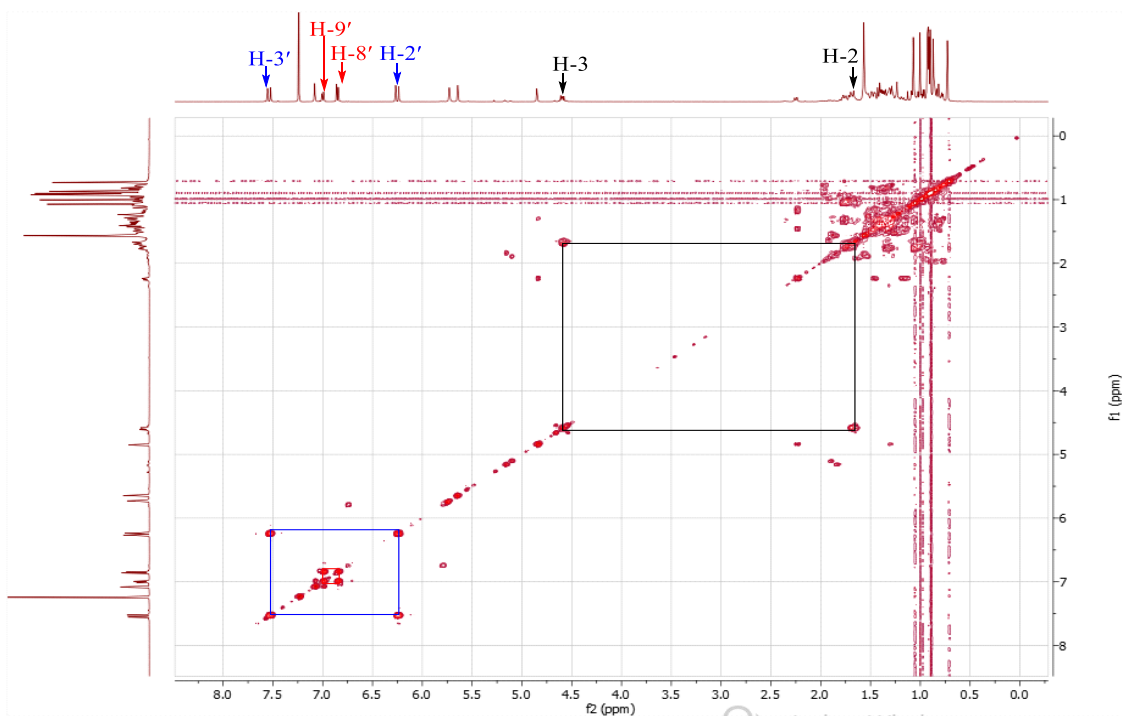
Figure 25: COSY spectrum of compound AL8
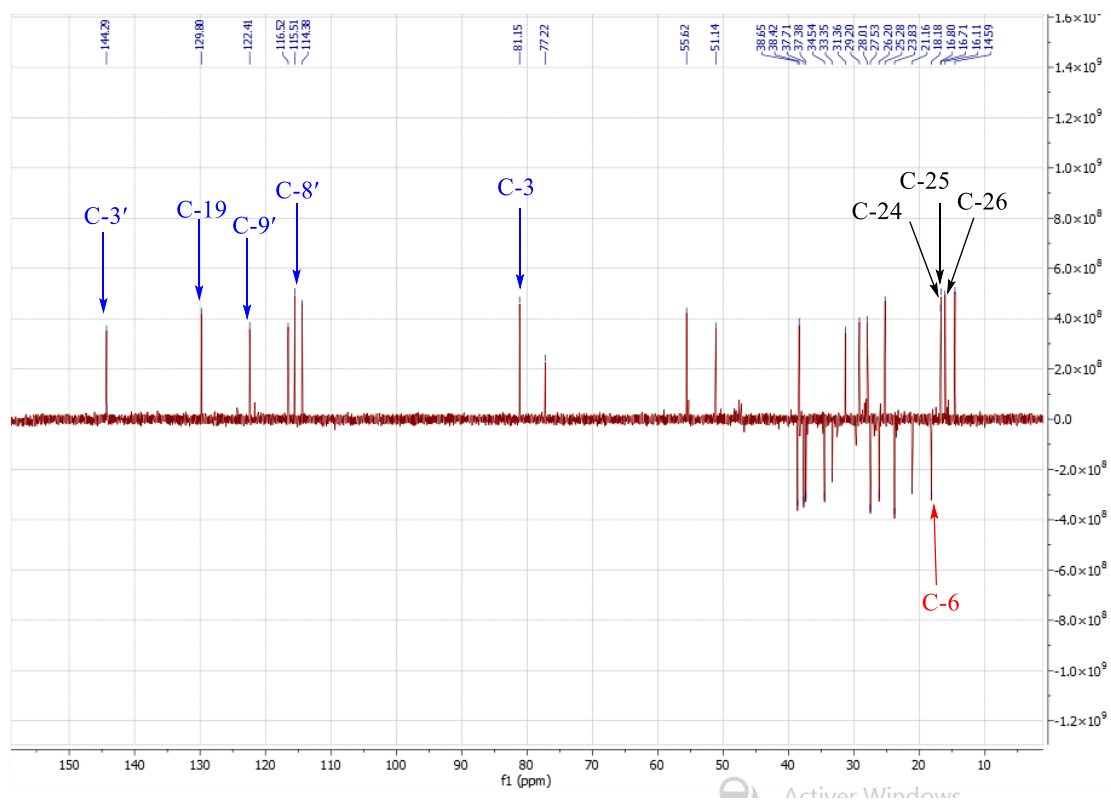
Figure 26: DEPT 135 spectrum of compound AL8

II.2.1.2.2 Identification of AL4 or ECT1 or ECF21

ECF21 was obtained as a white amorphous solid. It is soluble in dichloromethane and responds positively to the Liebermann-Burchard test, giving a red coloration, characteristic of triterpenes. Its HR-ESI (+) mass spectrum (Figure 27) gives the peak of the protonated ion $[M+H]^+$ at m/z 427.3964 corresponding to the molecular formula $C_{30}H_{50}O$ (calculated for 427.3940) and comprising six unsaturations.

On its broadband fully decoupled ^{13}C NMR spectrum (Figure 29), signals of 30 carbon atoms were distinguished and sorted using HSQC technique (Figure 30) into:

- eight methyl carbons including one appearing at δ_C 6.81 characteristic of the friedelane class and seven others at δ_C 8.7, 20.3, 17.9, 14.7, 32.1, 35.0 and 31.8 (Mahato and Kundu, 1994);

- four methine carbons at δ_C 58.2; 59.5; 53.1 and 42.8;

- eleven methylene carbons at δ_C 22.3; 41.5; 41.3; 18.2; 35.7; 30.5; 32.4; 36.0; 35.4; 32.8 and 39.3;

- seven quaternary carbons, including a carbon characteristic of the carbonyl of ketones at δ_C 213.3; and other quaternary carbons at δ_C 42.2, 37.5, 39.7, 38.3, 30.0 and 28.2.

Its ^1H NMR spectrum (Figure 28) shows signals of seven methyl singlets at δ_H 0.70; 0.93; 0.97; 0.98; 1.03; 1.16; 1.23 and one methyl appearing as a doublet at δ_H 0.86 ($J = 6.5$ Hz), which is reminiscent of methyl protons at position 23 of the pentacyclic triterpenes of the friedelane series (Sousa *et al.*, 2012). This assertion is reinforced by the presence of correlation on the COSY spectrum (Figure 31) between the signal of a doublet of three protons at δ_H 0.86 (3H, d, $J = 6.5$ Hz; CH$_3$-23) and that of a quadruple of a proton at δ_H 2.23 (1H; q; $J = 6.5$ Hz, H-4). The value of the chemical shift of the H-4 proton suggests that it is placed in α of a carbonyl.

The location of the carbonyl in C-3 was deduced from the correlations observed on the HMBC spectrum (Figure 32). Correlations were observed between:

-the H-4 proton (δ_H 2.23) and C-3 carbons (δ_C 213.3); C-23 (δ_C 6.8); C-24 (δ_C 14.7); C-5 (δ_C 42.2) and C-10 (δ_C 59.5) (scheme 12);

-The proton H-2 (δ_H 2.37) and the C-3 carbons (δ_C 213.3); C-4 (δ_C 58.2); C-10 (δ_C 59.5); and C-1 (δ_C 22.3).

Scheme 13: Selected HMBC and COSY correlations of ECF21

All these spectral data, compared to those of the literature (Table XXI), allowed us to attribute to ECF21 the structure (**56**), which is that of friedeline, previously isolated from leaves of *Matenus robusta* by Sousa and collaborators in 2012.

(**56**)

Table XXI: Spectral data of ^1H (500 MHz) and ^{13}C (125 MHz) of ECF21 in CDCl₃, compared to that of friedelin ^1H (400 MHz) and ^{13}C (100 MHz) in CDCl₃ (Sousa *et al.*, 2012)

Position	ECF21		Friedelin	
	δ_C	δ_H (nH, m, *J* in Hz)	δ_C	δ_H (nH, m, *J* in Hz)
1	22.3	1.94 (1H, m) / 1.66 (1H, m)	22.3	1.90 (1H, m) / 1.65 (1H, m)
2a	41.5	2.37 (1H, d, *J* = 8,5; 3,5 Hz)	41.5	2.38 (1H, d, *J* = 7,4 Hz) /
2b		2.36 (1H, m)		2.22 (1H, m)
3	213.3	-	212.9	-
4	58.5	2.23 (1H, q, *J* = 6,5 Hz)	58.3	2.18 (1H, q, *J* = 6,5 Hz)
5	42.2	-	42.8	-
6	41.5	1.75 (1H, m) /1.19 (1H, m)	41.3	1.66 (1H, m) / 1.21 (1H, m)
7	18.2	1.46 (1H, m) /1.32 (1H, m)	18.3	1.45 (1H, m) /1.35 (1H, m)
8	53.1	1.37 (1H, m)	52.9	1.35 (1H, m)
9	37.5	-	37.5	-
10	59.5	1.52 (1H, m)	59.5	1.48 (1H, m)
11	35.6	1.37 (1H, m) /1.20 (1H, m)	35.7	1.38 (1H, m) /1.19 (1H, m)
12	30.5	1.27 (1H, m) /1.26 (1H, m)	30.5	1.31 (1H, m) /1.24 (1H, m)
13	39.7	-	39.7	-
14	38.3	-	38.3	-
15	32.4	1.24 (1H, m) /1,46 (1H, m)	32.4	1.49 (1H, m) /1.27 (1H, m)
16	36.0	1.50 (1H, m) /1.25 (1H, m)	36.0	1.50 (1H, m) /1.28 (1H, m)
17	30.0	-	30.0	-

18	42.8	1.56 (1H, m)	42.9	1.51 (1H, m)
19	35.3	1.33 (1H, m) /1.18 (1H, m)	35.3	1.31 (1H, m) /1.14 (1H, m)
20	28.2	-	28.2	-
21	32.8	1.46 (1H, m) /1.33 (1H, m)	32.7	1.42 (1H, m) /1.37 (1H, m)
22	39.3	1.44 (1H, m) /0.93 (1H, m)	39.2	1.41 (1H, m) /0.90 (1H, m)
23	6.8	0.86 (3H, d, J = 6,5 Hz)	6.8	0.88 (3H, d, J = 6,6 Hz)
24	14.7	0.70 (3H, s)	14.7	0.72 (3H, s)
25	17.9	0.85 (3H, s)	17.9	0.87 (3H, s)
26	20.3	0.93 (3H, s)	20.2	1.01 (3H, s)
27	18.7	1.03 (3H, s)	18.7	1.05 (3H, s)
28	32.1	1.16 (3H, s)	31.9	1.18 (3H, s)
29	35.0	0.98 (3H, s)	35.0	0.95 (3H, s)
30	31.8	0.99 (3H, s)	31.7	1.00 (3H, s)
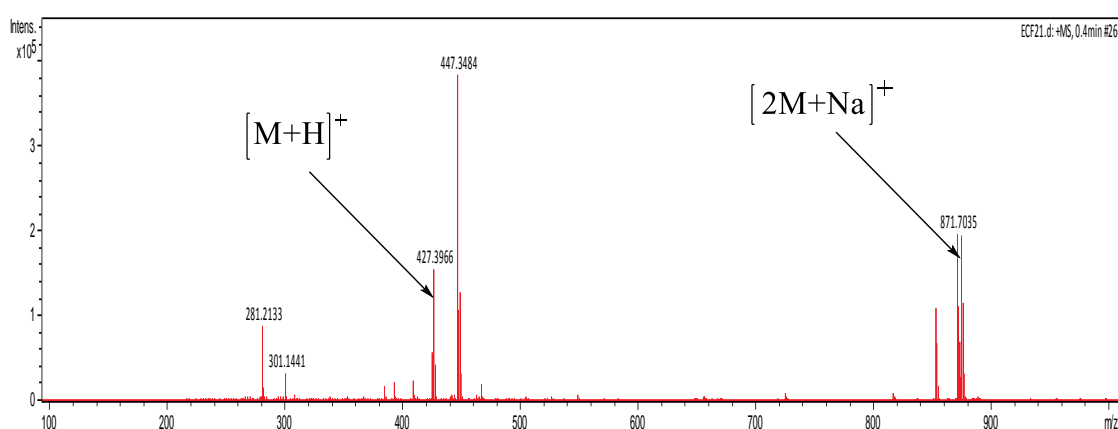
Figure 27: HR-ESI-MS spectrum of compound ECF21
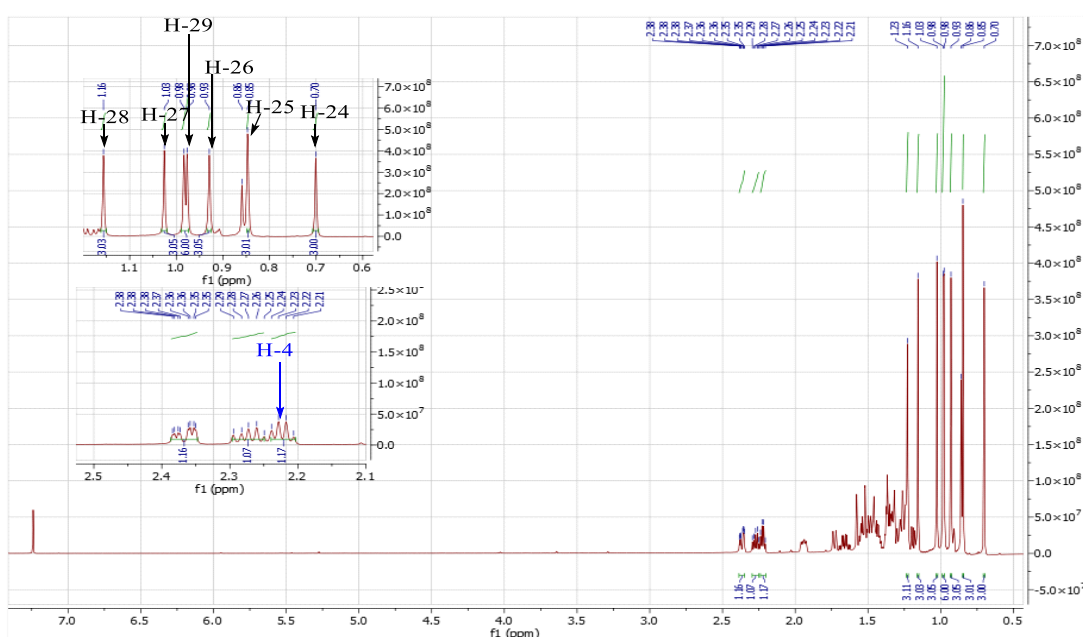
Figure 28: ^{1}H NMR spectrum (CDCl$_3$, 500 MHz) of compound ECF21
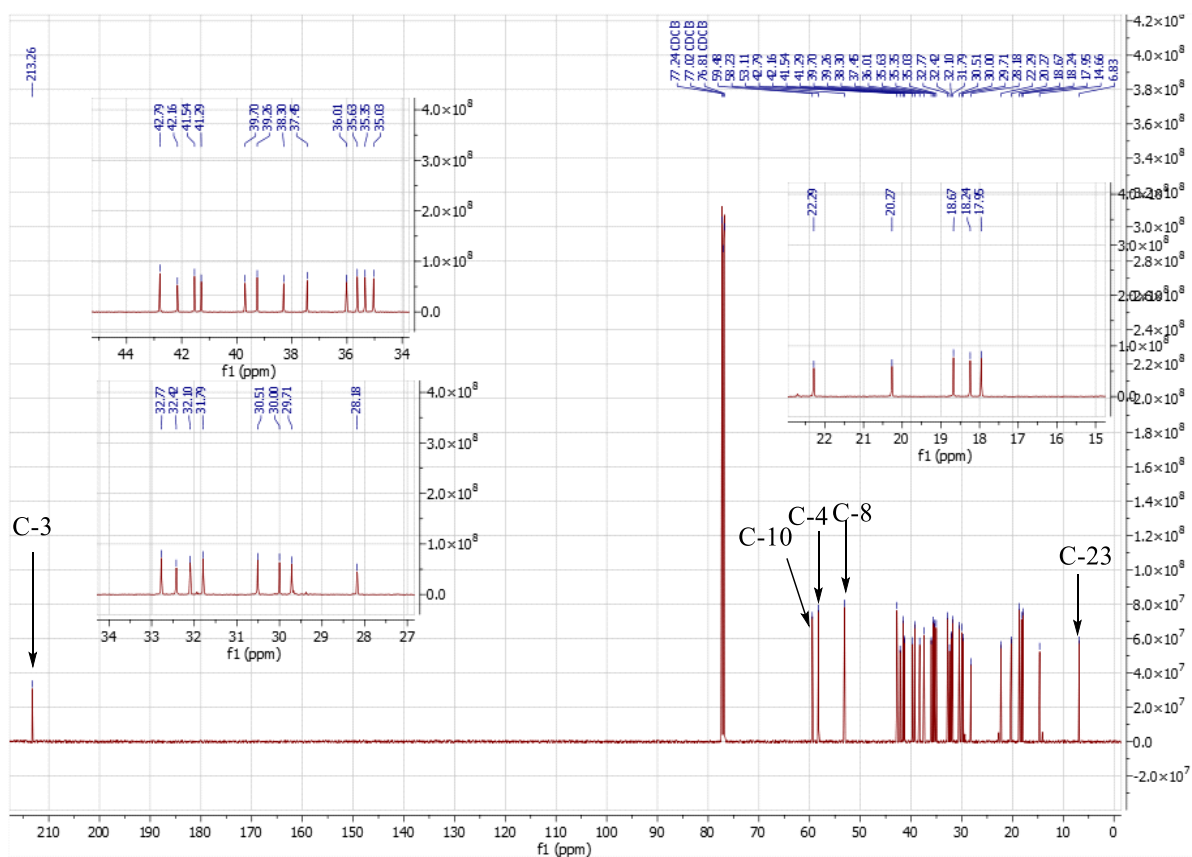
Figure 29: ^{13}C NMR spectrum (CDCl$_3$, 125 MHz) of compound ECF21
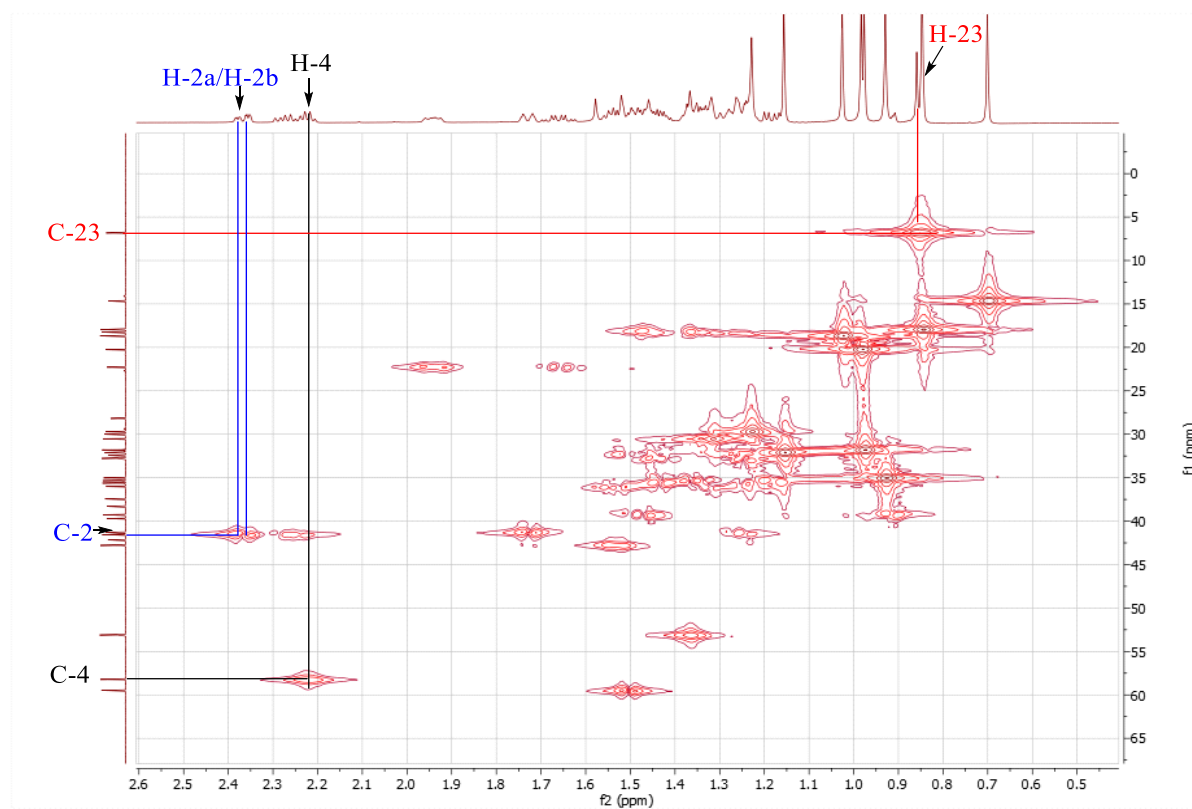
Figure 30: HSQC spectrum of compound ECF21
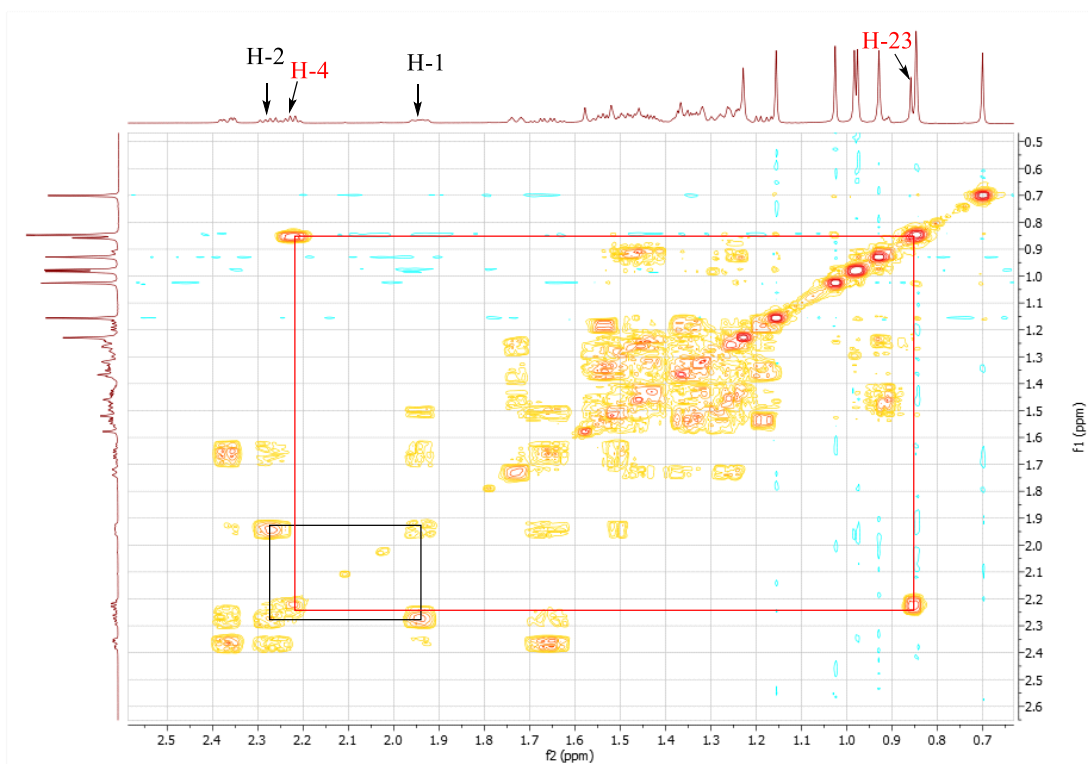
Figure 31: COSY spectrum of compound ECF21
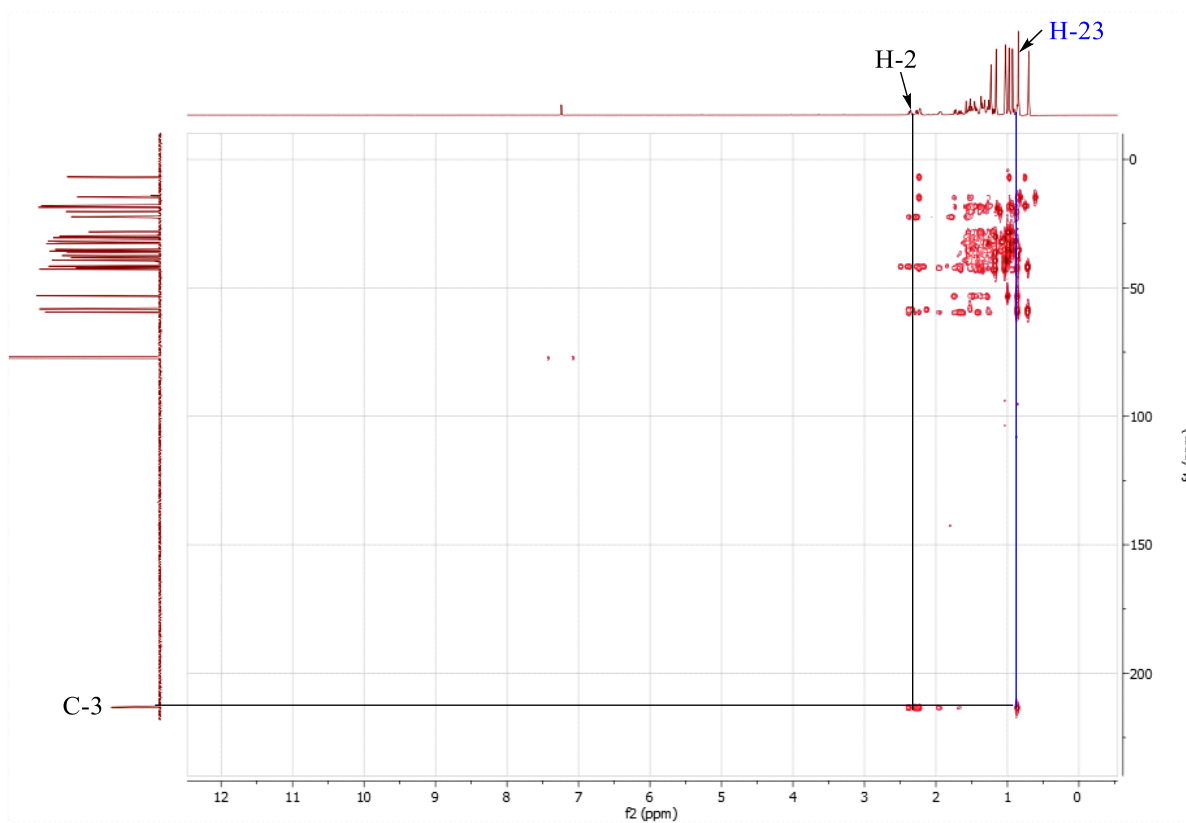
Figure 32: HMBC spectrum of compound ECF2

II.2.1.2.3 Identification of ECT2

ECT2 was obtained as a white amorphous solid. It is soluble in chloroform and responds positively to the Liebermann-Burchard test, giving a red coloration, characteristic of triterpenes.

Analysis of its ^{1}H and ^{13}C NMR spectra reveals that it has a friedelane-like backbone as ECTF21.

Indeed, its ^{1}H NMR spectrum (Figure 33) presents similarities to that of the compound ECF21. The observed difference was the presence of a broad singlet of two protons at δ_H 3.61 attributable to two protons of an oxygenated methylene group and the desappearance.of one singlet of methyl group.

On its ^{13}C NMR spectrum (Figure 34), signals corresponding to 30 carbon atoms are observed. Analysis of this spectrum and that of DEPT 135 (Figure 35) also showed similarities with the spectra of ECF21, and confirmed the presence of a oxymethylene carbon at δ_C 68.1.

The position of the oxymethylene group at C-28 was deduced from the HMBC spectrum (Figure 36), where correlation from H-16 proton (δ_H 1.84) to C-28 carbon (δ_C 68.1), and from H-28 proton (δ_H 3.61) to C-16 carbon (δ_C 29.1); C-22 (δ_C 35.1) carbon were observed (Scheme 14).
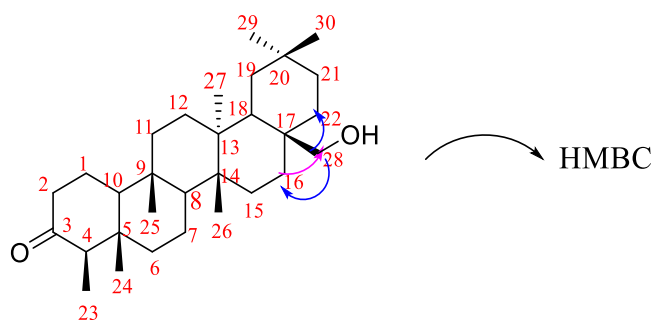
Scheme 14: Selected HMBC correlations of compound ECT2

All these spectral data, compared to those of the literature (Table XXII), allowed us to attribute to ECT2 the structure (**57**), which is that of canophyllol, previously isolated from stems of *Maytenus diversifolia* by Nozaki and collaborators (1986).

(**57**)
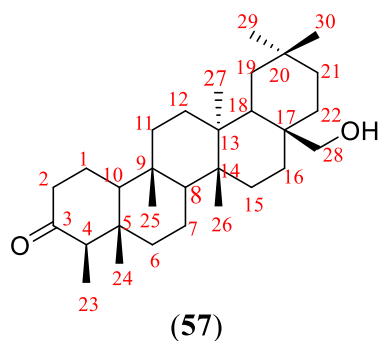
TableXXII: Spectral data of ¹³C (125 MHz) of ECT2 in CDCl₃, compared to that of canophyllol ¹³C (62.5 MHz) in CDCl₃ (Nozaki *et al.*, 1986).

Position	ECT2 δ_C	Canophyllol δ_C
1	22.3	22.1
2	41.2	41.3
3	213.2	212.6
4	58.2	57.8
5	42.1	41.9
6	41.5	41.0
7	18.2	18.1
8	52.3	52.2
9	37.5	37.3
10	59.5	59.1
11	35.4	35.3
12	30.1	29.9
13	39.4	39.1
14	38.2	38.0
15	31.2	31.3
16	29.1	29.0
17	34.5	35.1
18	39.5	39.2
19	35.2	34.4
20	28.2	27.9
21	31.4	31.4
22	33.3	33.2
23	6.8	6.7
24	14.7	14.5
25	18.1	18.0
26	19.1	18.9
27	19.2	19.1
28	68.1	67.0
29	32.9	32.9
30	34.3	34.2
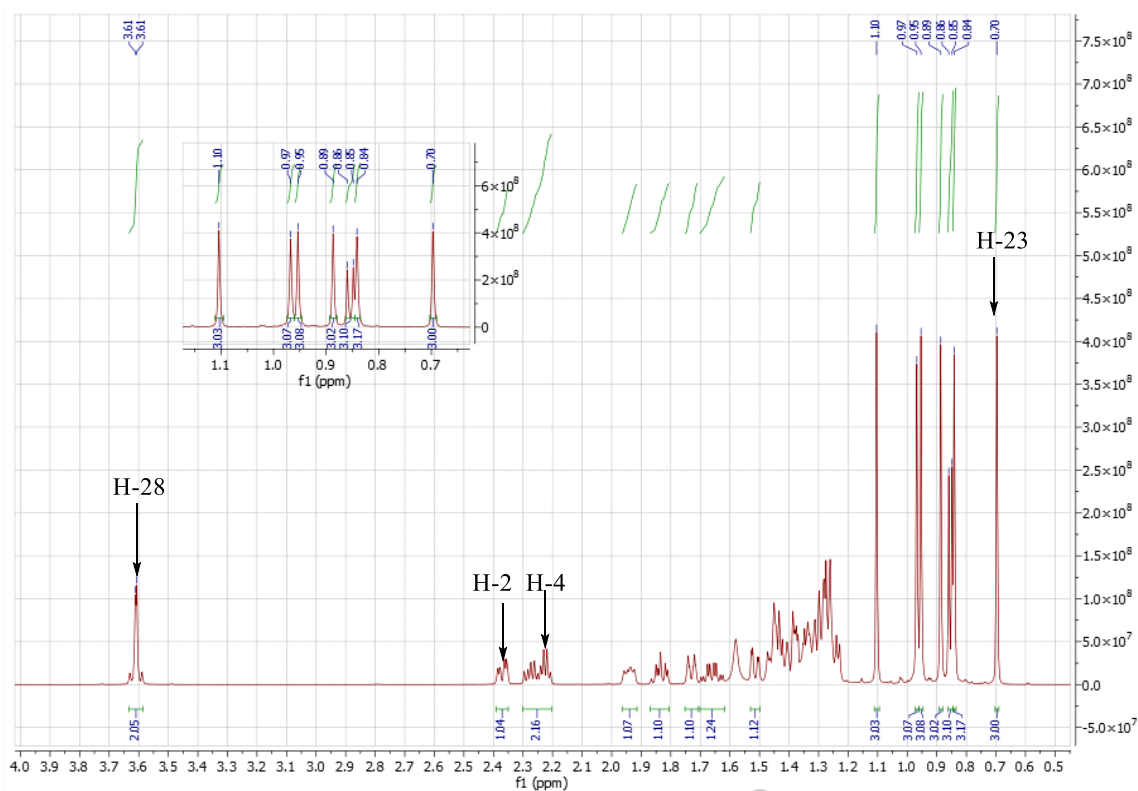
Figure 33: ^1H NMR spectrum (CDCl$_3$, 500 MHz) of compound ECT2
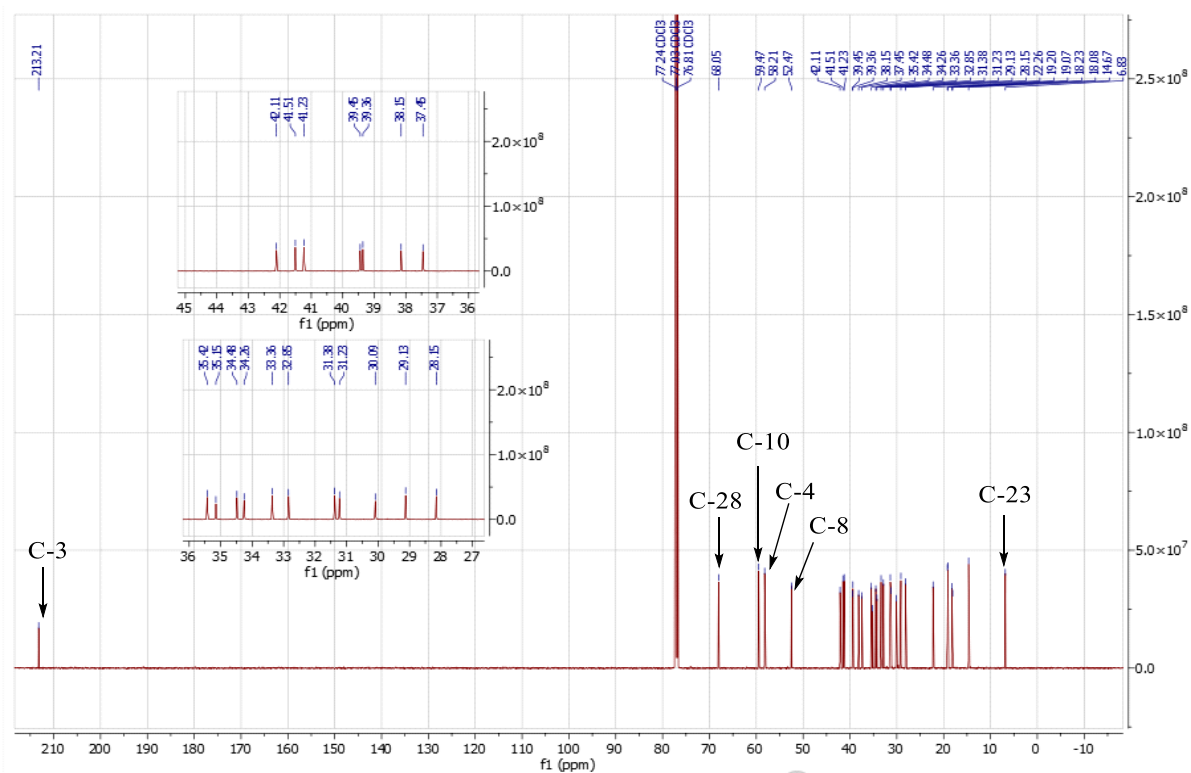
Figure 34: ^{13}C NMR spectrum (CDCl$_3$, 125 MHz) of compound ECT2
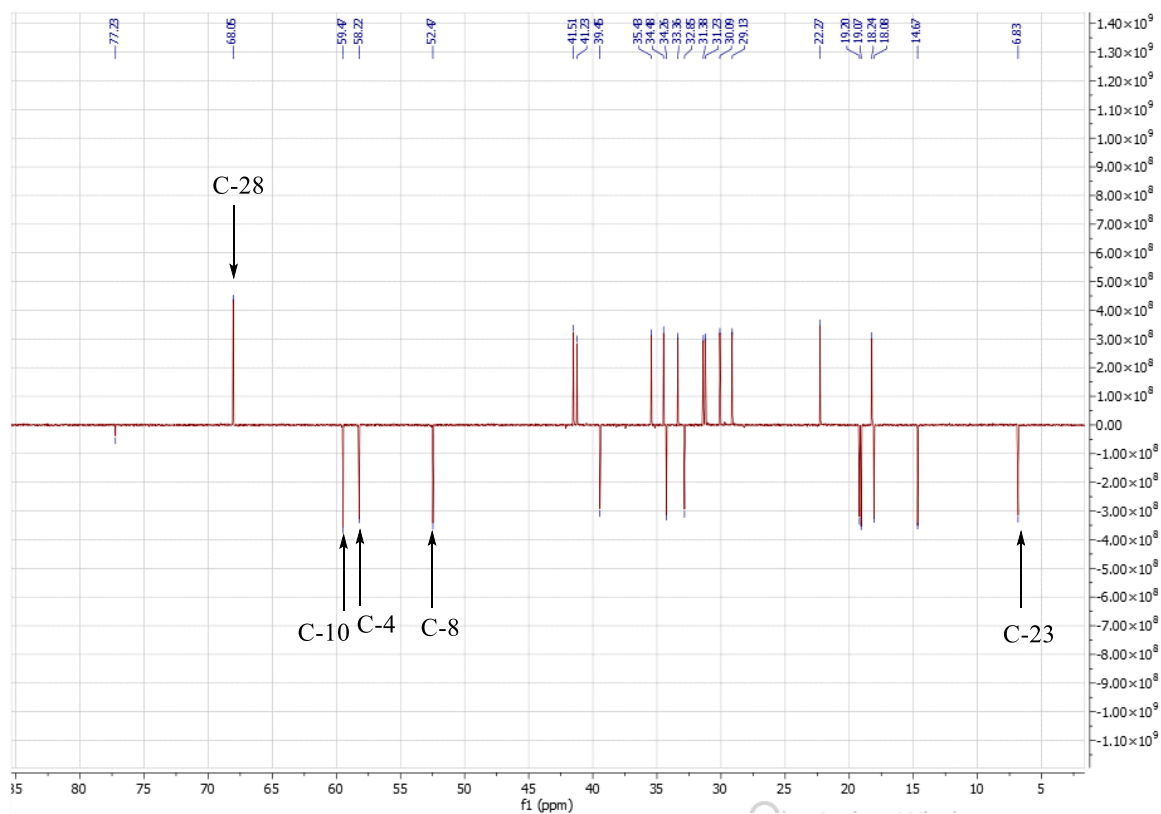
Figure 35: DEPT 135 spectrum of compound ECT2
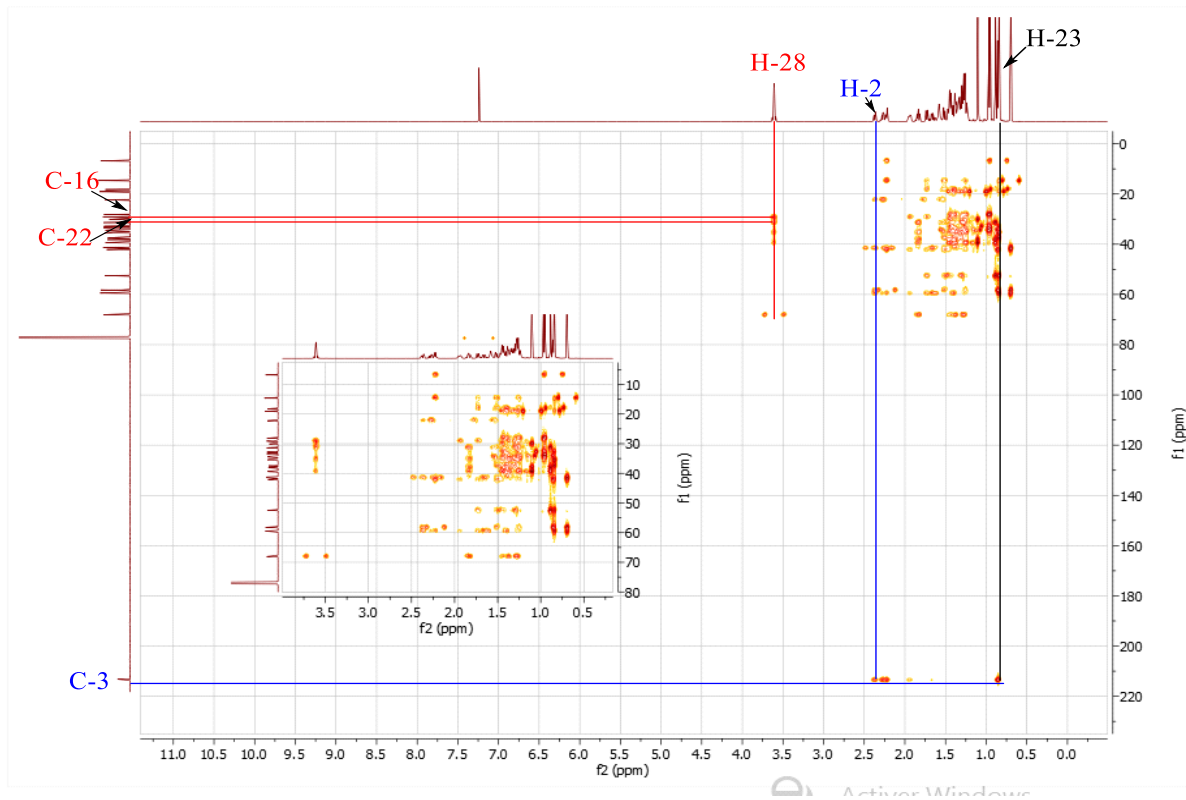
Figure 36: HMBC spectrum of compound ECT2

II.2.1.2.4 Identification of ECTF22

ECTF22 precipitates as a white amorphous solid. It is soluble in chloroform and responds positively to the Liebermann-Burchard test by giving a red coloration characteristic of triterpenes.

Its ^{1}H NMR spectrum (Figure 37) shows similarities with that of ECT2. The only difference observed is the appearance of a triplet at δ_H 3.80 (1H, dd, J = 11.7, 2.6 Hz) corresponding to an oxymethine proton.

Its ^{13}C NMR spectrum (Figures 38) shows chemical shifts identical to those of ECT2. The only difference is the presence of an oxygenated methine carbon at δ_C 77.0.

The position of oxymethine at C-2, was justified by the correlations observed on its HMBC spectrum (Figure 40), between the proton at δ_H 3.80 (H-2) and the carbons at δ_C 212.2 (C-3) on the one hand and the protons at δ_H 2.51 (H-1a), 2.37 (H-1b) and the carbons at δ_C 212.2 (C-3) and 77.0 (C-2) on the other hand (Scheme 15).
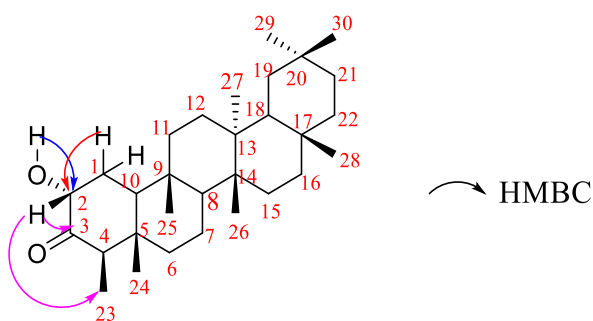
Scheme 15: Selected HMBC correlations of compound ECTF22

All these data compared to those of the literature (Table XXIII) allow us to identify ECTF22 as cerin (**58**) (Ngouamegne *et al.*, 2008).

(**58**)
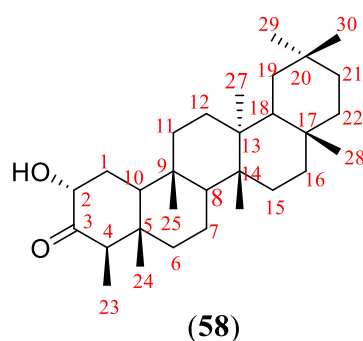
Table XXIII: Spectral data of ^{13}C (125 MHz) of ECTF22 in CDCl₃, compared to that of cerin ^{13}C (75 MHz) in CDCl₃/CD₃OD (4:1) (Ngouamegne *et al.*, 2008)

Position	ECTF22 δ_C	Cerin δ_C
1	36.1	37.3
2	77.0	74.2
3	212.2	215.7
4	53.1	52.6
5	54.5	53.2
6	43.0	43.2
7	17.8	18.7
8	53.1	53.5
9	38.3	38.7
10	60.6	56.6
11	35.5	35.7
12	30.2	30.4
13	40.8	41.5
14	39.9	40.2
15	30.5	30.7
16	36.4	36.4
17	30.2	30.9
18	43.0	43.8
19	35.3	35.3
20	32.9	33.2
21	28.4	28.5
22	37.8	39.7
23	10.8	6.6
24	14.3	14.3
25	17.6	18.3
26	18.8	19.0
27	20.4	20.6
28	32.3	32.0
29	32.6	32.8
30	31.9	32.4
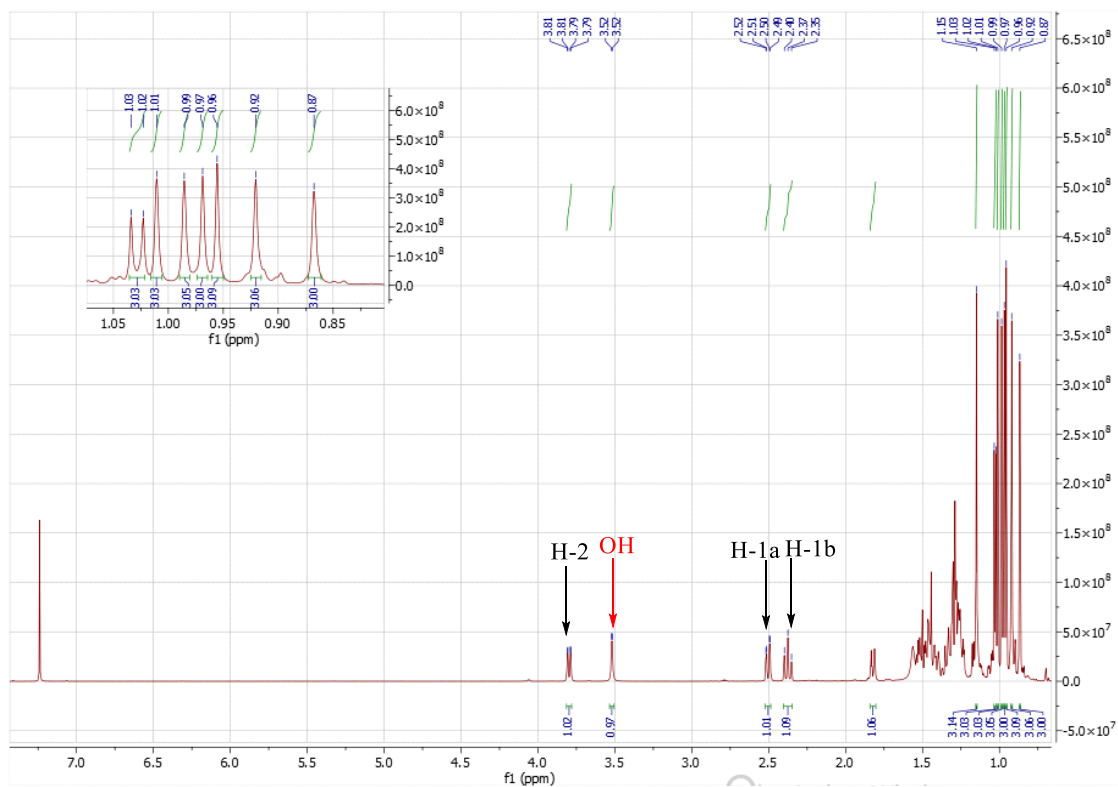
Figure 37: ^{1}H NMR spectrum (CDCl$_3$, 500 MHz) of compound ECTF22
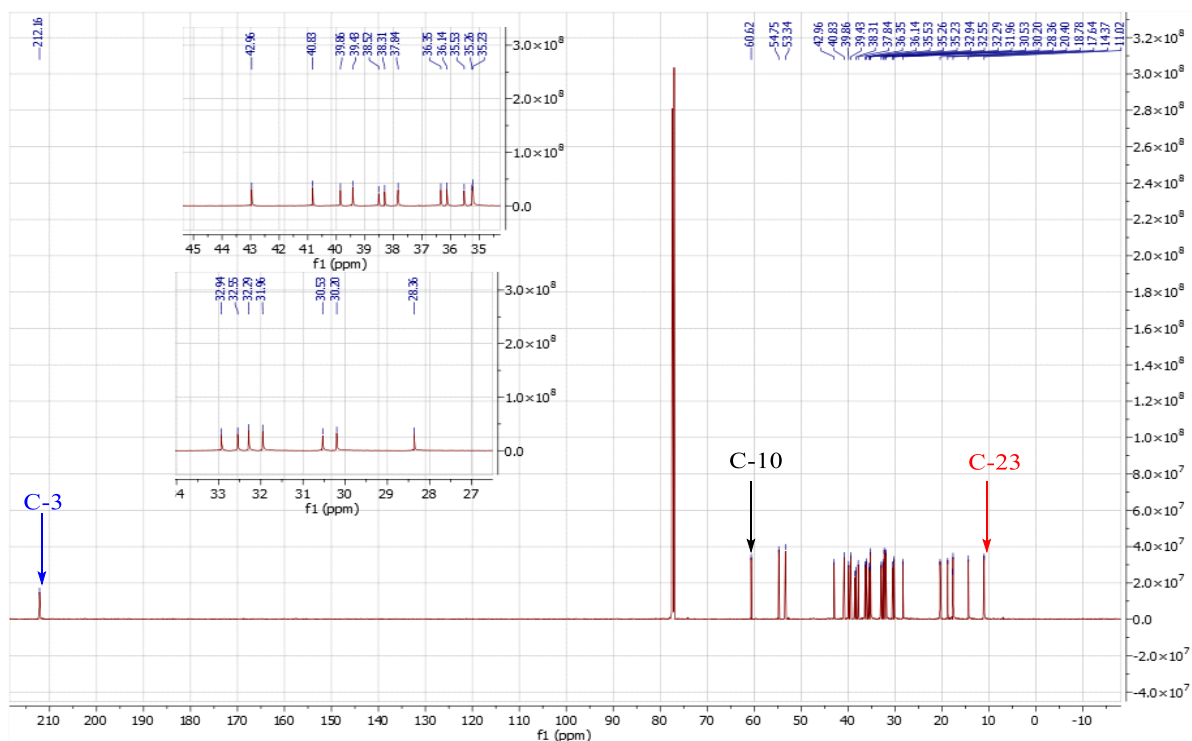
Figure 38: ^{13}C NMR spectrum (CDCl$_3$, 125 MHz) of compound ECTF22
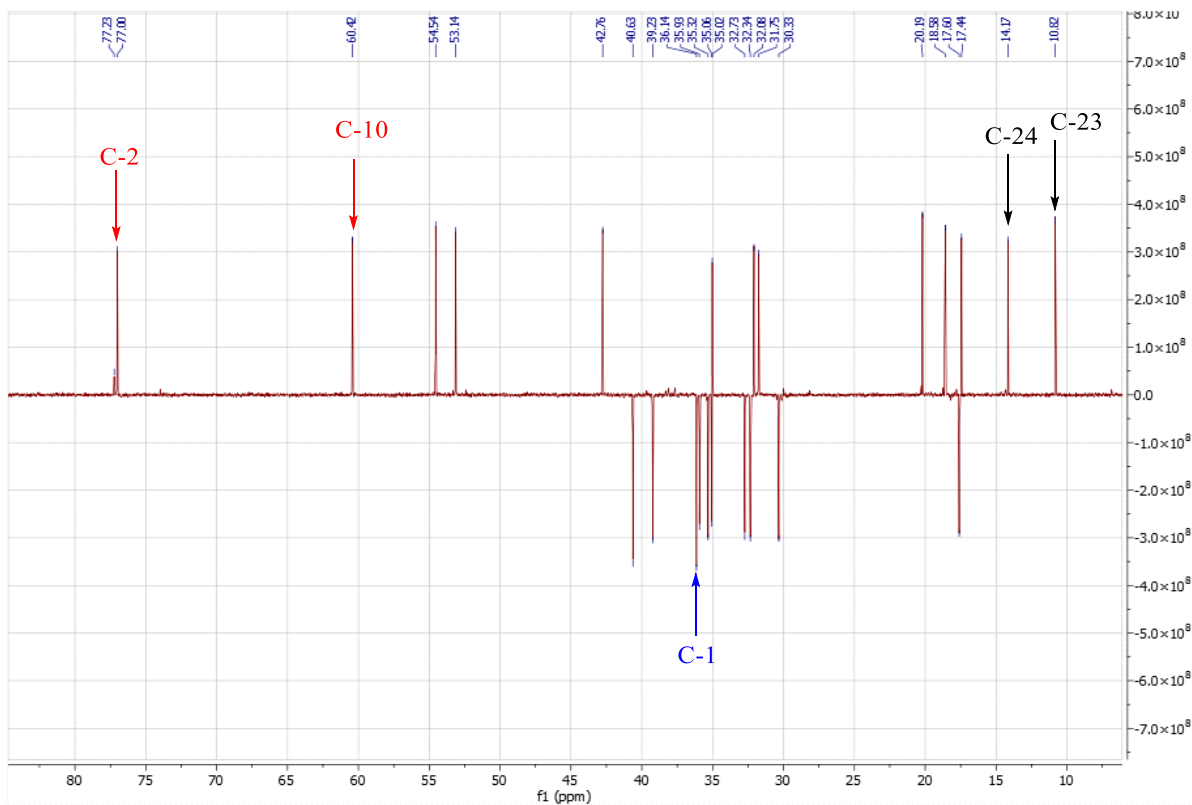
Figure 39: DEPT 135 spectrum of compound ECTF22

Figure 40: HMBC spectrum of compound ECTF22

II.2.1.2.5 Identification of ECTF21

Compound ECTF21 was obtained as a white amorphous solid. It is soluble in chloroform and responds positively to the Liebermann-Burchard test by giving a purplish red coloration, characteristic of triterpenes.

Its high resolution HR-ESI (+) mass spectrum (Figure 41) shows the peak of the protonated ion $[M+H]^+$ at m/z 483.3969 (calculated for $C_{32}H_{51}O_3$ at 483.3957), corresponding to the molecular formula $C_{32}H_{50}O_3$, containing eight unsaturations.

Its ^{13}C NMR spectrum (Figure 43), shows signals of 32 carbon atoms sorted using the HSQC technique as:

- eight methyl carbons at δ_C 33.7, 30.2, 29.9, 23.2, 27.0, 19.5, 17.0 and 16.6, of triterpene backbone.
- a methyl at δ_C 21.3 (OAc);
- seven methine carbons, amongst which an olefinic carbon at δ_C 118.9, an oxymethine carbon at δ_C 80.7 and 5 other methines at δ_C 54.7, 51.8, 53.4, 58.1 and 48.4;
- eight quaternary carbons including an olefinic carbon at δ_C 157.1 and an ester carbon at δ_C 170.8 and 6 other carbons at δ_C 38.9, 37.9, 36.6, 37.5, 35.3 and 29.9.

The chemical shifts of carbons at δ_C 158.1 and 117.0 are characteristic of pentacyclic triterpenes of the taraxerane series (Mahato and Kundu, 1994).

- Its ^1H NMR spectrum (Figure 42) exhibited:
- a signal of a proton at δ_H 5.52 (1H, dd, J = 8.2, 3.3 Hz), attributable to the proton of the ethylenic group carried by the carbon (C-15) of the type pentacyclic triterpene of the taraxer-14-ene (Ito and Lai, 1978);
- a signal of a proton at δ_H 4.50 (1H, dd, J =10.6; 5.7 Hz), attributable to the oxymethine of triterpenoid;
- two proton signals at δ_H 3.09 (1H, t, J = 5.1. Hz) and 2.78 (1H, d, J = 4.6. Hz), of two oxymethine proton;
- eight singlets methyl groups of pentacyclic triterpenes at δ_H 0.94 (H-23), 0.80 (H-29), 0.98 (H-24), 1.06 (H-26), 0.84 (H-30), 1.08 (H-27), 0.88 (H-25) and 0.85 (H-28);
- the proton of an acetyl group at δ_H 2.03.

All of these spectral data compared to that described in the literature clearly indicate that ECTF21 is a pentacyclic triterpene of the taraxer-14-ene type having, an ester group.

The positions of these substituents were deduced from the correlations observed on the HMBC spectrum (Figure 44, scheme 16). Infact on this spectra Correlations were observed between:

- The acetyl group was attached at C-3 follow the HMBC correlation from the proton at δ_H 4.50 (H-3) and the carbons at δ_C 170.9 (C-1′), 37.9 (C-1), 23.2 (C-2), 54.7 (C-5), 27.9 (C-23);

- the proton at δ_H 5.52 (H-15) and the carbons at δ_C 35.2 (C-16), 35.3 (C-17), 157.1 (C-14);

- the proton at δ_H 0.78 (H-27) and the carbons at δ_C 58.1 (C-12), 48.4 (C-18);

- the proton at δ_H 2.78 (H-12) and the carbons at δ_C 53.4 (C-11), 157.1 (C-14), 30.2 (C-27), 48.3 (C-18);

- the proton at δ_H 3.09 (H-11) and the carbons at δ_C 58.1 (C-12), 51.8 (C-9), 38.9 (C-8), 37.5 (C-10);

Its COSY spectrum (Figure 45) shows the correlation between the proton H-11 (δ_H 3.09) and the H-12 proton (δ_H 2.78). This information coupled to the mass spectrum indicated the 11, 12-epoxy group.

These informations clearly indicates that the epoxy group is formed with carbons (C-11) and (C-12), the double bond group is located $\Delta^{14,15}$ and the ester group is attach to carbon (C-3) (Ito and Lai, 1978).
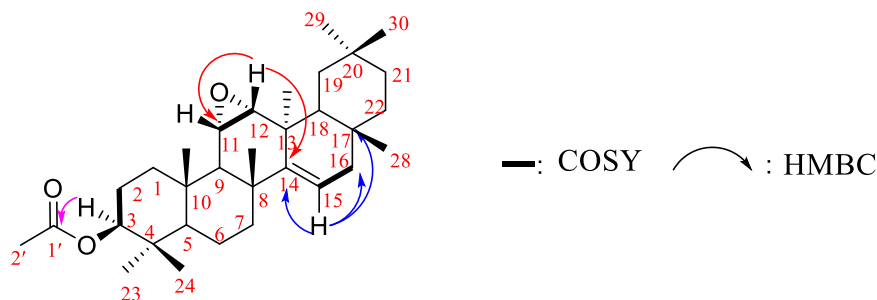
Scheme 16: Selected HMBC and COSY correlations of compound ECTF21

All these spectral data compared to that described in the literature table (XXIV) allow us to attribute to **ECTF21** the structure (**58**), which is that of marsformoxide B (11α,12α-oxidotaraxeryl acetate) previously isolated from *Euphorbia supina* (Euphorbiaceae) by Ito and collaborators (1978).

(59)
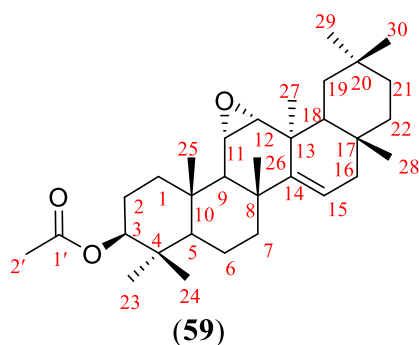
Table XXIV: Spectral data of ¹H (500 MHz) and ¹³C (125 MHz) of ECTF21 in CDCl₃, compared to that of marsformoxide B ¹H (300 MHz) and ¹³C (75 MHz) in CDCl₃ (Ito and Lai, 1978)

Position	ECTF21 δ_C	ECTF21 δ_H (nH, m, *J* in Hz)	Marsformoxide B δ_C	Marsformoxide B δ_H (nH, m, *J* in Hz)
1	37.9	/	37.9	/
2	23.2	/	23.2	/
3	80.1	4.50 (1H, dd, *J* = 10.6, 5.7 Hz)	80.7	4.50 (1H, dd, *J* =10.0, 6.5 Hz)
4	37.6	/	37.6	/
5	54.7	/	54.7	/
6	18.8	/	18.8	/
7	33.2	/	33.2	/
8	38.9	/	38.9	/
9	51.8	/	51.8	/
10	37.5	/	37.5	/
11	53.4	3.09 (1H, t, *J* = 5.1 Hz)	53.4	3.09 (1H, dd, *J* = 5.0, 5.7 Hz)
12	58.1	2.78 (1H, d, *J* = 4.6Hz)	58.1	2.77 (1H, d, *J* = 5.0 Hz)
13	36.6	/	36.6	/
14	157.1	/	157.1	/
15	118.9	5.52 (1H, dd, *J* = 8.2, 3.3 Hz),	118.9	5.51 (1H, dd, *J* = 8.0, 4.6 Hz)
16	35.2	/	35.2	/
17	35.3	/	35.4	/
18	48.3	/	48.1	/
19	40.2	/	40.2	/
20	28.7	/	28.7	/
21	36.5	/	36.5	/
22	38.2	/	38.2	/
23	27.9	0.94 (3H, s)	27.9	0.96 (3H, s)

24	17.0	0.98 (3H, s)	17.0	1.02 (3H, s)
25	16.6	0.88 (3H, s)	16.5	0.91 (3H, s)
26	27.0	1.06 (3H, s)	27.0	1.10 (3H, s)
27	30.2	1.08 (3H, s)	30.2	1.12 (3H, s)
28	29.9	0.85 (3H, s)	29.8	0.88 (3H, s)
29	33.7	0.80 (3H, s)	33.7	0.80 (3H, s)
30	19.5	0.84 (3H, s)	19.5	0.84 (3H, s)
OAc	170.9	/	170.8	/
Me(OAc)	21.3	2.03 (3H, s)	21.3	2.04 (3H, s)
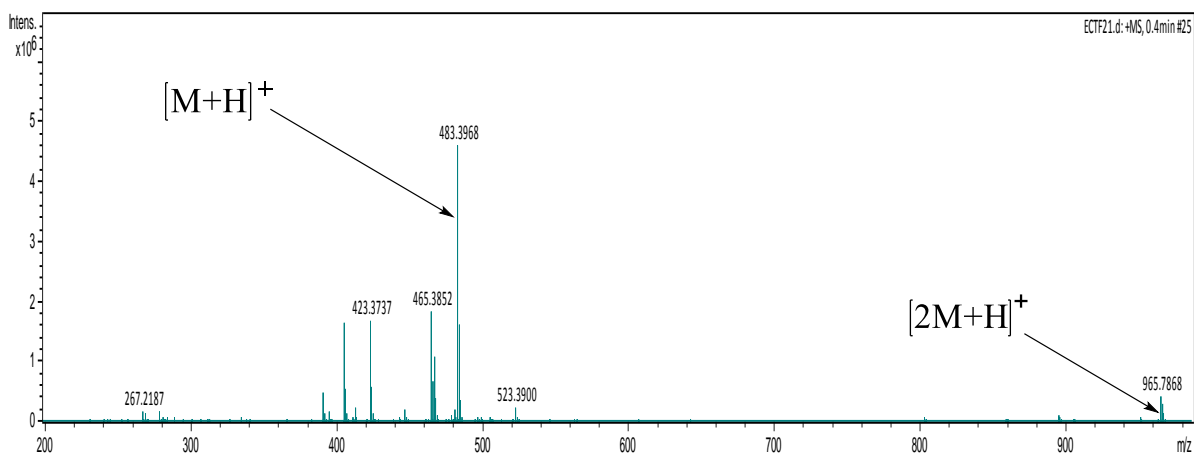
Figure 41: HR-ESI-MS spectrum of compound ECTF21
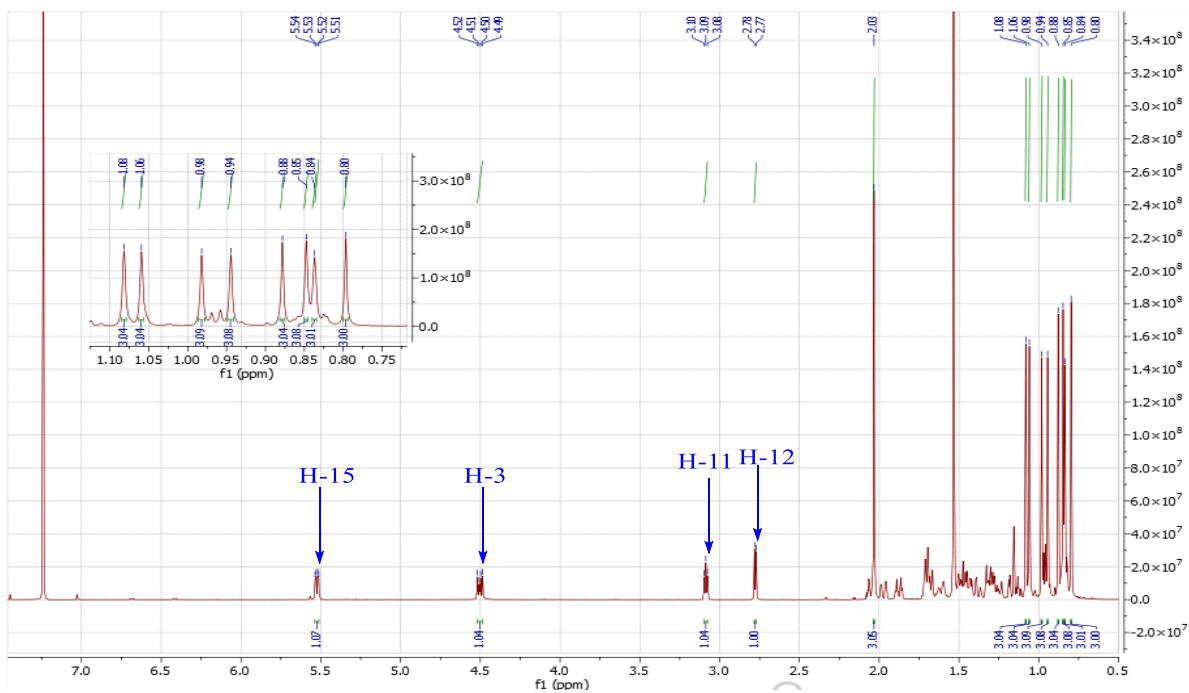
Figure 42: ^{1}H NMR spectrum (CDCl$_3$, 500 MHz) of compound ECTF21
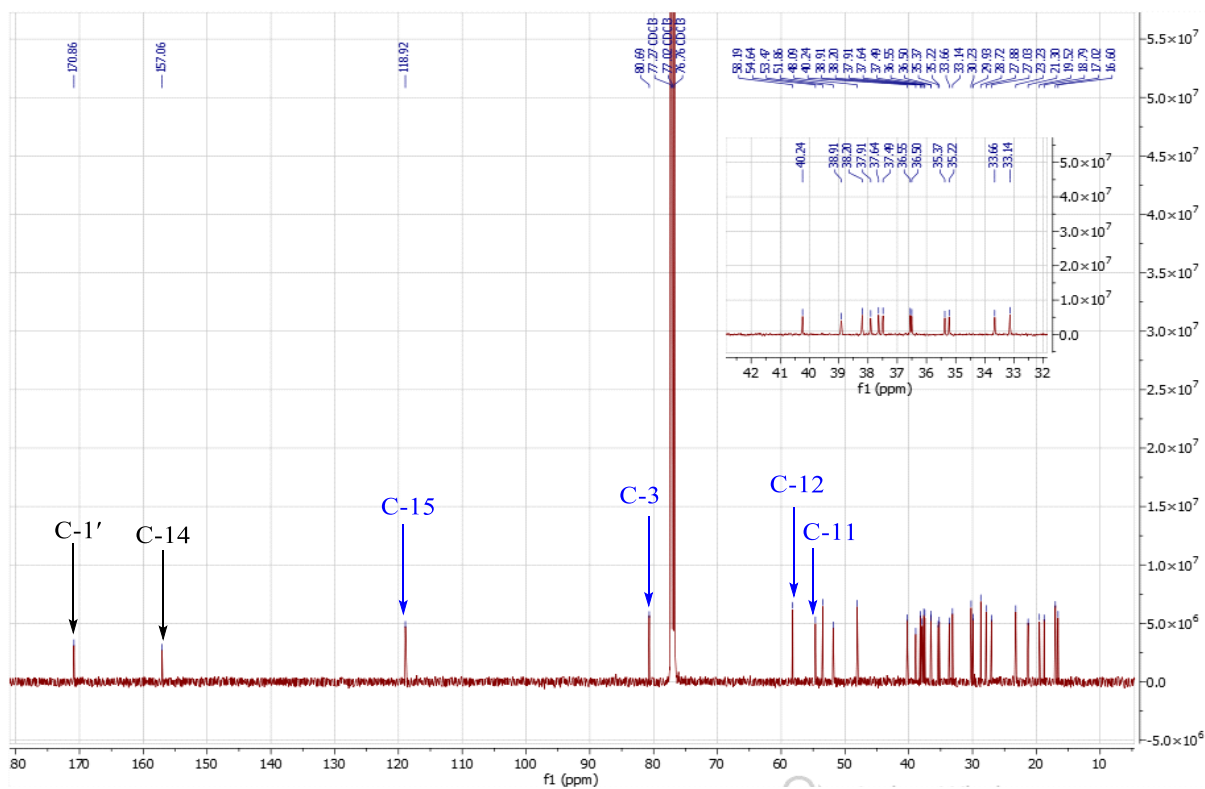
Figure 43: ^{13}C NMR spectrum (CDCl$_3$, 125 MHz) of compound ECTF21
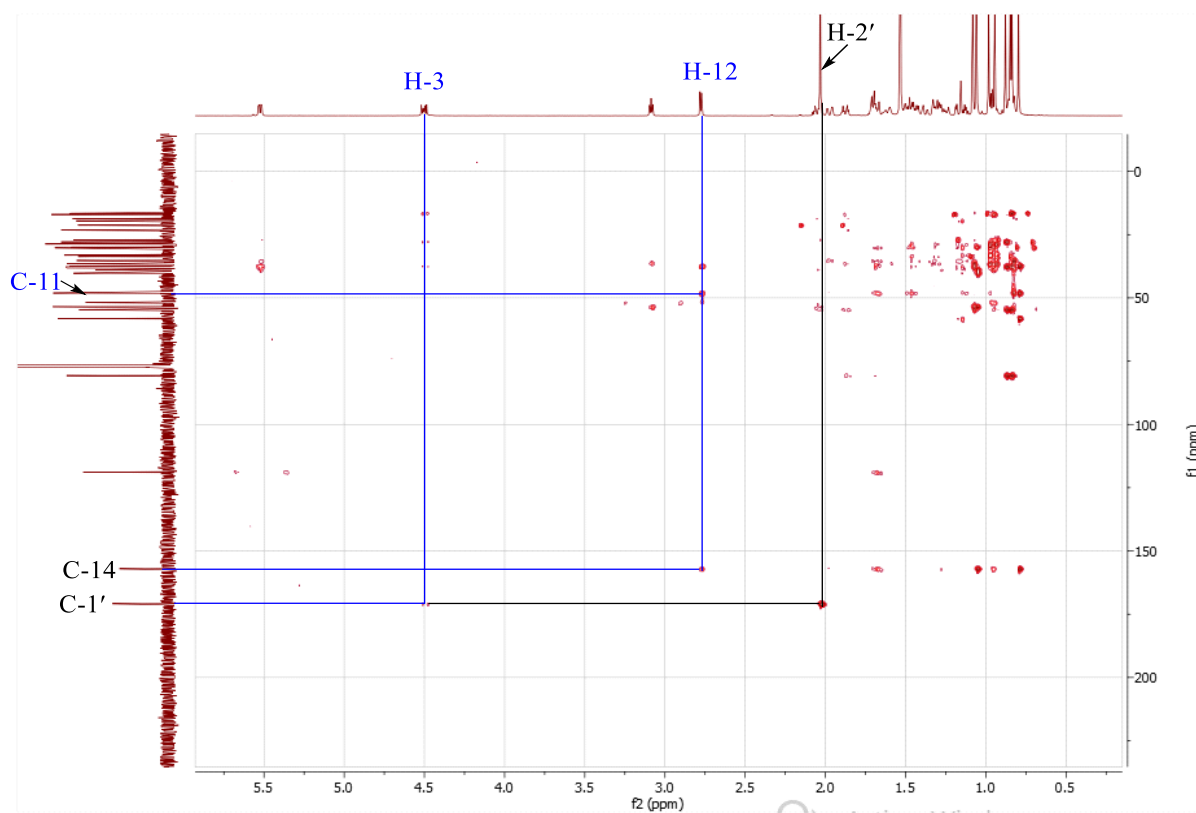
Figure 44: HMBC spectrum of compound ECTF21
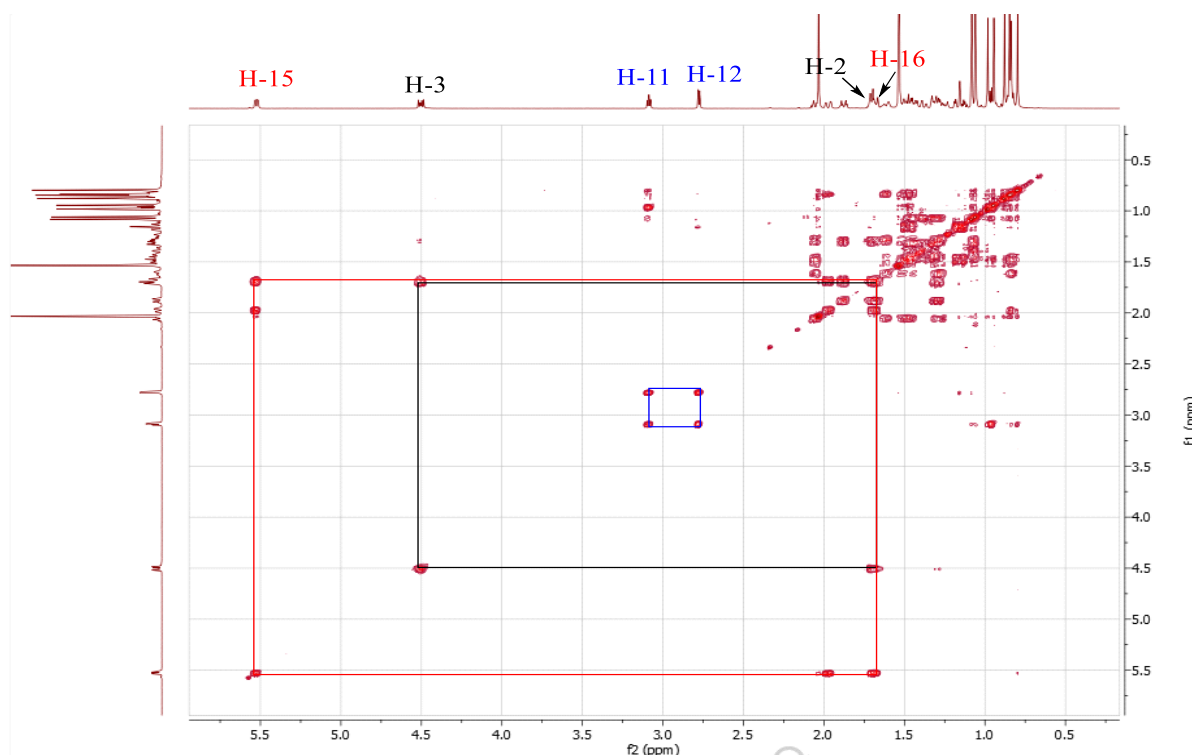
Figure 45: COSY spectrum of compound ECTF21

II.2.1.2.6 Identification of ECF23

ECF23 was obtained as a white amorphous solid. It is soluble in chloroform and reacts positively to the Liebermann-Burchard test, characteristic of triterpenes.

Its high resolution HR-ESI (+) mass spectrum (Figure 46) shows the peak of the protonated ion $[M+H]^+$, at *m/z* 427.3959 corresponding to the molecular formula $C_{30}H_{51}O$ (calculated for 427.3940), containing 6 degrees of unsaturation.
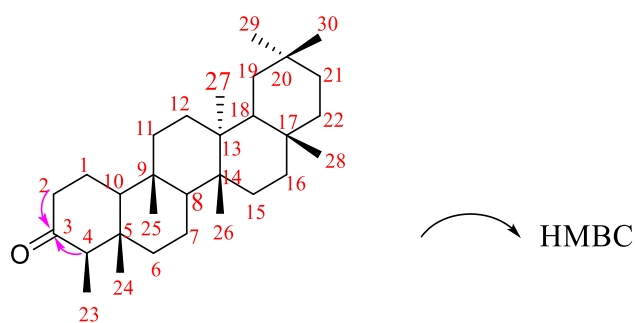
Its ^1H NMR spectrum (Figure 47), exhibited among others signals singlets of eight angular methyl protons at δ_H 1.11; 0.98; 0.95; 0.92; 0.85; 0.85; 0.81 and 0.77; a doubled doublet attributable to the H-3 proton of the triterpene backbone at δ_H 3.20 (1H, dd, *J* = 11.0; 4.4 Hz); and an olefinic proton attributable to a triplet at δ_H 5.16 (1H, t, *J* = 3.6 Hz).

The ^{13}C NMR spectrum (Figure 48) of ECF23 shows the signals of 30 carbon atoms amongst which those at δ_C 79.0 (C-3), 121.7 (C-12) and 145.2 (C-13).

The number of carbon atoms as well as the signals of the ethylenic carbons at δ_C 121.7 and 145.2 indicated that ECF23 is a triterpene belonging to the olean-12-ene series (Mahato and Kundu, 1994).

The spectroscopic data of ECF23 compared to those of the literature (Table XXV), coupled to its TLC profile with available *β*-amyrin, made it possible to identified ECF23 to *β*-amyrin (**60**), already isolated from *Alstonia boonei* (Okoye *et al.*, 2014).
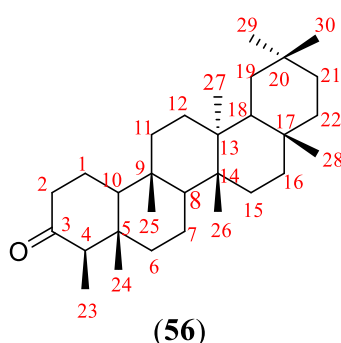
(**60**)
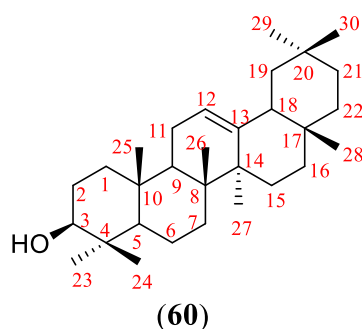
Table XXV: Spectral data of ^{1}H (500 MHz) and ^{13}C (125 MHz) of ECF23 in CDCl$_3$, compared to that of *β*-amyrin ^{1}H (400 MHz) and ^{13}C (100 MHz) in CDCl$_3$ (Okoye *et al.*, 2014)

| Position	ECF23		*β*-amyrin	
	δ_C	δ_H (nH, m, *J* in Hz)	δ_C	δ_H (nH, m, *J* in Hz)
1	38.8	/	38.8	/
2	27.3	/	27.4	/
3	79.0	3.20 (1H, dd, *J* = 11.0, 4.4 Hz)	79.2	3.20 (1H, dd, *J* = 11.5, 4.4 Hz)
4	39.8	/	39.9	/
5	55.2	/	55.4	/
6	18.4	/	18.6	/
7	32.7	/	32.8	/
8	39.8	/	40.2	/
9	47.2	/	47.4	/
10	37.2	/	37.2	/
11	23.5	/	23.8	/
12	121.7	5.16 (1H, t, *J* = 3.6 Hz)	121.9	5.16 (1H, t, *J* = 3.5 Hz)
13	145.2	/	145.4	/
14	41.7	/	41.9	/
15	26.2	/	26.4	/
16	26.9	/	27.1	/
17	32.5	/	32.7	/
18	47.6	/	47.8	/
19	46.8	/	47.0	/
20	31.1	/	31.3	/
21	37.2	/	37.4	/
22	34.7	/	34.9	/
23	15.5	0.77 (3H, s)	15.7	0.77 (3H, s)
24	28.1	0.98 (3H, s)	28.3	0.98 (3H, s)
25	15.6	0.92 (3H, s)	15.8	0.92 (3H, s)
26	16.8	0.95 (3H, s)	17.0	0.94 (3H, s)
27	26.0	1.11 (3H, s)	26.2	1.11 (3H, s)
28	28.4	0.81 (3H, s)	28.6	0.81 (3H, s)
29	33.4	0.85 (3H, s)	33.6	0.85 (3H, s)
30	23.7	0.85 (3H, s)	23.9	0.85 (3H, s)
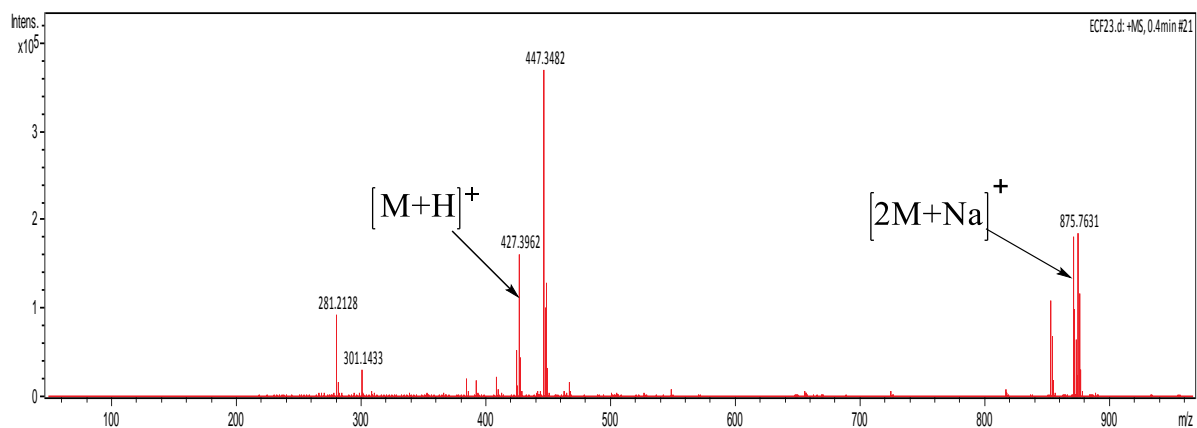
Figure 46: HR-ESI-MS spectrum of compound ECF23
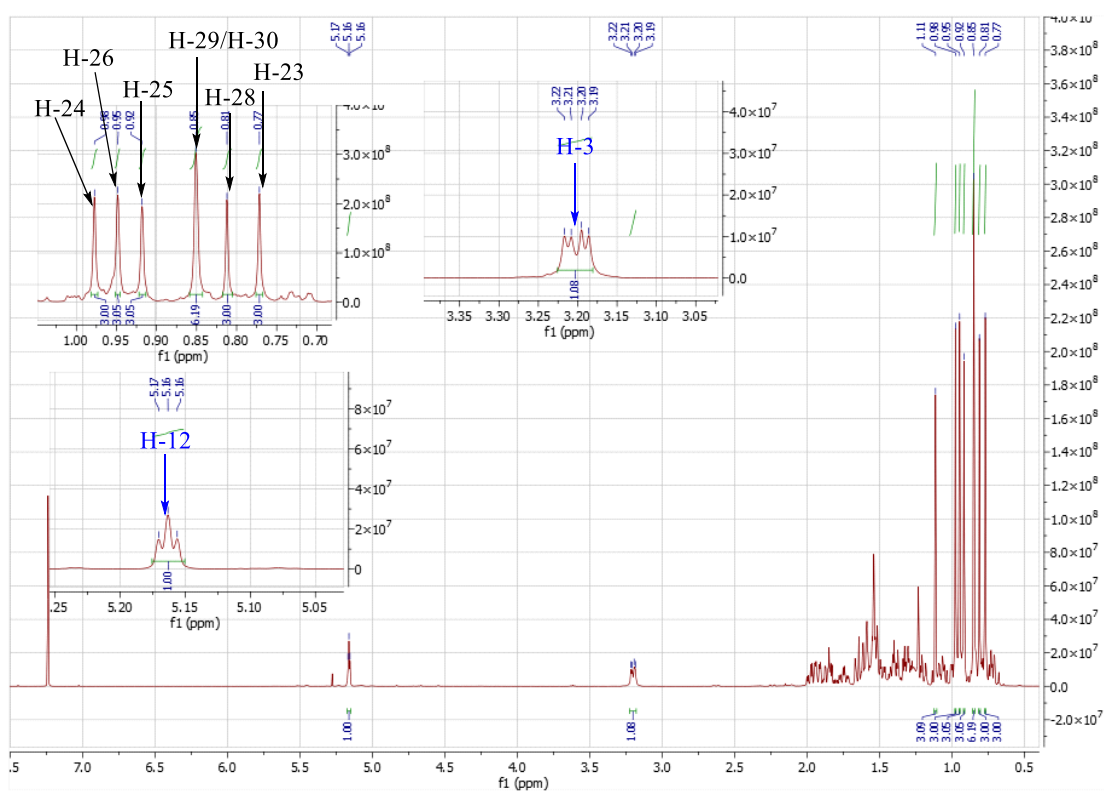
Figure 47: ¹H NMR spectrum (CDCl₃, 500 MHz) of compound ECF23
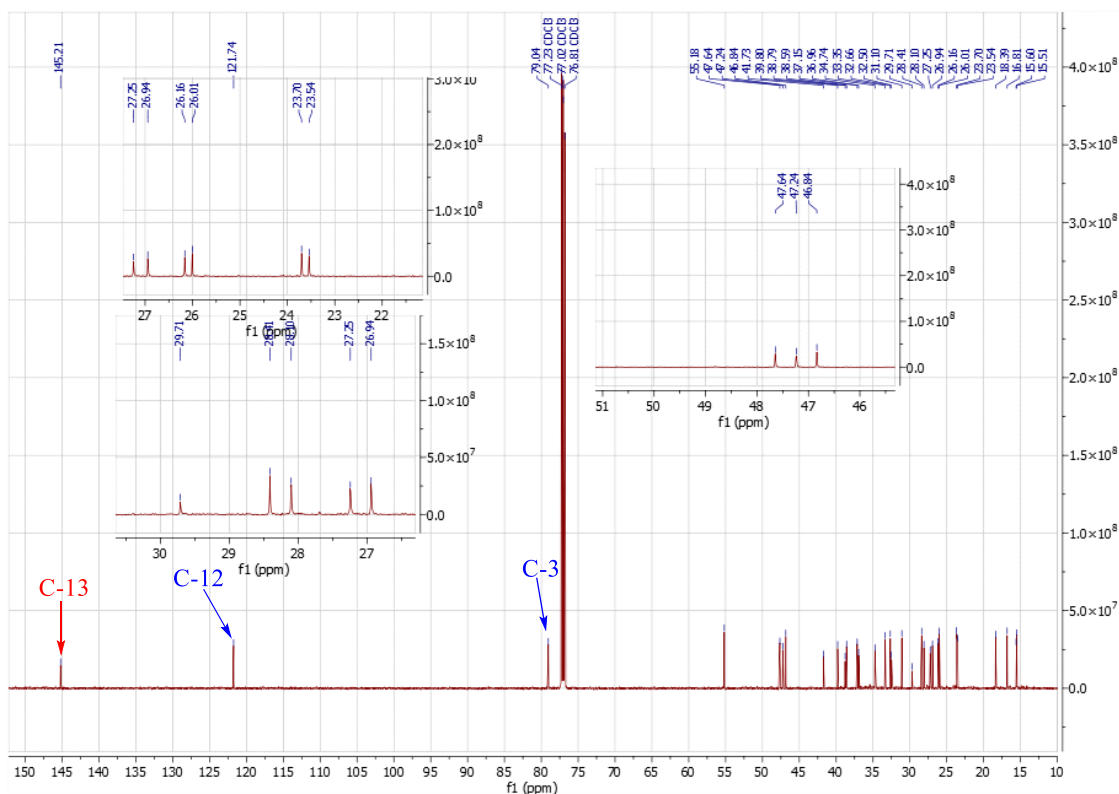
Figure 48: ^{13}C NMR spectrum (CDCl$_3$, 125 MHz) of compound ECF23

II.2.1.2.7 Identification of EC1

EC1 was obtained as a white amorphous solid. It is soluble in chloroform and reacts positively to the Liebermann-Burchard test, characteristic of triterpenes.

Its high resolution HR-ESI (+) mass spectrum (Figure 49) shows the peak of the sodium adduct [M+Na]$^+$, at *m/z* 687.6160 corresponding the molecular formula C$_{46}$H$_{80}$O$_2$Na (calculated for 687.6051), containing 7 degrees of unsaturation.

Its ^{1}H NMR spectrum (Figure 50), exhibited among others signals singlets of eight angular methyl protons at δ_H 1.16, 0.99, 0.99, 0.91, 0.89, 0.89, 0.86 and 0.85, a signal attributable to the H-3 proton of the triterpene backbone at δ_H 4.53 (1H, m); and an olefinic proton attributable to the H-12 proton at δ_H 5.21 (1H, t, J = 3.5 Hz). In addition, signals alkyl chain at δ_H 2.32 (2H, m), 1.28 (26H, m) and 0.90 (3H, m).

The ^{13}C NMR spectrum (Figure 51) of EC1 shows the signals of 46 carbon atoms, which were distinguished using the HSQC technique (Figure 52) into: two olefinic carbons at δ_C 121.7 (C-12) and 145.2 (C-13), one tertiary carbon signal at δ_C 80.6 (C-3), one quaternary carbon signal at δ_C 173.7 attributed to –C=O of fatty acid. The signal at δ_C 29.2-29.7 is assigned as (CH$_2$)$_{13}$ carbon signal of the fatty acid.

The junction of the fatty acid fragment at C-3 was established follow the correlations observed on its HMBC spectrum (Figure 53, scheme 17) where correlations from the proton at δ_H 4.53 (H-3) and the carbons at δ_C 173.7 (C-1′) and 16.8 (C-24) were observed.

HMBC — COSY
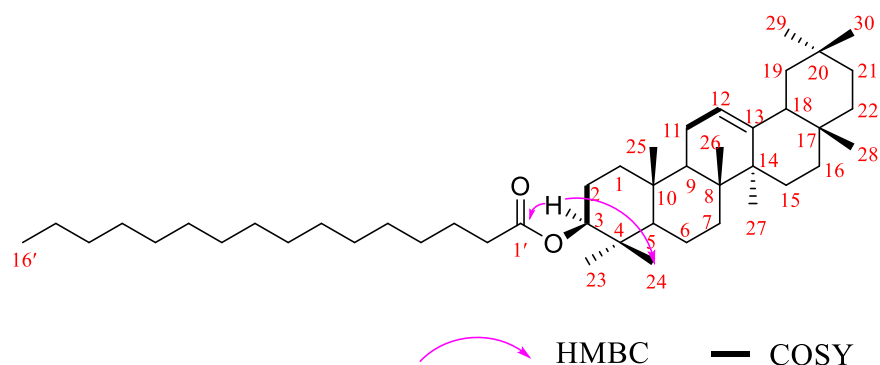
Scheme 17: Selected HMBC and COSY correlations of compound EC1

All these spectral data compared to that described in the literature (Table XXVI) allow us to attribute to **EC1** the structure (**61**), which is that of *β*-amyrin palmitate previously isolated from fruit of *Ficus aurata* by Nurhamidah and collaborators (2016).

(**61**)
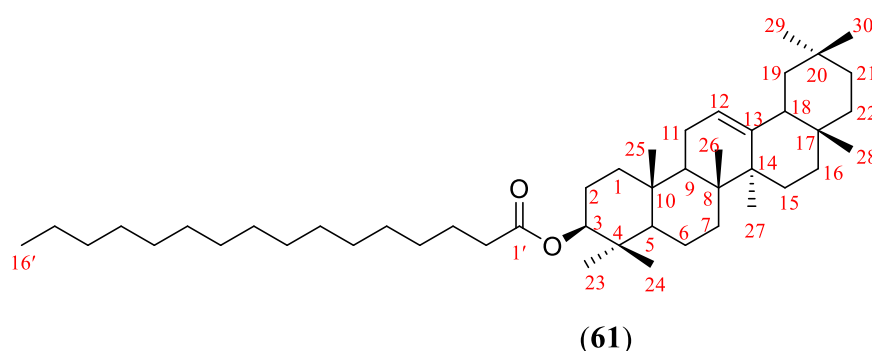
Table XXVI: Spectral data of ^{1}H (500 MHz) and ^{13}C (125 MHz) of EC1 in CDCl₃, compared to that of *β*-amyrin palmitate ^{1}H (400 MHz) and ^{13}C (100 MHz) in CDCl₃ (Nurhamidah *et al.*, 2016).

Position	EC1		*β*-amyrin palmitate	
	δ_C	δ_H (nH, m, *J* in Hz)	δ_C	δ_H (nH, m, *J* in Hz)
1	38.3	/	38.5	/
2	23.7	/	23.8	/
3	80.6	4.53 (1H, m)	80.8	4.50 (1H, t)
4	37.8	/	38.0	/
5	55.3	/	55.5	/
6	18.3	/	18.5	/
7	32.6	/	32.8	/
8	39.8	/	40.0	/
9	46.7	/	47.8	/
10	36.9	/	37.1	/
11	23.6	/	23.7	/
12	121.7	5.21 (1H, t, *J* = 3.5 Hz)	121.5	5.18 (1H, t)
13	145.2	/	145.4	/
14	41.7	/	41.9	/
15	26.9	/	27.1	/
16	26.1	/	26.3	/
17	32.6	/	32.7	/
18	47.6	/	47.4	/
19	46.8	/	47.0	/
20	31.1	/	31.3	/
21	34.9	/	35.1	/
22	37.2	/	37.3	/
23	28.4	0.89 (3H, s)	28.6	0.87 (3H, s)
24	15.4	0.85 (3H, s)	17.0	0.86 (3H, s)
25	15.6	0.99 (3H, s)	15.7	0.97 (3H, s)
26	16.8	0.91 (3H, s)	17.0	0.95 (3H, s)
27	26.1	1.16 (3H, s)	26.2	1.12 (3H, s)
28	28.4	0.89 (3H, s)	28.3	0.87 (3H, s)
29	33.3	0.89 (3H, s)	33.5	0.87 (3H, s)
30	23.7	0.86 (3H, s)	23.9	0.86 (3H, s)
1′	173.7	/	173.9	/
2′	34.9	2.31 (2H, m)	34.9	2.29 (2H, t)
3′	25.2	/	25.4	/
4′-13′	29.2-29.7	(20H, m)	29.4-29.9	(20H, m)
14′	31.9	/	32.1	/
15′	22.7	/	22.9	/
16′	14.1	0.90 (3H, m)	14.3	0.89 (3H, m)
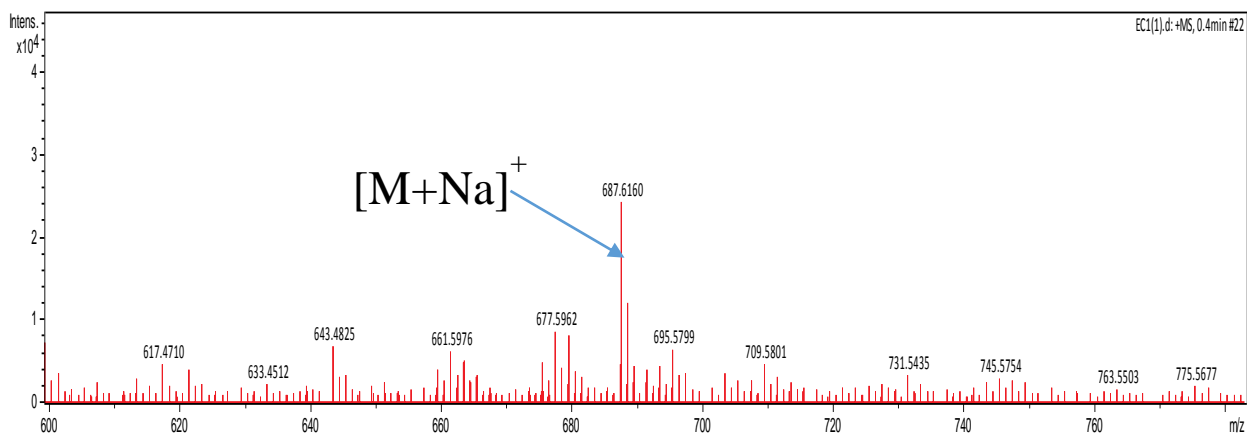
Figure 49: HR-ESI-MS spectrum of compound EC1
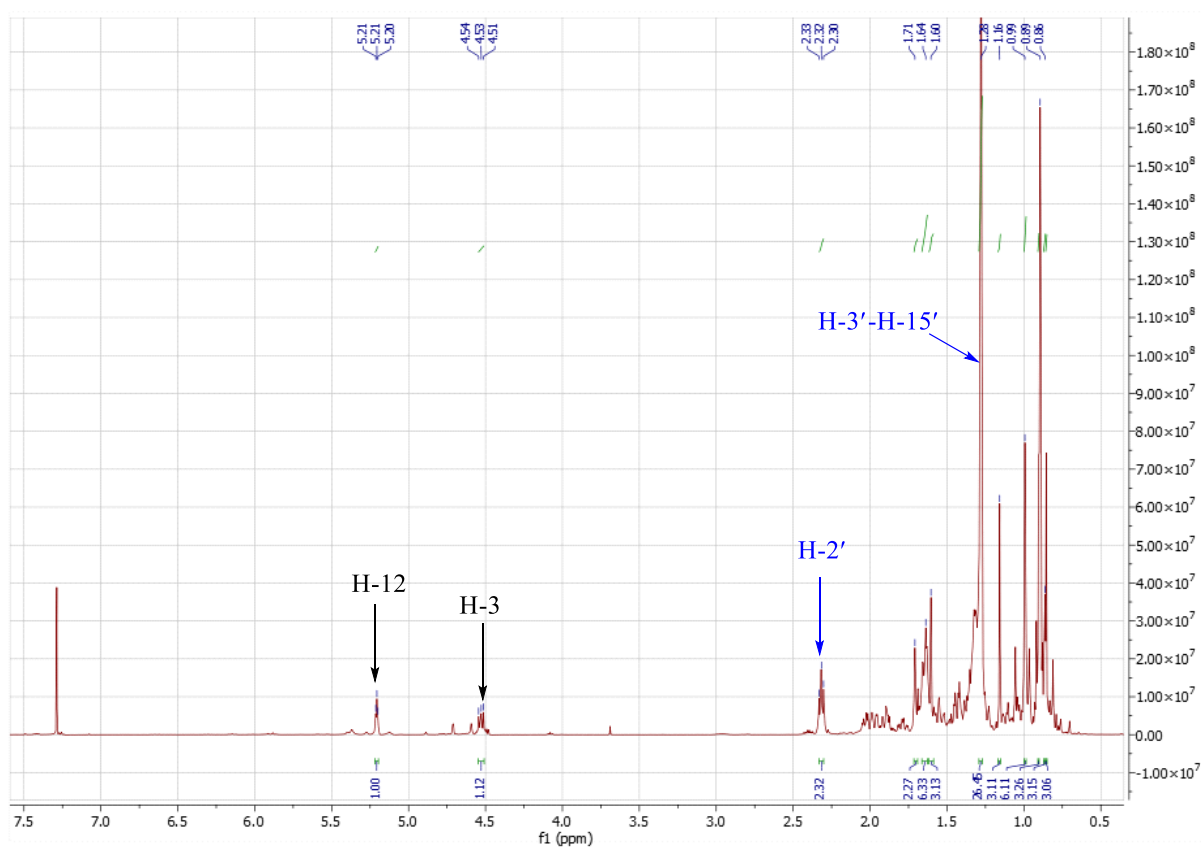
Figure 50: ^{1}H NMR spectrum (CDCl$_3$, 500 MHz) of compound EC1
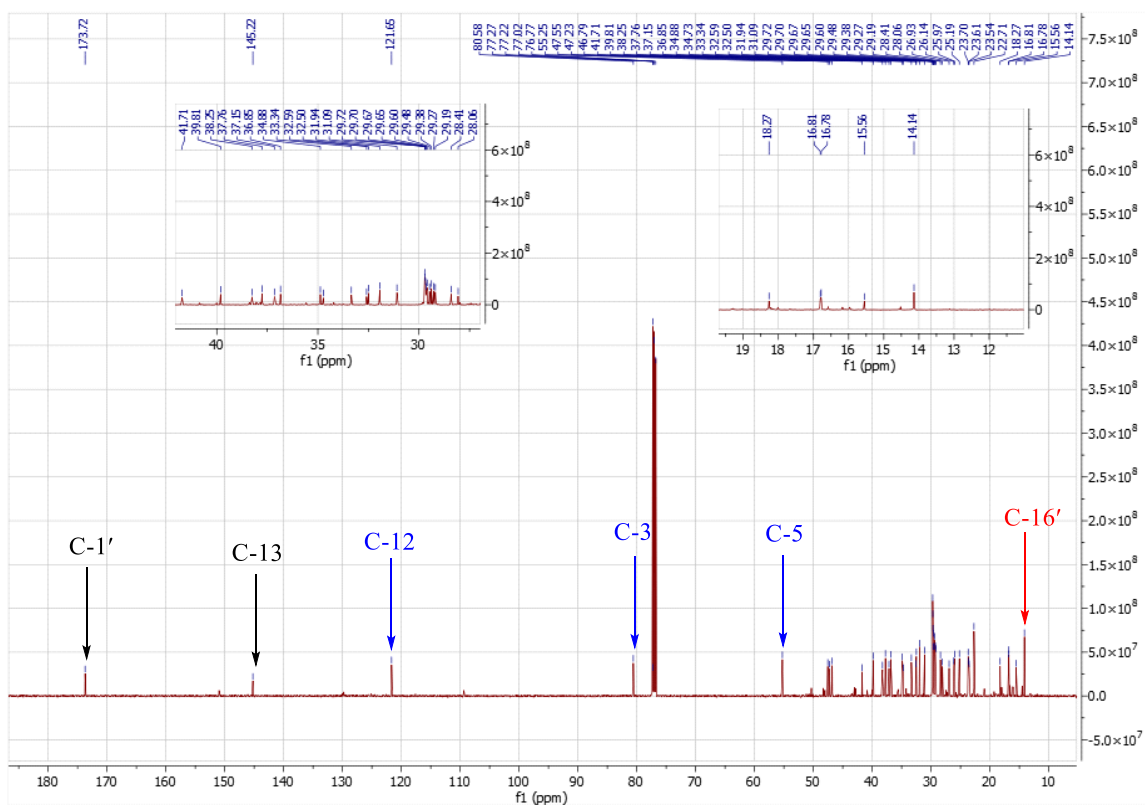
Figure 51: ¹³C NMR spectrum (CDCl₃, 125 MHz) of compound EC1
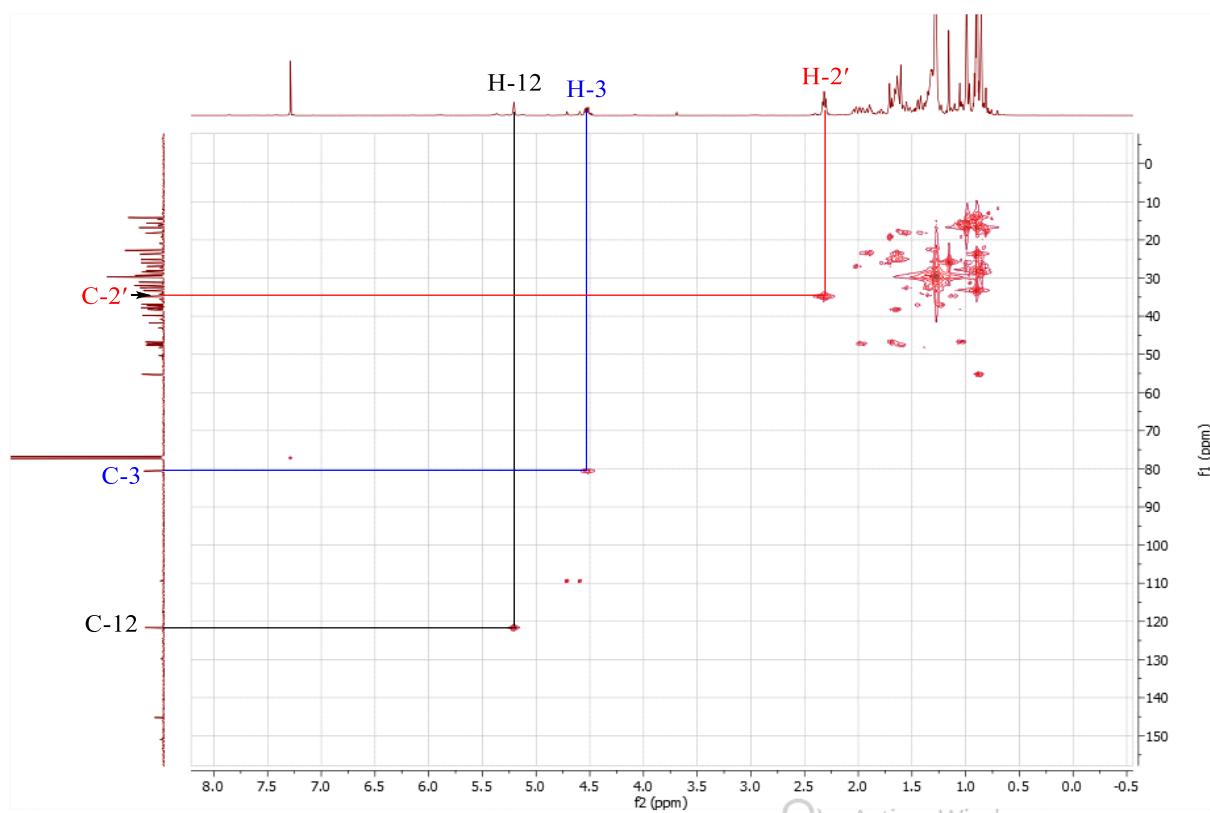
Figure 52: HSQC spectrum of compound EC1
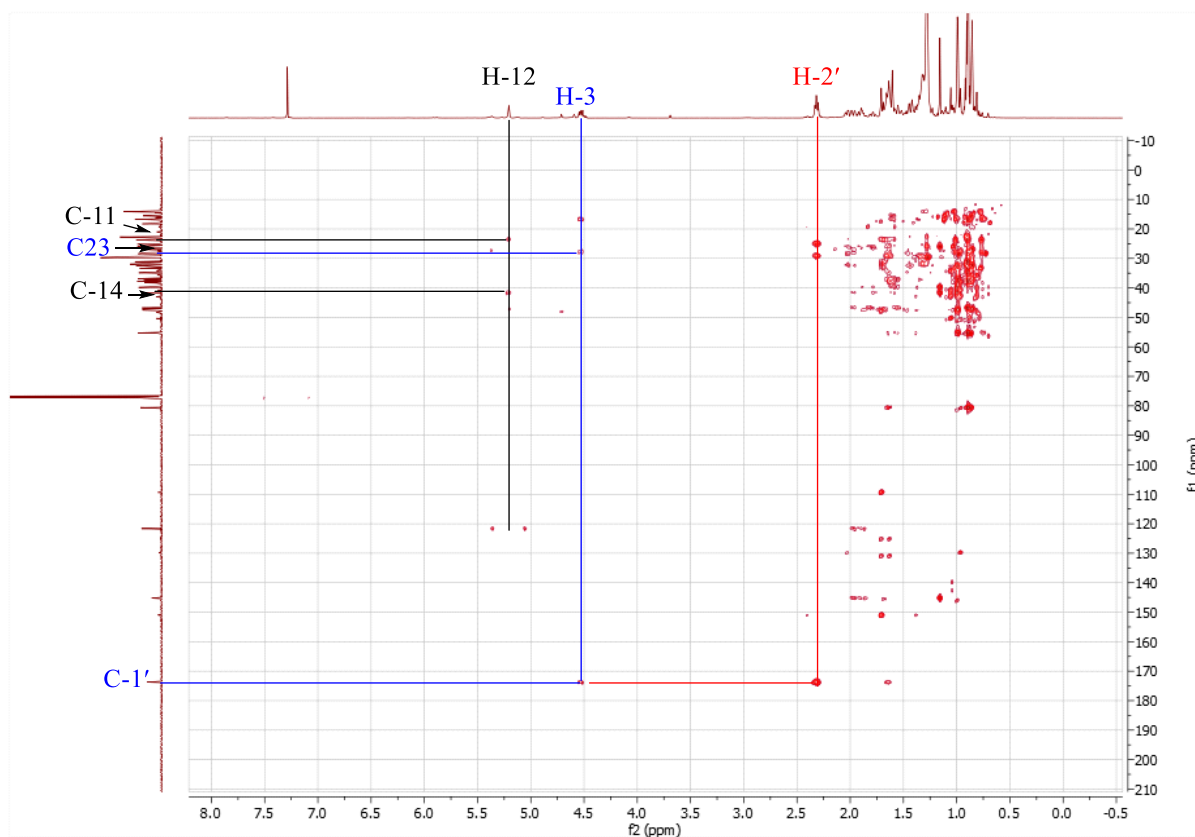
Figure 53: HMBC spectrum of compound EC1
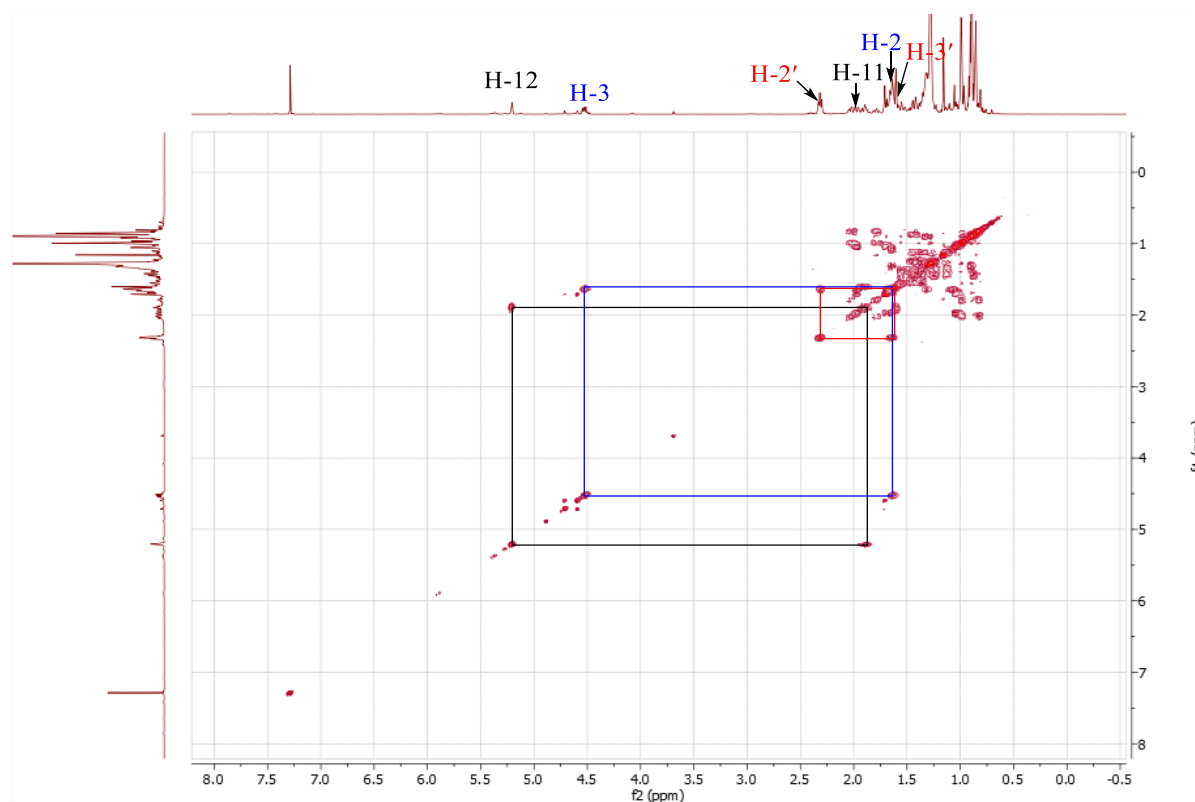
Figure 54: COSY spectrum of compound EC1

II.2.1.2.8 Identification of ECF1

Compound ECF1 was obtained as a white solid. It is soluble in chloroform and reacts positively to the Liebermann-Burchard test, reflecting its terpenoid nature.

Its ^{1}H NMR spectrum (Figure 55), from strong fields to weak fields, exhibited the following signals:

- six singlets of 3H each at δ_H 0.74, 0.77, 0.81, 0.92, 0.95 and 1.01 corresponding to the six angular methyl protons;

- a singlet of 3H at δ_H 1.66, characteristic of vinyl methyl;

- a doubled doublet of a proton at δ_H 3.17 (1H, dd, J = 11.4, 4.9) probably geminated to the hydroxyl group attach biogenetically to C-3;

- two doublets of exomethylene at δ_H 4.54 (1H, d, J = 2.3 Hz) and 4.67 (1H, d, J = 2.2 Hz).

Its ^{13}C NMR spectrum (56) shows the signals of 30 carbon atoms among which those at 151.0 (C-20) and 109.3 (C-29) characteristic of pentacyclic triterpenes of the lupane series (Mahato and Kundu, 1994).

The spectroscopic data of ECF1 compared to those of the literature (Table XXVII), allowed us to attributed the structure (**62**), which is that of lupeol already isolated from the stem bark of *Crataeva nurvala* (Haque *et al*., 2008).

(**62**)
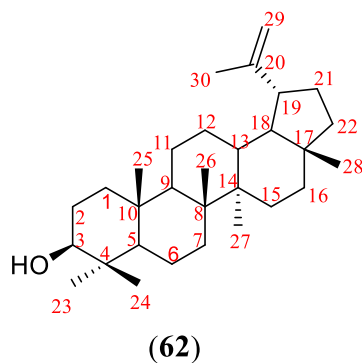
TableXXVII: Spectral data of ^{1}H (500 MHz) and ^{13}C (125 MHz) of ECF1 in CDCl$_3$, compared to that of lupeol ^{1}H (200.13 MHz) and ^{13}C (50.032 MHz) in CD$_3$OD (Haque *et al.*, 2008)

Position	ECF1		lupeol	
	δ_C	δ_H (nH, m, *J* in Hz)	δ_C	δ_H (nH, m, *J* in Hz)
1	38.1	/	38.0	/
2	27.4	/	27.4	/
3	79.0	3.17 (1H, dd, *J* = 11.4, 4.9 Hz)	78.0	3.18 (1H, dd, *J* = 9.6, 6.2 Hz)
4	38.7	/	38.7	/
5	55.3	/	55.3	/
6	18.3	/	18.3	/
7	34.3	/	34.0	/
8	40.8	/	40.1	/
9	50.4	/	50.4	/
10	37.2	/	37.7	/
11	20.9	/	20.9	/
12	25.4	/	25.1	/
13	38.9	/	38.0	/
14	42.8	/	42.8	/
15	27.5	/	27.4	/
16	35.6	/	35.6	/
17	43.0	/	42.8	/
18	48.3	/	48.2	/
19	48.0	/	48.0	/
20	151.0	/	150.8	/
21	28.5	/	28.5	/
22	40.0	/	40.0	/
23	28.0	0.77 (3H, s)	28.1	0.77 (3H, s)
24	15.4	0.81 (3H, s)	15.4	0.81 (3H, s)
25	16.1	0.92 (3H, s)	16.1	0.90 (3H, s)
26	15.9	0.95 (3H, s)	15.9	0.94 (3H, s)
27	14.6	1.01 (3H, s)	14.6	1.03 (3H, s)
28	18.0	0.74 (3H, s)	18.0	0.74 (3H, s)
29a		4.54 (1H, d, *J* = 2.3 Hz)		4.57 (1H, d, *J* = 2.4 Hz)
	109.3		109.3	
29b		4.67 (1H, d, *J* = 2.2 Hz)		4.67 (1H, d, *J* = 2.4 Hz)
30	19.3	1.66 (3H, s)	19.4	1.66 (3H, brs)
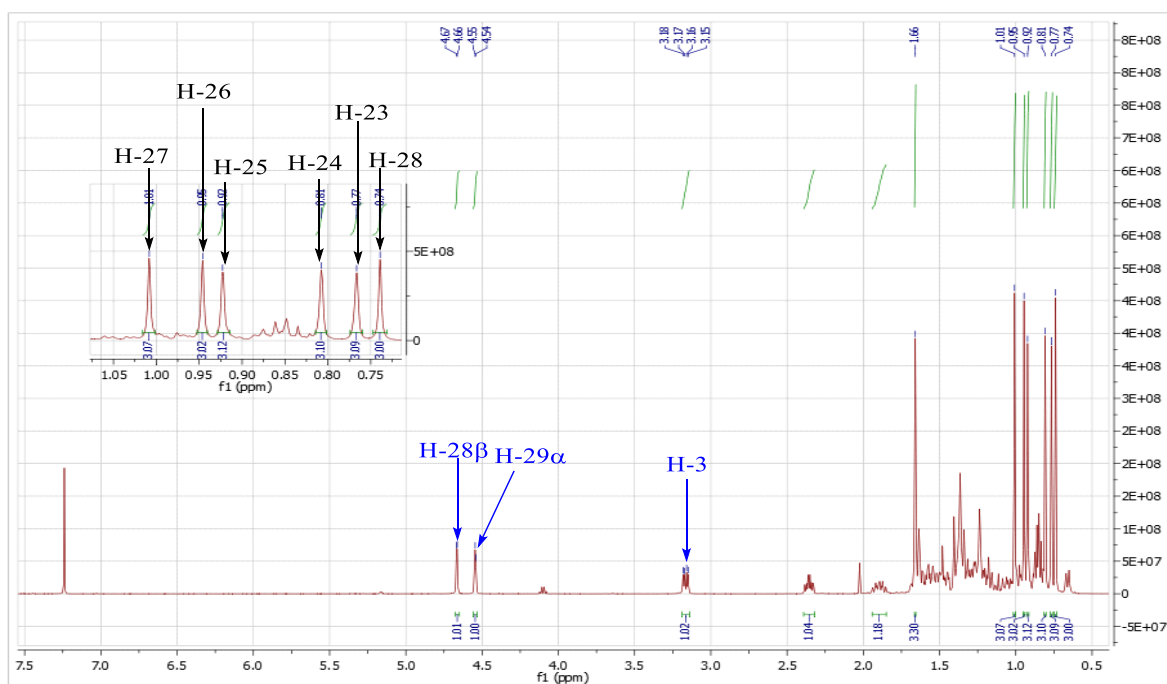
Figure 55: ¹H NMR spectrum (CDCl₃, 500 MHz) of compound ECF1
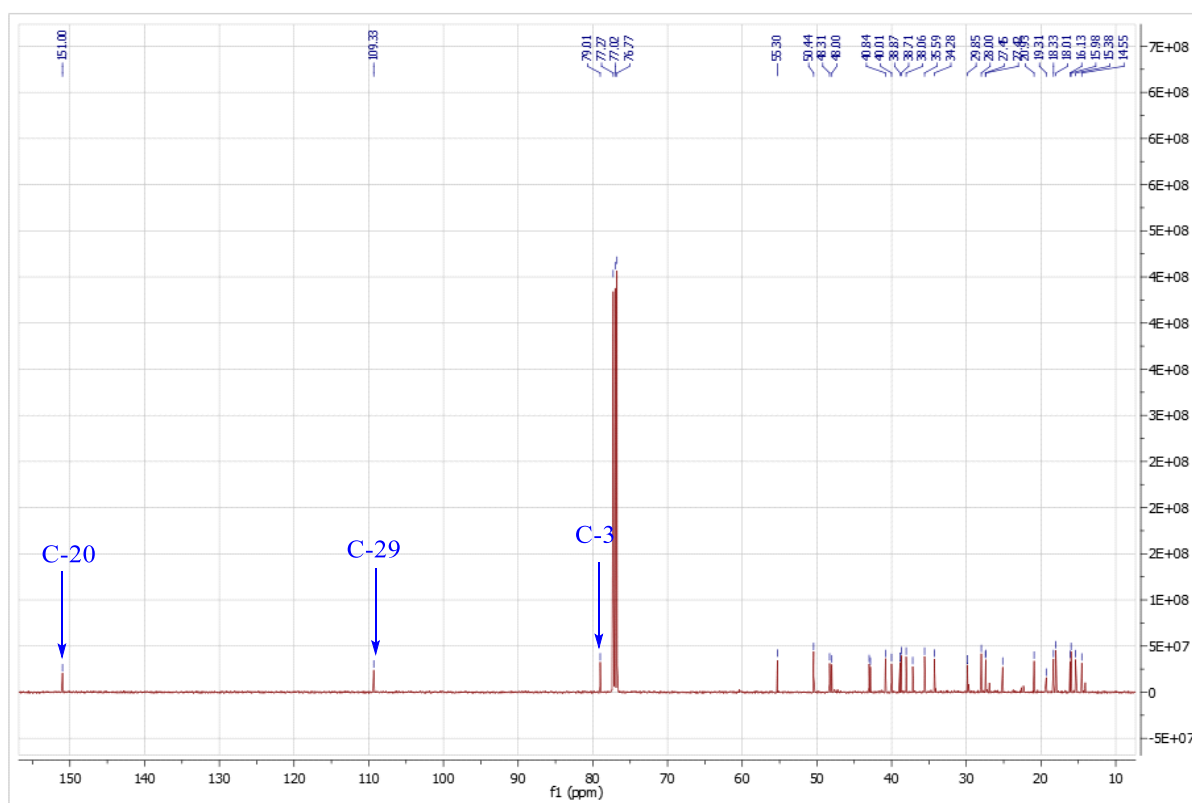
Figure 56: ¹³C NMR spectrum (CDCl₃, 125 MHz) of compound ECF1

II.2.1.2.9 Identification of ECTF23

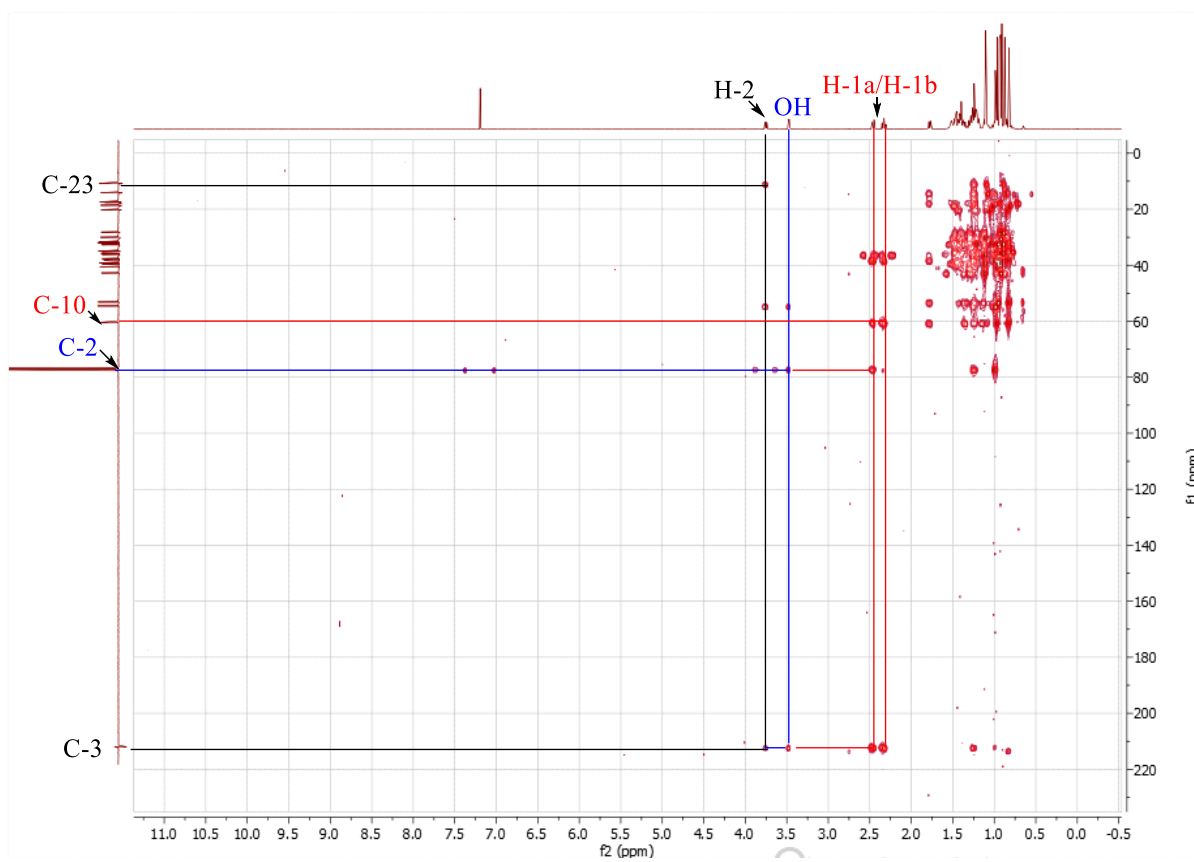Compound ECTF23 was obtained as a white amorphous solid. It is soluble in mchloroform and responds positively to the Liebermann-Burchard test, giving a red coloration, characteristic of triterpenes.

Its HR-ESI (+) mass spectrum (Figure 57) shows the peak of the protonated ion $[M+H]^+$ at m/z 425.3858 (calculated for $C_{30}H_{49}O$ at 425.3859), corresponding to the molecular formula $C_{30}H_{48}O$, containing seven unsaturations.

Its ^{13}C NMR spectrum (Figure 59), signals of 30 carbon atoms were distinguished, and were sorted using the HSQC technique (Figure 60) as:

- seven methyl carbons at δ_C 26.2, 21.1, 19.4, 17.5, 16.5, 16.2 and 15.2;

- five methine carbons at δ_C 54.9, 49.7, 48.8, 47.9 and 36.9;

- eleven methylene carbons including one oxomethylene at δ_C 109.5;

- seven quaternary carbons including one olefinic at δ_C 148.2 and a ketone carbonyl at δ_C 218.2.

Its ^1H NMR spectrum (Figure 58) shows:

- seven singlet signals each integrating for 3 protons at δ_H 0.67, 0.92, 0.93, 1.00, 1.01, 1.06 and 1.66 attributable to the seven methyl protons of the lupane series (Shiojima *et al*., 1995).

- signals of exomethylene at δ_H 4.68 denoting (1H, d, J = 2.5 Hz, H-29a) and at δ_H 4.65 (1H, d, J = 2.5 Hz, H-29b).

All of these data clearly indicate that ECTF23 is a pentacyclic triterpene of the lup-20 (29)-ene type carrying a carbonyl group.

The position of the carbonyl (C=O) was deduced from the correlations observed on the HMBC spectrum (Figure 61), where correlations were observed between:

- the proton at δ_H 1.06 (H-23), 1.01 (H-24) and carbons at δ_C 218.2 (C-3), 47.3 (C-4) and 54.9 (C-5).
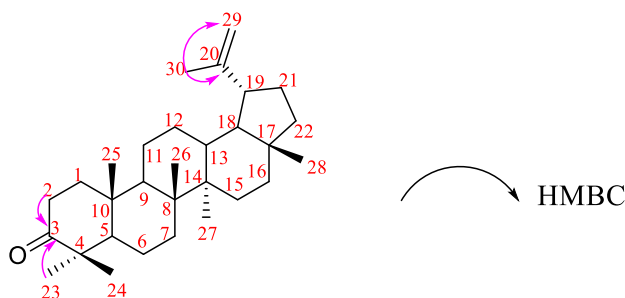
Scheme 18: Selected HMBC correlations of ECTF23

The combination of all these data with compared with those of the literature (table XXVIII) allowed us to attribute to ECTF23 the structure (**63**) which is that of lupenone, isolated previously from the roots of *Picris hieracioides* subsp, *japonica* (Shiojima *et al.*, 1995).

(**63**)
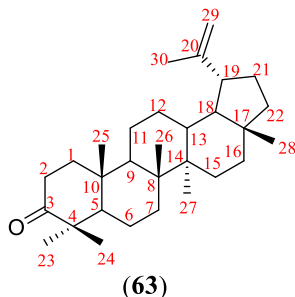
Table XXVIII: Spectral data of ^{13}C (125 MHz) of ECTF23 in CDCl$_3$, compared to that of lupenone ^{13}C (125 MHz) in CDCl$_3$ (Shiojima *et al.,* 1995).

Position	ECTF23	Lupenone
	δ_C	δ_C
1	39.6	39.6
2	34.2	34.2
3	218.2	218.2
4	47.3	47.3
5	54.9	54.9
6	19.7	19.7
7	34.9	33.6
8	40.2	40.8
9	49.7	49.8
10	36.9	36.9
11	21.7	21.5
12	25.4	25.2
13	32.9	32.2
14	44.2	43.0
15	26.6	27.4
16	35.6	35.5
17	42.3	42.9
18	48.8	48.3
19	47.9	48.0
20	148.2	150.9

21	29.7	29.8
22	40.2	39,6
23	26.2	26.7
24	21.1	21.0
25	16.2	16.0
26	16.5	15.8
27	15.2	14.7
28	17.5	18.0
29	109.5	109.4
30	19.4	19.3
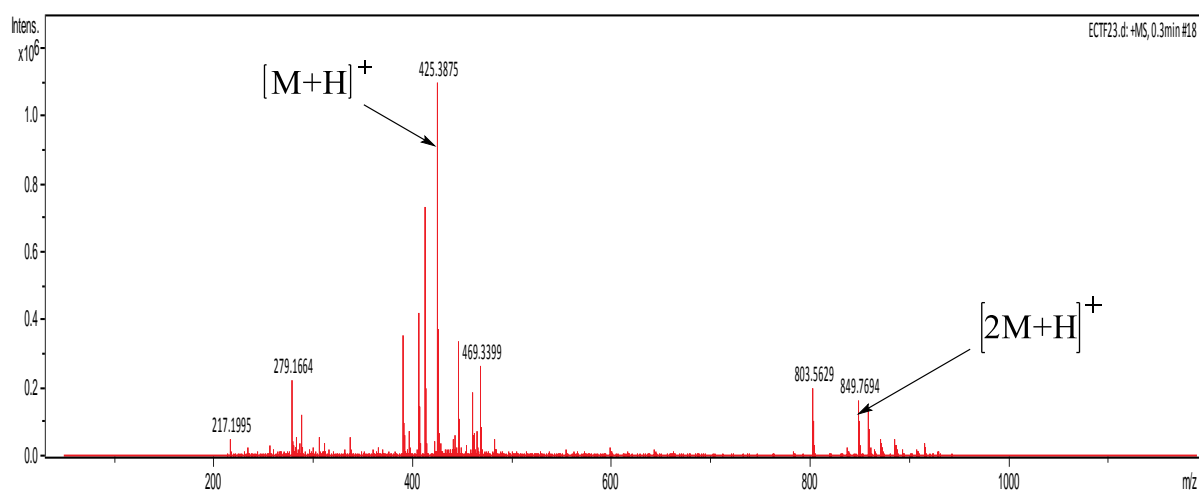
Figure 57: HR-ESI-MS spectrum of compound ECTF23
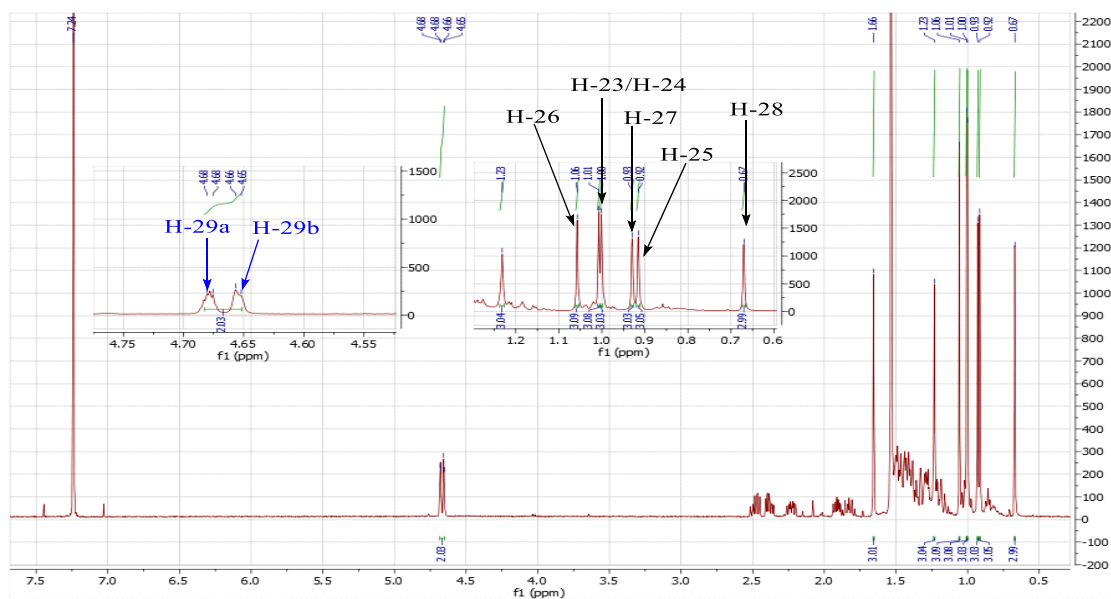
Figure 58: ^{1}H NMR spectrum (CDCl$_3$, 500 MHz) of compound ECTF23
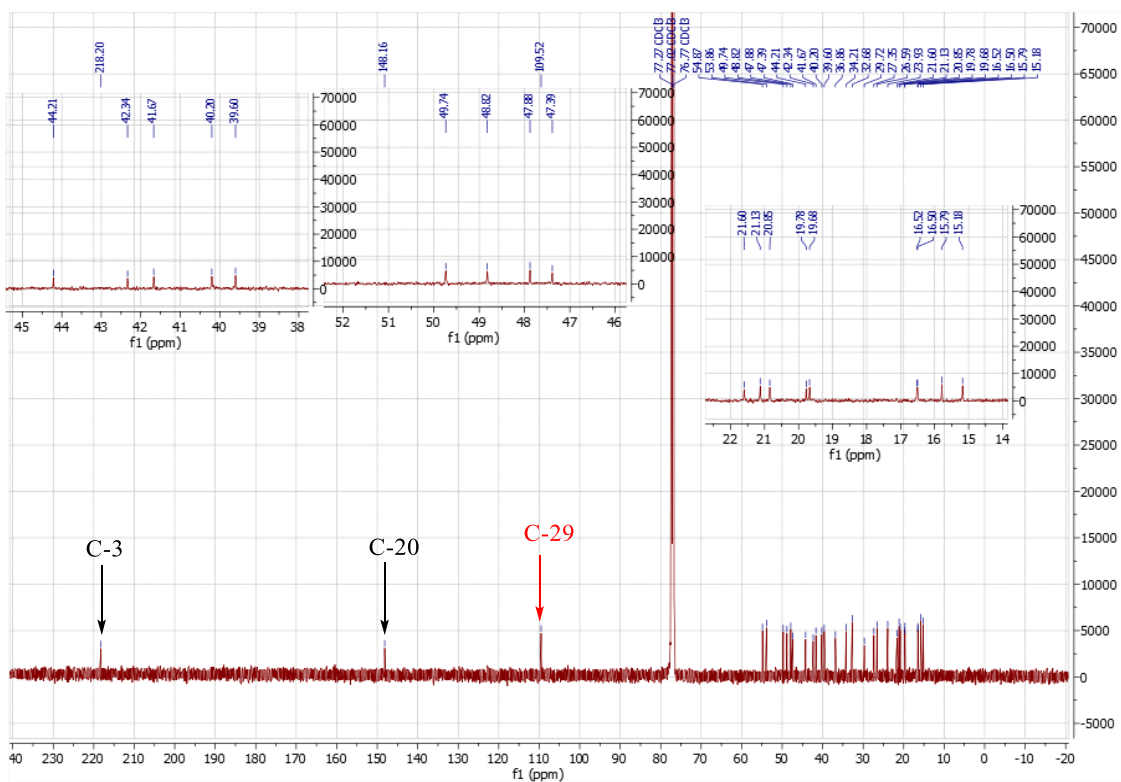
Figure 59: ¹³C NMR spectrum (CDCl₃, 125 MHz) of compound ECTF23
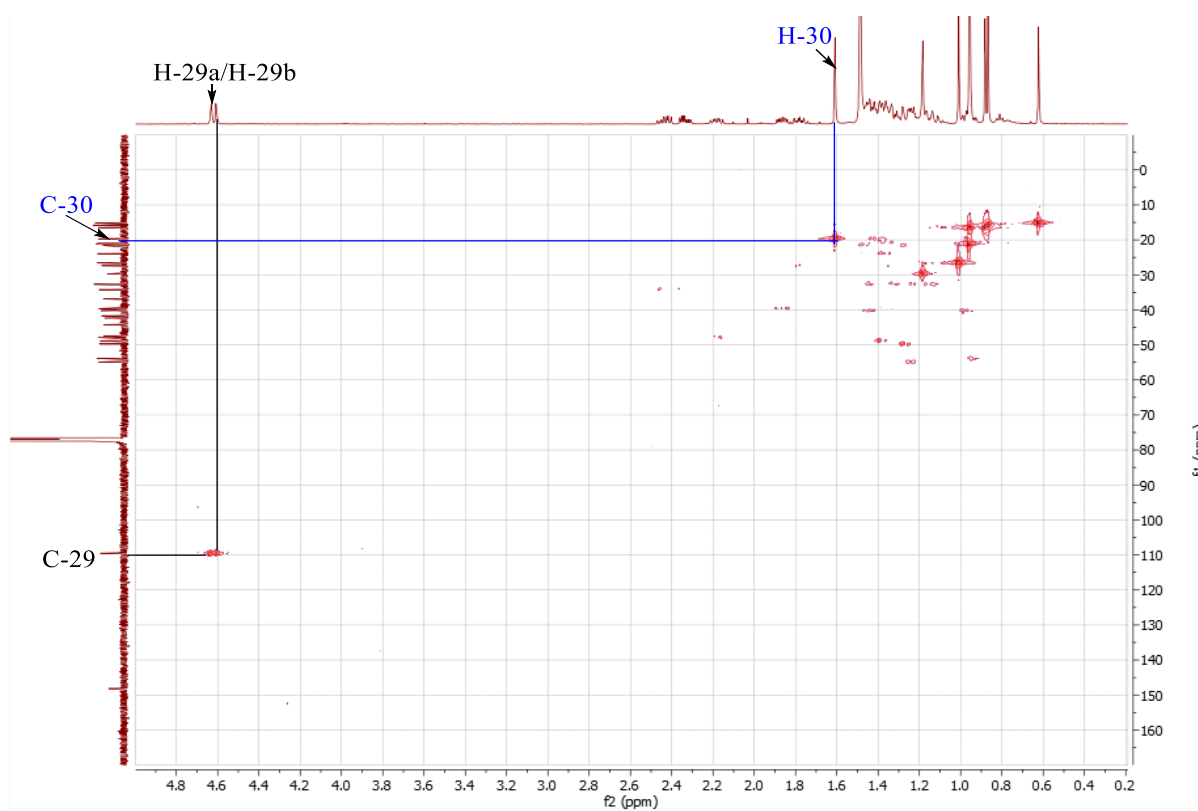
Figure 60: HSQC spectrum of compound ECTF23
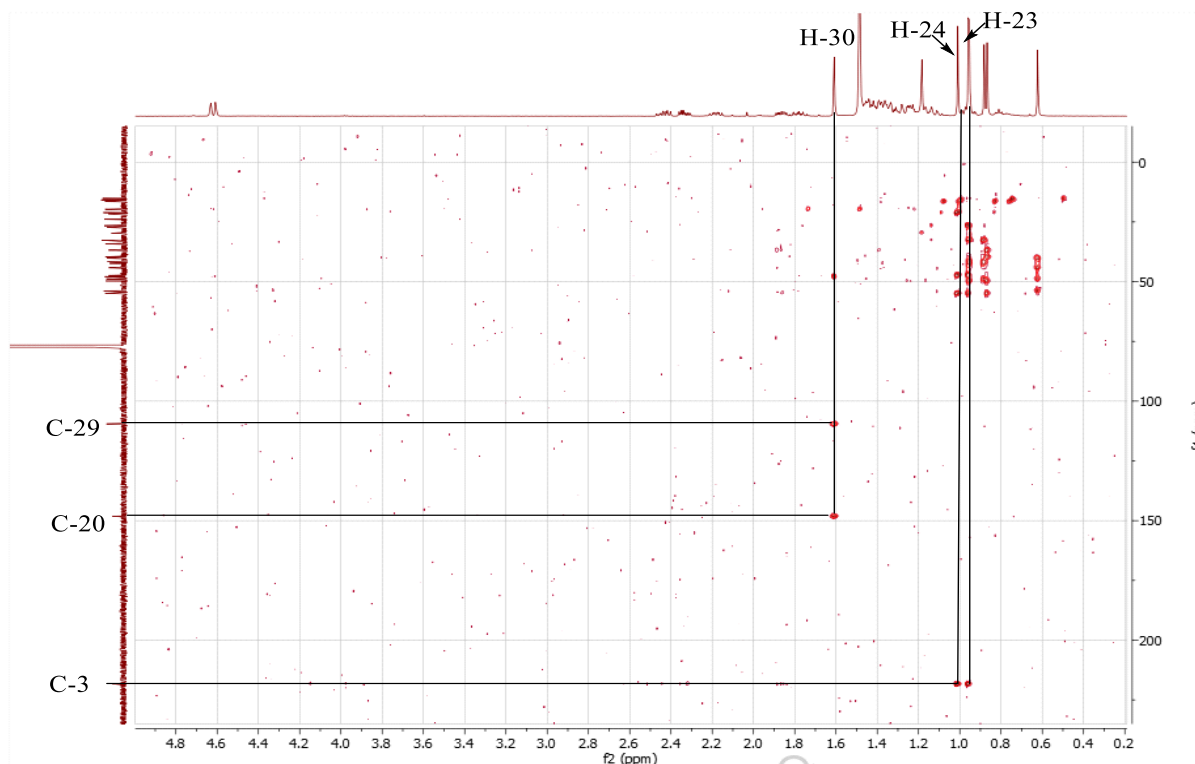
Figure 61: HMBC spectrum of compound ECTF23

II.2.1.2.10 Identification of PBE5

Compound PBE5 was obtained as a white amorphous solid. It is soluble in acetone and responds positively to the Liebermann-Burchard test by giving a red coloration, characteristic of triterpenes.

Its ^{1}H NMR spectrum (Figure 62), shows:

- six singlets of angular methyl protons at δ_H 0.78, 0.89, 0.99, 1.04, 1.09 and 1.72;

- a doubled doublet of a proton at δ_H 3.14 (1H, dd, J = 11.0, 5.1 Hz) attributable to a proton geminated to a hydroxyl group;

- two doublets of oxymethylene at proton at δ_H 3.32 (1H, d, J = 10.6 Hz) and 3.76 (1H, d, J = 10.3 Hz);

- two broad singlets of exomethylene proton at δ_H 4.58 and 4.71.

Its ^{13}C NMR spectrum (Figure 63) shows the signals of 30 carbon atoms which were sorted using HSQC technic into:

- six methyl carbons at δ_C 14.3, 15.1, 15.6, 15.7, 18.2 and 27.4;

- twelve methylene carbons including one olefinic at δ_C 109.0 and an oxymethylene at δ_C 59.1;

- six methine carbons amongst which an oxymethine at δ_C 77.7;

- six quaternary carbons including one olefinic at δ_C 150.8.

The signals at δ_C 150.8 and 109.0 are characteristic of the triterpenes of the lup-20(29)-ene series (Mahato and Kundu, 1994).

The position of oxymethylene was determined using correlations between its protons at δ_H 3.32 (H-28b) and 3.76 (H-28a) and carbons at δ_C 29.8 (C-16), 34.0 (C-22) and 48.7 (C-18) as observed on the HMBC spectrum (Figure 64).

All these data, compared to those of the literature (Table XXIX), allowed us to attribute to PBE5 the structure (**64**) which is that of betulin (Mahato and Kundu, 1994).

(**64**)
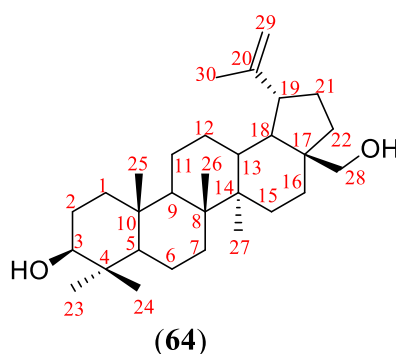
Table XXIX: Spectral data of ^{13}C (125 MHz) of PBE5 in C_3D_6O, compared to that of betulin ^{13}C (100 MHz) in CDCl$_3$ (Mahato and Kundu, 1994).

Position	PBE5	Betulin
	δ_C	δ_C
1	38.7	38.8
2	27.4	27.2
3	77.7	78.9
4	38.7	38.9
5	55.5	55.3
6	18.2	18.3
7	34.3	34.3
8	40.9	40.9
9	50.5	50.4
10	37.1	37.2
11	20.7	20.9
12	25.4	25.3
13	37.3	37.3
14	42.6	42.7
15	27.1	27.0
16	29.8	29.2
17	47.8	47.8
18	48.7	48.8
19	47.9	47.8

20	150.8	150.6
21	29.3	29.8
22	34.0	34.0
23	27.7	28.0
24	15.1	15.4
25	15.7	16.1
26	15.6	16.0
27	14.3	14.8
28	59.0	60.2
29	109.0	109.6
30	18.4	19.1
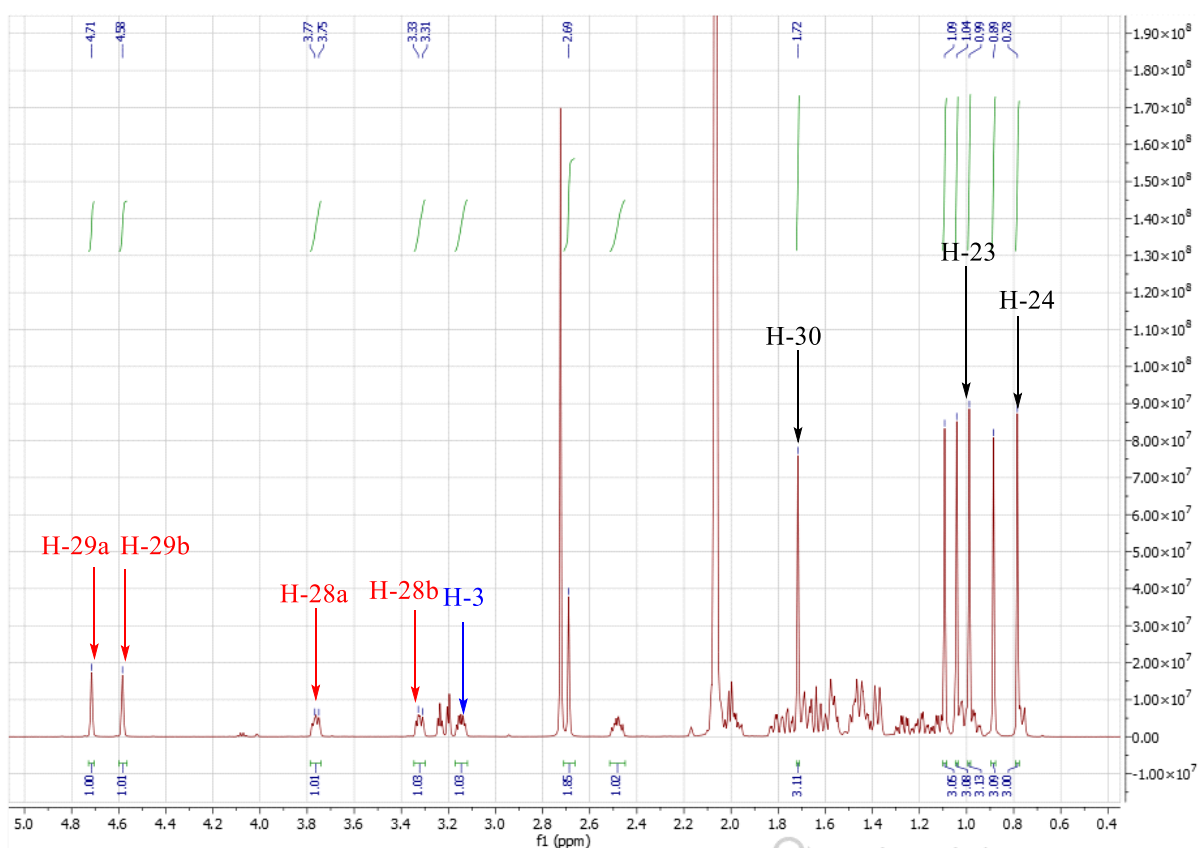
Figure 62: ^{1}H NMR spectrum (C$_3$D$_6$O, 500 MHz) of compound PBE5
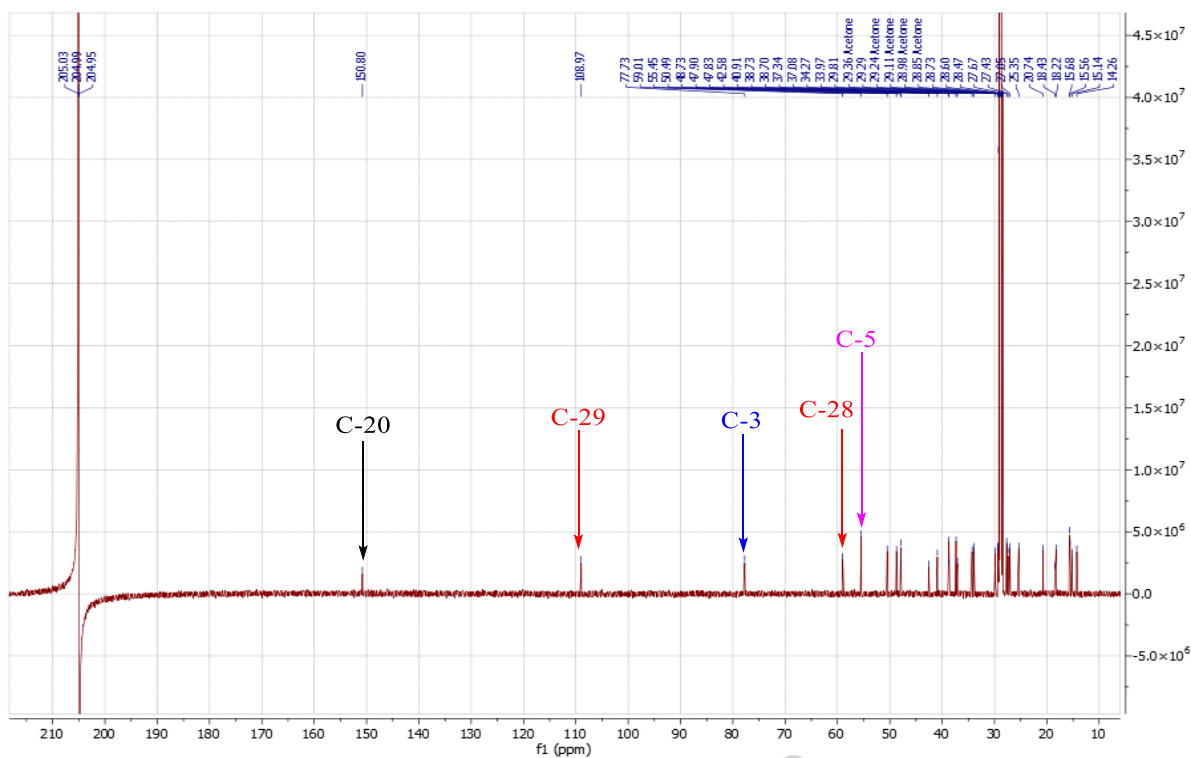
Figure 63: ^{13}C NMR spectrum (C$_3$D$_6$O, 125 MHz) of compound PBE5
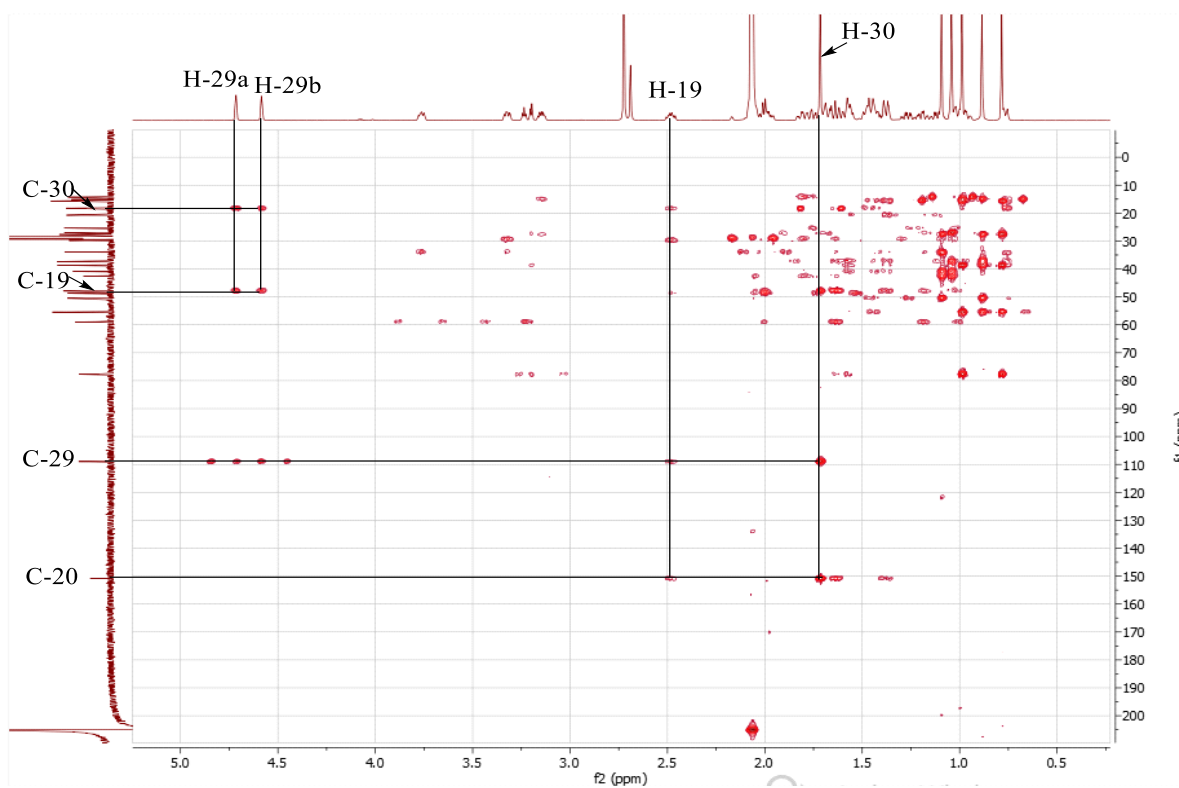
Figure 64: HMBC spectrum of compound PBE5

II.2.1.3. Flavonoids

II.2.1.3.1 Identification of ECF43

ECF43 was obtained as a yellowish amorphous solid and is soluble in acetone. It gives a purple color in the presence of ferric chloride, characteristic of phenolic compound. It also responds positively to the Shinoda test by giving a brick-red coloration characteristic of flavonoids.

Its HR-ESI mass spectrum in positive mode (Figure 65), shows the peak of the sodium adduct $[M+Na]^+$ at m/z 575.0919, corresponding to the molecular formula $C_{31}H_{20}NaO_{10}$ (calculated for 575.0949) and containing twenty-two degrees of unsaturations.

Its ^1H NMR spectrum (Figure 66) shows:

- an AA′BB′ aromatic system at δ_H 7.69 (2H, d, $J = 8.9$ Hz) and 6.94 (2H, d, $J = 8.9$ Hz);

- the signals of an ABX system at δ_H 7.16 (1H, d, $J = 8.8$ Hz), 8.00 (1H, d, $J = 2.3$ Hz) and 8.02 (1H, dd, $J = 8.5$ and 2.3 Hz);

- three singlets integrating for one proton each at δ_H 6.90, 6.42 and 6.84;

- a meta-coupled protons at δ_H 6.19 (1H, d, $J = 2.3$ Hz,) and 6.46 (1H, d, $J = 2.3$ Hz);

- a singlet at δ_H 3.77 (3H, s) attributable to protons of a methoxy group;

- two singlets of chelated hydroxyl groups at δ_H 13.08 (1H, s) and 12.98 (1H, s).

The presence of the AA′BB′, ABX and AX systems were confirmed by the couplings observed on the COSY spectrum (Figure 69):

- protons at δ_H 7.69 (2H, d, $J = 8.9$ Hz, H-3b′ and H-5b′) and 6.94 (2H, d, $J = 8.9$ Hz, H-2b′, H-6b′);

- protons at δ_H 7.16 (1H, d, $J = 8.8$ Hz, H-3a′), 8.00 (H-6a′, d, $J = 2.3$ Hz) and 8.02 (H-2a′, dd, $J = 8.5, 2.3$ Hz);

-the proton at δ_H 6.19 (1H, d, $J = 2.3$ Hz, H-8a) and 6.46 (1H, d, $J = 2.3$ Hz, H-6a).

Analysis of the ^{13}C NMR spectrum of ECF43 (Figure 67) brings out 31 signals of carbon atoms which were sorted using the DEPT 135 (Figure 68) technique as:

- seventeen quaternary carbons including two δ_C 182.6 (4a) and 182.2 (4b) flavonoid carbonyls (Suárez *et al.*, 2003) and the other carbons at δ_C 164.3 (2a), 163.7 (2a′), 162.7 (4b′), 161.9 (7b), 160.1 (4a′), 160.1 (5b), 157.8 (9a), 155.0 (9b), 123.4 (1b′), 121.4 (1a′), 120.5 (5a′), 104.5 (10b), 104.2 (10a) and 104.1 (8b);

- twelve methine carbons at δ_C 131.8 (6a′), 128.3 (2b′ and 6b′), 128.4 (2a′), 116.7 (3a′), 115.0 (3b′ and 5b′), 103.5 (3a), 103.7 (3b), 99.3 (6a), 94.5 (8a), 99.2 (6b);

- A signal of the methoxyl carbon at δ_C 56.0 (4b′-OCH$_3$).

On the HMBC spectrum of ECF43 (Figure 70) we observe correlations between:

- the proton H-11 (δ_H 3.77) and the carbon C-4b′ (δ_C 162.7);

- the proton H-3b′ (δ_H 7.69) and carbon C-2b′ (δ_C 1828.3);

- the proton H-6b′ (δ_H 6.94) and the carbons C-1b′ (δ_C 124.4) et C-5b′ (115.0), that led to built the substructure SSS1 below:

SSS₁
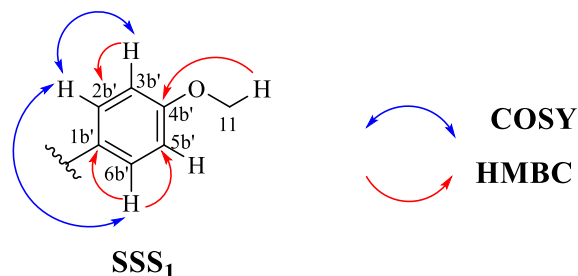
- the proton H-3b (δ_H 6.90) and the carbons C-4b (δ_C 182.2), C-10b (δ_C 104.5) and C-2b (δ_C 163.7);

- the proton H-6b (δ_H 6.42) and the carbons C-4b (δ_C 182.2), C-10b (δ_C 104.5) and C-8b (δ_C 104.1), that led to built the substructure SSS2 below:

SSS₂
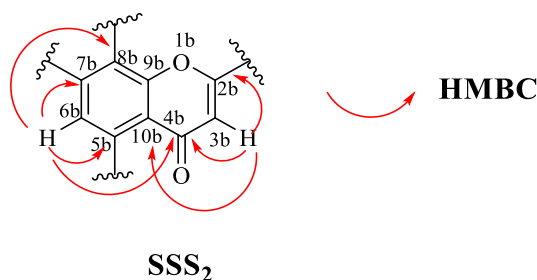
- the proton H-3a′ (δ_H 7.16) and the carbon C-4a′ (δ_C 116.7);

- the proton H-2a′ (δ_H 8.02) and the carbons C-3a′ (δ_C 160.1) and C-1a′ (δ_C 121.4);

- the proton H-6a′ (δ_H 8.00) and the carbons C-1a′ (δ_C 121.4) and C-5a′ (δ_C 120.5), that led to built the substructure SSS3.

SSS₃
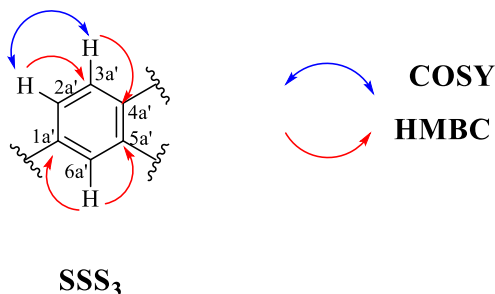
- the proton H-3a (δ_H 6.84) and the carbons at C-4a (δ_C 182.6), C-2a (δ_C 164.3) and C-10a (δ_C 104.2);

- the proton H-6a (δ_H 6.46) and the carbons C-4a (δ_C 182.6), C-7a (δ_C 164.6), C-10a (δ_C 104.2) and C-8a (δ_C 94.5);

- the proton H-8a (δ_H 6.19) and the carbons C-9a (δ_C 157.8) and C-7a (δ_C 164.6), which allowed the construction of the substructure SSS4.
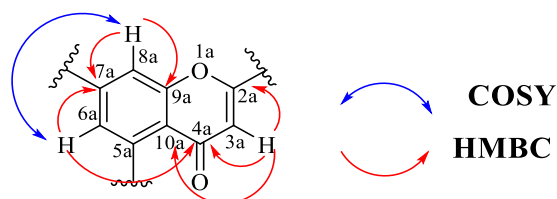
SSS$_4$

The junction between these substructures was made, base on the same HMBC spectrum, where additional correlations were observed between:

- the proton H-3b (δ_H 6.90) and carbon C-1b′ (δ_C 123,4) enabling us to link the SSS1 to SSS2 to yielding substructure SS1, on one hand and from the proton H-3a (δ_H 6.84) to the carbon C-1a′ (δ_C 121.4) enabling us to link the SSS3 to SSS4 to yielding substructure SS2, on the other hand.

SS$_1$ **SS$_2$**
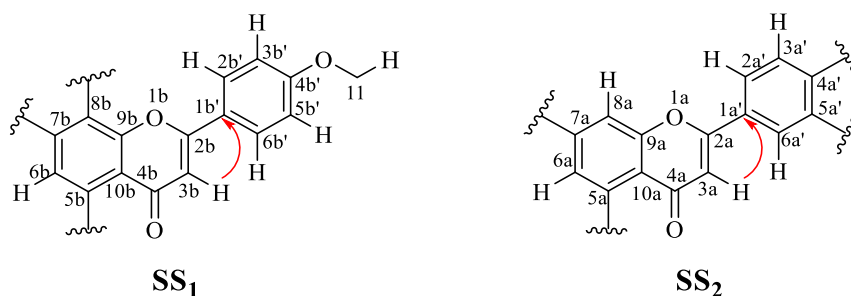
The HMBC spectrum of ECF43 also enabled the junction between the two flavone backbones (SS1 and SS2) from the correlation between the proton H-6a′ (δ_H 8.00) and the carbon C-8b (δ_C 104.1).
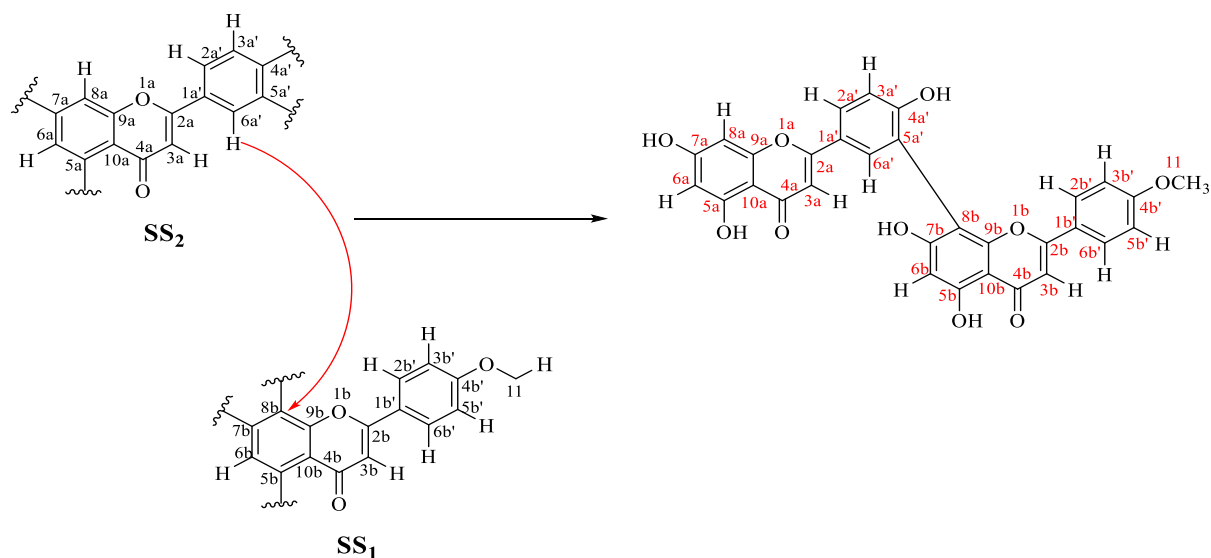
All these data, compared to those of the literature (table XXX), allowed us to attribute to ECF43 the structure (**65**), which is that of 4′-methylamentoflavone previously isolated from the leaves of *Podocalyx loranthoides* (Suárez *et al.,* 2003).

(**65**)
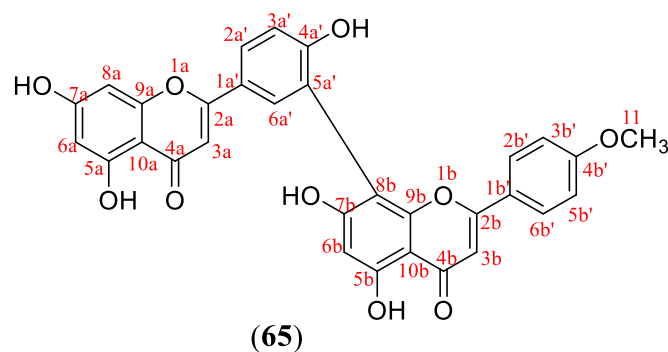
Table XXX: Spectral data of ^{1}H (500 MHz) and ^{13}C (125 MHz) of ECF44 in DMSO-d_6 compared with those of 4′-methylamentoflavone (DMSO-$d6$, 75 MHz) (Suárez *et al.,* 2003).

Position	ECF43		4′-methylamentoflavone
	δ_H (nH, m, *J* in Hz)	δ_C	δ_C
1a	/	/	/
2a	/	164.3	164.8
3a	6.84 (1H, s)	103.5	103.2
4a	/	182.6	182.9
5a	/	161.0	161.5
6a	6.46 (1H, d, 2.3)	99.3	99.7
7a		164.6	166.7
8a	6.19 (1H, d, 2.3)	94.5	94.8
9a	/	157.8	157.6

10a	/	104.2	103.9
1a′	/	121.4	121.6
2a′	8.02 (1H, dd, 8.5, 2.3)	128.4	127.9
3a′	7.16 (1H, d, 8.8)	116.7	114.5
4a′	/	160.1	159.4
5a′	/	120.5	121.3
6a′	8.00 (1H, d, 2.3)	131.8	131.3
1b	/	/	/
2b	/	163.7	164.5
3b	6.90 (1H, s)	103.7	104.1
4b	/	182.2	182.6
5b	/	161.0	161.5
6b	6.42 (1H, s)	99.2	99.7
7b	/	161.9	165.7
8b	/	104.1	104.1
9b	/	155.0	156.7
10b	/	104.5	104.1
1b′	/	123.4	121.6
2b′	6.94 (1H, d, 8.9)	128.3	127.8
3b′	7.69 (1H, d, 8.9)	114.9	114.5
4b′	/	162.7	162.3
5b′	7.69 (1H, d, 8.9)	114.9	114.5
6b′	6.94 (1H, d, 8.9)	128.3	127.8
11	3.77 (3H, s)	56.0	55.7
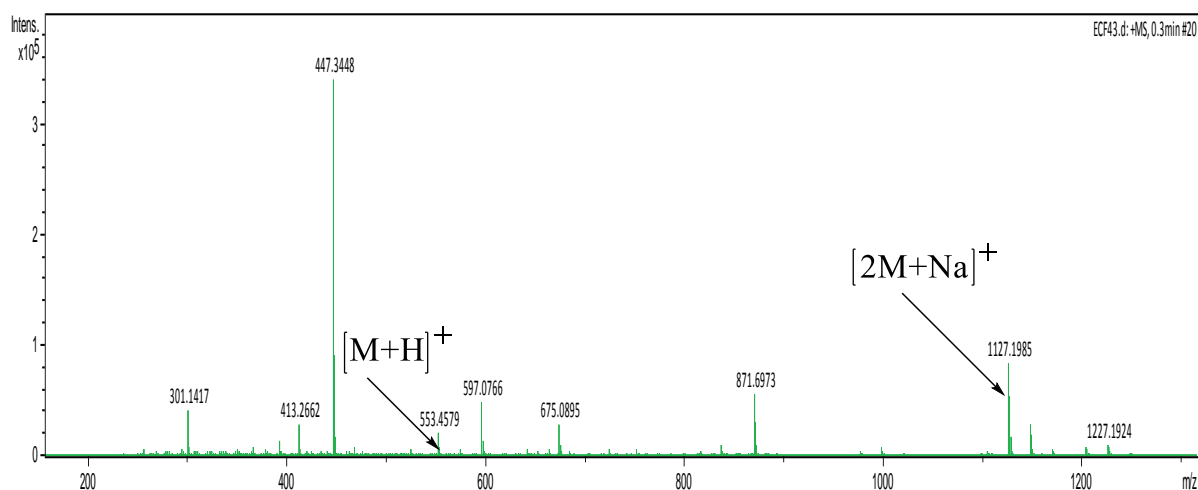
Figure 65: HR-ESI-MS spectrum of compound ECF43
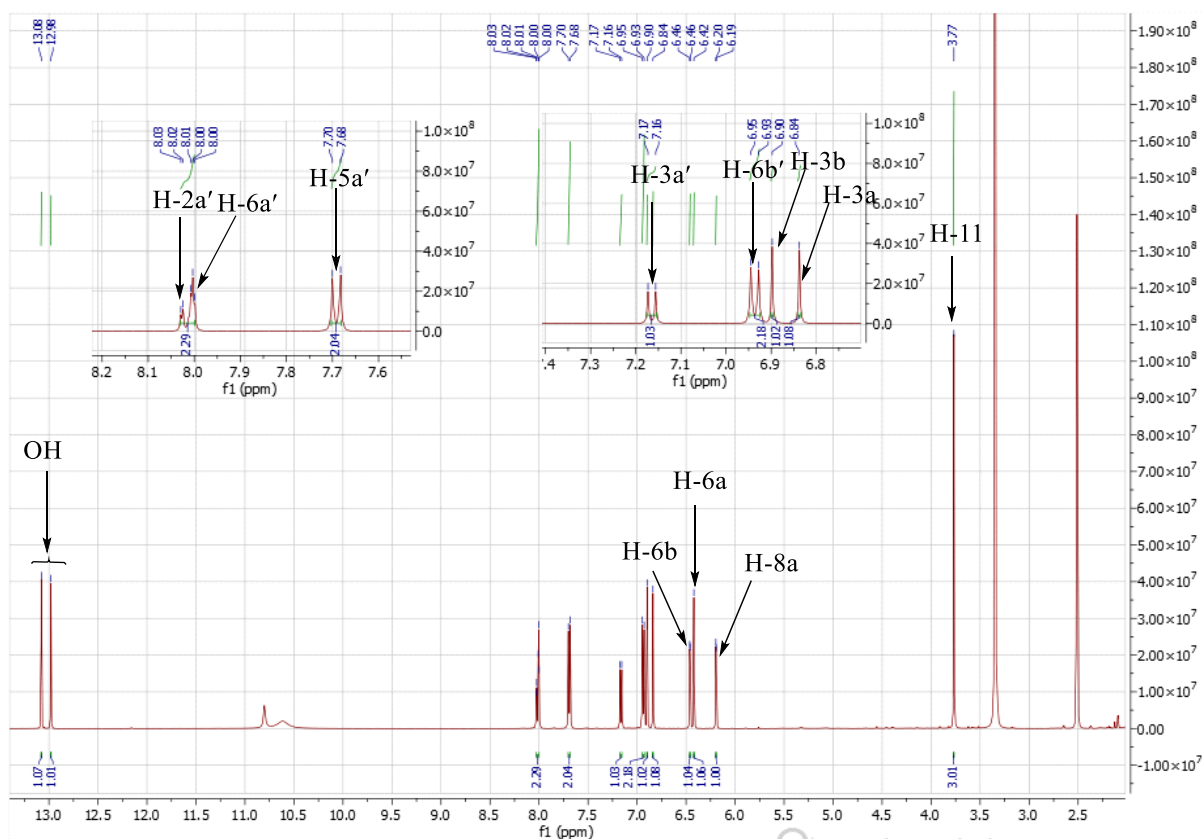
Figure 66: ^{1}H NMR spectrum (C$_2$D$_6$SO, 500 MHz) of compound ECF43
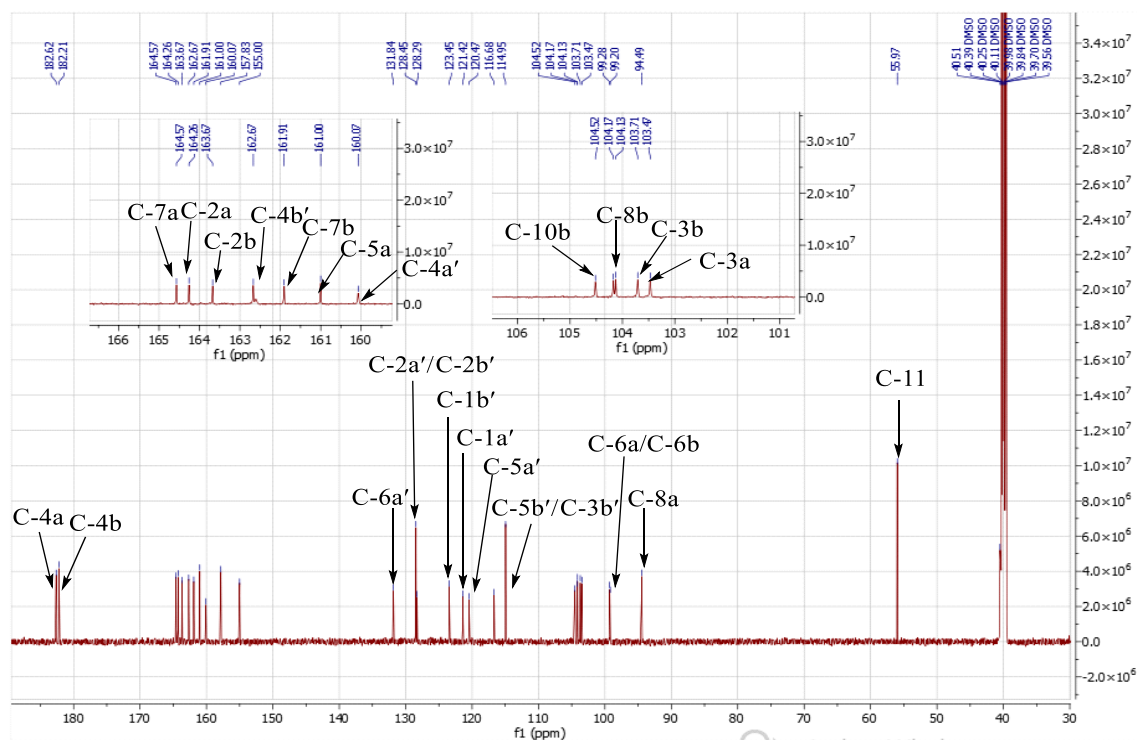
Figure 67: ^{13}C NMR spectrum (C$_2$D$_6$SO, 125 MHz) of compound ECF43
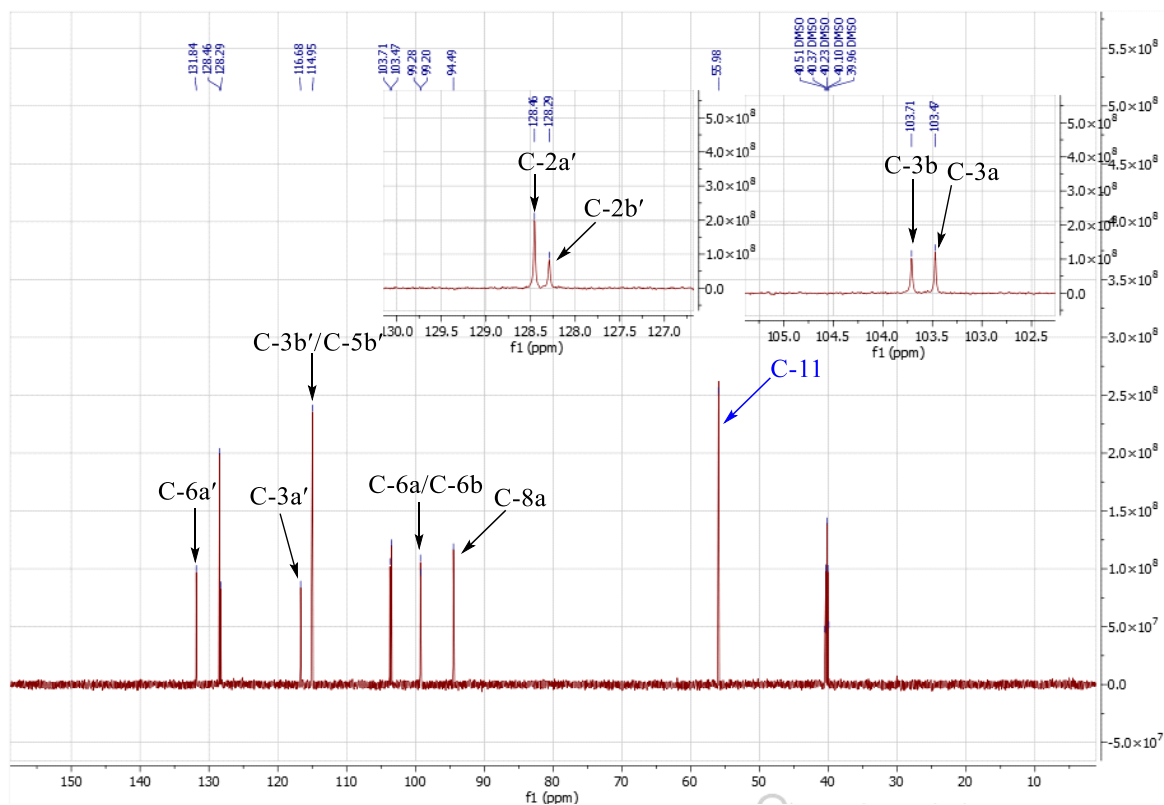
Figure 68: DEPT 135 spectrum of compound ECF43
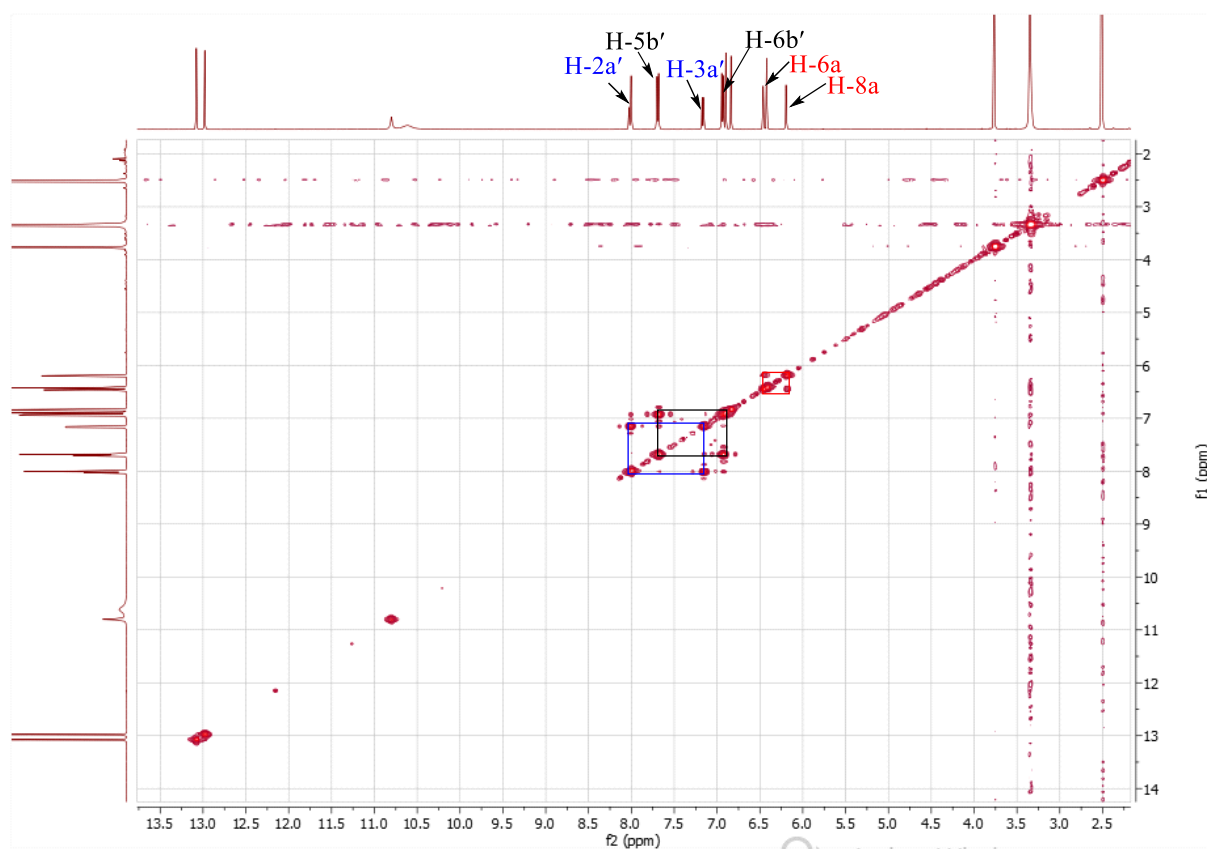
Figure 69: COSY spectrum of compound ECF43
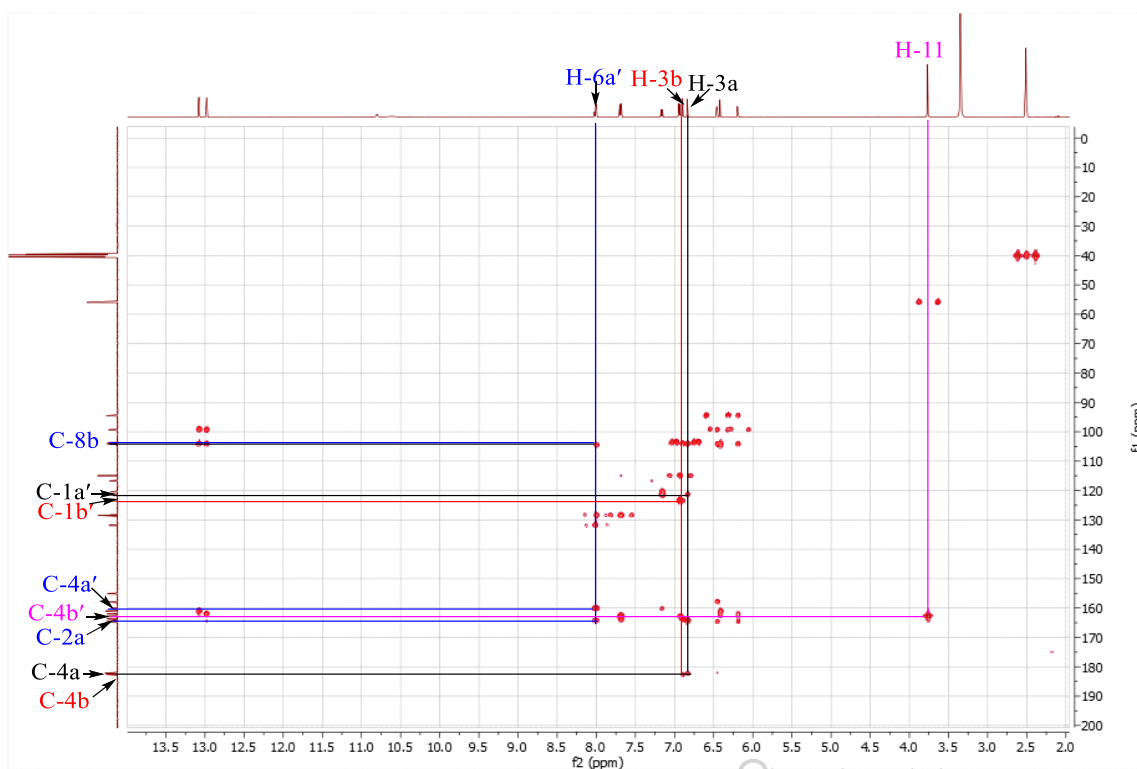
Figure 70: HMBC spectrum of compound ECF43

II.2.1.3.2 Identification of ECF44

ECF44 was isolated as yellowish amorphous solid, and was soluble in acetone. In the presence of ferric chloride, it gives a purple coloration, characteristic of phenolic compound. It also responds positively to the Shinoda test by giving a brick-red coloration characteristic of flavonoids.

Its high resolution ESI mass spectrum in positive mode (Figure 71), shows the peak of the protonated ion $[M+H]^+$ at m/z 539.0997, corresponding to the formula $C_{30}H_{18}O_{10}$ (calculated for 539.0978) and containing twenty-two degrees of unsaturations and has 14 mass unit less than ECF43, indicating the loss of methyl group.

Its ^1H NMR spectrum (Figure 72) shows almost the same signals as those of ECF43 except the absence of the methoxy protons. The observed proton signals are as follows:

- an AA′BB′ aromatic system at δ_H 7.59 (2H, d, $J = 8.8$ Hz) and 6.72 (2H, d, $J = 8.8$ Hz);

- the signals of an ABX system at δ_H 7.15 (1H, d, $J = 8.8$ Hz), 8.01 (1H, d, $J = 2.3$ Hz) and 8.02 (1H, dd, $J = 8.5, 2.3$ Hz);

- three singlets integrating for one proton each at δ_H 6.84, 6.40 and 6.80;

- a meta-coupled aromatic protons at δ_H 6.20 (1H, d, $J = 2.1$ Hz) and 6.47 (1H, d, $J = 2.1$ Hz);

- two singlets of chelated hydroxyl groups at δ_H 13.11 (1H, s) and 12.93 (1H, s).

Its HMBC spectrum (Figure 73) exhibited several correlation that enable to built the two flavone unit that were linked together follow the connectivity from H-6a′ to carbons C-5a′, C-1a′, C-4a′ and C-8b.

By comparison of the spectral data of ECF44 and with data from the literature (Table XXXI), allowed us to attribute the compound ECF44 the structure (**66**) which is that of the amentoflavone (Markham *et al*., 1987).

(**66**)
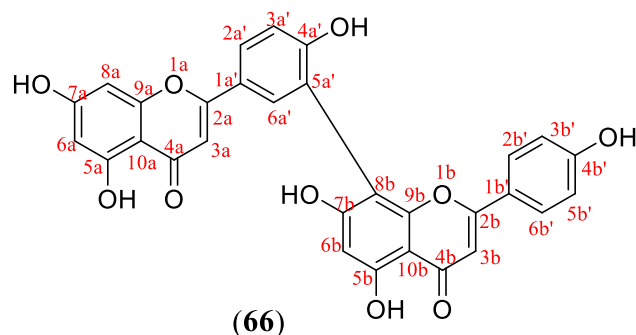
Table XXXI: Spectral data of ^{1}H (600 MHz) and ^{13}C (150 MHz) of ECF44 in DMSO-d_6 compared with those from amentoflavone (DMSO-$d6$, 5 MHz) (Markham *et al*., 1987)

Position	ECF44		Amentoflavone
	δ_H (nH, m, *J* in Hz)	δ_C	δ_C
1a	/	/	/
2a	/	164.2	164.3
3a	6.80 (1H, s)	103.1	103.2
4a	/	182.6	181.9
5a	/	161.9	161.6
6a	6.47 (1H, d, 2.1)	99.3	98.8
7a		164.6	163.9
8a	6.20 (1H, d, 2.1)	94.4	94.2
9a	/	157.9	157.6
10a	/	104.2	104.0
1a′	/	121.9	120.3
2a′	8.02 (1H, dd, 8.5, 2.3)	128.4	127.9
3a′	7.15 (1H, d, 8.8)	120.8	121.7
4a′	/	160.1	159.6
5a′	/	116.7	116.4
6a′	8.01 (1H, d, 2.3)	131.9	131.6
1b	/	/	/
2b	/	164.3	164.3
3b	6.84 (1H, s)	103.4	102.8
4b	/	182.3	182.2

5b	/	161.0	160.8
6b	6.40 (1H, s)	99.1	99.1
7b	/	162.3	161.9
8b	/	104.3	104.1
9b	/	157.2	154.7
10b	/	104.1	104.0
1b′	/	121.2	121.4
2b′	6.72 (1H, d, 8.8)	128.7	128.3
3b′	7.59 (1H, d, 8.8)	116.2	116.0
4b′	/	161.5	161.1
5b′	7.59 (1H, d, 8.8)	116.2	116.0
6b′	6.72 (1H, d, 8.8)	128.7	123.8
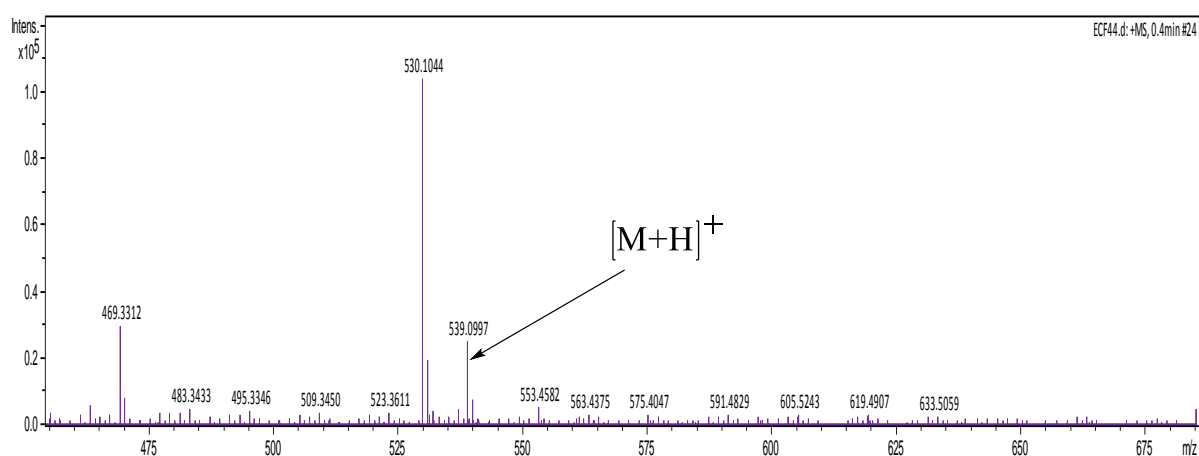
Figure 71: HR-ESI-MS spectrum of compound ECF44
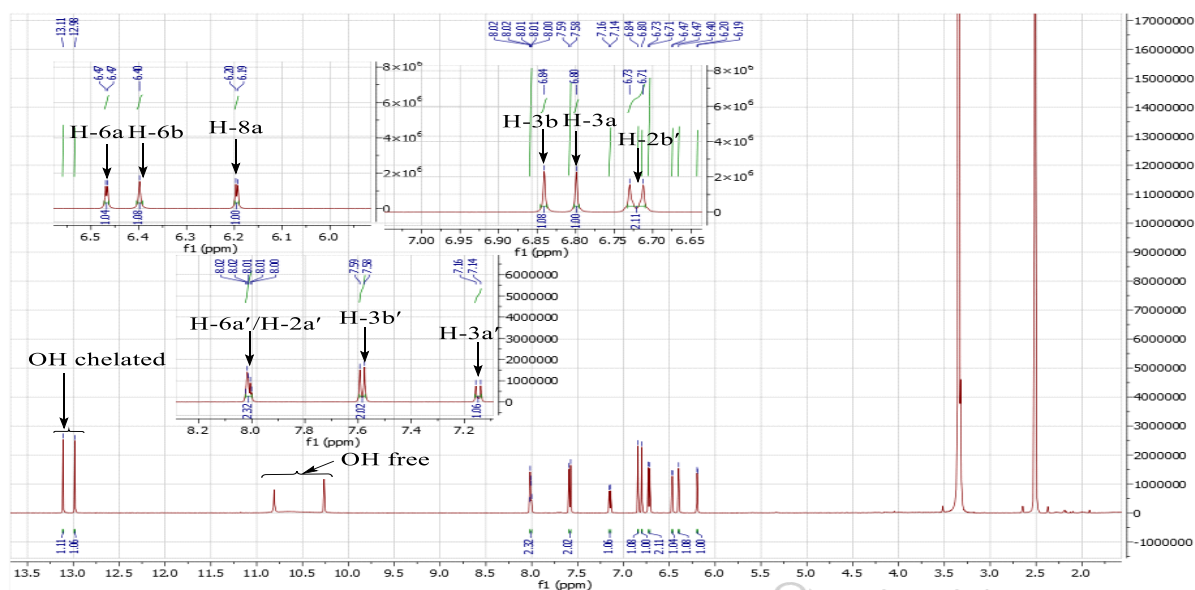
Figure 72: ^{1}H NMR spectrum (C$_2$D$_6$SO, 600 MHz) of compound ECF44
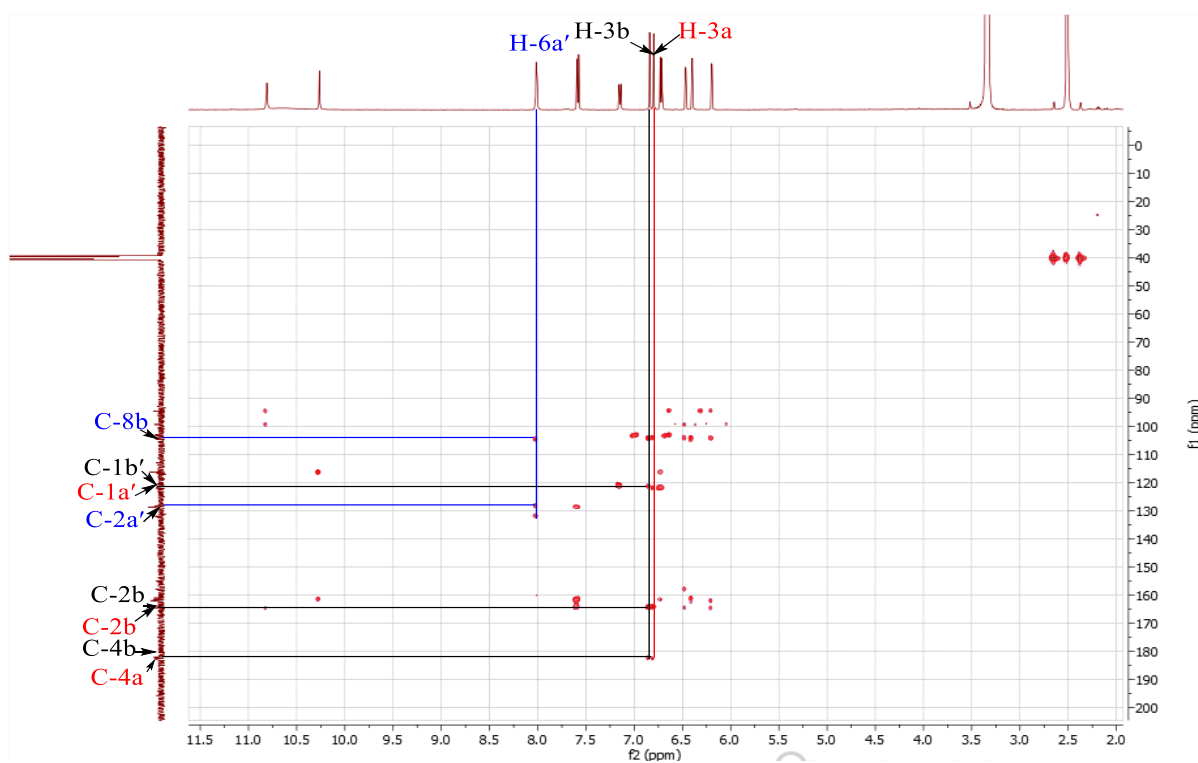
Figure 73: HMBC spectrum of compound ECF44
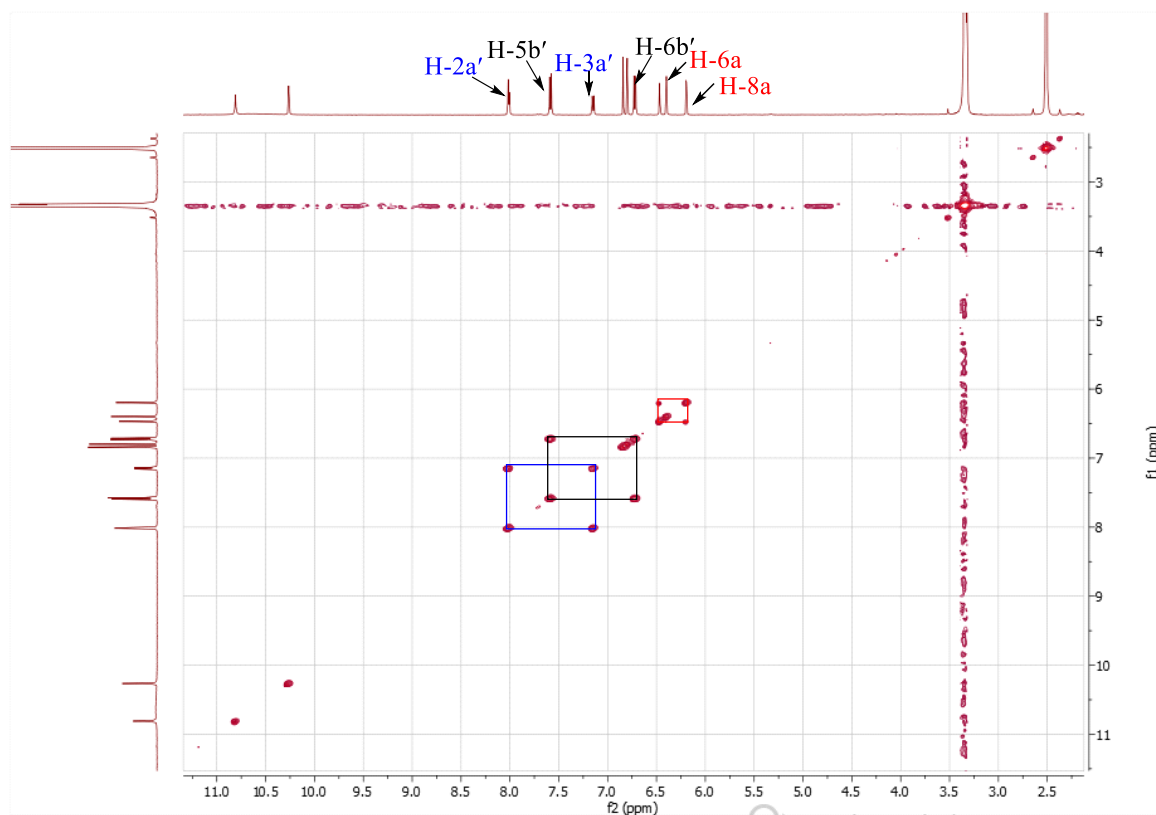
Figure 74: COSY spectrum of compound ECF44

II.2.1.3.3 Identification of ECTF33

ECTF33 was obtained as a yellow amorphous solid and was soluble in acetone. In the presence of ferric chloride, it gives a purple coloration, characteristic of phenolic compounds and responds positively to the Shinoda test, giving a brick-red coloration, characteristic of flavonoids.

Its HR-ESI$^+$ mass spectrum (Figure 75) shows the peak of the protonated ion $[M+H]^+$ at m/z 557.1070, corresponding to the molecular formula $C_{30}H_{20}O_{11}$ (calculated for 557.1078), containing twenty-one unsaturations.

Its ^{1}H NMR spectrum (Figure 76) shows duplicated signals. This phenomenon is observed in flavanone (3→8″)-flavanone and flavanone (3→8″)-flavone, when the NMR spectra are recorded at room temperature. Indeed, at room temperature, the molecule adopts several preferential conformations resulting from strong intra- and intermolecular hydrogen bonds of the various hydroxyl groups (Li *et al.*, 2002). In the case of compound ECTF33, there are two conformers at room temperature. It is only assigned signals that matched the majority of conformers and the structure (**67**) was attributed.

(**67**)
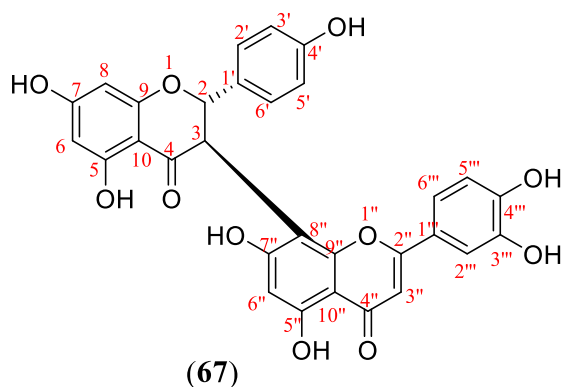
Thus it is observed on its ^{1}H NMR spectrum:

-two singlets of chelated hydroxyl groups at δ_H 13.16 (s, OH) and 12.35 (s, OH);

- two doublets of one proton each at δ_H 5.88 (1H, d, J = 12.0 Hz, H-2) and 5.01 (1H, d, J = 12.0 Hz, H-3), suggesting the existence of a flavanone backbone. The value of the coupling constant J = 12.0 Hz indicates the *trans* configuration of the two protons;

- signals of a trisubstituted 1,3,4-aromatic nucleus at δ_H 7.51 (1H, brs, H-2‴), 7.03 (1H, d, J = 8.3 Hz, H-5‴) and 7.53 (1H, d, J = 8.3 Hz, H-6‴);

- signals of an AA′BB′ system at δ_H 7.26 (2H, d, J = 8.3 Hz, H-2′) and 6.55 (2H, d, J = 8.3 Hz, H-3′);

- three singlets of a proton each at δ_H 6.03 (1H, brs, H-8), 6.03 (1H, brs, H-6) and 6.34 (1H, s, H-6″);

- a singlet of a proton at δ_H 6.48 (1H, s, H-3″).

On its fully decoupled broad band ^{13}C NMR spectrum (figure 77), 28 signals of 30 carbon atoms were distinguished, and were sorted using the DEPT135 technique (80) in:
- thirteen methine carbons at δ_C 49.1 (C-3), 81.5 (C-2), 95.2 (C-6), 96.3 (C-8), 98.7 (C-6″), 102.8 (C-3″), 145.5 (C-3‴), 114.6 (C-3′/C-5′), 113.2 (C-2‴), 119.7 (C-6‴) and 128.5 (C-2′/C-6′);
- seventeen quaternary carbon signals including two carbonyls of ketone at δ_C 196.4 (C-4); 182.3 (C-4″), olefinic and aromatic hydroxylated carbons at δ_C 149.3 (C-4‴), 115.8 (C-5‴), 155.9 (C-9″), 157.6 (C-4′), 161.4 (C- 9), 161.7 (C-7″), 163.4 (C-7), 164.0 (C-2″), 164.7 (C-5″) and 166.4 (C-5), aromatic carbons at δ_C 100.5 (C-8″), 102.0 (C-10) and 122.3 (C-1‴).

On the HMBC spectrum (Figure 78) of ECTF33, it is observe correlations between:
-the proton H-2 (δ_H 5.87) and the carbons C-3 (δ_C 49.1), C-4 (δ_C 196.4), C-2′ (δ_C 128.5);
- the proton H-6 (δ_H 6.03) and the carbons C-10 (δ_C 102.0), C-4 (δ_C 196.4), C-5 (δ_C 166.4), C-7 (δ_C 163.4);
- the proton H-8 (δ_H 6.11) and the carbons C-9 (δ_C 161.4), C-10 (δ_C 102.0), C-7 (δ_C 163.4);
- the proton H-2′ (δ_H 7.26) and the carbons C-2 (δ_C 81.5), C-4′ (δ_C 157.6), C-3′ (δ_C 114.6);
- the proton H-3′ (δ_H 6.55) and the carbons C-2′ (δ_C128.5), C-4′ (δ_C 157.6).

These data confirm the existence of a flavanone-type substructure (SS1)

SS₁
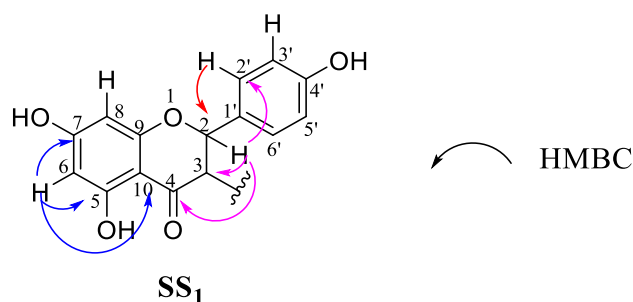
This HMBC spectrum also showed the correlations between:
- the proton H-5″ (δ_H 6.34) and the carbons C-3 (δ_C 49.1), C-8″ (δ_C 100.5), C-4 (δ_C 196.4);
- the proton H-2 (δ_H 5.87) and the carbons C-3 (δ_C 49.1), C-4 (δ_C 196.4), C-2′ (δ_C 129.3);
- the proton H-3″ (δ_H 6.48) and the carbons C-1‴ (δ_C 122.3), C-4″ (δ_C 182.3), C-2″ (δ_C 164.0);
- the proton H-3‴ (δ_H 7.51) and the carbons C-4‴ (δ_C 149.3), C-5‴ (δ_C 115.8), C-2″ (δ_C 164.0);
- the proton H-2‴ (δ_H 7.51) and the carbons C-2″ (δ_C 164.0), C-4‴ (δ_C 149.3), C-3‴ (δ_C 145.5);
- the proton H-6‴ (δ_H 7.53) and the carbons C-2″ (δ_C 164.0), C-5‴ (δ_C 115.8).

These data show the existence of a flavone-type substructure (SS2)

SS2
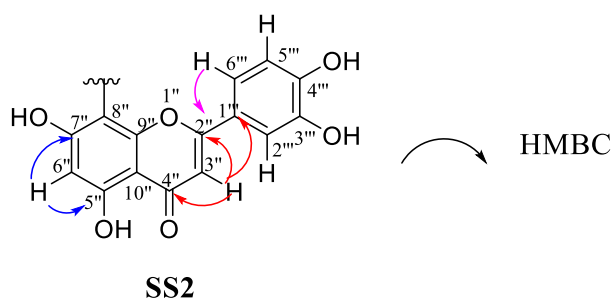
All of these data clearly indicates that ECTF33 is a biflavonoid. The junction between the two substructures is established to be C-3→C-8″. This flavanone-flavone junction was confirmed by the correlations between the proton H-3 (δ_H 5.01) and the carbons C-8″ (δ_C 100.5), C-7″ (δ_C 161.7), C-9″ (δ_C 155.9), C-2 (δ_C 81.5) and C-4 (δ_C 196.4) observed on the HMBC spectrum (Figure 80, scheme 19):
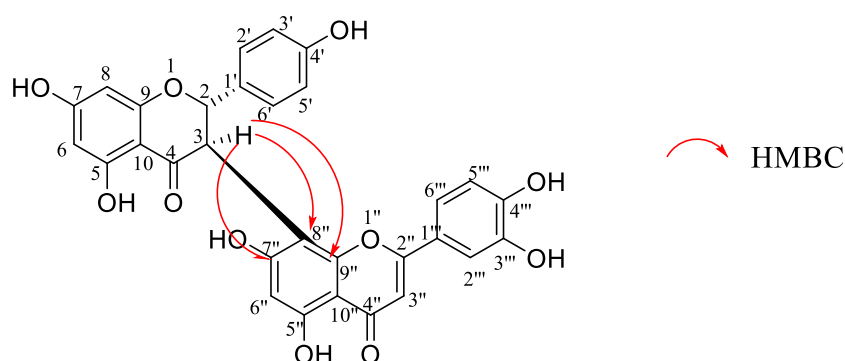
Scheme 19: Selected HMBC correlations of compound ECTF33

All these data, compared with those described in the literature (Table XXXII), see the previous structure (**67**) to be (+)-morelloflavone (Karanjgaokar *et al*., 1967).

Table XXXII: Spectral data of ^{1}H (500 MHz) and ^{13}C (125 MHz) of ECTF33 in C$_3$D$_6$O compared with those of morelloflavone (DMSO-d_6, 125 MHz) (Li *et al*., 2002)

Position	ECTF33		Morelloflavone	
	δ_C	δ_H (nH, m, *J* in Hz)	δ_C	δ_H (nH, m, *J* in Hz)
2	81.5	5.87 (1H, d, 12.0)	81.0	5.71 (1H, d, 12.0)
3	49.1	5.01 (1H, d, 12.0)	48.4	4.89 (1H, d, 12.0)
4	196.4	/	196.3	/
5	161.4	/	161.8	/
6	95.2	6.03 (1H, brs)	95.4	5.97 (1H, brs)

7	163.4	/	163.6	/
8	96.3	6.03 (1H, brs)	96.3	5.97 (1H, brs)
9	166.4	/	166.6	/
10	102.0	/	101.6	/
1′	129.3	/	128.2	/
2′/ 6′	128.5	7.26 (2H, d, 8.3)	128.6	7.15 (2H, d, 8.3)
3′/ 5′	114.6	6.55 (2H, d, 8.3)	114.5	6.39 (2H, d, 8.3)
4′	157.6	/	157.4	/
2″	164.0	/	163.8	/
3″	102.8	6.48 (1H, s)	102.3	6.76 (1H, s)
4″	182.3	/	181.7	/
5″	161.7	/	160.6	/
6″	98.7	6.34 (1H, s)	98.7	6.59 (1H, s)
7″	164.7	/	162.9	/
8″	100.5	/	100.6	/
9″	155.9	/	155.3	/
10″	103.9	/	103.2	/
1‴	122.3	/	121.1	/
2‴	113.2	7.51 (1H, brs)	113.3	7.42 (1H, brs)
3‴	145.5	/	145.7	/
4‴	149.3	/	149.8	/
5‴	115.8	7.03 (1H, d, 8.3)	116.1	6.91 (1H, d, 8.1)
6‴	119.7	7.53 (1H, d, 8.3)	119.4	7.43 (1H, d, 8.0)
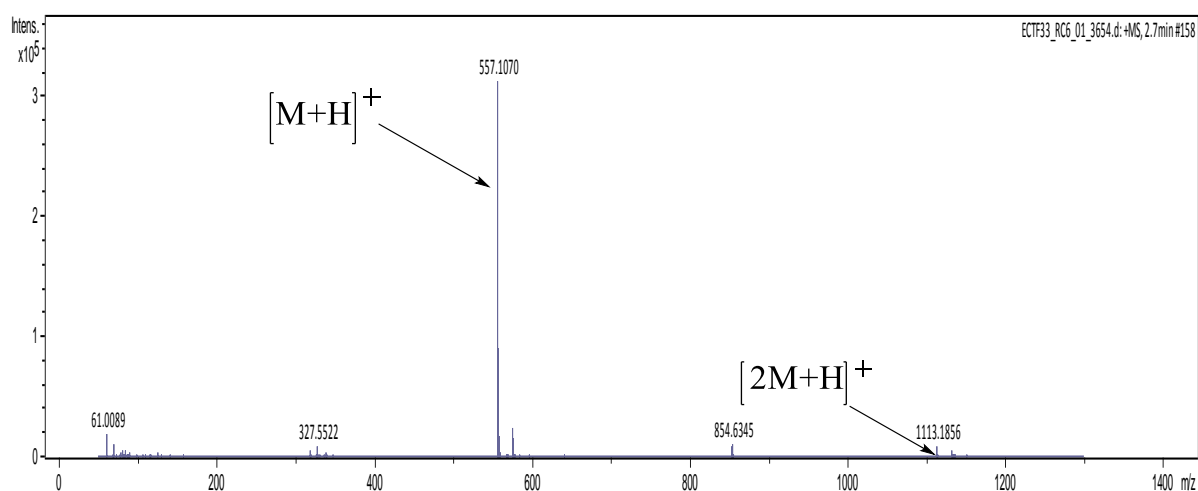
Figure 75: HR-ESI-MS spectrum of compound ECTF33
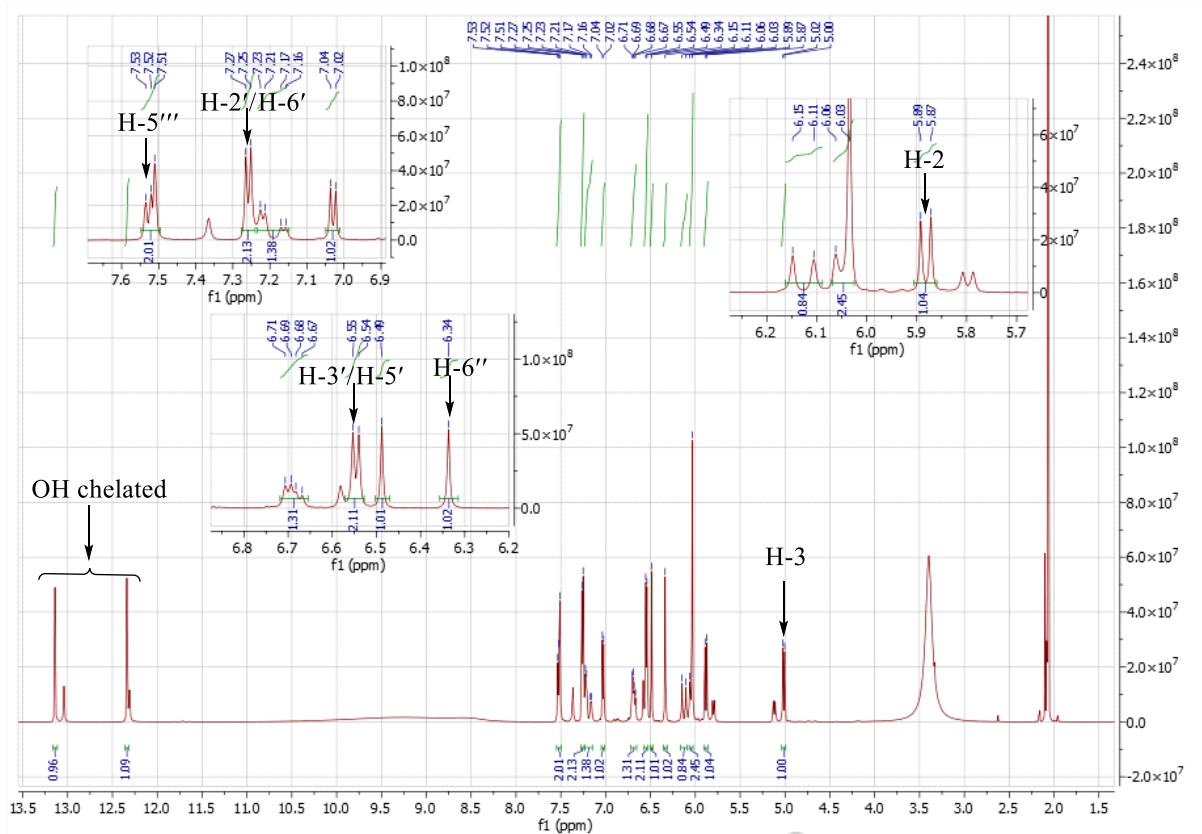
Figure 76: ¹H NMR spectrum (C₃D₆O, 500 MHz) of compound ECTF33
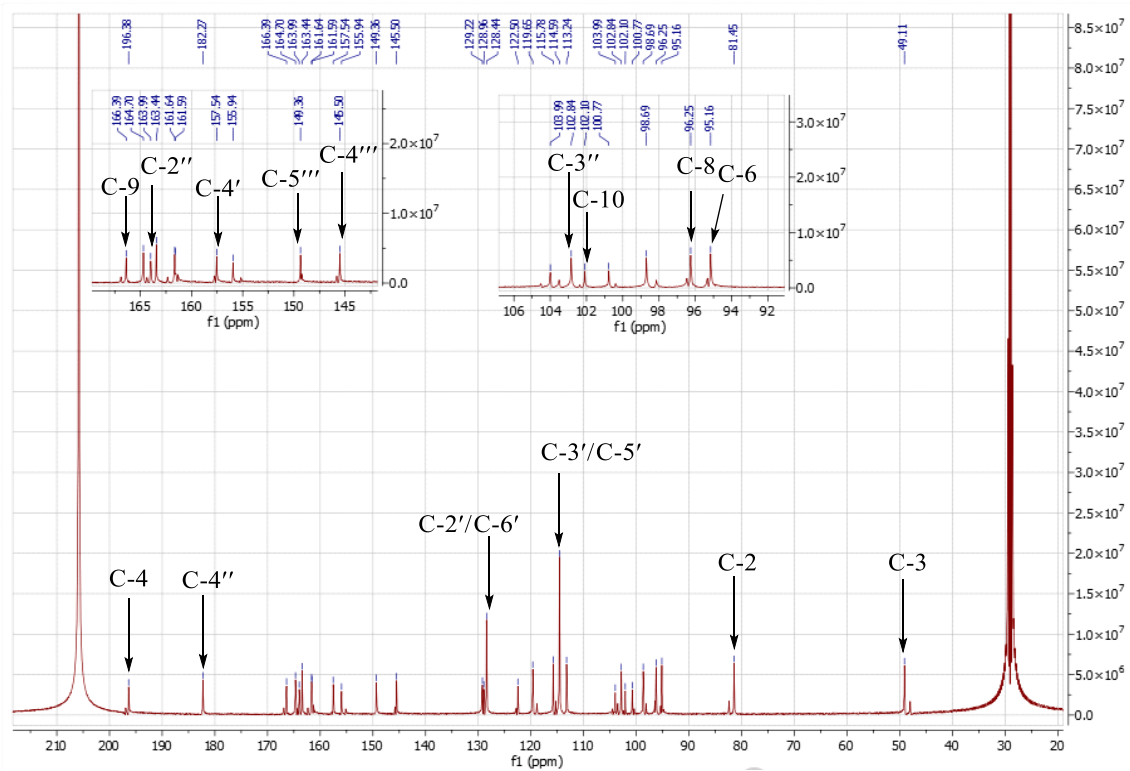
Figure 77: ¹³C NMR spectrum (C₃D₆O, 125 MHz) of compound ECTF33
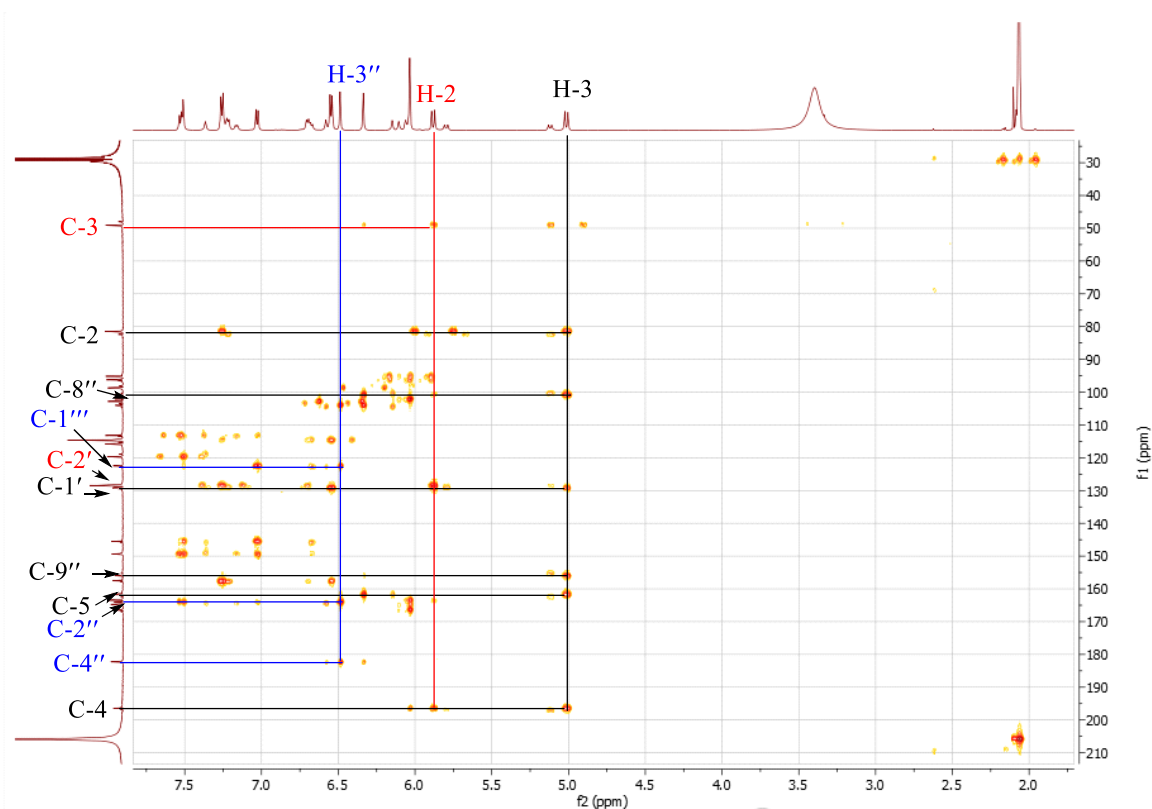
Figure 78: HMBC spectrum of compound ECTF33

II.2.1.3.4 Identification of PBER2

Compound PBER2 was obtained as yellow amorphous solid and was soluble in methanol. It gives a blue color when treated with ferric chloride, characteristic of phenolic compounds, and a brick-red coloration with the mixture of magnesium and concentrated hydrochloric acid (Shinoda test), and thus indicating its flavonoid nature.

Its HR-ESI$^+$ mass spectrum (Figure 79) showed the peak of the protonated ion [M+H]$^+$ at *m/z* 291.0873 corresponding to the molecular formula $C_{15}H_{14}O_6$ (calculated for 291.0863), containing nine degrees of unsaturation.

Its ^{1}H NMR spectrum (Figure 80) showed:

- two aromatic *meta*-coupled protons to δ_H 5.96 (1H, d, *J* = 2.3 Hz, H-6) and 5.94 (1H, d, *J* = 2.3 Hz, H-8) attribute to ring A of flavonoids;

- an ABX system protons at δ_H 6.99 (1H, d, *J* = 2.0 Hz), 6.82 (1H, dd, *J* = 8.2, 2.0 Hz), 6.78 (1H, d, *J* = 8.1 Hz) attribute to the ring B;

- four aliphatic protons at δ_H 4.74 (1H, brs), 4.20 (1H, m), 2.88 (1H, dd, *J* = 16.7, 4.6 Hz) and 2.75 (1H, dd, *J* = 16.8, 4.5Hz), characteristics of flavan-3-ol (Jang *et al*., 2009).

Its ^{13}C NMR spectrum (Figure 81) shows the signals of 15 carbon atoms which were distinguished by the HSQC technique (Figure 82) into:

- seven quaternary carbons, four of which are hydroxylated at δ_C 156.6, 156.3, 144.6, 144.4;

- seven methines, five of which correspond to aromatic carbons at δ_C 108.0, 114.5, 113.9, 95.0, 94.5;

- a methylene at δ_C 28.0.

PBF3 is a flavan with cis-2,3 stereochemistry, this was supported by the small value for the coupling (<1Hz) between protons H-2 (δ_H 4.84) and H-3 (δ_H 4, 20), which appeared as a large singlet (Usman et al., 2016).

The COSY spectrum (Figure 84, scheme 20) showed correlations between H-3 (δ_H 4.20) and H-2 (δ_H 4.84), and also between H-3 and H-4. These positions were further confirmed by long-range coupling observed in the HMBC (Figure 86) between proton H-2 and carbons C-1′ (δ_C 130.9), C-4 (δ_C 27.8), H-4 and carbons C-5 (δ_C 156.6), C-3 (δ_C 66.1). This spectrum also shows the correlation between the H-8 proton and the carbon C-9 (δ_C 156.0).
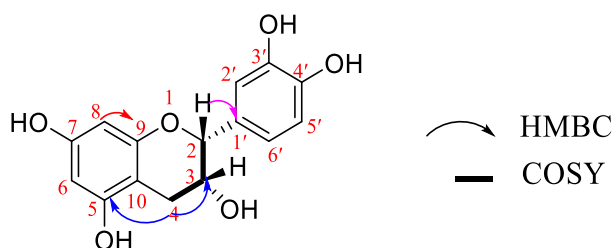
Scheme 20: Selected HMBC and COSY correlations of PBER2

All these spectral, compared with those in the literature (table XXXIII), enabled us to attribute to PBER2 the structure (**68**) which is that of epicatechin, previously isolated from the whole seeds of *Trichilia emetica* (Usman *et al*., 2016).

(**68**)
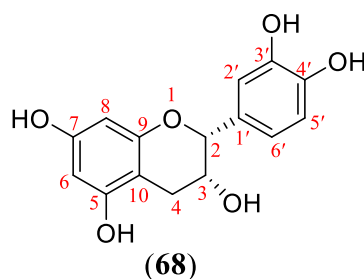
Table XXXIII: ^{1}H (500 MHz) and ^{13}C (125 MHz) NMR spectral data of PBR2 in CD$_3$OD compared to those of epicatechin [^{13}C NMR (100 MHz) and ^{1}H NMR (400 MHz) in CD$_3$OD] (Usman *et al.*, 2016)

Position	PBER2		Epicatechin	
	δ_C	δ_H (nH, m, *J* in Hz)	δ_C	δ_H (nH, m, *J* in Hz)
1	/	/	/	/
2	78.5	4.84 (1H, brs)	79.9	4.82 (1H, brs)
3	66.1	4.20 (1H, m)	67.5	4.19 (1H, m)
4a	27.8	2.88 (1H, dd, *J* =16.7, 4.6)	29.3	2.86 (1H, dd, *J* =16.8, 4.5)
4b		2.75 (1H, dd, *J* =16.8, 3.0)		2.73 (1H, dd, *J* =16.8, 3.0)
5	156.6	/	157.4	/
6	95.0	5.94 (1H, d, *J* = 2.3)	96.4	5.93 (1H, d, *J* = 2.3)
7	156.3	/	157.9	/
8	94.5	5.96 (1H, d, *J* = 2.3)	95.9	5.96 (1H, d, *J* = 2.3)
9	156.0	/	157.7	/
10	98.7	/	100.1	/
1′	130.9	/	132.3	/
2′	114.5	6.99 (1H, d, *J* = 2.0)	115.3	6.99 (1H, d, *J* = 1.7)
3′	144.6	/	145.9	/
4′	144.4	/	145.8	/
5′	113.9	6.78 (1H, d, *J* = 8.1)	115.9	6.77 (1H, d, *J* = 8,2)
6′	118.0	6.82 (1H, dd, *J* = 8.2, 2.0)	119.4	6.81 (1H, dd, *J*=8.2, 1,7)
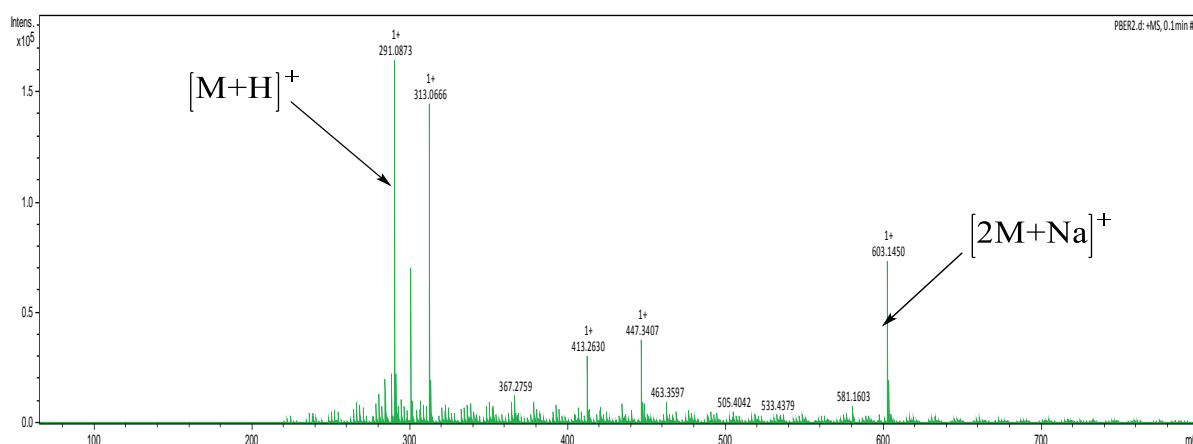
Figure 79: HR-ESI-MS spectrum of compound PBER2
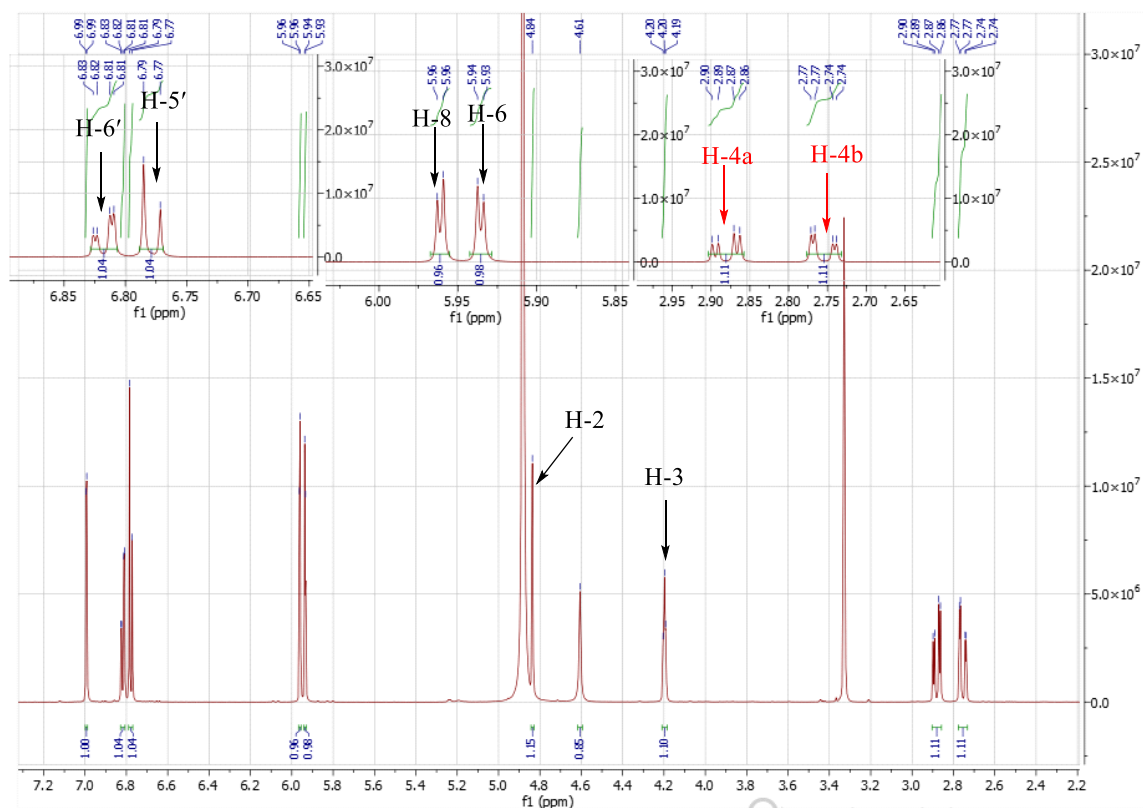
Figure 80: ¹H NMR spectrum (CD₃OD, 500 MHz) of compound PBER2
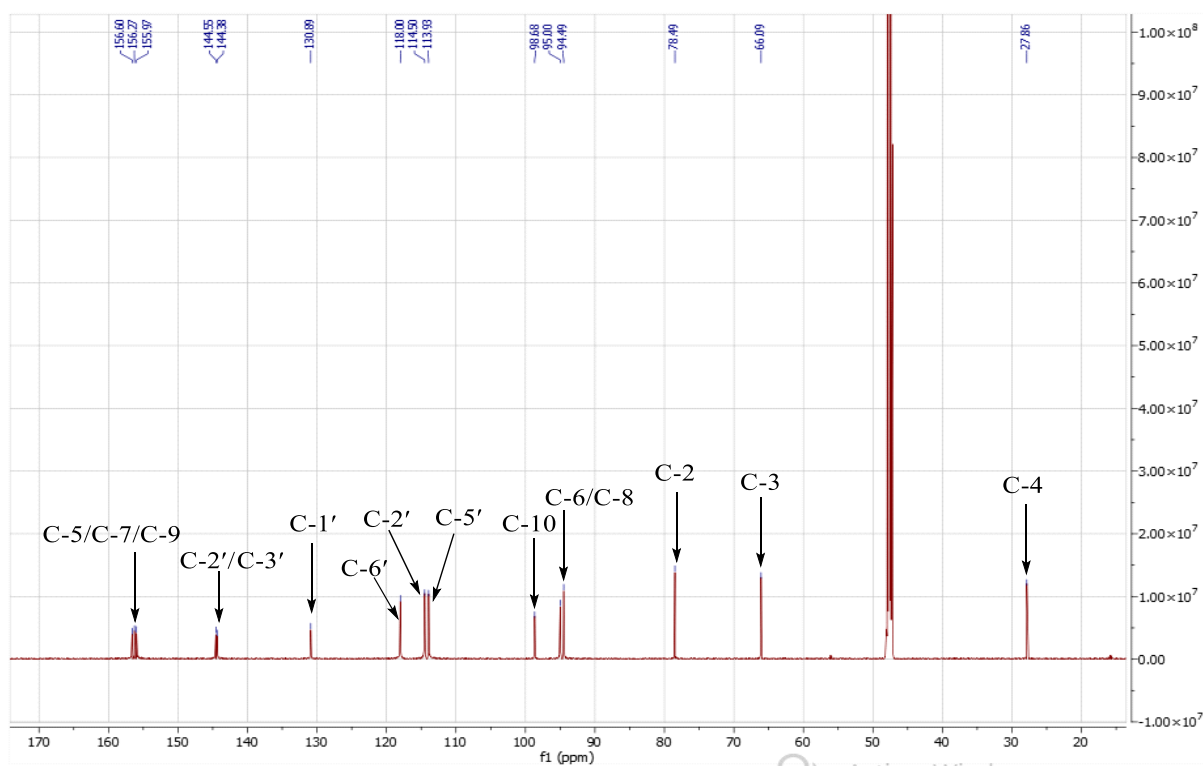
Figure 81: ¹³C NMR spectrum (CD₃OD, 125 MHz) of compound PBER2
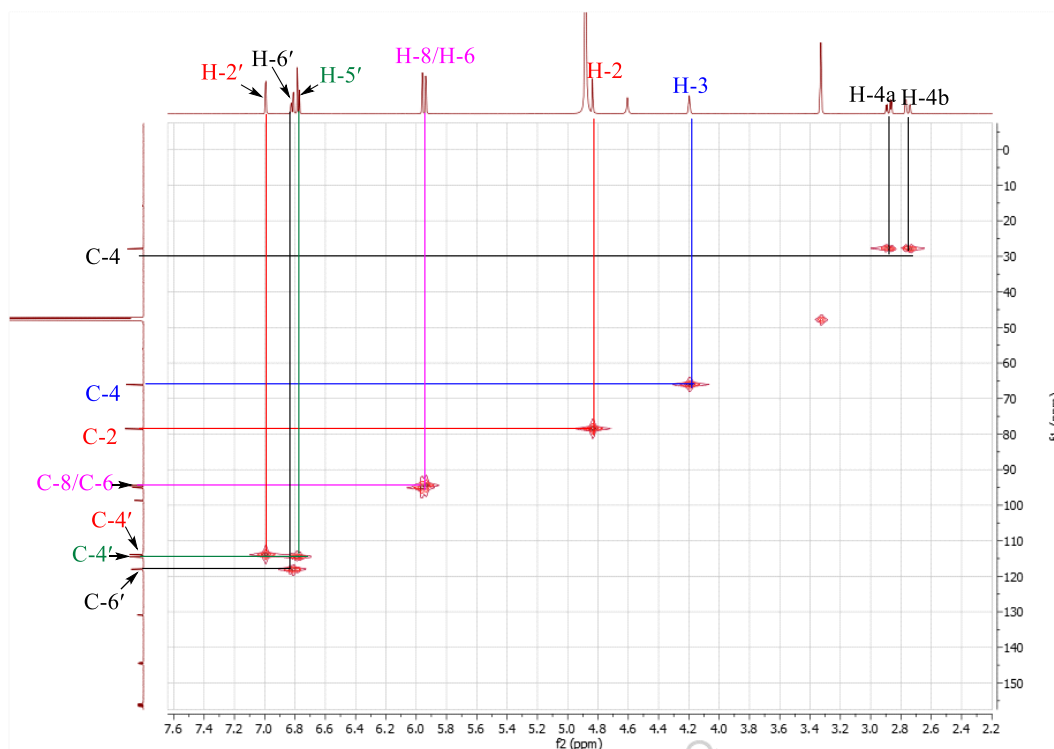
Figure 82: HSQC spectrum of compound PBER2
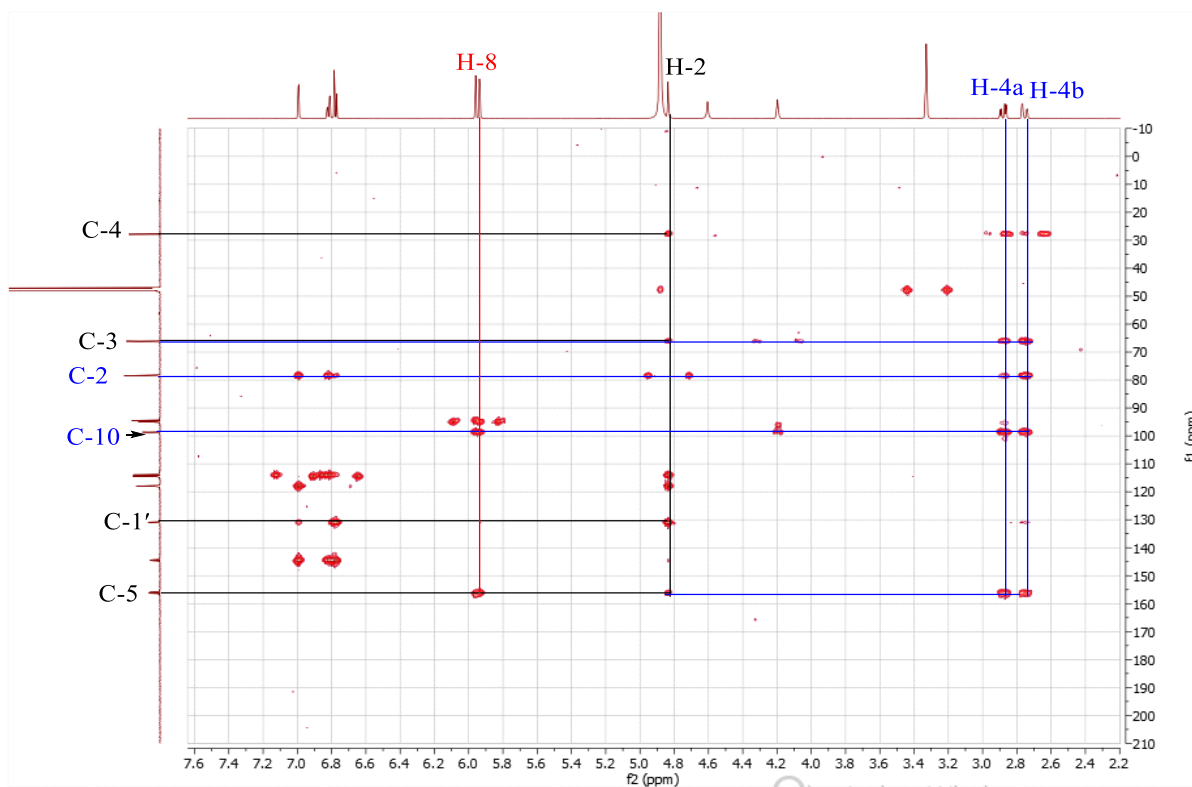
Figure 83: HMBC spectrum of compound PBER2
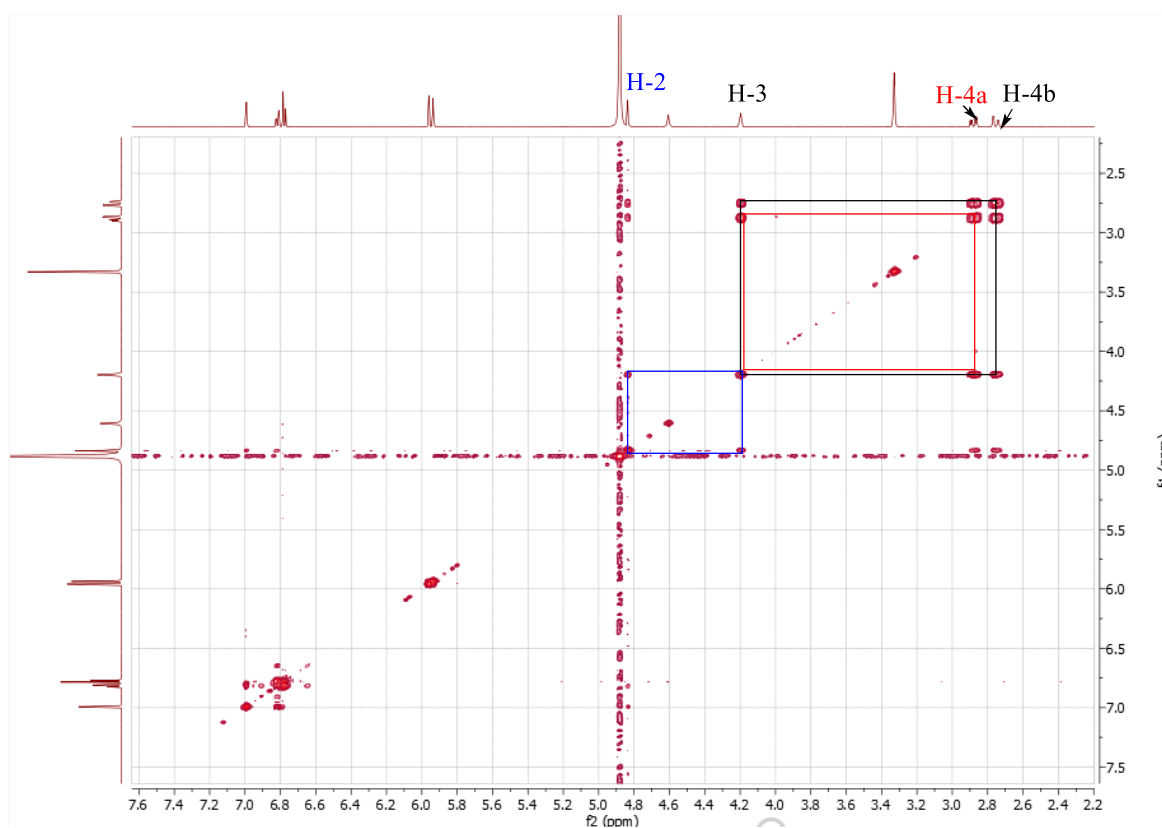
Figure 84: COSY spectrum of compound PBER2

II.2.1.4. Benzophenone

II.2.1.4.1 Identification of ECTF3

ECTF3 was obtained as a white amorphous solid. It gives a purple color with a methanolic solution of ferric chloride indicating its phenolic nature. Analysis of all its spectral data allowed us to assign to this compound the structure (**69**), corresponding to a mixture of two regioisomers in the proportion (1:1). The presence on its LC-MS profile (Figure 87) showed a single peak confirming that the two compounds are isomers.

(**69a**)   (**69b**)
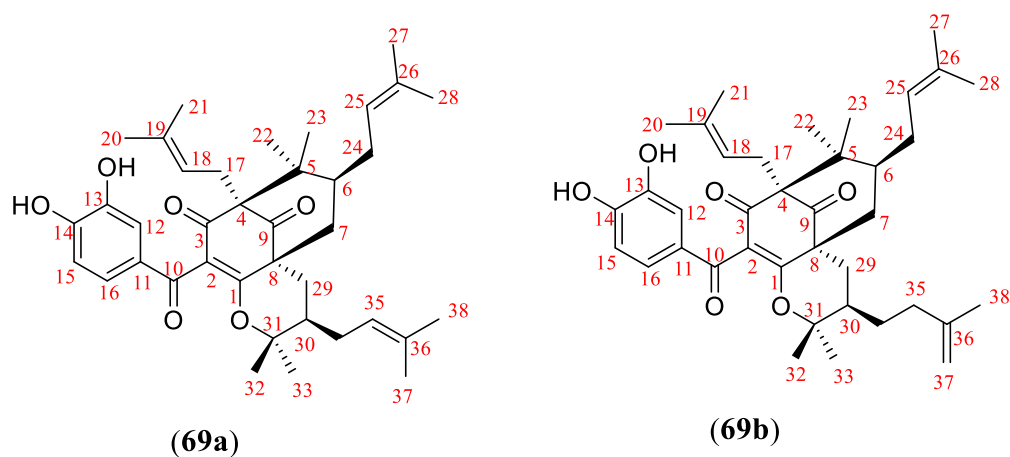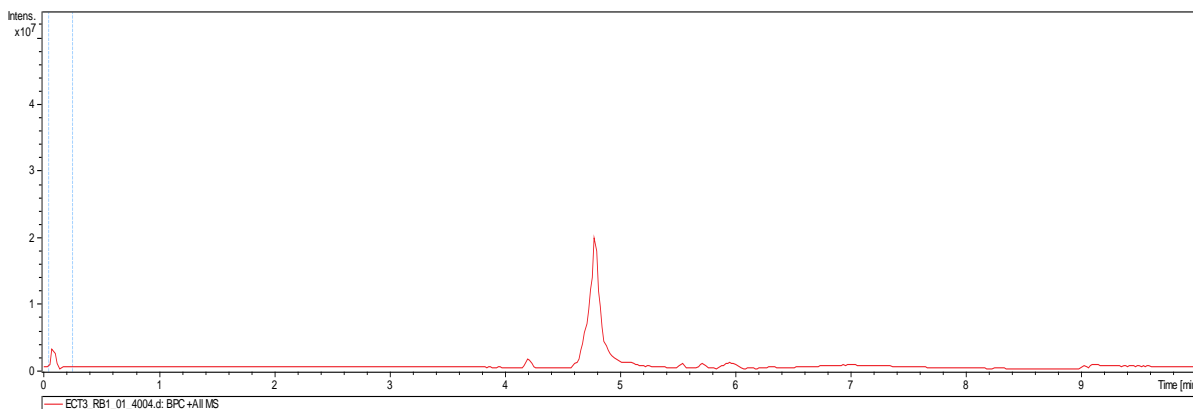
Figure 85: LC-MS profile of compound ECTF3

Its HR-ESI (+) mass spectrum in positive mode (Figure 86) shows a single peak corresponding to the protonated ion $[M+H]^+$ at *m/z* 603.3686 (calculated *m/z* 603.3680) corresponding to the molecular formula $C_{38}H_{50}O_6$ containing fourteen degrees of unsaturation.

Its ^1H NMR spectrum (Figures 87) showed two AMX systems, one at δ_H 7.33 (1H, d, *J* = 2.0 Hz, H-12), 7.03 (1H, dd, *J* = 8.2, 2.0 Hz, H-16) and 6.79 (1H, d, *J* = 8.2 Hz, H-15), the other at δ_H 7.30 (1H, d, *J* = 2.0 Hz, H-12), 6.96 (1H, dd, *J* = 8.4, 2.0 Hz, H-16) and 6.75 (1H, d, *J* = 8.2 Hz, H-15).

It is also noted the presence of five vinyl protons at δ_H 4.95 (2H, t, *J* = 6.2 Hz, H-18), 5.23 (1H, t, *J* = 6.9 Hz, H-35) and 4.96 (2H, brs, H-25), one terminal methylenic protons at δ_H 4.78 (2H, d, *J* = 4.8 Hz, H-37), five allylic methylene protons in the region δ_H 2.26 to 2.72 and seven vinyl methyl protons. This suggests the presence in the structure of five isopent-2-enyl groups and one isopent-3-enyl groups (Sub-structures 1 and 2).
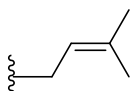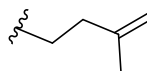
SS1   SS2

Its ^{13}C NMR spectrum (Figures 88) showed more than thirty eight carbon signals. Indeed, some signals are accompanied by a very close chemical shift signal of the same intensity. Analysis of the of DEPT 135 spectrum was used (Figure 89) to distinguish six aromatic carbons including three methine carbons at δ_C 151.3 (C-14), 145.6 (C-13), 129.6 (C-11), 122.2 (C-16), 115.1 (C-12), 114.8 (C-15) and a carbonyl conjugated carbon at δ_C 191.6 (C-10), suggesting the presence of a 3,4-dihydroxybenzoyl group (substructure 3) characteristic of benzophenones (Gustafson *et al.*, 1992).
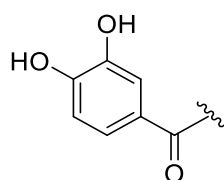
SS3

This same spectrum also shows, the signals of an unconjugated carbonyl of a ketone at δ_C 206.7 (C-9), three quaternary carbons at δ_C 67.9 (C-4), 51.4 (C-8) and 45.8 (C- 5), a ketone at δ_C 193.6 (C-3), the carbons of an enol function at δ_C 120.7 (C-2) and 170.6 (C-3), a methine carbon at δ_C 46.0 (C-6) and a methylene carbon at δ_C 38.4 (C-7). All these signals indicate the presence of a bicyclo[3.3.1]nonane unit (Substructure 4) characteristic of guttiferones (Gustafson *et al.*, 1992).
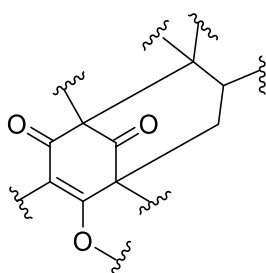
SS4

The confirmation of these substructures was established based to the correlations observed on the HMBC spectrum (Figure 90), that were observed between:

-the proton at δ_H 7.33 (H-12) and the carbons at δ_C 191.6 (C-10), 145.6 (C-13), 129.6 (C-11);

-the proton at δ_H 6.79 (H-15) and the carbons at δ_C 151.3 (C-14), 129.6 (C-11), 122.2 (C-16);

-the proton at δ_H 7.03 (H-16) and the carbons at δ_C 191.6 (C-10), 114.8 (C-15), 129.6 (C-11).

Hence the following substructure was established (SS3):
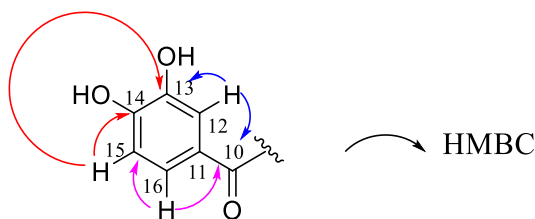
SS3

The same spectrum presents correlations between:

- the pronton at δ_H 2.25 (H-7) and the carbons at δ_C 206.7 (C-9), 170.6 (C-1) and 45.8 (C-5);

- the proton δ_H 1.13 (H-22) and carbons at δ_C 67.9 (C-4), 51.1 (C-5);

- the proton at δ_H 0.98 (H-23) and the carbon at δ_C 51.1 (C-5);

That led to the following substructure (SS4):
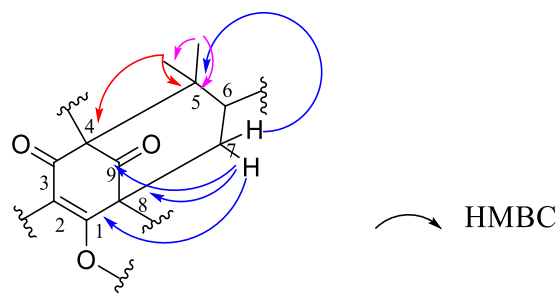
SS4

This spectrum also showed correlations between:

- the proton at δ_H 1.55 (H-21) and the carbons at δ_C 133.2 (C-19), 120.8 (C-18);

- the proton at δ_H 4.91 (H-18) and the carbons at δ_C 25.4 (C-17), 17.6 (C-21);

- the proton at δ_H 4.96 (H-25) and the carbons at δ_C 132.9 (C-26), 25.5 (C-27);

- the proton at δ_H 2.72 (H-24) and the carbons at δ_C 132.9 (C-26), 125.5 (C-25);

- the proton at δ_H 2.26 (H-34) and the carbon at δ_C 145.0 (C-36).

- the proton at at δ_H 1.73 (H-38) and carbon at δ_C 110.7 (C-37).

Hence the following substructures:

SS1′   SS1″   SS1‴   SS2′
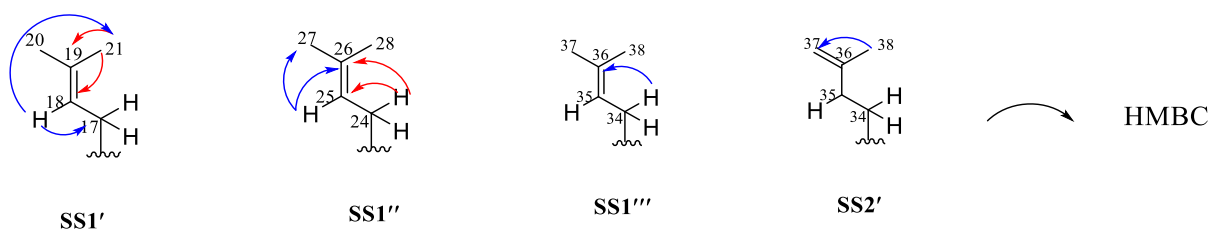
The junctions of these substructures were established based to the correlations observed on the HMBC spectrum (Figure 90, scheme 21), That were observed between:

-the proton at δ_H 2.60 (H-17) and the carbons at δ_C 67.9 (C-4), 193.6 (C-3);

- the proton at δ_H 2.72 (H-24) and the carbon at δ_C 38.4 (C-7);

- the proton at δ_H 2.25 (H-7) and the carbon at δ_C 29.2 (C-24);

- the proton at δ_H 2.26 (H-29) and the carbon at δ_C 170.6 (C-1).

a Δ^{35}

b Δ^{36}
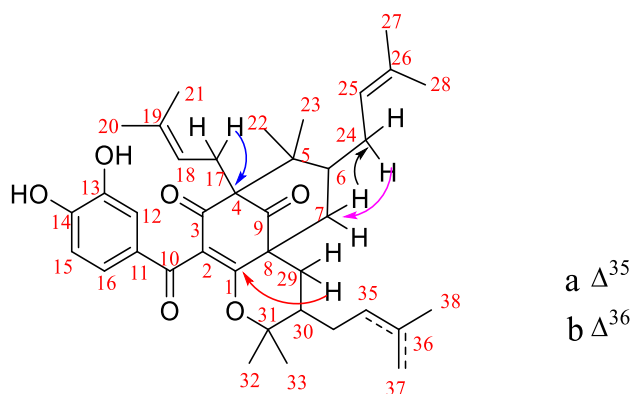
Scheme 21: Seleted HMBC corrélations of compound ECTF3

All these data, compared with those described in the literature (Table XXXIV), enabled to assign to ECTF3 structure (**69**) see the previous, which is the mixture (1:1) of isoxanthochymol and cycloxanthochymol, isolated previously from the fruits of *Garcinia pyrifera* (Roux *et al*., 2000).

Table XXXIV: Spectral data of ^1H (500 MHz) and ^{13}C (125 MHz) of ECTF3 in C_3D_6O compared with those from the mixture of isoxanthochymol (a)/ cycloxanthochymol (b) (DMSO-d_6, 75 MHz). (Roux *et al*., 2000)

Position	ECTF3		Isoxanthochymol (a)/ cycloxanthochymol (b)	
	δ_C	δ_H (nH, m, *J* in Hz)	δ_C	δ_H (nH, m, *J* in Hz)
1	170.6	/	172.4	/
2	120.7	/	119.6	/
3	193.8(**a**), 193.6 (**b**)	/	193.1	/
4	67.7	/	68.3	/
5	51.1	/	51.3 (**a**), 51.5 (**b**)	/
6	46.0 (**a**), 45.9 (**b**)	1.51 (m)	46.4 (**a**), 46.3 (**b**)	1.50 (m)
7	38.4 (**a**), 38.7(**b**)	2.24, 2.25 (m)	39.9	1.81, 2.51 (m)
8	51.5	/	53.4	/
9	206.7	/	209.0	/
10	191.6 (**a**), 191.5 (**b**)	/	194.8	/
11	129.7(**a**), 129.6 (**b**)	/	130.0	/
12	115.1 (**a**), 115.4 (**b**)	7.33 (d, *J* = 2.0 Hz)	114.9	7.41 (d, *J* = 2.1 Hz)
13	145.6 (**a**), 145.7 (**b**)	/	144.1	/
14	151.3	/	150.1	/
15	114.8	6.79 (d, *J* = 8.2 Hz)	114.3	6.70 (d, *J* = 8,0 Hz)
16	122.2 (**a**), 122.4 (**b**)	7.03 (dd, *J* = 8.0, 2.0 Hz)	124.1 (**a**), 124.0 (**b**)	7.03 (dd, *J* = 8.0, 2.1 Hz)
17	25.4	2.40, 2.60 (m)	25.6	2.51, 2.63 (m)
18	120.8 (**a**), 120.7 (**b**)	4.95 (brs)	121.3	4.83 (m)
19	133.9 (**a**), 133.0 (**b**)	/	134.7	/
20	25.3 (**a**), 25.4 (**b**)	1.59 (s)	26.1	1.55 (s)
21	17.6	1.55 (s)	18.1	1.66 (s)
22	21.9	1.13 (s)	22.5	0.99 (s)
23	26.2 (**a**), 26.2 (**b**)	0.98 (s)	26.8 (**a**), 26.7 (**b**)	0.99 (s)
24	28.3 (**a**), 28.1(**b**)	2.10, 2.72 (m)	28.2 (**a**), 28.0 (**b**)	2.20, 2.59 (m)
25	125.5 (**a**), 125.4 (**b**)	4.96 (m)	124.9 (**a**), 124.8 (**b**)	4.92 (m)
26	132.9	1.68 (s)	133.6	1.68 (s)
27	25.5 (**a**), 25.4 (**b**)	1.77 (s)	25.9 (**a**), 25.7 (**b**)	1.68 (s)
28	17.9 (**a**), 17.5 (**b**)	1.55 (s)	18.0 (**a**), 17.9 (**b**)	1.58 (s)

29	38.6 (**a**), 38.4 (**b**)	2.27 (m)	39.6 (**a**), 39.8 (**b**)	1.88, 2.08 (m)
30	42.7 (**a**), 41.7 (**b**)	1.47 (m)	42.9 (**a**), 42.1 (**b**)	3.06 (m)
31	86.8 (**a**), 86.4 (**b**)	/	87.1 (**a**), 86.9 (**b**)	/
32	21.0	1.25 (s)	21.2	1.17 (s)
33	28.4 (**a**), 28.2 (**b**)	0.87 (s)	28.6 (**a**), 28.4 (**b**)	0.90 (s)
34	29.2(**a**), 29.4 (**b**)	2.12 (**a**) (m), 2.05 (**b**) (m)	29.6 (**a**), 29.4 (**b**)	2.11(**a**) (m), 1.47 (**b**) (m)
35	122.0 (**a**), 35.2 (**b**)	5.23 (**a**) (m), 2.25 (**b**) (m)	121.3 (**a**), 35.2 (**b**)	5.09 (**a**) (m), 1.85 (**b**) (m)
36	133.2 (**a**), 145.0 (**b**)	/	133.2 (**a**), 144.9 (**b**)	/
37	26.2 (**a**), 110.7 (**b**)	1.98 (s) (**a**), 4.78 (d, J = 4.6 Hz)	26.8 (**a**), 110.6 (**b**)	1.68 (**a**) (s), 4.76 (**b**) (brs)
38	17.9 (**a**), 22.0 (**b**)	1.68 (**a**) (s), 1.73 (**b**) (s)	18.1 (**a**), 22.5 (**b**)	1.56 (**a**) (s), 1.68 (**b**) (s)
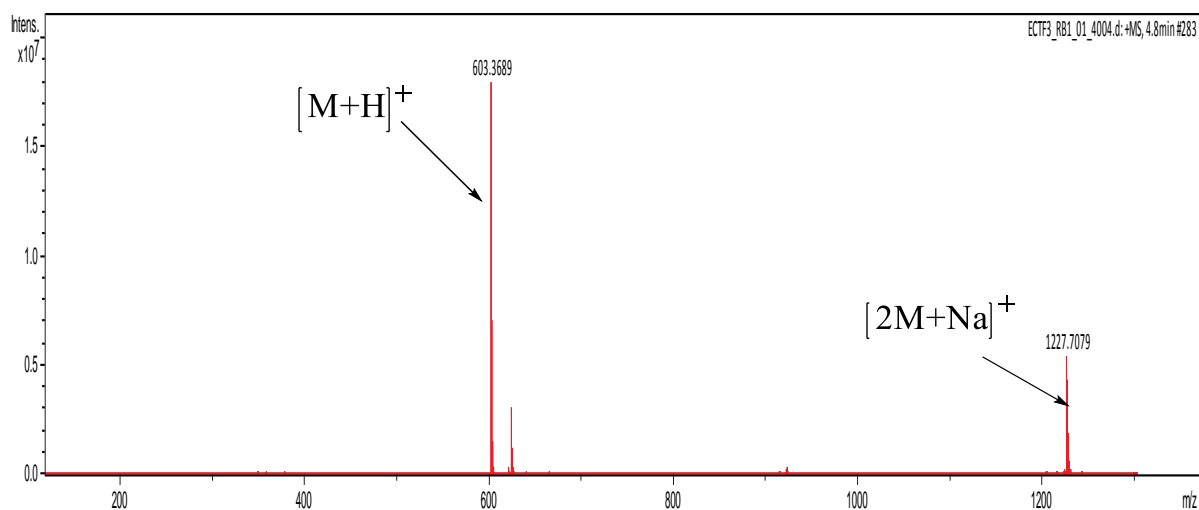
Figure 86: HR-ESI-MS spectrum of compound ECTF3
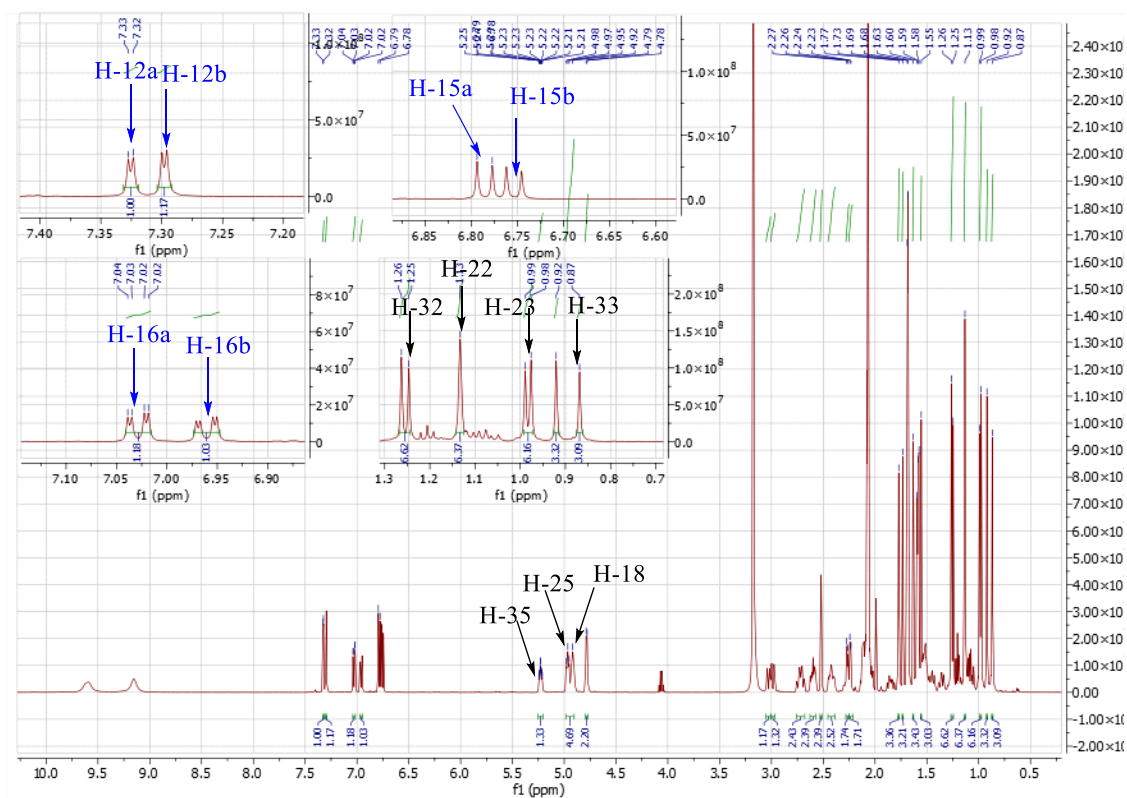
Figure 87: ^{1}H NMR spectrum (C$_3$D$_6$O, 500 MHz) of compound ECTF3
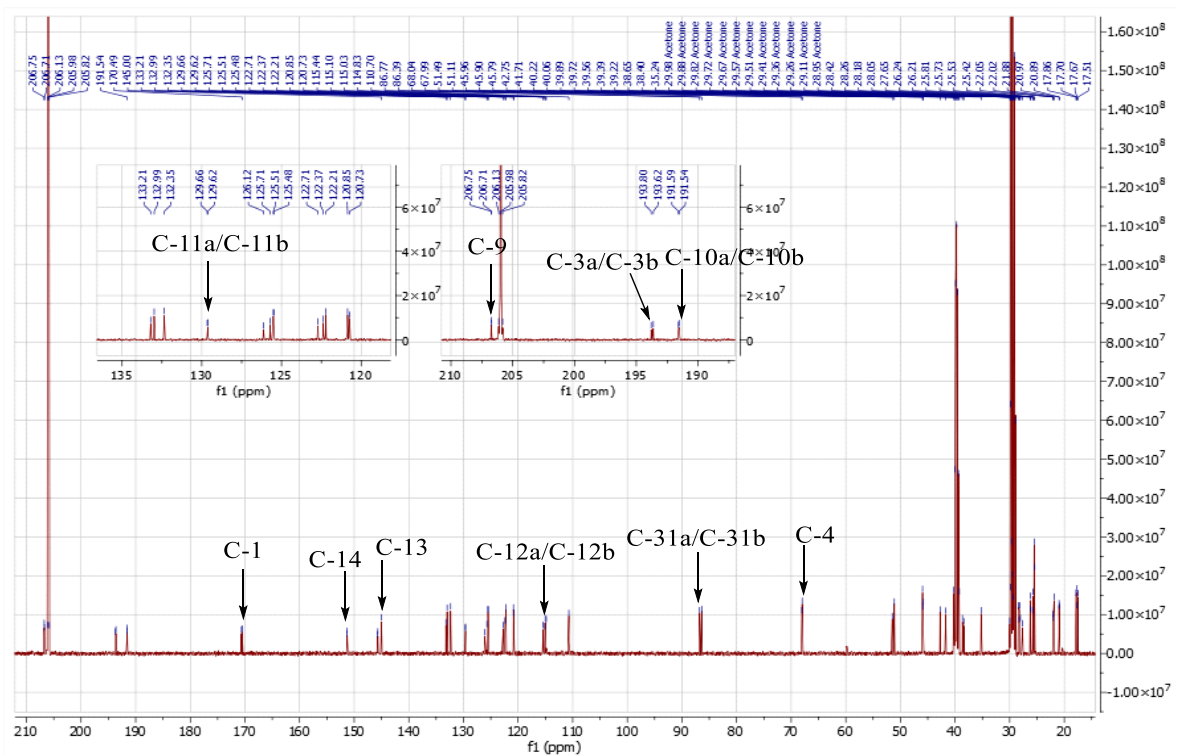
Figure 88: ^{13}C NMR spectrum (C$_3$D$_6$O, 125 MHz) of compound ECTF3
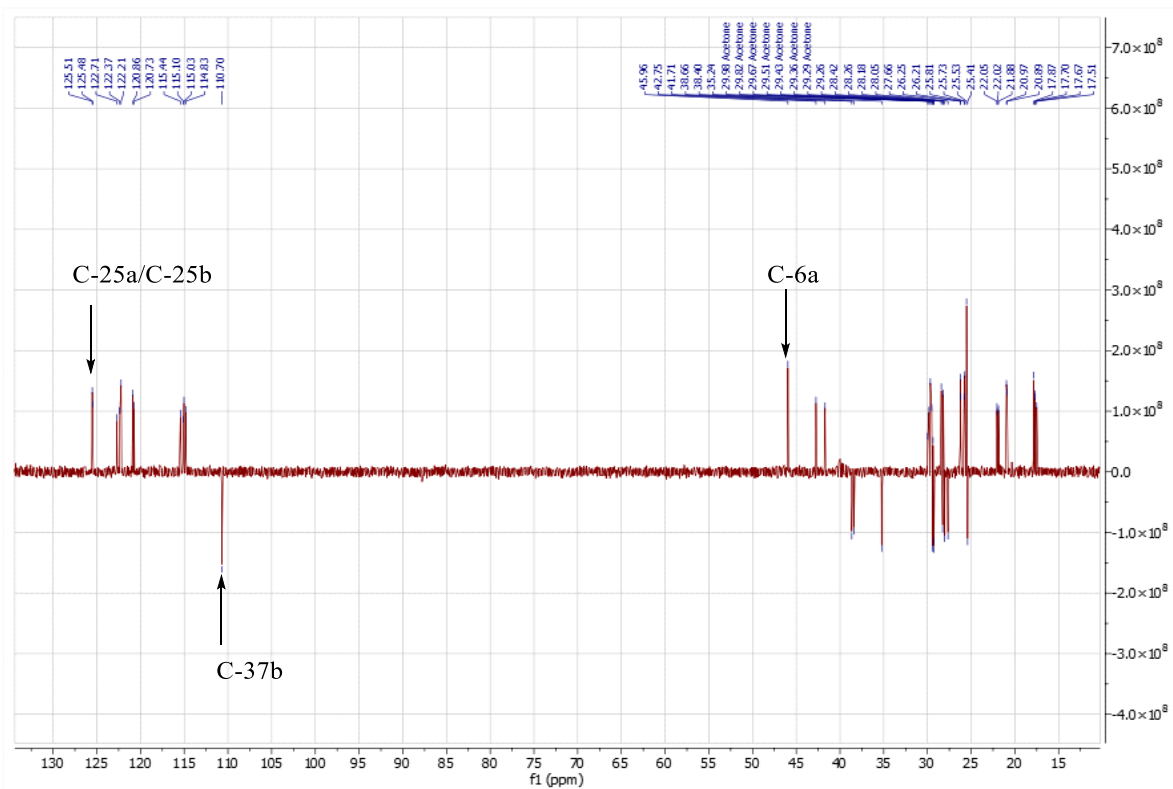
Figure 89: DEPT135 spectrum of compound ECTF3
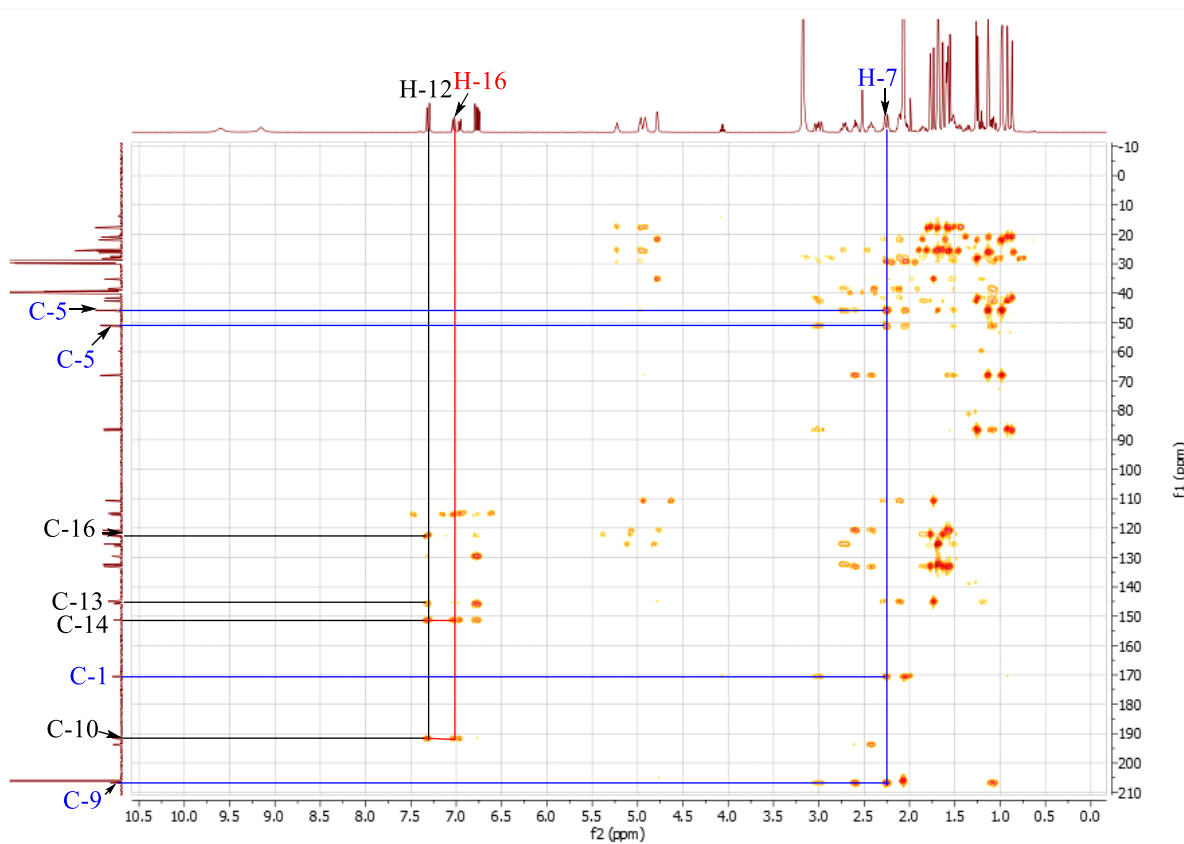
Figure 90: HMBC spectrum of compound ECTF3

II.2.1.5. Glucosylated sesquiterpenoid

II.2.1.5.1 Identification of ECTF44

ECTF44 was obtained as a brown oil. It is soluble in methanol and respond positively to the Molish test, giving a red coloration characteristic of sugars.

Its HR-ESI (+) mass spectrum (Figure 91) showed the protonated ion $[M+H]^+$ at m/z 443.1911 corresponding to the molecular formula $C_{21}H_{30}O_{10}$ (calculated for 443.1912), containing seven unsaturations.

All these data, compared with those described in the literature (table XXXV), enabled the attribution of structure (**70**) to ECTF44, which is that of absicic acid β-D-glucoside, previously isolated from *Persea americana* (Ramos *et al*., 2004).

(**70**)
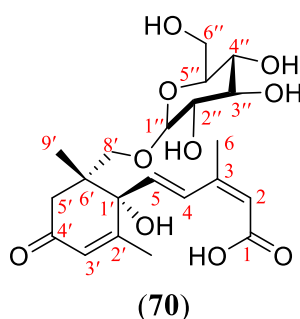
Indeed, on its ^{13}C NMR spectrum (Figure 93), signals of 21 carbon atoms were distinguished and sorted using DEPT 135 technique (Figure 94) in:

- three methyl carbon at δ_C 18.3 (C-7′), 18.9 (C-9′), and 19.1 (C-6);

- three methylene group including two linked to a hydroxyl group at δ_C 61.3 (C-6″), and 73.2 (C-8′), and one linked to the carbonyl at δ_C 43.9 (C-5′);

- four methine carbon signals attributable to ethylenic carbons at δ_C 126.5 (C-3′), 127.9 (C-2), 129.6 (C-4) and 131.1 (C-5), and five methine carbons attributable to sugar unit at δ_C 103.3 (C-1″), attributable to anomeric carbon; and those at δ_C 70.1 (C-4″), 73.8 (C-2″), 76.5 (C-5″), 76.6 (C-3″);

- six quatenary carbon signals amongst which the signal of a carbonyl carbon at δ_C 199.8 (C-4′); one carboxyl at δ_C 174.3 (C-1); and others at δ_C 45.3 (C-6′), 78.6 (C-1′), 138.2 (C-3), 165.3 (C-2′).

Its ^1H NMR spectrum (Figure 92) showed:

- the signals of the protons of a double bond of *trans* configuration at δ_H 5.94 (1H, d, $J = 16.1$ Hz, H-5) and δ_H 7.57 (1H, d, $J = 16.1$ Hz, H-4);

- a singlet of methyl protons at δ_H 1.09 (H-9′);

- two signals integrating for three protons at δ_H 1.94 (3H, brs, H-6) and δ_H 1.92 (3H, brs, H-7′) attributable to methyls in α of an olefinic group;

- signals at δ_H 5.87 (1H, s, H-2) and δ_H 5.93 (1H, s, H-3′) attributable to protons bound to *sp2* carbons;

- the signals of two diastereotopic protons of a methylene at δ_H 2.72 (1H, d, J = 17.1 Hz, H-5′α) and δ_H 2.42 (1H, d, J = 17.1 Hz, H-5′β) attributable to protons bound to an α carbon of the carbonyl;

- the signals of two diastereotopic protons of a methylene at δ_H 3.62 (1H, d, J = 10.0 Hz, H-8′) and δ_H 3.97 (1H, d, J = 10.0 Hz, H-8′) attributable to the protons of an oxidized methylene;

- The signals of two diastereotopic protons of a methylene at δ_H 3.68 (1H, dd, J = 11.9, 2.2Hz, H-6″) and δ_H 3.86 (1H, dd, J = 11.9, 2.2 Hz, H-6″) attributable to the protons of an oxidized methylene;

- signals between δ_H 3.16 (1H, dd, J = 9.0, 7.9 Hz, H-2″) and δ_H 3.68 (1H, dd, J = 10.0, 5.0 Hz, H-6″) attributable to the protons of a glycosidic unit;

The HMBC spectrum (Figure 95) of ECTF44, exhibits the correlations between:

-the proton H-2 (δ_H 5.87) and carbons C-4 (δ_C 129.6), C-6 (δ_C 19.1);

- the proton H-4 (δ_H 7.57) and the carbons C-3 (δ_C 138.2), C-1′ (δ_C 78.6), C-6 (δ_C 19.1);

- the proton H-3′ (δ_H 5.93) and the carbons C-2′ (δ_C 165.3), C-7′ (δ_C 18.3), C-1′ (δ_C 78.6);

- the proton H-5′ (δ_H 2.42) and the carbons C-4′ (δ_C 199.8), C-6′ (δ_C 45.3), C-1′ (δ_C 78.6), C-8′ (δ_C 73.2), C-9′ (δ_C 18.9);

- the proton H-5′ (δ_H 2.72) and the carbons C-4′ (δ_C 199.8), C-6′ (δ_C 45.3), C-1′ (δ_C 78.6), C-3′ (δ_C 126.5);

 - the proton H-9′ (δ_H 1.09) and the carbons C-5′ (δ_C 43.9), C-6′ (δ_C 45.3), C-1′ (δ_C 78.6), C-8′ (δ_C 73.2):

- the proton H-8′ (δ_H 3.62) and carbon C-9′ (δ_C 18.9);

- the proton H-8′ (δ_H 3.97) and the carbons C-5′ (δ_C 43.9), C-1″ (δ_C 103.3), C-1′ (δ_C 78.6).

These data show the existence of a substructure of the abscisic acid type (SS1), with characteristic cortrelations observed on its COSY spectrum (Figure 96):

-the proton H-4 (δ_H 7.57) and the proton H-5 (δ_H 5.94).
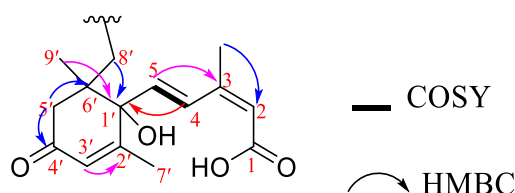
Scheme 22: Selected HMBC and COSY correlations of the abscissic group

In addition, the signal at δ_H 4.17 (1H, d, J = 7.8 Hz) attributable to the proton of the anomeric carbon. This glycosidic unit has been identified as β-glucose based on the chemicals NMR data and coupling constant of anomeric proton (Agrawal, 1992).

The HMBC spectrum (Figure 95) also shows the correlations in the glucosidic unit between:

- the proton H-4″ (δ_H 3.36) and the carbons C-6″ (δ_C 61.3), C-3″ (δ_C 76.6), C-5″ (δ_C 76.5);

- the proton H-3″ (δ_H 3.41) and the carbon C-4″ (δ_C 70.1);

- the proton H-2″ (δ_H 3.16) and the carbons C-1″ (δ_C 103.3), C-4″ (δ_C 70.1), C-3″ (δ_C 76.6);

- the proton H-6″ (δ_H 3.86) and the carbons C-4″ (δ_C 70.1), C-5″ (δ_C 76.5).

This last correlations led to the glucosidic type substructure (SS2), of which the COSY spectrum (Figure 96), shows correlations between:

- the proton H-1″ (δ_H 4.17) and the proton H-2″ (δ_H 3.16);

- the proton H-6″ (δ_H 3.86) and the proton H-5″ (δ_H 3.22);

- the proton H-5″ (δ_H 3.22) and the proton H-6″ (δ_H 3.68);

- the proton H-2″ (δ_H 3.16) and the proton H-3″ (δ_H 3.36).
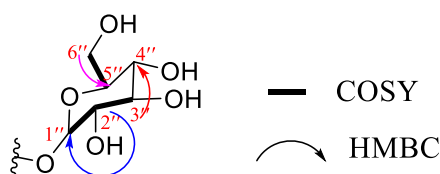
Scheme 23: Selected HMBC and COSY correlations of the glucosidic group

The junction between sugar unit anr the absicic acid skeleton was established based on the correlations observed on its HMBC spectrum (Figure 95, scheme 24) between:

- the proton H-1″ (δ_H 4.17) and carbons C-8′ (δ_C 73.2), and C-3″ (δ_C 76.6);

- the proton H-8′ (δ_H 3.62) and the carbon C-1′ (δ_C 103.3).
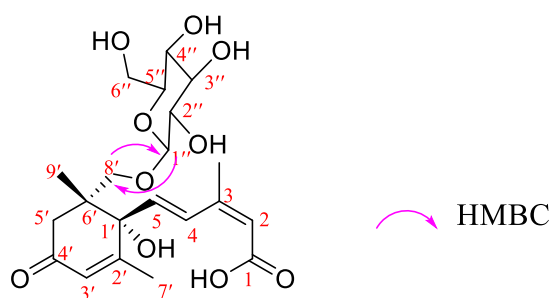
Scheme 24: Selected HMBC corrélations of the compound ECTF44

Table XXXV: ¹H NMR (500 MHz) and ¹³C (125 MHz) spectral data of ECTF44 in CD₃OD compared to those of absicic acid [¹³C NMR (75 MHz) and ¹H NMR (300 MHz)] in CD₃OD (Ramos *et al.*, 2004)

Position	ECTF44		absicic acid β-D-glucoside	
	δ_C	δ_H (nH, m, *J* in Hz)	δ_C	δ_H (nH, m, *J* in Hz)
1	174.3	/	/	/
2	127.9	5.87 (1H, s)	121.2	5.78 (1H, s)
3	138.2	/	150.0	/
4	129.6	7.57 (1H, d, *J* = 16.1 Hz)	129.6	7.75 (1H, d, *J* = 16.0 Hz)
5	131.1	5.94 (1H, d, *J* = 16.1 Hz)	136.3	6.15 (1H, d, *J* = 16.0 Hz)
6	19.1	1.92 (3H, s)	20.8	2.01 (3H, s)
1′	78.6	/	80.0	/
2′	165.3	/	166.3	/
3′	126.5	5.93 (1H, s)	127.9	5.94 (1H, s)
4′	199.8	/	200.5	/
5′	43.9	2.42 (1H, d, *J* = 17.1 Hz) 2.72 (1H, d, *J* = 17.1 Hz)	45.2	2.41 (1H, d, *J* = 17.0 Hz) 2.66 (1H, d, *J* = 17.0 Hz)
6′	45.3	/	46.6	/
7′	18.3	1.92 (3H, s)	19.3	1.93 (3H, s)
8′	73.2	3.62 (1H, d, *J* =10.0 Hz) 3.97 (1H, d, *J* =10.0 Hz)	74.4	3.62 (1H, d, *J* =10.0 Hz) 3.97 (1H, d, *J* =10.0 Hz)
9′	18.9	1.09 (3H, s)	20.0	1.08 (3H, s)
1″	103.3	4.17 (1H, d, *J* = 7.8 Hz)	104.4	4.16 (1H, d, *J* = 8.0 Hz)
2″	73.8	3.16 (1H, dd, *J* = 9.0, 7.9Hz)	74.9	3.15 (1H, dd, 8.5, 8.0Hz)
3″	76.6	3.36 (1H, d, *J* = 8.9 Hz)	77.8	3.27 (1H, d, *J* = 8.9 Hz)
4″	70.1	3.29 (1H, m)	71.3	3.30 (1H, m)
5″	76.5	3.22 (1H, d, *J* = 8.9 Hz)	77.7	3.24 (1H, d, *J* = 8.9 Hz)
6″	61.3	3.68 (1H, dd, *J* = 10.0, 5.0 Hz) 3.86 (1H, dd, *J* = 10.0, 2.0 Hz)	62.5	3.66 (1H, dd, *J* = 10.0, 5.0 Hz) 3.85 (1H, dd, *J* = 10.0, 2.0 Hz)
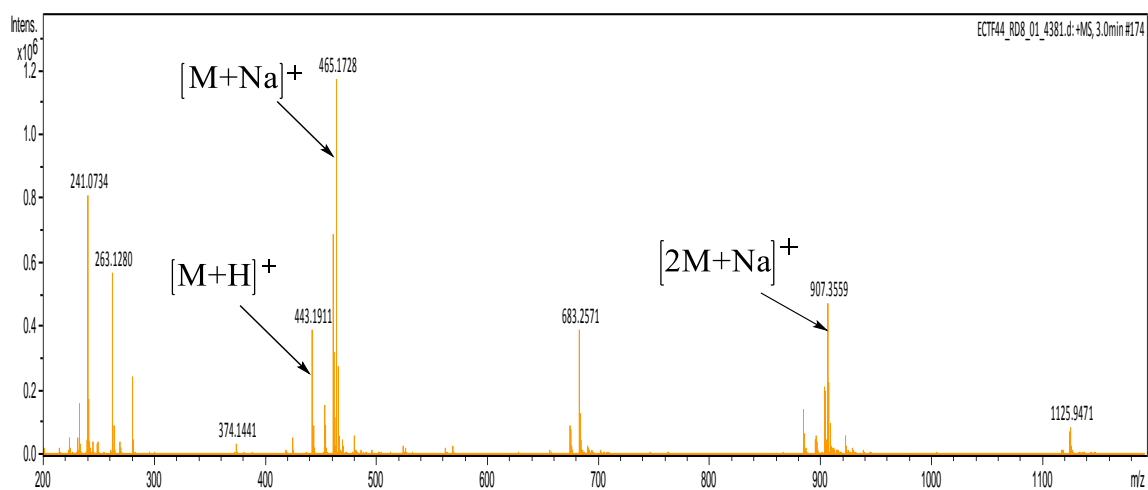
Figure 91: HR-ESI-MS spectrum of compound ECTF44
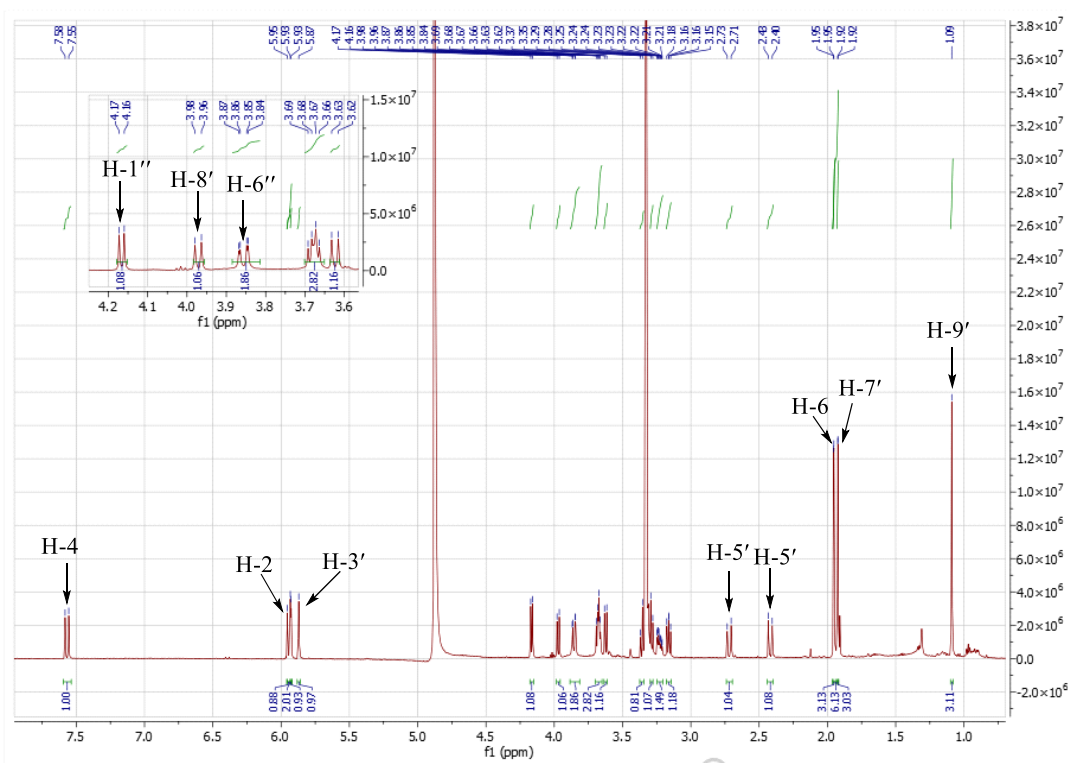
Figure 92: ¹H NMR spectrum (CD₃OD, 500 MHz) of compound ECTF44
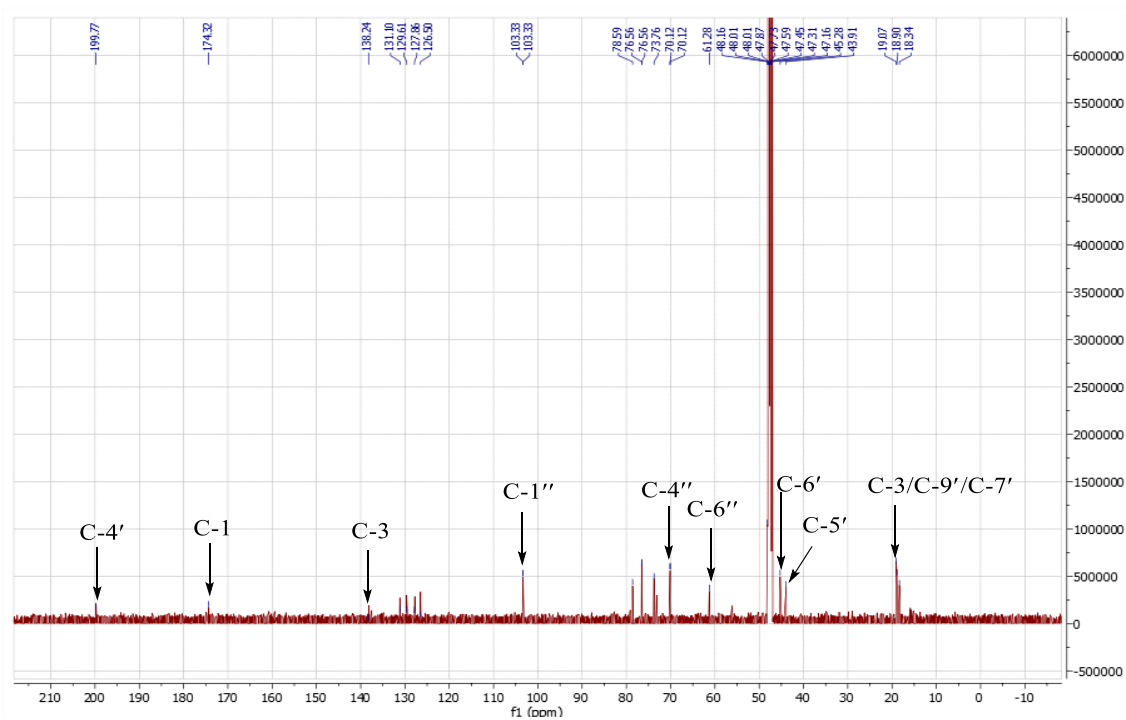
Figure 93: ^{13}C NMR spectrum (CD$_3$OD, 125 MHz) of compound ECTF44
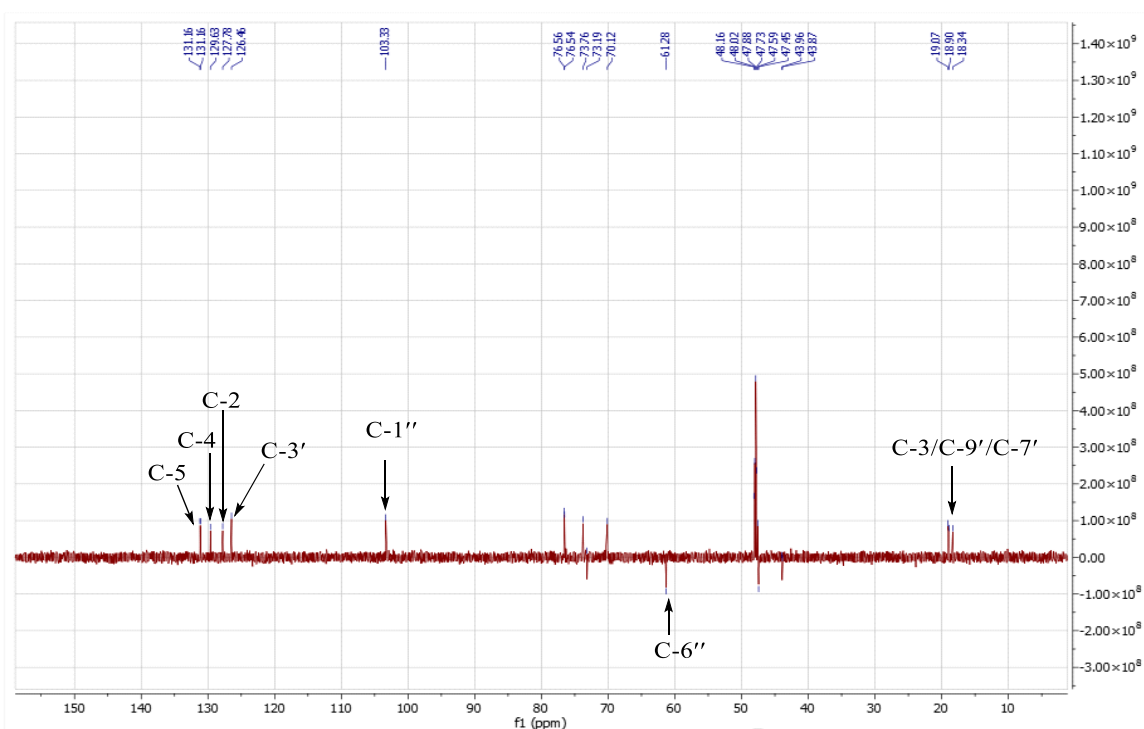
Figure 94: DEPT135 spectrum of compound ECTF44
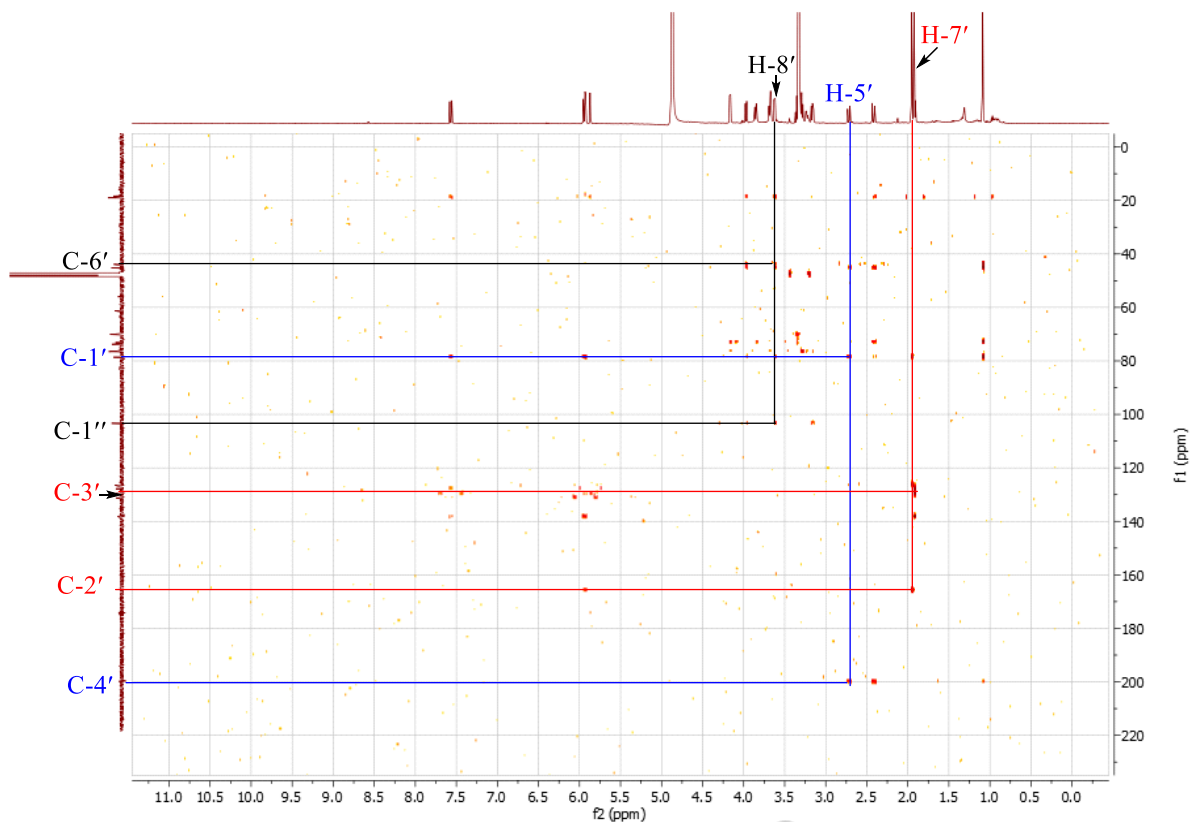
Figure 95: HMBC spectrum of compound ECTF44
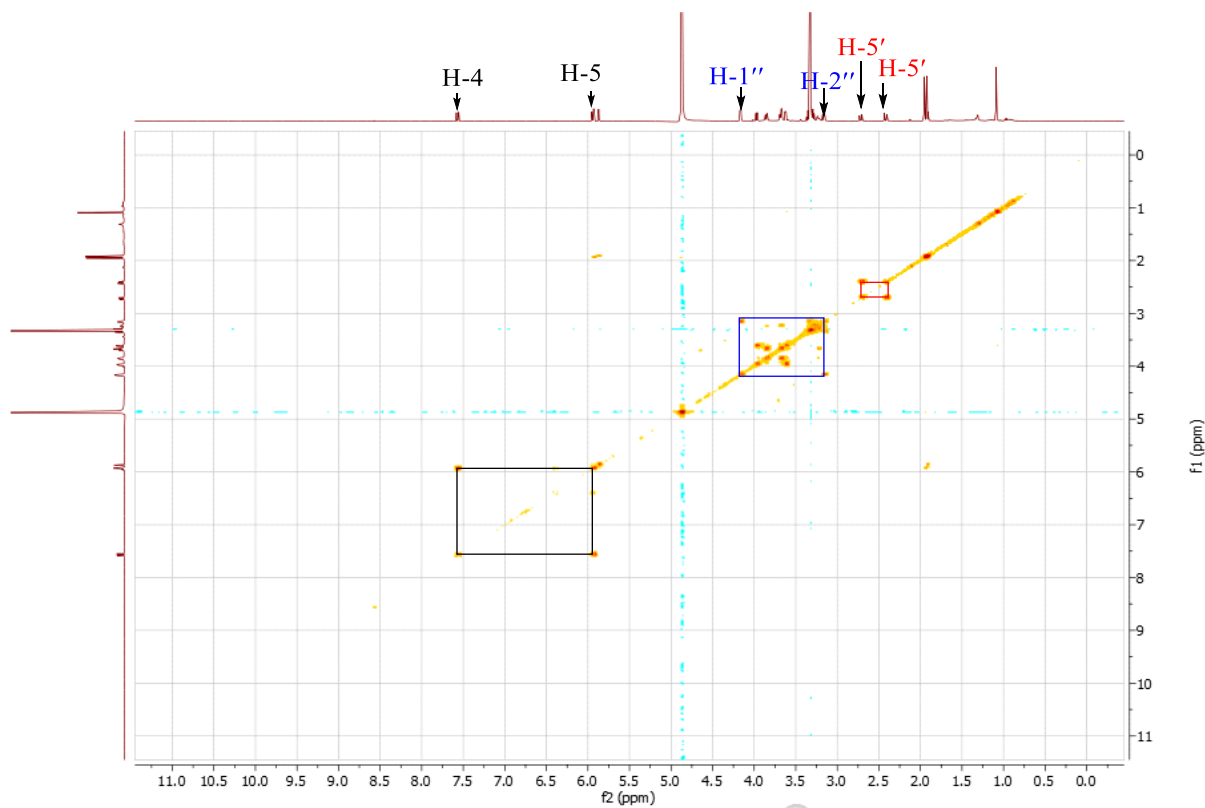
Figure 96: COSY spectrum of compound ECTF44

II.2.1.6. Phenolic compounds

II.2.1.6.1 Identification of ECTF41

ECTF41 was obtained as a brown oil. It was soluble in methanol and responds positively to the Molish test, giving a red color, characteristic of sugars and a blue coloration with a methanolic solution of ferric chloride indicating its phenolic nature.

Its ESI$^+$ mass spectrum (Figure 97) showed the peak of the sodium adduct [M+Na]$^+$ at m/z 325.11. This value, combined with the NMR data, gives the molecular formula $C_{13}H_{18}O_8$, containing five unsaturations.

All these data, compared with those described in the literature (Table XXXVI), allow the structure (**71**) to be attributed to ECTF41, which is that of tachioside.

(**71**)
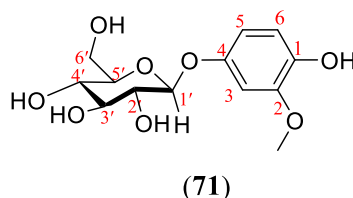
Its ^{1}H NMR spectrum (Figure 98) exhibited:

- an ABX aromatic signals at δ_H 6.60 (1H, dd, J = 8.6, 2.7 Hz, H-5), δ_H 6.72 (1H, d, J = 8.6 Hz, H -6) and δ_H 6.82 (1H, d, J = 2.7 Hz, H-3);

- signals of sugar unit were observed between δ_H 3.38 (1H, d, J = 8.3 Hz, H-4′) and δ_H 3.70 (1H, dd, J = 12.0, 2.1 Hz, H-6′), with the β-anomeric proton at δ_H 4.76 (1H, d, J = 7.8 Hz, H-1′).

-The methoxy group at δ_H 3.85 (O-CH3) were also observed.

Its ^{13}C NMR spectrum (Figure 99), signals of 13 carbon atoms were observed and using DEPT135 techniques (Figure 100) assigned as:

- 1 signal of a methoxyl carbon at δ_C 55.0 (OMe).

- 3 signals of methine carbons characteristic of an aromatic ring at δ_C 114.6 (C-6), 108.6 (C-5), and 102.4 (C-3);

- 3 hydroxylated quaternary signals belonging to an 1,2,4-trisubstituted aromatic ring at δ_C 141.5 (C-1), 147.8 (C-2), and 151.4 (C-4);

We also observed the following signals of carbons of a glucosidic group at δ_C 102.4 (C-1′), attributable to anomeric carbon; and those at δ_C 70.2 (C-4′), 73.6 (C-2 ′), 76.7 (C-5′), and 76.8 (C-3′) (Agrawal, 1992).

The HMBC spectrum (Figure 101), support the trisubstituted aromatic ring while the glucosidic unit is linked at para position based on the HMBC correlation from H-1′ (δ_H 4.76), H-3 (δ_H 6.82) and H-5 (δ_H 6.60) to C-4 (δ_C 151.4).

The methoxy group was linked at ortho position, following the HMBC correlation from the proton of the methoxy (δ_H 3.85) to carbon C-2 (δ_C 147.8).

The ROESY (Figure 102, scheme 25) correlation between H-1′ and H-3, confirm the proposed substitution.
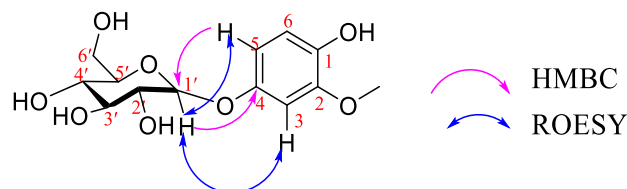
Scheme 25: Selected HMBC and ROESY correlations of ECTF41

All these data, compared with those described in the literature (Table XXXVI), enabled to assign to ECTF41 structure (**71**) see the previous, which is the tachioside, isolated previously from the stems of *Berchemia racemosa* (Inoshiri *et al.*, 1987).

Table XXXVI: ^{1}H NMR (500 MHz) and ^{13}C (150 MHz) spectral data of ECTF41 in CD$_3$OD compared to those of tachioside [^{13}C NMR (25 MHz)] in DMSO-d_6 (Inoshiri *et al.*, 1987).

Position	ECTF41		Tachioside
	δ_C	δ_H (nH, m, J in Hz)	δ_C
1	141.6	/	141.2
2	147.8	/	147.7
3	102.4	6.82 (1H, d, J = 2.7 Hz)	102.4
4	151.4		150.6
5	108.6	6.60 (1H, dd, J = 8.6, 2.7 Hz)	107.9
6	114.6	6.71 (1H, d, J = 8.6 Hz)	115.1
1′	102.4	4.76 (1H, d, J = 7.4 Hz)	101.6
2′	73.6	3.44 (1H, d, J = 7.8 Hz)	73.2
3′	76.8	3.41 (1H, d, J =7.8 Hz)	76.9
4′	70.2	3.38 (1H, d, J = 8.3 Hz)	69.9
5′	76.7	3.41 (1H, dd, J = 5.7, 2.0 Hz)	76.6
6′	61.3	3.92 (1H, d, J=2.1 Hz), 3.70 (1H, d, J = 5.7 Hz)	60.8
-OMe	55.0	3.84 (s)	55.4
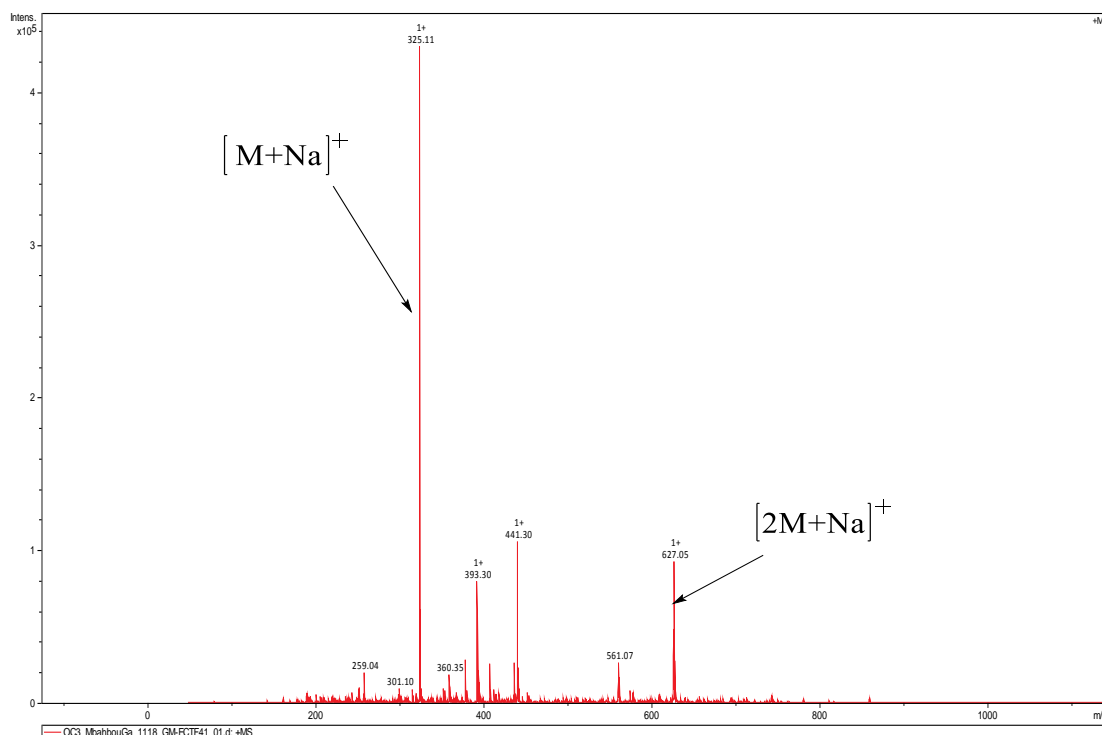
Figure 97: ESI-MS spectrum of compound ECTF41
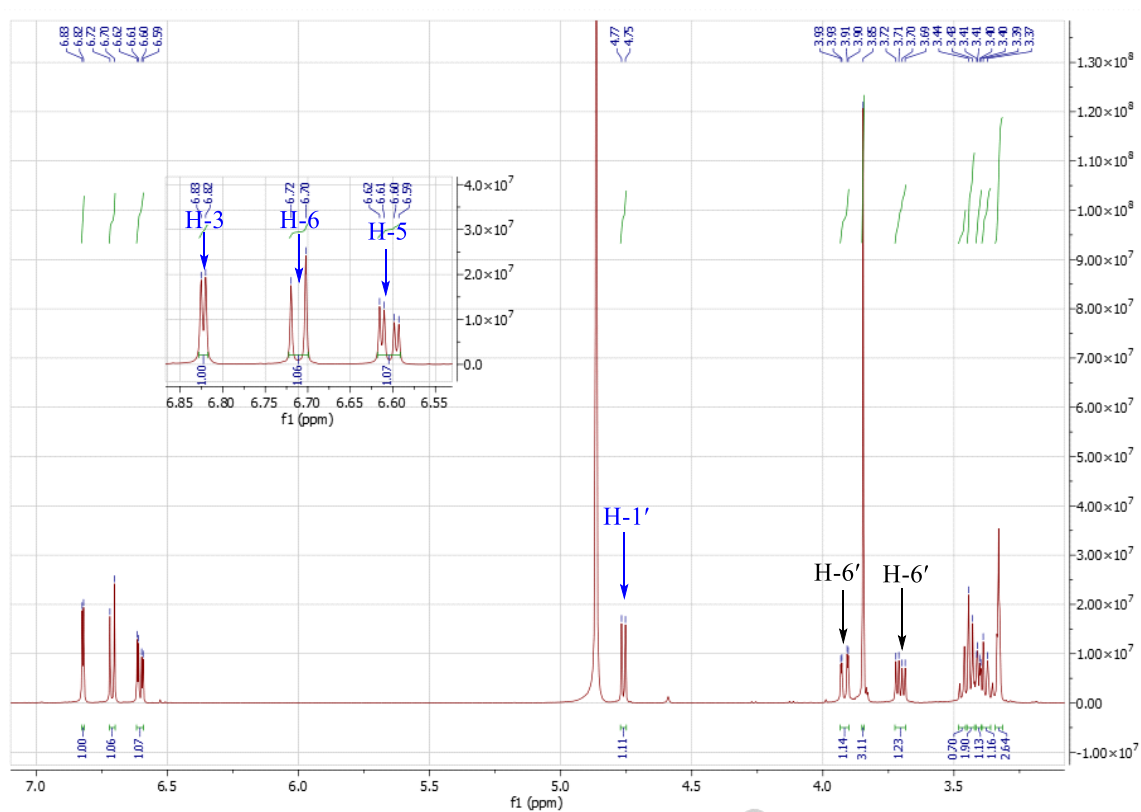
Figure 98: ¹H NMR spectrum (CD₃OD, 500 MHz) of compound ECTF41
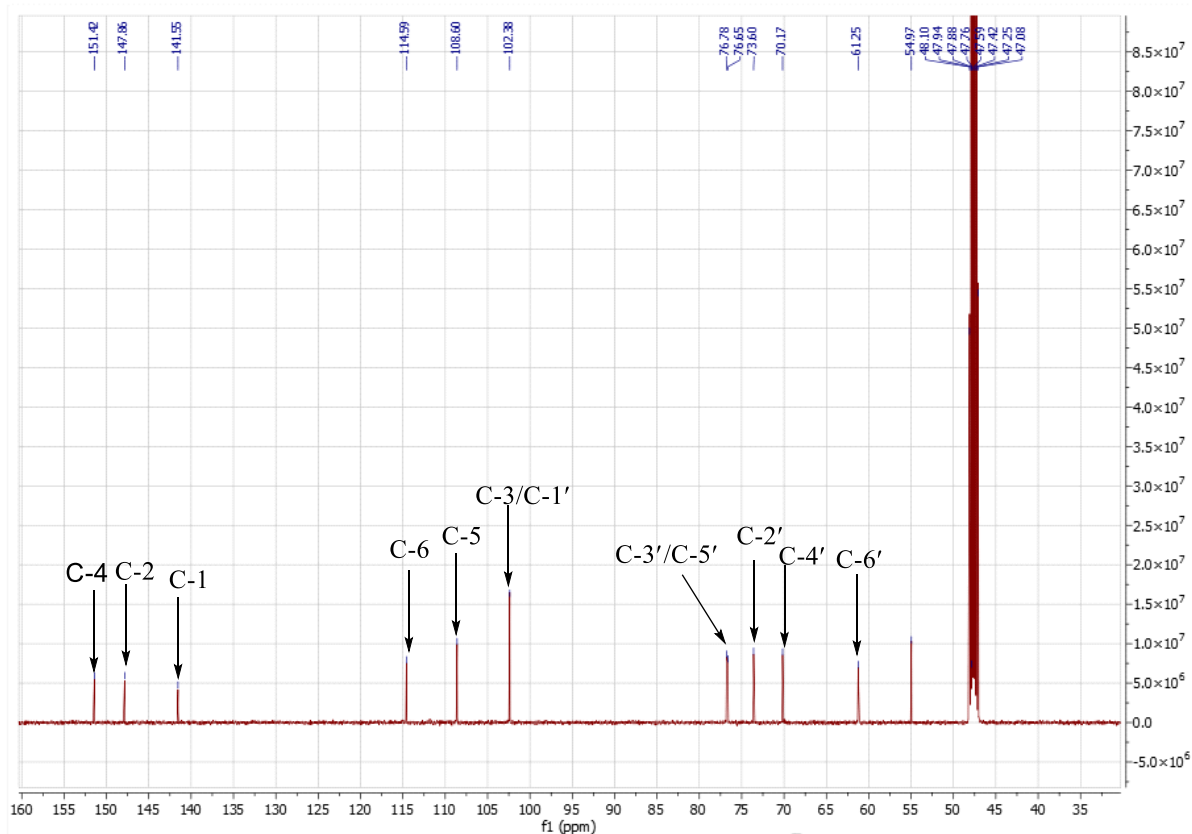
Figure 99: ^{13}C NMR spectrum (CD$_3$OD, 125 MHz) of compound ECTF41

Figure 100: DEPT 135 spectrum of compound ECTF41
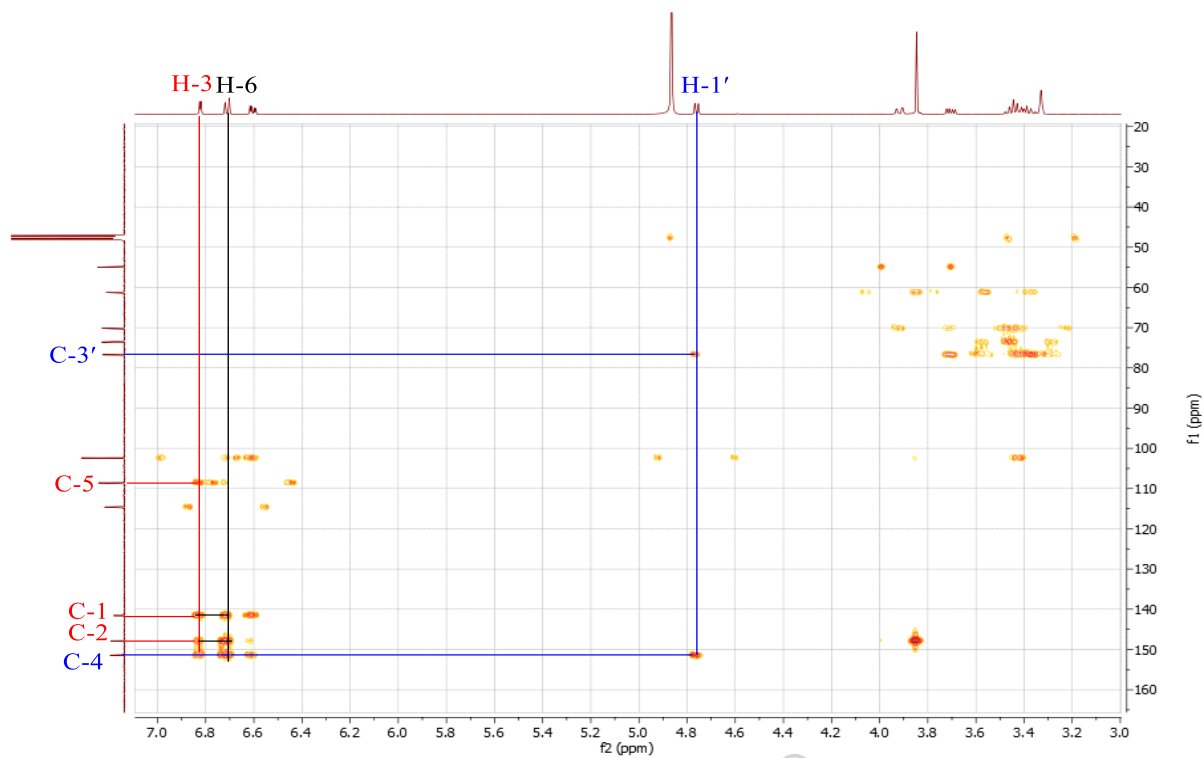
Figure 101: HMBC spectrum of compound ECTF41
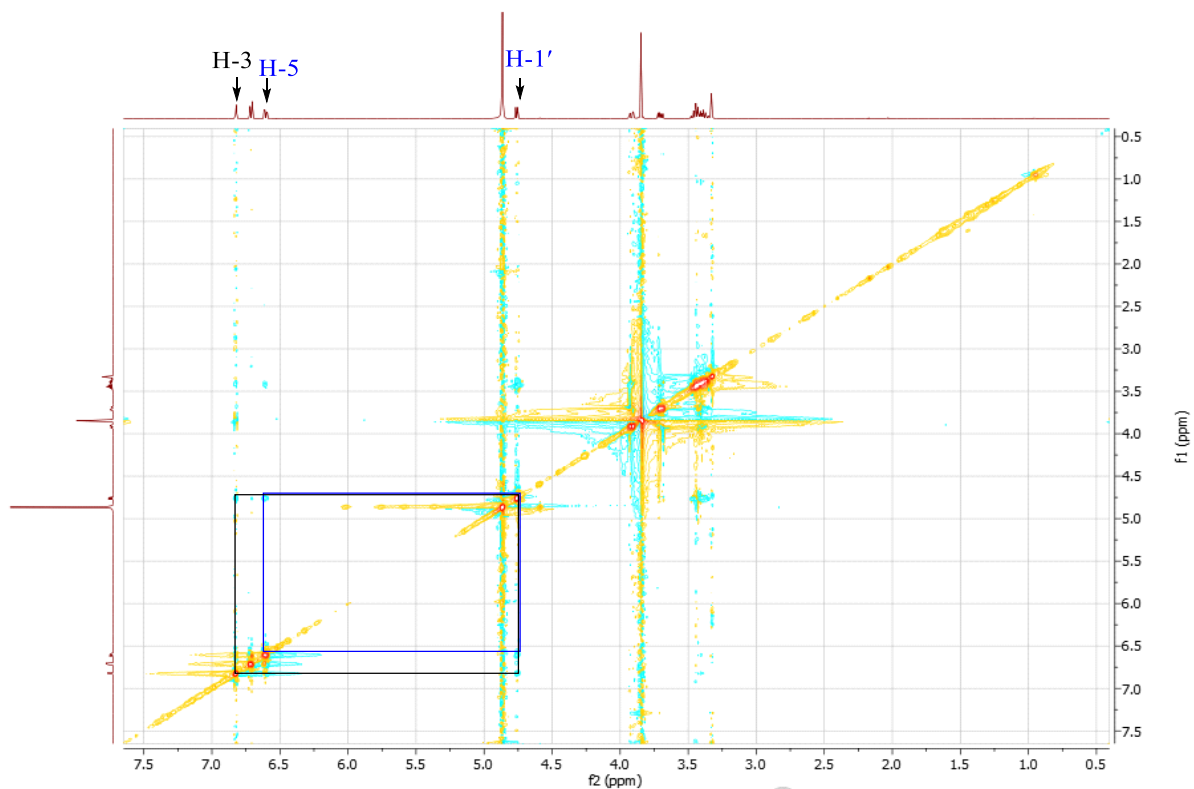
Figure 102: ROESY spectrum of compound ECTF41

II.2.1.6.2 Identification of ECTF42

ECTF42 was obtained as a brown oil. It is soluble in pyridin and responds positively to the Molish test, giving a red color, characteristic of sugars. It also gives a purple coloration with a methanolic solution of ferric chloride indicating its phenolic nature.

Its ESI (+) mass spectrum (Figure 103) shows the peak of the sodium adduct $[M+Na]^+$ at *m/z* 325.14. This value, combined with the NMR data, coroborates the molecular formula $C_{13}H_{18}O_8$, containing five unsaturations.

The ^{1}H and ^{13}C NMR spectra (Figures 104 and 105) of ECTF42 are similar to those of ECTF41. It is observed the duplication of signals, and ABX system, sugar unit and methoxy group.

Analysis of all its spectral data allowed us to assign the structure (**72**) to it, corresponding to a mixture of tachioside and isotachioside, in the proportions (1:3) (Inoshiri *et al.*, 1987).

(**71**)   (**72**)
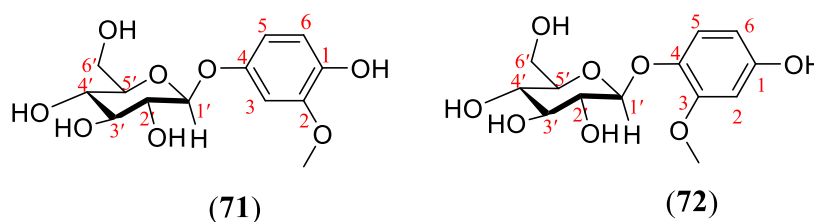
Table XXXVI: ^{1}H NMR (500 MHz) and ^{13}C (150 MHz) spectral data of ECTF42 in C₅D₅N compared to those of isotachioside [^{13}C NMR (25 MHz)] in DMSO-*d₆* (Inoshiri *et al.*, 1987).

Position	ECTF42a	Isotachioside
	δC	δC
1	151.1	152.6
2	96.1	100.8
3	148.9	149.8
4	142.8	139.3
5	116.0	117.2
6	108.9	105.9
1′	103.3	101.4
2′	74.7	73.2
3′	78.6	76.8

4′	71.2	69.7
5′	78.2	76.7
6′	60.7	62.1
-OMe	55.8	55.5
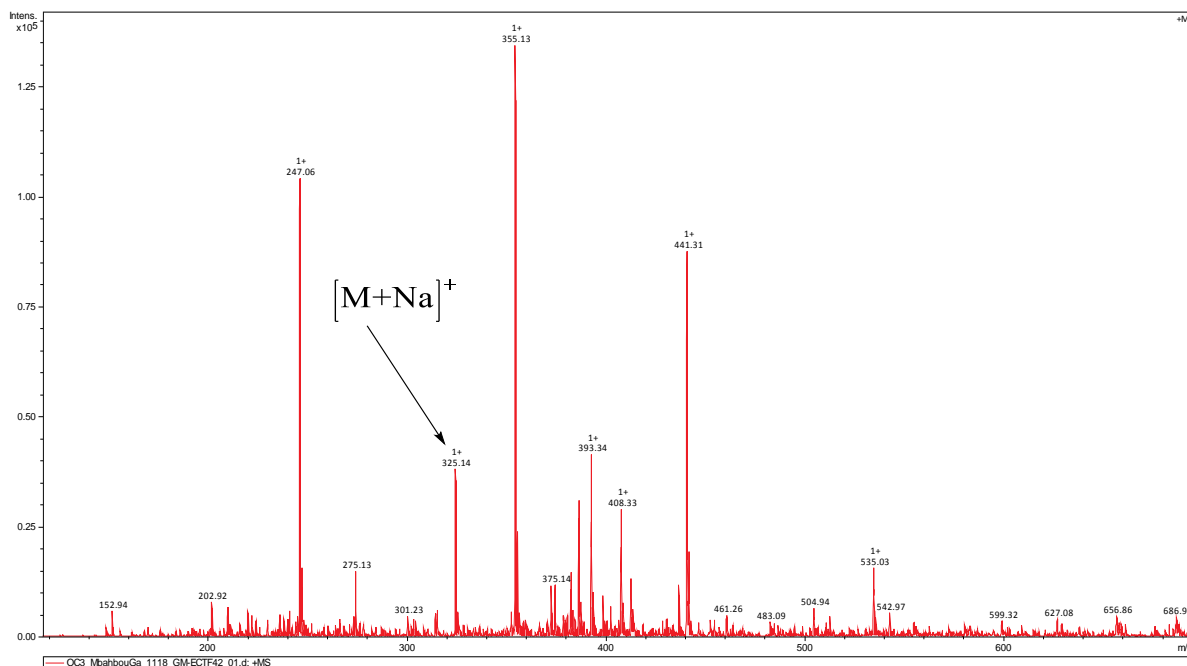
Figure 103: ESI-MS spectrum of compound ECTF42
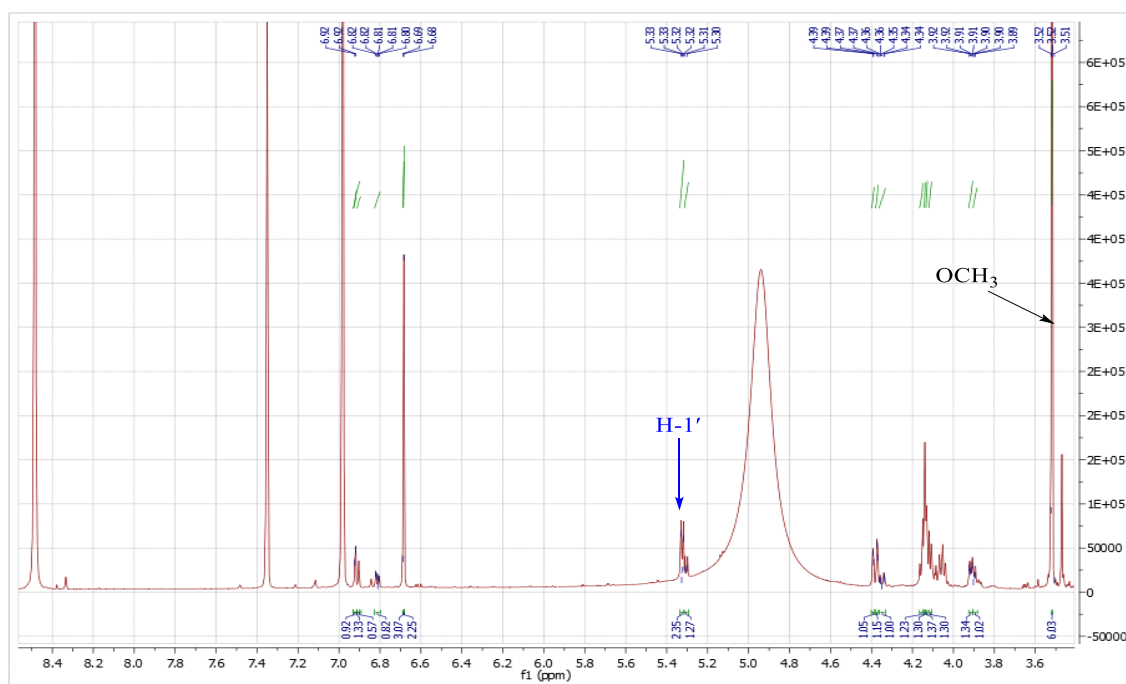
Figure 104: ^{1}H NMR spectrum (C$_5$D$_5$N, 500 MHz) of compound ECTF42
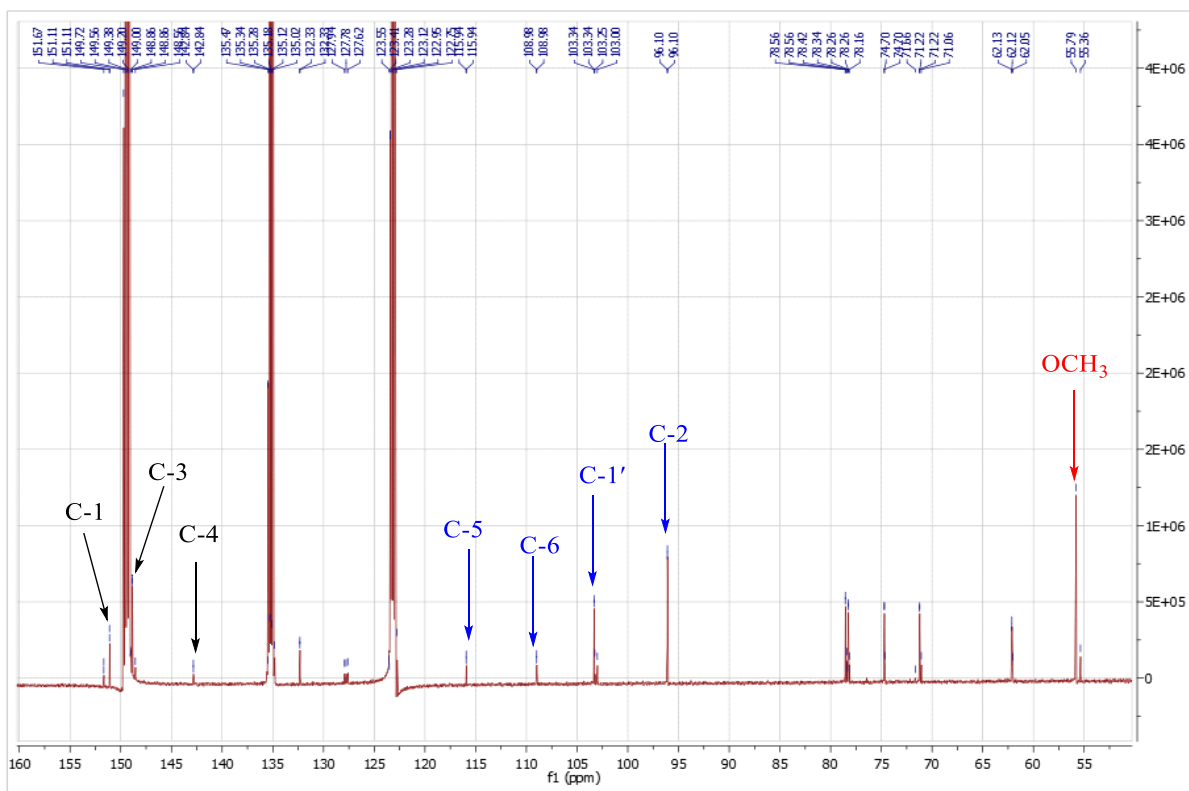
Figure 105: ^{13}C NMR spectrum (C$_5$D$_5$N, 125 MHz) of compound ECTF42

II.2.1.6.3 Identification of ECTF93

ECTF93 was obtained as brown amorphous. It is soluble in pyridin and responds positively to the Molish test, giving a red color, characteristic of sugars. It also gives a purple coloration with a methanolic solution of ferric chloride indicating its phenolic nature.

The analysis of its ^{1}H and ^{13}C NMR spectra (Figures 106 and 107) combined with data from the literature allowed us to assign it the molecular formula $C_{14}H_{20}O_9$, with five degrees of unsaturation.

All of these data, compared with those described in the literature (Table XXXVIII), allow the structure (**73**) to be attributed to ECTF93, which is that of koaburaside.

(**73**)
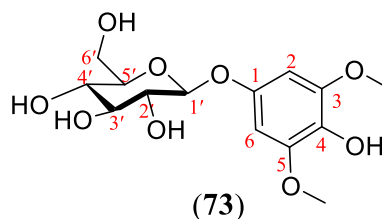
Its ^{13}C NMR spectrum (Figure 107), 11 signals of 14 carbon atoms were observed and using DEPT135 techniques (Figure 108) were sorted as:

- 1 signal of the methoxyl group at δ_C 56.0 (OMe).

- 2 signal of methine group from an aromatic ring at δ_C 96.3 (C-2 and C-6);

- 4 hydroxylated quaternary signals belonging to a 1,3,4,5-tetrabstituted aromatic ring at δ_C 132.6 (C-4), 149.5 (C-3 and C-5), and 151.3 (C-1);

- We also observed the following signals of carbons of a glucosidic group at δ_C 103.6 (C-1′), attributable to anomeric carbon; and those at δ_C 75.0 (C-2′), 78.8 (C-3′), 71.4 (C-4′), 78.5 (C-5′), and 62.4 (C-6′) (Agrawal, 1992).

　　　Its ^{1}H NMR spectrum (Figure 106) showed:

- meta coupled proton of a tetrasubstitued simetric ring at δ_H 6.90 (2H, brs, H-2 and H-6);

- the signal of β-anomeric proton at δ_H 5.56 (1H, d, J = 6.5 Hz, H-1′) of the sugar unit;

- The methoxy group at δ_H 3.73 (O-CH$_3$) were also observed.

　　　The HMBC spectrum (Figure 109, scheme 26) of ECTF93, support the tetrasubstituted aromatic ring while the glucosidic unit is linked at position 1 based on the HMBC correlation from H-1′ (δ_H 5.56), H-2 (δ_H 6.90) and H-6 (δ_H 6.90) to C-1 (δ_C 151.3).

　　　The methoxy groups were linked at position 3 and 5, following the HMBC correlations from the protons of the methoxy groups (δ_H 3.73) to carbons C-3 (δ_C 149.5) and C-5(δ_C 149.5).
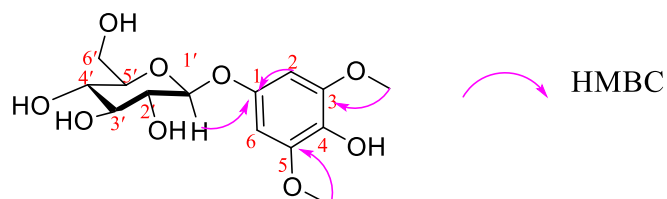
Scheme 26: Selected HMBC correlations of the compound ECTF93

　　　All of these data, compared with those described in the literature (Table XXXVIII), allow the structure (**73**) to be attributed to ECTF93 see the previous, which is that of koaburaside, previously isolated from *Canthium berberidifolium* (Wen *et al*., 2012).

Table XXXVIII: ^{1}H (500 MHz) and ^{13}C (125 MHz) NMR spectral data of ECTF93 in C$_5$D$_5$N compared to koaburaside ^{1}H (600 MHz) and ^{13}C (150 MHz) NMR in CD$_3$OD (Wen *et al.*, 2012)

Position	ECTF93		Koaburaside	
	δ_C	δ_H (nH, m, *J* in Hz)	δ_C	δ_H (nH, m, *J* in Hz)
1	151.3	/	156.0	/
2	96.3	6.90 (1H, s)	94.6	6.13 (1H, s)
3	149.5	/	154.8	/
4	132.6	/	129.7	/
5	149.5	/	154.8	/
6	96.3	6.90 (1H, s)	94.6	6.13 (1H, s)
1′	103.6	5.56 (1H, d, *J* = 6.5 Hz)	106.2	4.66 (1H, d, *J* = 7.4 Hz)
2′	75.0	/	75.8	/
3′	78.8	/	78.3	/
4′	71.4	/	71.4	/
5′	78.5	/	77.8	/
6′	62.4	/	62.6	/
-OMe	56.0	3.73 (3H, s)	56.8	3.79 (3H, s)
-OMe	56.0	3.73 (3H, s)	56.8	3.79 (3H, s)
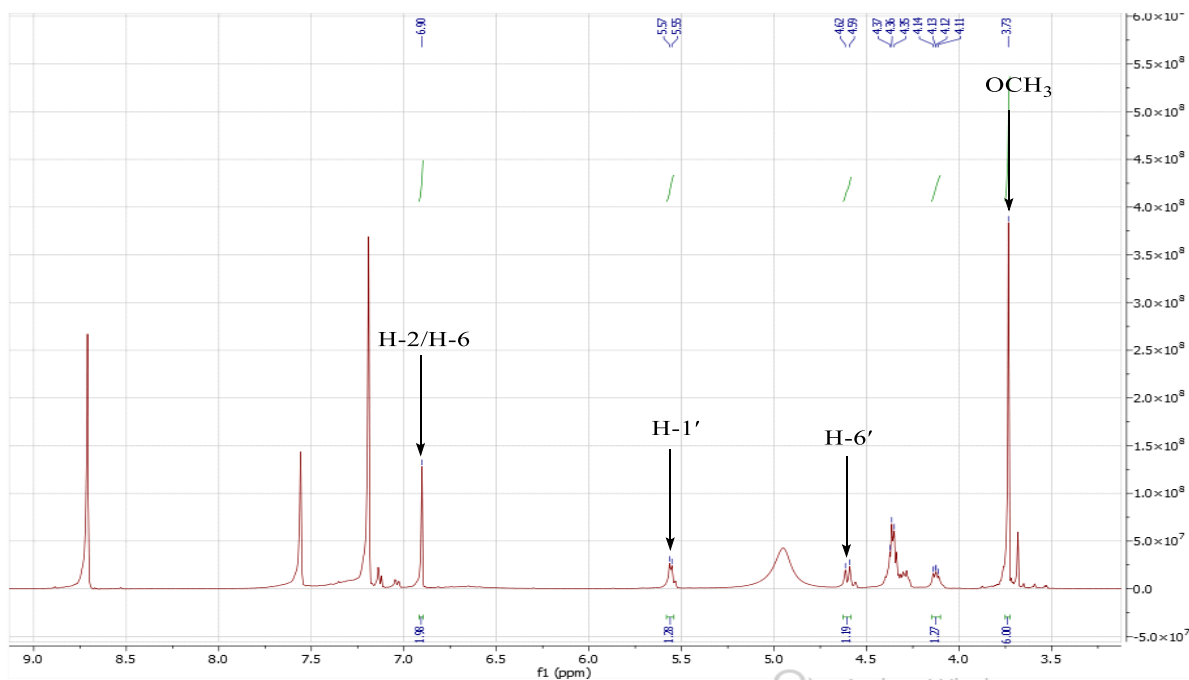
Figure 106: ¹H NMR spectrum (C₅D₅N, 500 MHz) of compound ECTF93
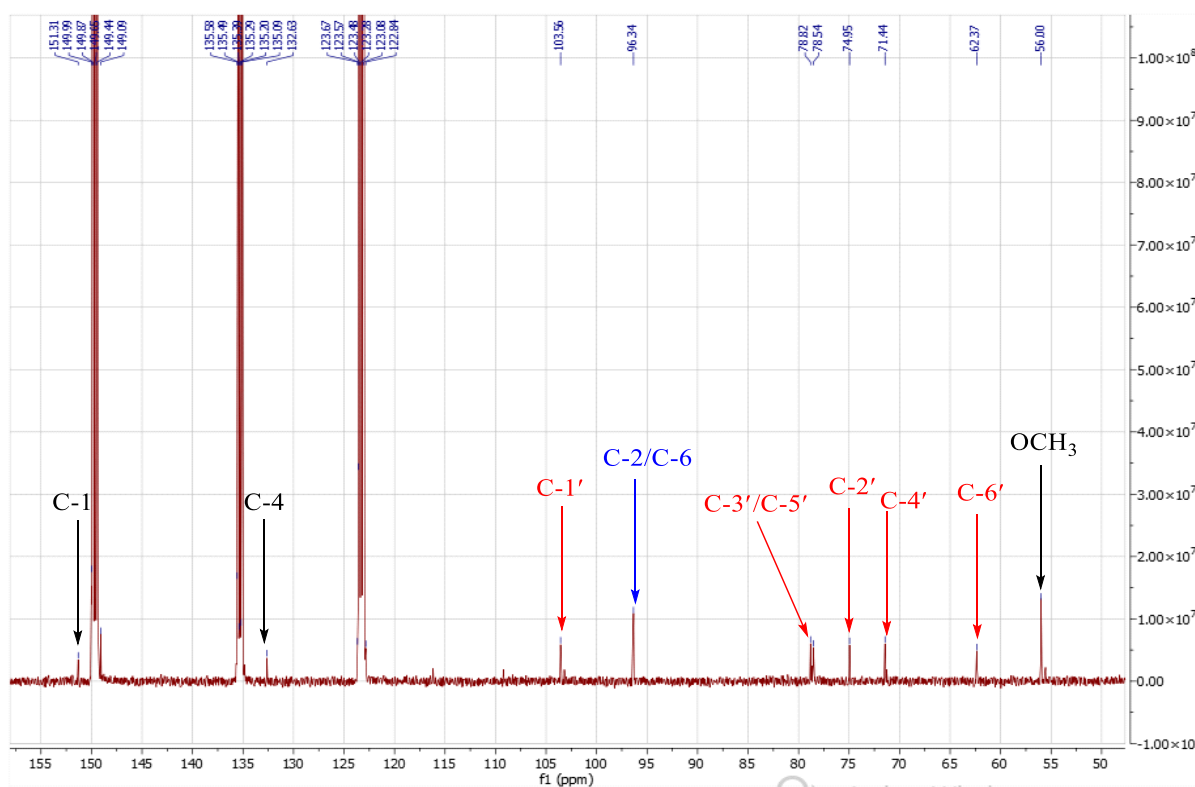
Figure 107: ¹³C NMR spectrum (C₅D₅N, 125 MHz) of compound ECTF93
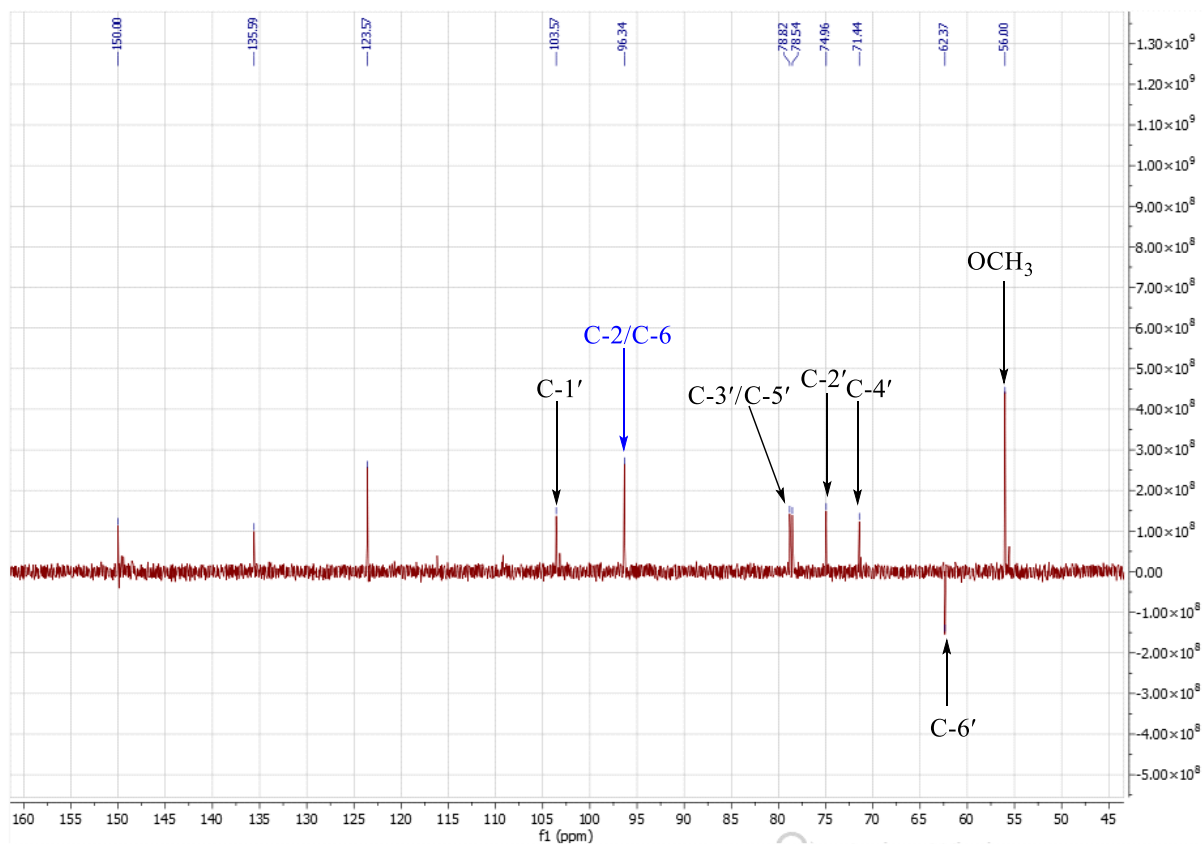
Figure 108: DEPT 135 spectrum of compound ECTF93
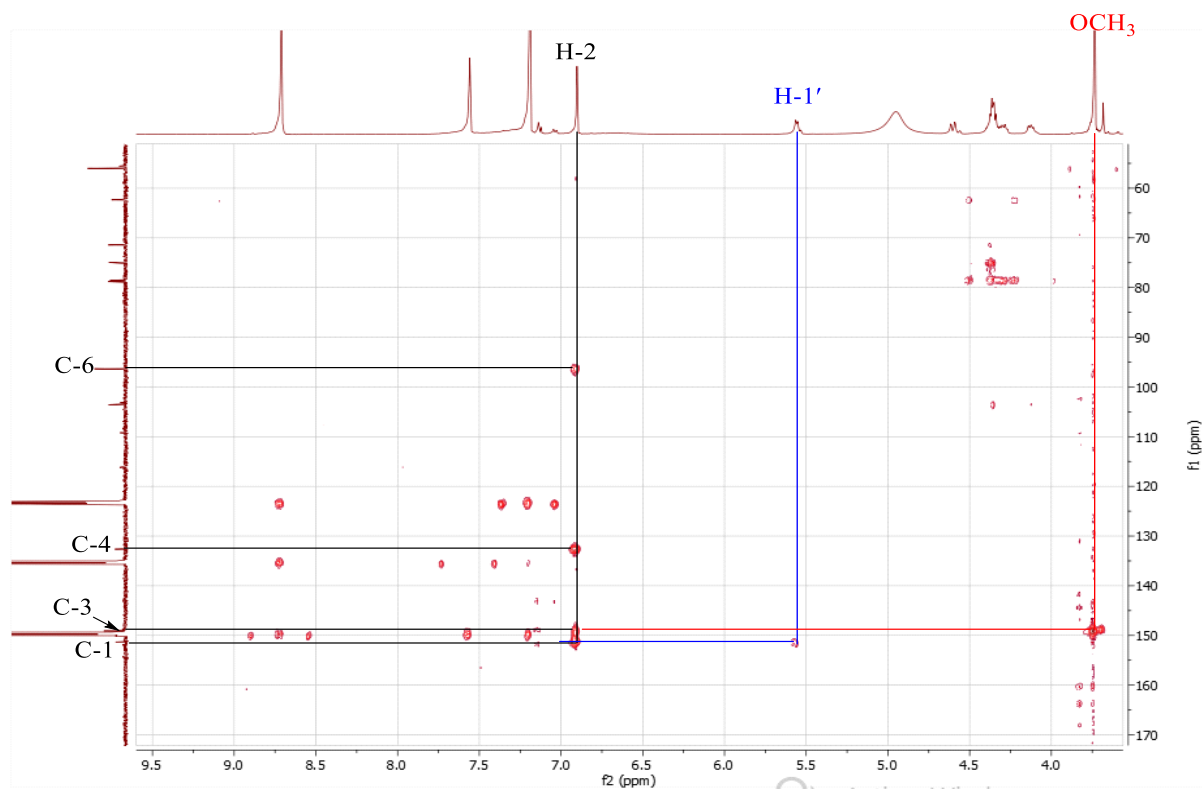
Figure 109: HMBC spectrum of compound ECTF93

II.2.1.6.4 Identification of ALB3

The compound ALB3 was obtained as a yellow amorphous solid and it is soluble in pyridine. It gives a blue coloration with a solution of iron (III) chloride, which is characteristic of phenolic compounds.

Analysis of its 1D and 2D NMR spectra enabled to attribute the molecular formula $C_8H_8O_4$, containing 5 degrees of unsaturation.

Its ^1H NMR spectrum (Figure 110), exhibited:

- an ABX aromatic system at δ_H 8.04 (1H, brs), 8.11 (1H, brd, J = 8.1 Hz) and 7.30 (1H, brd, J = 8.1 Hz);

- a singlet of a methoxy protons at δ_H 3.77.

Its ^{13}C NMR spectrum (Figure 111) presented signals correcponding to 8 carbon atoms which were distinguished using its DEPT 135 spectrum (Figure 112) into:

- four quartenary carbons amongst which that of carbonyl at δ_C 170.5;
- three aromatic methine carbons at δ_C 126.1, 117.3 and 115.1;
- an oxymethyl carbon at δ_C 57.1.

These information indicates that the compound ALB3 is a benzoic acid derrivative with an methoxy group attached to it. Looking at the above data and its molecular formula we deduce that in addition to the methoxy group, hydroxyl group attached to the benzoic acid.

The positions of the hydroxyl and methoxy groups were determined thanks to correlations observed on the HMBC spectrum (Figure 113) of ALB3. The following correlations were observed between:

The proton H-2 (δ_H 8.04) and the oxymethyl protons at δ_H 3.77 and the carbon C-3 (δ_C 149.6); between the proton H-5 (δ_H 7.30) and the carbons C-3 (δ_C 149.6) et C-4 (δ_C 154.0); equally between the protons H-2 (δ_H 8.04) and H-6 (δ_H 8.11) and the carboxyl C-7 (δ_C 170.5), enabling the fixation of the hydroxyl group at position 4 and the methoxyl group at position 3.

These data indicate clearly that the hydroxyl and methoxyl groups are located at C-4 and C-3 respectively.
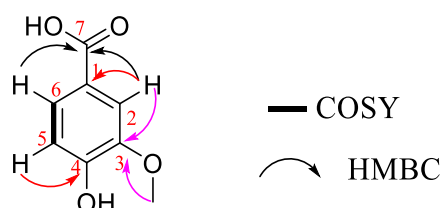
Scheme 27: Selected HMBC and COSY correlations of ALB3

All these spectral data put together compared with those described in the literature (table XXXIX) enabled us to attribute the structure (**74**) to compound ALB3 which is that of 3-methoxy-4-hydroxybenzoic acid (Vanillic acid), previously isolated from *Bathysa australis* (Sang *et al*., 2009).

(74)
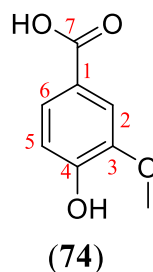
Table XXXIX: ^{1}H NMR (500 MHz) and ^{13}C (125 MHz) spectral data of ALB3 in C_5D_5N compared to those of vanillic acid [^{13}C NMR (125 MHz), ^{1}H NMR (500 MHz) in CD_3OD] (Sang *et al*., 2009)

Position	ALB3		Vanillic acid	
	δ_H (nH, m, *J* in Hz)	δ_C	δ_H (nH, m, *J* in Hz)	δ_C
1	/	124.4	/	124.1
2	8.04 (1H, brs)	115.1	7.58 (1H, d, *J* = 2.0)	114.6
3	/	149.6	/	147.5
4	/	154.0	/	151.4
5	7.30 (1H, d, *J* = 7.7)	117.3	6.82 (1H, d, *J* = 8.5)	116.5
6	8.11 (1H, brd, *J* = 7.9)	126.1	7.54 (1H, dd, *J* = 8.5, 2.0)	122.9
7	/	170.5	/	167.6
3-OCH$_3$	3.77 (3H, s)	57.1	3.90 (3H, s)	55.2
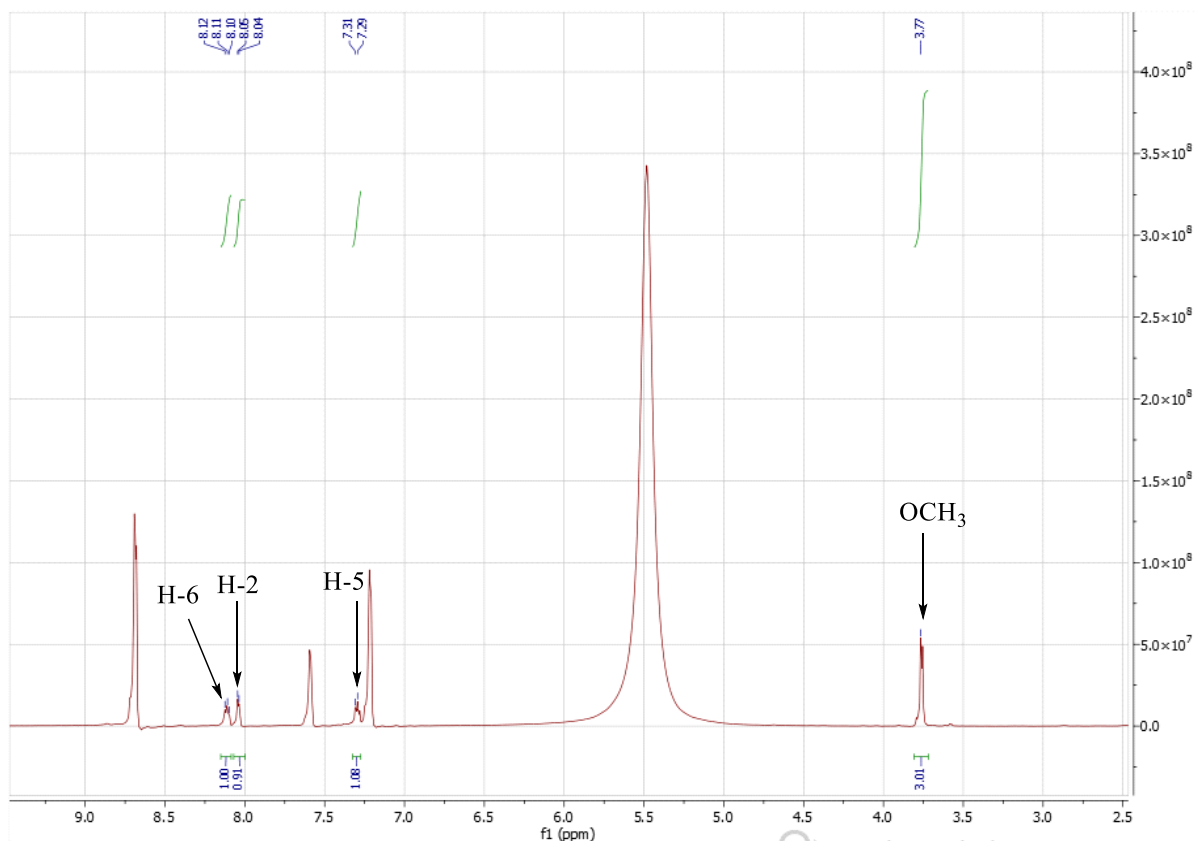
Figure 110: ^{1}H NMR spectrum (C$_5$D$_5$N, 500 MHz) of compound ALB3
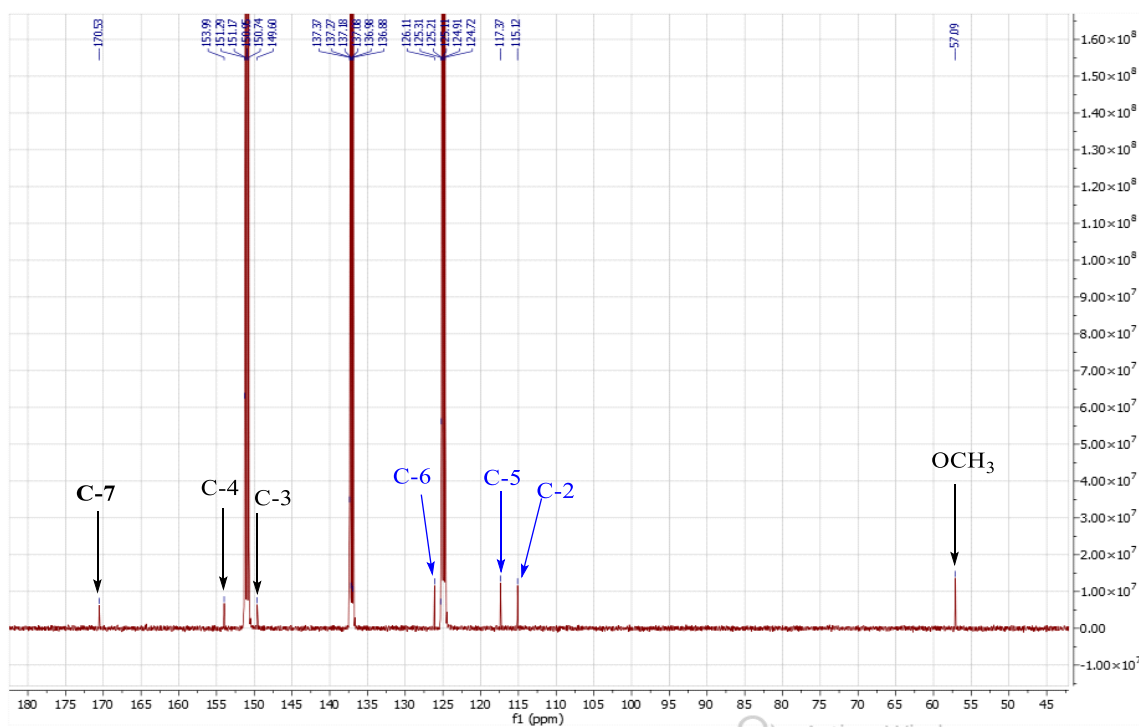
Figure 111: ^{13}C NMR spectrum (C$_5$D$_5$N, 125 MHz) of compound ALB3
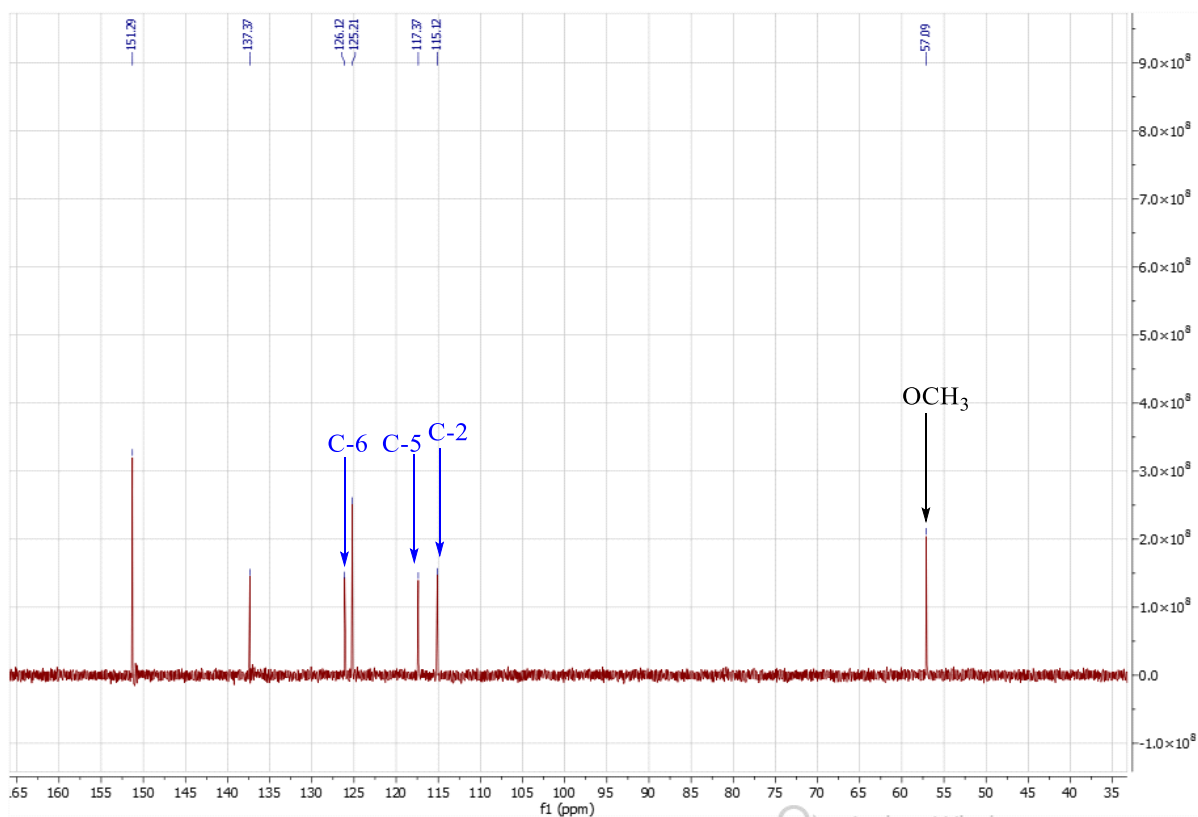
Figure 112: DEPT 135 spectrum of compound ALB3
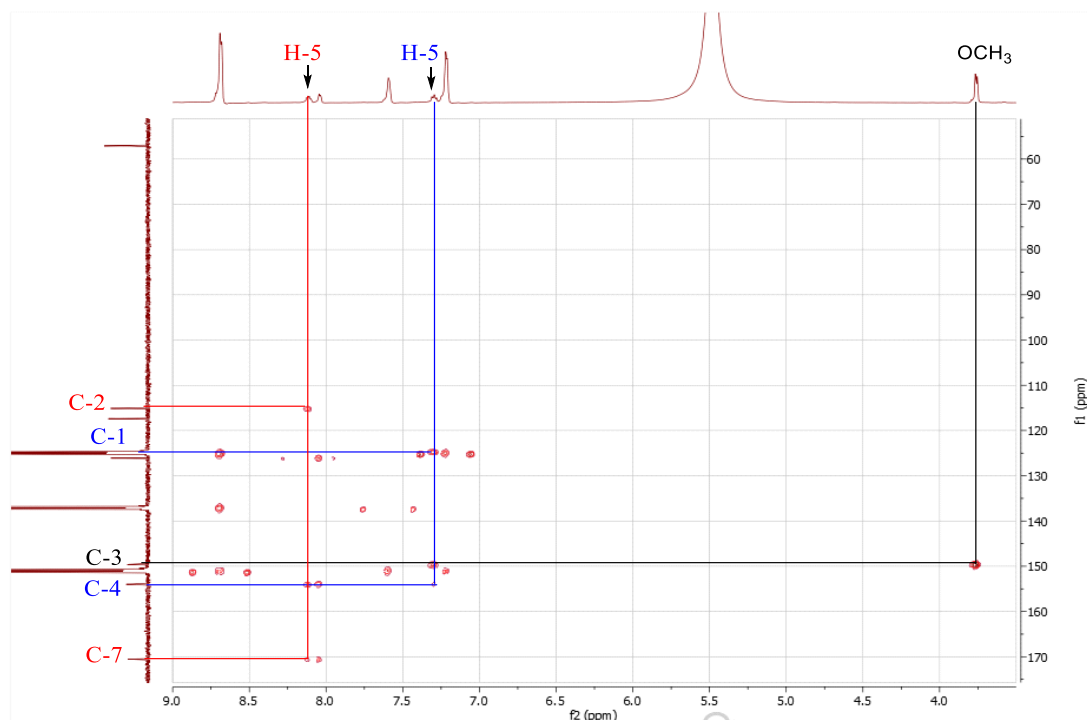
Figure 113: HMBC spectrum of compound ALB3
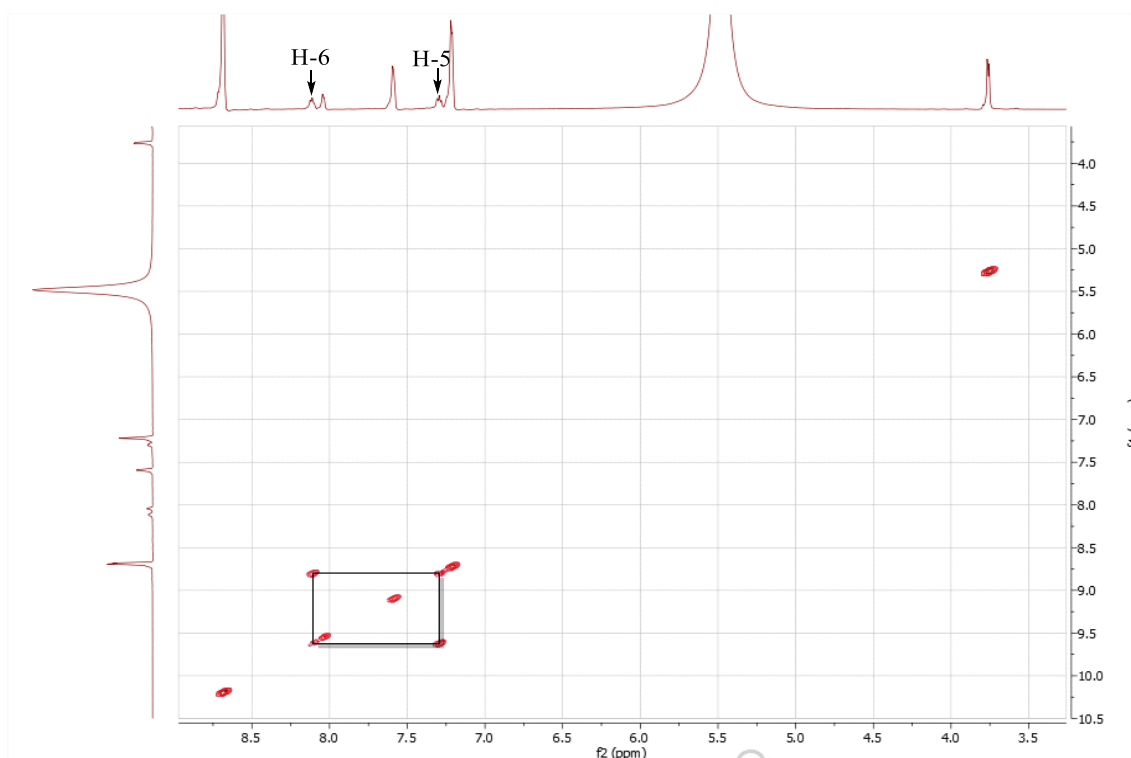
Figure 114: COSY spectrum of compound ALB3

II.2.1.7. Xanthones

II.2.1.7.1 Identification of ECTF24

ECTF24 was isolated as a yellowish amorphous solid, and was soluble in acetone. Analysis of its ^{1}H and ^{13}C NMR spectrum combined with data from the literature allowed us to assign the molecular formula $C_{14}H_{10}O_5$ that contains ten degrees of unsaturation. In the presence of ferric chloride, it gives a purple coloration, characteristic of phenolic compound.

All these spectral data taken together, compared with those described in the literature (Table XL), allowed us to attribute to ECTF24 the structure (**75**) which is that of 1,5-dihydroxy-3-metoxyxanthone, previously isolated from *Centaurium erythraea* (Valentão *et al*., 2002).

(**75**)
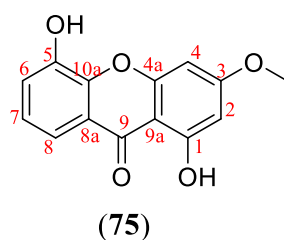
Indeed, its ^{1}H NMR spectrum (Figure 115) showed:

- a singlet of a proton at δ_H 13.01 (1H, s) attributable to a proton of a chelated hydroxyl group;

- A *meta*-coupled protons at δ_H 6.35 (1H, d, $J = 2.3$ Hz, H-2) and 6.59 (1H, $J = 2.3$ Hz, H-4);

- an oxymethyl singlet at δ_H 3.98.

The ^{13}C NMR spectrum of ECTF24 (Figure 116) showed the signals of 14 carbon atoms which were distinguished using the DEPT 135 technique (Figure 117) into: -
eight quaternary carbons including one carbonyl at δ_C 181.3 (C-9), the others at δ_C 167.0 (C-1), 163.1 (C-3), 157.6 (C-4a), 146.1 (C-5), 145.2 (C-10a), 121.3 (C-8a), and 103.3 (C-9a);

- five methines at δ_C 124.0 (C-7), 120.5 (C-6), 115.2 (C-8), 97.0 (C-2), and 92.5 (C-4).

- a methoxyl group signal at δ_C 55.5 (C-3-OCH$_3$).

The HMBC spectrum of ECTF24 (Figure 118, scheme 28) led to built the xanthone skeleton following correlations between:

- the proton at δ_H 7.31 (H-6) with the carbons at δ_C 146.1 (C-5) and 145.2 (C-10a);

- the proton at δ_H 7.27 (H-7) with the carbon at δ_C 120.5 (C-6);

- the proton at δ_H 7.65 (H-8) with the carbons at δ_C 124.0 (C-7), 121.3 (C-8a) and 145.2 (C-10a);
- the proton at δ_H 6.59 (H-4) with the carbons at δ_C 163.1 (C-3) and 157.6 (C-4a);
- the proton at δ_H 6.35 (H-2) with the carbons at δ_C 163.1 (C-3), 167.0 (C-1) and 103.3 (C-9a);
- the methoxy group was linked at C-3 following the HMBC correlation from O-CH$_3$ (δ_H 3.94), H-2 and H-4 to carbon C-3 (δ_C 163.1).
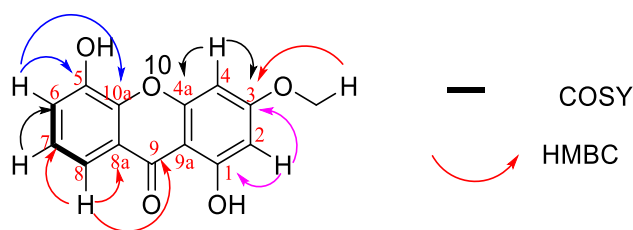
Scheme 28: Selected HMBC and COSY correlations of ECTF24

Table XL: ^{1}H (500 MHz) and ^{13}C (150 MHz) NMR spectral data of ECTF24 in Acetone-d_6 compared to those of 1,5-dihydroxy-3-metoxyxanthone [^{13}C NMR (100 MHz) and ^{1}H NMR (400 MHz) in C$_2$D$_6$SO] (Valentão *et al.*, 2002)

Position	ECTF24		1,5-dihydroxy-3-metoxyxanthone	
	δ_H (nH, m, J in Hz)	δ_C	δ_H (nH, m, J in Hz)	δ_C
1	/	163.1	/	162.6
2	6.35 (1H, d, 2.3 Hz)	97.0	6.40 (1H, d, 2.2 Hz)	97.1
3	/	167.0	/	166.1
4	6.59 (1H, d, 2.2 Hz)	92.5	6.64 (1H, d, 2.2 Hz)	92.8
4a	/	157.6	/	156.8
5	/	146.1	/	146.3
6	7.31 (1H, dd, 7.8, 1,6 Hz)	120.5	7.33 (1H, dd, 7.8, 1.8 Hz)	120.9
7	7.27 (1H, t, 7.8 Hz)	124.0	7.27 (1H, t, 1.8 Hz)	124.3
8	7.65 (1H, dd, 7.8, 1.6 Hz)	115.2	7.56 (1H, dd, 7.8, 1.8 Hz)	114.5
8a	/	121.3	/	120.6
9	/	181.3	/	181.2
9a	/	103.3	/	103.0
10	/	/	/	/
10a	/	145.2	/	147.1
11	3.94 (3H, s)	55.5	3.93 (3H, s)	56.2
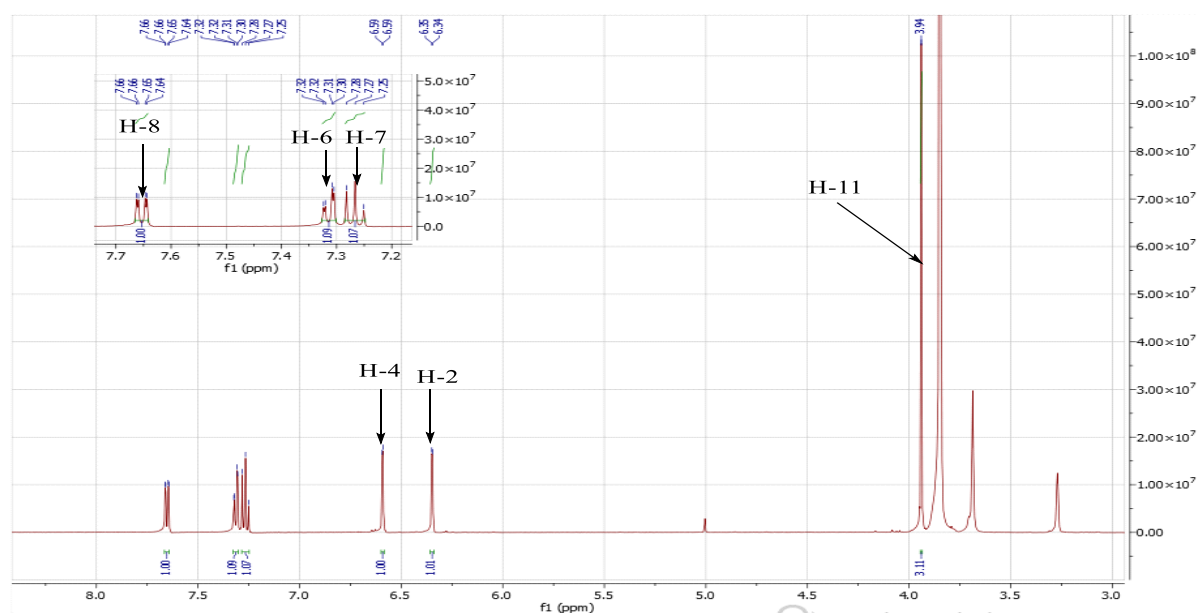
Figure 115: ^{1}H NMR spectrum (CD$_3$COCD$_3$, 500 MHz) of compound ECTF24
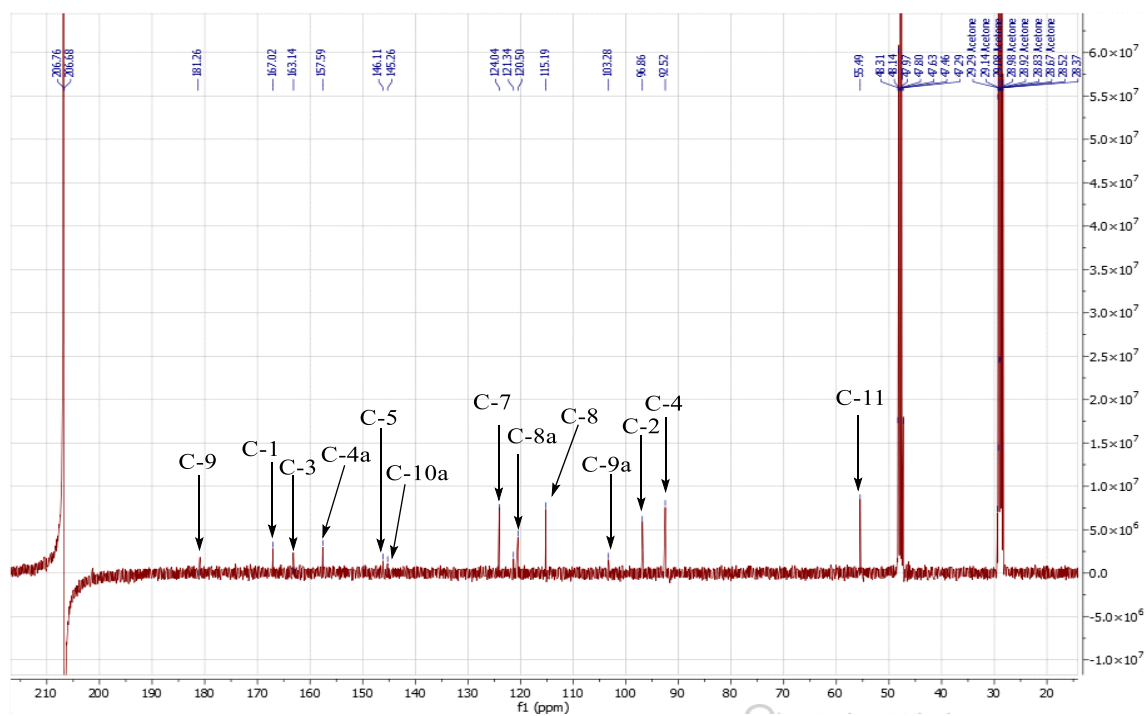
Figure 116: ^{13}C NMR spectrum (CD$_3$COCD$_3$, 500 MHz) of compound ECTF24

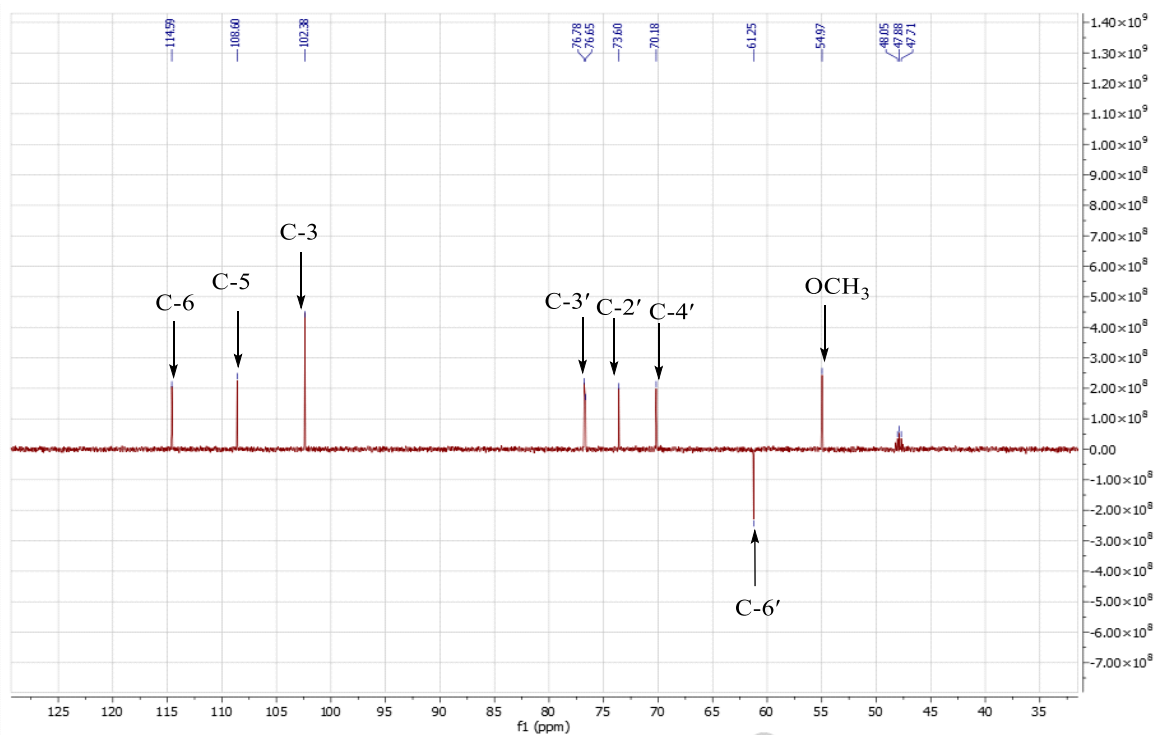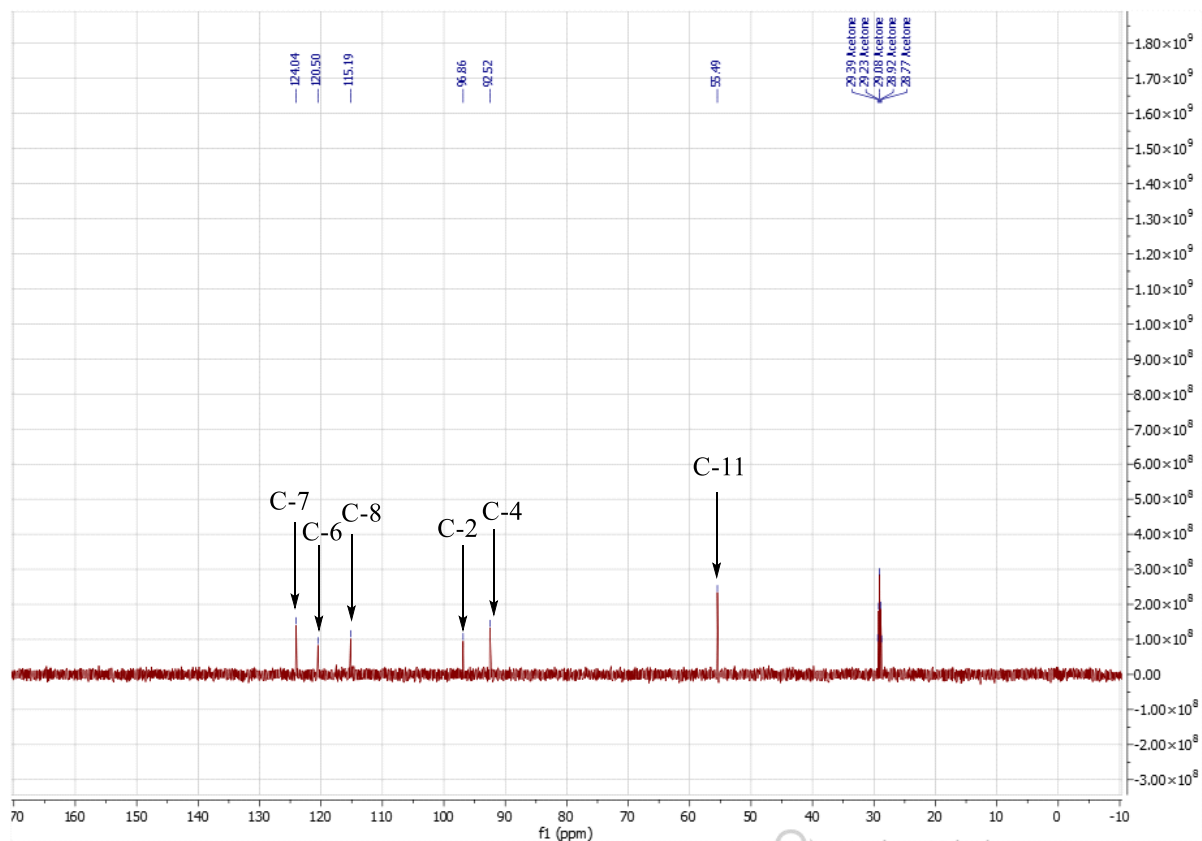**Figure 117: DEPT 135 spectrum of compound ECTF24**
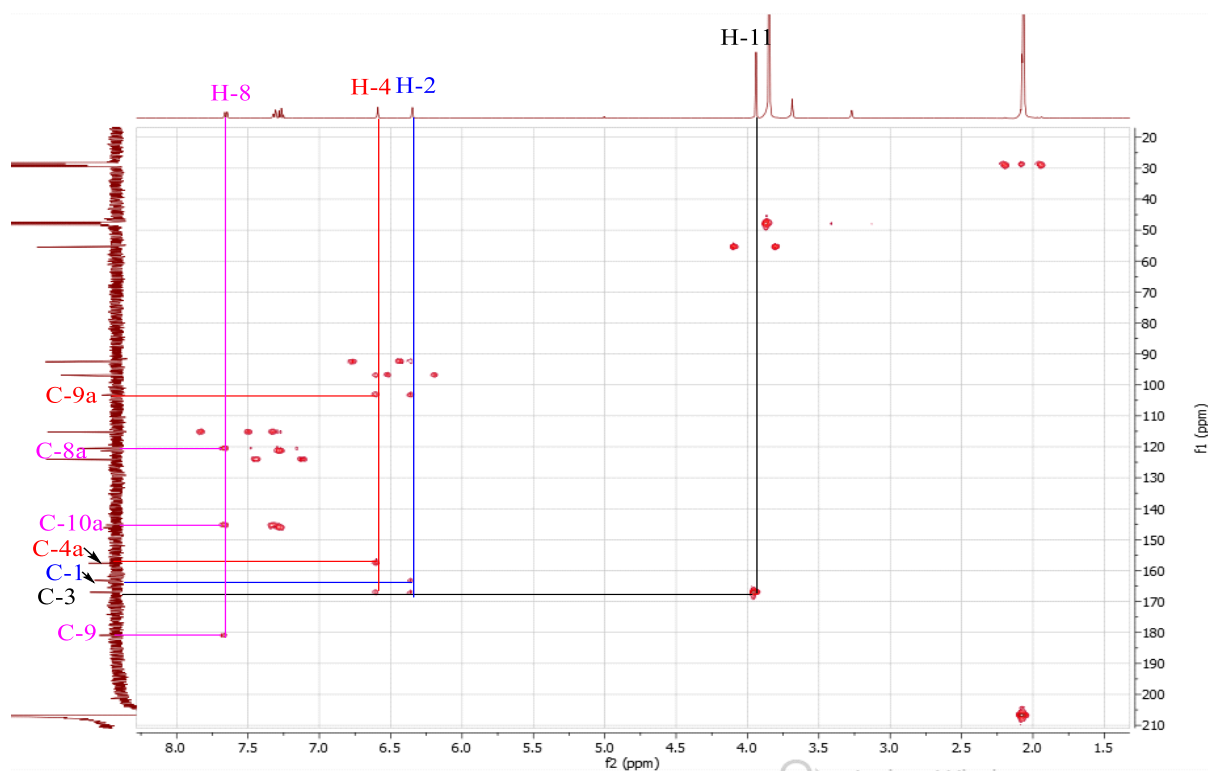
Figure 118: HMBC spectrum of compound ECTF24
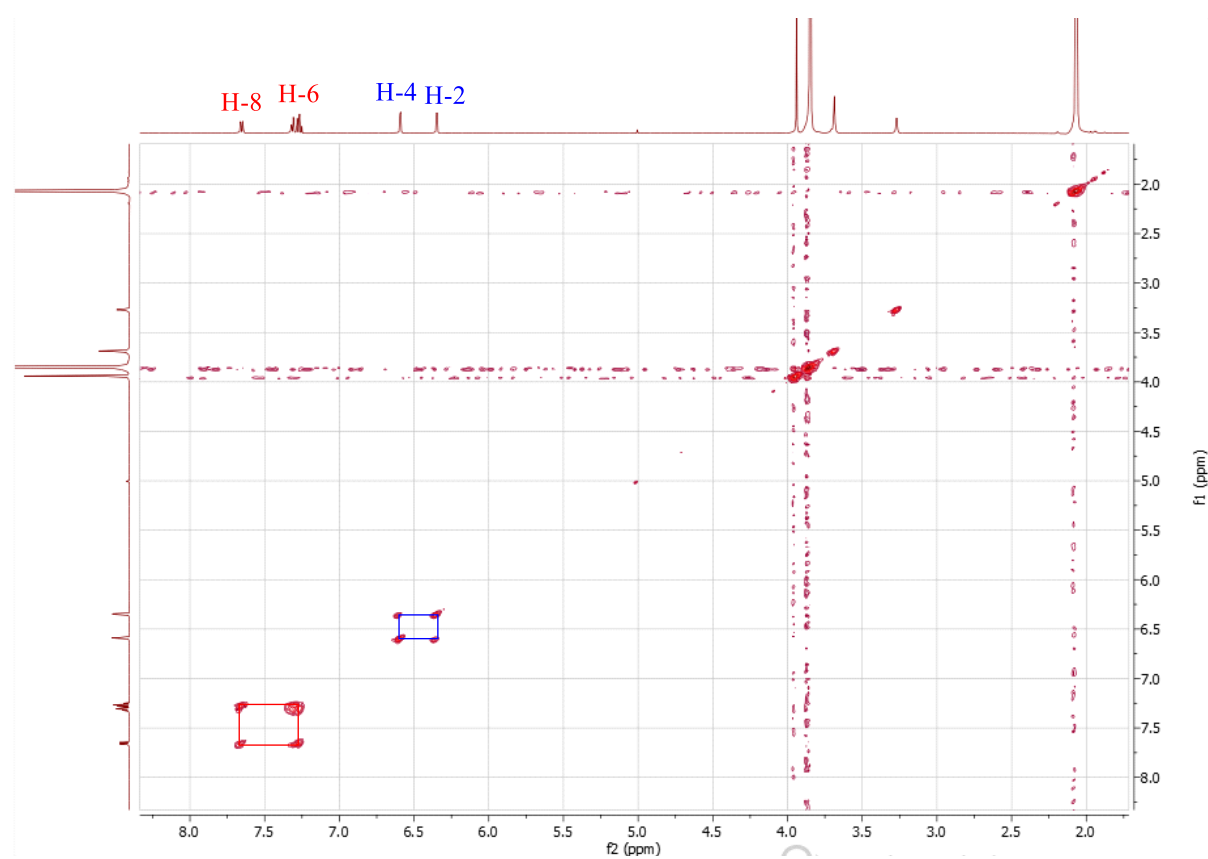
Figure 119: COSY spectrum of compound ECTF24

II.2.1.7.2 Identification of PBER1

PBER1 was isolated as a yellowish amorphous solid, and was soluble in dimethyl sulfoxide. In the presence of ferric chloride, it gives a blue coloration, characteristic of phenolic compound.

Its HR-ESI (+) mass spectrum (Figure 120) shows the peak of the protonated ion $[M+H]^+$ at *m/z* 261.0414 corresponding to the molecular formula $C_{13}H_9O_6$ (calculated for 261.0394), contains ten degrees of unsaturations.

From these spectral data, the compound PBER1 was found to be 1,3,6,7-tetrahydroxylated xanthone (Table XLI), know as norathyriol, previously isolated from the leaves of *Garcinia mackeaniana* (Ninh *et al.*, 2020).

(**76**)
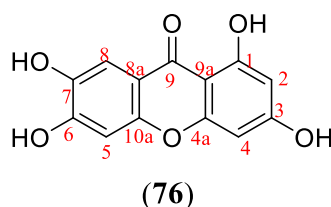
Indeed, the ^{1}H-NMR spectrum (Figure 121) of PBER1 contain the pattern of a simple xanthone, which includ:

- a singlet of chelated proton at δ_H 13.16 (1H, s);

-two singlet of one proton each at δ_H 6.83 (1H, s, H-5), and 7.45 (1H, s, H-8);

- A *meta*-coupled protons at δ_H 6.16 (1H, d, *J* = 2.2 Hz, H-2) and 6.31 (1H, *J* = 2.2 Hz, H-4).

Analysis of the ^{13}C NMR spectrum of PBER1 (Figure 122) brings out the signals of 13 carbon atoms which were distinguished using the HSQC technique (Figure 125) into:

- four aromatic methines at δ_C 94.0 (C-4), 97.3 (C-2), 102.1 (C-5), and 107.7 (C-8);

- six oxygenated quaternary carbons at δ_C 164.9 (C-3), 163.0 (C-1), 151.8 (C-7), 144.1 (C-6), 158.0 (C-4a), and 153.9 (C-10a) and one carbonyl at δ_C 179.7 (C-9);

-two aromatic carbons at δ_C 112.5 (C-8a), and 101.9 (C-9a).

The structure of PBER1 was confirmed by the HMBC spectrum (Figure 123, scheme 29). The methine proton H-2 has correlations with the carbons C-9 (δ_C 179.7), C-3 (δ_C 164.9), C-1 (δ_C 163.0), C-9a (δ_C 103.5) and 94.0 (C- 4) while the H-4 methine proton crossed the peak with C-3, C-4a (δ_C 158.0) and C-9a. In the remaining aromatic ring, the methine proton H-5 induced the key correlation with the carbons C-9 (δ_C 179.7), C-6 (δ_C 144.1) and C-10a (δ_C 153.9). Likewise, the H-8 methine proton correlates with carbons C-6, C-7 (δ_C 151.8), C-9 and C-10a (Ninh *et al.*, 2020).
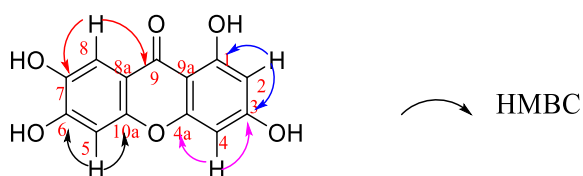
Scheme 29: Selected HMBC correlations of PBER1

Table XLI: ^{1}H (500 MHz) and ^{13}C (125 MHz) NMR spectral data of PBER1 in DMSO-d_6 compared to those of norathyriol [^{13}C NMR (125 MHz) and ^{1}H NMR (500 MHz) in CD$_3$OD] (Ninh *et al.*, 2020)

Position	PBER1		norathyriol	
	δ_H (nH, *m*, *J* in Hz)	δ_C	δ_H (nH, *m*, *J* in Hz)	δ_C
1	/	163.0	/	164.4
2	6.16 (1H, d, 2.2 Hz)	97.3	6.16 (1H, d, 2.0 Hz)	98.8
3	/	165.0	/	166.5
4	6.31 (1H, d, 2.2 Hz)	94.0	6.30 (1H, d, 2.0 Hz)	94.7
4a	/	158.0	/	159.5
5	6.83 (1H, s)	102.1	6.83 (1H, s)	103.5
6	/	144.1	/	144.9
7	/	151.8	/	153.3
8	7.45 (1H, s)	107.7	7.46 (1H, s)	109.1
8a	/	112.5	/	113.8
9	/	179.7	/	181.2
9a	/	103.5	/	103.5
10	/	/	/	/
10a	/	153.9	/	155.5
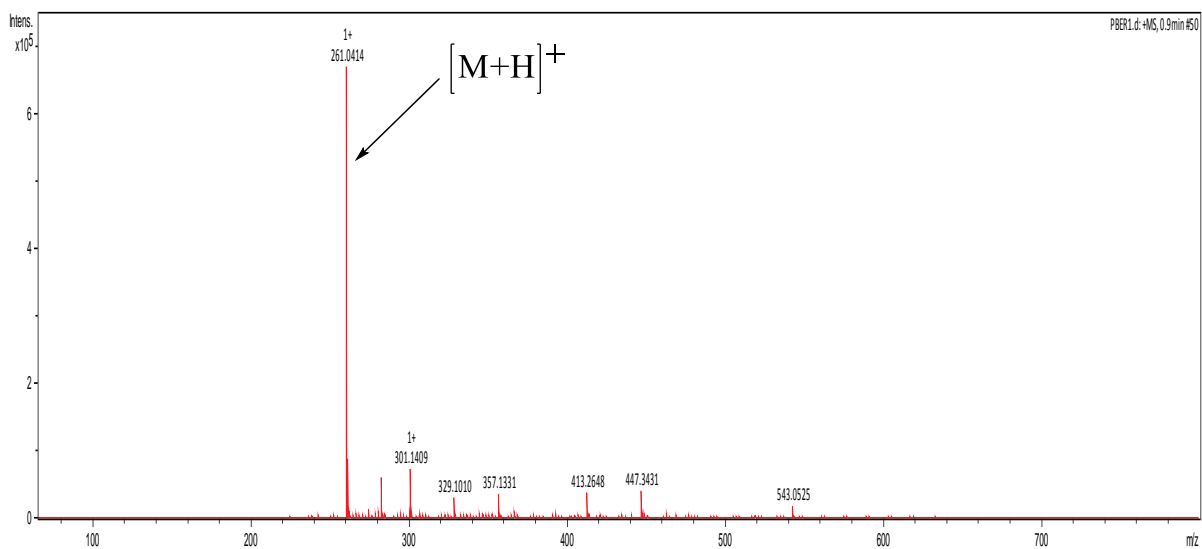
Figure 120: HR-ESI-MS spectrum of compound PBER1
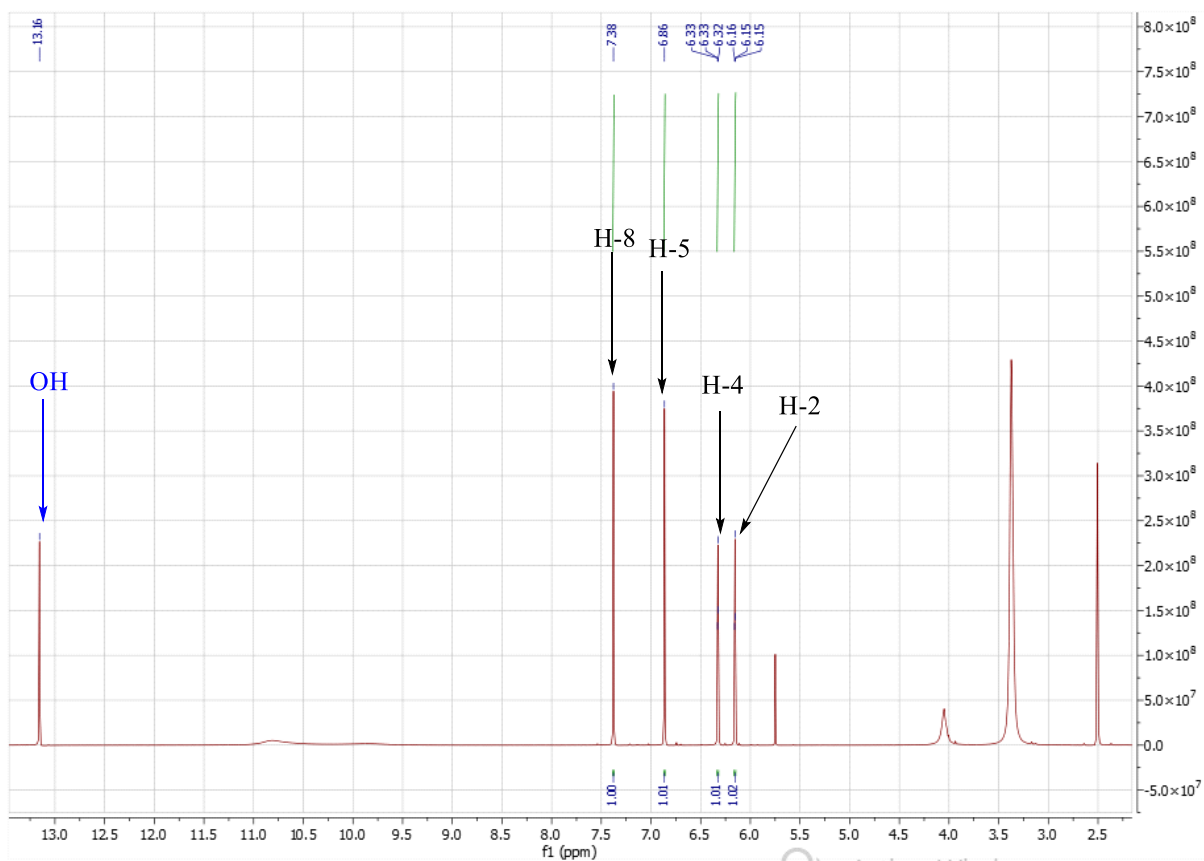
Figure 121: ^{1}H NMR spectrum (C$_2$D$_6$SO, 500 MHz) of compound PBER1
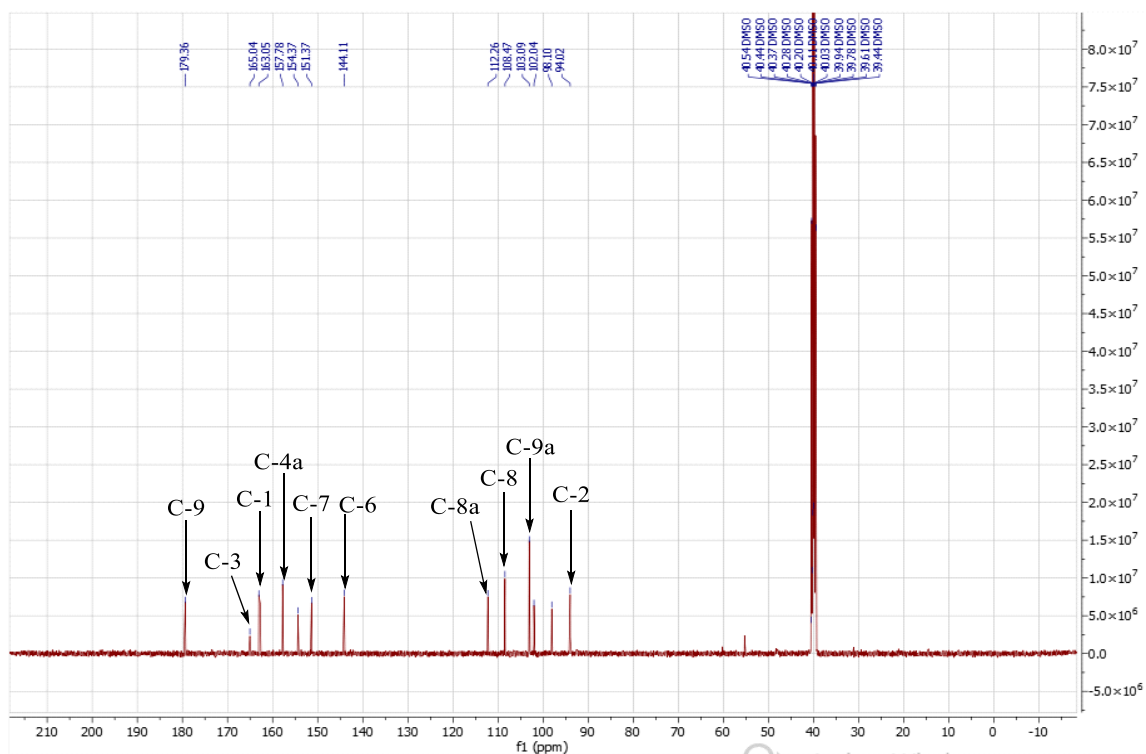
Figure 122: ^{13}C NMR spectrum (C_2D_6SO, 125 MHz) of compound PBER1
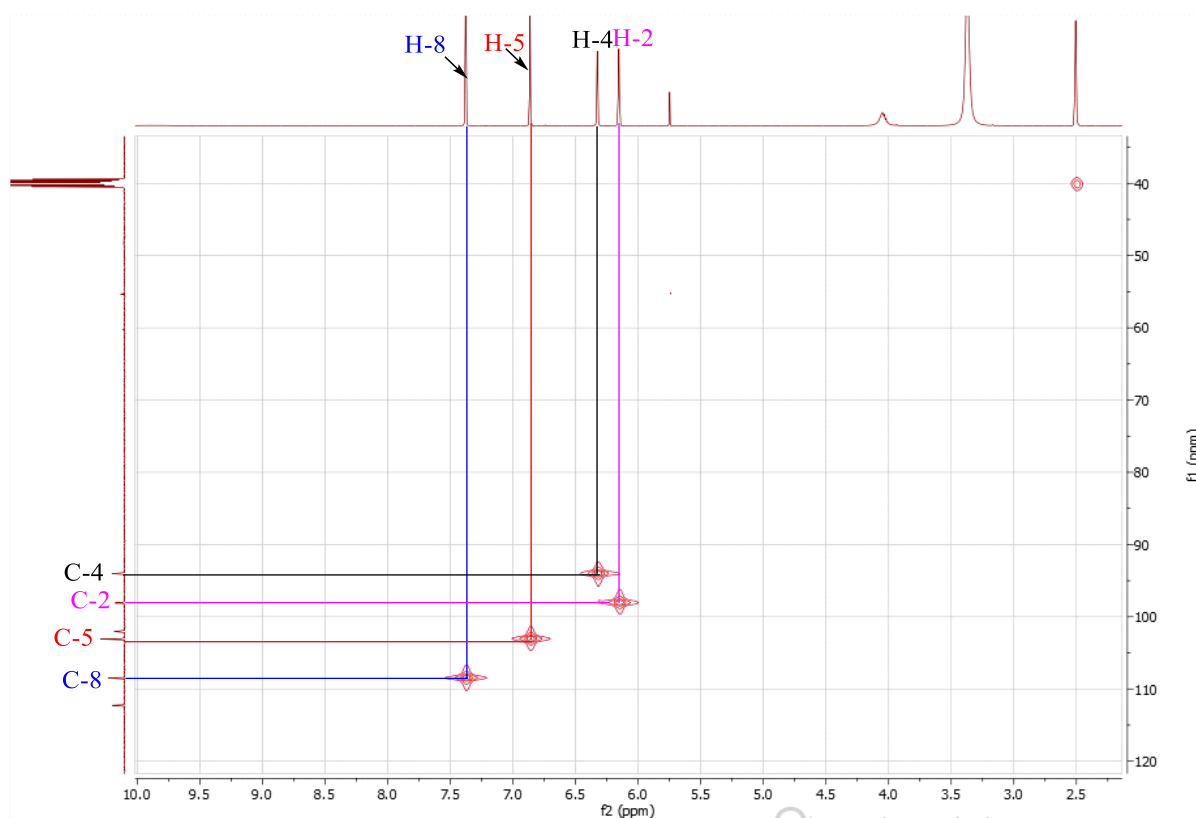
Figure 123: HSQC spectrum of compound PBER1
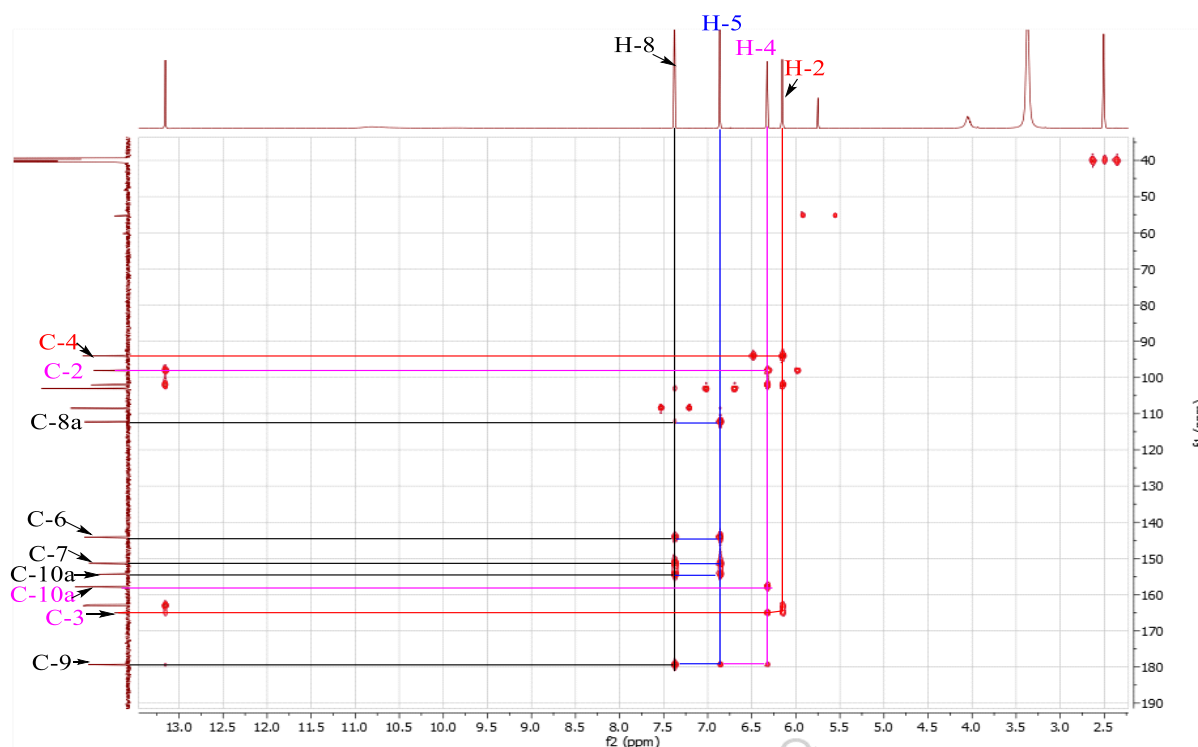
Figure 124: HMBC spectrum of compound PBER1

II.2.1.7.3 Identification of PBF1

PBF1 was isolated as a yellowish amorphous solid, and soluble in dimethyl sulfoxide. In the presence of ferric chloride, it gives a blue coloration, characteristic of phenolic compound.

Analysis of its ^1H and ^{13}C NMR spectrum combined with data from the literature allowed us to assign it the molecula formula $C_{14}H_{10}O_6$ containing ten degrees of unsaturations.

All these spectral data taken together, compared with those in the literature (Table XLII), allowed us to attribute to PBF1 the structure (**77**) which is that of daphnifolin, previously isolated from *Mesua daphnifolia* (Ee *et al*., 2006).

(**77**)
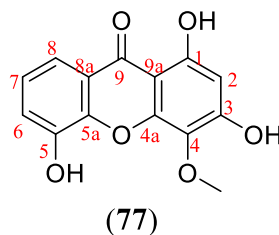
Indeed, the ^{1}H-NMR spectrum (Figure 125) of PBF1 contain the pattern of a simple xanthone, which includ:

An ABC system at δ_H 7.66 (1H, dd, J = 7.8, 1.7 Hz), 7.25 (1H, dd, J = 7.8, 1.7Hz) and 7.21 (1H, t, J = 7.8 Hz) which were assigned to the aromatic protons H-8, H-6 and H-7, respectively. The proton H-2 gave a singlet at δ_H 6.58 and the remaining singlet at δ_H 3.91 (3H, s) was therefore attributed to the methoxy protons.

Analysis of the ^{13}C NMR spectrum of PBF1 (Figure 126) showed signals of 14 carbon atoms which were distinguished using the DEPT 135 technique (Figure 127) into:
- four aromatic methines at δ_C 94.1 (C-2), 115.0 (C-8), 120.8 (C-6), and 123.5 (C-7);
- nine quaternary carbons including one carbonyl at δ_C 181.3 (C-9) and others at δ_C 158.7 (C-1), 154.0 (C-3), 153.2 (C-3), 145.8 (C-4a), 145.4 (C-5a), 130.7 (C-4) 121.7 (C-8a), and 103.9 (C-9a);

- one methoxy carbon at δ_C 59.8.

The structure of PBF1 was further confirmed by COSY (Figure 129) and HMBC (Figure 128, scheme 30) spectral data. From the HMBC spectrum, it was observed that the proton (H-2) correlated with three oxygenated quaternary carbons C-1(δ_C 158.7), C-3(δ_C 153.2), C-4(δ_C 130.7) and C-9a (δ_C 103.9). Both the protons H-6 and H-8 correlated with a aromatic carbon C-5a (δ_C 145.4). Connectivity was also observed between proton H-8 and carbon C-9 (δ_C 181.3) and thus confirmed the location of the hydroxyl group at C-5. The presence of the ABC system protons in the xanthone ring B was confirmed by the ^{1}H-^{1}H COSY spectral data, which showed correlations between H-6 and H-7, and H-7 and H-8. This was further supported by their similar coupling constant value in the ^{1}H NMR spectrum.
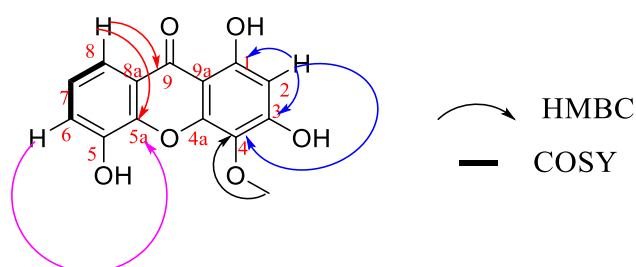
Scheme 30: Selected HMBC and COSY correlations of PBF1

Table XLII: ^{1}H (500 MHz) and ^{13}C (125 MHz) NMR spectral data of PBF1 in CD$_3$OD compared to those of daphnifolin [^{13}C NMR (125 MHz) and ^{1}H NMR (500 MHz) in C$_3$D$_6$O] (Ee *et al.*, 2006)

Position	PBF1		Daphnifolin	
	δ_H (nH, *m*, *J* in Hz)	δ_C	δ_H (nH, *m*, *J* in Hz)	δ_C
1	/	158.7	/	159.4
2	6.58 (1H, s)	94.1	6.51 (1H, s)	94.8
3	/	153.8	/	153.8
4		130.7	/	131.5
4a	/	145.8	/	146.9
5		154.0	/	155.3
5a	/	145.4	/	146.1
6	7.25 (1H, dd, *J* = 7.8, 1.7Hz)	120.8	7.30 (1H, dd, *J* = 7.4, 1.8Hz)	121.3
7	7.21 (1H, t, *J* = 7.8 Hz)	123.5	7.24 (1H, t, *J* = 7.4 Hz)	124.8
8	7.66 (1H, dd, *J* = 7.8, 1.7 Hz)	115.0	7.63 (1H, dd, *J* =7.4, 1.8 Hz)	116.0
8a	/	121.7	/	121.7
9	/	181.3	/	182.1
9a	/	103.9	/	103.9
OMe	3.91 (3H, s)	59.8	3.83 (3H, s)	60.7
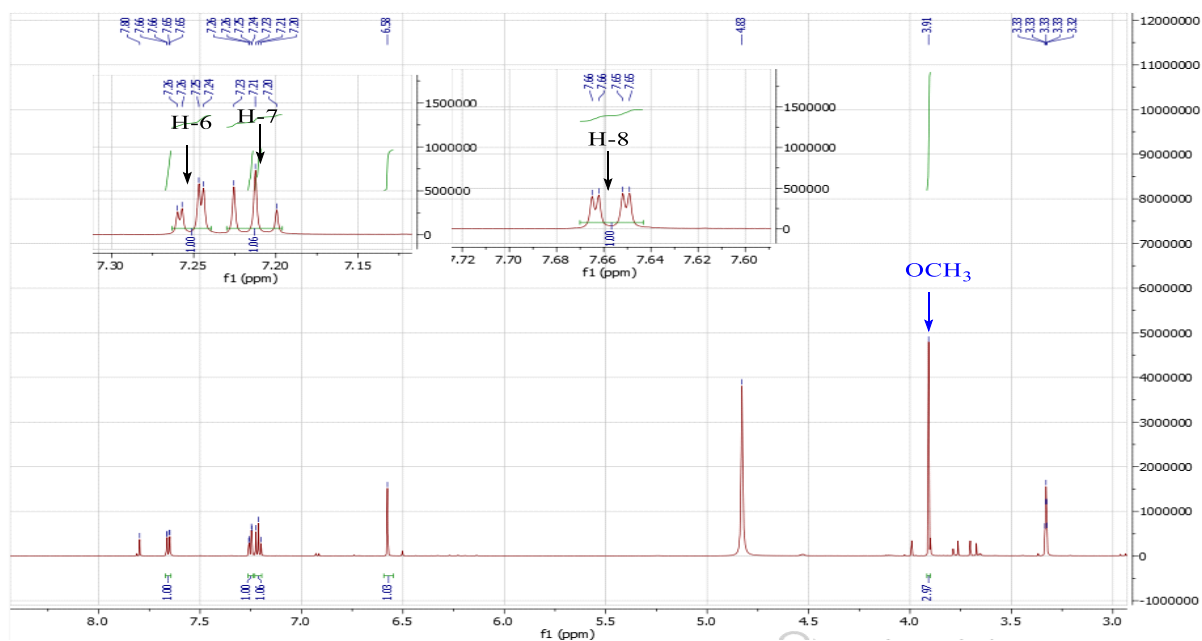
Figure 125: ^{1}H NMR spectrum (C$_3$D$_6$O, 500 MHz) of compound PBF1
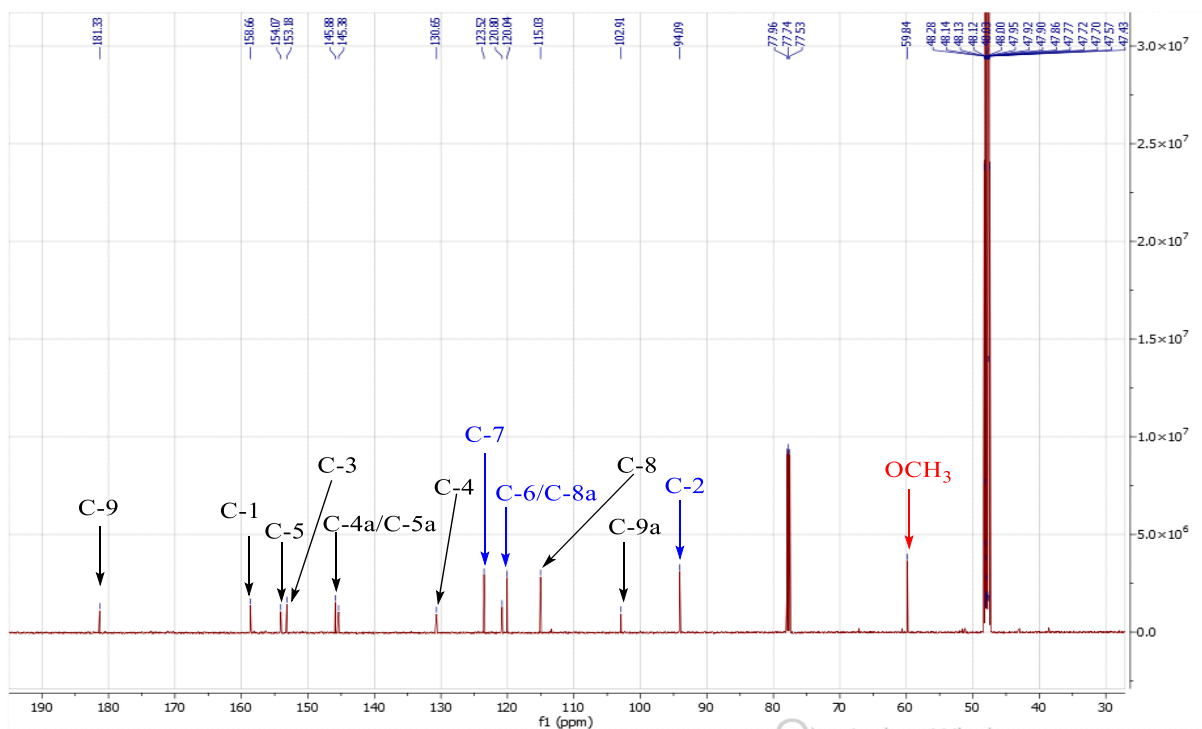
Figure 126: ^{13}C NMR spectrum (C$_3$D$_6$O, 125 MHz) of compound PBF1
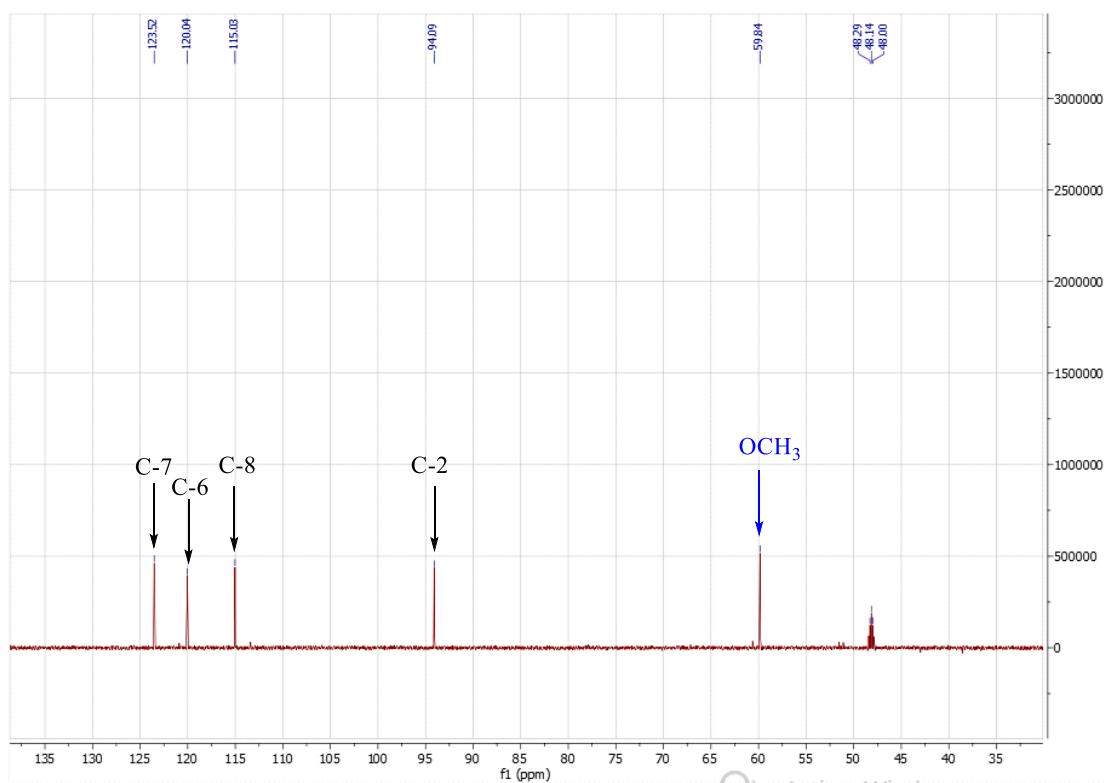
Figure 127: DEPT 135 spectrum of compound PBF1
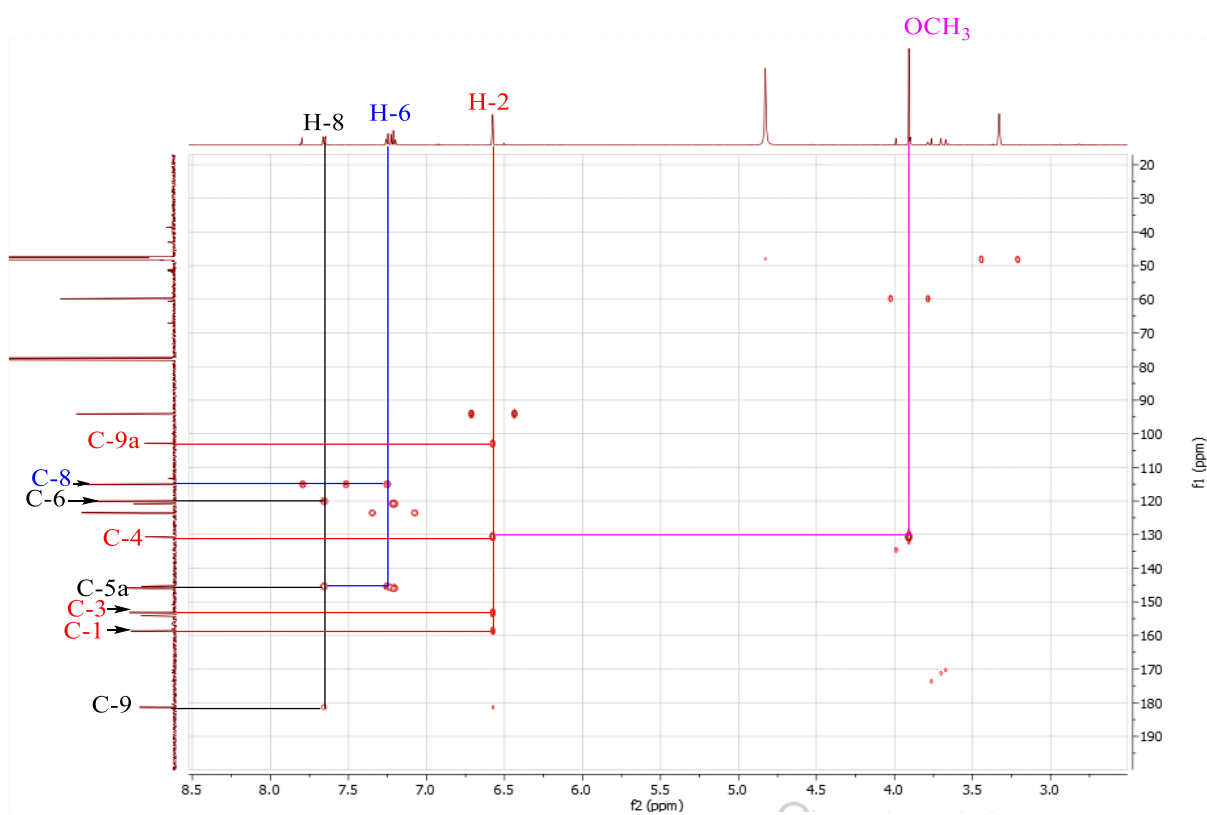
Figure 128: HMBC spectrum of compound PBF1

Figure 129: COSY spectrum of compound PBF1

II.2.1.7.4 Identification of PBHF3

PBHF3 was isolated as a yellowish amorphous solid, and is soluble methanol. In the presence of ferric chloride, it gives a purple coloration, characteristic of phenolic compounds.

Analysis of its ^{1}H and ^{13}C NMR spectrum combined with data from the literature allowed us to assign it the molecular formula $C_{14}H_{10}O_6$ containing ten degrees of unsaturation.

The ^{1}H and ^{13}C NMR spectra (Figures 130 and Figure 131) are almost identical to those of PBF1 but the difference lies in the position of the methoxy group at the ring A.

Indeed the HMBC spectrum (Figures 133, scheme 31) showed spots of correlations between:
The proton H-4 (δ_H 6.56) and the carbons C-9 (δ_C 181.2), C-3 (δ_C 158.7), C-4a (δ_C 153.1), C-2 (δ_C 130.7) and C-9a (δ_C 102.7). Then the protons of the methoxy group OCH$_3$ (δ_H 3.90) and the carbon C-2 (δ_C 130.7). All this information justifies the position of the methoxy group in position 2.
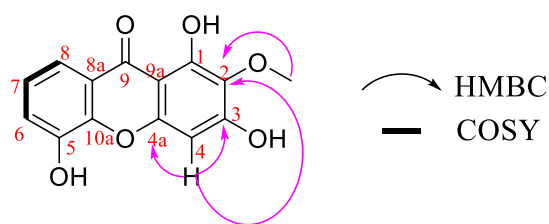
Scheme 31: Some keys correlations observed on the HMBC and COSY spectra of PBHF3

All these spectral data taken together, compared with those in the literature (Table XLIII), allowed us to attribute to PBHF3 the structure (**78**) which is that of tovopyrifolin C, previously isolated from *Mesua daphnifolia* (Ee *et al.*, 2009).

(**78**)
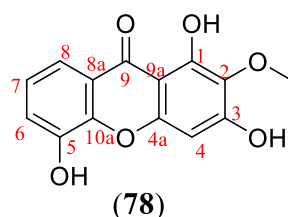
Table XLIII: ^{1}H (500 MHz) and ^{13}C (125 MHz) NMR spectral data of PBHF3 in CD$_3$OD compared to those of tovopyrifolin C [^{13}C NMR (100 MHz) and ^{1}H NMR (400 MHz) in CDCl$_3$] (Ee *et al.*, 2009)

Position	PBHF3		Tovopyrifolin C	
	δ_H (nH, *m*, *J* in Hz)	δ_C	δ_H (nH, *m*, *J* in Hz)	δ_C
1	/	154.1	/	155.3
2	/	130.7	/	131.5
3	/	158.7	/	159.2
4	6.56 (1H, s)	93.9	6.52 (1H, s)	94.7
4a	/	153.1	/	153.8
5		146.0	/	146.9
6	7.26 (1H, dd, *J* = 7.8, 1.7Hz)	120.0	7.34 (1H, dd, *J* = 8.2, 1.8Hz)	121.3
7	7.23 (1H, t, *J* = 7.8 Hz)	123.5	7.28 (1H, t, *J* = 7.5 Hz)	124.8
8	7.66 (1H, dd, *J* =7.8, 1.8 Hz)	115.0	7.64 (1H, dd, *J* = 7.5, 1.8 Hz)	116.1
8a	/	120.7	/	121.7
9	/	181.2	/	182.1
9a	/	102.7	/	104.0
10a		145.4		146.1
OMe	3.90 (3H, s)	59.6	3.86 (3H, s)	60.7
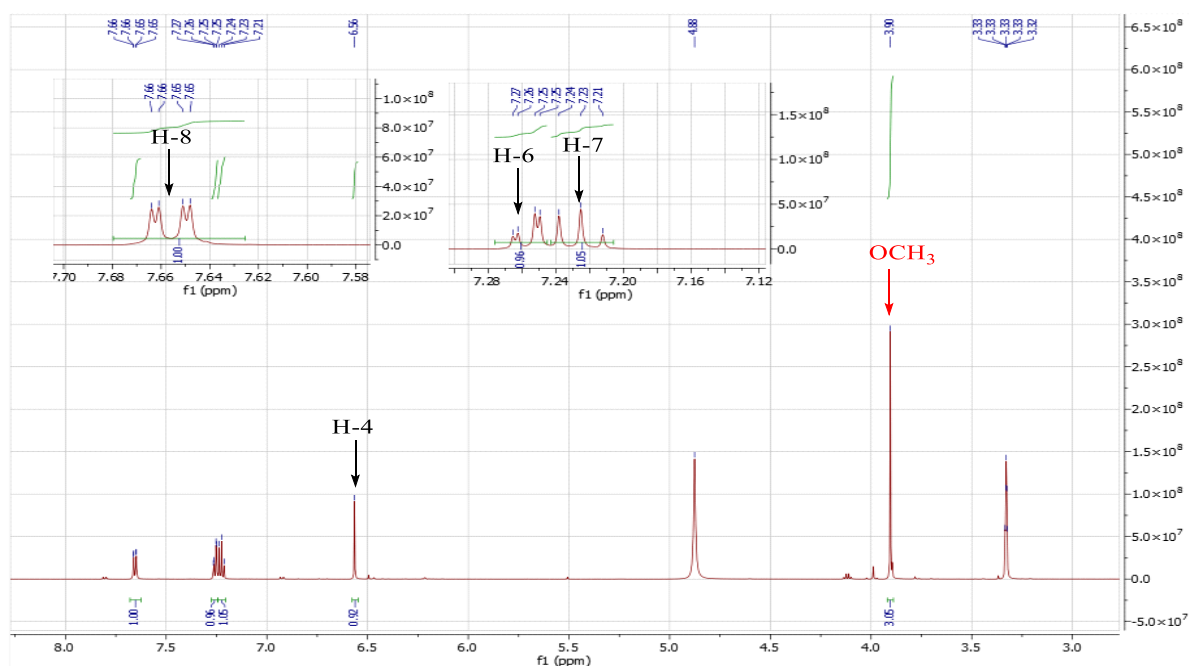
Figure 130: ^{1}H NMR spectrum (CD₃OD, 500 MHz) of compound PBHF3
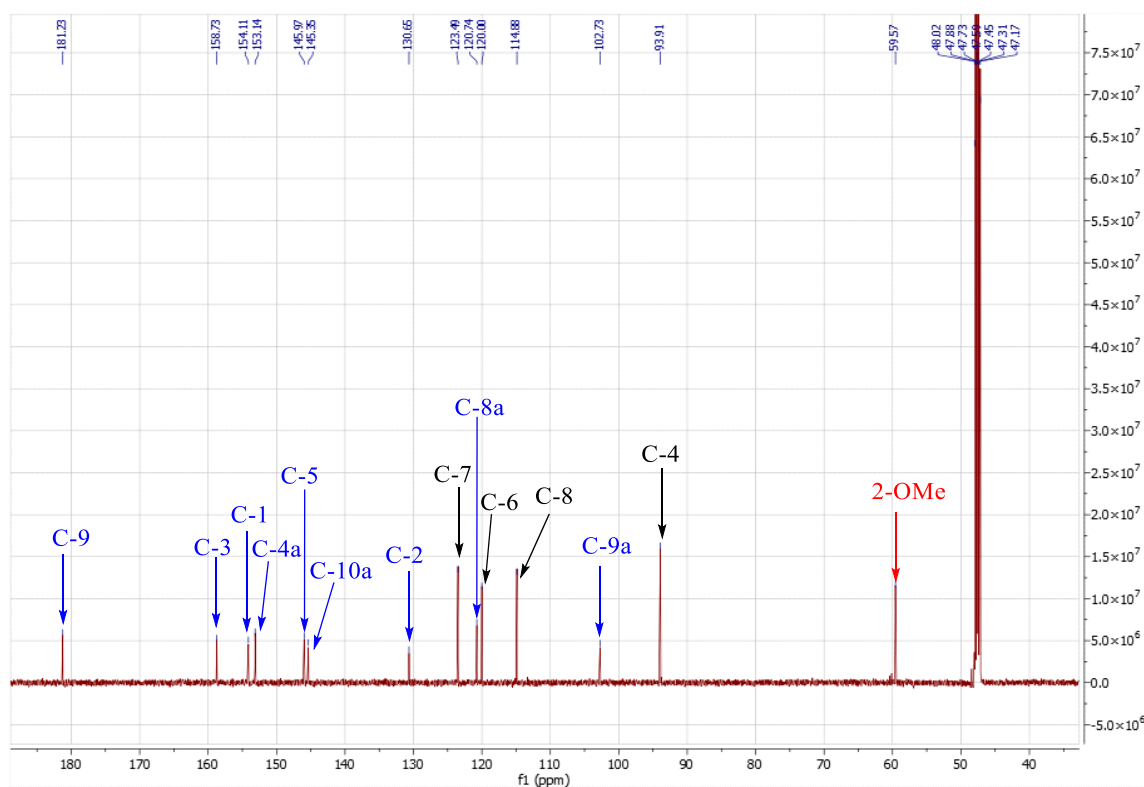
Figure 131: ^{13}C NMR spectrum (CD₃OD, 125 MHz) of compound PBHF3
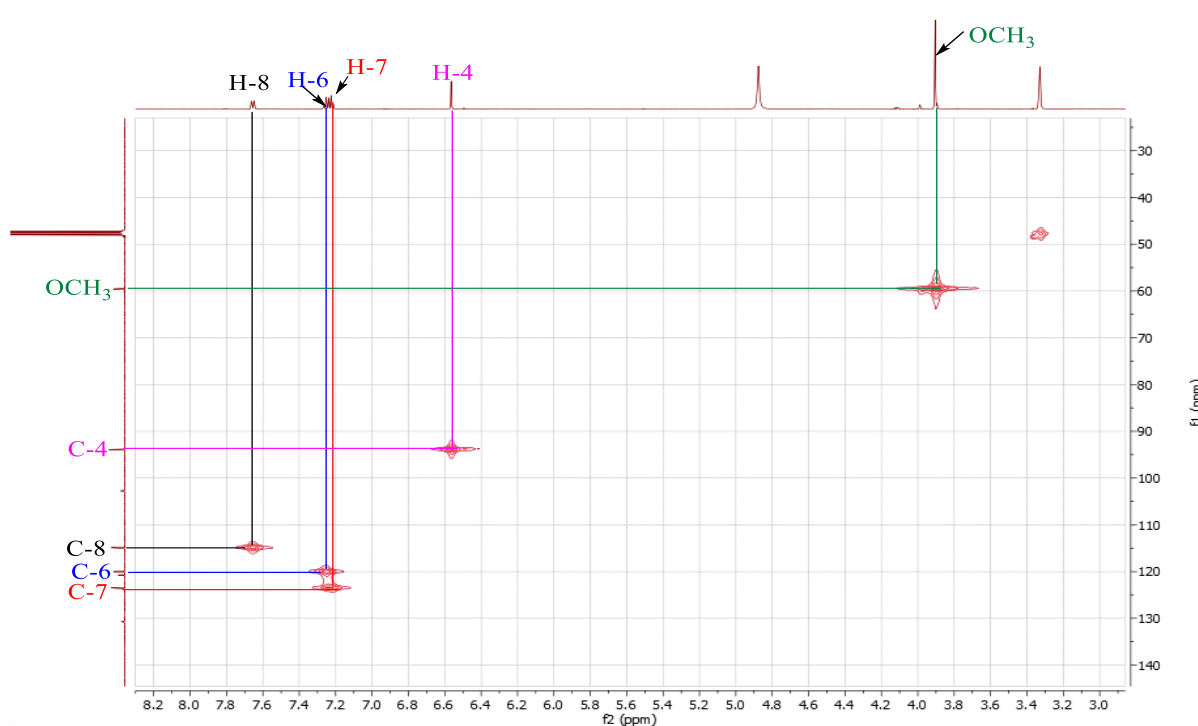
Figure 132: HSQC spectrum of compound PBHF3
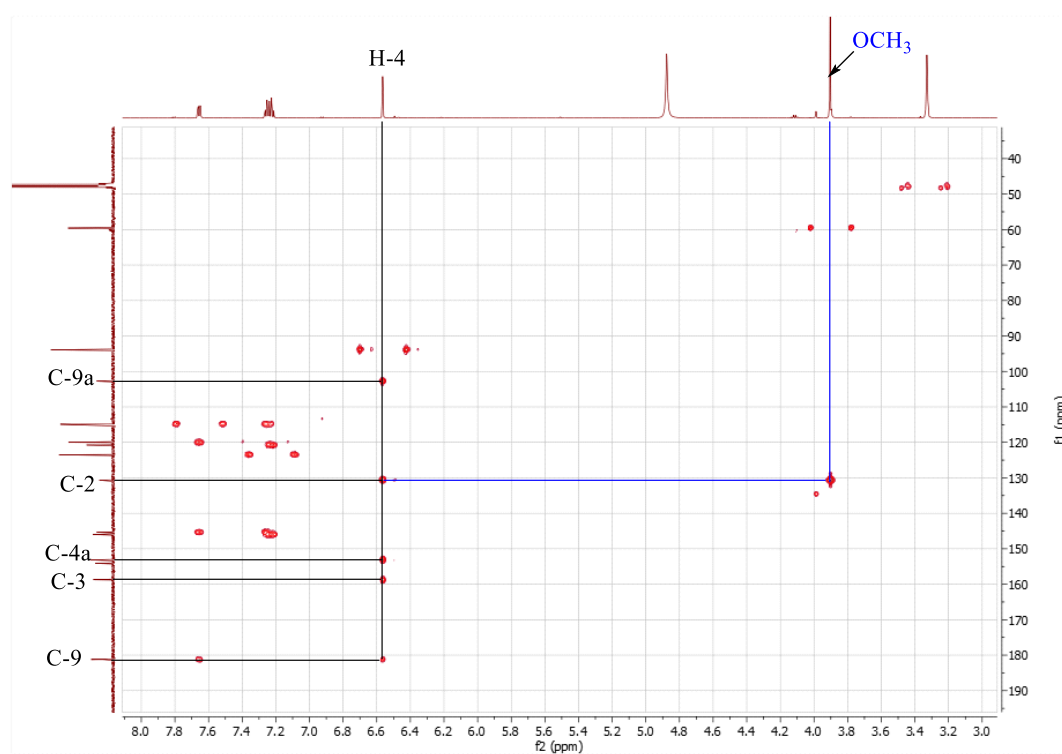
Figure 133: HMBC spectrum of compound PBHF3
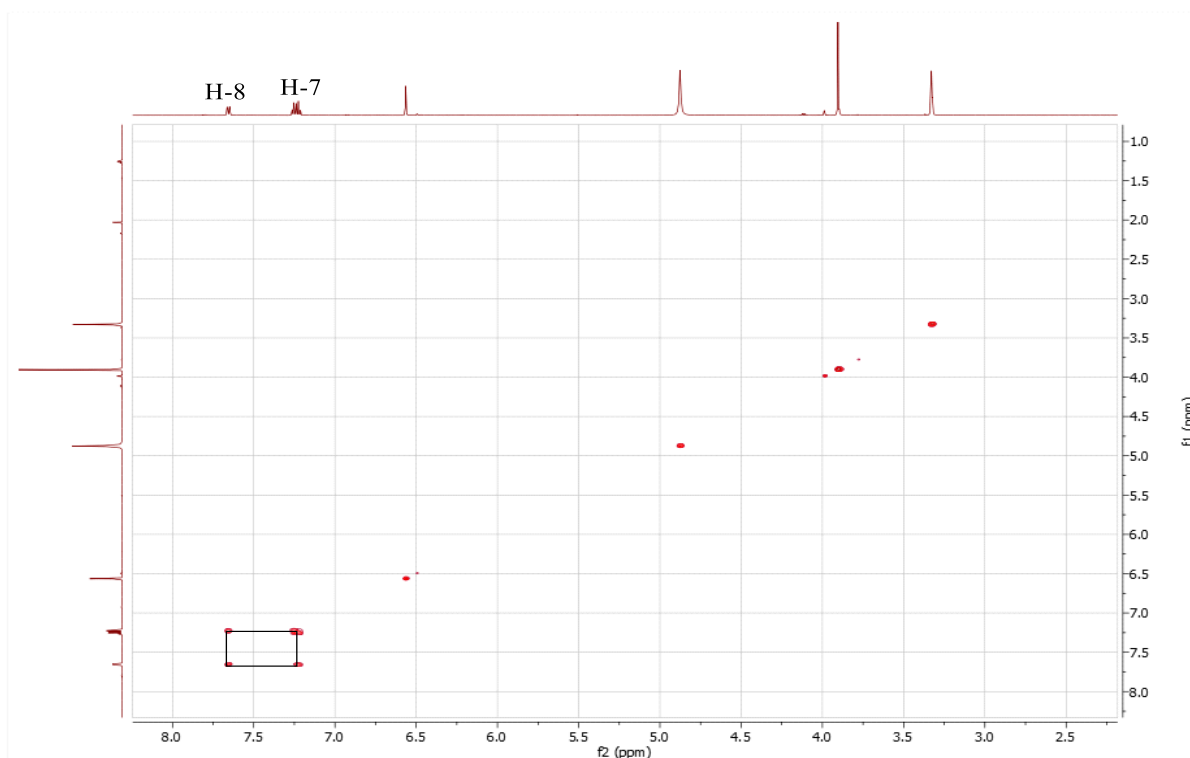
Figure 134: COSY spectrum of compound PBHF3

II.2.1.7.5 Identification of PBE2=PBHF9

PBHF9 was isolated as a yellowish amorphous solid, and is soluble in chloroform. In the presence of ferric chloride, it gives a purple coloration, characteristic of phenolic compound.

Its high-resolution ESI (+) mass spectrum (Figure 135) shows the peak of the sodium adduct ion $[M+Na]^+$ at m/z 433.1647 (calculated 433.1622 for $C_{24}H_{26}O_6Na$) corresponding to the molecular formula $C_{24}H_{26}O_6$, containing twelve unsaturations.

All these spectral data taken together, compared with those in the literature (Table XLIV), allowed us to attribute to PBHF9 the structure (**79**) which is that of α-mangostin, previously isolated from the fruits of *Garcinia mangostana* (Yu *et al*., 2007).

(**79**)
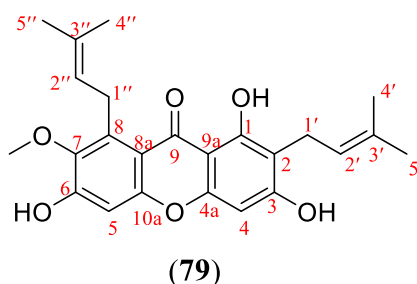
Indeed, the ^{1}H-NMR spectrum (Figure 136) of PBHF9 showed:

- one chelated hydroxyl group at δ_H 13.71;

- two aromatic singlets of one proton at δ_H 6.26 (1H, s, H-4) and 6.76 (1H, s, H-5);

- characteristic signals of two prenyl unit were exhibited at δ_H [5.24 (1H, m, H-2′), 3.31 (2H, brd, J = 7.1 Hz, H-1′), 1.69 (3H, s, H-5′), and 1.68 (3H, s, H-4′)] and [5.24 (1H, m, H-2″), 4.02 (2H, brd, J = 6.3 Hz, H-1″), 1.84 (3H, s, H-5″), and 1.80 (3H, s, H-4″)].

Analysis of the ^{13}C NMR spectrum of PBHF9 (Figure 137) brings out the signals of 24 carbon atoms which were distinguished using the HSQC technic (Figure 138) into:

- two aromatic methines at δ_C 91.5 (C-4), and 101.2 (C-5);

- seven quarternary carbon signals including a carbonyl of ketone at δ_C 182.1 (C-9), six oxygenated aromatic carbons at δ_C 162.4 (C-3), 160.1 (C-1), 156.5 (C-10a), 155.8 (C-4a), 154.8 (C-6), and 143.5 (C-7);

- one methoxy carbon at δ_C 62.1;

- four methyl of carbons at δ_C 24.3 (C-4′), 16.9 (C-5′), 24.3 (C-4″) and 16.4 (C-5″) belonging to the two prenyl groups.

The structure of PBHF9 was further confirmed by HMBC (Figure 139, scheme 32) spectrum. It was observed that the prenyl unit was linked to C-2 (δ_C 109.8) and C-8 (δ_C 137.3) by the correlation between H-1′ (δ_H 3.36) and C-1 (δ_C 160.1), C-2 (δ_C 109.8) and C-3 (δ_C 162.4), and H-1″ (δ_H 4.02) and C-7 (δ_C 143.5), C-8 (δ_C 137.3) and C-8a (δ_C 111.1).

This spectrum also shows correlation spots between the proton H-4 and the carbons C-3 (δ_C 162.4), C-2 (δ_C 109.8), then H-5 and the carbons C-6 (δ_C 154.8), C-7 (δ_C 143.5), confirming the position of the hydroxyl groups at position C-1, C-2 and C-6 and the methoxy group at position C-7.
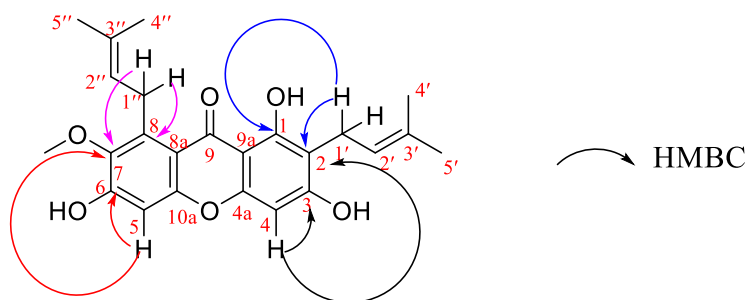
Scheme 32: Selected HMBC correlations of PBHF9

Table XLIV: ¹H (500 MHz) and ¹³C (125 MHz) NMR spectral data of PBHF9 in CDCl₃ compared to those of α-mangostin [¹³C NMR (125 MHz) and ¹H NMR (500 MHz) in C₃D₆O] (Yu et al., 2007)

Position	PBHF9		α-Mangostin	
	δ_H (nH, m, J in Hz)	δ_C	δ_H (nH, m, J in Hz)	δ_C
1	/	160.1	/	160.3
2	/	109.8	/	110.2
3	/	161.7	/	162.3
4	6.26 (1H, s)	91.5	6.41 (1H, s)	91.9
4a	/	155.8	/	154.9
5	6.76 (1H, s)	101.2	6.83 (1H, s)	101.6
6	/	154.8	/	156.6
7	/	143.5	/	143.5
8	/	137.3	/	137.2
8a	/	111.1	/	111.0
9	/	182.1	/	181.8
9a	/	102.8	/	102.6
10a	/	156.5	/	155.4
1′	3.36 (2H, brd, J = 7.1 Hz)	21.5	3.38 (2H, d, J = 6.0 Hz)	21.2
2′	5.24 (1H, m)	123.9	5.28 (1H, m)	122.7
3′		130.3		130.6
4′	1.68 (3H, s)	24.3	1.65 (3H, s)	26.0
5′	1.69 (3H, s)	16.9	1.67 (3H, s)	16.9
1″	4.02 (2H, brd, J = 6.3 Hz)	26.0	4.16 (2H, dd, J= 18, 10 Hz)	25.0
2″	5.24 (1H, m)	122.4	5.28 (1H, m)	123.9
3″		130.4		130.4
4″	1.80 (3H, s)	24.3	1.80 (3H, s)	25.0
5″	1.84 (3H, s)	16.4	1.85 (3H, s)	17.3
OMe	3.78 (3H, s)	62.1	3.81 (3H, s)	60.2
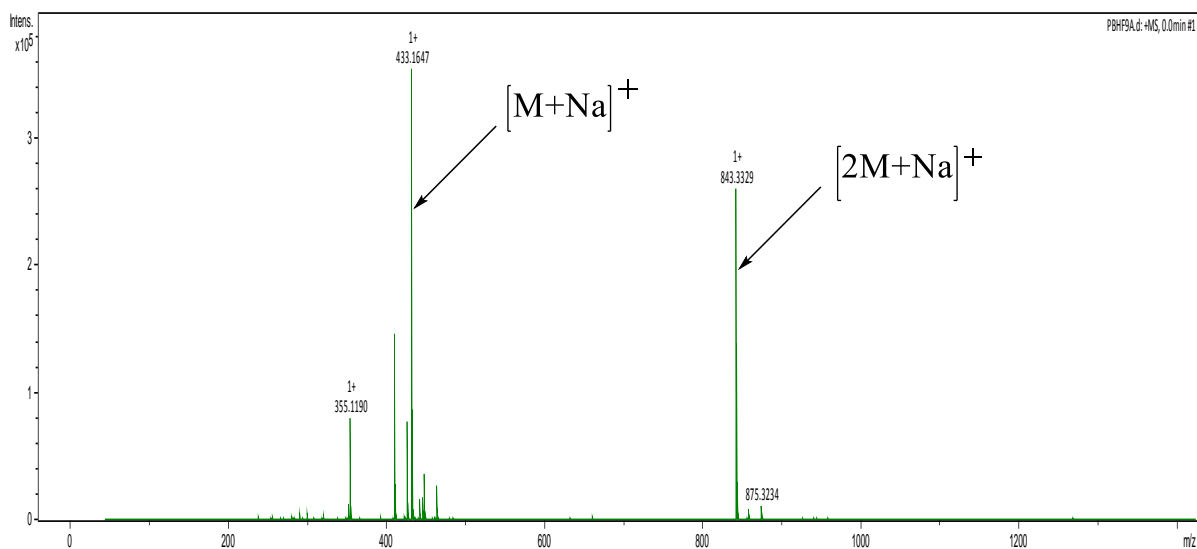
Figure 135: HR-ESI-MS spectrum of compound PBHF9
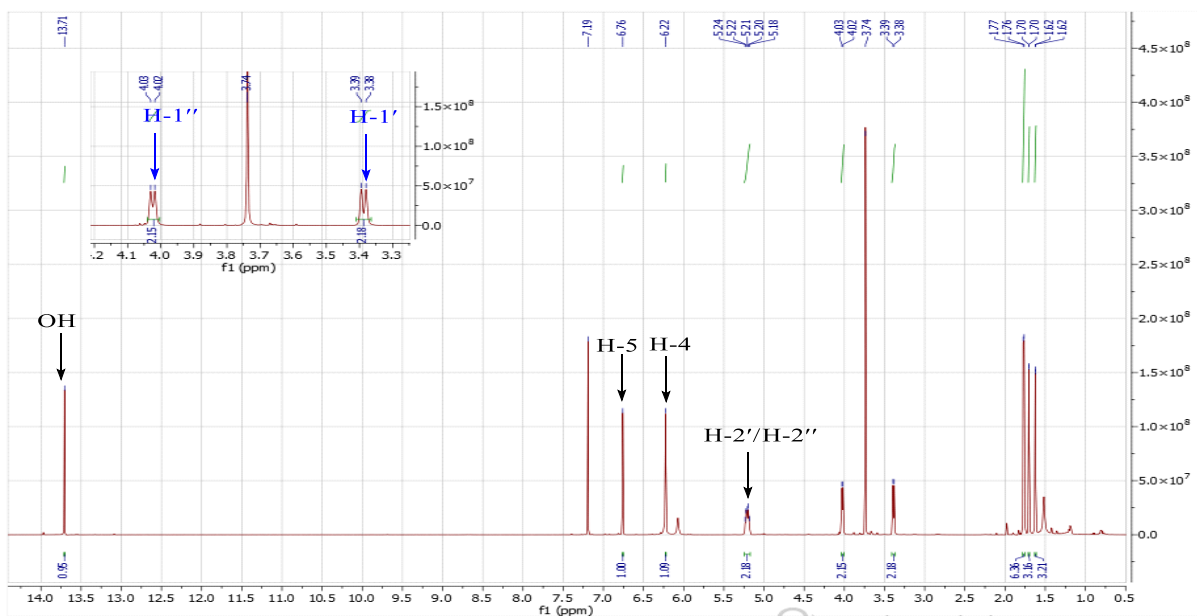
Figure 136: ^{1}H NMR spectrum (CDCl$_3$, 500 MHz) of compound PBHF9

Figure 137: ¹³C NMR spectrum (CDCl₃, 125 MHz) of compound PBHF9
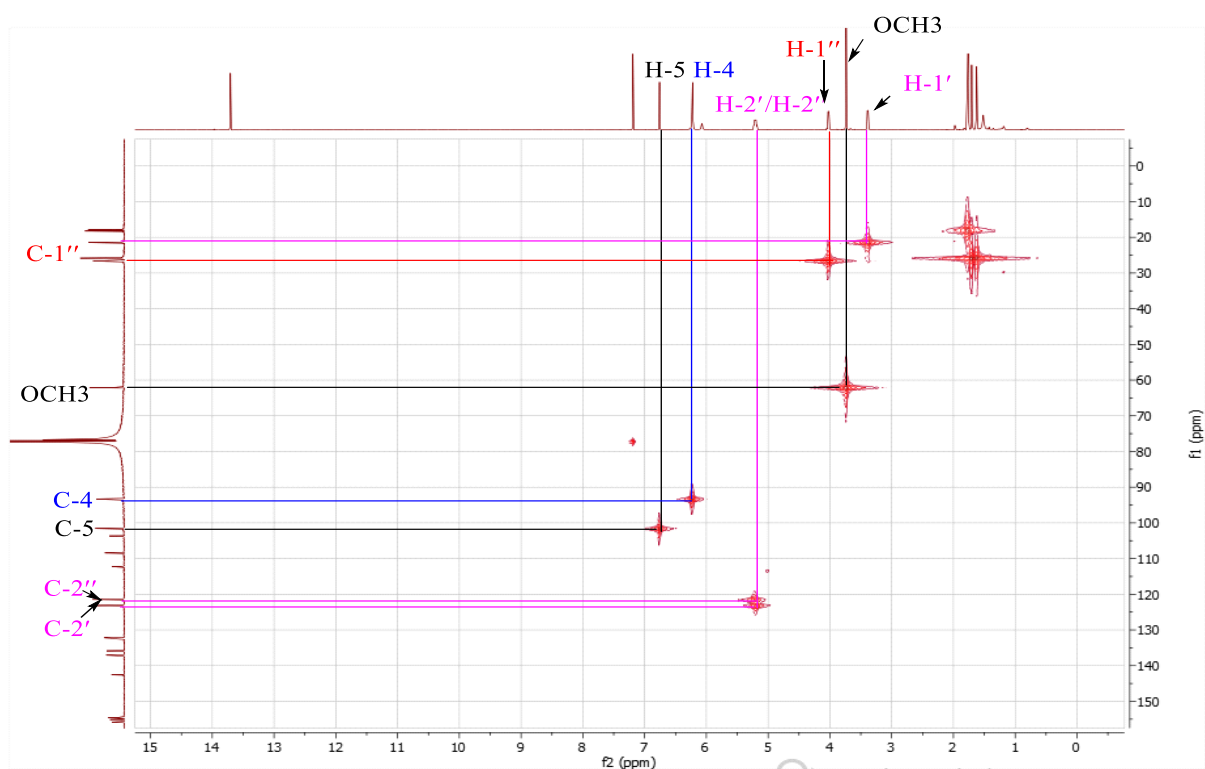
Figure 138: HSQC spectrum of compound PBHF9

Figure 139: HMBC spectrum of compound PBHF9

II.2.1.7.6 Identification of PBHF4

PBHF4 was obtained as a yellow amorphous solid, and is soluble in chloroform. It reacts positively to the ferric chloride test indicating its phenolic nature.

Its HR- ESI positive-mode mass spectrum (Figure 140) shows the peak of protonated ion $[M+H]^+$ at m/z 357.1333, corresponding to the molecular formula $C_{20}H_{21}O_6$ (calculated for 357.1333), containing 11 degrees of unsaturation.

The ^1H NMR spectrum (Figure 141) showed:

-a singlet of a proton characteristic of a chelated hydroxyl at δ_H 13.10 (OH, s);

-the signals of three aromatic protons at δ_H 7.63 (1H, s), 6.45 (1H, s) and 6.36 (1H, s);

-the signals of two methoxy groups at δ_H 3.95 (s, OCH$_3$) and 4.04 (s, OCH$_3$);

-the signals of a 3,3-dimethylallyl group at δ_H [5.26 (1H, t, J = 7.1Hz), 3.40 (2H, d, J = 7.0Hz); 1.83 (3H, s) and 1.71 (3H, s)].

Analysis of its ^{13}C NMR spectrum (Figure 142) brings out the signals of 20 carbon atoms which were distinguished using the DEPT 135 technique (Figure 143) into:

- eleven quaternary carbons including one carbonyl at δ_C 179.9;

-four carbons of methine groups, three of which correspond to aromatic carbons (δ_C 104.6, 102.5 and 89.6), and one attributable to the olefinic carbon of prenyl (δ_C 122.2);

-a methylene group at δ_C 21.4;

-four carbons of methyl groups including two at δ_C 25.8 and 17.8 belonging to the prenyl group and two at δ_C 56.5 and 55.9 belonging to the methoxy group.

The positions of the prenyl, methoxy and hydroxyl groups were established based on the correlations observed on the HMBC spectrum (Figure 144, scheme 33) between: the H-8 proton (δ_H 7.63) and the C-9 carbon (δ_C 179.9) of the carbonyl, shows that the chelated hydroxyl is bonded to the C-1 (δ_C 159.3) carbon. The proton H-4 (δ_H 6.45) and the carbons C-3 (δ_C 163.8), C-2 (δ_C 111.7). Likewise the proton H-1′ (δ_H 3.40) and the carbons C-1, C-3 and C-2, confirm the positions of the chelated hydroxyl groups, prenyl and methoxy in C-1, C-2 and C-3 respectively. Then the proton H-5 (δ_H 6.96) and the carbons C-6 (δ_C 152.4), C-8 (δ_C 104.6), confirming the positions of the free hydroxyl and methoxy groups at C-6 and C-7 respectively.
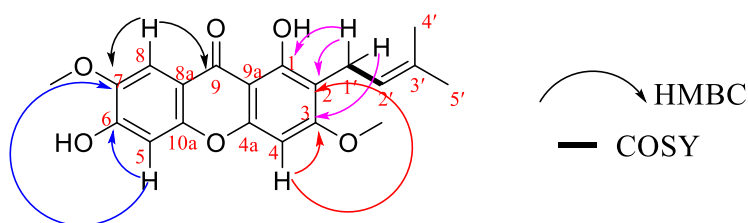
Scheme 33: Selected HMBC and COSY correlations of PBHF4

All these spectral data taken together, compared with those in the literature (Table XLV), allowed us to attribute to PBHF4 the structure (**80**) which is that of cowagarcinone B, previously isolated from *Garcinia cowa* (Mahabusarakam *et al*., 2005).
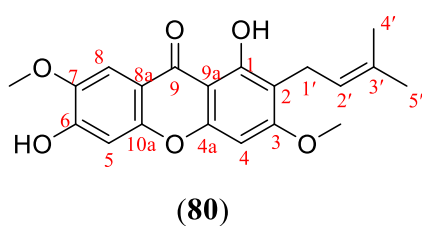
(**80**)

Table XLV: ^{1}H (500 MHz) and ^{13}C (125 MHz) NMR spectral data of PBHF4 in CDCl$_3$ compared to those of cowagarcinone B [^{13}C NMR (125 MHz) and ^{1}H NMR (500 MHz) in CDCl$_3$] (Mahabusarakam *et al.*, 2005)

Position	PBHF4		Cowagarcinone B	
	δ_H (nH, *m*, *J* in Hz)	δ_C	δ_H (nH, *m*, *J* in Hz)	δ_C
1	/	159.3	/	159.4
2	/	111.7	/	111.8
3	/	163.8	/	163.9
4	6.45 (1H, s)	89.6	6.43 (1H, s)	89.6
4a	/	156.2	/	156.2
5	6.96 (1H, s)	102.5	6.94 (1H, s)	102.5
6	/	152.4	/	152.4
7	/	144.3	/	144.3
8	7.63 (1H, s)	104.6	7.61 (1H, s)	104.6
8a	/	113.6	/	113.6
9	/	179.9	/	179.9
9a	/	103.4	/	104.6
10a	/	152.5	/	152.5
1′	3.40 (2H, d, *J* = 7.1 Hz)	21.4	3.37 (2H, d, *J* = 7.0 Hz)	21.4
2′	5.26 (1H, t, *J* = 7.1 Hz)	122.2	5.28 (1H, br t, *J* = 7.0 Hz)	122.2
3′		131.9		131.8
4′	1.83 (3H, s)	17.8	1.80 (3H, s)	17.8
5′	1.71 (3H, s)	25.8	1.68 (3H, s)	25.8
3-OMe	4.04 (3H, s)	55.9	4.01 (3H, s)	55.9
7-OMe	3.95 (3H, s)	56.5	3.92 (3H, s)	56.5
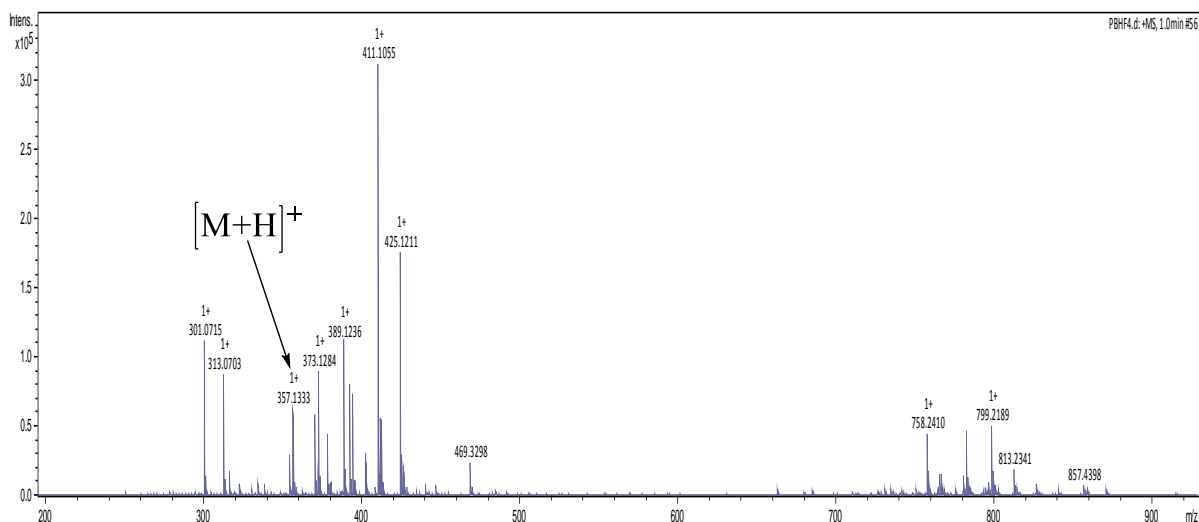
Figure 140: HR-ESI-MS spectrum of compound PBHF4
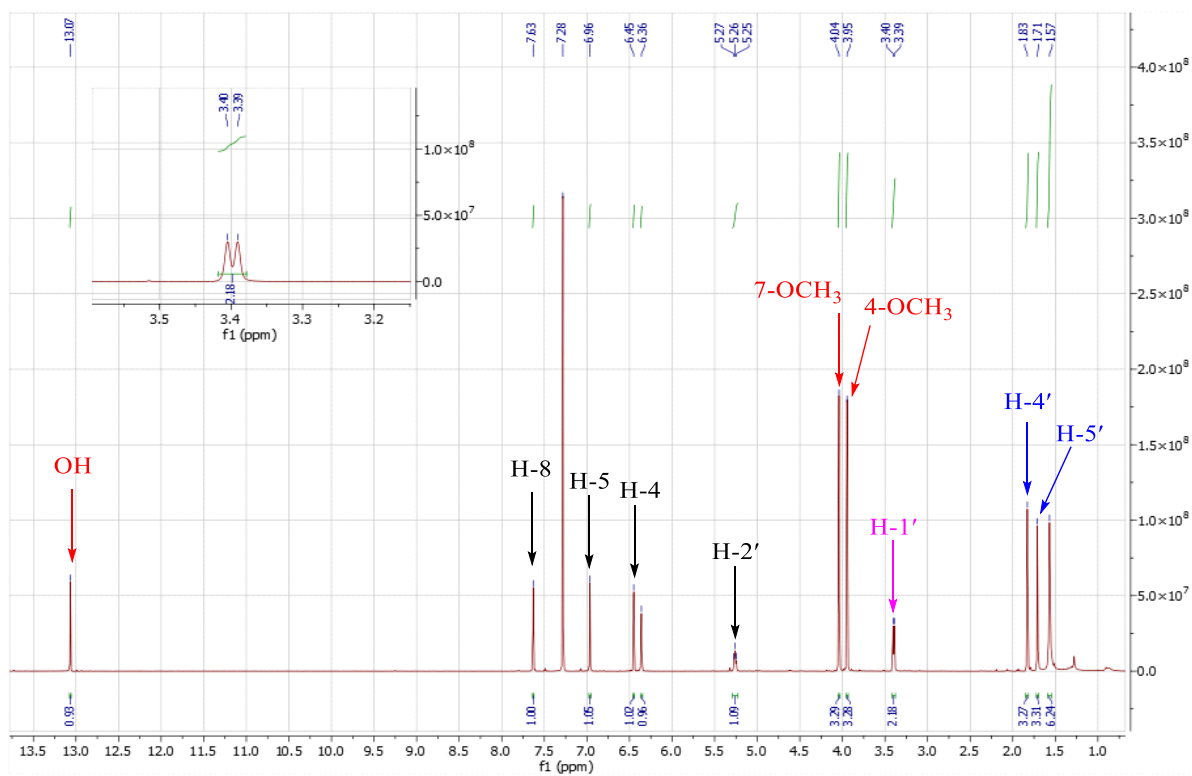
Figure 141: ^{1}H NMR spectrum (CDCl$_3$, 500 MHz) of compound PBHF4
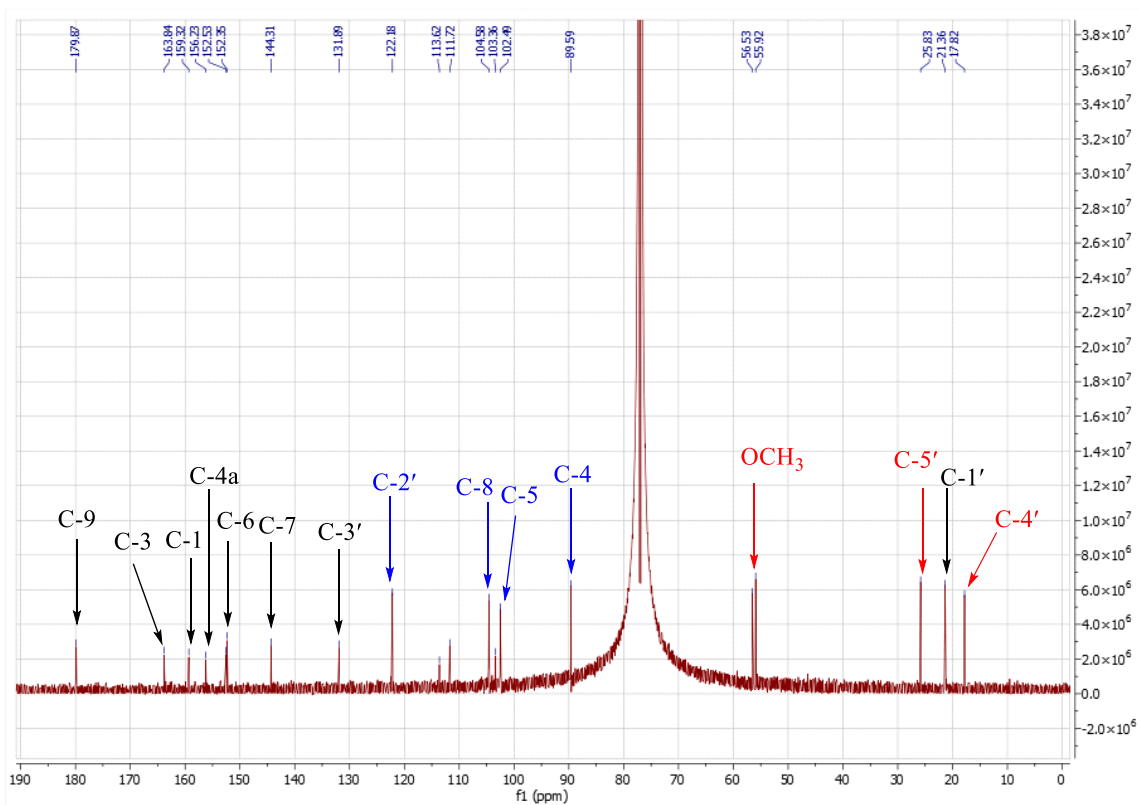
Figure 142: ^{13}C NMR spectrum (CDCl$_3$, 125 MHz) of compound PBHF4

Figure 143: DEPT 135 spectrum of compound PBHF4

Figure 144: HMBC spectrum of compound PBHF4

Figure 145: COSY spectrum of compound PBHF4

II.2.1.7.7 Identification of PBE13

PBE13 was obtained as a yellow amorphous solid and is soluble in chloroform. It reacts positively to the ferric chloride test, indicating its phenolic nature.

Analysis of its ^{1}H and ^{13}C NMR spectrum combined with data from the literature allowed us to assign molecular formula $C_{24}H_{24}O_6$ containing thirteen degrees of unsaturation.

All these spectral data taken together, compared with those in the literature (Table XLVI), allowed us to attribute to PBE13 the structure (**81**) which is that of 9-hydroxycalabaxanthone, previously isolated from the seed cases of *Garcinia mangostana* (Ryu *et al.*, 2010).

(**81**)
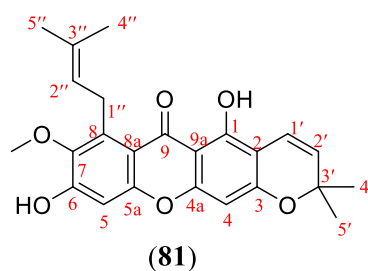
Indeed, the ^{1}H NMR spectrum of PBE12 (Figure 146) showed:

- the signal of a singlet of a chelated hydroxyl proton at δ_H 13.62 (1H, s, OH-1);

- the signals of two aromatic singlets at δ_H 6.17 (1H, s, H-4), 6.76 (1H, s, H-5);

- the signals of the protons of a 3,3-dimethylallyl moiety at δ_H [5.19 (1H, br t, *J* = 5.0 Hz, H-2″), 4.02 (2H, d, *J* = 6.2 Hz, H-1″), 1.62 (3H, s, H-4″), and 1.76 (3H, s, H-5″)];

- the signals of the protons of a dimethyl pyran ring at δ_H 6.66 (1H, d, *J* = 10.0 Hz, H-1′), 5.49 (1H, d, *J*= 10.0 Hz, H-2′), and 1.39 (6H, s, H-4′ and H-5′) (Ngouela *et al.*, 2006);

- the signal of singlet of one methoxy group at δ_H 3.73 (3H, s, OCH$_3$-7).

The ^{13}C NMR spectrum (Figure 147) of PBE13 showed the signals of 24 carbon atoms which were distinguished using the HSQC technique (Figure 148) into:
- thirteen quaternary carbons including a carbonyl of 1-hydroxylated xanthone at δ_C 182.0 (C-9) (Silva and Pinto., 2005) and the others at δ_C 157.9 (C-1), 104.5 (C-2), 159.9 (C-3), 156.3 (C-4a), 154.6 (C-6), 142.7 (C-7), 137.0 (C-8), 112.2 (C-8a), 103.7 (C-9a), 155.8 (C-10a), 77.9 (C-3′) and 132.2(C-3″);

- four carbons of methine groups including three olefinics at δ_C 115.7 (C-1′), 127.2 (C-2′) and 123.1 (C-2″), two aromatics at δ_C 94.2 (C-4) and 101.7 (C-5);

- one carbon of methylene group at δ_C 26.6 (C-1″);

- four carbons of methyl groups at δ_C 28.3 (C-4′ and C-5′), 25.8 (C-4″) and 18.2 (C-5″);

- one carbon of methoxy group at δ_C 62.1 (OCH₃-7).

All of this data shows that the compound PBE13 is a xanthone carrying one methoxy group, a prenyl and a dimethyl pyran ring.

The position of these groups on the xanthone skeleton was determined using correlations observed on the HMBC spectrum (Figure 149, scheme 34). In fact, on this spectrum, cross peaks were observed between;

- the methoxy protons 7-OCH₃ (δ_H 3.73) and H-1″ (δ_H 4.02) to carbon C-7 (δ_C 142.7) suggesting the attachment of the methoxy group to the position C-7;

- the protons of the methylene group H-1″ (δ_H 4.02) and carbons C-8 (δ_C 137.0), C-7 (δ_C 142.7), and C-8a (δ_C 112.2), confirming the attachment of the 3,3-dimethylallyl moiety to the C-8;

- the olefinic proton of the dimethyl pyran ring H-1′ (δ_H 6.66) and carbons C-3′ (δ_C 28.3), C-3 (δ_C 159.9), and C-2 (δ_C 104.5), confirming the linear cyclisation and the attachment of the dimethyl pyran ring to C-2 and C-3;

- the chelated hydroxy proton 1-OH (δ_H 13.62) and carbons C-1 (δ_C 157.9), and C-9 (δ_C 182.0), confirming the attachment of the hydroxy chelated proton to the C-1;

- the aromatic proton H-5 (δ_H 6.76) and C-6 (δ_C 154.6), and C-7 (δ_C 142.7), confirming the attachment of the free hydroxy proton to the C-6.
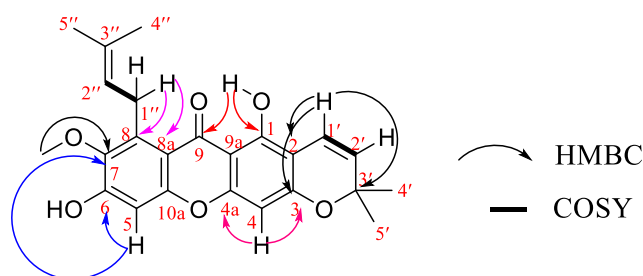
Scheme 34: Selected HMBC and COSY correlations of PBE13

Table XLVI: ^{1}H (500 MHz) and ^{13}C (125 MHz) NMR spectral data of PBE13 in CDCl$_3$ compared to those of 9-hydroxycalabaxanthone [^{13}C NMR (125 MHz) in CDCl$_3$] (Ryu *et al.*, 2010)

Position	PBE13		9-hydroxycalabaxanthone
	δ_H (nH, *m*, *J* in Hz)	δ_C	δ_C
1	/	157.9	158.3
2	/	104.5	104.9
3	/	159.9	160.3
4	6.17 (1H, s)	94.2	94.6
4a	/	156.3	154.9
5	6.76 (1H, s)	101.7	102.0
5a	/	155.8	156.2
6	/	154.6	156.7
7	/	142.7	143.0
8	/	137.0	137.4
8a	/	112.2	112.6
9	/	182.0	182.4
9a	/	103.7	104.2
1′	6.66 (1H, d, *J* = 10.0 Hz)	115.7	116.1
2′	5.49 (1H, d, *J* = 10.0 Hz)	127.2	127.6
3′	/	77.9	78.3
4′	1.39 (3H, s)	28.3	28.7
5′	1.39 (3H, s)	28.3	28.7
1″	4.02 (2H, d, *J* = 6.2 Hz)	26.6	26.2
2″	5.19 (1H, br t, *J* = 5.0 Hz)	123.1	123.5
3″	/	132.2	132.6
4″	1.62 (3H, s)	25.8	27.0
5″	1.76 (3H, s)	18.2	18.6
7-OMe	3.73 (3H, s)	62.1	62.5
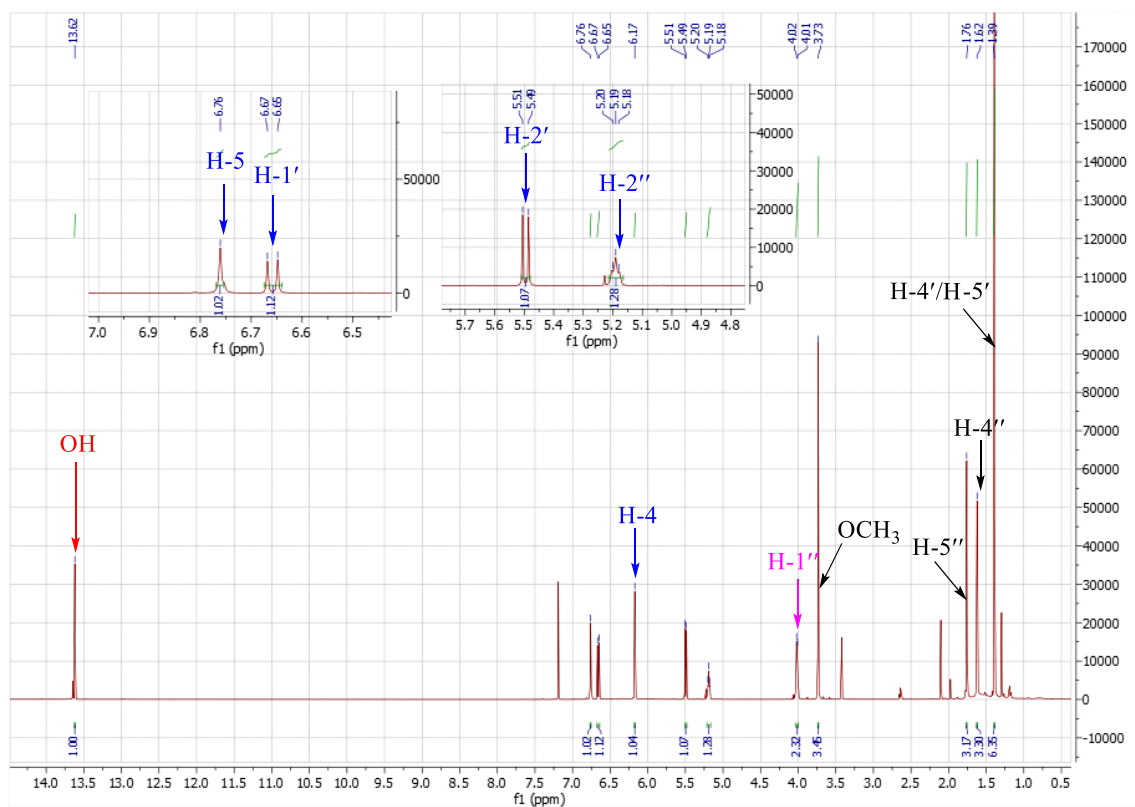
Figure 146: ^{1}H NMR spectrum (CDCl$_3$, 500 MHz) of compound PBE13
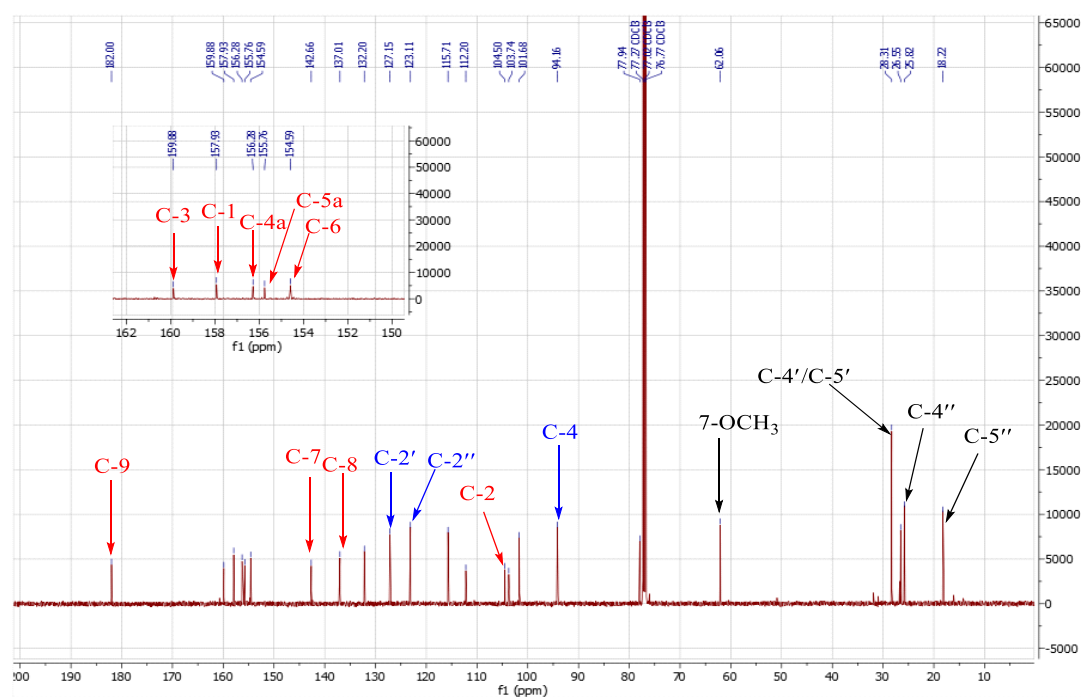
Figure 147: ^{13}C NMR spectrum (CDCl$_3$, 125 MHz) of compound PBE13
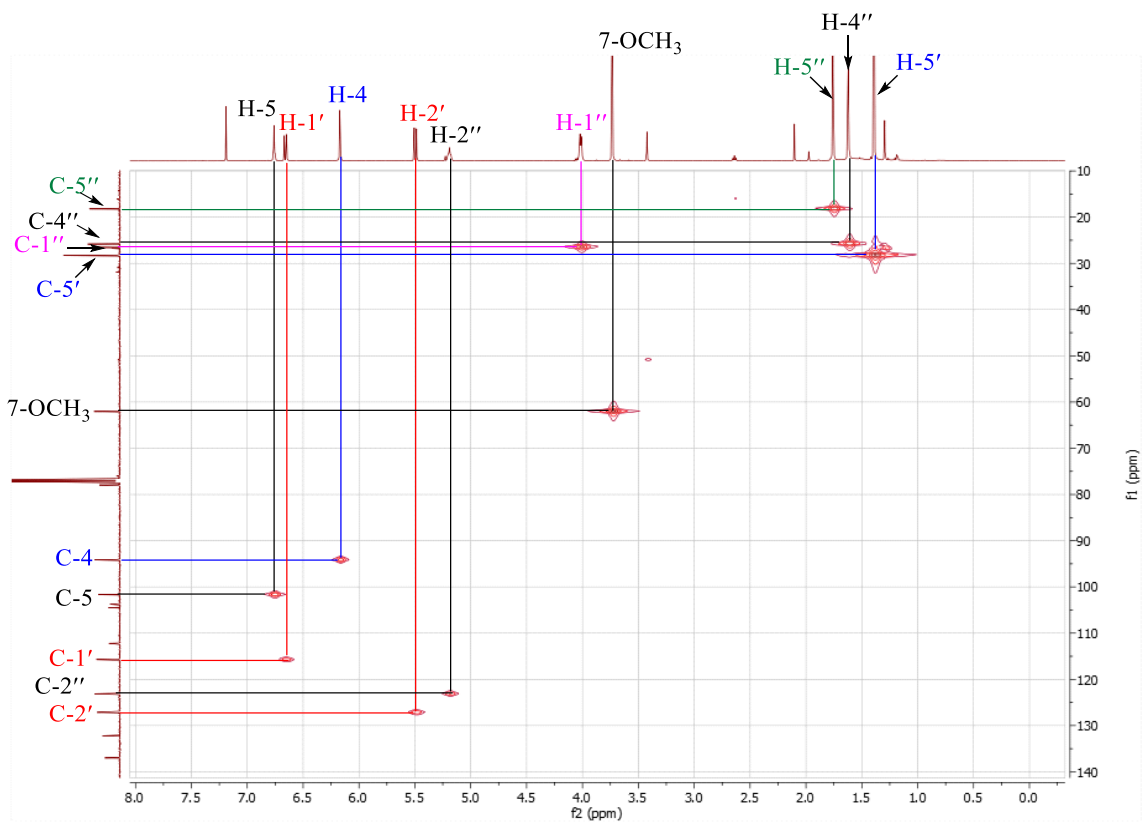
Figure 148: HSQC spectrum of compound PBE13
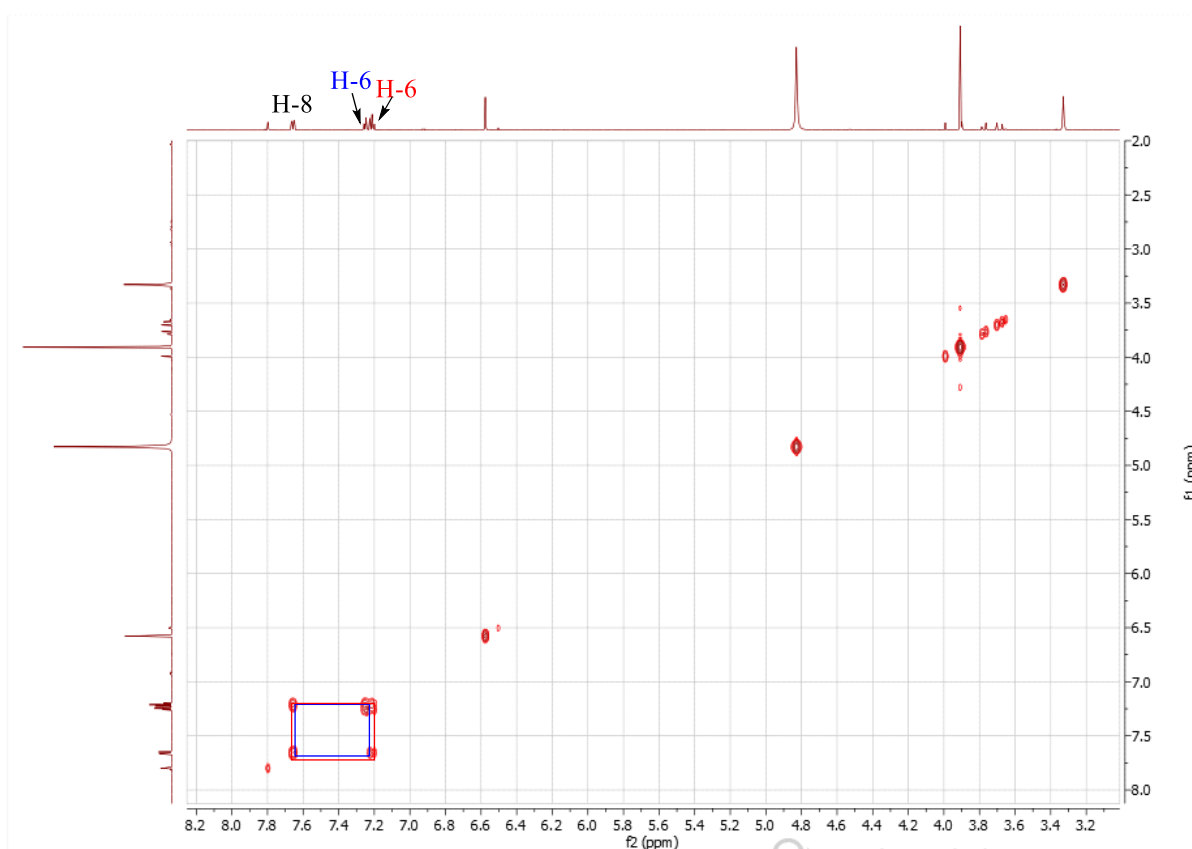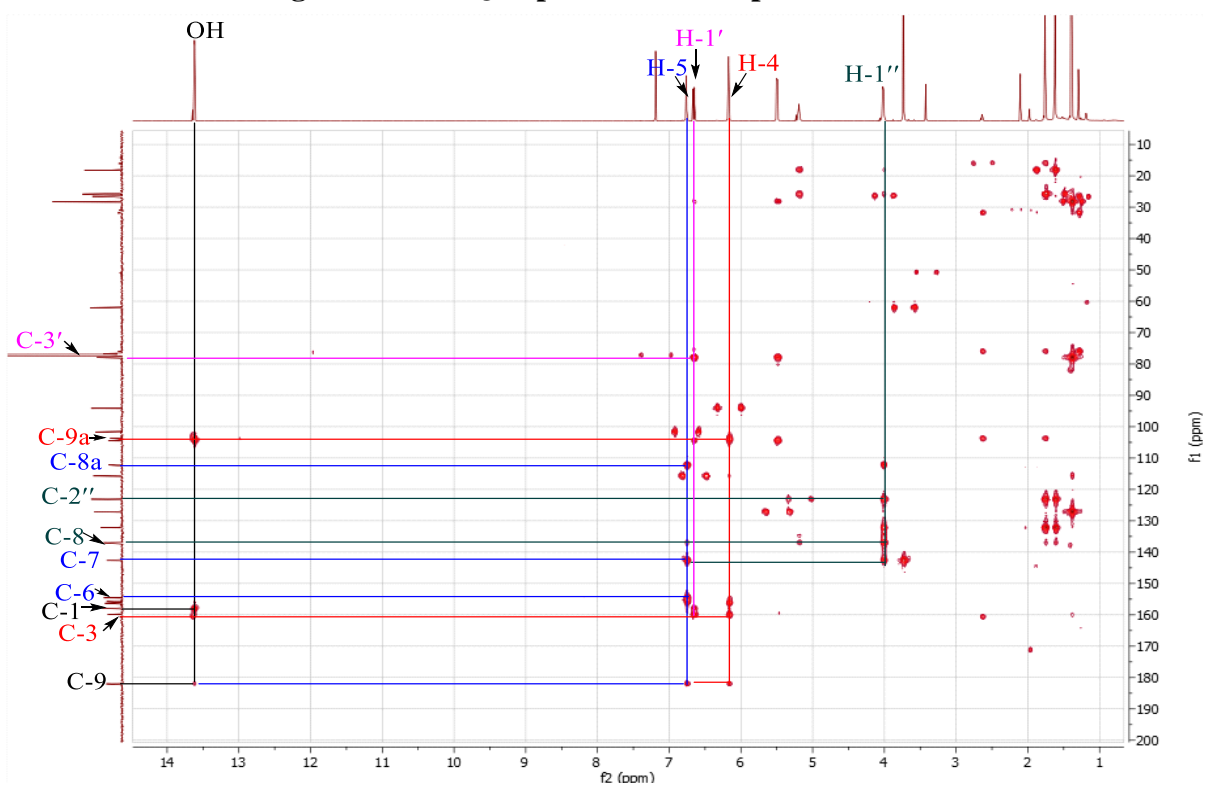

Figure 149: HMBC spectrum of compound PBE13
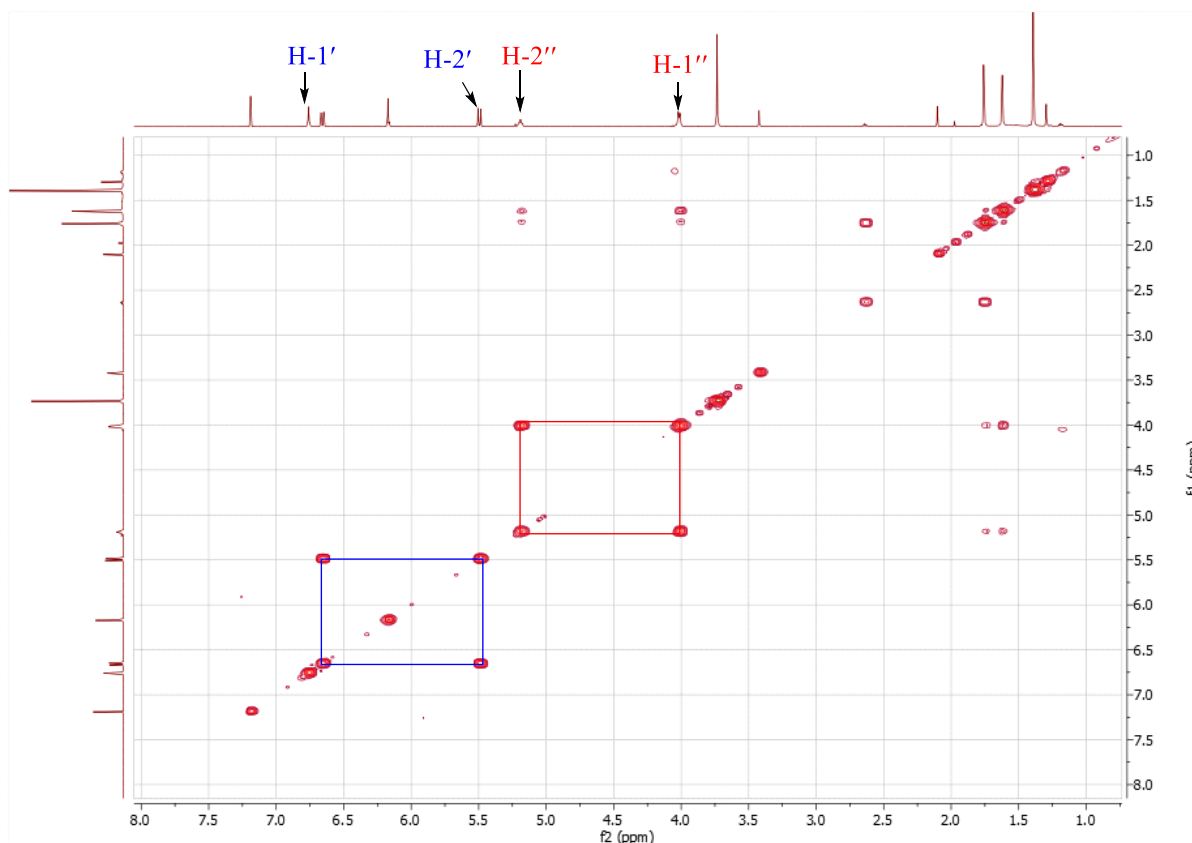
Figure 150: COSY spectrum of compound PBE13

II.2.1.7.8 Identification of PBE6

PBE6 was obtained as a yellow amorphous solid and is soluble in chloroform. It reacts positively to the ferric chloride test, indicating its phenolic nature.

Analysis of its ^1H and ^{13}C NMR spectrum combined with data from the literature allowed us to assign it the molecular formula $C_{28}H_{30}O_6$ containing fourteen degrees of unsaturation.

All these spectral data taken together, compared with those in the literature (Table XLVII), allowed us to attribute to PBE6 the structure (**82**) which is that of tovophyllin A, previously isolated from *Garcinia mangostana* (Al-Massarani *et al.*, 2013).

(**82**)
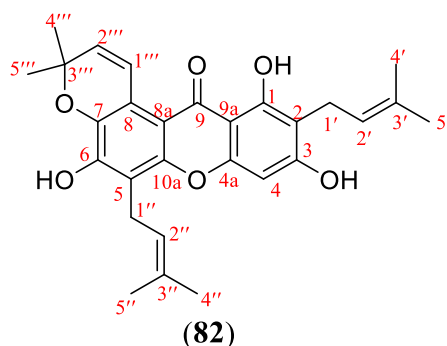
Indeed, the ^{1}H NMR spectrum of PBE6 (Figure 151) showed:

- the signal of a singlet of a chelated hydroxyl proton at δ_H 13.79 (1H, s, OH-1);

- the signal of one aromatic singlet at δ_H 6.37 (1H, s, H-4);

- the signals of the protons of two 3,3-dimethylallyl moiety at δ_H [5.31 (1H, t, J = 7.2 Hz, H-2′), 3.49 (2H, d, J = 7.2 Hz, H-1′), 1.71 (3H, s, H-4′), and 1.90 (3H, s, H-5′)] and [5.31 (2H, t, J = 7.2 Hz, H-2″), 3.60 (2H, d, J = 7.3 Hz, H-1″), and 1.80 (3H, s, H-4″), 1.87 (3H, s, H-5″)];

- the signals of the protons of a dimethyl pyran ring at δ_H 5.79 (1H, d, J =10.2 Hz, H-1‴), 8.03 (1H, d, J =10.2 Hz, H-2‴), and 1.51 (6H, s, H-4‴ and H-5‴) (Ngouela *et al.*, 2006).

The ^{13}C NMR spectrum (Figure 152) of PBE6 shows the signals of 28 carbon atoms which were distinguished using the HSQC technique (Figure 153) into:
- fifteen quaternary carbons including a carbonyl of 1-hydroxylated xanthone at δ_C 182.9 (C-9) (Silva and Pinto, 2005) and the others at δ_C 160.4 (C-1), 108.2 (C-2), 161.7 (C-3), 155.3 (C-4a), 115.2 (C-5), 136.5 (C-6), 136.5 (C-7), 117.2 (C-8), 108.4 (C-8a), 103.7 (C-9a), 151.0 (C-10a), 131.3 (C-3′), 132.6 (C-3″) and 76.4 (C-3‴);

- five carbons of methine groups including three olefinics at δ_C 121.5 (C-2′), 121.1 (C-2″), 136.0 (C-1‴) and 121.0 (C-2‴), one aromatic at δ_C 93.4 (C-4);

- two carbons of methylene groups at δ_C 22.6 (C-1′) and 21.5 (C-1″);

- six carbons of methyl groups at δ_C 25.9 (C-4′) and 18.0 (C-5′), 25.8 (C-4″) and 17.9 (C-5″), 27.4 (C-4‴ and C-5‴).

All of this data shows that the compound PBE6 is a xanthone carrying two prenyl groups and a dimethyl pyran ring.

The position of these groups on the xanthone skeleton was determined using correlations observed on the HMBC spectrum (Figure 154, scheme 35). In fact, on this spectrum, cross peaks were observed between;
- the protons of the methylene group H-1′ (δ_H 3.49) and carbons C-2 (δ_C 108.2), C-2′ (δ_C 121.5), C-1 (δ_C 160.4) and C-3 (δ_C 161.7), which is in line with the attachment of the first 3,3-dimethylallyl moiety to the C-2;

- the protons of the methylene group H-1″ (δ_H 3.60) and carbons C-5 (δ_C 115.2), C-3″ (δ_C 132.6), C-6 (δ_C 148.6) and C-10a (δ_C 151.0), which is in line with the attachment of the

second 3,3-dimethylallyl moiety to the C-5 and the attachment of the free hydroxy proton to the C-6;

- the olefinic proton of the dimethyl pyran ring H-1‴ (δ_H 5.79) and carbons C-3‴ (δ_C 76.8) and C-8 (δ_C 117.2), confirming the angular cyclisation and the attachment of the dimethyl pyran ring to C-7 and C-8;

- the chelated hydroxy proton 1-OH (δ_H 13.79) and carbons C-9a (δ_C 103.7), C-2 (δ_C 108.2) and C-1 (δ_C 160.4), confirming the attachment of the hydroxy chelated proton to the C-1;

- the aromatic proton H-4 (δ_H 6.37) and carbons C-2 (δ_C 108.2), C-4a (δ_C 155.3) and C-3 (δ_C 161.7), confirming the attachment of the free hydroxy proton to the C-3.
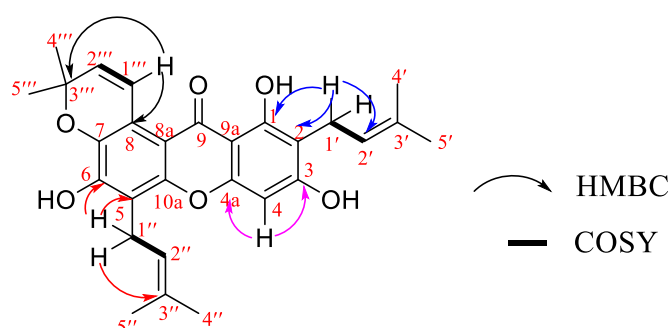
Scheme 35: Selected HMBC and COSY correlations of PBE6

Table XLVII: ¹H (500 MHz) and ¹³C (125 MHz) NMR spectral data of PBE6 in CDCl₃ compared to those of tovophyllin A [¹H (500 MHz) and ¹³C (125 MHz) NMR in CDCl₃] (Al-Massarani *et al.*, 2013)

Position	PBE6		Tovophyllin A	
	δ_H (nH, *m*, *J* in Hz)	δ_C	δ_H (nH, *m*, *J* in Hz)	δ_C
1	/	160.4	/	160.4
2	/	108.2	/	108.4
3	/	161.7	/	161.6
4	6.37 (1H, s)	93.4	6.37 (1H, s)	93.4
4a	/	155.3	/	155.3
5	/	115.2	/	115.2
6	/	148.6	/	151.0
7	/	136.5	/	136.5
8	/	117.2	/	117.2
8a	/	108.4	/	108.4
9	/	182.9	/	182.9

9a	/	103.7	/	103.7
10a	/	151.0	/	151.0
1′	3.49 (2H, d, J = 7.2 Hz)	22.6	3.48 (2H, d, J = 6.0 Hz)	22.6
2′	5.31 (1H, t, J = 7.2 Hz)	121.5	5.31 (1H, t, J = 7.0 Hz)	121.0
3′		131.3		131.3
4′	1.71 (3H, s)	25.9	1.71 (3H, s)	25.8
5′	1.90 (3H, s)	18.0	1.79 (3H, s)	17.9
1″	3.60 (2H, d, J = 7.3 Hz)	21.5	3.59 (2H, d, J = 6.0 Hz)	21.4
2″	5.31 (2H, t, J = 7.2 Hz)	121.1	5.31 (2H, t, J = 7.0 Hz)	121.4
3″		132.6		132.6
4″	1.80 (3H, s)	25.8	1.87 (3H, s)	25.8
5″	1.87 (3H, s)	17.9	1.89 (3H, s)	17.9
1‴	5.79 (1H, d, J =10.2 Hz)	136.0	5.79 (1H, d, J = 10.0 Hz)	135.8
2‴	8.03 (1H, d, J =10.2 Hz)	121.0	8.00 (1H, d, J = 10.0 Hz)	121.0
3‴		76.4		77.1
4‴	1.51 (3H, s)	27.4	1.51 (3H, s)	27.4
5‴	1.51 (3H, s)	27.4	1.51 (3H, s)	27.4
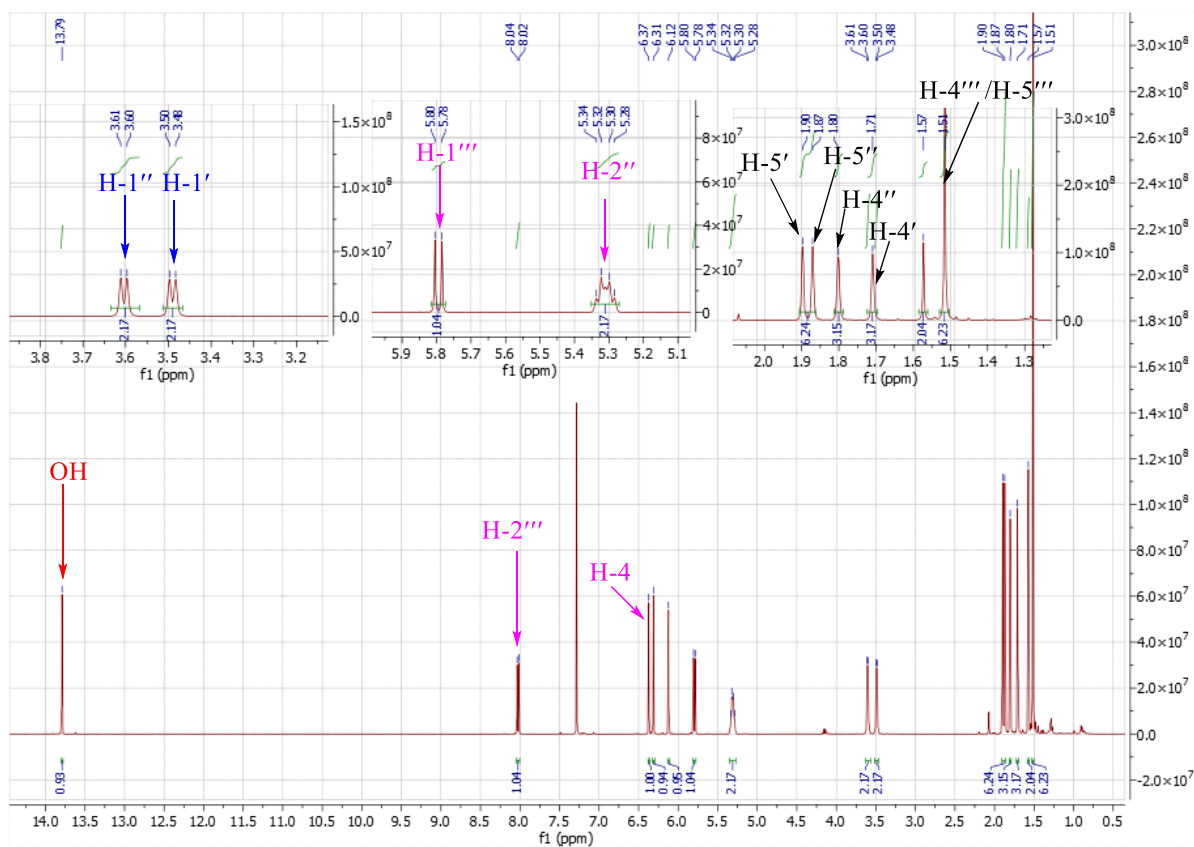
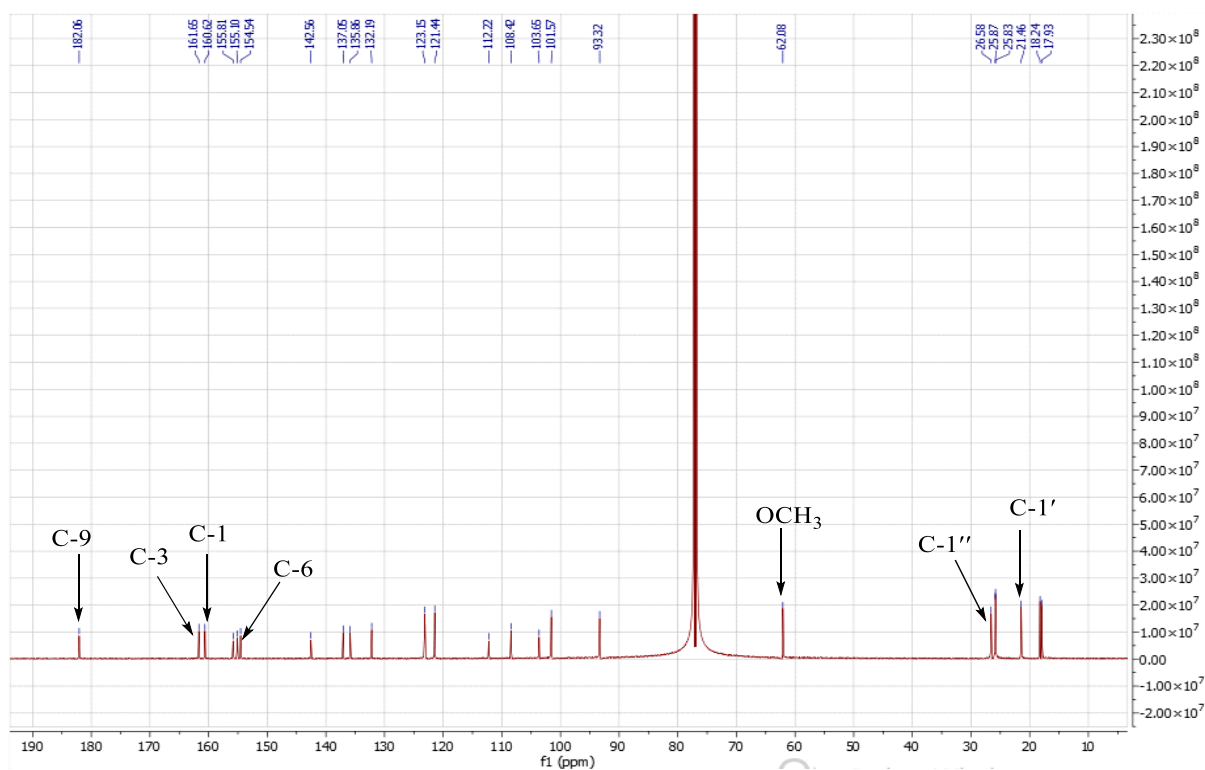**Figure 151: ^{1}H NMR spectrum (CDCl$_3$, 500 MHz) of compound PBE6**
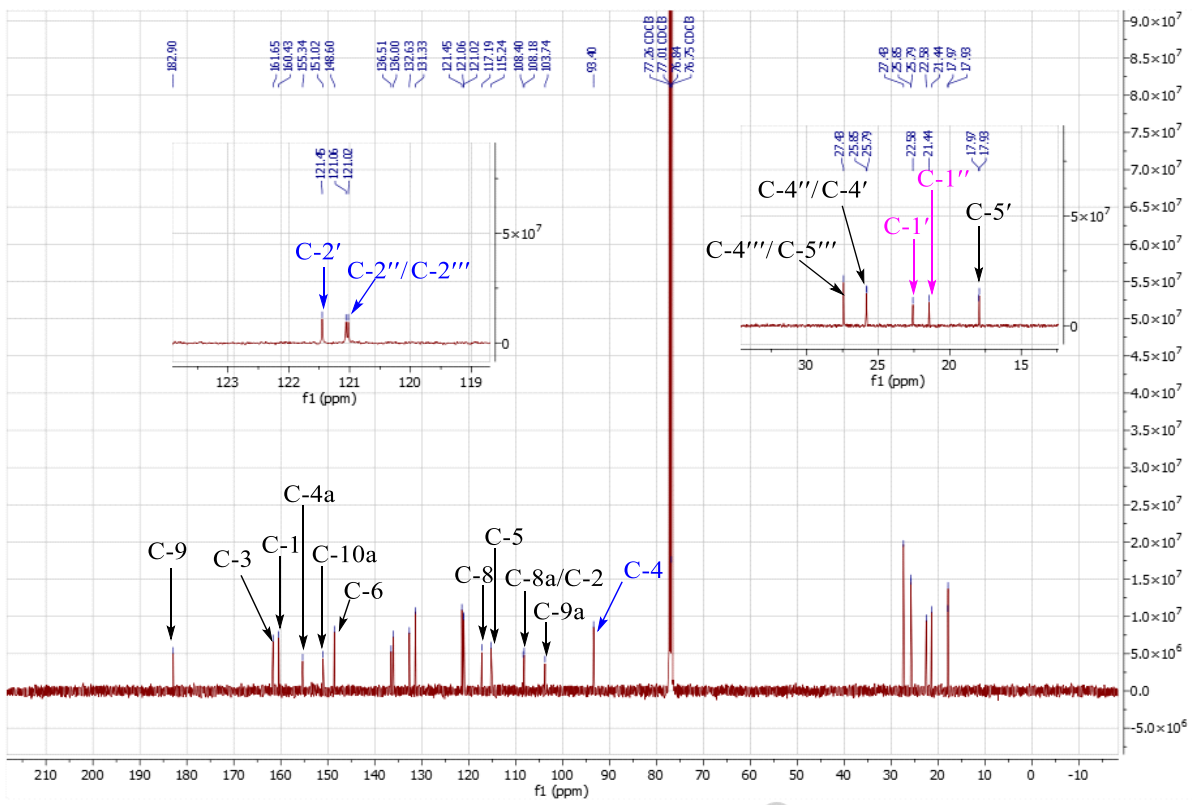
Figure 152: ^{13}C NMR spectrum (CDCl$_3$, 125 MHz) of compound PBE6
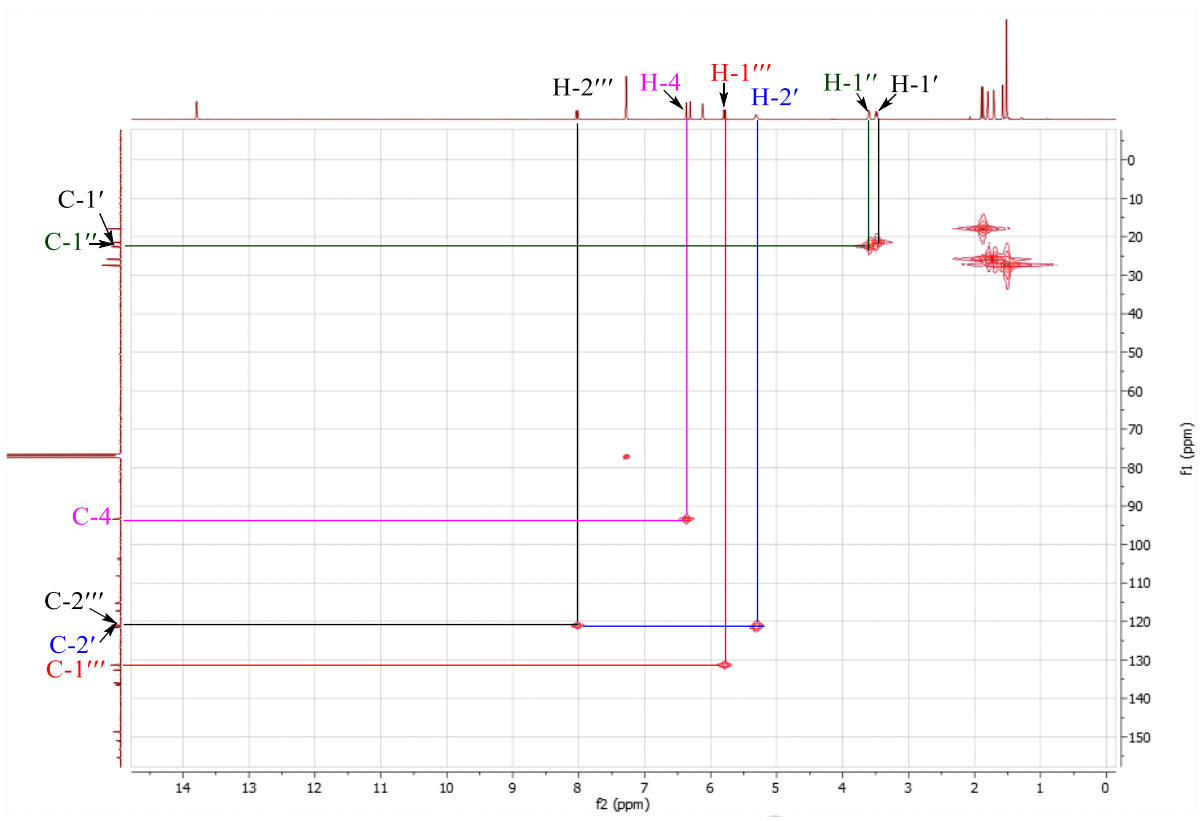
Figure 153: HSQC spectrum of compound PBE6
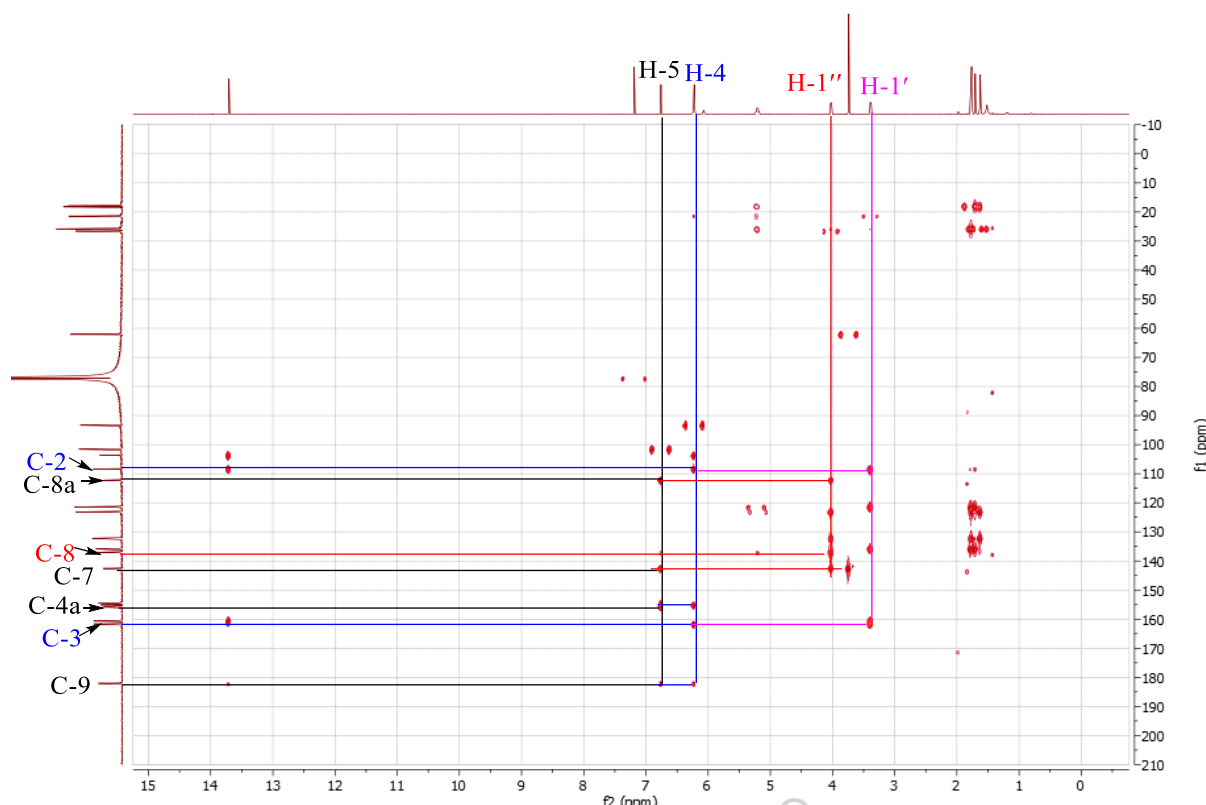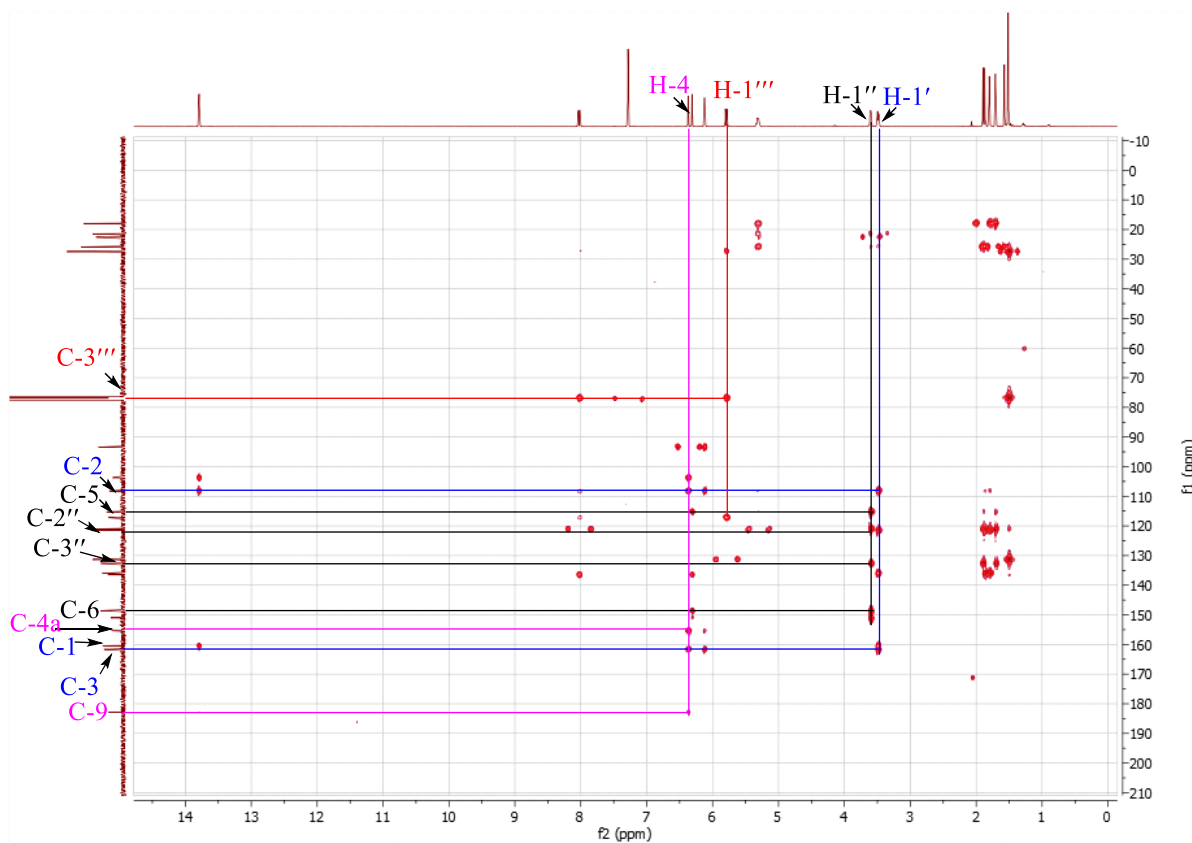
Figure 154: HMBC spectrum of compound PBE6
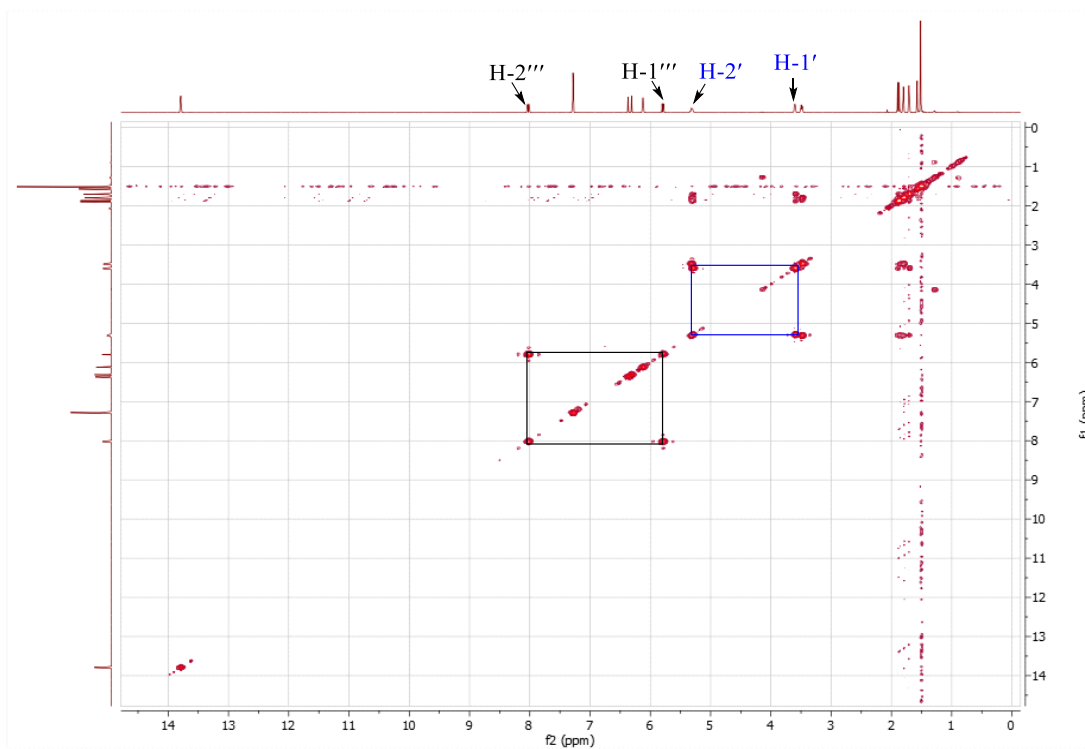
Figure 155: COSY spectrum of compound PBE6

II.2.1.7.9 Identification of PBE12

PBE12 was obtained as a yellow amorphous solid and is soluble in methanol. It reacts positively to the ferric chloride test, indicating its phenolic nature.

Analysis of its ^1H and ^{13}C NMR spectrum combined with data from the literature allowed us to assign it the molecula formula $C_{13}H_8O_5$ containing ten degrees of unsaturation.

The ^1H NMR spectrum of PBE12 (Figure 156) showed:

- A *meta*-coupled protons at δ_H 6.19 (1H, d, $J = 2.1$ Hz) and 6.33 (1H, d, $J = 2.1$ Hz);

- the signals of the protons of an 1,2,3-trisubstituted aromatic ring at δ_H 7.26 (1H, dd, $J = 9.0$, 3.0 Hz); 7.38 (1H, d, $J = 9.0$Hz) and 7.50 (1H, d, $J = 3.0$Hz).

The ^{13}C NMR spectrum (Figure 157) of PBE12 showed the signals of 13 carbon atoms which were distinguished using the HSQC technique (Figure 158) into:

-nine quaternary carbons including carbonyl at δ_C 180.4;

-five aromatic methines at δ_C 93.4, 97.7, 118.4, 120.8, and 123.9.

These data indicate that PBE12 is a xanthone (Silva *et al.*, 2005).

The positions of the free hydroxyl groups were deduced from the correlations observed in HMBC spectrum (Figure 159, scheme 36), between the H-2 proton (δ_H 6. 19) and the carbons C-3 (δ_C 165.8), C-1 (δ_C 163.3) the H-4 proton (δ_H 6.33) and the C-3 carbons (δ_C 165.8) and C-4a (δ_C 158.0), the proton H-6 (δ_H 7.26) and carbon C-7 (δ_C 154.0).
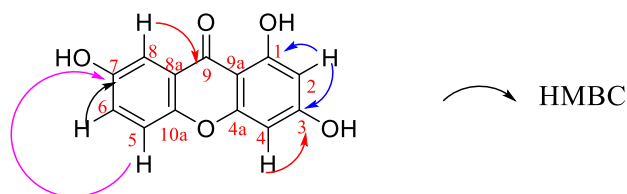
Scheme 36: Some keys correlations observed on the HMBC spectrum of PBE12

All of these data, compared with that of the literature (Table XLVIII), enabled us to attribute to the compound PBE12, the structure (**82**) which is that of 1,3,7-trihydroxyxanthone (Mukulesh *et al.*, 2006).

(**83**)
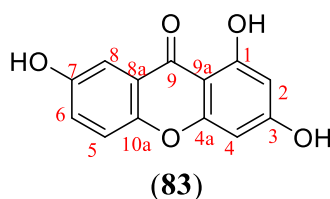
Table XLVIII: ¹H (500 MHz) and ¹³C (125 MHz) NMR spectral data of PBE12 in CD₃OD compared to those of 1,3,7-trihydroxyxanthone [¹³C NMR (50 MHz) and ¹H NMR (200 MHz) in C₂D₆SO] (Mukulesh *et al.*, 2006)

Position	PBE12		1, 3,7-trihydroxyxanthone	
	δ_C	δ_H (nH, *m*, *J* in Hz)	δ_C	δ_H (nH, *m*, *J* in Hz)
1	165.8	/	162.7	/
2	97.5	6.19 (1H, d, *J* = 2.1 Hz)	98.0	6.18 (1H, d, *J* = 2.1 Hz)
3	163.3	/	163.0	/
4	93.4	6.33 (1H, d, *J* = 2.1 Hz)	93.9	6.35 (1H, d, *J* = 1.9 Hz)
5	118.4	7.38 (1H, d, *J* = 9.0Hz)	119.1	7.45 (1H, d, *J* = 9.1 Hz)
6	123.9	7.26 (1H, dd, *J* = 9.0, 3.0 Hz)	124.6	7.27 (1H, dd, *J* = 9.0, 3.0 Hz)
7	153.9	/	154.1	/
8	108.0	7.50 (1H, d, *J* = 2.9 Hz).	108.2	7.40 (1H, d, *J* = 2.9 Hz)
9	180.0	/	179.9	/
4a	158.4	/	157.7	/
8a	120.8	/	120.6	/
9a	102.3	/	102.1	/
10a	149.8	/	149.2	/
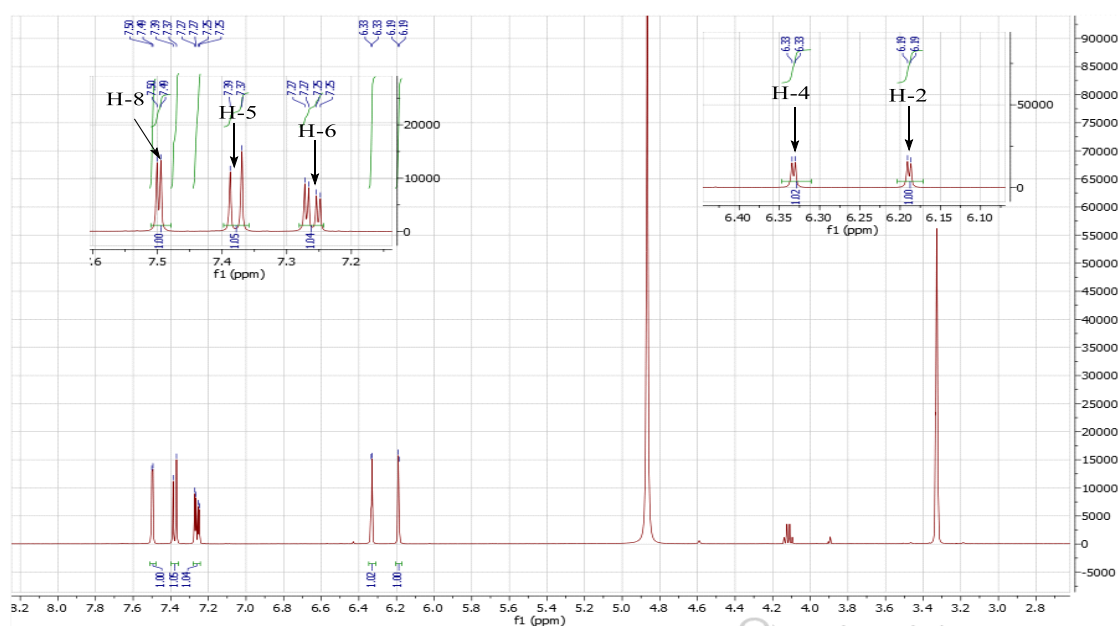
Figure 156: ¹H NMR spectrum (CD₃OD, 500 MHz) of compound PBE12
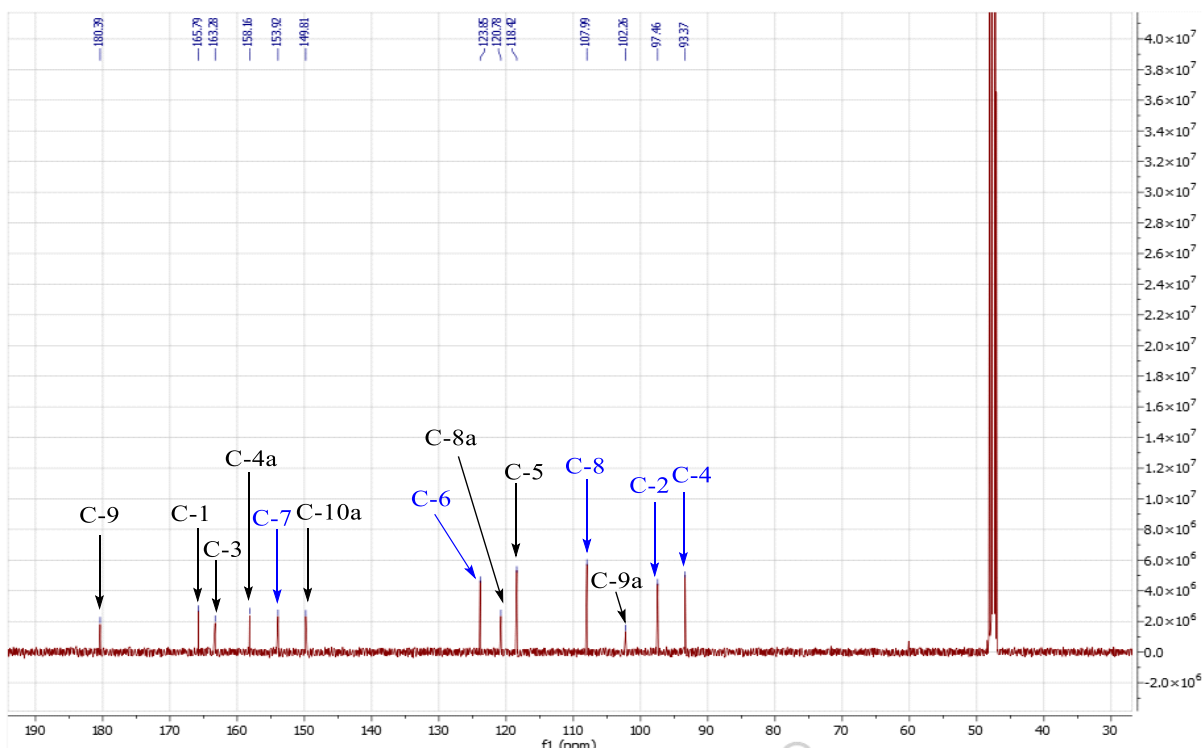
Figure 157: ^{13}C NMR spectrum (CD₃OD, 125 MHz) of compound PBE12
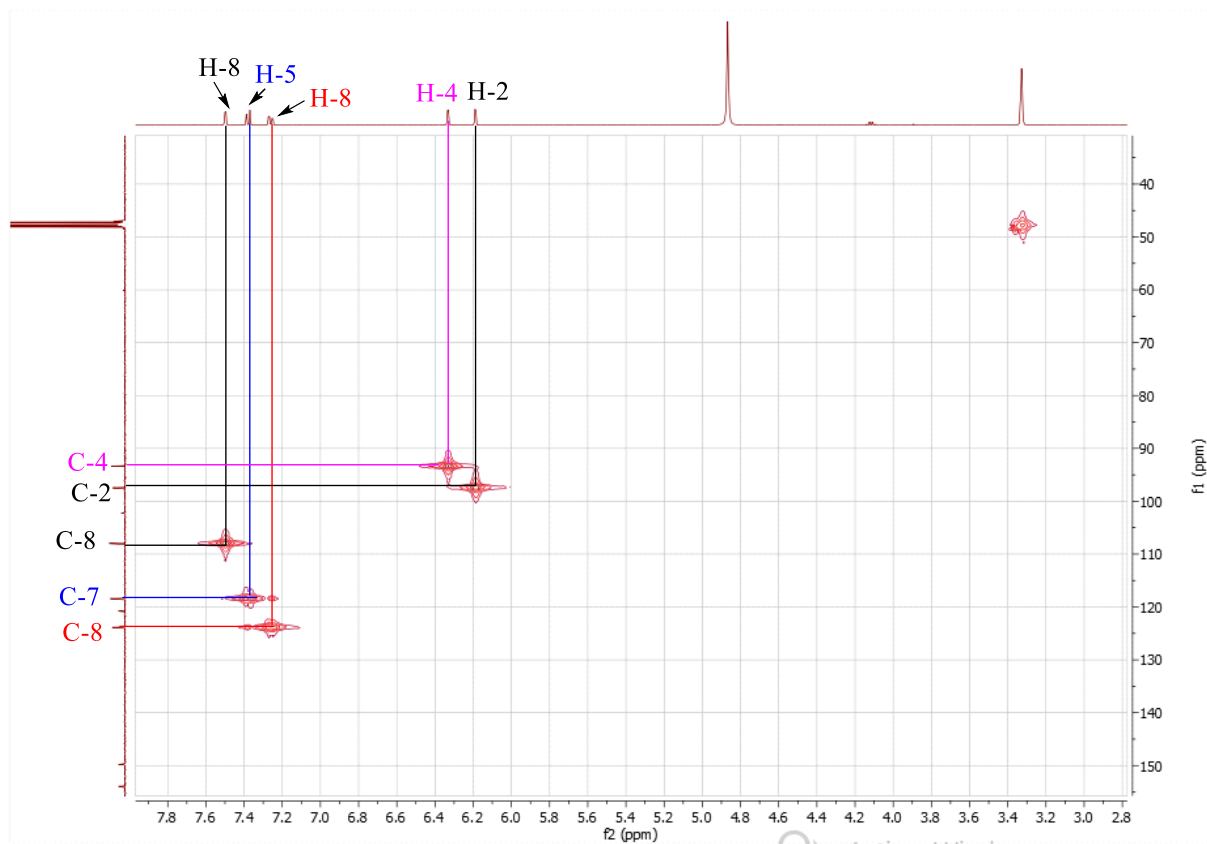
Figure 158: HSQC spectrum of compound PBE12
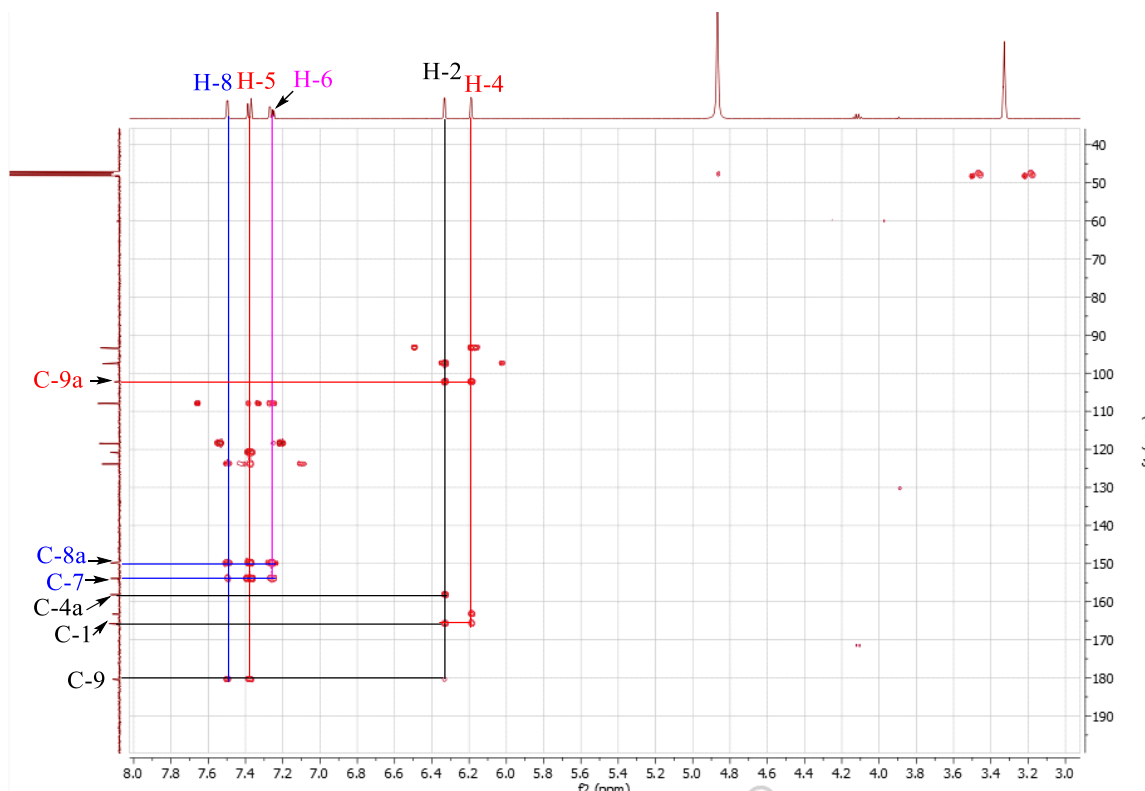
Figure 159: HMBC spectrum of compound PBE12

II.2.1.8. Fatty acid

II.2.1.8.1 Identification of PBF4

PBF4 was obtained as a white amorphous solid and was soluble in methanol.

Its high resolution HR-ESI (+) mass spectrum (Figure 160) shows the peak of the sodium adduct [M+Na]$^+$ at m/z 229.0302 corresponding to the formula $C_7H_{10}O_7$ (calculated for 229.0319) and containing three degrees of unsaturation.

Its ^{1}H NMR spectrum (Figure 161) showed:

-a singlet of a methoxyl group at δ_H 3.77 (3H, s);

- a geminal system of two integrating doublets for one proton each: at δ_H 2.78 (2H, d, $J = 15.6$ Hz) and δ_H 2.93 (2H, d, $J = 15.6$ Hz);

Its ^{13}C NMR spectrum (Figure 162) showed five signals of seven carbon atoms, which were distinguished using the DEPT 135 spectrum (Figure 163), which is in line with the symmetry in the molecule, into:

- four quaternary carbon comprising two carbonyls at δ_C 171.9 and 174.1 and the other quaternary carbon at δ_C 73.1;

- a signal counting as two methylene groups at δ_C 42.8;

- a methoxyl group at δ_C 51.6 (OCH$_3$).

All of this data indicates that PBF4 is a citrate with two carboxylic acid groups and one ester group (Li *et al.*, 2007). The positions of these substituents were deduced from the HMBC correlations (Figure 164, scheme 37).

Indeed this spectrum shows the correlations between:

- the proton at δ_H 3.77 of the methoxyl group and the C-1′ carbon (δ_C 174.1);
- the protons H-2a (δ_H 2.93) and H-2b (δ_H 2.78) of the methylene groups and the C-1′ carbons (δ_C 174.1); C-1 (δ_C 171.9) and C-3 (δ_C 73.1).

Its COSY spectrum (Figure 168) shows the coupling between the proton H-2a (δ_H 2.78) and the proton H-2b (δ_H 2.93).
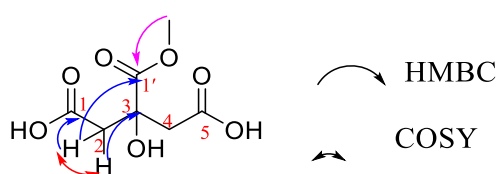
Scheme 37: Selected HMBC and COSY correlations of PBF4

All these spectral data taken together, compared with those in the literature (Table XLIX), enabled us to attribute to PBEF4 the structure (**84**) which is that of methyl citrate (Li *et al.*, 2007).

(84)
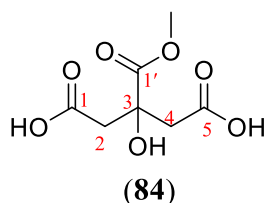
Table XLIX: ^{1}H (500 MHz) and ^{13}C (125 MHz) NMR spectral data of PBF4 in CD₃OD

Position	PBEF4 (Li *et al.*, 2007)	
	δ_C	δ_H (nH, m, *J* in Hz)
1, 5	171.9	/
2, 4	42.8	2.78 (2H, d, *J* = 15.6 Hz)
		2,93 (2H, d, *J* = 15.6 Hz)
3	73.1	/
1′	174.1	/
OCH₃	51.6	3.77 (3H, s)
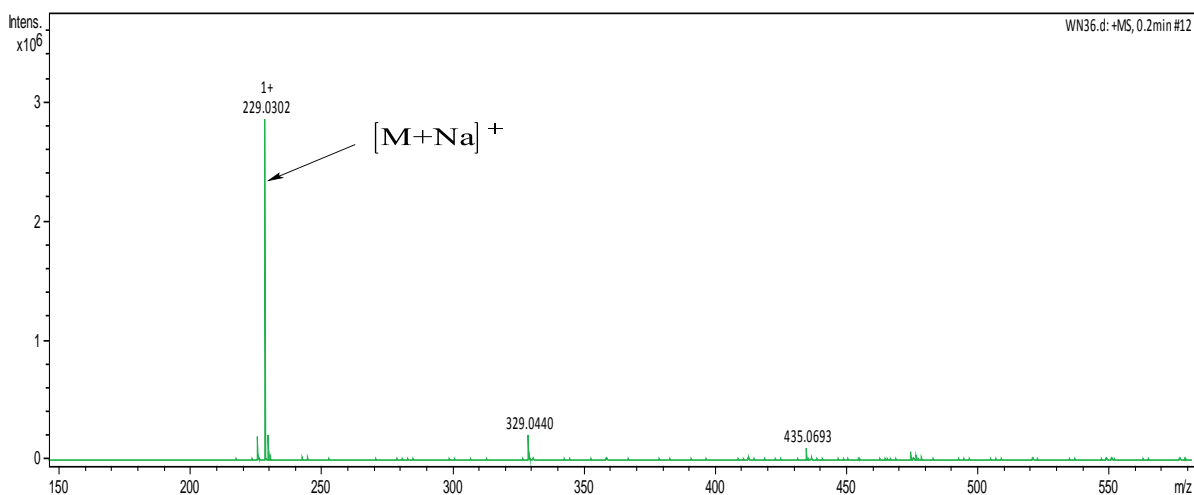
Figure 160: HR-ESI-MS spectrum of compound PBEF4
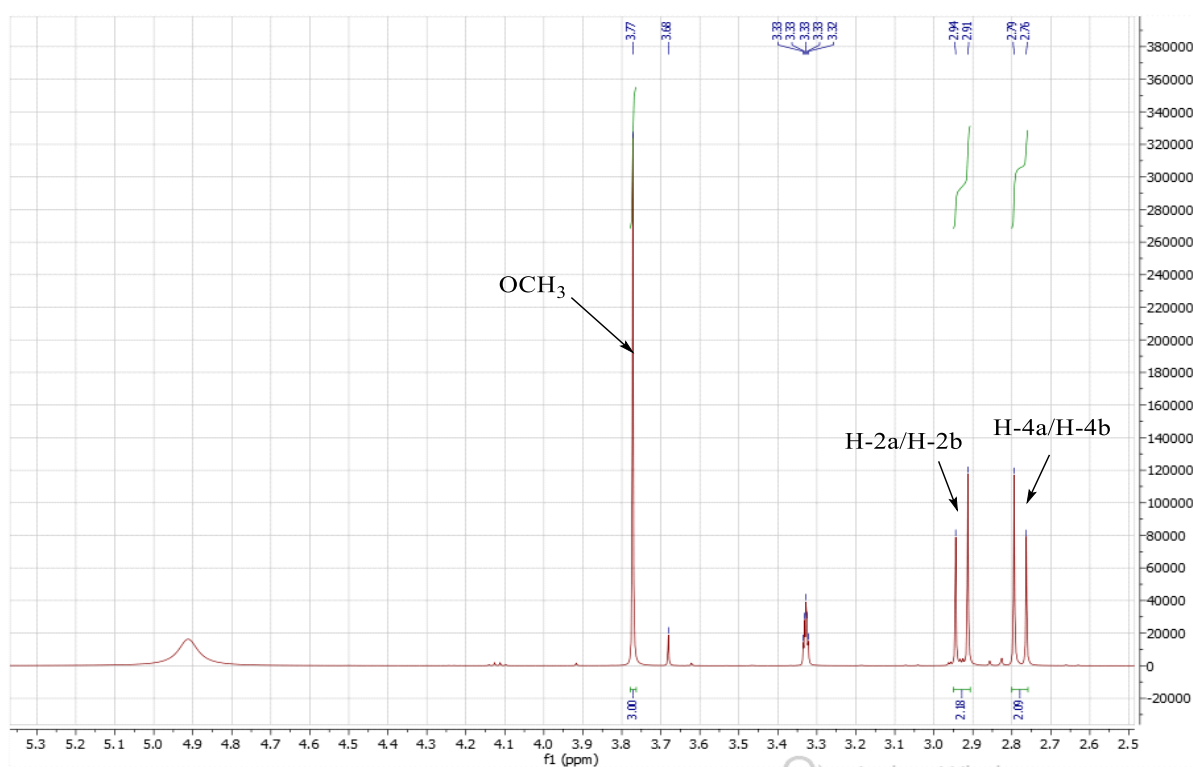
Figure 161: ^{1}H NMR (CD₃OD, 500 MHz) spectrum of compound PBEF4
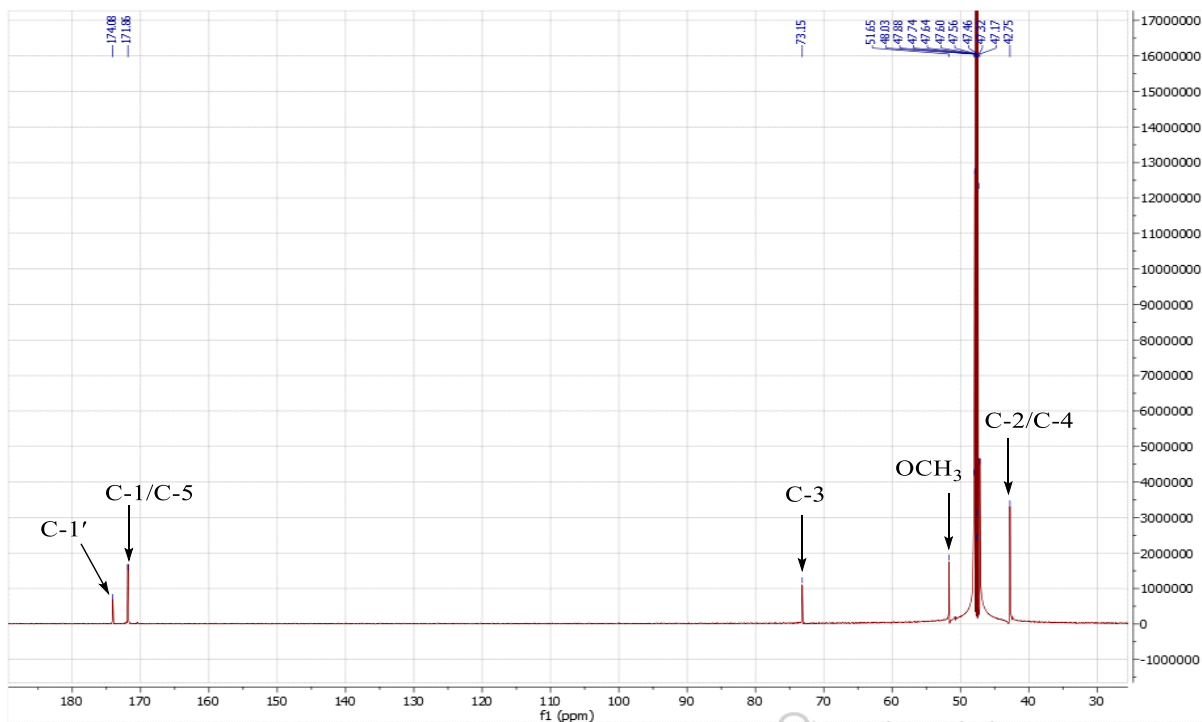
Figure 162: ^{13}C NMR (CD₃OD, 125 MHz) spectrum of compound PBEF4
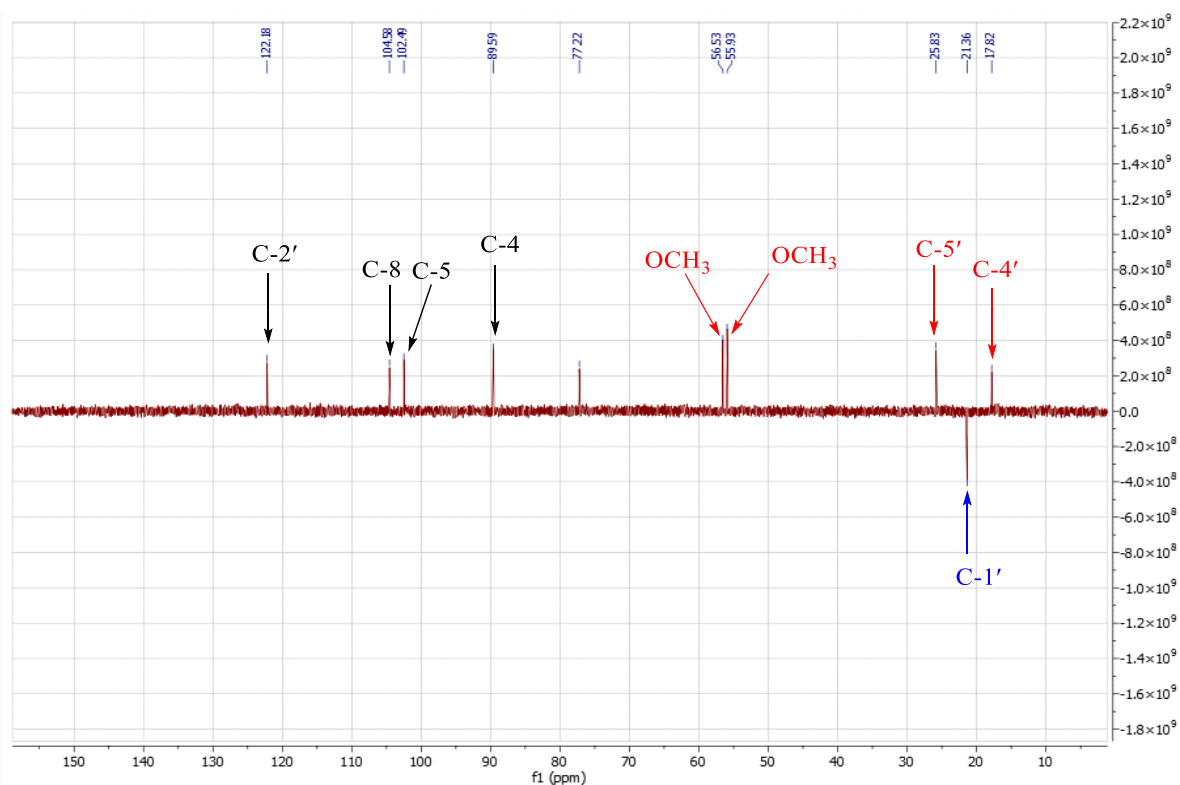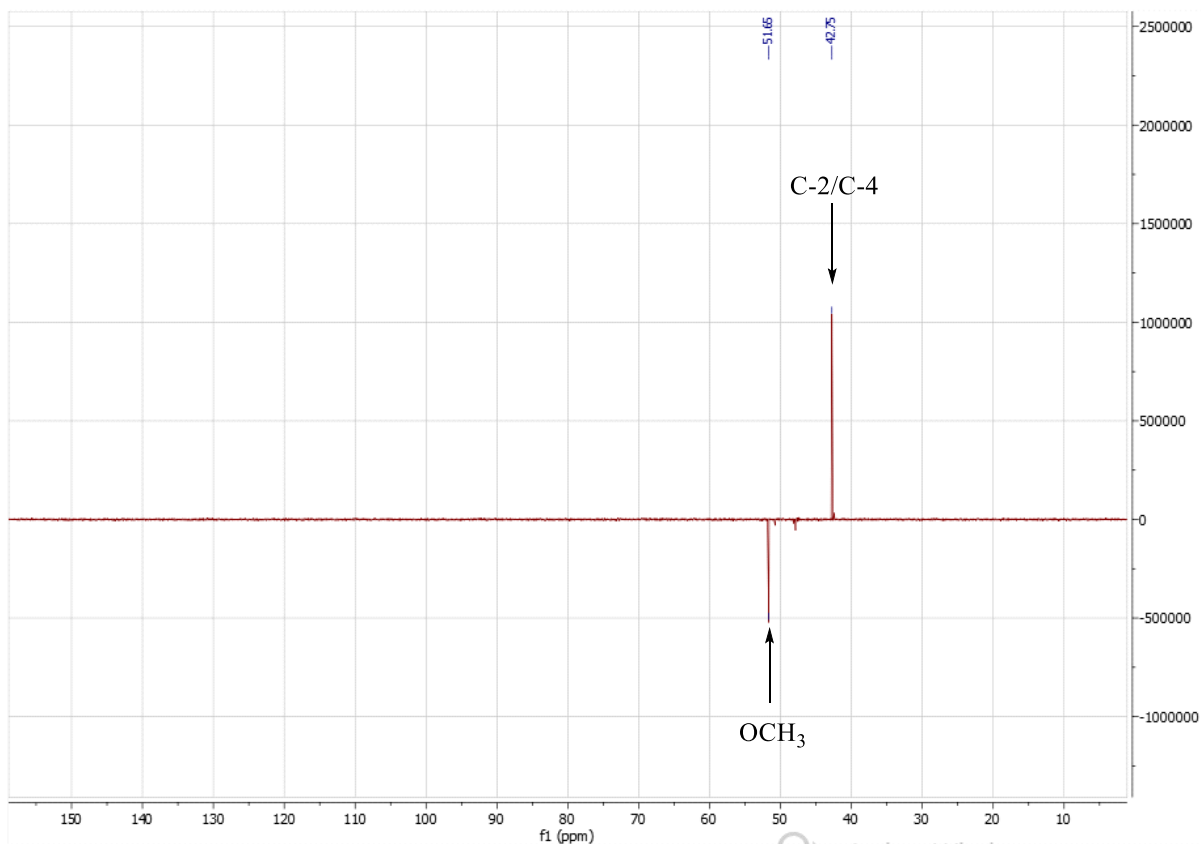

Figure 163: DEPT 135 spectrum of compound PBEF4
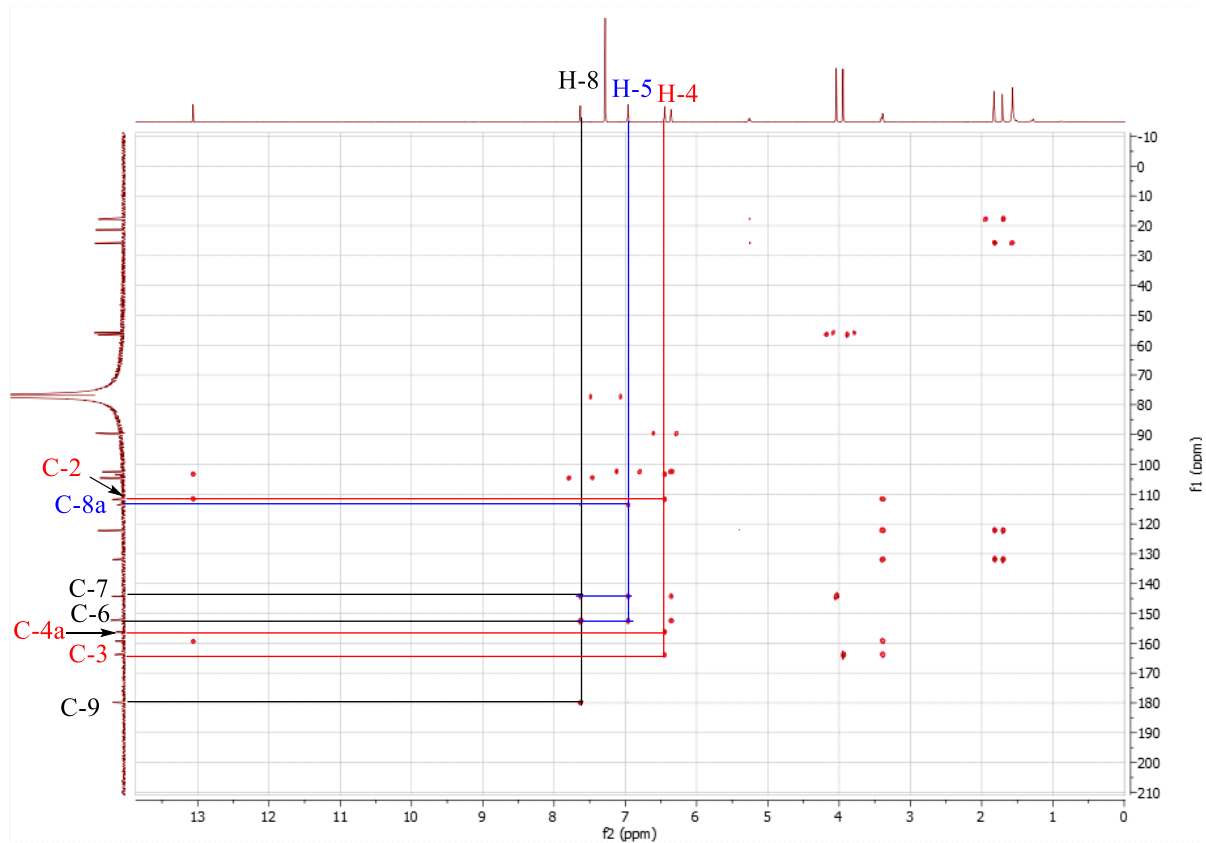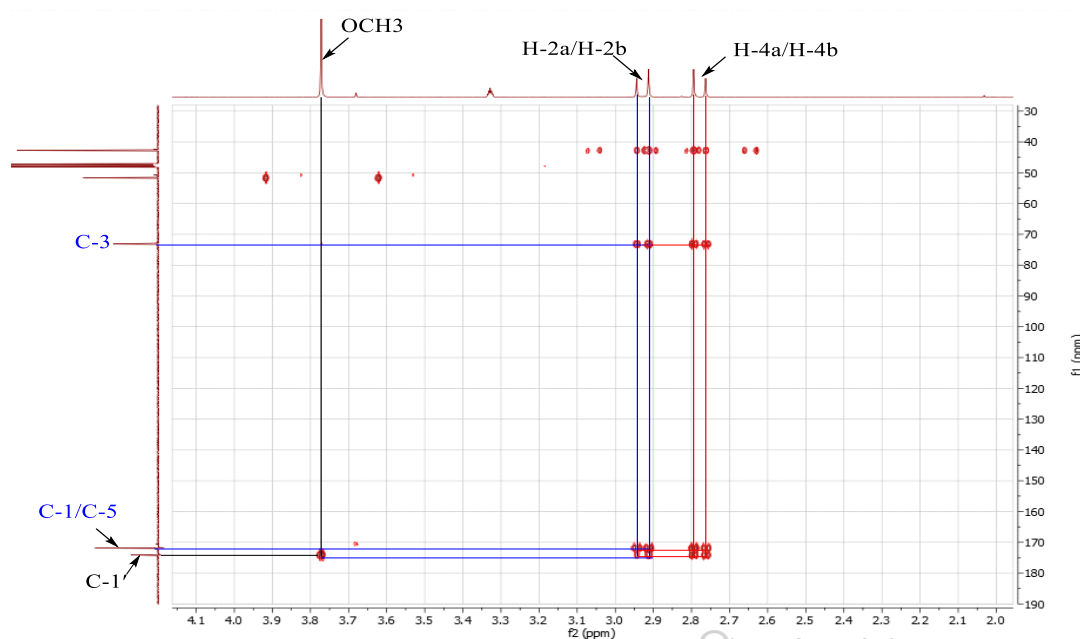
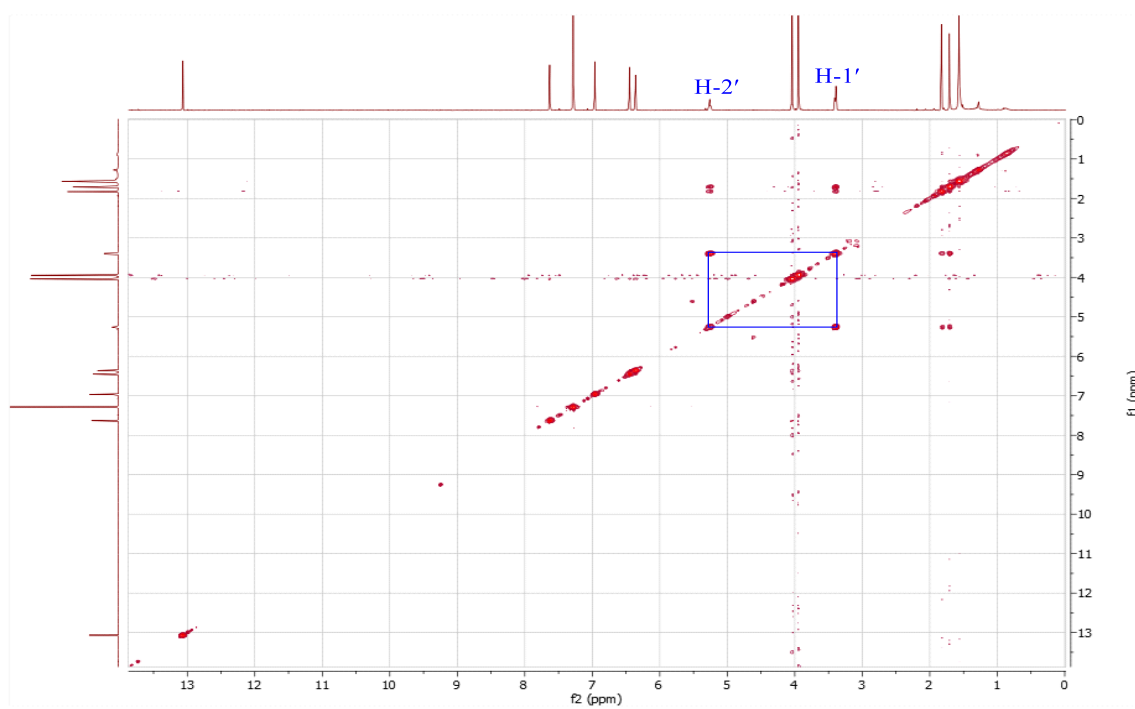**Figure 164: HMBC spectrum of compound PBEF4**
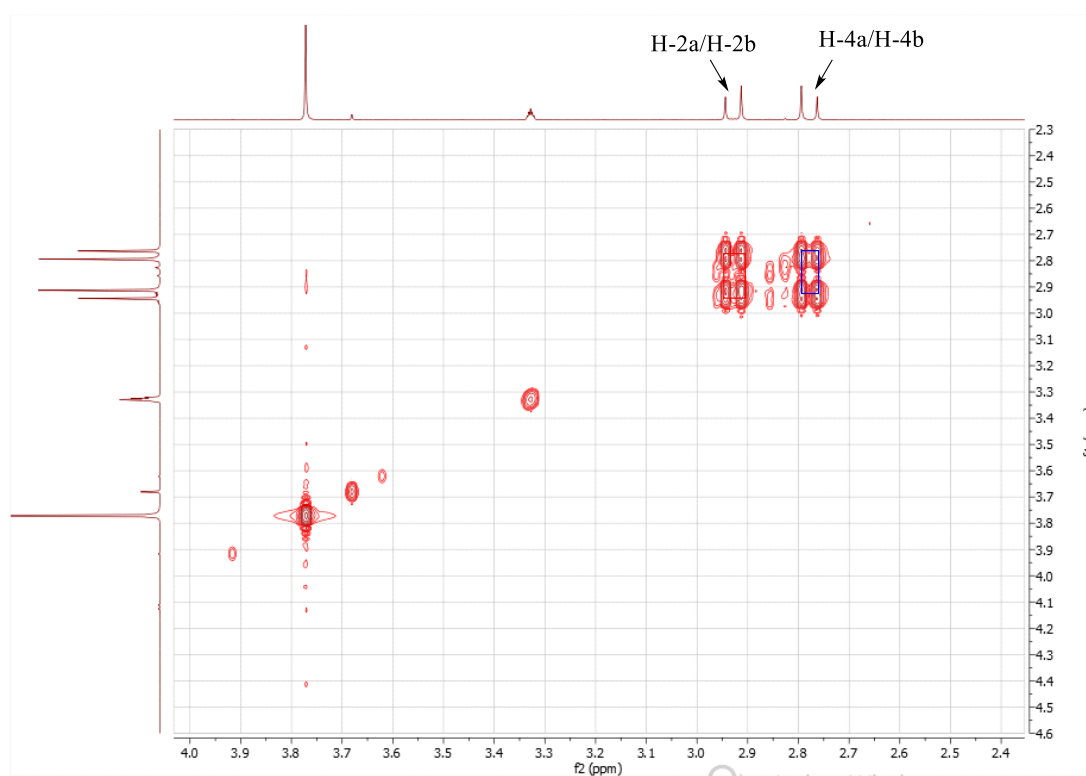
Figure 165: COSY spectrum of compound PBEF4

II.2.1.8.2 Identification of EC8

EC8 was obtained as a white amorphous solid. It is soluble in chloroform. Its high-resolution, negative-mode ESI mass spectrum (Figure 166) shows the peak of the

deprotonated ion [M-H]⁻ at *m/z* 423.4252, corresponding to the molecular formula $C_{28}H_{56}O_2$ (calculated for 424.4280), containing a degree of unsaturation.

Its ^1H NMR spectrum (Figure 167) reveals the presence:

- methylene groups between δ_H 1.10 and 2.30 among which one in α of the carboxyl with δ_H 2.28 (2H, t, *J* = 7.5 Hz);

- a triplet of a terminal methyl at δ_H 0.81 (3H, t, *J* = 6.9 Hz).

All these spectral data taken together, compared with those in the literature, allow EC8 to be assigned the structure (**85**) which is that of octacosanoic acid (Himanshu *et al.*, 2009).

(**85**)
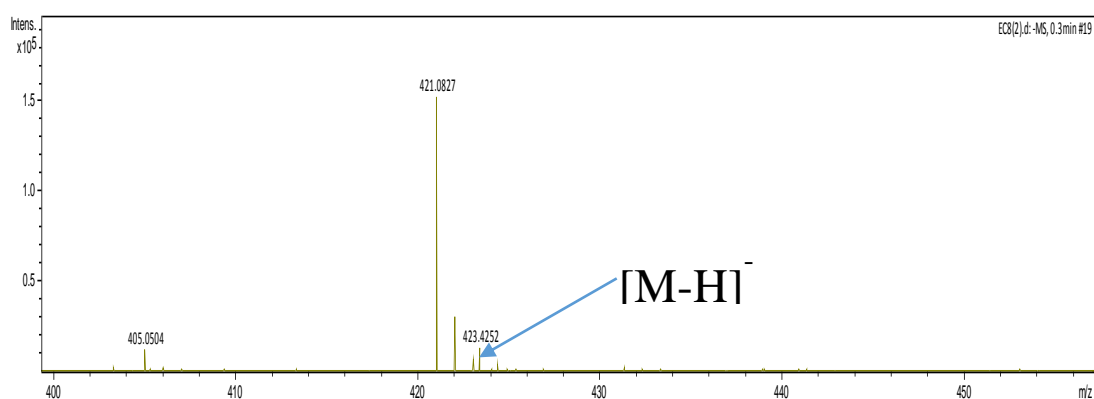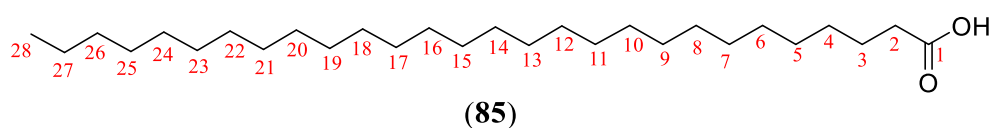
Figure 166: HR-ESI-MS spectrum of compound EC8
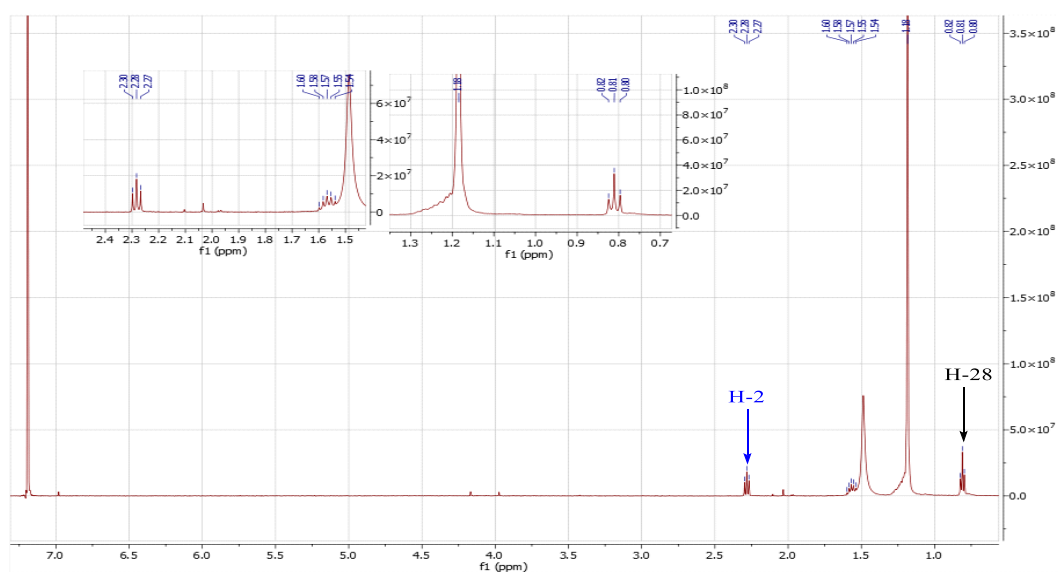
Figure 167: ^1H NMR (CD₃OD, 500 MHz) spectrum of compound EC8

II.2.1.8.3 Identification of AL3

AL3 was obtained as a white amorphous powder. It is soluble in chloroform. Its high-resolution, negative-mode ESI mass spectrum (Figure 168) shows the peak of the deprotonated ion [M-H]$^-$ at m/z 367.3634, corresponding to the molecular formula $C_{24}H_{48}O_2$ (calculated for 368.3654), containing a degree of unsaturation.

Its ^{1}H NMR spectrum (Figure 169) reveals the presence:

- methylene groups between δ_H 1.10 and 2.30 among which one in α of the carboxyl with δ_H 2.28 (2H, t, $J = 7.5$ Hz);

- a triplet of a terminal methyl at δ_H 0.81 (3H, t, $J = 6.9$ Hz).

The data for the ^{1}H NMR spectrum (Figure 169) are similar to those for octacosanoic acid (EC8). The difference lies in the number of methylenes constituting the long chain. Based on all the data and comparison with those in the literature, the structure of AL3 was determined to be that of tetracosanoic acid (**86**) (Reis *et al.*, 2018).

(**86**)
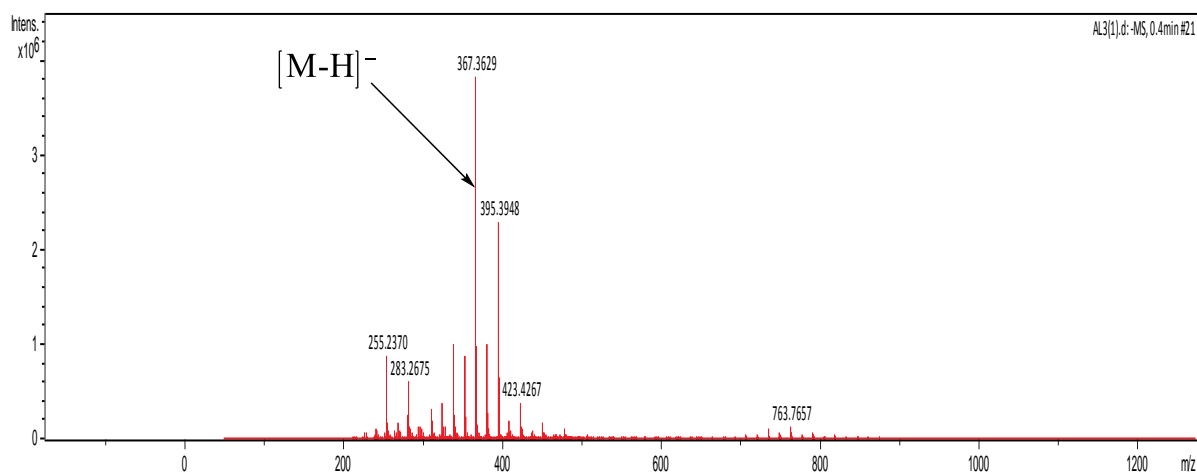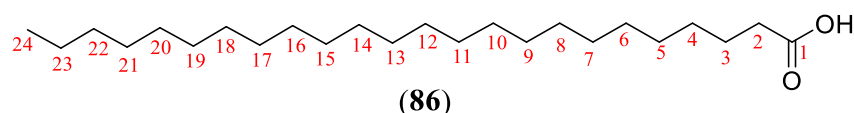
Figure 168: HR-ESI-MS spectrum of compound AL3
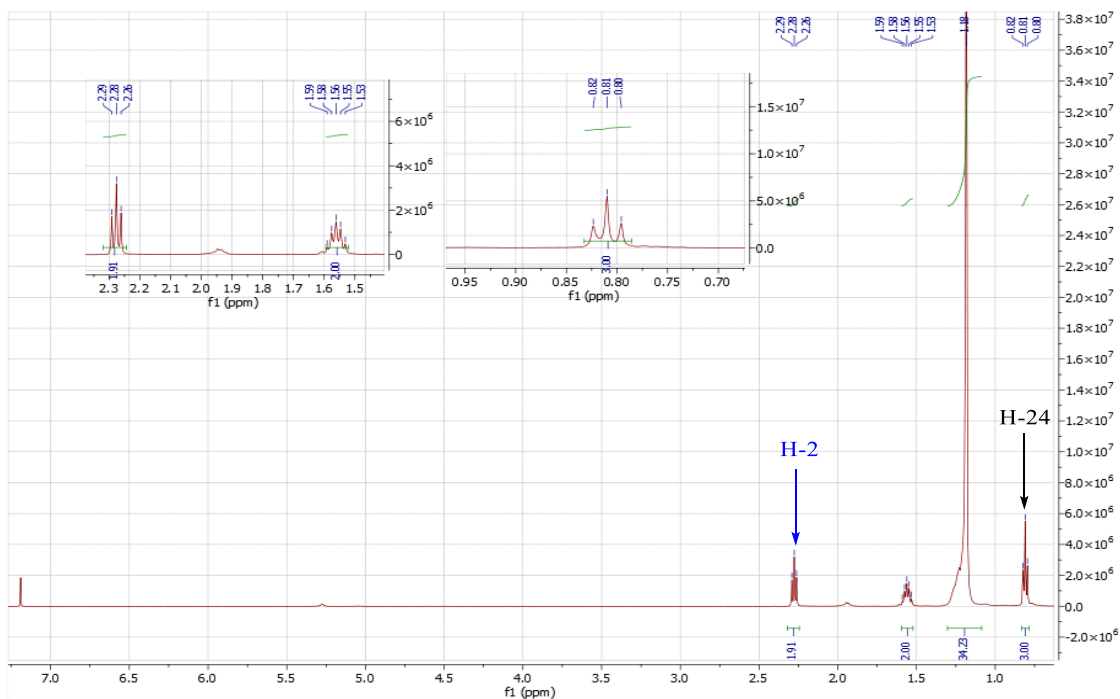
Figure 169: ^{1}H NMR (CD$_3$OD, 500 MHz) spectrum of compound AL3

II.2.1.9. Monoglyceride

II.2.1.9.1 Identification of ECT14

ECT14 was obtained as a white amorphous powder and is soluble in pyridine. Its molecular formula C$_{33}$H$_{66}$O$_4$, containing an unsaturation was deduced after analysis of its mass spectrum ESI in positive mode at high resolution (Figure 170), which shows the peak of the potassium adduct [M+K]$^+$ at *m/z* 565.2966 (calculated for 565.2993).

Its ^{1}H NMR spectrum (Figure 171) exhibits:

- two doublets of one proton each at δ_H 4.71 (1H, dd, *J* = 11.0, 4.5 Hz, H-1′a) and 4.64 (1H, dd, *J* = 11.1, 6.2 Hz, H-1′b) attributable to the diastereotopic protons of oxymethylene close to the carbonyl of a glycerolipid;

- a multiplet of oxymethine at δ_H 4.44 (1H, m, H-2′)

- a doublet of oxymethylene at δ_H 4.11 (2H, d, *J* = 5.3 Hz, H-3′);

- a triplet of two protons at δ_H 2.34 (2H, t, *J* = 7.4 Hz, H-2) attributable to the methylene group in the α position of a carbonyl;

- a multiplet of a methylene group at δ_H 1.62 (2H, m, H-3);

- a broad singlet of several methylenes belonging to the long hydrocarbon chain between δ_H 1.20-1.40;

- a triplet of a terminal methyl at δ_H 0.84 (3H, *J* = 6.7 Hz).

Its COSY spectrum (Figure 172) shows the couplings between oxymethylene protons at δ_H 4.71 (H-1′a) and 4.64 (H-1′b); the protons of oxymethine at δ_H 4.44 (H-2′) and oxymethylene at δ_H 4.11 (H-3′); the methylene protons at δ_H 2.34 (H-2), 1.62 (H-3), the long chain between δ_H 1.20-1.40 and the terminal methyl at δ_H 0.84 (H-30).

Its HMBC spectrum (Figure 173, scheme 38), shows among other things correlations between the proton at δ_H 2.34 (H-2) and the carbon at δ_C 25.0 (C-3), the protons of oxymethylene at δ_H 4.64 (H-1′b), 4.71 (H-1′a) and δ_C carbons 63.6 (C-3′), 70.5 (C-2′) and 173.5 (C-1).

↷ HMBC ▬ COSY
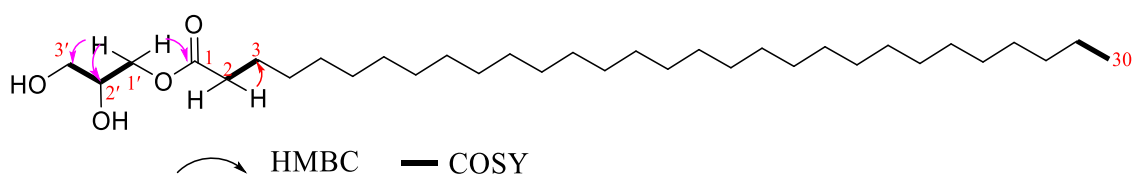
Scheme 38: Some keys correlations observed on the HMBC and COSY spectra of ECT14

The previous data, compared with those in the literature (Table L), allow the structure (**87**) to be attributed to ECT14, which is that of 2′,3′-dihydroxypropyl triacontanoate (Matsumaru *et al*., 2019).

(**87**)
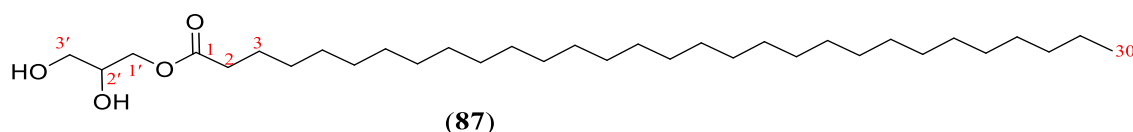
Table L: ^{1}H (500 MHz) and ^{13}C (125 MHz) NMR spectral data of PBR2 in C$_5$D$_5$N compared to those of 2′,3′-dihydroxypropyl tetracosanoate [^{13}C NMR (75 MHz) and ^{1}H NMR (300 MHz) in CDCl$_3$] (Sabudak *et al*., 2007)

Position	ECT14		2′,3′-dihydroxypropyl tetracosanoate	
	δ_H (nH, m, *J* in Hz)	δ_C	δ_H (nH, m, *J* in Hz)	δ_C
1	/	173.5	/	174.5
2	2.34 (2H, t, *J* = 7.4 Hz, H-2)	34.1	2.33 (2H, t, *J* = 7.5 Hz)	34.3
3	1.62 (2H, m, H-3)	25.1	1,61 (2H, m)	25.1
1′	4.71 (1H, dd, *J* = 4.5, 11.0 Hz, H-1′a)	66.4	4.19 (1H, dd, *J* = 4.8 et 11.7 Hz, H-1′a)	65.3
	4.64 (1H, dd, *J* = 6.2, 11.1 Hz, H-1′b)		4.13 (1H, dd, *J* = 6.0 et 11.7 Hz, H-1′b)	
2′	4.44 (1H, m)	70.5	3,19 (1H, m)	70.5
3′	/	63.6	/	63.5
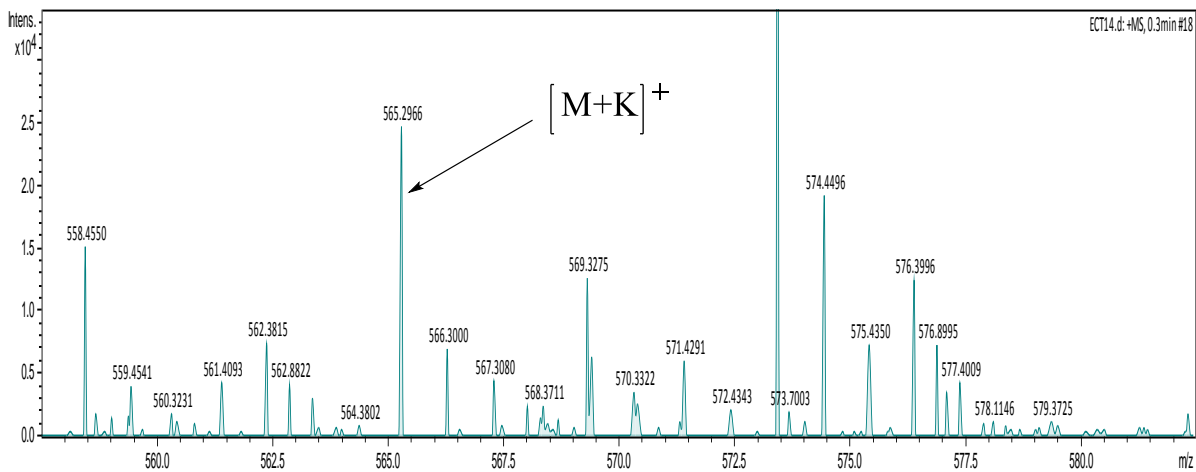
Figure 170: HR-ESI-MS spectrum of compound ECT14
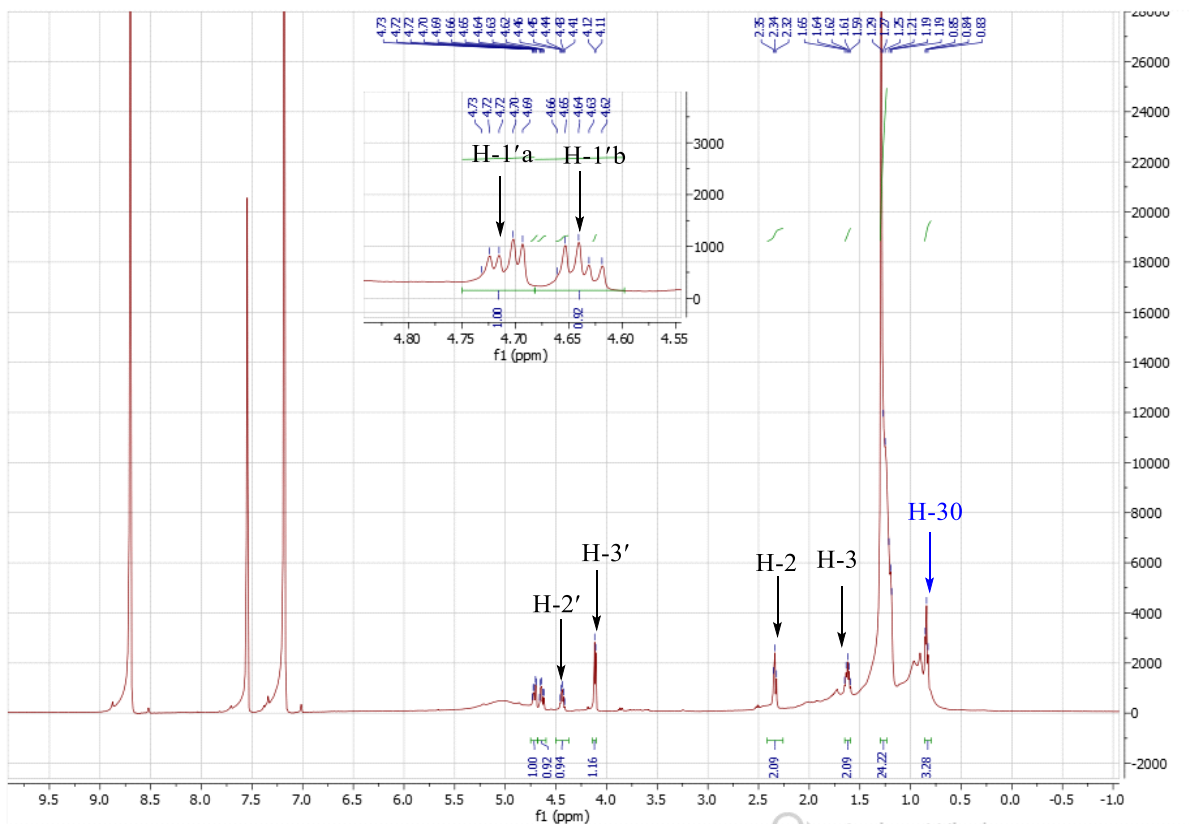
Figure 171: ^{1}H NMR (C$_5$D$_5$N, 500 MHz) spectrum of compound ECT14
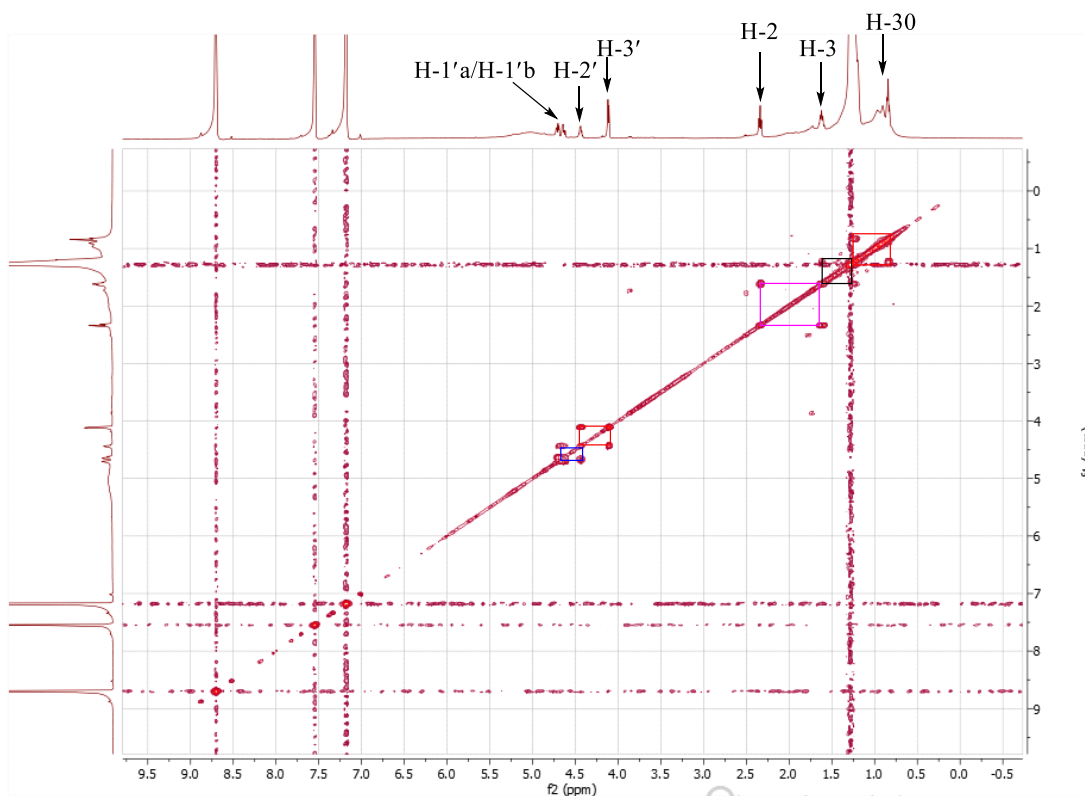
Figure 172: COSY spectrum of compound ECT14
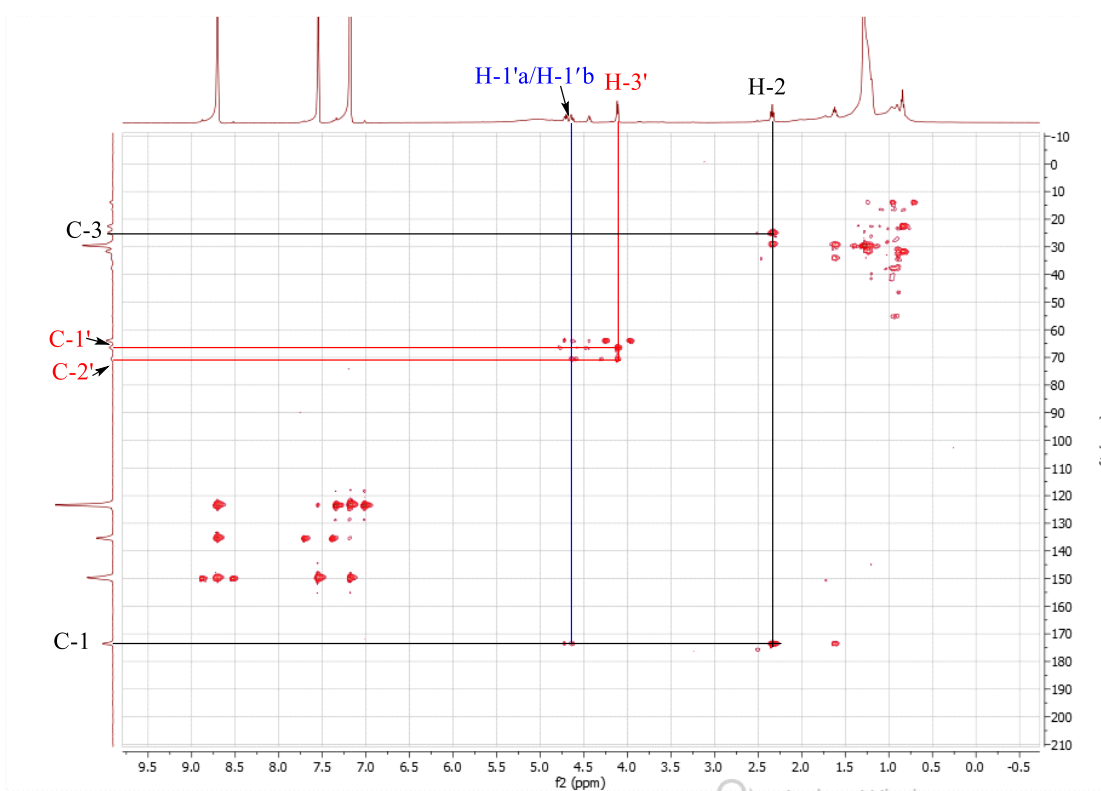
Figure 173: HMBC spectrum of compound ECT14

II.2.1.10 Sugar

II.2.1.10.1 Identification of AL7

AL7 was obtained as a white amorphous powder. It is soluble in pyridine and responds positively to the Molish test and manifests itself by the appearance of a purplish red ring at the interface, characteristic of sugars.

Its high-resolution ESI$^+$ mass spectrum (Figure 174) shows the peak of the potassique adduct [M+K]$^+$ at *m/z* 221.0334 (calculated for 221.0322) corresponding to the molecular formula $C_6H_{14}O_6$, containing no unsaturation.

Its ^{13}C NMR spectrum (figure 176) shows 3 signals which were distinguished thanks to the DEPT 135 spectrum (Figure 177) into:
-2 carbons of methine groups each linked to a hydroxyl group at δ_C 72.0 and 73.1;
- 1 carbon of methylene group linked to a hydroxyl group at δ_C 65.4.

The presence of 3 signals for 6 carbons indicates that there is symmetry in the molecule.

On its ^1H NMR spectrum (Figure 175), we observe:
- a signal at δ_H 4.62 (1H, s), corresponding to the proton of the hydroxyl group;
- a doubled doublet of at δ_H 4.83 (1H, dd, *J* = 7.6, 2.8 Hz), corresponding to the proton link to the carbon at δ_C 73.1;
- a doubled doublet at δ_H 4.53 (1H, dd, *J* = 7.6, 3.6 Hz), corresponding to the proton link to the carbon at δ_C 72.0;
- a signal at δ_H 4.35 (1H, ddd, *J* = 7.6, 3.6, 2.8 Hz), corresponding to the proton link to the carbon at δ_C 65.4.

The positions of these substituents were deduced from the correlations observed on the HMBC spectrum (Figure 178, scheme 39) of AL7. Indeed, on this spectrum, we observe the correlations between:
- the proton at δ_H 4.35 (H-1) and the carbons at δ_C 72.0 (C-2), 73.1 (C-3).
- the proton at δ_H 4.53 (H-2) and the carbons at δ_C 65.4 (C-1), 73.1 (C-3).
- the proton at δ_H 4.83 (H-3) and the carbons at δ_C 65.4 (C-1), 73.1 (C-3).

The structure was confirmed thanks to the correlations observed on the COSY spectrum (Figure 179). Indeed this spectrum presents among others:
- the proton at δ_H 4.35 (H-1) and the proton at δ_H 4.53 (H-2)
- the proton at δ_H 4.35 (H-1) and the proton at δ_H 4.62 (H-3)
- the proton at δ_H 4.53 (H-2) and the proton at δ_H 4.62 (H-3)
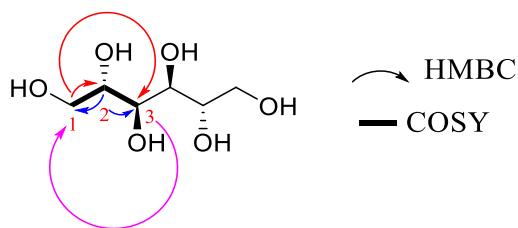
Scheme 39: Selected HMBC and COSY correlations of AL7

The previous data, compared with those in the literature (Table LI), allow the structure (**88**) to be attributed to AL7, which is that of D-mannitol (Kerimli *et al*., 2016).

(88)
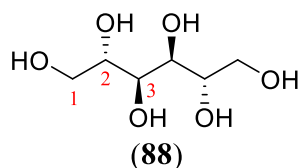
Table LI: ^{1}H (500 MHz) and ^{13}C (125 MHz) NMR spectral data of AL7 in C$_5$D$_5$N compared to those of D-mannitol [^{13}C NMR (75 MHz) and ^{1}H NMR (300 MHz) in C$_2$D$_6$SO] (Kerimli *et al*., 2016)

Position	AL7	D-mannitol
	δ_C	δ_C
1	65.4	**64.3**
2	71.9	**70.1**
3	**73.0**	**71.7**
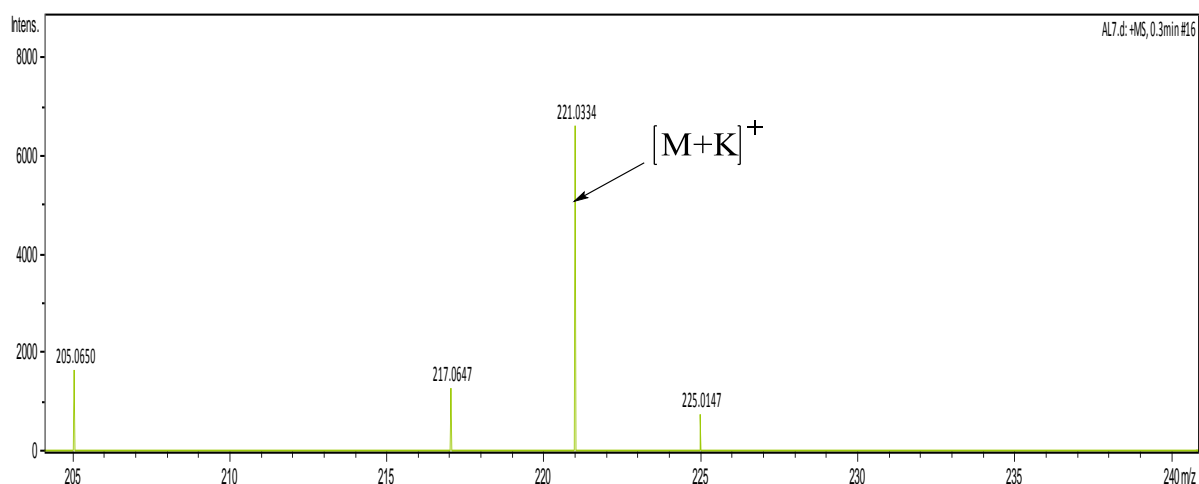
Figure 174: HR-ESI-MS spectrum of compound AL7
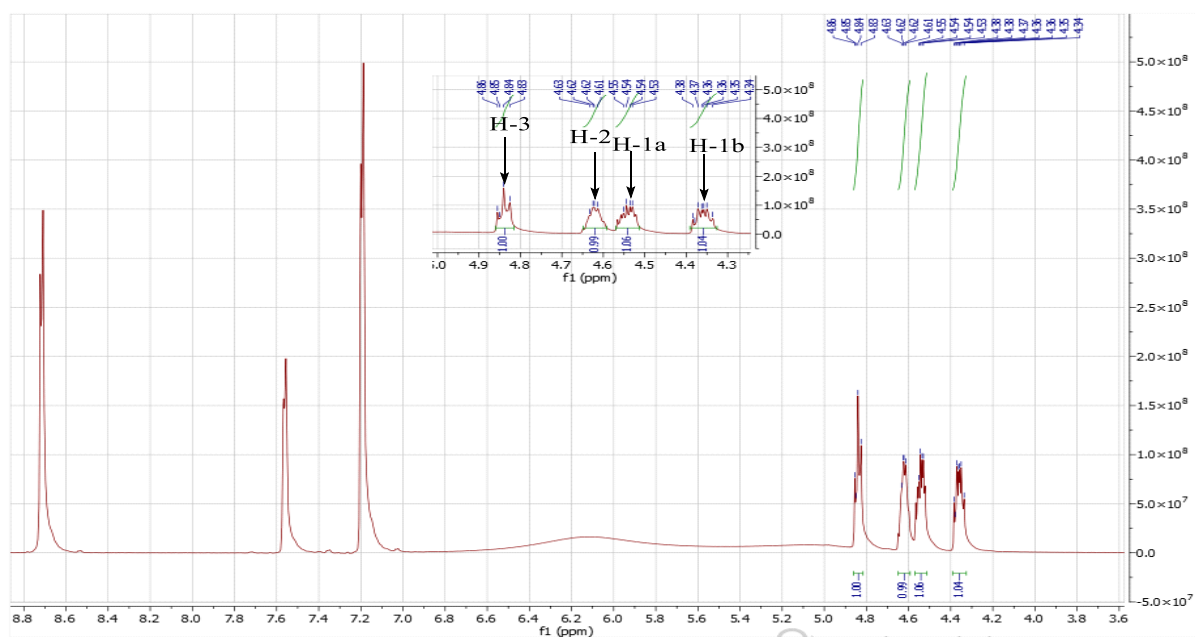
Figure 175: ^{1}H NMR spectrum (C$_5$D$_5$N, 500 MHz) of compound AL7
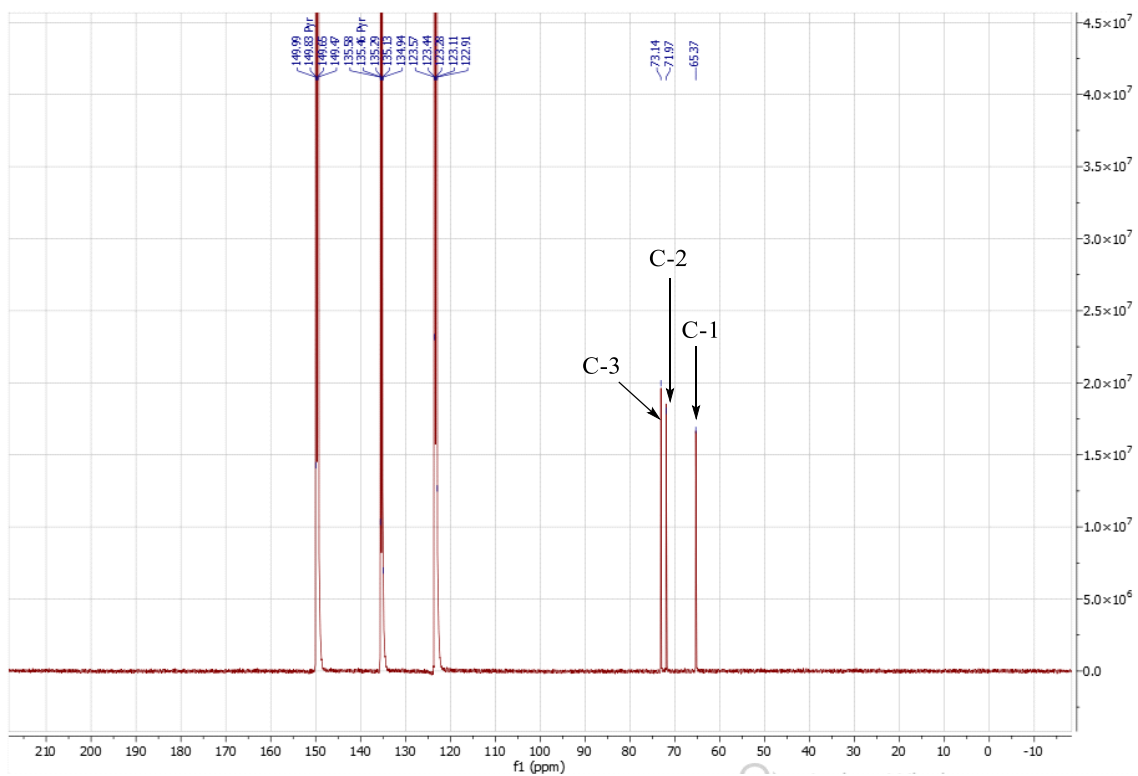
Figure 176: ^{13}C NMR (C$_5$D$_5$N, 125 MHz) spectrum of compound AL7
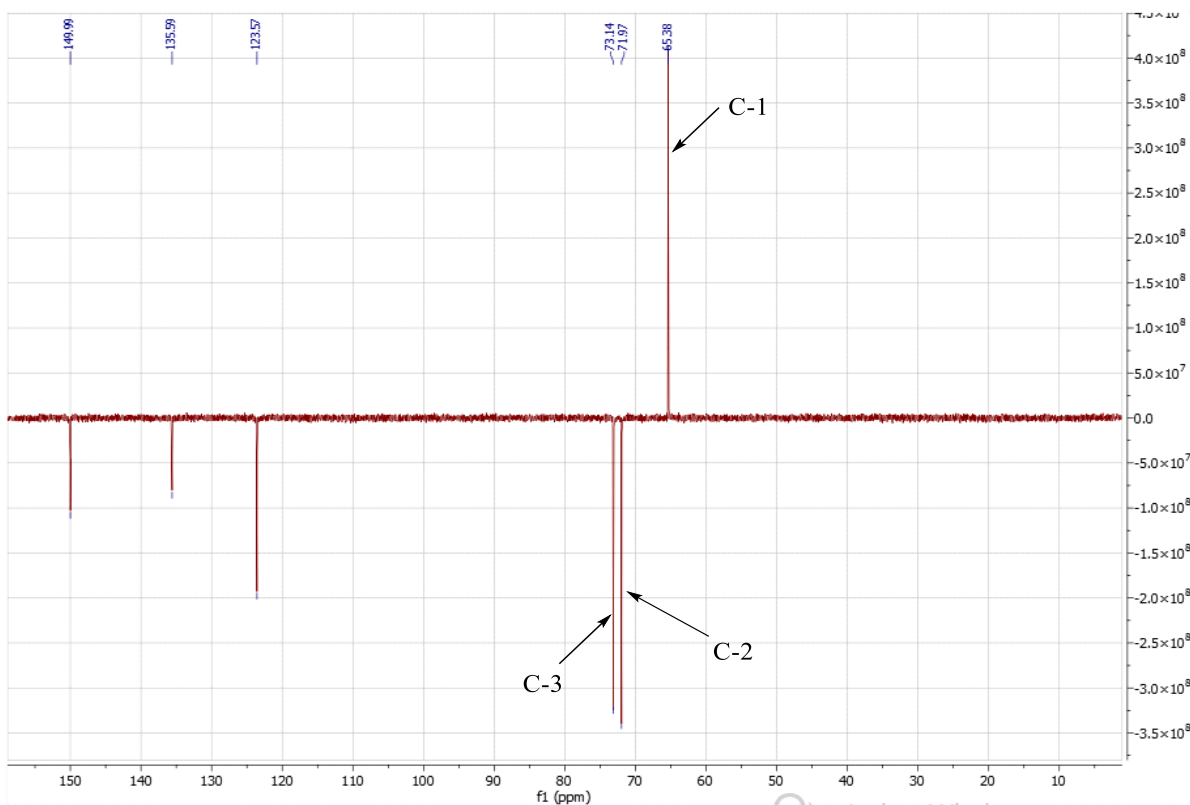
Figure 177: DEPT 135 spectrum of compound AL7
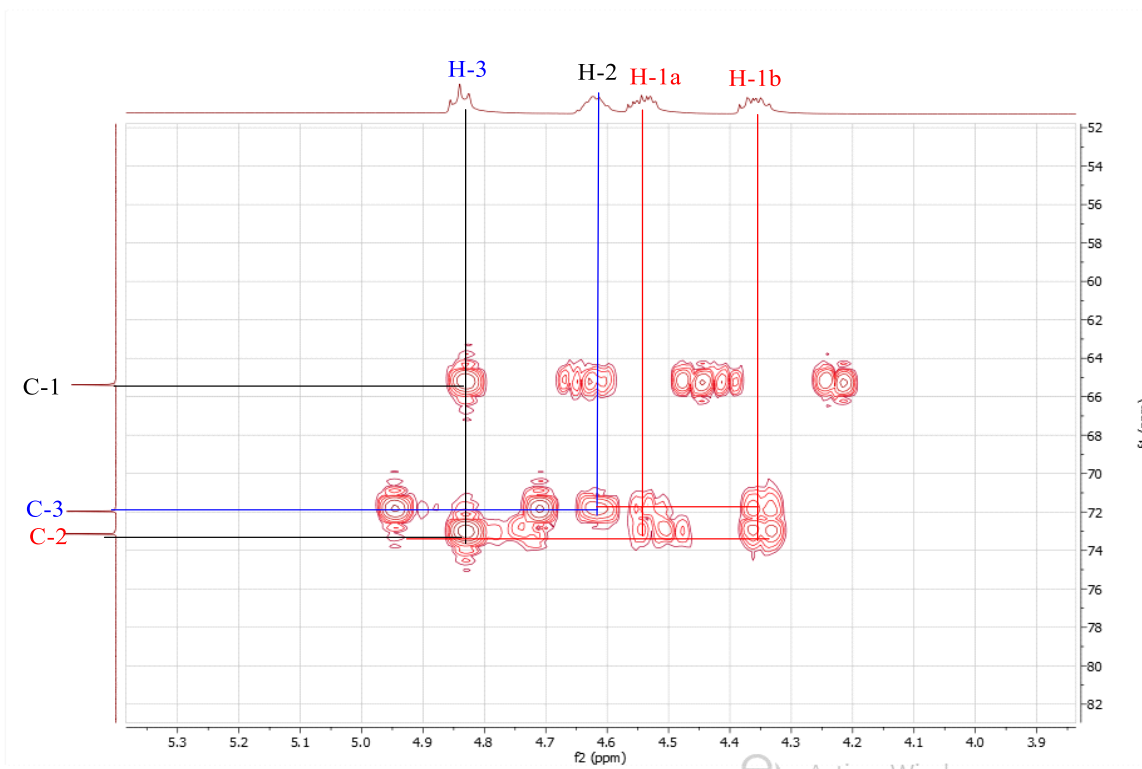
Figure 178: HMBC spectrum of compound AL7
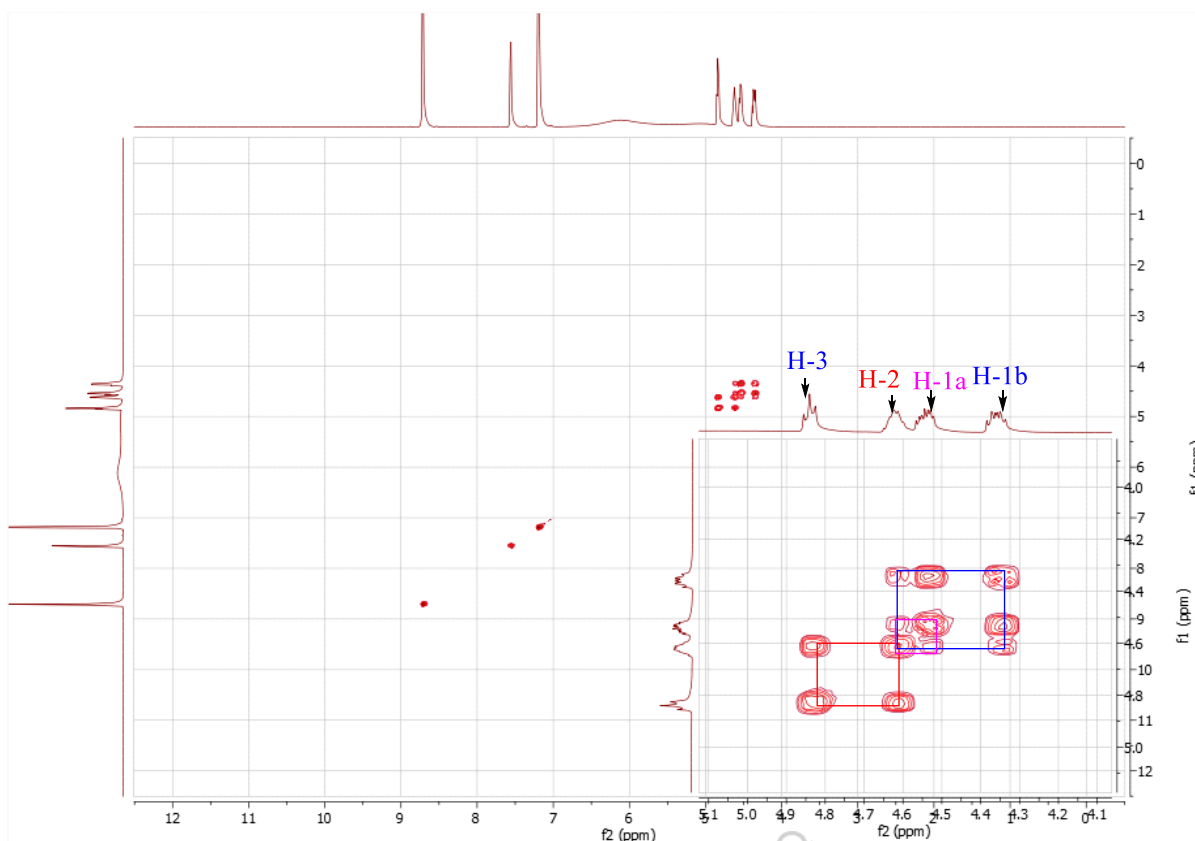
Figure 179: COSY spectrum of compound AL7

II.2.1.11 Ellagic acid

II.2.1.11.1 Identification of EC9

EC9 was obtained as a yellow amorphous powder. It is soluble in pyridine and responds positively to the ferric chloride test, characteristic of phenols.

Its high-resolution ESI (-) mass spectrum (Figure 180) shows the peak of the deprotonated ion [M-H]⁻ at *m/z* 329.0311 (calculated for 329.0376) corresponding to the molecular formula $C_{16}H_{10}O_8$, containing twelve unsaturations.

Its ^1H NMR spectrum (Figure 181) shows the signal of two aromatic protons at δ_H 8.04 (2H, s, H-5 and H-5′) and the signal of two methoxyl groups at δ_H 4.20 (6H, s), characteristics of a methoxylated ellagic acid type backbone (Khac *et al.*, 1990).

These data, compared with those in the literature, enable us to identify the compound EC9 with a dimethoxylated derivative of ellagic acid, 3,3′-*O*-dimethylellagic acid (**89**) (Khac *et al.*, 1990).

(89)
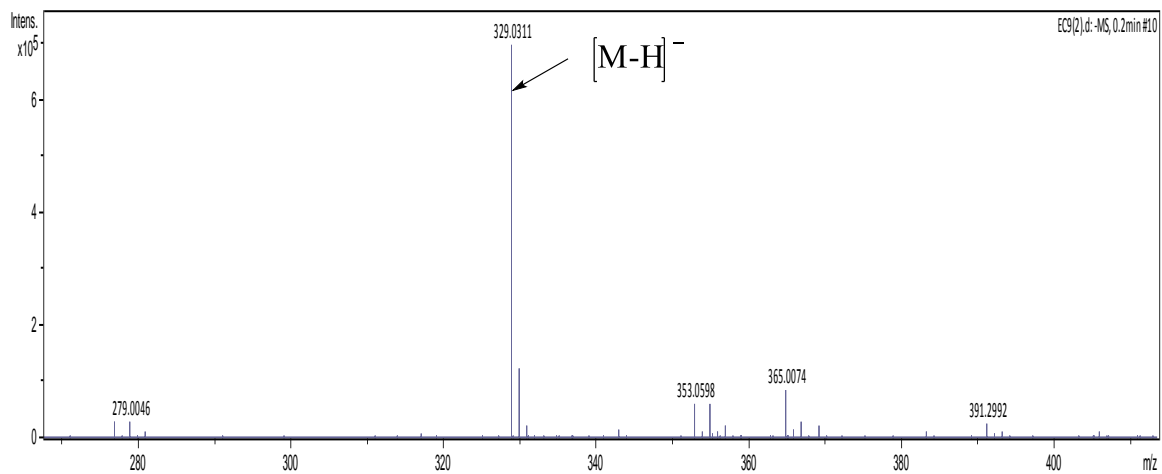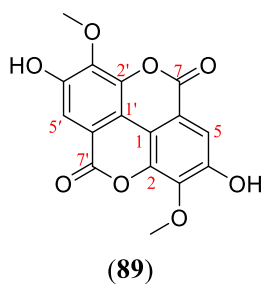
Figure 180: HR-ESI-MS spectrum of compound EC9
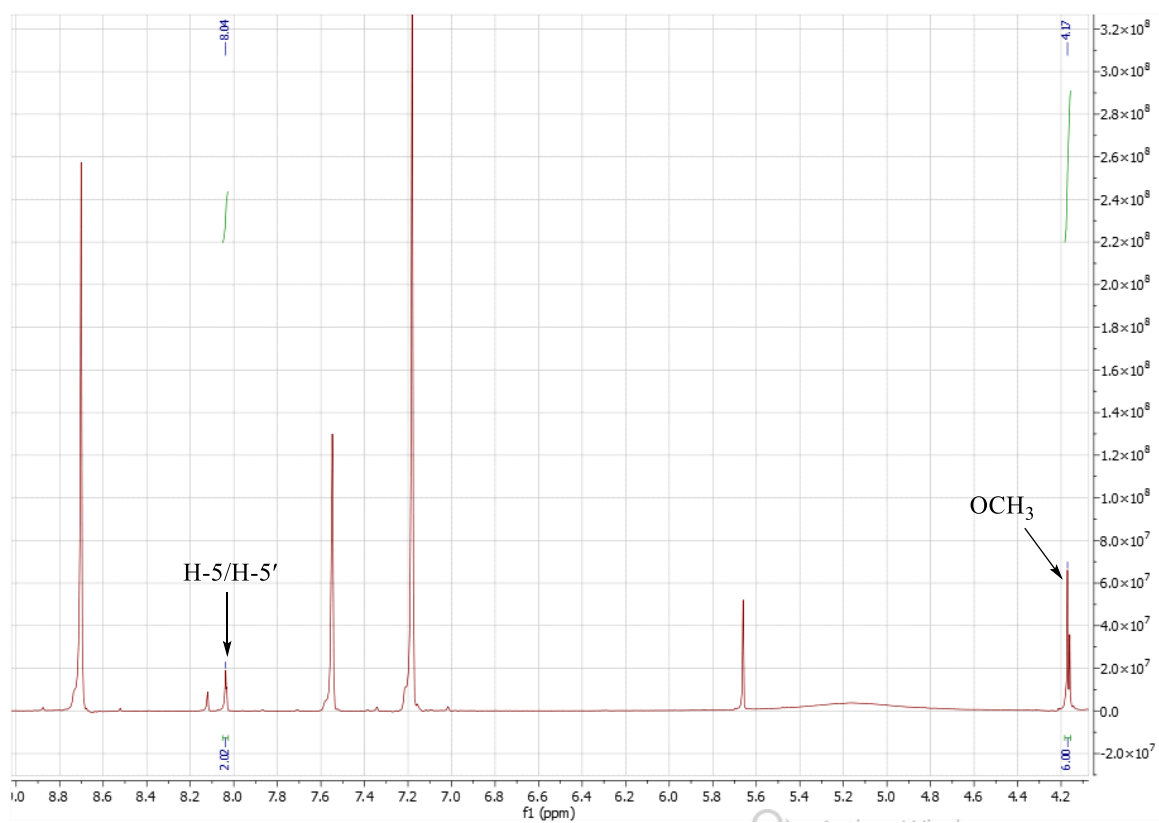
Figure 181: ^{1}H NMR (C$_5$D$_5$N, 500 MHz) spectrum of compound EC9

II.2.1.12 Steroids

II.2.1.12.1 Identification of PBF5

PBF5 was obtained as white needles and is soluble in chloroform. It reacts positively to the Liebermann-Burchard test, giving a blue color which quickly turns dark green, characteristic of sterols.

Its high resolution positive mode ESI mass spectrum (Figure 182) shows the peak of the protonated ion $[M+H]^+$ at *m/z* 413.2736 (calculated for 413.2778), corresponding to the molecular formula $C_{29}H_{48}O$, containing 6 unsaturations.

Its ^1H NMR spectrum (Figure 183), showed the signals at δ_H 5.40 (H-6), 3.55 (H-3) and the signals of the protons H-22 and H-23 in the *trans* position of the stigmasterol at δ_H 5.07 (1H, dd, J = 15.2, 8.6 Hz) and 5.20 (1H, dd, J = 15.2 Hz, 8.7 Hz). This was confirmed by its ^{13}C NMR spectrum (Figure 184) which shows the signals of ethylenic carbons at δ_C 140.8 (C-5), 121.7 (C-6), 138.3 (C-22) and 129.3 (C-23), as well as the carbon signal of an oxymethine at δ_C 71.8 (C-3) (Chaturvedula *et al*., 2012).

PBF5 was therefore identified with stigmasterol (**90**) thanks to its spectroscopic (table LII), physical data and by comparison by TLC with a sample available in our laboratory.

(**90**)
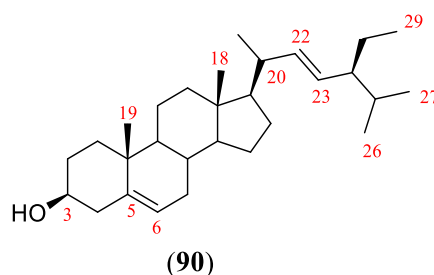
Table LII: ^1H (500 MHz) and ^{13}C (125 MHz) NMR spectral data of PBF5 in CDCl₃ compared to those of stigmasterol [^{13}C NMR (150 MHz) and ^1H NMR (600 MHz) in CDCl₃] (Chaturvedula *et al.*, 2012)

Position	PBF5	stigmasterol
	δ_C	δ_C
1	37.3	37.6
2	31.9	32.1
3	71.8	72.1
4	42.3	42.4
5	140.8	141.1

6	121.7	121.8
7	31.7	31.8
8	31.7	31.8
9	50.2	50.2
10	36.5	36.6
11	21.1	21.5
12	39.7	39.9
13	32.9	42.4
14	56.8	56.8
15	24.4	24.4
16	29.0	29.3
17	56.1	56.2
18	40.5	40.6
19	21.2	21.7
20	138.3	138.7
21	129.3	129.6
22	45.9	46.1
23	25.4	25.4
24	12.1	12.1
25	29.0	29.6
26	19.4	20.2
27	19.0	19.8
28	17.5	18.9
29	12.3	12.2
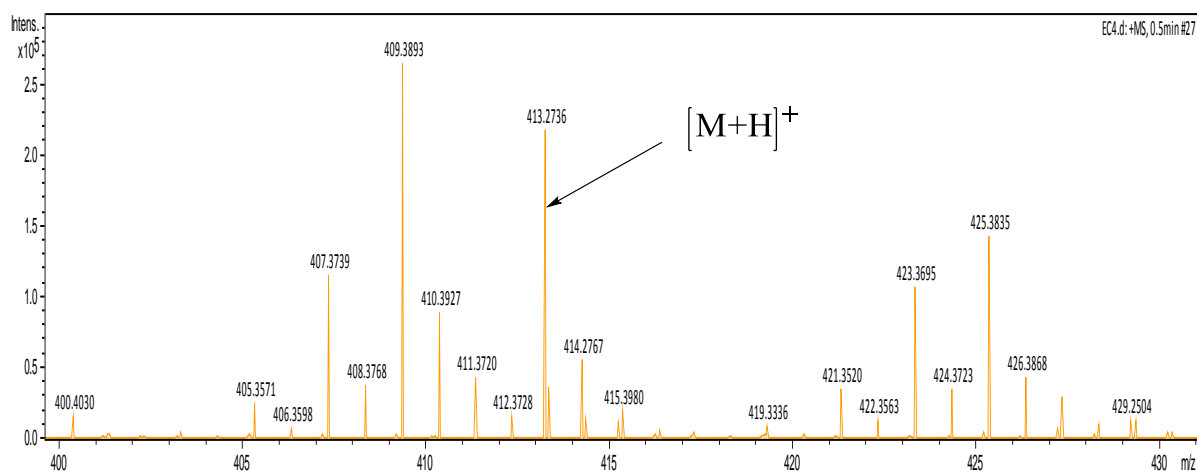
Figure 182: HR-ESI-MS spectrum of compound PBF5
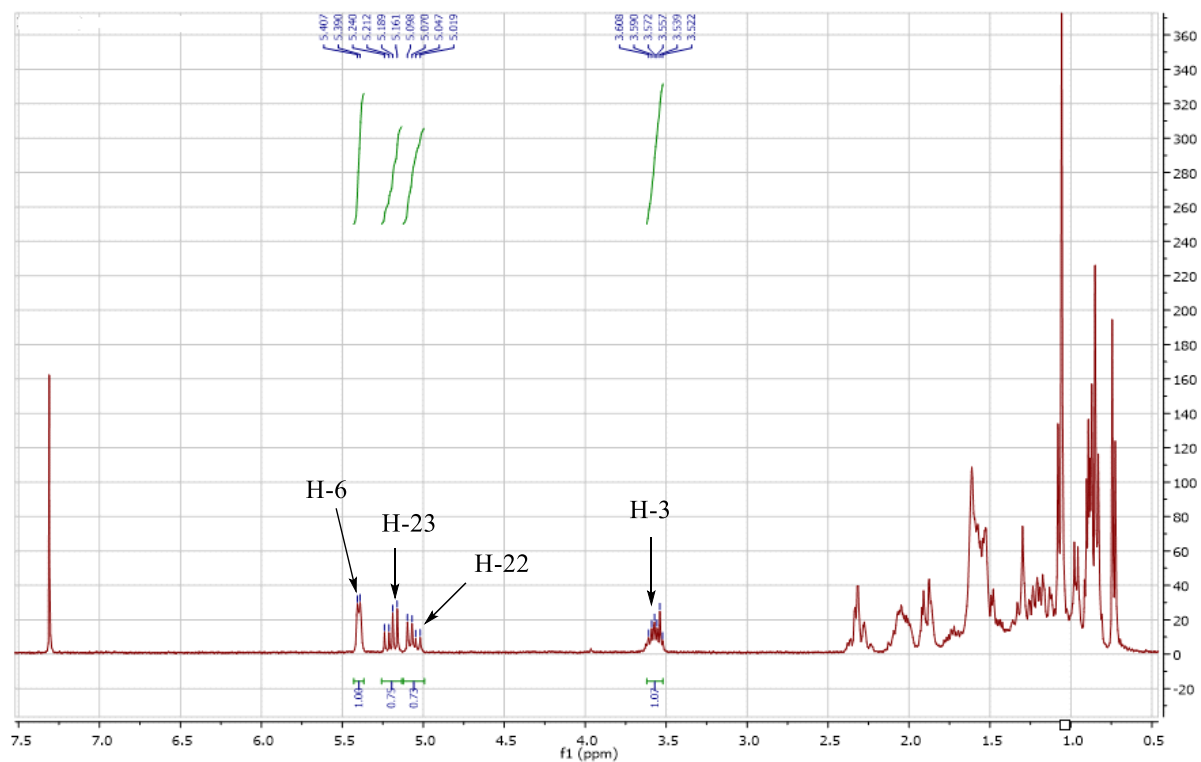
Figure 183: ¹H NMR (CDCl₃, 500 MHz) spectrum of compound PBF5
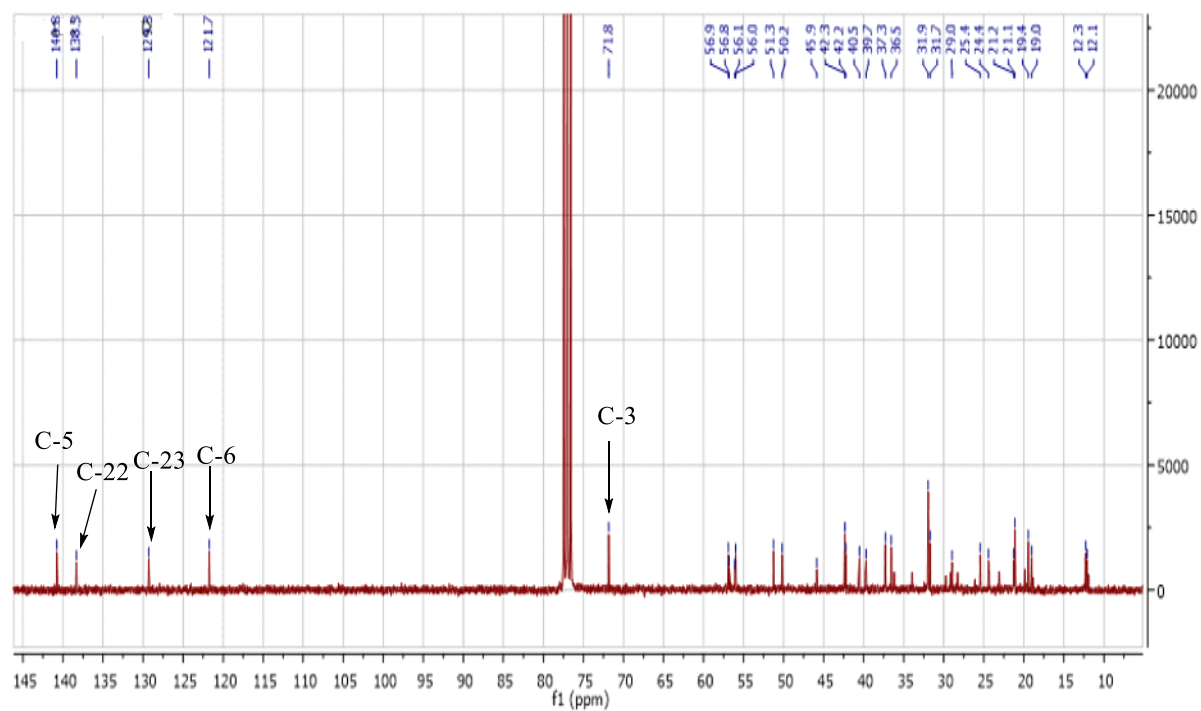
Figure 184: ¹³C NMR (CDCl₃, 125 MHz) spectrum of compound PBF5

II.2.1.12.2 Identification of EC4

EC4 was obtained as a white amorphous powder. It is soluble in chloroform. It reacts positively to the Liebermann-Burchard test by giving a blue color which quickly turns to the green characteristic of sterols.

EC4 has been identified as a mixture of phytosterols consisting of stigmasterol (**90**) and *β*-sitosterol (**91**) (Kovganko *et al.*, 1999) thanks to its NMR data. Indeed, on its proton spectrum (Figure 185), we observe the signal of the H-6 protons of these phytosterols at δ_H 5.28, that of their H-3 protons at δ_H 3.45 and the signals of the H-22 protons and H-23 of stigmasterol at δ_H 5.09 and 4.94.
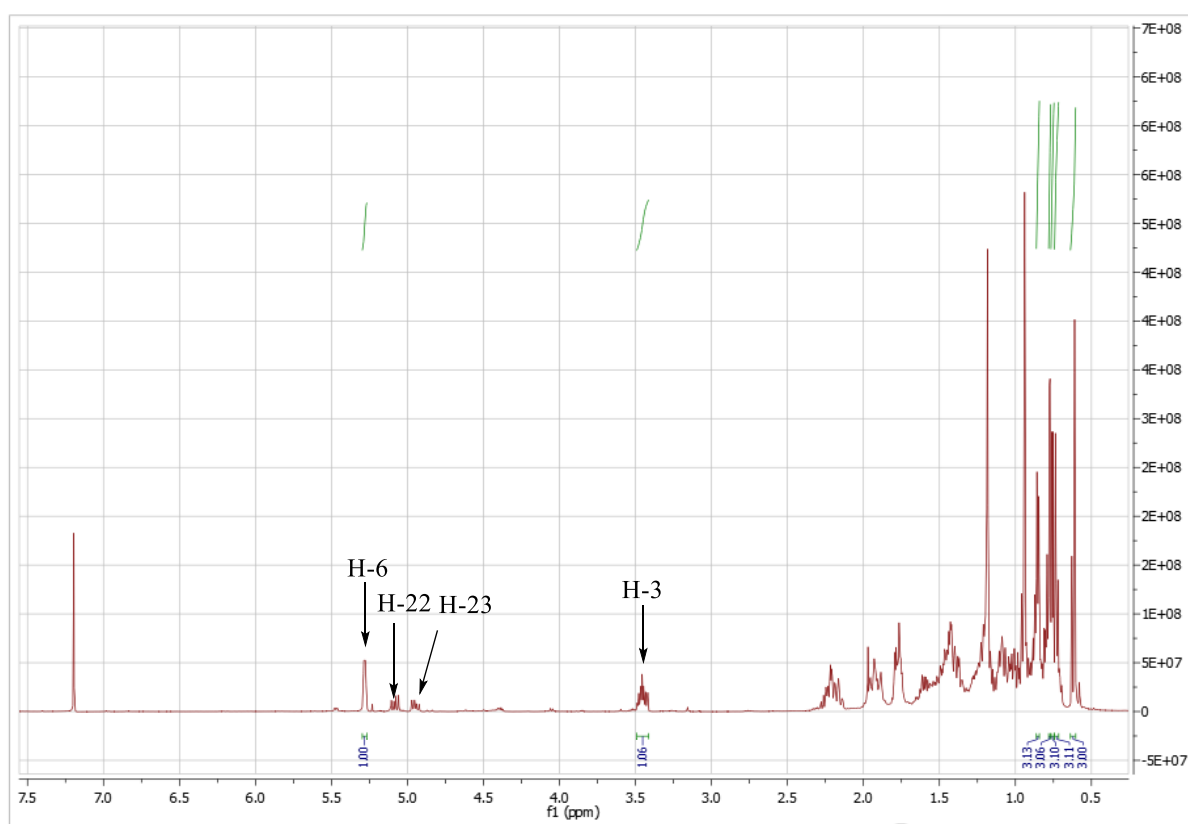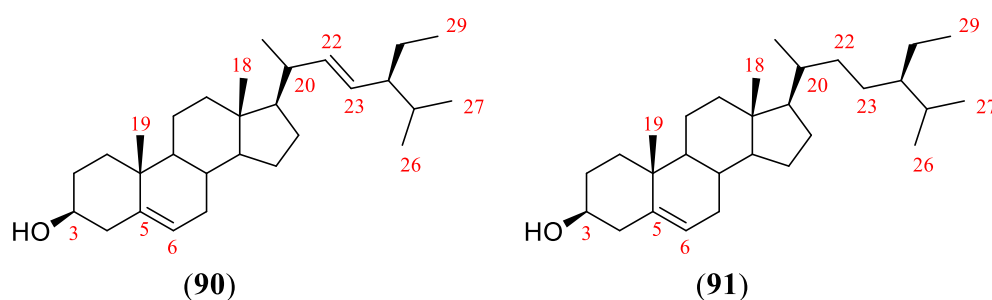
Figure 185: ¹H NMR (CDCl₃, 500 MHz) spectrum of compound EC4

II.2.1.12.3 Identification of EC6=PBF6

EC6 was obtained as a white powder. It is soluble in pyridine and reacts positively to the Molish and Liebermann-Burchard tests, characteristic of sugars and sterols, respectively.

Its high-resolution ESI (+) mass spectrum (Figure 186) gives the peak sodium adduct $[M+Na]^+$ at *m/z* 599.4522 (calculated for 599.4282), corresponding to the molecular formula $C_{35}H_{60}O_6$ containing six degrees of unsaturation.

Its ^{1}H NMR spectrum (Figure 187), compared to that of EC6 shows between δ_H 3.70 and 5.10 a set of signals characteristic of a sugar whose β-anomeric proton resonates at δ_H 5.05 (d, $J = 7.6$ Hz).

Based on these data and TLC with an authentic sample available in the laboratory, EC6 was identified as β-sitosterol-3-*O*-β-D-glucopyranoside (**92**) (Khatun *et al*., 2012).
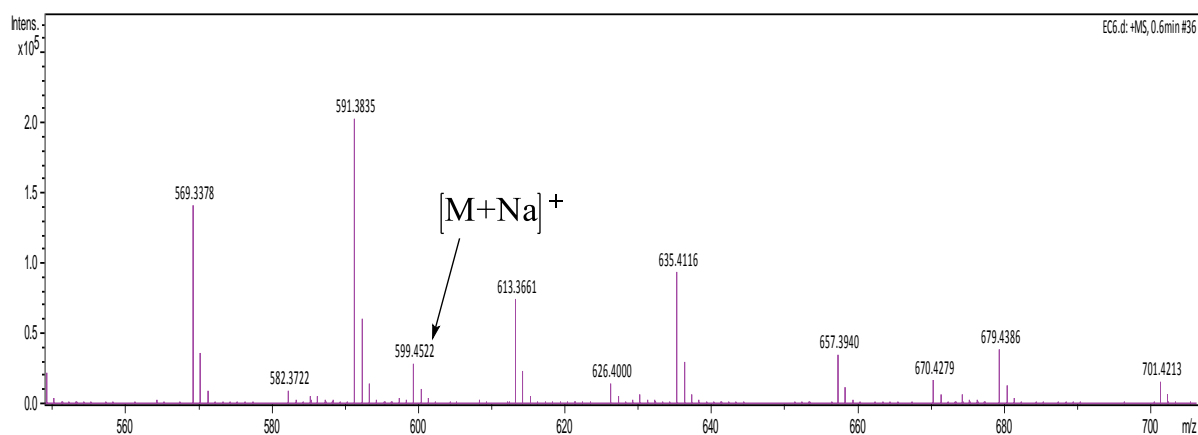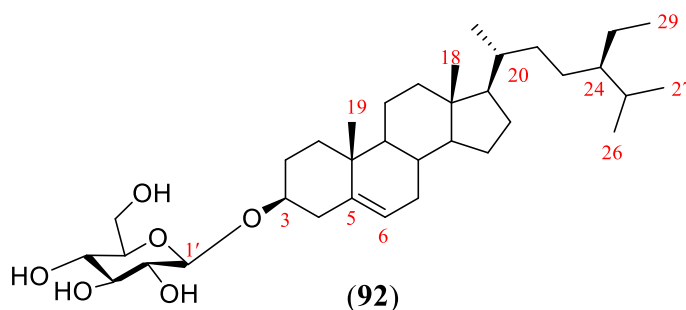
Figure 186: HR-ESI-MS spectrum of compound EC6
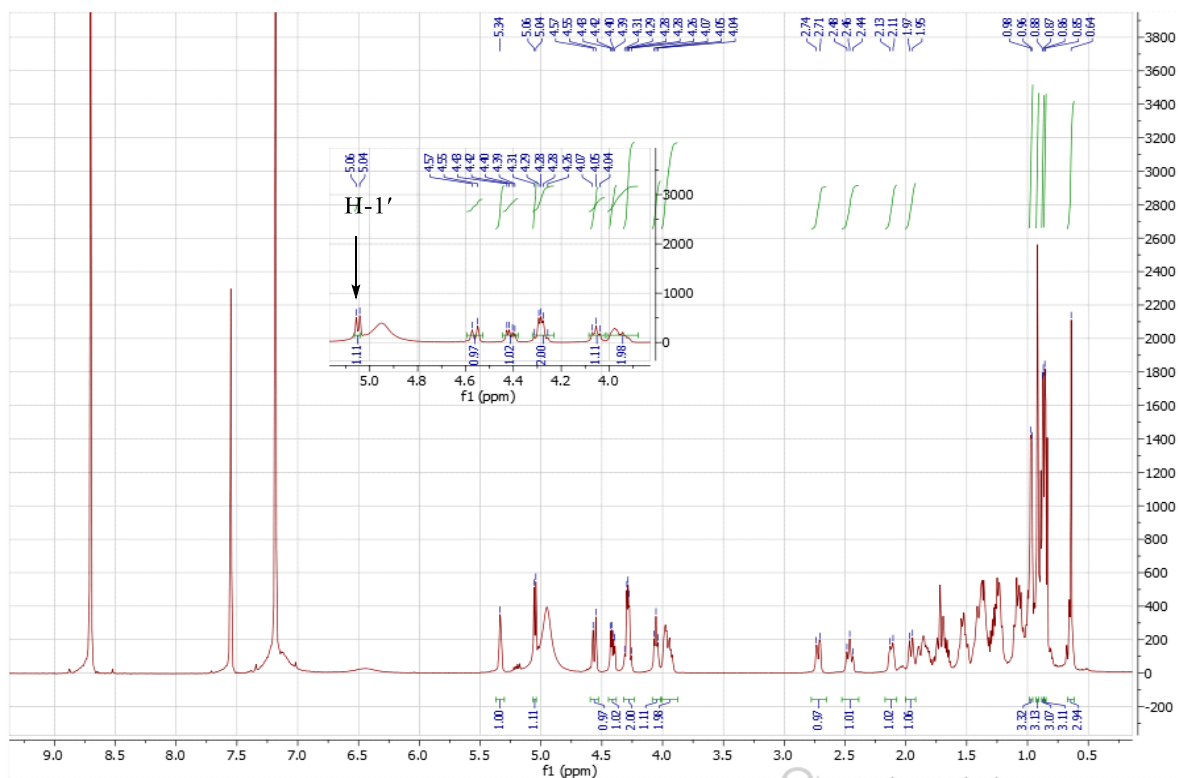
Figure 187: ^{1}H NMR (C$_5$D$_5$N, 500 MHz) spectrum of compound EC6

II.3. Biological activities

The antileishmanial activity of CH$_2$Cl$_2$/MeOH (1:1) extracts of *E. calophylloides*, *P. butyracea* and *A. lobata*, were evaluated based on their ethnobotanical used as skin parasitic phytomedecine and in the manufacture of soap for healing qualities, filariae and hemorrhoids.

The antileishmanial results showed in Table LII à LVI, were discussed according to the classification established by Camacho *et al*. (2003) (**IC$_{50}$ <10 μg/mL**, extract is **highly active**; **10<IC$_{50}$<50 μg/mL**, extract is **good active**; **50<IC$_{50}$<100 μg/mL**, extract is **moderately active**; **IC$_{50}$>100 μg/mL**, extract is **inactive**). And the cytoxicity according to the classification established by Mosmann (1983) (**SI>1:** extract or fraction or compound is **selective** and **SI<1:** extract or fraction or compound is **non-selective**).

II.3.1 Antileishmanial activity

II.3.1.1 Antileishmanial activity and cytotoxicity from the CH$_2$Cl$_2$/MeOH (1:1) crude extract of the fruits and stem bark of *P. butyracea* against *Leishmania donovani* 1S (MHOM/SD/62/1S) promastigotes

Table LIII: Antileishmanial activity and cytotoxicity of the extract, fractions and compounds from the fruits *P. butyracea*

Extracts/compounds	Antileishmanial activity $IC_{50} \pm SD$ (μg/mL)	Macrophages $CC_{50} \pm SD$ (μg/mL)	Selectivity Index (SI ± SD) (CC_{50}/IC_{50})
CH_2Cl_2/MeOH (1:1) extract	5.96 ± 0.05[d]	398.70 ±10.18[d]	66.89±1.14[g]
n-hexane fraction	17.37 ± 0.28[i]	106.35 ±7.14[c]	6.11±0.31[b]
n-hex/EtOAc (1:1) fraction	25.97 ± 0.32[l]	397.25 ± 0.64[d]	15.29±0.16[c]
EtOAc fraction	12.94 ± 0.21[g]	485.55 ± 0.07[f]	37.52±0.60[f]
EtOAc/MeOH (8:2) to MeOH fraction	18.88 ± 0.12[j]	465.50 ±18.24[e]	24.33±0.85[d]
Daphnifolin (**77**)	2.01 ± 0.19 [b]	66.68 ± 4.89[b]	33.21±0.71[e]
Norathyriol (**76**)	16.59 ± 0.48 [h]	22.18 ± 0.67[a]	1.33±0.00[a]
Epicatechin (**68**)	9.09 ± 0.23[e]	>100	ND
Methyl citrate (**84**)	21.47 ± 0.25[k]	>100	ND
Stigmasterol (**90**)	27.00 ± 0.23[m]	>100	ND
β-sitosterol-3-*O*-*β*-D-Glucopyranoside (**92**)	NA	ND	ND
Tovopyrifolin C (**78**)	11.04 ± 0.11[f]	75.50 ± 6.05[b]	6.83±0.47[b]
Cowagarcinone B (**80**)	>50	ND	
α-mangostin (**79**)	3.37 ± 0.20[c]	80.79 ± 0.12[b]	24.02±1.39[d]
Amphotericin B	0.22 ± 0.36[a]	-	ND

ND: not determined; Data points are means from triplicate experiments. SD = Standard Deviation; Activity values were obtained from sigmoidal dose-response curves of concentration versus response. Along the columns values with different letter superscript are significantly different; Waller Ducan at p ≤ 0.05.

PBF: P. butyracea fruit extract; PBFF1-4: P. butyracea fruit fractions.

Legends: IC_{50} values against *Leishmania donovani* 1S(MHOM/SD/62/1S) promastigotes

■= Highly active   ■ = Good active   ■= moderately active   □ = Inactive

Table LIV: Antileishmanial activity and cytotoxicity of the extract, fractions and compounds from the stem bark of *P. butyracea*

Extracts/compounds	Antileishmanial activity (IC_{50} in μg/mL)	Macrophages $CC_{50} \pm SD$ (μg/mL)	Selectivity Index (SI) (CC_{50}/IC_{50})
CH_2Cl_2/MeOH (1:1) extract	26.43 ± 0.05[k]	148.81 ± 17.96[e]	5.62 ± 0.66[c]
n-hexane fraction	7.91 ± 0.17[f]	106.35 ± 7.15[d]	13.45 ± 0.61[d]
n-hex/EtOAc (1:1) fraction	12.56 ± 0.30[i]	48.775 ± 5.60[b]	3.77 ± 0.22[b]
EtOAc fraction	2.71 ± 0.38[c]	75.58 ±7.09[c]	28.01 ± 1.32[f]
EtOAc/MeOH (9:1) fraction	12.75 ± 0.39[i]	405.80 ±16.25[g]	31.82 ± 0.30[g]
EtOAc/MeOH (7.5:2.5)-MeOH fraction	10.88 ± 0.49[h]	305.00 ±10.47[f]	28.04 ± 0.30[f]
Lupeol (**62**)	> 50	31.22 ± 1.64[ab]	ND
Betulin (**64**)	> 50	ND	ND
Tovophylin A (**82**)	> 50	ND	ND

1,3,7-trihydroxyxanthone (**83**)	> 50	78.23 ± 7.81^c	ND
9-hydroxycalabaxanthone (**81**)	6.87 ± 0.33^e	16.81 ± 0.67^a	2.45 ± 0.02^{ab}
Amphotericin B	0.22 ± 0.36^a	-	

ND: not determined; Data points are means from triplicate experiments. SD = Standard Deviation; Activity values were obtained from sigmoidal dose-response curves of concentration versus response. Along the columns values with different letter superscript are significantly different; Waller Ducan at $p \leq 0.05$.

PBB: *P. butyracea* stem bark extract; PBBF1-5: *P. butyracea* stem bark fractions.

Legends: IC_{50} values against *Leishmania donovani* 1S(MHOM/SD/62/1S) promastigotes

■= Highly active   ■ = Good active   ■= moderately active   □ = Inactive

The fruit crude extract (PBF) was about four times more active than the stem bark extract (PBB). The fractionation of the PBF extract resulted in a decrease in the *antileishmanial* activity, while the fractionation of PBB extract led to an increase of activity, indicating the synergistic and antagonistic effect of fractions, respectively. The antileishmanial activity of daphnifolin (**77**) and *α*-mangostin (**79**) as well as 9-hydroxycalabaxanthone (**81**) corroborated with some previous results on xanthone derivative (Silva *et al*., 2013; Azebaze *et al*., 2008). Indeed, *α*-mangostin isolated from the fruits of *Garcinia mangostana* showed good activity against intracellular amastigotes of *L. infantum*, with IC_{50} value 8 μM (Al-Massarani *et al*., 2013). Daphnifolin (**77**) and *α*-mangostin (**79**), could be probably the main active principles isolated from both extracts. This result could justify the use of *P. butyracea* in the treatment of the parasitic diseases of the skin (Raponda-Walker and Sillans, 1961).

II.3.1.2 Antileishmanial activity and cytotoxicity from the the CH_2Cl_2/MeOH (1:1) crude extract of the leaves and stem bark of *E. calophylloides* against *Leishmania donovani* 1S (MHOM/SD/62/1S) promastigotes

Table LV: Antileishmanial activity and cytotoxicity of extract, fractions, and isolates of stem bark of *E. calophylloides*

Part	Extract, fraction or compound	$IC_{50} \pm SD$ (μg/mL)	CC_{50} on Vero Cells (μg/mL $\pm$ SD)	SI (CC_{50}/IC_{50})
	CH_2Cl_2/MeOH (1:1) extract	24.33 ± 0.01	>100	>4.11
	n-hexane fraction	21.91 ± 0.02	26.62 ± 1.90	1.22
	Dichloromethane fraction	21.31 ± 0.02	22.97 ± 1.97	1.08

bark	Ethyl acetate fraction	**9.19 ± 0.19**	>100	>10.88
	n-butanol fraction	**45.77 ± 0.04**	>100	>2.18
	Water soluble residue	>100	NA	ND
	Friedelin (**56**)	>50	NA	ND
	Absicic acid β-D-glucoside (**70**)	>50	NA	ND
	Tachioside (**71**) and isotachioside (**72**)	**8.66 ±0.15**	33.77 ± 0.13	3.9
	Morelloflavone (**67**)	>50	NA	ND
	Lupenone (**63**)	>50	NA	ND
	2′,3′-dihydroxypropyl triacontanoate (**87**)	>50	NA	ND
	1,5-dihydroxy-3-methoxyxanthone (**75**)	**44.24 ± 0.09**	>100	>2.26
	Marsformoxide B (**59**)	>50	NA	ND
	Isoxanthochymol (**69a**) and cycloxanthochymol (**69b**)	**4.77 ± 0.15**	7.88 ± 0.55	1.65
	Koaburaside (**73**)	>50	NA	ND
	Amphotericin B	**0.14 ± 0.13**		

SD: Standard deviation; IC$_{50}$: Inhibition concentration 50%; CC$_{50}$: Cytotoxic concentration 50%; SI: Selectivity Index; NA: Not Applicable; ND: Not determined.

Legends: IC$_{50}$ values against *Leishmania donovani* 1S(MHOM/SD/62/1S) promastigotes

■ = Highly active   ■ = Good active   ■ = moderately active   □ = Inactive

Table LVI: Antileishmanial activity and cytotoxicity of extracts, fractions, and isolates of leaves of *E. calophylloides*

Part	Extract, fraction or compound	IC$_{50}$ ± SD (µg/mL)	CC$_{50}$ on Vero Cells (µg/mL ± SD)	SI (CC$_{50}$/IC$_{50}$)
	CH$_2$Cl$_2$/MeOH (1:1) extract	**17.75 ± 0.17**	>100	>5.63
	n-hexane fraction	>100	NA	ND
	n-hex/EtOAc (3:1) fraction	**22.74 ± 0.09**	34.40 ± 10.79	1.51
	n-hex/EtOAc (1:1-1:3) fraction	**47.77 ± 0.05**	29.89 ± 10.24	0.63
Leaves	EtOAc fraction	>100	NA	ND
	EtOAc/MeOH (9:1) fraction	>100	NA	ND
	EtOAc/MeOH (3:1) fraction	>100	NA	ND
	MeOH fraction	>100	NA	ND
	Lupeol (**62**)	**44.43± 0.03**	37.64±0.30	0.85
	β-amyrin (**60**)	>50	NA	ND
	4′-methylamentoflavone (**65**)	>50	NA	ND
	Amentoflavone (**66**)	>50	NA	ND
	3,3′-*O*-dimeyhylellagic acid (**89**)	>50	NA	ND

Amphotericin B	**0.14 ± 0.13**

SD: Standard deviation; IC$_{50}$: Inhibition concentration 50%; CC$_{50}$: Cytotoxic concentration 50%; SI: Selectivity Index; NA: Not Applicable; ND: Not determined.

Legends: IC$_{50}$ values against *Leishmania donovani* 1S(MHOM/SD/62/1S) promastigotes

■ = Highly active   ■ = Good active   ■ = moderately active   □ = Inactive

The metabolites present in the stem bark and the leaves of *E. calophylloides* were also assessed for their antileishmanial potential against the same strain. These extracts showed good activity with IC$_{50}$ values of 24.33 and 17.75 µg/mL, respectively. The antileishmanial activity of all obtained fractions were also evaluated and, the *n*-hexane, dichloromethane, ethyl acetate and *n*-butanol fractions from the stem bark and *n*-hex/EtOAc (3:1) fraction and *n*-hex/EtOAc (1:1-1:3) fraction from leaves of the same plant showed good to moderate antileishmanial activity with IC$_{50}$ values ranges from 9.19 to 47.77 µg/mL. Ethyl acetate fraction was the most active (IC$_{50}$ = 9.19 µg/mL) with the good selectivity (SI>10), the compounds obtained from these active fractions globally showed potent antileishmanial activity with IC$_{50}$ values range from 8.66 to 50 µg/mL. The (1:1) mixture of tachioside (**71**) and isotachioside (**72**) (IC$_{50}$ = 8.66 µg/mL), (1:1) mixture of isoxanthochymol (**69a**) and cycloxanthochymol (**69b**) (IC$_{50}$ = 4.77 µg/mL) and lupeol (**62**) exhibited the best activity with an IC$_{50}$ value of 44.43 µg/mL. From these results, the good activity of CH$_2$Cl$_2$-MeOH (1:1) extract could be due to the synergetic effect of it constituents. Previous works carried out by other research groups on other plant isolates gave results that corroborate with those obtained from this study. In effect, isoxanthochymol isolated from the stem bark of *Garcinia griffithii* was reported to exhibit activity against *L. infantum*, with an IC$_{50}$ value of 1.22 µg/mL (Elfita *et al.*, 2009). Thus, the activity of the (1:1) mixture of isoxanthochymol (**69a**) and cycloxanthochymol (**69b**) could be due to antagonist effect.

II.3.1.3 Antileishmanial activity and cytotoxicity from the CH$_2$Cl$_2$/MeOH (1:1) crude extract of stem bark of *A. lobata* against *Leishmania donovani* 1S (MHOM/SD/62/1S) promastigotes

Table LVII: Antileishmanial activity and cytotoxicity of the crude extract, fractions, and isolates of the stem bark of *A. lobata*

Extract, fraction or compounds	$IC_{50} \pm SD$ (μg/mL)	CC_{50} on Vero Cells (μg/mL $\pm$ SD)	SI (CC_{50}/IC_{50})
CH_2Cl_2/MeOH extract	21.17 ± 0.05	>100	>4.72
n-hexane fraction	>100	NA	ND
Dichloromethane fraction	>100	NA	ND
Ethyl acetate fraction	34.42 ± 0.13	>100	>2.91
n-butanol fraction fraction	>100	NA	ND
methanol fraction	>100	NA	ND
Adeniamide (**54**)	>50	NA	ND
D-mannitol (**88**)	>50	NA	ND
Germanicol ester caffeoyl (**55**)	6.03 ±0.19	>100	>16.58
Vanillic acid (**74**)	>50	NA	ND
β-sitosterol-3-*O*-*β*-D-glucopyranoside (**92**)	>50	NA	ND
Stigmasterol (**90**) and *β*-sitosterol (**91**)	>50	NA	ND
Amphotericin B	**0.14 ± 0.13**		

Legends: IC_{50} values against *Leishmania donovani* 1S(MHOM/SD/62/1S) promastigotes

■= Highly active   ■ = Good active   ■= moderately active   □ = Inactive

The stem bark extract of *A. lobata* showed good activity against *Leishmania donovani* 1S (MHOM/SD/62/1S) promastigotes with an IC_{50} value of 21.17 μg/mL. The fractionation of this crude extract yielded five fractions among which ethyl acetate fraction exhibited the best potency with IC_{50} value of 34.42 μg/mL. Germanicol caffeoyl ester (**55**) obtained from this fraction, displayed the best activity against *L. donovani* with an IC_{50} value of 6.03 μg/mL (Table LVII). However, most of the tested samples were selective (SI >1) against Vero cells. Additionally, the results obtained from the crude extract in this study were in line with those obtained by others authors in the literature. In fact, Okpekon and collaborators (2004) demonstrated that leaves and stem methanol extracts of *A. lobata* were inactive on *L. donovani* promastigotes with EC_{50}>100 μg/mL but the methylene chloride extract of the leaves of *A. lobata* was active on the same strain with EC_{50} values of 50 μg/mL (Okpekon *et al.*, 2004).

Other biological activities where carried out in our work in collaboration with biochemists and biologists.

II.3.2 Antiplasmodial activity

The thresholds for the antiplasmodial activity were based on the established criteria by Batista and collaborators. According to these authors, **IC$_{50}$<1μM** indicates compound with **excellent/potent** activity; IC$_{50}$ of **1-20 μM**, **good** activity; IC$_{50}$ of **20-100 μM**, **moderate** activity; IC$_{50}$ of **100-200 μM**, **low** activity; and **IC$_{50}$ > 200 μM**, **inactive** (Batista *et al*., 2009).

For the crude extract, we have **Highly** activity if **IC$_{50}$ ≤ 5 μg/mL**; **Promisingly** activity if **IC$_{50}$ 5.1-10 μg/mL**; **Good** activity if **IC$_{50}$ 10.1-20 μg/mL**; **Moderate** activity if **IC$_{50}$ 20.1-40 μg/mL**; **Marginal potency** if **IC$_{50}$ 40.1-70 μg/mL** and **Poor or Inactive** if **IC$_{50}$ 70.1-100 μg/mL** (Singh *et al*., 2015).

II.3.2.1 Antiplasmodial activity and selectivity of stem bark and leaves extracts and compounds of *E. calophylloides* against *Plasmodium falciparum* 3D7 and Dd2

Table LVIII: Antiplasmodial activity and selectivity of stem bark of *E. calophylloides* against *P. falciparum* 3D7 and Dd2

Plant part	Extract, fractions and compounds	EC$_{50}$ ± SD (µg/mL) Pf3D7	EC$_{50}$ ± SD (µg/mL) PfDd2	CC$_{50}$ on Vero Cells (µg/ml± SD)	SI Pf3D7 (PfDd2)
Stem bark of *E. calophylloi des*	CH$_2$Cl$_2$-MeOH crude extract	4.96±1.33	8.54±3.36	> 100	-
	Hexan fraction	4.66±1.50	5.16±0.43	26.62±1.90	5.71 (5.15)
	CH$_2$Cl$_2$ fraction	5.85±0.64	3.82±0.88	22.97±1.97	3.93 (6.01)
	EtOAc fraction	0.45±0.08	5.98±1.83	>100	>222.22 (>16.71)
	n-butanol fraction	41.25±0.00	25.98±0.13	>100	>2.42 (>3.85)
	Canophyllol (**57**)	>20	10.69±0.00	-	-
	Mixture of ixoxanthochymol (**69a**) and cycloxanthochymol (**69b**)	1.34±0.21	0.78±0.28	7.88±0.55	5.88 (10.10)
	Morellofavone (**67**)	16.79±0.14	5.99±0.21	>50	>2.98 (>8.35)
	Friedelin (**56**)	>20	>20	-	-
	β-amyrin palmitate (**61**)	> 20	> 20	-	-
	3,3´-*O*-dimethylellagic acid (**89**)	1.40±0.14	0.45±0.50	>50	-
	Marsformoxide B (**59**)	> 20	>20	-	-
	Lupenone (**63**)	> 20	> 20	-	-
References drugs	**Artemisinin (*µ*M)**	**0.014±0.0001**	**0.018±0.0003**	**NA**	
	Chloroquine(*µ*M)	**0.018±0.0002**	**0.449±0.065**	**NA**	
	Podophyllotoxine	**NA**	**NA**	**1.89±0.38**	

Pf: *Plasmodium falciparum*; NA: not applicable; EC$_{50}$: 50% Effective Concentration; CC$_{50}$: 50% Cytotoxicity Concentration; Selectivity Index SI calculated as CC$_{50}$Cell line/EC$_{50}$*Plasmodium* strain

Legends: EC$_{50}$ values aginst *Plasmodium falciparum* 3D7 and Dd2
■= Highly active   ■ = Good active   ■= moderately active   □ = Inactive

Table LIX: Antiplasmodial activity and selectivity of leaves of *E. calophylloides* against *Plasmodium falciparum* 3D7 and Dd2

Part plant	Solvent or Name of Compound	EC$_{50}$ ± SD (μg/mL) *Pf*3D7	EC$_{50}$ ± SD (μg/mL) *Pf*Dd2	CC$_{50}$ on Vero Cells (μg/ml± SD)
Leaves of *E. calophylloides*	CH$_2$Cl$_2$-MeOH crude extract	15.91 ± 0.67	11.77 ± 2.59	> 100
	n-hexane fraction	> 50	> 50	NA
	n-Hex/ EtOAc (3:1) fraction	7.62 ± 0.21	5.00 ± 1.20	34.40 ± 10.79
	n-Hex/ EtOAc (1:1-1:3) fraction	8.53 ± 0.28	5.81 ± 0.58	29.89 ± 10.24
	EtOAc fraction	> 50	> 50	NA
	EtOAc /MeOH (9:1) fraction	25.98± 2.61	31.61± 0.00	NA
	EtOAc /MeOH (75:25) fraction	> 50	> 50	NA
	MeOH fraction	> 50	> 50	NA
	Lupeol (**62**)	> 20	> 20	NA
	β-amyrin (**60**)	> 20	> 20	NA
	4′-methylamentoflavone (**65**)	> 20	11.06±1.2	NA
	Amentoflavone (**66**)	> 20	8.58±2.21	NA
References drugs	**Artemisinin (μM)**	**0.014±0.001**	**0.018±0.003**	**NA**
	Chloroquine(μM)	**0.018±0.002**	**0.449±0.065**	**NA**
	Podophyllotoxine	**NA**	**NA**	**1.89±0.38**

Pf: *Plasmodium falciparum*; NA: not applicable; EC$_{50}$: 50% Effective Concentration; CC$_{50}$: 50% Cytotoxicity Concentration; Selectivity Index SI calculated as CC$_{50}$Cell line/EC$_{50}$ *Plasmodium* strain

Legends: EC$_{50}$ values aginst *Plasmodium falciparum* 3D7 and Dd2

■= Highly active   ■ = Good active   ■= moderately active   □ = Inactive

    The methanolic stem bark and leaves extracts of *E. calophylloides* exhibited promising antiplasmodial efficacy against both chloroquine sensitive *P. falciparum* 3D7 and chloroquine resistance *P. falciparum* Dd2 strains. These results corroborate those of Ngouamegne *et al* who showed that hexane, ethyl acetate and methanol crude extracts from stem bark of *E. calophylloides* exhibited potent antiplasmodial score against the chloroquine-resistant W2 strain of *P. falciparum* with respective IC$_{50}$ values 9.3±1.0; 7.4±0.6 and 12.8±1.0 μg/mL (Ngouamegne *et al.*, 2008).

    3,3′-*O*-dimethylellagic acid (**89**) exhibited the best antiplasmodial effect against both *P. falciparum* parasite species and it did not show significant signs of cytotoxicity. However,

this compound belongs to the ellagic acid, a class of polyphenol compounds, well recognized by their antiplasmodial properties. In fact, ellagic acid and it derivatives have been reported by many authors to display *in vitro* as well as *in vivo* antiplasmodial activities without toxicity (Banzouzi *et al*., 2002; Ndjonka *et al*., 2012; Reddy *et al*., 2007; Simões-Pires *et al*., 2009; Soh *et al*., 2009). On the other hand, Kunert *et al* (2008), showed that the amamentoflavone exhibited an $IC_{50} > 9.3$ μg/mL on the *P. falciparum* K1 strain, which corroborates with our result. Likewise, 4´-*O*-methylamentoflavone showed good activity on the same strain with an IC_{50} value of 0.3 μg/mL and Ngouamegne and collaborators, showed that morelloflavone exhibited a good activity against *P. falciparum* W2 with an IC_{50} value of 23.6 μM (Ngouamegne *et al*., 2008).

II.3.2.2 Antiplasmodial activity of stem bark of *A. lobata* against *Plasmodium falciparum* 3D7

Table LX: EC$_{50}$ of extract and fractions of *A. lobata* (μg/mL) against *Pf* 3D7

	Sample	EC$_{50}$ (μg/mL)
Extract	CH$_2$Cl$_2$-MeOH (1:1)	27.58 ±3.25
Fractions	*n*-Hex	>50
	CH$_2$Cl$_2$	>50
	EtOAc	**7.39±0.38**
	n-BuOH	**16.99±2.47**
	methanol	>50
Artemisinin (nM)*	Art	**14.47±1.84**

Legends: Antiplasmodial activity (EC$_{50}$ in μg/mL)

■= Highly active   ■ = Good active   ■= moderately active   □ = Inactive

The CH$_2$Cl$_2$-MeOH (1:1) crude extract inhibited parasite growth with EC$_{50}$ value of 27.58 ± 3.25 μg/mL, meanwhile, two out the five obtained fractions, EtOAc and *n*-BuOH soluble fractions exhibited interesting activities with EC$_{50}$ of 7.39 ± 0.38 and 16.99 ± 2.47 μg/mL, respectively. None of the isolates was active. The antiplasmodial efficacy of the active fractions seems to be increased with regard to the crude extract. Likely explanation is that the activities of the fractions may be due to the minor constituents or to the antagonism effect of the components within the crude extract. Our findings justify the use of *A. lobata* in ethnomedicine for the treatment of malaria and related symptoms such as fever (Kipré *et al*., 2017; Kipré *et al*., 2018; Fowa *et al*., 2019).

II.3.3 Antibacterial activity

The activity of plant extracts is classified as **significant** if **(MIC < 100 µg/mL),** **moderate** if **(100 < MIC≤ 625 µg/mL)** and **weak** if **(MIC > 625 µg/ mL)** and the antibacterial activity of compound is **strong**, **moderate** and **weak** if the MIC of the plants is **≤ 10 µg/mL**, **10 < MIC ≤ 100 µg/mL** and **> 100 µg/mL**, respectively (Kuete *et al.*, 2011).

II.3.3.1 Antibacterial activity (MIC, µg/mL) of extracts and compounds from the stem bark and fruits of *P. butyracea*

Table LXI: Antibacterial activity (MIC, µg/mL) of extracts and compounds from the stem bark and fruits of *P. butyracea*.

Extracts/ compounds	Antibacterial activity (MIC in µg/mL)					
	S. thyphi	*S. aureus*	*E. cloacae*	*P. aeruginosa*	*S. pneumoniae*	*E. coli*
CH₂Cl₂-MeOH (1:1) fruits extract	-	125	500	500	500	500
CH₂Cl₂-MeOH (1:1) stem bark extract	7.8	15.6	7.8	7.8	31.2	15.6
Daphnifolin (**77**)	-	-	500	-	-	-
Norathyriol (**76**)	250	31.2	62.5	250	-	125
Epicathechin (**68**)	-	250	500	-	-	-
β-sitosterol-3-*O*-*β*-D-glucopyranoside (**92**)	-	250	-	250	250	500
Tovopyrifolin C (**78**)	-	-	250	-	-	-
Cowargarcicone (**80**)	125	15	125	250	125	125
α-mangostin (**79**)	< 3.9	< 3.9	3.9	3.9	3.9	3.9
Ciprofloxacin	0.03	0.15	0.06	0.07	0.03	0.03

*Salmonella typhi (CPC and CHU), Enterobacter cloacae (CPC), Pseudomonas aeruginosa HM801, Staphylococcus aureus (CPC), Streptococcus pneumoniae ATCC 491619; E coli ATCC 25322
* CPC: "Centre Pasteur" of Cameroon
* CHU: "Centre Hospitalier Universitaire" of Cameroon.

Legends: Antibacterial activity (MIC in µg/mL)
■= Highly active   ■ = Good active   ■= moderately active   □ = Inactive

The fruits and stem bark extracts as well as some of the isolates were assessed for their antibacterial activity on six bacteria strains*: Escherichia coli* ATCC 25322, *Streptococcus pneumoniae* ATCC 491619, *Pseudomonia aeruginosa* HM801, *Salmonela typhi* (CPC and CHU), *Enterobacter cloacae* (CPC), and *Staphylococcus aureus* (CPC). The stem bark extract exhibited significant activity against the six strain*s*, with MICs values ranging from 7.8 to 15.6 µg/mL, while fruits extract was moderately active (Table LXI). *α*-mangostin (**79**) showed a good activity against the six strains with MICs ≤ 3.9 µg/mL. These results are quite similar

with those obtained by Koh and collaborator (2013) which showed that, α-mangostin isolated from the fruits of *G. mangostana* exhibited good activity against Gram-positive pathogens with MICs values between 0.78 and 1.56 μg/mL (Koh *et al*., 2013). These evidences contribute to reinforce the knowledge on the potential of xanthone as potent antibacterial agents and thus, should draw awareness in the perspective of the search for new broad spectrum antibacterial agent from plant origin. In addition, it provides an insight that can justify the use of this plant in traditional medicine to treat skin and bacterial diseases (Araújo *et al*., 2019; Dharmaratne *et al*., 2013).

II.3.4 Acute toxicity

II.3.4.1 Effects on some clinical parameters on rats

Table LXII: Effects on some clinical parameters

Parameters	Witness			EC 2000 mg/kg			EC 5000 mg/kg		
	30 min	4 hours	14 days	30 min	4 hours	14 days	30 min	4 hours	14 days
Number of deaths	0	0	0	0	0	0	0	0	0
Thrill	-	-	-	-	-	-	-	-	-
Aggressiveness	-	-	-	-	-	-	-	-	-
Mobility	+	+	+	+	+	+	+	+	+
Appearance of faeces	N	N	N	N	N	N	N	N	N
Horripilation	-	-	-	-	-	-	-	-	-
Touch sensitivity	+	+	+	+	+	+	+	+	+
Noise sensitivity	+	+	+	+	+	+	+	+	+

N= normal, + = Present, - = Absent

The table LXII above shows the effects of the administration in rats of *E. calophylloides* extract at doses of 2000 and 5000 mg/kg on some clinical signs observed during the 14 days of the experiment. According to this table, it is noted that the plant extract was not harmless or showed no sign of toxicity with regard to the clinical parameters evaluated. Animals given the hydroethanolic plant extract did not show aggression and chills. In addition, animals that received the plant extract in the same way as normal animals that received distilled water show normal stool appearance, sensitivity to sound and touch, and mobility. The extract also shows zero lethality at doses of 2000 and 5000 mg/kg.

II.3.4.2 Effects on weight gain
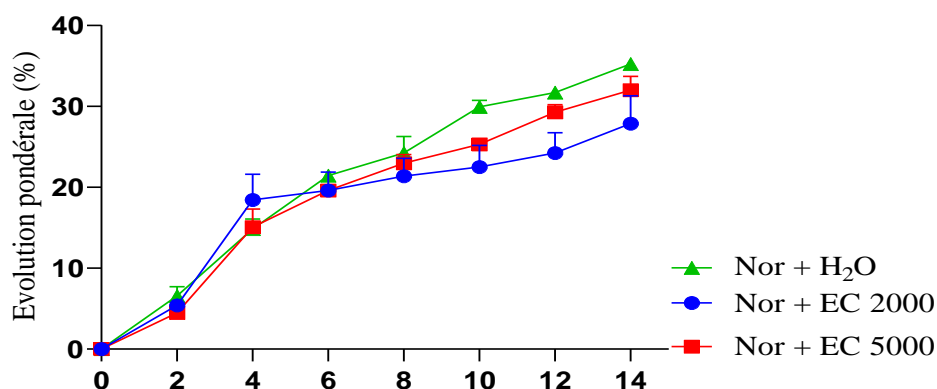
Each value represents the mean ± ESM; n = 3; Nor + H$_2$O: healthy rats treated with distilled water; Nor + EC 2000, Nor + EC 5000: rats treated with hydroethanolic extract of *E. calophylloides* at the respective doses of 2000 and 5000 mg/kg.

Figure 188: Effects of the hydroethanolic extract of *E. calophylloides* on the weight development of acutely toxic rats

The figure above shows the effects of the administration of the hydroethanolic extract of *E. calophylloides* on the weight gain of rats. According to this figure, there is a non-significant variation in body weight from day 0 to day 14 in normal rats treated having received the plant extract at different doses of 2000 and 5000 mg/kg compared to normal rats treated with distilled water.

II.3.4.3 Effects on the relative weight of certain organs
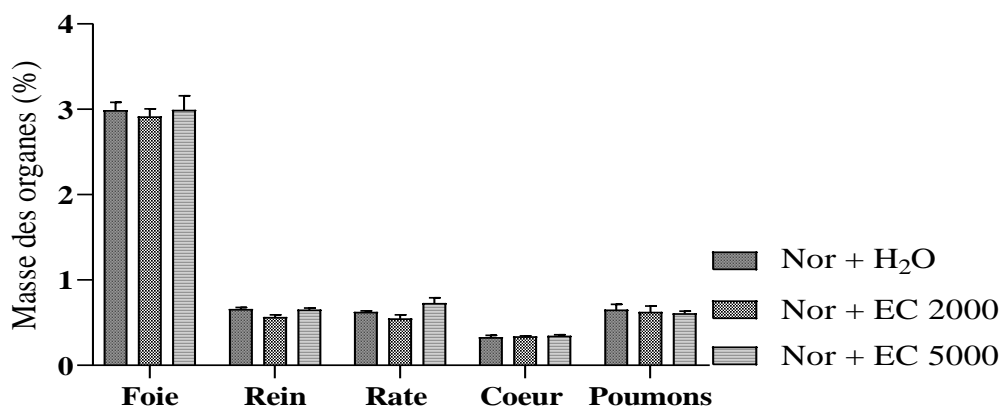
Each value represents the mean ± ESM; n = 3; Nor + H$_2$O: healthy rats treated with distilled water; Nor + EC 2000, Nor + EC 5000: rats treated with hydroethanolic extract of *E. calophylloides* at the respective doses of 2000 and 5000 mg/kg.

Figure 189: Effects of the hydroethanolic extract of *E. calophylloides* on the relative weight of rats in acute toxicity

The figure above is an illustration of the effects of administration of the extract on the relative mass of the liver, kidney, heart and lung of rats treated with the hydrethanolic extract of acutely toxic *E. calophylloides*. According to this figure, the administration for 14 days of the plant extract did not cause any significant variation in the relative mass of the various organs mentioned above compared to normal animals given distilled water.

The present study was also conducted to assess the toxic effects of acute toxicity of hydroethanolic extract of *E. calophylloides* in female rats. This extract at the tested limit doses of 2000 and 5000 mg/kg did not cause any death during the 14 days of experimentation, indicating that the Lethal Dose 50 (LD$_{50}$) of *E. calophylloides* is greater than 5000 mg/kg. In addition, no apparent signs of toxicity, neither on the behavior of the animals, nor on the clinical signs observed, nor on the body weight of the animals, nor on the relative weight of the organs involved in the toxicity were noted. In addition, slight differences in color observed on the macroscopic appearance of the organs after dissection are believed to be due to the specific physiology of each animal. Indeed, WHO has reported that almost all medicinal plants are non-toxic due to their regular and common use in traditional pharmacopoeia (OMS, 2000). Our results are in close agreement with WHO data suggests that the hydroethanolic extract of *E. calophylloides* would be classified according to the Globally Harmonized Classification System (SCGH) as category 5 of substances of low or no toxicity (OCDE, 2001).

II.3.5 Pre-formulation assay

The objective of this work was, among other things, to develop a phytomedicine. The evaluation of the activities of the extracts (evaluation of the antileishmanial activity and of the acute toxicity) having led to encouraging results, it seemed judicious to us to attempt a pre-formulation.

After carrying out the *in vitro* tests on the *Leishmania donovani* 1S (MHOM/SD/62/1S) promastigotes strain, the results obtained showed that the stem bark of *E. calophylloides* was a good candidate for the pre-formulation of a phytomedicine. Thus, the acute toxicity test was first performed as well as the *in vivo* test. At the end of these tests, the extract showed no sign of toxicity, and it also shows zero lethality at doses of 2000 and 5000 mg/kg. To optimize the use of our plant material, we have preformulated our phytomedicine using the smallest curative dose 3.43 mg/kg. The protocol used was that of Reagan-Shaw and collaborators, set up in 2007, entitled "Dose translation from animal to human studies revisited". The following formula was used:

Formula for Dose Translation Based on BSA
HED (mg/kg) = Animal dose (mg/kg) $\times \dfrac{Animal\ Km}{Human\ Km}$

In the present case, animal dose is 3.43 mg/kg. From the above formula, the Km factor are constant and known. The animal Km vary from one animal to another according to the species (Km of rat is 6 while the human Km is 37 for adult and 25 for child). Our phytodrug has been pre-formulated as a syrup (Reagan-Shaw *et al*., 2007), with the consumable doses evaluated as follows. This operation has several steps:

1er step: Human effective dose calculation

HED = 3.4× 6/ 37 = 0.556 mg/kg.

2nd step: Calculation of the daily dose for an adult

D = HED × 60 = 0.556× 60 = 33.3729 mg/day

3th step: Preparation of simple syrup

The standard formula for a syrup saturated 6.7g of sugar for 3.3g of water. A total of 10g of simple syrup. It is advisable to use demineralized or deionized water.

4th step: Determination of quantity of each ingredient

- **Extract (active ingredient)**

The daily dose is 33.3729 mg for an adult. The normal concentration of the active ingredient is 1.3mg/mL. One teaspoon is 15 mL; i.e. a concentration of 19.5 g/15 mL. For our extract, we will have 33.3729 /3 = 11.1243 mg;

((11.1243/19500) × 15) = 0.0085 mg= of active ingredient per spoon in 15 mL of teaspoon

In a box of 100 mL we will have:

((0.0085 /15) × 100) = 0.057mg

- **Conservator or stabilizer (Sodium benzoate)**

It is advisable to vary the percentage of stabilizers in order to determine which stabilizes the product over a long period. This percentage varies between 0.05 and 0.5%.

- **For orange essence:** The percentage is standard for essences and is 0.5%.

- **For Aroma:** The percentage is also standard for aromas and is 0.1%.

- **Simple syrup:**

Its percentage is deducted from the percentages of the other ingredients:

% syrup = 100% - (% extract +% stabilizer +% orange essence +% flavor)

= 100% - (0.057% + 0.3% + 0.5% + 0.1%)

= 99.043

So, in 100 mg of phytomedicine, we will have 99.043 mg of saturated simple syrup (excipient), 0.057 mg of crude extract (active principle), 0.3 mg of sodium benzoate (preservative), 0.5 mg of orange oil (ingredient) and 0.1 mg of flavor (ingredient).

Figure 190: Phytodrugs preformulation trial

CONCLUSION AND PERSPECTIVES

This work focused on the chemical study of three Cameroonian medicinal plants with antileishmanial potency: *Endodesmia calophylloides* (Clusiaceae); *Pentadesma butyracea* (Clusiaceae) and *Adenia lobata* (Passifloraceae).

The aim was to search for active and non-toxic extracts, fractions or molecules that could be used in the pre-formulation of new therapeutic agents for the treatment of leishmaniasis.

The chemical investigation of these plant extracts carried out led to the isolation of 40 compounds characterized using the usual spectroscopic techniques (HR-ESI-MS, IR, 1D NMR and 2D NMR) and divided into 12 classes: 01 ceramide [among which a new derivative, adeniamide (**54**)], 09 xanthones, 10 triterpenoids, 04 flavonoids, 05 phenolic compounds, 02 benzophenones, 03 steroids, 03 fatty acids, 01 ellagic acid derivative, 01 Sugar, 01 monoglyceride.

The crude extracts of *E. calophylloides* (Clusiaceae), *P. butyracea* (Clusiaceae) and *A. lobata* (Passifloraceae), showed potent antiparasitic activity *in vitro* during preliminary screening against *Leishmania donovani* 1S (MHOM/SD/62/1S) promastigotes with IC_{50} values ranging from 5.96-26.43 μg/mL and for their good selectivity towards Raw 264.7 macrophage and Vero Cells (SI>4.11). The bioguided fractionation of extracts of *E. calophylloides* (Stem bark and leaves), *P. butyracea* (Stem bark and fruits) and *A. lobata* (Stem bark) led to fractions which showed good to moderate activities with IC_{50} values ranging from 2.71 to 100 μg/mL. Daphnifolin (**77**), epicathechin (**68**), α-mangostin (**79**), 9-hydroxycalabaxanthone (**81**), germanicolcaffeoyl ester (**55**), mixture (1:1) of isoxanthochymol (**69a**)/cycloxanthochymol (**69b**) and mixture (1:3) of tachioside (**71**)/isotachioside (**72**) exhibited potent antileismanial activity against *L. donovani* 1S (MHOM/SD/62/1S) promastigotes with IC_{50} values of 2.01, 9.09, 3.37, 6.87, 6.03, 4.77 and 8.66 μg/mL, respectively and good selectivity towards Raw 264.7 macrophage cells and Vero Cells (SI> 2.4).

In addition, the hydroethanolic extract of *E. calophylloides* at the tested limit doses of 2000 and 5000 mg / kg did not cause any death during the 14 days of experimentation, indicating that the Lethal Dose 50 (LD_{50}) is greater than 5000 mg/kg. Absicic acid β-D-glucoside (**70**) was

isolated for the first time from the Guttiferae family and interestingly, all the isolated compounds are herein reported for the first time from the genus *Adenia* and therefore provide new perspectives on the chemical diversity of plants of this genus. This result could justify the use of *P. butyracea, E. calophylloides* and *A. lobata*, in the treatment of the parasitic diseases of the skin and others infectious diseases.

We envisage in our perspectives:

- Continue with sub acute and chronic toxicities
- Continue to search a good galenic form for the suitable for the phytodrug
- Testing our syrup on *wistar* strain rats infected with leishmaniasis
- Preformulate the phytodrug

CHAPTER III: MATERIALS ET METHODS

CHAPTER III: MATERIALS ET METHODS

III.1 General experimental procedures

III.1.1 Chromatographic methods

The IR spectrum was obtained on a Tensor 27 FT-IR spectrometer (Bruker), while the high resolution mass spectra were obtained with an Agilent 6220 time-of-flight mass spectrometer (Agilent Technologies, Santa Clara, CA, USA) in extended dynamic range mode equipped with a Dual-ESI source, operating with a spraying voltage of 2.5 kV. ^{1}H and ^{13}C NMR spectra were recorded on 500 MHz and 125 MHz Bruker DRX 500 NMR spectrometer (Bruker, Rheinstetten, Germany), with tetramethylsilane (TMS) as internal reference, giving the chemical shifts in ppm and the coupling constants in Hertz. Column chromatography was performed on 230-400 mesh silica gel (Merck, Darmstadt, Germany), 70-230 mesh silica gel (Merck, Darmstadt, Germany), C_{18}-reversed phase silica gel (Sigma-Aldrich, Munich, Germany), and Sephadex LH-20 (Sigma-Aldrich, Munich, Germany). Thin layer chromatography (TLC) was performed on Merck 60 pre-coated silica gel on aluminum foil F254 (Merck). The crude extracts were concentrated on Heidolph rotary evaporators with a Vaccuubrand pump (PC 500 series) and using Lauda microcool (MC 250), as a water recycler. The extracts were lyophilized using Freeze dryer alpha 2-4 LD plus (Christ, Germany). Compounds were visualized under UV light at 254 or 365 nm, followed by spraying with dilute sulfuric acid solution (10%) and heating. All reagents used were of analytical quality. The various masses obtained were measured on an electronic balance of the "Cobos" type (for the plant material, the crude extract and the various fractions) and Ohaus-Pioneer "type of precision 0.0001 (for the compounds obtained).

III.1.2 *In vitro* antileishmanial assay

Leishmania donovani 1S(MHOM/SD/62/1S) promastigotes were cultivated at 28°C in axenic M199 culture medium (Sigma Aldrich) supplemented with 10% heat-inactivated fetal bovine serum (FBS) (Sigma Aldrich) and 1% streptomycin/penicillin (Sigma Aldrich). The antileishmananial activity of test samples were determined as previously described (Siqueira-Neto *et al.*, 2010), using the resazurin-based assay. Compounds were serially diluted in incomplete M199 medium and 10 μL of each compound were introduced in 90 μL of *L. donovani* promastigotes (4×10^5 parasites) from an exponential phase culture in complete medium. They were all screened at final concentrations of 100-0.16 μg/mL for extracts and fractions and 5-0.08 μg/mL for compounds and test plates were incubated for 28 h at 28°C, followed by the addition of 1 mg/mL resazurin. The negative and positive controls were 0.1%

DMSO and amphotericin B (10-0.016 μg/mL), respectively. After an additional incubation of 44 h, plates were then read on a Magelan Infinite M200 fluorescence multi-well plate reader (Tecan) at an excitation and an emission wavelength of 530 and 590 nm, respectively. For each sample, growth percentages were calculated and dose-response curves were constructed to determine the 50% inhibitory concentration (IC$_{50}$) using the GraphPad-version 5.0 software. The results showed in table between LII and LVI, were discussed according to the classification established by Camacho *et al*. (2003) (IC$_{50}$ <10 μg/mL, extract is highly active; 10<IC$_{50}$<50 μg/mL, extract is good active; 50<IC$_{50}$<100 μg/mL, extract is moderately active; IC$_{50}$>100 μg/mL, extract is inactive) (Camacho *et al*., 2003).

III.1.3 *In vitro* antiplasmodial assay

The Chloroquine-sensitive 3D7 (MRA-102) and resistant *P. falciparum* Dd2 (MRA-150) strains were cultured in fresh O$^+$ human red blood cells at 3% haematocrit in complete RPMI 1640 medium [500 mL RPMI 1640 (Gibco, UK) supplemented with 25 mM HEPES (Gibco, UK), 0.50% Albumax I (Gibco, USA), 1X hypoxanthine (Gibco, USA) and 20µg/mL gentamicin (Gibco, China)] and incubating at 37°C in a humidified atmosphere with 5% CO$_2$. The culture medium was renewed daily to propagate the culture. The giemsa-stained thin blood smears were examined microscopically under oil immersion to monitor cell cycle transition and parasitaemia.

Before each experiment, synchronized ring stage parasites were obtained by 5% sorbitol (v/v) treatment as previously described (Lambros *et al*., 1979). The experiment with synchronized ring stage culture provided distinct observing growth inhibitory effect without a rise in parasitemia during the ring-trophozoite-schizont transitions.

The parasite susceptibility was determined in 96-well microtitration plates using the SYBR green I fluorescence-based method with some modifications (Smilkstein *et al*., 2004). Briefly, sorbitol-synchronized ring stage parasites (hematocrit: 1.5%, parasitemia: 1%) were incubated in the presence of two-fold diluted extracts (0.78-100µg/mL, DMSO 0.5%), fractions (0.39-50µg/mL, DMSO 0.5%) or compounds (0.15-20µg/mL, DMSO 0.5%). Artemisinin (98%, Sigma-Aldrich, Germany) and Chloroquine (98%, Sigma-Aldrich, Germany) were used as reference compounds at concentration ranges from 7.81-1000 nM. Drug-free culture wells in 0.5% DMSO were considered as positive growth controls. After 72h of incubation, 50 μL of SYBR Green I lysis solution [Tris (20 mM; pH 7.5)(Sigma-Aldrich), EDTA (5 mM)(Sigma-Aldrich), saponin (0.008%, w/v) (Sigma–Aldrich), Triton X-100 (0.08%, v/v) (Sigma-Aldrich) and SYBR Green (2×) (Life technologies)] were added to

each well and the plate was incubated in the dark at 37°C for 30 min. SYBR green I fluorescence was measured using a Fluoroskan Ascent multi-well plate reader (Thermo scientific) with excitation and emission wavelength bands set at 485 and 538 nm, respectively. The parasite growth percentages were generated via Microsoft excel, then a non-linear regression was used to determine the effective concentration (EC_{50}) that reduced 50% of parasite growth using GraphPad Prism software version 5.0 (San Diego, California).

III.1.4 *In vitro* antibacterial Assay

Antibacterial activity assays were conducted on a total of six bacterial strains, two from American type culture collection, *Escherichia coli* ATCC 25322 and *Streptococcus pneumoniae* ATCC 491619, one from BEI resources namely *Pseudomonia aeruginosa* HM801 and finally three clinical isolate strains from laboratory collection namely *Salmonela typhi* (CPC and CHU), *Enterobacter cloacae* (CPC), and *Staphylococcus aureus* (CPC). They were assessed for their susceptibility to extracts/compounds. The tests were performed in duplicate, following the method by Eloff (1998) (Eloff, 1998). In a 96-well microplate, 100 μL of sterile culture broth (MHB) were introduced. Then 100 μL of each stock sample solution (2000 μg/mL) were added to the first wells and then distributed to all other wells, with concentrations ranging from 3.8 to 500 μg/mL and < 0.15 to 500 μg/mL for ciprofloxacin. Then 100 μL of liquid culture medium (MHB) inoculated with the test organism (2×10^6 CFU/mL) were introduced into the wells in order to obtain a final concentration of 10^6 CFU/mL. Ciprofloxacin was used as reference. The negative controls consisted of wells containing only the culture medium, and wells containing a mixture of culture broth and test organism. The culture microplates were covered and incubated at 37°C (18 hours). Twenty microliters (20 μL) of resazurin were then introduced into both and then incubated again at 37°C for 24h (Mativandlela *et al*., 2006). The antibacterial activity of compound is strong, moderate and weak if the MIC of the plants is ≤ 10 μg/mL, 10 < MIC ≤ 100 μg/mL and > 100 μg/mL, respectively. Whereas, the activity of plant extracts is classified as significant if (MIC < 100 μg/mL), moderate if (100 < MIC≤ 625 μg/mL) and weak if (MIC > 625 μg/ mL) (Kuete *et al*., 2011).

III.1.5 Cytotoxicity Assay

The cytotoxicity of active natural products was assessed according to the protocol described by (Mosmann, 1983). The African green monkey normal kidney Vero cells (ATCC CRL 1586) and murine macrophages *Raw* 264.7cell (ATCC #TIB-71) were maintained in T-25 flasks (Corning Incorporated, USA) using complete Dulbecco's Modified Eagle's Medium

(Sigma-Aldrich, Germany), supplemented with, 10% Fetal Bovine Serum (Sigma-Aldrich, Germany), 0.2% sodium bicarbonate (w/v) (Sigma-Aldrich, Germany) and 1% (v/v) Penicillin-Streptomycin (Sigma-Aldrich, Germany). The cells were kept at 37°C for 72 hours in 5% CO_2 incubator, and the medium was renewed every 72 h and the cell density monitored under the inverted fluorescent microscope Etaluma 520 (Etaluma, USA) until the formation of a monolayer. Confluent culture (nearly 90%) was trypsinized (0.05% Trypsin-EDTA, Sigma-Aldrich, Germany), then centrifuged at 1800 rpm for 5 minutes and the resulting pellet was re-suspended in culture medium. Cells at 10^4cells per well were seeded (100μL) in 96-well culture plates (Costar, USA) and incubated overnight to allow cell adhesion. Thereafter, 10 μL of serially diluted extracts, fractions (≤200 μg/mL), and compounds (≤50 μg/mL) were added to plate wells in duplicate. The plates were incubated in a humidified and 5% CO_2 atmosphere at 37°C for 48h. Podophyllotoxin at 20μM was added as positive control and wells containing untreated cells were included as 100% growth control. Ten microliters of Resazurin stock solution (0.15 mg/mL in sterile PBS), were added to each well, and incubated for an additional 4 h. Fluorescence was then read using a Magelan Infinite M200 fluorescence multi-well plate reader (Tecan) with excitation and emission wavelengths at 530 and 590 nm, respectively. The percentage of cell viability was calculated with regard to the negative control, and subsequently used to determine the concentration that reduced 50% of cell viability (CC_{50}) by non-linear regression using the GraphPad Prism software version 5.0 (San Diego, California).

III.1.6 Acute toxicity

The study was performed according to the protocol of OCDE (2001) according to guideline 423. For this toxicity study, 9 adult, non-pregnant female rats were used. These animals were randomly divided into 3 groups of 3 animals each, of which group 1, taken as a test control, was treated with distilled water at a single dose of 10 mg/kg; the other two groups (test batches) for their part received the extract at the respective single doses of 2000 and 5000 mg/kg. The animals were fasted without water 12 hours before the start of the experiment and 4 hours after. Oral administration of the extract and distilled water was done through a gastric tube. After administration, animals were observed individually for the first 4 hours and daily for 14 days after treatment. Particular care should be taken during the first 30 minutes after administration of the substance. Any signs of immediate toxicity such as aggressiveness, mobility, possible tremors, changes in coat, convulsions and other apparent signs of toxicity were noted during the experiment as well as changes in body weight. At the

end of the experiment, the animals were sacrificed, their organs (liver, kidneys, spleen, lungs and heart) were removed and weighed in order to perform a macroscopic autopsy (OCDE, 2001).

III.2 Some characteristic tests used in the identification of secondary metabolites

III.2.1 Libermann-Burchard test

The purpose of this test is to identify triterpenoids and steroids. The reagents used are chloroform ($CHCl_3$), acetic anhydride [$(CH_3CO)_2O$], and concentrated sulfuric acid (H_2SO_4).

Procedure: The dry residue was dissolved in 3 mL of chloroform. After having stirred it, the mixture was filtered and then distributed into 2 test tubes, the first of which serves as a control. Two drops of acetic anhydride were added in the second tube. The mixture is slightly stirred, then few drops of H_2SO_4 (36 N) have been added it.

Results and interpretation: The evolution of the coloration is observed for 15 min. The greenish coloration indicates the presence of steroids, while the appearance of a red or pink color indicates the presence of triterpenoids.

III.2.2 Shinoda test

The purpose of this test is to identify flavonoids. The reagents used are methanol, concentrated hydrochloric acid (HCl), magnesium shavings (Mg).

Procedure: In 4 mL of methanol contained in a test tube, a small amount of the extract or compound was dissolved. To the resulting solution were added a few drops of concentrated hydrochloric acid (HCl) and few shavings of magnesium.

Results and interpretation: The presence of flavonoids is evidenced by the appearance of a brick-red or violet color.

III.2.3 Ferric chloride test

The purpose of this test is to identify phenolic compounds. The reagents used are ethanol and ferric (III) chloride ($FeCl_3$).

Procedure: In 5 mL of ethanol contained in a test tube, a small amount of the extract or compound was dissolved. Then a few drops of the ferric chloride ($FeCl_3$) solution were added to the solution obtained.

Results and interpretation: Gradually, the reaction medium takes on a blue or purple color (transient or permanent) due to the formation of a complex of the type $[Fe(ArO)_6]^{3-}$, which indicates the presence of hydroxyl groups free phenolics. The formation of this complex is done according to the equation:

$$6 \text{ Ar-OH} + \text{FeCl}_3 \longrightarrow [\text{Fe(Ar-O)}_6]^{3-} + 3\text{H}^+ + 3\text{HCl}$$

III.2.4 Molish test

The purpose of this test is to identify sugars. The reagents used are ethanol (C_2H_5OH), α-naphthol $C_{10}H_8O$ and concentrated sulfuric acid (H_2SO_4).

Procedure: In a tube, a small amount of the product was dissolved with a solution of 1% ethanol-α-naphthol. Then on the walls of the tube, few drops of concentrated sulfuric acid were allowed to run.

Results and interpretation: The presence of sugars was indicated by the appearance of a purplish red ring at the interphase.

III.3 Harvesting, extraction, fractionation and isolation of compounds

III.3.1 Harvesting

The stem bark and leaves of *E. calophylloides* Benth., the stem bark and fruits of *P. butyracea* Sabine and the stem bark of *A. lobata* (Jacq.) Engl. were harvested in May-October 2018 at Mbalmayo, Bazou and Ngoumou, respectively, in the Center and West Region of Cameroon. The plant materials were identified by Mr. Victor Nana, botanist at the National Herbarium of Cameroon, by comparison with the voucher specimens formerly kept at the National Herbarium under the registration number 29528/HNC, 6861/SRF/Cam and 43292/HNC, respectively.

III.3.2 Extraction

III.3.2.1 Preparation of extracts of *E. calophylloides*

The leaves of *E. calophylloides* were dried and then crushed, the bark of the trunk were cut up, dried and then crushed. The powders obtained: 5.2 kg (leaves), and 5.2 kg (bark of the trunk) were extracted separately by maceration in MeOH twice for 48 hours. The volumes of the solvents are: 35 L (leaves), 30 L (stem bark) at room temperature (about 25°C). After evaporation of the various filtrates on a rotary evaporator, 341.9 g and 587.2 g of extracts were obtained respectively.

III.3.2.2 Preparation of extracts of *P. butyracea*

The fruits and stem bark of *P. butyracea* were chopped into pieces, air dried under shade, and ground to give 4.8 and 3.5 kg of powder, respectively, and were separately macerated with (1:1) CH_2Cl_2/MeOH (3×5 L) twice for 48 hours at room temperature (26°C).

The extracts of fruits and stem bark were freed from solvent under vacuum to yield 210.7 and 190.8 g, respectively.

III.3.2.2 Preparation of extracts of *A. lobata*

The stem bark of *A. lobata* was chopped, air-dried and ground. The resulting powder (1.1 kg) was extracted by maceration with CH_2Cl_2-MeOH (1:1) (10 L) (2 days, repeated three times) at room temperature (about 26°C). The extract was freed from solvent under vacuum at low temperature (40°C) to give 114.1 g.

III.3.3 Fractionation and isolation of compounds

III.3.3.1 Fractionation and isolation of compounds of *E. calophylloides* (stem bark and leaves)

III.3.3.1.1 Fractionation and isolation of compounds of stem bark of *E. calophylloides*

The stem bark crude extract was submitted to bioguided fractionation towards *L. donovani* 1S (MHOM/SD/62/1S) promastigotes strain. 340.1 g was partitioned in different solvents to give five fractions including the *n*-hexane fraction (F1, 32.1 g), the dichloromethane fraction (F2, 29.3 g), the ethyl acetate fraction (F3, 93.9 g), the *n*-butanol fraction (F4, 85.4 g), and the water-soluble residue (F5, 95.8 g) (Table LXII). All these fractions were assessed for their antileishmanial activity against *L. donovani* strain and all fractions except the aqueous residue, showed good activity. The four active fractions were investigated using usual chromatographic methods of separation to afford 15 compounds.

Table LXIII: Chromatogram of MeOH extract of the stem bark of *E. calophylloides*

Solvent	Series	Fractions	Remarks
n-Hex	1-8	F$_1$	Mixture of oily products
CH_2Cl_2	9-14	F$_2$	Mixture of about six compounds
EtOAc	15-19	F$_3$	Mixture of about five compounds

	20-23	F$_4$	Mixture of about seven compounds
n-butanol			
Aqueous residus	24-28	F$_5$	Complex mixture

III.3.3.1.1.1 Chromatography of the fraction F1

Fraction F1 was dissolved in dichloromethane, then fixed on silica and chromatographed on a silica gel column. The 100 mL sub-fractions (in total 167) collected by elution with the *n*-hexane/EtOAc (1:0-0:1) polarity gradient system, have were collected and grouped on the basis of TLC profiles. By simple filtration, we obtained 4 products indexed **ECT1** (137.3 mg), **ECT2** (15.2 mg), ECT3 (150.1 mg) and **ECTF21** (15.5 mg) in the form of white powder (Table LXIV).

Table LXIV: Chromatogram of the *n*-hexane fraction

Eluent	Sub fractions	Remarks
n-Hex	1-29	Oily mixture from which **ECT1** precipitates
n-Hex/EtOAc (9:1-17:3)	30-91	Mixture of at least 3 products from which **ECT2** precipitates
n-Hex/EtOAc (4:1-3:2)	92-143	Mixture of at least 3 products including **ECT3** precipitates
n-Hex/EtOAc (1:1-0:1)	144-167	Complex mixture including **ECTF21** precipitates

III.3.3.1.1.2 Chromatography of the fraction F2

Fraction F2 was dissolved in methanol, then fixed on silica and chromatographed on a silica gel column. The 100 mL sub-fractions (in total 200) collected by elution with the *n*-hexane/EtOAc (95:5-0:1), and EtOAc/MeOH (1:0-0:1) polarity gradient system, have were collected and grouped on the basis of TLC profiles. By simple filtration, we obtained 3 products indexed **ECTF22** (4.4 mg), **ECT14** (5.1 mg) and **ECT23** (3.8 mg) in the form of white powder (Table LXV).

Table LXV: Chromatogram of the dichloromethane fraction

Eluent	Sub fractions	Remarks
n-Hex/EtOAc (19:1-17:3)	1-45	Mixture of at least 2 products from which **ECTF22** precipitates
n-Hex/EtOAc (4:1-7:3)	46-115	Mixture of at least 2 products from which **ECT23** precipitates
n-Hex/EtOAc (3:2-2:3)	116-153	Mixture of at least 3 products including **ECT14** precipitates

n-Hex/EtOAc (1:1-0:1) and EtOAc/MeOH (1:0-0:1)	154-200	Complex mixture

III.3.3.1.1.3 Chromatography of the fraction F3

Fraction F3 was dissolved in methanol, then fixed on on silica, was equally subjected to CC over silica gel and eluted with n-hexane/EtOAc (9:1-0:1), and EtOAc/MeOH mixture (1:0-0:1) and yielded subfraction F_{31} (mixture of 3 compounds) (152.3 mg). This subfraction was further subjected to Sephadex LH-20, eluted with CH_2Cl_2/MeOH (3:7) and led to obtained 3 products indexed **ECTF33** (659.2 mg), **ECTF24** (15.7 mg) and **EC9** (49.8 mg) in the form of yellow powder.

Table LXVI: Chromatogram of the ethyl acetate fraction

Eluent	Sub fractions	Remarks
n-Hex/EtOAc (1:1-3:7)	1-120	Mixture of 3 products whose separation was made by sephadex LH-20 and **ECTF33**, **ECTF24** and **EC9** were obtained.
EtOAc/MeOH (1:0-0:1)	121-241	

III.3.3.1.1.3 Chromatography of the fraction F4

Fraction F4 was subjected to purification using an open column chromatography over silica gel, C_{18}-reversed phase, and Sephadex LH-20 successively and eluted with the mixtures of n-hexane/EtOAc (3:2-0:1), EtOAc/MeOH (1:0-9:1), EtOAc/MeOH/H_2O, (18:2:1-7:3:1) MeOH/H_2O (1:1), and CH_2Cl_2/MeOH (3:7) to afford 4 compouds, indexed **ECTF41** (7.9 mg), **ECTF42** (5.2 mg), **ECTF93** (10.8 mg) and **ECTF44** in the form of marrone oil.

Table LXVII: Chromatogram of the n-butanol fraction

Eluent	Sub fractions	Remarks
EtOAc/MeOH (9:1)	1-35	Mixtures of several compounds
EtOAc/MeOH/H_2O (18:2:1)	36-112	About 3 products of which **ECTF41** precipitates after a reverse phase chromatography column, followed by LH-20 sephadex.
EtOAc/MeOH/H_2O (8:2:1)	113-195	About 4 products including **ECTF42** and **ECTF93** precipitate after a reverse phase chromatography column, followed by LH-20 sephadex

EtOAc/MeOH/H₂O (7:3:1)	196-215	About 2 products of which **ECTF44** precipitates after a reverse phase chromatographic column, followed by LH-20 sephadex

III.3.3.1.2 Fractionation and isolation of compounds of leaves of *E. calophylloides*

The leaves crude extract was submitted to bioguided fractionation towards *L. donovani* 1S (MHOM/SD/62/1S) promastigotes strain. 580.1 g was subjected to vacuum liquid chromatography and successively eluted with *n*-hexane, the mixtures of *n*-hexane/EtOAc (1:0-0:1), EtOAc and EtOAc /MeOH (1:0-0:1) of increasing polarities to give six fractions: F1 (*n*-hexane, 17.1 g); F2 [*n*-Hex/EtOAc (3:1), 83.5 g)]; F3 [*n*-HexEtOAc (1:1-1:3), 18.6 g]; F4 (EtOAc, 21.2 g), F5 [EtOAc/MeOH (9:1-4:1), 33.1 g]; F6 [EtOAc/MeOH (1:1-0:1), 20.5 g] (Table LXVII). All these fractions were assessed for their antileishmanial activity against *L. donovani* strain and fractions F2 and F3, displayed significant activity and were subjected to purification using an open column chromatography on silica gel. These active fractions gave 5 compounds.

Table LXVIII: Chromatogram of MeOH extract of leaves of *E. calophylloides*

Solvent	Series	Fractions	Remarks
n-hexane	1-15	F₁	Mixture of oily products
n-Hex/EtOAc (3:1)	16-28	F₂	Mixture of about three compounds
n-Hex/EtOAc (1:1-1:3)	29-64	F₃	Mixture of about five compounds
EtOAc	65-74	F₄	Complex mixture
EtOAc/MeOH (9:1-4:1)	75-81	F₅	Complex mixture
EtOAc/MeOH (1:1-0:1)	81-111	F₆	Complex mixture

III.3.3.1.2.1 Chromatography of the fraction F2

Fraction F2 was dissolved in dichloromethane, then fixed on silica and chromatographed on a silica gel column. The 100 mL sub-fractions (in total 229) collected by elution with the *n*-hexane/EtOAc (1:0-0:1) polarity gradient system, have were collected and grouped on the basis of TLC profiles. By simple filtration, we obtained 2 products indexed **ECF1** (15.6 mg) and **ECF23** (18.2 mg) in the form of white powder (Table LXVIII).

Table LXIX: Chromatogram of the *n*-hexane/EtOAc (3:1) fraction

Eluent	Sub fractions	Remarks
n-Hex	1-30	Oily mixture
n-Hex/EtOAc (9:1-8:2)	31-95	Mixture of at least 3 products from which **ECF23** precipitates
n-Hex/EtOAc (7:3-3:2)	92-138	Mixture of at least 3 products including **ECF1** precipitates
n-Hex/EtOAc (1:1-0:1)	139-167	Complex mixture

III.3.3.1.2.2 Chromatography of the fraction F3

Fraction F3 was dissolved in methanol, then fixed on silica and chromatographed on a silica gel column. The 100 mL sub-fractions (in total 274) collected by elution with the *n*-hexane/ CH_2Cl_2 (3:2-3:7), CH_2Cl_2/MeOH (1:0-4:1) polarity gradient system, have were collected and grouped on the basis of TLC profiles. By simple filtration, we obtained 3 products indexed **ECF43** (178.9 mg), **ECF44** (3.0 mg) and **EC6** (500.2 mg) in the form of yellow, yellow and white powders respectively (Table LXX).

Table LXX: Chromatogram of the *n*-Hex/EtOAc (1:1-1:3) fraction

Eluent	Sub fractions	Remarks
n-Hex/ CH_2Cl_2 (7:3)	1-60	Complex mixture
n-Hex/CH_2Cl_2 (3:2-3:7)	61-111	About 5 spots including **ECF43** obtained using the microcolumn
CH_2Cl_2/MeOH (1:0-9:1)	112-205	About 2 spots including **ECF44** obtained after a column of LH-20 sephadex
CH_2Cl_2/MeOH (4:1)	206-274	About 2 spots of which **EC6** crystallizes

III.3.3.2 Fractionation and isolation of compounds of *P. butyracea* (stem bark and fruits)

III.3.3.2.1 Fractionation and isolation of compounds of fruits of *P. butyracea*

The fruits crude extract was submitted to bioguided fractionation towards *L. donovani* 1S (MHOM/SD/62/1S) promastigotes strain. 205.1 g was subjected to flash chromatography over silica gel to afford four main fractions PBFF$_1$ [*n*-Hex/EtOAc (1:0), 80.5 g], PBFF$_2$ [*n*-Hex/EtOAc (1:1), 70.8 g], PBFF$_3$ [*n*-Hex/EtOAc (0:1), 15.6 g], and PBFF$_4$ [EtOAc/MeOH (4:1) to MeOH, 30.9 g] (Table LXXI). The four active fractions were investigated using usual chromatographic methods of separation to afford 15 compounds.

Table LXXI: Chromatogram of the mixture CH₂Cl₂/MeOH (1:1) extract of fruits of *P. butyracea*

Solvent	Series	Fractions	Remarks
n-hexane	1-15	F$_1$	Mixture of oily about three products
n-Hex/EtOAc (1:1)	16-28	F$_2$	Mixture of about six compounds
n-Hex/EtOAc (0:1)	29-64	F$_3$	Mixture of about seven compounds
EtOAc/MeOH (4:1-0:1)	75-81	F$_4$	Complex mixture

III.3.3.2.1.1 Chromatography of the fraction F1

Fraction F1 was dissolved in dichloromethane, then fixed on silica and chromatographed on a silica gel column. The 100 mL sub-fractions (in total 120) collected by elution with the *n*-hexane/EtOAc (1:0-0:1), and CH₂Cl₂/MeOH (1:0-8:1) polarity gradient system, have were collected and grouped on the basis of TLC profiles. By simple filtration, we obtained 2 products indexed **PBE4** (19.5 mg) and **PBE5** (14.2 mg) in the form of yellow powder (Table LXXII).

Table LXXII: Chromatogram of the *n*-hexane fraction

Eluent	Sub fractions	Remarks
n-Hex	1-6	Oily mixture
n-Hex/EtOAc (9:1-2:3)	7-91	Mixture of at least 3 products from which **PBE4** precipitates
n-Hex/EtOAc (3:7-0:1)	92-143	Mixture of at least 2 products from which PBE5 was obtained at a microcolumn with the CH₂Cl₂/MeOH (9:1) mixture as eluent
EtOAc/MeOH (9:1-0:1)	144-167	Complex mixture

III.3.3.2.1.2 Chromatography of the fraction F2

Fraction F2 was chromatographed on a silica gel column with mixtures *n*-Hex/EtOAc (7:3-0:1) as eluent. 100 mL sub-fractions (total 225) were collected and pooled based on the TLC profiles. The sub-fractions obtained were chromatographed on a Sephadex LH-20 gel column with a mixture of CH₂Cl₂/MeOH (9:1-4:1) as eluent and made it possible to obtain 4 compounds indexed **PBHF2** (9.5 mg), **PBE2** (14.2 mg), **PBHF4** (5.4 mg) and **PBHF** (340.0 mg), as a yellow powder (Table LXXIII).

Table LXXIII: Chromatogram of the *n*-Hex/EtOAc (1:1) fraction

Eluent	Sub fractions	Remarks
n-Hex/EtOAc (19:1-9:1)	1-25	Mixture of at least 3 products from which **PBHF2** precipitates
n-Hex/EtOAc (4:1-7:3)	26-98	Mixture of at least 2 products from which **PBE2** precipitates
n-Hex/EtOAc (3:2-0:1)	99-168	Mixture of at least 2 products from which **PBHF4** was obtained at a microcolumn with the CH_2Cl_2/MeOH (4:1) mixture as eluent
EtOAc/MeOH (9:1-0:1)	169-225	Mixture of at least 2 products from which **PBHF3** was obtained at a microcolumn with the CH_2Cl_2/MeOH (4:1) mixture as eluent

III.3.3.2.1.3 Chromatography of the fraction F3

Fraction F3 was chromatographed on a silica gel column with *n*-Hex/EtOAc (7:3-0:1) mixtures as eluent. 100 ml sub-fractions (total 299) were collected and pooled based on the TLC profiles. The sub-fractions obtained were chromatographed on a silica gel microcolumn with a mixture *n*-Hex/EtOAc (9:1-4:1) as eluent and made it possible to obtain 5 compounds indexed **PBF1** (9.5 mg), **PBER1** (6.5 mg), **PBF3** (68.4 mg), **PBF4** (420.0 mg) and **PBEF5**, as a yellow powder (Table LXXIV).

Table LXXIV: Chromatogram of the EtOAc fraction

Eluent	Sub fractions	Remarks
n-Hex/EtOAc (95:5-9:1)	1-29	Mixture of at least 2 products from which **PBEF5** precipitates
n-Hex/EtOAc (4:1-7:3)	30-99	Mixture of at least 3 products from which **PBER1** and **PBF1** precipitates
n-Hex/EtOAc (3:2-0:1)	100-174	Mixture of at least 2 products from which **PBF3** precipitates
EtOAc/MeOH (9:1-0:1)	175-299	Mixture of at least 2 products from which **PBF4** precipitates

III.3.3.2.2 Fractionation and isolation of compounds of stem bark of *P. butyracea*

The fruits crude extract was submitted to bioguided fractionation towards *L. donovani* 1S (MHOM/SD/62/1S) promastigotes strain. 190.8 g of crude extract was submitted to flash column chromatography and afforded five fractions PBBF$_1$ [*n*-Hex/EtOAc (1:0), 15.3 g), PBBF$_2$ [*n*-Hex/EtOAc (1:1), 85.6 g], PBBF$_3$ [*n*-Hex/EtOAc (0:1), 19.7 g], PBBF$_4$ [EtOAc/MeOH (9:1), 19.5 g], and PBBF$_5$ [EtOAc/MeOH (3:1) to MeOH (0:1), 30.3 g] (Table LXXV). The most active fractions was submitted to CC over silica gel, and eluted with the mixtures of *n*-Hex/EtOAc (3:7-0:1) and afforded 11 compounds.

Table LXXV: Chromatogram of the mixture CH₂Cl₂/MeOH (1:1) extract of stem bark of *P. butyracea*

Solvent	Series	Fractions	Remarks
n-hexane	1-25	F₁	Mixture of oily
n-Hex/EtOAc (1:1)	26-41	F₂	Mixture of about eleven compounds
n-Hex/EtOAc (0:1)	42-53	F₃	Mixture of about five compounds
EtOAc/MeOH (9:1)	54-88	F₄	Complex mixture
EtOAc/MeOH (3:1-0:1)	89-139	F₅	Complex mixture

III.3.3.2.2.1 Chromatography of the fraction F2

Fraction F2 was chromatographed on a silica gel column with mixtures *n*-Hex/EtOAc (1:0-0:1) as eluent. 100 mL sub-fractions (total 301) were collected and pooled based on the TLC profiles. The sub-fractions obtained were chromatographed on a Sephadex LH-20 gel column with a mixture of CH₂Cl₂/MeOH (9:1-8:2) as eluent and made it possible to obtain 8 compounds indexed **PBER4** (5.1 mg), **PBF3** (4.2 mg), **PBE4** (41.1 mg), **PBE12** (25.0 mg), **PBE5** (10.2 mg), **PBE2** (136.9 mg), **PBE13** (3.8 mg) and **PBF5** (158.5 mg) as a yellow and white powders (Table LXXVI).

Table LXXVI: Chromatogram of the *n*-Hex/EtOAc (1:1) fraction

Eluent	Sub fractions	Remarks
n-Hex/EtOAc (1:0-17:3)	1-45	Mixture of at least 4 products from which **PBE1** (lupeol) and **PBE2** precipitates
n-Hex/EtOAc (4:1-3:2)	46-98	Mixture of at least 3 products from which **PBE4** and **PBF5** precipitates
n-Hex/EtOAc (1:1-3:7)	99-201	Mixture of at least 5 products from which **PBE5**, **PBE13** precipitates
EtOAc/MeOH (9:1-0:1)	202-301	Mixture of at least 5 products from which **PBER4**, **PBE12** and **PBF3** precipitates

III.3.3.2.2.2 Chromatography of the fraction F3

Fraction F3 was chromatographed on a silica gel column with mixtures *n*-Hex/EtOAc (1:0-0:1) as eluent. 100 mL sub-fractions (total 200) were collected and pooled based on the TLC profiles. The sub-fractions obtained were chromatographed on a Sephadex LH-20 gel column with a mixture of CH₂Cl₂/MeOH (9:1-4:1) as eluent and made it possible to obtain 3

compounds indexed **PBER1** (25.6 mg), **PBER4** (96.6 mg) and **PBF5** (8.0 mg) as a yellow powders (Table LXXVII).

Table LXXVII: Chromatogram of the EtOAc fraction

Eluent	Sub fractions	Remarks
***n*-Hex/EtOAc (1:0-4:1)**	1-35	Complex mixture
***n*-Hex/EtOAc (7:3-3:2)**	36-92	Mixture of at least 5 products from which PBER4 and PBER1 precipitates
***n*-Hex/EtOAc (1:1-3:7)**	93-128	Mixture of at least 2 products from which PBF5 precipitates
EtOAc/MeOH (9:1-0:1)	202-301	Complex mixture

III.3.3.3 Fractionation and isolation of compounds of stem bark *A. lobata*

The stem bark crude extract was submitted to bioguided fractionation towards *L. donovani* 1S (MHOM/SD/62/1S) promastigotes strain. 110.0 g was subjected to liquid-liquid extraction with different solvents and gave five fractions including the *n*-hexane fraction (F1, 1.8 g), the dichloromethane fraction (F2, 14.9 g), the ethyl acetate fraction (F3, 36.7 g), the *n*-butanol fraction (F4, 25.4 g), and the water-soluble residue (F5, 20.1 g) (Table LXXVIII). These fractions were assessed for their antileishmanial activity against *L. donovani* strain and fraction F3, was active.

Table LXXVIII: Chromatogram of MeOH extract of the stem bark of *A. lobata*

Solvent	Series	Fractions	Remarks
***n*-Hex**	1-10	F_1	Mixture of oily products
CH$_2$Cl$_2$	11-17	F_2	Mixture of about three compounds
EtOAc	18-29	F_3	Mixture of about eight compounds
***n*-butanol**	30-48	F_4	Mixture of about two compounds
Aqueous résidue	49-50	F_5	

III.3.3.3.1 Chromatography of the fraction F3

This fraction (F3) was subjected to CC over silica gel eluting with *n*-hexane, mixtures of *n*-HexEtOAc (1:0-0:1), EtOAc and EtOAc/MeOH (1:0-0:1) of increasing polarities. 100 mL sub-fractions (total 348) were collected and combined based on the TLC profiles, to afford 6 compounds indexed **AL3** (7.5 mg), **AL4** (5.1 mg), **AL5** (50.5 mg), **AL6** (11.0 mg), **AL7** (15.7 mg) and **AL8** (136.9 mg) as a white powders (Table LXXIX).

Table LXXIX: Chromatogram of the EtOAc fraction

Eluent	Sub fractions	Remarks
n-Hex/EtOAc (9:1-7:3)	1-39	Mixture of at least 3 products from which **AL3** and **AL4** precipitates
n-Hex/EtOAc (3:2-3:2)	40-159	Mixture of at least 3 products from which **AL8** precipitates
n-Hex/EtOAc (1:1-3:7)	160-229	Mixture of at least 2 products from which **AL5** precipitates
EtOAc/MeOH (9:1-0:1)	230-348	Mixture of at least 4 products from which **AL6** and **AL7** precipitates

III.3.3.3.2 Chromatography of the fraction F2

Fraction F2 was dissolved in dichloromethane, then fixed on silica and chromatographed on a silica gel column. The 100 mL sub-fractions (in total 150) collected by elution with the *n*-Hex/EtOAc (1:0-0:1) polarity gradient system, have were collected and grouped on the basis of TLC profiles. By simple filtration, we obtained 2 products indexed **AL1** (49.5 mg) and **AL2** (18.7 mg) in the form of white powder (Table LXXX).

Table LXXX: Chromatogram of the dichloromethane fraction

Eluent	Sub fractions	Remarks
n-Hex/EtOAc (1:0-4:1)	1-59	Mixture of at least 2 products from which and **AL1** precipitates
n-Hex/EtOAc (7:3-3:2)	60-111	Mixture of at least 2 products from which **AL2** precipitates
n-Hex/EtOAc (1:1-0:1)	112-150	Complex mixture

III.3.3.3.3 Chromatography of the fraction F4

Fraction F4 was subjected to purification using an open column chromatography over silica gel, and Sephadex LH-20 successively and eluted with the mixtures of *n*-hexane/EtOAc (3:2-0:1), EtOAc/MeOH (1:0-9:1), EtOAc/MeOH/H$_2$O, (9:1:0.5-7:3:1) and CH$_2$Cl$_2$/MeOH (3:7) to afford 1 compouds, indexed **ALB3** (10.9 mg) in the form of yellow powder (Table LXXXI).

Table LXXXI: Chromatogram of the *n*-butanol fraction

Eluent	Sub fractions	Remarks
n-Hex/EtOAc (3:2-0:1)	1-49	Complex mixture
EtOAc/MeOH (1:0-9:1)	60-112	Mixture of at least 2 products from which **ALB3** precipitates
EtOAc/MeOH/H$_2$O (18:2:1-7:3:1)	113-152	Complex mixture

III.4 Physicochemical characteristics of isolated compounds

III.4.1 The new derivative
AL6: Adeniamide (**54**)
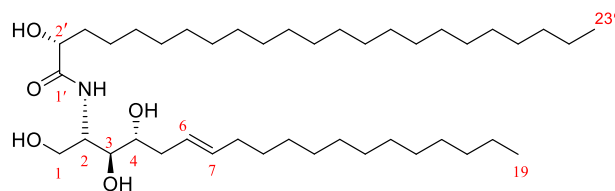
Physical appearance: white amorphous powder;

$[\alpha]_D^{24}$ –5.9 (c 0.001, MeOH);

IR (KBr): υ_{max} 3398 cm^{-1} (OH), 1638 cm^{-1} (CO), 1463 cm^{-1} (C=C);

(+)-HR-ESI-MS: [M+H]$^+$ at *m/z* 682.6352 (calcd 682.6349 for C$_{42}$H$_{84}$NO$_5$);

^{13}C NMR (125 MHz, C$_5$D$_5$N): Table XVIII

^{1}H NMR (500 MHz, C$_5$D$_5$N): Table XVIII

III.4.2 Known derivatives

AL8: germanicol caffeoyl ester (**55**)
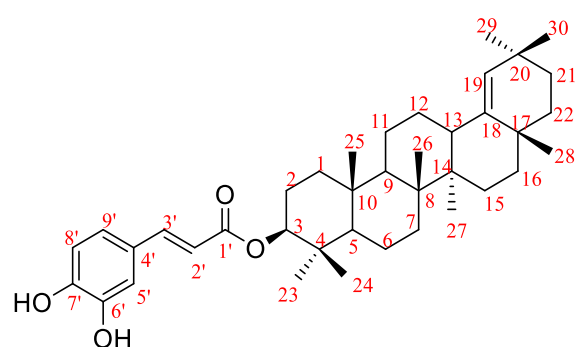
Molecular formula:	C$_{39}$H$_{56}$O$_4$
(+)-HR ESI-MS: [M+H]$^+$	*m/z* 611.4114
Physical appearance:	White powder
Positive test:	Liebermann-Burchard
^{1}H NMR (500 MHz, CDCl$_3$):	Table XIX
^{13}C NMR (125 MHz, CDCl$_3$):	Table XIX

ECF21: friedelin (**56**)
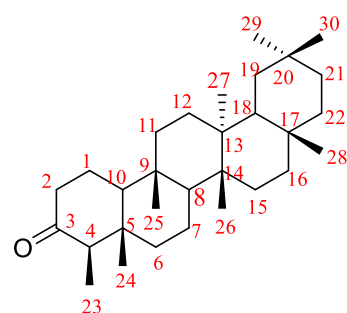
Molecular formula:	C$_{30}$H$_{50}$O
(+)-HR ESI-MS: [M+H]$^+$	*m/z* 427.3964
Physical appearance:	White powder
Positive test:	Liebermann-Burchard
^{1}H NMR (500 MHz, CDCl$_3$):	Table XX
^{13}C NMR (125 MHz, CDCl$_3$):	Table XX

ECT2: canophyllol (**57**)
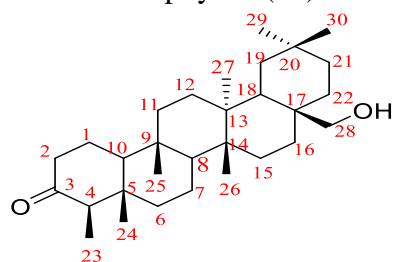
Molecular formula:	$C_{30}H_{50}O_2$
Physical appearance:	White powder
Positive test:	Liebermann-Burchard
^{13}C NMR (125 MHz, CDCl$_3$):	Table XXI

ECTF22: cerin (**58**)
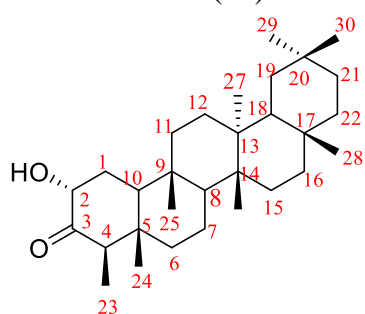
Molecular formula:	$C_{30}H_{50}O_2$
Physical appearance:	White powder
Positive test:	Liebermann-Burchard
^{13}C NMR (125 MHz, CDCl$_3$):	Table XXII

ECTF21: marsformoxide B (**59**)
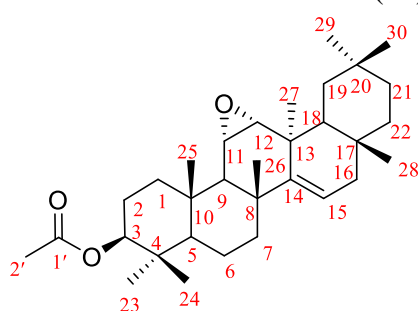
Molecular formula:	$C_{32}H_{50}O_2$
(+)-HR ESI-MS: [M+H]$^+$	*m/z* 483.3969
Physical appearance:	White powder
Positive test:	Liebermann-Burchard
^1H NMR (500 MHz, CDCl$_3$):	Table XXIII
^{13}C NMR (125 MHz, CDCl$_3$):	Table XXIII

ECF23: *β*-amyrin (**60**)
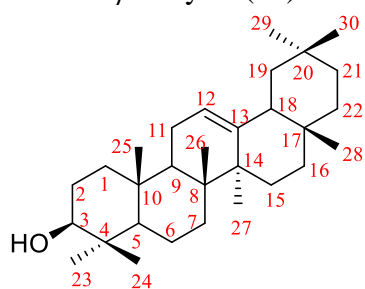
Molecular formula:	$C_{30}H_{50}O$
(+)-HR ESI-MS: [M+H]$^+$	*m/z* 427.3959
Physical appearance:	White powder
Positive test:	Liebermann-Burchard
^1H NMR (500 MHz, CDCl$_3$):	Table XXIV
^{13}C NMR (125 MHz, CDCl$_3$):	Table XXIV

EC1: *β*-amyrin palmitate (**61**)
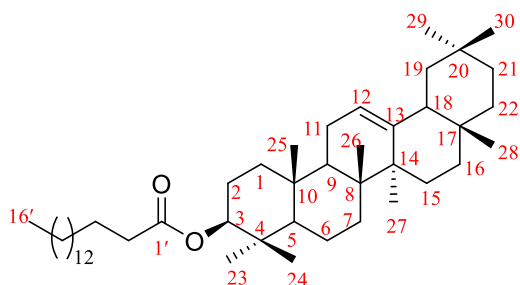
Molecular formula:	$C_{46}H_{80}O_2$
(+)-HR ESI-MS: $[M+Na]^+$	*m/z* 687.6160
Physical appearance:	White powder
Positive test:	Liebermann-Burchard
^1H NMR (500 MHz, CDCl$_3$):	Table XXV
^{13}C NMR (125 MHz, CDCl$_3$):	Table XXV

ECF1: lupeol (**62**)
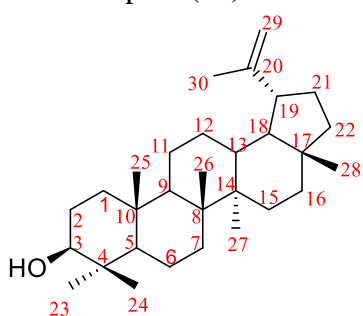
Molecular formula:	$C_{30}H_{50}O$
Physical appearance:	White powder
Positive test:	Liebermann-Burchard
^1H NMR (500 MHz, CDCl$_3$):	Table XXVI
^{13}C NMR (125 MHz, CDCl$_3$):	Table XXVI

ECTF23: lupenone (**63**)
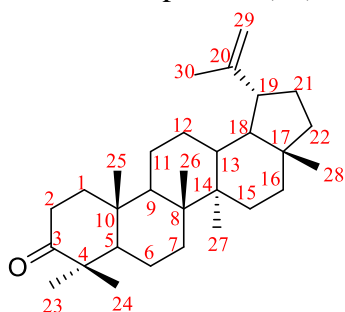
Molecular formula:	$C_{30}H_{48}O$
(+)-HR ESI-MS: $[M+H]^+$	*m/z* 425.3858
Physical appearance:	White powder
Positive test:	Liebermann-Burchard
^{13}C NMR (125 MHz, CDCl$_3$):	Table XXVII

PBE5: betulin (**64**)
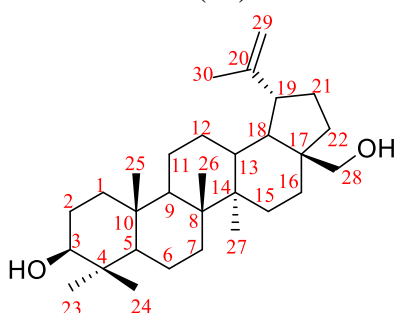
Molecular formula:	$C_{30}H_{50}O_2$
Physical appearance:	White powder
Positive test:	Liebermann-Burchard
^{13}C NMR (125 MHz, CDCl$_3$):	Table XXVIII

ECF43: 4′-methylamentoflavone (**65**)
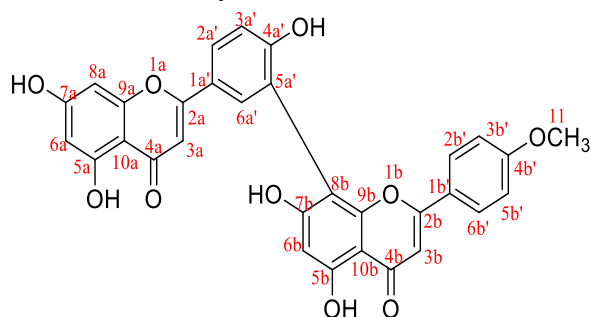
Molecular formula:	$C_{30}H_{20}O_{11}$
(+)-HR ESI-MS: [M+H]$^+$	*m/z* 557.1070
Physical appearance:	yellow powder
Positive test:	Shinoda
^{1}H NMR (500 MHz, $C_3D_3O_6$):	Table XXIX
^{13}C NMR (125 MHz, $C_3D_3O_6$):	Table XXIX

ECF44: amentoflavone (**66**)
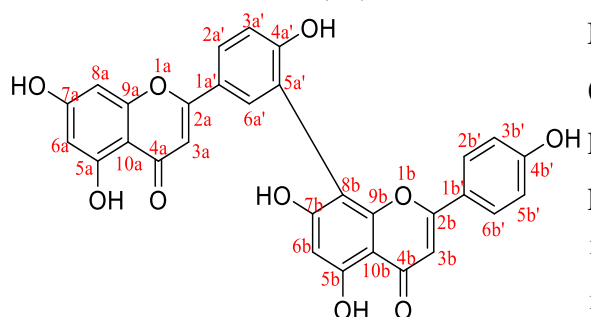
Molecular formula:	$C_{30}H_{18}O_{10}$
(+)-HR ESI-MS: [M+H]$^+$	*m/z* 539.0997
Physical appearance:	yellow powder
Positive test:	Shinoda
^{1}H NMR (500 MHz, $C_3D_3O_6$):	Table XXX
^{13}C NMR (125 MHz, $C_3D_3O_6$):	Table XXX

ECTF33: morelloflavone (**67**)
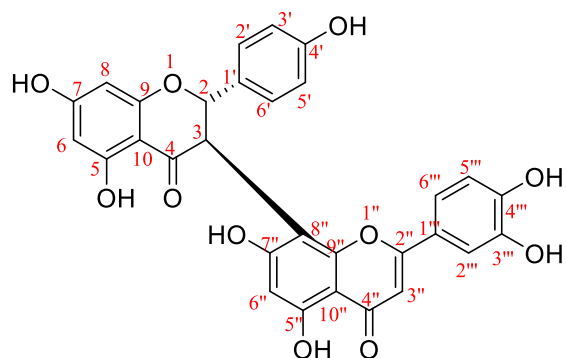
Molecular formula:	$C_{31}H_{20}O_{10}$
(+)-HR ESI-MS: [M+Na]$^+$	*m/z* 575.0919
Physical appearance:	yellow powder
Positive test:	Shinoda
^{1}H NMR (500 MHz, $C_3D_3O_6$):	TableXXXI
^{13}C NMR (125 MHz, $C_3D_3O_6$):	Table XXXI

PBER2: epicatechin (**68**)
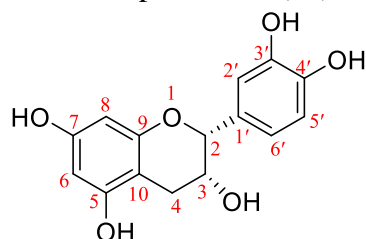
Molecular formula:	$C_{15}H_{14}O_6$
(+)-HR ESI-MS: [M+H]$^+$	291.0873
Physical appearance:	Yellow powder
Positive test:	Shinoda and FeCl$_3$
^{1}H NMR (500 MHz, CD$_3$OD):	Table XXXII
^{13}C NMR (125 MHz, CD$_3$OD):	Table XXXII

ECTF3: mixture (1:1) of Isoxanthochymol (**69a**)/Cycloxanthochymol (**69b**)
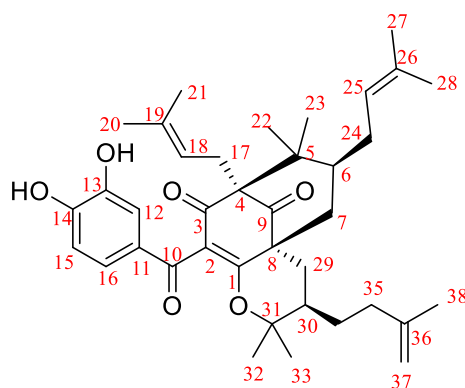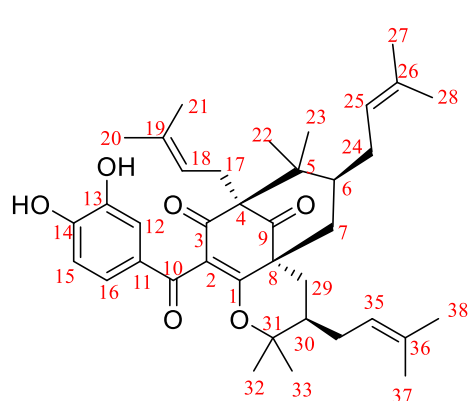
Molecular formula:	$C_{38}H_{50}O_{11}$
(+)-HR ESI-MS: [M+H]$^+$	*m/z* 603.3686
Physical appearance:	White powder
Positive test:	Shinoda
^{1}H NMR (500 MHz, $C_3D_3O_6$):	Table XXXIII
^{13}C NMR (125 MHz, $C_3D_3O_6$):	Table XXXIII

ECTF44: absicic acid (**70**)
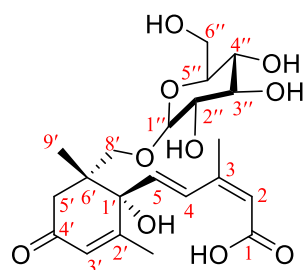
Molecular formula:	$C_{21}H_{30}O_{10}$
(+)-HR ESI-MS: [M+H]$^+$	*m/z* 443.1911
Physical appearance:	Brown oil
Positive test:	Molish and $FeCl_3$
^{1}H NMR (500 MHz, CD_3OD):	Table XXXIV
^{13}C NMR (125 MHz, CD_3OD):	Table XXXIV

ECTF41: tachioside (**71**)
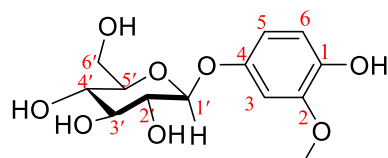
Molecular formula:	$C_{13}H_{18}O_8$
(+)-ESI-MS: [M+Na]$^+$	*m/z* 325.11
Physical appearance:	Brown oil
Positive test:	Molish and $FeCl_3$
^{1}H NMR (500 MHz, CD_3OD):	Table XXXV
^{13}C NMR (125 MHz, CD_3OD):	Table XXXV

ECTF42: mixture (1:3) of tachioside (**71**)/ isotachioside (**72**)
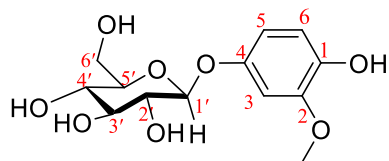
Molecular formula:	$C_{13}H_{18}O_8$
(+)-ESI-MS: [M+Na]$^+$	*m/z* 325.14
Physical appearance:	Brown oil
Positive test:	Molish and $FeCl_3$
^{13}C NMR (125 MHz, C_5D_5N):	Table XXXVI
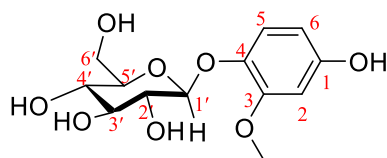
ECTF93: koaburaside (**73**)
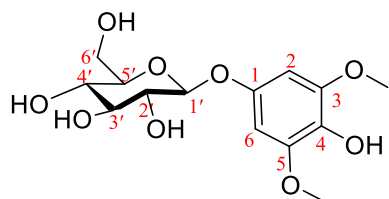
Molecular formula:	$C_{14}H_{20}O_9$
Physical appearance:	Brown powder
Positive test:	Molish and $FeCl_3$
^1H NMR (500 MHz, C_5D_5N):	Table XXXVII
^{13}C NMR (125 MHz, C_5D_5N):	Table XXXVII

ALB3: vanillic acid (**74**)
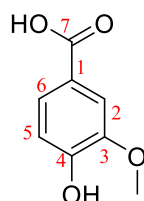
Molecular formula:	$C_8H_8O_4$
Physical appearance:	Yellow powder
Positive test:	$FeCl_3$
^1H NMR (500 MHz, C_5D_5N):	Table XXXVIII
^{13}C NMR (125 MHz, C_5D_5N):	Table XXXVIII

ECTF24: 1,5-dihydroxy-3-methoxyxanthone (**75**)
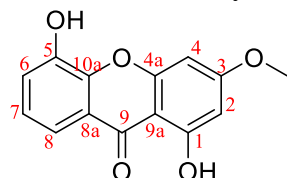
Molecular formula:	$C_{14}H_{10}O_5$
Physical appearance:	Yellow powder
Positive test:	$FeCl_3$
^1H NMR (500 MHz, C_3D_6O):	Table XXXIX
^{13}C NMR (125 MHz, C_3D_6O):	TableXXXIX

PBER1: norathyriol (**76**)
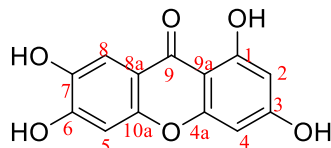
Molecular formula:	$C_{14}H_{10}O_5$
Physical appearance:	Yellow powder
Positive test:	$FeCl_3$
^1H NMR (500 MHz, C_2D_6SO):	Table XL
^{13}C NMR (125 MHz, C_2D_6SO):	Table XL

PBF1: daphnifolin (**77**)
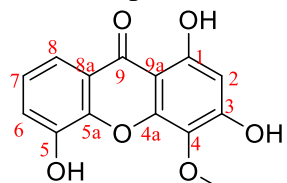
Molecular formula:	$C_{14}H_{10}O_5$
Physical appearance:	Yellow powder
Positive test:	$FeCl_3$
^1H NMR (500 MHz, CD_3OD):	Table XLI
^{13}C NMR (125 MHz, CD_3OD):	Table XLI

PBHF3: tovopyrifolin C (**78**)
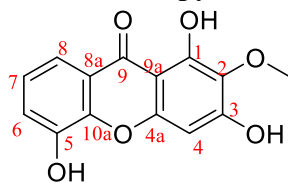
Molecular formula:	$C_{14}H_{10}O_5$
Physical appearance:	Yellow powder
Positive test:	$FeCl_3$
^1H NMR (500 MHz, CD_3OD):	Table XLII
^{13}C NMR (125 MHz, CD_3OD):	Table XLII

PBHF9: α-mangostin (**79**)
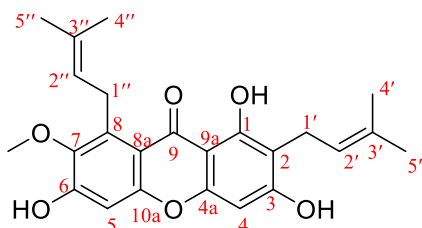
Molecular formula:	$C_{14}H_{10}O_5$
(+)-HR ESI-MS: [M+H]$^+$	433.1647
Physical appearance:	Yellow powder
Positive test:	$FeCl_3$
^1H NMR (500 MHz, $CDCl_3$):	Table XLIII
^{13}C NMR (125 MHz, $CDCl_3$):	Table XLIII

PBHF4: cowagarcinone (**80**)
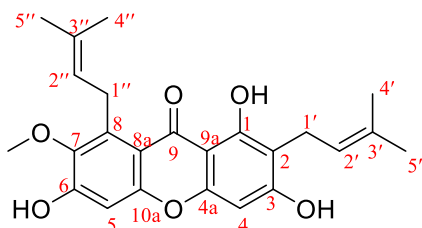
Molecular formula:	$C_{24}H_{26}O_6$
(+)-HR ESI-MS: [M+Na]$^+$	433.1647
Physical appearance:	Yellow powder
Positive test:	$FeCl_3$
^1H NMR (500 MHz, $CDCl_3$):	Table XLIV
^{13}C NMR (125 MHz, $CDCl_3$):	TableXLIV

PBE13: 9-hydroxycalabaxanthone (**81**)
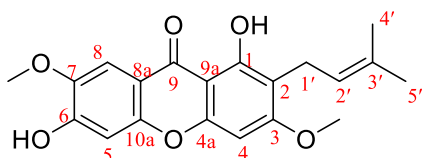
Molecular formula:	$C_{20}H_{21}O_6$
(+)-HR ESI-MS: [M+H]$^+$	357.1333
Physical appearance:	Yellow powder
Positive test:	$FeCl_3$
^1H NMR (500 MHz, $CDCl_3$):	Table XLV
^{13}C NMR (125 MHz, $CDCl_3$):	Table XLV

PBE6: tovophyllin A (**82**)
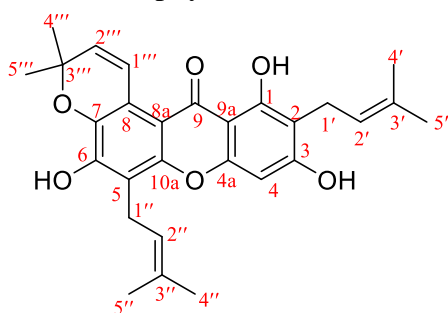
Molecular formula:	$C_{28}H_{30}O_6$
Physical appearance:	Yellow powder
Positive test:	$FeCl_3$
^1H NMR (500 MHz, $CDCl_3$):	Table XLVI
^{13}C NMR (125 MHz, $CDCl_3$):	Table XLVI

PBE12: 1,3,7-trihydroxyxanthone (**83**)
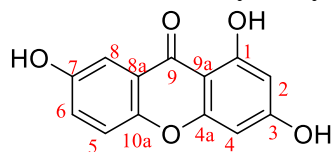
Molecular formula:	$C_{13}H_8O_5$
Physical appearance:	Yellow powder
Positive test:	$FeCl_3$
^{1}H NMR (500 MHz, $CDCl_3$):	Table XLVII
^{13}C NMR (125 MHz, $CDCl_3$):	Table XLVII

PBEF4: methyl citrate (**84**)
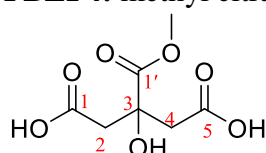
Molecular formula:	$C_7H_{10}O_7$
(+)-HR ESI-MS: $[M+Na]^+$	229.0302
Physical appearance:	White powder
^{1}H NMR (500 MHz, CD_3OD):	Table XLVIII
^{13}C NMR (125 MHz, CD_3OD):	Table XLVIII

EC8: octacosanoic acid (**85**)
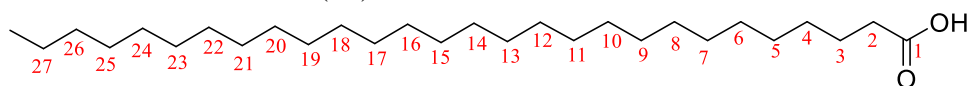
Molecular formula:	$C_{28}H_{56}O_2$
(-)-HR ESI-MS: $[M-H]^-$	423.4252
Physical appearance:	White powder
^{1}H NMR (500 MHz, $CDCl_3$):	Figure 170

AL3: tetracosanoic acid (**86**)
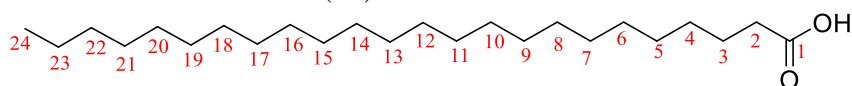
Molecular formula:	$C_{24}H_{48}O_2$
(-)-HR ESI-MS: $[M-H]^-$	367.3634
Physical appearance:	White powder
^{1}H NMR (500 MHz, $CDCl_3$):	Figure 172

ECT14: 2′,3′-dihydroxypropyltriacontanoate (**87**)
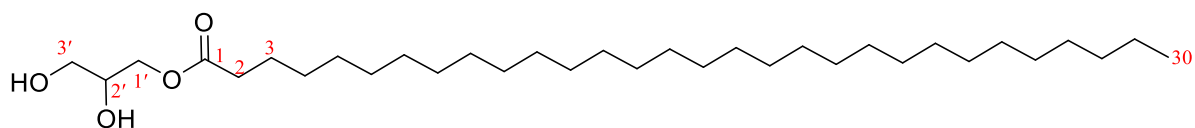
Molecular formula:	$C_{33}H_{66}O_4$
(+)-HR ESI-MS: $[M+K]^+$	565.2966
Physical appearance:	White powder
^{1}H NMR (500 MHz, C_5D_5N):	Figure 174

AL7: D-mannitol (**88**)

EC9: 3,3′-dimethylellagic acid (**89**)

PBF5: stigmasterol (**90**)
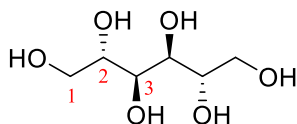
Molecular formula:	$C_6H_8O_6$
(+)-HR ESI-MS: $[M+K]^+$	221.0334
Physical appearance:	White powder
^{13}C NMR (125 MHz, C_5D_5N):	Table L
Molecular formula:	$C_{16}H_{10}O_8$
(-)-HR ESI-MS: $[M-H]^-$	329.0311
Positive test :	$FeCl_3$
Physical appearance:	Yellow powder
^1H NMR (500 MHz, C_5D_5N):	Figure 184
Molecular formula:	$C_{29}H_{48}O$
(+)-HR ESI-MS: $[M+H]^+$	413.2736
Positive test :	Liebermann-Burchard
Physical appearance:	White powder
^{13}C NMR (125 MHz, $CDCl_3$):	Table LI
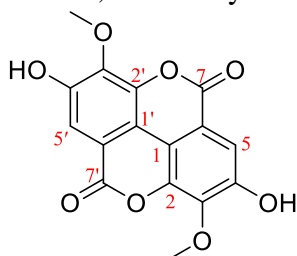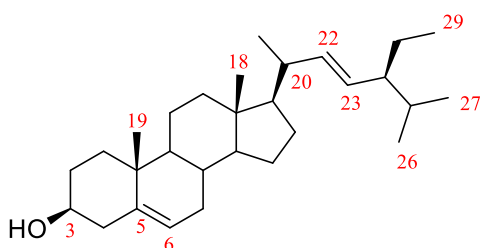
AL1: mixture (1:4) of stigmasterol (**90**)/β-sitosterol (**91**)
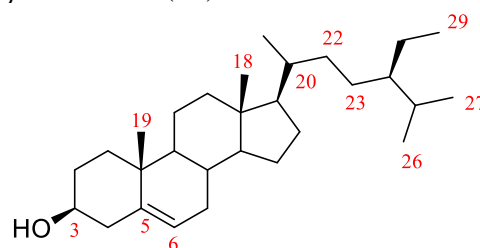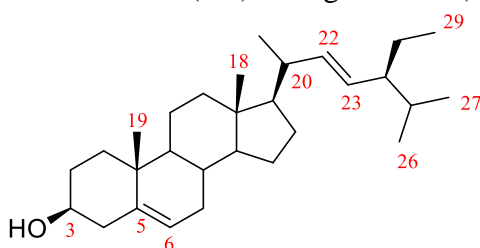
Molecular formula:	$C_{29}H_{48}O$
Positive test :	Liebermann-Burchard
Physical appearance:	White powder
^1H NMR (500 MHz, $CDCl_3$):	Figure 186

EC6: β-sitosterol-3-O-β-D-glucopyranoside (**92**)
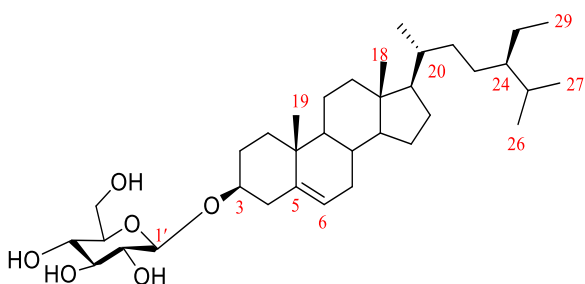
Molecular formula:	$C_{29}H_{48}O$
(+)-HR ESI-MS: $[M+Na]^+$	599.4522
Positive test :	Liebermann-Burchard and Molish
Physical appearance:	White powder
^1H NMR (125 MHz, $CDCl_3$):	Figure 190

BIBLIOGRAPHICAL REFERENCES

BIBLIOGRAPHICAL REFERENCES

Adam J. G., **1971**. Flore Descriptive des Monts Nimba. Muséum National d'histoire Naturelle, Ed. Paris Ve Tome XX, pp. 317-324.

Adjanohoun J., Ahyi A., Aké assi I., Akpagana K., Chibon P., El-Adji A., Eymé J., Garba M., Gassitan N., Gbeassor M., Goudote E., Guinko S., Hodouto K., Houngnon P., Keita A., Keoula Y., Hodouto P., Issa L., Siamevi M., Taffame K., **1986**. Contributions aux études ethnobotaniques et floristiques au Togo. Médecine Traditionnelle et pharmacopée. Agence de coopération culturelle et Technique, Paris, France, p. 671.

Adjanohoun J., Aké assi L., **1979**. Contribution au recensement des plantes médicinales de Côte d'Ivoire. Centre National de Floristique, Abidjan, Côte d'Ivoire p. 358.

Agrawal P. K., **1992**. NMR Spectroscopy in the structural elucidation of oligosaccharides and glycosides. *Phytochemistry* 31(10), 3307–3330. doi:10.1016/0031-9422(92)83678-r.

Ai-Qun J., Xu Y., Wei-Xin W., Yong-Hong J., **2010**. Glycocerebroside bearing a novel long-chain base from *Sagina japonica* (caryophyllaceae). *Fitoterapia* 81(6), 540–545.

Aké assi L., Abeye J., Guinko S., Riguet R., Bangavou X., **1985**. Contribution aux études ethnobotaniques et floristiques en République centrafricaine. Agence de coopération culturelle et Technique, Paris, France, p. 140.

Al-Massarani S., El Gamal A., Al-Musayeib N., Mothana R., Basudan O., Al-Rehaily A., Farag M., Assaf M. H., El Tahir K. H., Maes L., **2013**. Phytochemical, antimicrobial and antiprotozoal evaluation of *Garcinia Mangostana* Pericarp and α-mangostin, Its major xanthone serivative. *Molecules* 18(9), 10599-10608.

Anofel (Association Française des Enseignants de Parasitologie et Mycologie), **2014**. Leishmanioses. Université Médicale Virtuelle francophone. pp. 1-16.

Araújo J., Fernandes C., Pinto M., Tiritan M. E., **2019**. Chiral derivatives of xanthones with antimicrobial activity. *Molecules* 24, 314.

Atindehou K., Terreaux C., Traoré D., Hpstettmann K., Dosso M., **2002**. Evaluation of the antimicrobial potential of medicinal plants from the Ivory Coast. *Phytotherapy Research* 16(5), 497-502.

Aubreville A., **1950**. Flore Forestière Soudano-Guinenne A.O.F. Cameroun A.E.F. Société d´Edition Géographique, Maritime et Coloniale, Paris, pp. 148-150.

Aubry Pierre., Gaüzère Bernard-Alex., **2020**. Leishmanioses, centre René Labusquière, université de Bordeaux, 33076 Bordeaux (France), Institut de Médecine Tropicale, p. 1-12.

Azebaze A. G. B., Ouahouo B. M. W., Vardamides J. C., Valentin A., Kuete V., Acebey L., Beng V. P., Nkengfack A. E., Meyer M., **2008**. Antimicrobial and antileishmanial xanthones from the stem bark of *Allanblackia gabonensis*. *Chemistry of Natural Compounds* 44, 582-587.

Bamps P., **1970**. Flore du Congo, du Rwanda et du Burundi : Spermatophytes, Guttiferae. Jardin Botanique National de Belgique, Bruxelles, pp. 1-61.

Bankeu J. J. K., Mustafa S. A. A., Gojayev A. S., Lenta D. B., Noungoué T. D., Ngouela A. S., Asaad K., Choudhary M. I., Prigge S., Guliyev A. A., Nkengfack A. E., Tsamo E., Shaiq Ali M., **2010**. Ceramide and cerebroside from the Stem Bark of *Ficus mucuso* (Moraceae). *Chemical Pharmaceutical Bulletin* 58(12), 1661-1665.

Banzouzi J. T., Prado R., Menan H., Valentin A., Roumestan C., Mallie M., Pelissier Y., Blache Y., **2002**. *In vitro* antiplasmodial activity of extracts of *Alchornea cordifolia* and identification of an active constituent : Ellagic acid. *Journal of Ethnopharmacology*, 81(3), 399−401. https://doi.org/10.1016/S0378-8741(02)00121-6.

Batista R., De Jesus S. J. A., De Oliveira A., **2009**. Plant-derived antimalarial agents: New leads and efficient phytomedicines. Part II. Non-Alkaloidal Natural Products. *Molecules* 14, 3037-3072.

Bennett G. J., Lee H. H., **1989**. Xanthones from Guttiferae**.** *Phytochemistry* 28, 967-998.

Biomnis., **2012**. Précis de bio pathologie analyses médicales spécialisées p. 1-2.

Bittrich V., Amaral., **1996**. Flower morphology and pollination biology of some *Clusia* species from the Gran Sabana (Venezuela). *Kew Bulletin* 51, 681–694.

Borghi S. M., Fattori V., Conchon-Costa I., Pinge-Filho P., Pavanelli W. R., Verri W. A., **2016**. Leishmania infection: painful or painless? *Parasitology Research* 116(2), 465-475. doi:10.1007/s00436-016-5340-7.

Bouquet A., Debray M., **1974**. Plantes médicinales de la Côte d'Ivoire. orstom, Paris, France. Travaux et Documents N° 32, P. 231.

Bruneton J., **1999**. Pharmacognosie, phytochimie et plantes médicinales. 4e édition, revue et augmentée, Technique et Documentation - Éditions médicales internationales, Paris, p. 1288.

Burkill H. M., **1985**. The useful plants of west tropical Africa. Volume 2, Kew: Royal Botanic Gardens, 1985-2004.

Burkill M., **1997**. The useful plants of west Tropical Africa. 2nd Edition. Volume 4, Families M-R. Royal Botanic Gardens, Kew, Richmond, United Kingdom, p. 969.

Busson F., **1965**. Plantes Alimentaires de l'Ouest Africain : Etude Botanique, Biologique et Chimique. Edition Le Conte, Marseille, pp. 211- 215.

Camacho M. D. R., Phillipson J. D., Croft S. L., Solis P. N., Marshall S. J., Ghazanfar S. A., **2003**. Screening of plant extracts for antiprotozoal and cytotoxic activities. *Journal of Ethnopharmacology* 89, 185-191.

Cateni F., Zilic J., Falsone G., Scialino G., Banfi E., **2003**. New cerebrosides from *Euphorbia peplis* L.: antimicrobial activity evaluation. *Bioorganic & Medicinal Chemistry Letters* 13(24), 4345-4350. doi:10.1016/j.bmcl.2003.09.044.

Chaouli N., **2013**. Intoxication par les plantes cyanogènes, these en vue de l'obtention du diplôme national de docteur en pharmacie, universite de monastir faculte de pharmacie de Monastir, année universitaire: 2011-2012 N° d'ordre:207.

Chaturvedula V. S. P., Prakash I., **2012**. Isolation of Stigmasterol and *β*-Sitosterol from the dichloromethane extract of *Rubus suavissimus*. *International Current Pharmaceutical Journal* 1(9), 239-242.

Courtin O., **1986**. Cosmetic preparation to retard the ageing skin. *European Patents Applications* CODEN:EPXXDW EP 180505 A1 19860507, p. 13.

Dah-Dovonon Z., **2002**. Rapport du Bénin. In: Eyog Matip O, Gaoué OG et Dossou B, (éds). Programme de ressources génétiques forestières en Afrique au Sud du Sahara. Réseau "Espèces Ligneuses Alimentaires". Compte rendu de la première réunion du Réseau tenue 11-13 Décembre 2000 au CNSF Ouagadougou, Burkina Faso. Institut International des Ressources Phytogénétiques, Rome, Italie. p. 12.

De Wilde O., **1975**. Passifloraceae. In: Polhill, R.M. (Editor). Flora of Tropical East Africa. Crown Agents for Oversea Governments and Administrations, London, United Kingdom, p.71.

Dedet J. P., **2001**. Leishmanies, leishmanioses. Biologie, clinique et thérapeutique, maladies infectieuses. *Encyclopedie Medico-Chirurgical* 8, p. 11.

Dedet J. P., **2003**. *Leishmania* (atteinte cutanée de l'ancien monde). *Encyclopedy Medicine and Biology Elsevier Paris* 9, p. 11.

Dedet J. P., **2003**. *Leishmania* (atteinte cutanée et cutanéomuqueuse du nouveau monde). *Encyclopedy Medicine and Biology Elsevier Paris* 9, p. 11.

Dencausse L., Nsourankoua H., Artaud J., Clamou J.L., **1995**. Comparaison des compositions lipidiques des beurres de *Pentadesma* et de Karité. *OCL* 2, 143-147.

Dharmaratne H. R. W., Sakagami Y., Piyasena K. G. P., Thevanesam V., **2013**. Antibacterial activity of xanthones from *Garcinia mangostana* (L.) and their structure–activity relationship studies. *Natural Product Research* 27, 938-941.

Ebede G. R., Ndongo J. T., Mbing J. N., Kenfack H. C. M., Pegnyemb D. E., Bochet C. G., **2019**. Contortamide, a new anti-colon cancer cerebroside and other constituents from *Tabernaemontana contorta* Stapf (Apocynaceae). *Natural Product Research*, 1-9. doi:10.1080/14786419.2019.1636243.

Ee G. C. L., Jong V. Y. M., Sukari M. A., Rahmani M., Kua A. S. M., **2009**. Xanthones from *Calophyllum inophyllum*. *Pertanika Journal* of *Science and Technology*17 (2), 307-312.

Ee G. C. L., Lim C. K., Ong G. P., Sukari M. A., Lee H. L., **2006**. Daphnifolin, a new xanthone from *Mesua daphnifolia* (Guttiferae). *Journal of Asian Natural Products Research* 8, 567-570.

Elfita E., Muharni M., Latief M., Darwati D., Widiyantoro A., Supriyatna S., Bahti H. H., Dachriyanus D., Cos P., Maes L., Foubert K., Apers S., Pieters L., **2009**. Antiplasmodial and other constituents from four Indonesia *Garcinia* spp. *Phytochemistry* 70, 907-912.

Elmahallawy E. K., Sampedro Martínez A., Rodriguez-Granger J., Hoyos-Mallecot Y., Agil A., Navarro Mari J. M., Gutierrez Fernández J., **2014**. Diagnosis of leishmaniasis. *The Journal of Infection in Developing Countries* 8(08), 961-972. doi:10.3855/jidc.4310.

Eloff J. N., **1998**. A sensitive and quick microplate method to determine the minimal inhibitory concentration of plant extracts for bacteria. *Planta Medica* 64, 711-713.

Ewédjè E.E., **2012**. Biologie de la reproduction, phylogéographie et diversité de l'arbre à beurre *Pentadesma butyracea* Sabine (Clusiaceae). Implications pour sa conservation au Béni. Thèse de doctorat, Université d'Abomey-Calavi, Bénin, pp. 1-227.

Fernandes R., Fernandes A., **1978**. Passifloraceae. In: Launert, E (Editor). Flora Zambesiaca. Flora Zambesiaca Managing Committee, London, United Kongdom. Volume 4, pp. 368-411.

Feuillet C., **1989**. Diversity and distribution of Guianan Passifloraceae. In: Tropical forests, eds l.b. holm- nielsen; nielsen i.c. 81 h. balsln, Academic Press, London: 31, P. 1-31.

Fowa A. B., Djoueudam F. G., Njateng G. S. S., Ngoudjou T., Sokoudjou J. B., Kodjio N., Gatsing D., **2019**. *In vitro* antisalmonellal activities of leaf extracts of *Adenia lobata* Jacq. (Passifloraceae) and mechanism of action of the most active extract on *Salmonella typhi* ATCC6539. *International Journal of Biology Research* 4, 18-25.

Frahm, A. W., Chaudhuri R. K., **1979**. ^{13}C NMR spectroscopy of substituted xanthones-II. *Tetrahedron* 35 (17), 2035-2038. doi:10.1016/s0040-4020(01)88974-2.

Gentilini M., **1993**. Les leishmanioses, in medecine tropicale. *Paris Flammarion* 5, p. 141.

Goto H., Lindoso J. A. L., **2010**. Current diagnosis and treatment of cutaneous and mucocutaneous leishmaniasis. *Expert Review* of *Anti-infective Therapy* 8, 419-433.

Gustafson K. R., Blunt J. W., Munro M. H. G., Fuller R. W., McKee T. C., Cardellina II J. H., McMahon J. B., Cragg G. M., Boyd M. R., **1992**. The guttiferones, HIV-inhibitory benzophenones from *Symphonia globulifera*, *Garcinia livingstonei*, *Garcinia ovalifolia* and *Clusia rosea*. *Tetrahedron* 48, 10093-10102.

Haque E., Islam N., Gupta D. D., Hossain M., Hossain U. S., Shibib B. A., **2008**. Triterpenoids from the stem bark of *Crataeva nurvala*. *Journal of Pharmaceutical Sciences* 7, 71-74.

Hearn J., **2006**. *Adenia* (Passifloraceae) and its Adaptive Radiation: Phylogeny and Growth form diversification. *Systematic Botany* 31, 805-821.

Héfin L., **1980**. Etude sur la forêt et le bois du Cameroun, Librairie Larousse, Paris Veme, pp. 55- 56.

Heitz H., **1943**. *La Forêt du Gabon*, Larousse, Paris, pp. 53-66

Himanshu J., Joshi A. B., Hemlata S., Gururaja M. P., Prajwal R. S., Subrahmanyam E. V. S., Satyanaryana D., **2009**. Fatty acids from *Memecylon umbellatum* (Burm.). *Asian Journal of Research in Chemistry* 2(2), 178-180.

Huang XZ, Yin Y, Dai JH, Liang H, Dai Y, Bai L. **2010**. Two new ceramides from the stems of *Piper betle* L. *Chinese Chemical Letters* 21(4):433–436.

Hutchinson J., **1973**. The Families of Flowering Plants, Oxford University Press, London, p. 336.

Hutchinson L. L., Dalziel J. M., **1954**. Flora of West Tropical Africa. 2nd Edition, Vol. 1, Oxford University Press, London, pp. 286-287.

Inoshiri S., Sasaki M., Kohda H., Otsuka H., Yamasaki K., **1987**. Aromatic glycosides from *Berchemia racemose*. *Phytochemistr*y 26, 2811-2814.

Ito K., Lai J., **1978**. Studies on the constituents of *Marsdenia formosana* Masamure II. Structure of marsformoxide A and marsformoxide B. *Chemical and Pharmaceutical Bulletin* 26 (6), 1908-1916.

Iwu, M.M., **1993**. Handbook of African Medicinal Plants. CRC Press, London36–37.

Jang D. S., Lee G. Y., Lee Y. M., Kim Y. S., Sun H., Kim D. H., Kim J. S., **2009**. Flavan-3-ols having a γ-lactam from the roots of *Actinidia arguta* inhibit the formation of advanced glycation end products *in vitro*. *Chemical and Pharmaceutical Bulletin* 57, 397-400.

Jaroszewski., Jerzy W., Birthe J., **1985**. Deidaclin and tetraphyllin A, epimeric glucosides of 2-cyclopentenone cyanohydrin, in *Adenia globosa* Engl. (Passifloraceae):Crystal structure of deidaclin tetraacetate. *Acta Chemica Scandinavica* 39, 867-875.

Kagho D.U.K., Fongang Y.S.F., Awantu A.F., Bankeu J.J.K., Toghueo R.M.K., Ngouela A.S., Sewald N., Lenta B.N., Mehreen L., Ali M.S., **2020**. Ceramides and other bioactive compounds from *Celtis tessmannii* Rendle. *Chemical Data Collections* 28, 1-10.

Kamga J., Louis P., Sandjo H. M., Ngameni P. B., Shiono Y., Yemloul M., Rincheval V., Ngadjui B. T., Kirsch G., **2010**. Politamide, a new constituent from the stem bark of *Ficus polita* Vahl (Moraceae). *Arkivoc* (ii), 323-329.

Karanjgaokar C. G., Radhakrishnan P. V., Venkataraman K., **1967**. Morelloflavone, a 3-(8-) flavonylflavanone, from the heartwood of *Garcinia morella*. *Tetrahedron Letters* 33, 3195-3198.

Kerimli E.G.O., Serkerov S.V., **2016**. D-mannitol from the *Fraxinus excelsior*. *Chemical Plant Raw Material* 1, 191-194.

Khac D. D., Tran-Van S., Campos A. M., Lallemand J. Y., Fetizon M., **1990**. Ellagic compounds from *Diplopanax stachyanthus*. *Phytochemistry* 29, 251-256.

Khatun M., Billah M., Quader M. A., **2012**. Sterols and sterol glucoside from *Phyllanthus* species. *Dhaka University Journal of Sciences* 60, 5-10.

Kihara A., **2016**. Synthesis and degradation pathways, functions, and pathology of ceramides and epidermal acylceramides. *Progress in Lipid Research* 63, 50-69. doi:10.1016/j.plipres.2016.04.001.

Killip P., **1938**. The American species of Passifloraceae. Field Museum of Natural History, Botanical series, Chicago, vol 2, p. 52-68.

Kimutai A., Ngure K. P., Tonui K. W., Gicheru M. M., Nyamwamu B. L., **2009**. Leishmaniasis in northern and Western Africa: A reviews 1. *African Journal* of *Infectious Diseases* 3(1), 14-25.

Kipré G. R., Offoumou R. M., Silue K. D., Bouable G. M., Zirihi G. N., Djaman A. J., **2017**. Enquête ethnopharmacologique des plantes antipaludiques dans le département d'Agboville, sud-est de la Cote d'Ivoire. *Journal of Applied Biosciences* 09, 10618-10629.

Kipré G. R., Offoumou R. M., Silué K. D., Bouablé G. M., Zirihi G. N., Djaman A. J., **2018**. Antiplasmodial activity and phytochemical screening of *Adenia lobata*, *Cola gigantea* VAR.GLABRESCENS and *Entada mannii,* three traditional plants. *International journal of applied biology* and *pharmaceutical technology* 9, 12-14.

Koh J. J., Qiu S., Zou H., Lakshminarayanan R., Li J., Zhou X., Tang C., Saraswathi P., Verma C., Tan D. T. H., Tan A. L., Liu S., Beuerman R. W., **2013**. Rapid bactericidal action of alpha-mangostin against MRSA as an outcome of membrane targeting. *Biochimica Biophysica Acta* 1828, 834-844.

Kolter T., Sandhoff K., **1999**. Sphingolipids-Their Metabolic Pathways and the pathobiochemistry of neurodegenerative diseases. *Angewandte Chemie International Edition* 38(11), 1532-1568. doi:10.1002/(sici)1521-3773(19990601)38:11<1532::aid-anie1532>3.0.co;2-u

Konkon N. G., Adjoungoua A. L., Ouattara D., Simaga D., Koné B., N'guessan K. E., Kouakou T. H., **2012**. Anti-hemorrhoidal activity of leaf extract of *Adenia lobata* (Jacq.) Engl. (Passifloraceae). *Research Journal* of *Pharmacy and Technology* 5, 63-67.

Kovganko N. V., Kashkan Z. N., Borisov E. V., Batura E. V., **1999**. ^{13}C NMR spectra of *β*-sitosterol derivatives with oxidized rings A and B. *Chemistry of Natural Compounds* 35, 646-649.

Kuete V., Alibert-Franco S., Eyong K. O., Ngameni B., Folefoc G. N., Nguemeving J. R., Tangmouo J. G., Fotso G. W., Komguem J., Ouahouo B. M. W., Bolla J. M., Chevalier J., Ngadjui B. T., Nkengfack A. E., **2011**. Antibacterial activity of some natural products against bacteria expressing a multidrug-resistant phenotype. *International Journal* of *Antimicrobial Agents* 37, 156-161.

Kunert O., Swamy R. C., Kaiser M., Presser A., Buzzi S., Appa Rao A. V. N., Schühly W., **2008**. Antiplasmodial and leishmanicidal activity of biflavonoids from Indian *Selaginella bryopteris. Phytochemistry Letters* 1, 171-174.

Lambros C., Vanderberg J. P., **1979**. Synchronization of *Plasmodium falciparum* erythrocytic stages in culture. *The Journal of Parasitology* 65, 418.

Lenta N. B., Kamdem L., Ngouela S., Tantangmo F., Devkota K., Boyom F., Rosenthal P. J., Tsamo E., **2011**. Antiplasmodial constituents from the Fruit Pericarp of *Pentadesma butyracea. Planta Medica* 77(04), 377-379. doi:10.1055/s-0030-1250384.

Lenta N. B., Vonthron-Sénécheau C., Weniger B., Devkota P. K., Ngoupayo J., Kaiser M., Naz Q., Choudhary I. M., Tsamo E., Sewald N., **2007**. Leishmanicidal and

chlolinesterase inhibiting activities of phenolic compounds from *Allanblackia monticola* and *Symphonia globulifera*. *Molecules* 12, 1548-1557.

Letouzey R., **1982**. Manuel de Botanique Forestière, Afrique Tropical, Centre Technique Forestier Tropical, Tome 2A, Part.1, pp. 122-123.

Li M., Wang Y., Fu D., Liu X., **2007**. 6-methyl citrate from *Dioscorea opposite* Thunb. *Acta Crystallographica* Section *E* 63, 4497.

Li X. C., Joshi A. S., Tan B., ElSohly H. N., Walker L. A., Zjawiony J. K., Ferreira D., **2002**. Absolute configuration, conformation, and chiral properties of flavanone-(3→8″)-flavone biflavonoids from *Rheedia acuminata*. *Tetrahedron* 58(43), 8709-8717. doi:10.1016/s0040-4020(02)01096-7.

Liu B., Falkenstein-Paul H., Schmidt W., Beerhues L., **2003**. Benzophenone synthase and chalcone synthase from *Hypericum androsaemum* cell cultures: cDNA cloning, functional expression, and site-directed mutagenesis of two polyketide synthases. *Plants Journal* 34, 847-855.

Liu H, Orjala J, Sticher O, Rali T., **1999**. Acylated flavonol glycosides from leaves of *Stenochlaena palustris*. *Journal of Natural Products* 62(1), 70-75.

Mahabusarakam W., Chairek P., Taylor W. C., **2005**. Xanthones from *Garcinia cowa* Roxb. latex. *Phytochemistry* 66, 1148-1153.

Mahato S. B., Kundu A. P., **1994**. ^{13}C NMR spectra of pentacyclic triterpenoids. A compilation and some salient features. *Phytochemistry* 37, 1517-1575.

Markham K. R., Sheppard C., Geiger H., **1987**. ^{13}C NMR studies of some naturally occurring amentoflavone and hinokiflavone bioflavonoids. *Phytochemistry* 26, 3335-3337.

Marshall S. J., Russell P. F., Phillipson J.D., Kirby G. C., Warhurst D. C., Wright C. W., **2000**. Antiplasmodial and antiamoebic activities of medicinal plants from Sierra Leone. *Phytotherapy Research* 14, 356-358.

Marty P., **2010**. Leishmaniose viscérale : épidémiologie, diagnostic et traitement. *La Lettre de l'Infectiologue* 25, 186-190.

Masters K. S., Bräse S., **2012**. Xanthones from fungi, lichens, and bacteria. *Natural Products and their Synthesis* 112, 3717-3776.

Masuda Y., Mori K., **2005**. Synthesis and absolute configuration of 6-hydroxylated new ceramides in human skin, ceramides B, 4, 7 and 8. *European Journal of Organic Chemistry* 22, 4789-4800. doi:10.1002/ejoc.200500357.

Mativandlela S. P. N., Lall N., Meyer J. J. M., **2006**. Antibacterial, antifungal and antitubercular activity of (the roots of) *Pelargonium reniforme* (CURT) and

Pelargonium sidoides (DC) (Geraniaceae) root extracts. *South African Journal of Botany* 72, 232-237.

Matsumaru T., Ikeno R., Shuchi Y., Iwamatsu T., Tadokoro T., Yamasaki S., Fujimoto Y., Furukawa A., Maenaka K., **2019**. Synthesis of glycerolipids containing simple linear acyl chains or aromatic rings and evaluation of their Mincle signaling activity. *Chemical Communications* 55, 711-714.

Merrill A. H., Sandhoff K., **2002**. Sphingolipids: metabolism and cell signalling. In: Biochemistry of Lipids, Lipoproteins and Membranes, 4th Edition, Elsevier. Amsterdam, Netherlands, 373-407.

Morah F. N. I., **1988**. Tetraphyllin B from *Adenia cissampeloides. Phytochemistry* 27(9), 2985-2986. doi:10.1016/0031-9422(88)80704-0.

Mosmann, T., **1983**. Rapid colorimetric assay for cellular growth and survival: Application to proliferation and cytotoxicity assays. *Journal of Immunological Methods*, 65(1-2), 55–63. doi:10.1016/0022-1759(83)90303-4

Mukulesh M., Vedavati G. P., Narshinha P. A., **2006**. Facile synthesis of 1,3,7-trihydroxyxanthone and its regioselective coupling reactions with prenal: simple and efficient access to osajaxanthone and nigrolineaxanthone F. *Journal of Organic Chemistry* 71, 4992-4995.

Muralidhar P., Kumar M. M., Krishna N., Rao C. B., Rao D. V., **2005**. New sphingolipids and a Sterol from a *Lobophytum* Species of the Indian Ocean. *Chemical Pharmaceutical Bulletin* 53(2), 168-171. doi:10.1248/cpb.53.168.

Ndjonka D., Bergmann B., Agyare C., Zimbres F. M., Lüersen K., Hensel A., Wrenger C., Liebau E. **2012**. *In vitro* activity of extracts and isolated polyphenols from West African medicinal plants against *Plasmodium falciparum*. *Parasitology Research* 111(2), 827-834. https://doi.org/10.1007/s00436-012-2905-y.

Negi J. S., Bisht V. K., Singh P., Rawat M. S. M., Joshi G. P., **2013**. Naturally occurring xanthones: chemistry and biology. *Journal of Applied Chemistry*, 1-9 http://dx.doi.org/10.1155/2013/621459.

Neuwinger D., **2000**. African traditional medicine: a dictionary of plant use and applications. *Medpharm Scientific*, Stuttgart, Germany, p. 589.

Neuwinger D., **2004**. Plants used for poison fishing in tropical Africa. *Toxicon* 44(4), 417-430.

Ngouamegne T. E., **2008**. Etude phytochimique et activité antiplasmodiale *de Endodesmia calophylloïdes* Benth (Guittiferae). Thèse de doctorat, Université de yaoundé I, pp. 1-223.

Ngouamegne T. E., Fongang R., Ngouela S., Fekam F., Rohmer M., Tsamo E., Gut J., Rosenthal P., **2008**. Endodesmiadiol, a friedelane triterpenoid, and other antiplamodial compounds from *Endodesmia calophylloïdes*. *Chemical and Pharmaceutical Bulletin* 56, 374-377.

Ngouateu O. B., Dondji B., **2022**. Leishmaniasis in Cameroon and neighboring countries: An overview of current status and control challenges. *Current Research in Parasitology & Vector-Borne Diseases* 2, 100077.

Ngouela S., Lenta B. N., Noungoue D. T., Ngoupayo J., Boyom F. F., Tsamo E., Gut J., Rosenthal P. J., Connolly J. D., **2006**. Anti-plasmodial and antioxidant activities of constituents of the seed shells of *Symphonia globulifera* Linn f. *Phytochemistry* 67, 302-306.

Ninh T. S., Nguyen T. T. H., Pham V. C., Le T. A., Nguyen T. T., Ba T. C., **2020**. Antimicrobacterial xanthones from *Garcinia mackeaniana* leaves. *Vietnam Journal of Chemistry* 58, 343-48.

Normand D., **2014**. Anatomie des bois de *Endodesmia* et de *Lebrunia*. *Bulletin* of the Botanical *Society* of France 91, 245-246.

Nozaki H., Suzuki H., Hirayama T., kasai R., Wu R. Y., Lee H. K., **1986**. Antitumour triterpenes of *Maytenus diversifolia*. *Phytochemistry* 25(2), 479-485.

Nurhamidah., Nurdin H., Manjang Y., Dharma A., Suryati., **2016**. Isolation and characterization of *β*-amyrin palmitate from fruit of *Ficus aurata* (Miq.) Miq. *Journal of Chemical and Pharmaceutical Research* 8(4), 677-679.

OCDE., **2001**. Toxicité orale aiguë-méthode par classe de toxicité aiguë. *Ligne directrice de l'OCDE pour les essais de produits chimiques*, *Ligne directrice* 423, p.14.

Office national de développement des forêts du Cameroun., **1998**. Liste des essences par ordre alphabétique des noms commerciaux et locaux, pp. 10-15.

Okoye N. N., Ajaghaku D. L., Okeke H. N., Ilodigwe E. E., Nworu C. S., Okoye F. B. C., **2014**. *beta*-Amyrin and *alpha*-amyrin acetate isolated from the stem bark of *Alstonia boonei* display profound anti-inflammatory activity. *Pharmaceutical Biology* 52(11), 1478-1486. doi:10.3109/13880209.2014.898078

Okpekon T., Yolou S., Gleye C., Roblot F., Loiseau P., Bories C., Grellier P., Frappier F., Laurens A., Hocquemiller R., **2004**. Antiparasitic activities of medicinal plants used in Ivory Coast. *Journal of Ethnopharmacology* 90, 91-97.

OMS., **2000**. Principes méthodiques généraux pour la recherche et l'évaluation relative à la médécine traditionnelle 2015: Résumé. *WHO/EDT/TRMP. Organisation mondiale de la Santé, Genève, Suisse*, p. 87.

Ouattara N., **1999**. Evolution du taux de germination de semences oléagineuses en fonction du mode et de la durée de conservation. Cas du *Pentadesma butyracea* Sabine (Lami). In: Ouédraogo AS, Boffa J-M (eds) Vers une approche régionale des ressources génétiques forestières en Afrique sub-saharienne. Actes de l'atelier sur la conservation et l'utilisation durable des ressources génétiques forestières en Afrique de l'Ouest, Afrique Centrale et Madagascar, Ouagadogou, Burkina-Faso. IPGRI, Rome, Italie, pp. 170-174.

Pellegrin F., **1959**. Guttifères d'Afrique Equatoriale. *Bulletin* of the Botanical *Society France* 2, 217-218.

Peters S., Schmidt W., Beerhues L., **1997**. Regioselective oxidative phenol couplings of 2,3',4,6-tetrahydroxybenzophenone in cell cultures of *Centaurium erythraea* RAFN and *Hypericum androsaemum L. Planta* 204, 64-69.

Quotig-info., **2011**. Plantes botaniques. N° 10, p. 1-2.

Rachman O., Balfas T., Sifat P. K., **1987**. Machining properties of wood species from West-Java. *Journal Penelitian Hasil Hutan* 4, 54-64.

Ragasa C. Y., Espineli D. L., Shen C. C., **2011**. New triterpenes from *Barringtonia asiatica*. *Chemical and Pharmaceutical Bulletin* 59, 778-782.

Ramos M. d. R., Jerz G., Villanueva S., López-Dellamary F., Waibel R., Winterhalter P., **2004**. Two glucosylated abscisic acid derivates from avocado seeds (*Persea americana* Mill. Lauraceae cv. Hass). *Phytochemistry* 65, 955-962.

Raponda-Walker A., Sillans R., **1961**. Les plantes utiles du Gabon. Paul Lechevalier, Paris, France p. 614.

Reagan-Shaw S., Nihal M., Ahmad N., **2007**. Dose translation from animal to human studies revisited. *The FASEB Journal* 22(3), 659-661. doi:10.1096/fj.07-9574lsf.

Reddy M., Gupta S., Jacob M., Khan S., Ferreira D., **2007**. Antioxidant, antimalarial and antimicrobial Activities of tannin-rich fractions, ellagitannins and phenolic acids from *Punica granatum* L. *Planta Medica* 73(5), 461-467. https://doi.org/10.1055/s-2007-967167

Reis M. Á., Novaes R. D., Baggio S. R., Viana A. L. M., Salles B. C. C., Duarte S. M. da S., Rodrigues M. R., Paula F. B. de A., **2018**. Hepatoprotective and Antioxidant Activities of Oil from Baru Almonds (*Dipteryx alata* Vog.) in a Preclinical Model of Lipotoxicity and Dyslipidemia. *Evidence-Based Complementary and Alternative Medicine* 1-11. doi:10.1155/2018/8376081.

Robyns A., **1995**. Passifloraceae. In: Bamps, P. (Editor). Flore d'Afrique centrale. Spermatophytes. *Jardin botanique national de Belgique,* Brussels, Belgium, p. 75.

Rocha L. G., Almeida J. R. G. S., Macêdo R. O., Barbosa-Filho J. M., **2005**. A review of natural products with antileishmanial activity. *Phytomedicine* 12(6-7), 514-535. doi:10.1016/j.phymed.2003.10.006

Rodrigues K. A. D. F., Amorim L. V., Dias C. N., Moraes D. F. C., Carneiro S. M. P., Carvalho F. A. D. A., **2015**. *Syzygium cumini* (L.) Skeels essential oil and its major constituent *α*- pinene exhibit anti-leishmania activity through immunomodulation *in vitro*. *Journal of Ethnopharmacology* 160, 32-40.

Roux D., Hadi H. A., Thoret S., Guénard D., Thoison O., Païs M., Sévenet T., **2000**. Structure-activity relationship of polyisoprenylated benzophenones from *Garcinia pyrifera* on the tubilin/microtubule system. *Journal of Natural Products* 63, 1070-1076.

Ryu H. W., Curtis-Long M. J., Jung S., Jin Y. M., Cho J. K., Ryu Y. B., Lee W. S., Park K. H., **2010**. Xanthones with neuraminidase inhibitory activity from the seedcases of *Garcinia mangostana. Bioorganic and Medicinal Chemistry* 18(17), 6258-6264. doi:10.1016/j.bmc.2010.07.033.

Sabudak T., Isik E., Oksuz S., **2007**. Lipid constituents of *Trifolium resupinatum* var. *microcephalum. Natural Product Research* 21, 828-833.

Saddoughi S. A., Song P., Ogretmen B., **2008**. Roles of bioactive sphingolipids in cancer biology and therapeutics. *Lipids in Health and Disease* 413-440. doi:10.1007/978-1-4020-8831-516.

Sang W. C., Ki H. K., II K. L., Sang U. C., Shi Y. R., Kang R. L., **2009**. Phytochemical constituents of *Bistorta manshuriensis. Natural Product Sciences* 15, 234-240.

Sarah J., Peter F., David P., Geoffrey C., David C., Colin W., **2000**. Antiplasmodial and antiamoebic activities of medicinal plants from Sierra Leone. *Phytotherapy Research* 14, 356-358.

Sarkodie A. J., Fleischer C. T., Edoh A.D., Dickson A. R., Mensah L. K., Annan K., Woode E., Koffour A. G., Appiah A. A., Brew-Daniels H., **2013**. Antihyperglycaemic activity

of ethanolic extract of the stem of *Adenia lobata* ENGL (Passifloraceae). *International Journal of Pharmaceutical Sciences* and *Research* 4, 1370-1377.

Schmidt W., Peters S., Beerhues L., **2000**. Xanthone 6-hydroxylase from cell cultures of *Centaurium erythraea* RAFN and *Hypericum androsaemium* L. *Phytochemistry* 53, 427-431.

Schultes E., Raffauf F., **1990**. The Healing Forest - Medicinal and toxic plants of the Northwest Amazonia. Dioscorides Press, Portland, Oregon (USA), p. 484.

Scmelzer A., Arro R., Bosh C., Ruijter A., Simmonds M., Lemmens R., Chauvet M., **2008**. Ressources végétales de l'Afrique tropicale; plantes médicinales. Fondation Prota, backlurgs pubishers, cta, wageninpen, Pays-bas, p. 42.

Scmelzer G., Gurib-fakim A., **2008**. Ressources végétales de l'Afrique tropicale (11). Plantes médicinales (1), Wageningen, *Backhuys Publishers*, p. 869.

Shaiq Ali M., Ahmed W., Saleem M., Khan T., **2006**. Longifoamide-A and B: two new ceramides from *Mentha longifolia* (Lamiaceae*). Natural Product Research* 20(10), 953-960. doi:10.1080/14786410500445186.

Shiojima K., Masuda K., Suzuki H., Lin T., Ooishi Y., Ageta H., **1995**. Composite constituents: forty-two triterpenoids including eight novel compounds isolated from *Picris hieracioides* subsp, *japonica. Chemical and Pharmaceutical Bulletin* 43, 1634-1639.

Silva E. M., Araújo R. M., Freire-Filha L. G., Silveira E. R., Lopes N. P., de Paula J. E., Braz-Filhof R., Espindola L. S., **2013**. Clusiaxanthone and tocotrienol Series from *Clusia pernambucensis* and their antileishmanial activity. *Journal* of the *Brazilian Chemical Society* 24, 1314-1321.

Silva S.M.A., Pinto A.G.C.D., **2005**. Structure elucidation of xanthone derivatives: studies of nuclear magnetique resonnance spectroscopy. *Current Medecinal Chemistry* 12(21), 2481-2497. doi:10.2174/092986705774370718.

Simões-Pires C. A., Vargas S., Marston A., Ioset J. R., Paulo M. Q., Matheeussen A., Maes L., **2009**. Ellagic acid derivatives from *Syzygium cumini* Stem Bark : Investigation of their antiplasmodial activity. *Natural Product Communications* 4(10), 1934578X0900401. https://doi.org/10.1177/1934578X0900401012.

Singh N., Kaushik N. K., Mohanakrishnan D., Tiwari S. K., Sahal D., **2015**. Antiplasmodial activity of medicinal plants from Chhotanagpur plateau, Jharkhand. India. *Journal of Ethnopharmacology* 165, 152-162.

Sinsin B., Sinadouwirou T. A., **2003**. In Cahiers Agricultures. John Libbey Eurotext: Montrouge, Vol. 12, No. 2, pp. 75-79.

Siqueira-Neto J. L., Song O. R., Oh H., Sohn J. H., Yang G., Nam J., Jang J., Cechetto J., Lee C. B., Moon S., Genovesio A., Chatelain E., Christophe T., Freitas-Junior L. H., **2010**. Antileishmanial high-throughput drug screening reveals drug candidates with new scaffolds. *PLOS Neglected Tropical Diseases* 4, 675.

Smilkstein M., Sriwilaijaroen N., Kelly J. X., Wilairat P., Riscoe M., **2004**. Simple and inexpensive fluorescence-based technique for High-Throughput antimalarial drug screening. *Antimicrobial Agents and Chemotherapy* 48, 1803-1856.

Soh P. N., Witkowski B., Olagnier D., Nicolau M. L., Garcia-Alvarez M. C., Berry A., Benoit-Vical F., **2009**. *In vitro* and *in vivo* Properties of ellagic acid in Malaria Treatment. *Antimicrobial Agents and Chemotherapy* 53(3), 1100‑1106. https://doi.org/10.1128/AAC.01175-08.

Sousa G., Duarte L., Alcântara A., Silva G., Vieira-Filho S., Silva R., Oliveira D., Takahashi J., **2012**. New triterpenes from *Maytenus robusta*: Structural elucidation based on NMR experimental data and theoretical calculations. *Molecules* 17(11), 13439-13456. doi:10.3390/molecules171113439.

Spencer K. C., Seigler D. S., **1987**. Passicoriacin and epipassicoriacin: C-4 epimers of tetraphyllin B and epitetraphyllin B from *Passiflora coriacea*. *Phytochemistry* 26(6), 1661-1663. doi:10.1016/s0031-9422(00)82265-7.

Stevens P. F., **1980**. A revision of the Old World species of *Calophyllum* (Guttiferae). *Journal of the Arnold Arboretum* 61, 117-699.

Sturm N., Hu Y., Zimmermann H., Fritz-Wolf K., Wittlin S., Rahlfs S., Becker K., **2009**. Compounds Structurally Related to Ellagic Acid Show Improved Antiplasmodial Activity. *Antimicrobial Agents and Chemotherapy* 53(2), 622‑630.

Suárez A. I., Beth D. M., Monache F. D., Compagnone R. S., **2003**. Biflavonoids from *Podocalyx loranthoides*. *Fitoterapia* 74, 473-475.

Sultanbawa M. U. S., **1980**. Xanthonoids of tropical plants. *Tetrahedron* 36, 1465-1506.

Taher M., Idris M. S., Ahmad F., Arbain D., **2005**. A polyisoprenylated ketone from *Calophyllum enervosum*. *Phytochemistry* 66, 723-726.

Tala M. F., Wabo H. K., Zeng G. Z., Ji C. J., Tane P., Tan N. H., **2013**. A prenylated xanthone and antiproliferative compounds from leaves of *Pentadesma butyracea*. *Phytochemistry Letters* 6, 326-330.

Tantisewie B., Ruijgrok H. W. L., Hegnauer R., **1969**. Cyanogenic compounds in Parietales and some further species. V. Distribution of hydrocyanic acid in cormophytes. *Pharmaceutisch Weekblad* 109, 1341-1355.

Tchobo F., Natta A., Barea B., Barouh N., Piombo G., Pina M., Villeneuve P., Soumanou M., Sohounhloue D., **2007**. *Journal* of the *American Oil* Chemists' *Society* 84, 755-760.

Teinkela J. E. M., Noundou X. S., Fannang S., Song A. M., Nguedia J. C. A., Heinrich C.H., Rui W. M. K., **2019**. Terminaliamide, a new ceramide and other phytoconstituents from the roots of *Terminalia mantaly* H. Perrier and their biological activities. *Natural Product Research*. doi: 10.1080/14786419.2019.1647425.

Thakur S., Joshi J., Kaur S., **2020**. Leishmaniasis diagnosis: an update on the use of parasitological, immunological and molecular methods. *Journal of Parasitic Diseases* 44(2), 253-272. doi:10.1007/s12639-020-01212-w.

Torres-Guerrero E., Quintanilla-Cedillo M. R., Ruiz-Esmenjaud J., Arenas R., **2017**. Leishmaniasis: a review. *F1000 Research* 6, 1-15.

Troupin G., **1978**. Flore du Rwanda. Vol. 1, Institut National de la Recherche Scientifique de la République Rwandaise, Musée Royal de l'Afrique Centrale, Tervurin, Belgique, pp. 297-307.

Ullah N., Nadhman A., Siddiq S., Mehwish S., Islam A., Jafri L., Hamayun M., **2016**. Plants as Antileishmanial Agents: Current Scenario. *Phytotherapy Research* 30(12), 1905-1925. doi:10.1002/ptr.5710.

Ulubeblen A., Oksuz S., Mabry J., Dellamonica G., Chopin J., **1982**. C-glycosylflavnoids from *Passiflora pittieri*, *P. alata*, *P. ambigua* and *Adenia mannii. Journal of Natural Products* 45, 783.

Usman A., Thoss V., Nur-e-Alam M., **2016**. Isolation of (-) - epicatechin from *Trichilia emetica* whole seeds. *American journal of organic chemistry* 6, 81-85.

Valentão P., Andrade P. B., Silva E., Vicente A., Santos H., Bastos M. L., Seabra R. M., **2002**. Methoxylated xanthones in the quality control of small centaury (*Centaurium erythraea*) Flowering Tops. *Journal of Agricultural and Food Chemistry* 50(3), 460-463. doi:10.1021/jf0109571.

Wabo H. K., Kikuchi H., Katou Y., Tane P., Oshima Y., **2010**. Xanthones and a benzophenone from the roots of *Pentadesma butyracea* and their antiproliferative activity. *Phytochemistry Letters* 3, 104-107.

Waterman P. G., **1986**. A phytochemist in the african rain forest. *Phytochemistry* 25, 3-17.

Wen Q., Lin X., Liu Y., Xu X., Liang T., Zheng N., Kintoko K., Huang R., **2012**. Phenolic and Lignan glycosides from the butanol extract of *Averrhoa carambola* L. Root. *Molecules* 17(10), 12330-12340. doi:10.3390/molecules171012330.

White L., Albernethy K., **1996**. Guide de la végétation de la réserve de la Lopé. Traduit de l'anglais par Benoît Fontaine & Anne Rouvière, p. 224.

WHO., **2018**. Global leishmaniasis surveillance in the WHO European region. vol 93, 521-530.

WHO., **2020**. Weekly epidemiological record. N°25, vol 95, 265-280.

Yaoita Y., Kohata R., Kakuda R., Machida K., Kikuchi M., **2002**. *Ceramide Constituents from Five Mushrooms. Chemical and Pharmaceutical Bulletin* 50(5), 681-684. doi:10.1248/cpb.50.681.

Yemeli D. L., Domche A., Djeunga N. C. H., Nanga L. G. C., Tabah N. E., Nko'Ayissi B. G., Kamgno J., **2021**. Leishmaniasis in Cameroon: what is known and is done so far? A protocol for systematic review. *BMJ Open* 11, 1-4.

Yong Y. J., **1992**. A flavonoid study of the *lauraceae.* Thesis of Master of Science, Departement of Botany, The Faculty of Graduate Studies, The University of British Columbia, p. 19.

Yu L., Zhao M., Yang B., Zhao Q., Jiang Y., **2007**. Phenolics from hull of *Garcinia mangostana* fruit and their antioxidant activities. *Food Chemistry* 104, 176-181.

Zelefack F., Guilet D., Fabre N., Bayet C., Chevalley S., Ngouela S., Lenta B. N., Valentin A., Tsamo E., Geneviève M., Dijoux F., **2009**. Cytotoxic and antiplasmodial xanthones from *Pentadesma butyracea*. *Journal of Natural Products* 72, 954-957.

Zhu Y., Soroka D. N., Sang S., **2013**. Structure elucidation and chemical profile of sphingolipids in wheat bran and their cytotoxic effects against human colon cancer cells. *Journal of Agricultural and Food Chemistry* 61(4), 866-874. doi:10.1021/jf3047863.

ANNEX

Publications resulting from this work

1. **Jean Garba Koffi**., Rodrigue Keumoe., Cyrille Armel Njanpa Ngansop., Donald Ulrich Kenou Kagho., Billy Toussie Tchegnitegni., Yannick Stéphane Fongang Fotsing., Jean Jules Kezetas Bankeu., Fabrice Fekam Boyom., Norbert Sewald., Bruno Ndjakou Lenta., 2021. Constituents of *Endodesmia calophylloides* Benth and *Adenia lobata* (Jacq.) Engl. with antileihsmanial activities. *Chemeical Data Collections* 35, 100751.

2. **Jean Koffi Garba**., Ruland Tchuinkeu Nguengang., Gwladys Tatiana Youmbi., Joel Njopnu Menatche., Cyrille Armel Njanpa Ngansop., Jean Jules Kezetas Bankeu., Jean Rodolphe Chouna., Fabrice Fekam Boyom., Norbert Sewald., Bruno Ndjakou Lenta., 2021. Antileishmanial, antibacterial and cytotoxicity activity of extracts, fractions and compounds from the fruits and stem bark extract of *Pentadesma butyracea* Sabine. *Zeitschrift fur Naturforschung B*, 1-7.